Anatomy, Relationships, and Paleobiology of *Cambaytherium* (Mammalia, Perissodactylamorpha, Anthracobunia) from the lower Eocene of western India

Kenneth D. Rose , Luke T. Holbrook , Kishor Kumar , Rajendra S. Rana , Heather E. Ahrens , Rachel H. Dunn , Annelise Folie , Katrina E. Jones & Thierry Smith

Published online: 05 Nov 2020.

Submit your article to this journal

View related articles

View Crossmark data

ANATOMY, RELATIONSHIPS, AND PALEOBIOLOGY OF *CAMBAYTHERIUM* (MAMMALIA, PERISSODACTYLAMORPHA, ANTHRACOBUNIA) FROM THE LOWER EOCENE OF WESTERN INDIA

KENNETH D. ROSE, [*,1] LUKE T. HOLBROOK, [2] KISHOR KUMAR, [3] RAJENDRA S. RANA, [4]
HEATHER E. AHRENS,[5] RACHEL H. DUNN, [6] ANNELISE FOLIE,[7] KATRINA E. JONES, [8] and THIERRY SMITH [9]

[1]Center for Functional Anatomy and Evolution, The Johns Hopkins University School of Medicine, 1830 E. Monument Street, Baltimore, Maryland 21205, U.S.A., kdrose@jhmi.edu;

[2]Department of Biological Sciences, Rowan University, Glassboro, New Jersey 08028, U.S.A., holbrook@rowan.edu;

[3]Wadia Institute of Himalayan Geology, Dehradun 248001, Uttarakhand, India, kishorsri@gmail.com;

[4]Department of Geology, H. N. B. Garhwal University, Srinagar 246175, Uttarakhand, India, Rajendra.Rana1@gmail.com;

[5]Department of Biology, High Point University, High Point, North Carolina 27268, U.S.A., hahrens@highpoint.edu;

[6]Department of Anatomy, Des Moines University, Des Moines, Iowa 50312, U.S.A., Rachel.Dunn@dmu.edu;

[7]Scientific Survey of Heritage, Royal Belgian Institute of Natural Sciences, Rue Vautier 29, B-1000 Brussels, Belgium, annelise.folie@naturalsciences.be;

[8]Department of Organismic & Evolutionary Biology, Harvard University, Cambridge, Massachusetts 02138, U.S.A., katrinajones@fas.harvard.edu;

[9]Directorate Earth and History of Life, Royal Belgian Institute of Natural Sciences, Rue Vautier 29, B-1000 Brussels, Belgium, thierry.smith@naturalsciences.be

ABSTRACT—The anatomy of *Cambaytherium*, a primitive, perissodactyl-like mammal from the lower Eocene Cambay Shale Formation of Gujarat, India, is described in detail on the basis of more than 350 specimens that represent almost the entire dentition and the skeleton. *Cambaytherium* combines plesiomorphic traits typical of archaic ungulates such as phenacodontids with derived traits characteristic of early perissodactyls. *Cambaytherium* was a subcursorial animal better adapted for running than phenacodontids but less specialized than early perissodactyls. The cheek teeth are bunodont with large upper molar conules, not lophodont as in early perissodactyls; like perissodactyls, however, the lower molars have twinned metaconids and m3 has an extended hypoconulid lobe. A steep wear gradient with heavy wear in the middle of the tooth row suggests an abrasive herbivorous diet. Three species of *Cambaytherium* are recognized: *C. thewissi* (~23 kg), *C. gracilis* (~10 kg), and *C. marinus* (~99 kg). Body masses were estimated from tooth size and long bone dimensions. Biostratigraphic and isotopic evidence indicates an age of ca. 54.5 Ma for the Cambay Shale vertebrate fauna, the oldest Cenozoic continental vertebrate assemblage from India, near or prior to the initial collision with Asia. Cambaytheriidae (also including *Nakusia* and *Perissobune*) and Anthracobunidae are sister taxa, constituting the clade Anthracobunia, which is sister to Perissodactyla. We unite them in a new higher taxon, Perissodactylamorpha. The antiquity and occurrence of *Cambaytherium*—the most primitive known perissodactylamorph—in India near or before its collision with Asia suggest that Perissodactyla evolved during the Paleocene on the Indian Plate or in peripheral areas of southern or southwestern Asia.

INTRODUCTION

Cambaytherium is a medium-sized, bunodont, perissodactyl-like mammal from the lower Eocene Cambay Shale Formation of Gujarat, India. Initially based primarily on lower dentitions, the genus was described as a perissodactyl by Bajpai et al. (2005a), who remarked on its bunodonty. Soon after *Cambaytherium* was named, Rose et al. (2006) described *Indobune vastanensis*, based on bunodont upper teeth, and assigned it to the family Anthracobunidae, then considered to be stem tethytheres or basal proboscideans (Gheerbrant et al., 2005b). Additional specimens demonstrated that these two genera were synonymous, with *Cambaytherium* having priority. However, neither of these earlier reports recognized the

phylogenetic and paleobiogeographic significance of *Cambaytherium*; and were it not for subsequent discoveries of most of the skeleton, the taxon might have been relegated to comparative obscurity as an endemic taxon of little relevance to placentals outside of India. The present study provides a detailed account of the dental and skeletal anatomy of *Cambaytherium* and demonstrates that it occupies a key phylogenetic position with respect to the origin and relationships of the order Perissodactyla. Its phylogenetic relationships in turn have significant paleobiogeographic implications for the origin of the order Perissodactyla and the early diversification of Euungulata.

Initial comparison of *Indobune* upper teeth with those of the supposed anthracobunid *Nakusia shahrigensis* from the lower Eocene Ghazij Formation of Pakistan (Ginsburg et al., 1999) indicated a close relationship and was part of the evidence cited to support allocation of *Indobune* to Anthracobunidae. In the 1980s and 1990s, anthracobunids—a group apparently confined

---

*Corresponding author.

to the Indian Plate—were thought to be either basal proboscideans or basal tethytheres (West, 1980; Wells and Gingerich, 1983). This interpretation was bolstered by discovery of an astragalus from Kashmir attributed to *Anthracobune* (Gingerich et al., 1990). With the realization that *Indobune* is a junior synonym of *Cambaytherium*, however, it is now clear that *Nakusia* is also a cambaytheriid, not an anthracobunid. Moreover, as discussed below, there is reason to question the allocation of the Kashmiri astragalus to Anthracobunidae. Subsequent field work in the Ghazij Formation has yielded another closely related cambaytheriid, *Perissobune* (with two species), which was originally assigned to Perissodactyla incertae sedis (Missiaen and Gingerich, 2014). These discoveries reveal a small radiation of cambaytheres that appears to be confined to the Indian Plate.

When they first described *Cambaytherium*, Bajpai et al. (2005a) proposed three similar-sized species from the same horizon at Vastan Lignite Mine, each based on lower dentitions. As will be shown below, it is probable that these three species are synonymous, and that the proper species name for all of them is *C. thewissi*. Bajpai et al. (2005a) also described an unnamed new species based on an isolated P2, whose published measurements are about 10% larger than the means for P2 in our sample; it probably represents a large individual of *C. thewissi* rather than a distinct taxon. The following year, Bajpai et al. (2006) described a rostrum of a new, large cambaythere they named *Kalitherium marinus*, also from Vastan Mine. Since 2004, we have collected substantial additional material of *C. thewissi* from Vastan Mine and the nearby Mangrol and Tadkeshwar mines, as well as a few specimens that probably represent the larger species. At least one additional significantly smaller species of *Cambaytherium* (*C. gracilis*) has recently been described from Tadkeshwar Mine (Smith et al., 2016). *Cambaytherium* is the most common mammal known from the Cambay Shale, being represented now by more than 350 specimens (including nearly 40 specimens reported by Bajpai et al., 2005a, 2006), which reveal the complete dentition and a substantial part of the postcranial skeleton. More than half of the specimens are craniodental. As more of the skeleton was discovered, it became evident that *Cambaytherium* possesses a mosaic of dental and postcranial features that are more or less intermediate between those of archaic ungulates, particularly phenacodontid condylarths (long regarded as the probable source of Perissodactyla), and basal perissodactyls. This suite of intermediate features placed *Cambaytherium* as the sister taxon of Perissodactyla (Rose et al., 2014b).

As noted above, Bajpai et al. (2005a, 2006) observed that cambaytheres share features in common with perissodactyls, whereas Rose et al. (2006) identified traits in common with anthracobunids. Both observations have proven to be correct. The relationships of anthracobunids themselves have long been controversial and poorly understood, various authors assigning them to Artiodactyla, Perissodactyla, Proboscidea, Sirenia, Tethytheria, Embrithopoda (Phenacolophidae), or order incertae sedis (see Wells and Gingerich, 1983, for a review). Two recent studies (Cooper et al., 2014; Rose et al., 2014b) provided more thorough analyses clarifying their affinities, and both concluded that Anthracobunidae and Cambaytheriidae are closer to Perissodactyla than to Proboscidea or Tethytheria, thus corroborating the prescient conclusions of Coombs and Coombs (1979) that *Pilgrimella* (= *Anthracobune*) had perissodactyl affinities. The analyses presented herein support a closer relationship between the two families, grouping *Cambaytherium* and other cambaytheres in a clade together with Anthracobunidae. In our analyses, this clade, Anthracobunia, is consistently the sister taxon of Perissodactyla.

The restriction of both Cambaytheriidae and Anthracobunidae to the Indian Plate strongly suggests that Anthracobunia

originated there, and this has profound implications for the geographic origin of its sister taxon, Perissodactyla. It has long been known that the 'modern' mammalian orders Perissodactyla, Artiodactyla, and Euprimates first appear at the beginning of the Eocene across the Laurasian continents (e.g., Simpson, 1947; McKenna, 1975; Rose, 1981), but only more recently has the abruptness of their appearance become apparent (e.g., Gingerich, 1989, 2006; Bowen et al., 2002; Smith et al., 2006; Rose et al., 2012). Despite substantial field exploration, the geographic source of these apparent immigrants is still a mystery, although it has been suggested (Hooker, 2005) that Asia was the likely center of origin. Previously, Krause and Maas (1990) postulated that the three orders could have originated on India during its northward drift, but no direct evidence then existed. This intriguing hypothesis provided the initial impetus for our field work in the early Cenozoic of India. With Eocene Anthracobunia restricted to the Indian Plate, and early Eocene cambaytheres probably predating India's initial collision with Asia, the possibility that Perissodactyla originated on the Indian Plate or somewhere along the adjacent periphery must be reconsidered.

The Cambay Shale fauna occupies a unique paleogeographic position. It is the only early Eocene biota known from peninsular India. Nearly all other known Eocene vertebrate faunas are from middle or high latitudes, which has long colored our perception of the Eocene biota. Eocene tropical faunas are rare, and the Cambay Shale fauna is undoubtedly the richest fauna known from near the equator (about 5–10°S latitude; e.g., Copley et al., 2010; Clementz et al., 2011) during the early Eocene. This fauna offers a new perspective on the early Eocene biota by providing data on an assemblage that formed under nearshore, continental tropical conditions.

Here, we present a detailed account of the anatomy of *Cambaytherium* and its functional implications, together with new, comprehensive phylogenetic analyses incorporating all the new anatomical data. These data are in turn used to reevaluate the phylogenetic, paleogeographic, and paleoenvironmental significance of this pivotal taxon.

Institutional Abbreviations—**AMNH**, American Museum of Natural History, New York, New York, U.S.A.; **GSP-UM**, Geological Survey of Pakistan–University of Michigan collection, Quetta, Pakistan; **GU**, Department of Geology, H. N. B. Garhwal University, Srinagar, Uttarakhand, India (GU is used throughout as shorthand for GU/RSR/VAS [Vastan], GU/RSR/MN [Mangrol], and GU/RSR/TAD [Tadkeshwar]; numbers in the 7000 series apply to Mangrol Mine, and those in the 9000 series apply to Tadkeshwar; all others apply to fossils from Vastan Mine); **H-GSP**, Howard University–Geological Survey of Pakistan, Quetta and Islamabad, Pakistan; **IITR/SB/VLM**, Vertebrate Paleontology Laboratory, Department of Earth Sciences, Indian Institute of Technology, Roorkee, India (IITR is used as an abbreviation herein); **IVPP**, Institute of Vertebrate Paleontology and Paleoanthropology of the Chinese Academy of Sciences, Beijing, China; **LUVP**, Lucknow University Vertebrate Paleontology collection, Department of Geology, Lucknow, India (collection transferred to Wadia Institute of Himalayan Geology, Dehradun, Uttarakhand, India); **MNHN**, Muséum national d'Histoire naturelle, Paris, France; **NHMUK**, Palaeontology Department, Natural History Museum, London, U.K.; **USGS**, United States Geological Survey, Denver, Colorado, U.S.A. (collection transferred to USNM); **USNM**, Department of Paleobiology, United States National Museum of Natural History, Smithsonian Institution, Washington, D.C., U.S.A.; **USNM-M**, Department of Mammalogy, United States National Museum of Natural History, Smithsonian Institution, Washington, D.C., U.S.A.; **WIF/A**, Wadia Institute of Himalayan Geology, Vertebrate Paleontology, Dehradun, Uttarakhand, India.

BACKGROUND

Geological Setting and Paleoecology

The Cambay Shale Formation is a lower Eocene deposit in the Cambay Basin, a narrow graben trending roughly north-south in western India. The basin covers more than 50,000 km^2 extending from Sanchor, Rajasthan, in the north to Surat, Gujarat, in the south. The Cambay Basin formed during the Early Cretaceous due to rifting along the Precambrian Dharwar tectonic trend (Biswas, 1987; Mohan, 1995; Rangarajan, 2008). The oldest sediments in the basin, which overlie the granitic basement, are of Early Cretaceous age. Deposition in the Cambay Basin was interrupted during the Late Cretaceous and early Paleocene by extensive basalt flows, the Deccan Traps (which covered a large part of western and central India), and resumed in the late Paleocene (Chandra and Chowdhary, 1969; Rao, 1969; Sudhakar and Basu, 1973). Today, the Cambay Basin is a rich hydrocarbon region of India, with the Cambay Shale Formation being a particularly important hydrocarbon source rock (Mohan, 1995).

The oldest Cenozoic sediments in the Cambay Basin nonconformably overlie the Deccan Traps and represent the syn-rift stage of deposition. These deposits comprise the upper Paleocene–lower Eocene Vagadkhol/Olpad and the lower Eocene Cambay Shale formations. Although they mostly occur in the subsurface, limited surface exposures are present on both sides of the Gulf of Cambay (= Khambhat)—to the west along the Saurashtra coast (southwestern Gujarat) and to the east between the Narmada and Tapi (= Tapti) rivers. The Vagadkhol Formation and its subsurface equivalent Olpad Formation were deposited on the Deccan Traps and underlie the Cambay Shale Formation. Surface exposures of the Vagadkhol Formation consist of clay and gritty sand or conglomerate, which have produced well-preserved leaves and petrified wood, but so far no vertebrates (Chandra and Chowdhary, 1969; Sudhakar and Basu, 1973; Singh et al., 2011). The Cambay Shale Formation consists mainly of greenish and gray to black mudstone and shale with multiple lignite seams; in the subsurface (see below), the formation also contains calcareous shales and thin limestones (McCann, 2010). Pandey et al. (1993) divided the Cambay Shale Formation into two units: the Older Cambay Shale and the Younger Cambay Shale, separated by an unconformity. The subsurface strata that have produced mammals and other vertebrates correspond to the upper part of the Older Cambay Shale (McCann, 2010). No vertebrate fossils have been reported from surface exposures of the Cambay Shale. Overlying the Cambay Shale is the upper Eocene nummulitic limestone and marl of the Amravati Formation (Sudhakar and Basu, 1973). Nummulitic clays at the top of the section at Tadkeshwar Mine recently produced an assemblage of ostracods that are predominantly middle Eocene in age (Nagori et al., 2013). The Cambay Shale Formation has yielded a great variety of plant and animal fossils (e.g., Singh et al., 2010, 2014, 2015; Kumar et al., 2011; Rao et al., 2013; updated lists of the vertebrate fauna, including references, are provided later in this section).

Subsurface beds of the Cambay Shale Formation are exposed in a series of open cast lignite mines distributed for about 20 km along a southwest–northeast line in the interfluve between the Narmada and Tapi rivers (Fig. 1). From south to north, these mines are Tadkeshwar, Vastan, Mangrol, and Valia. Fossil vertebrates have been found in the first three mines but not yet at Valia, and the most extensive samples have come from Vastan. Vastan Lignite Mine (Fig. 2) is situated about 29 km northeast of the city of Surat. It consists of two pits: Vastan North (latitude 21°25′47″N, longitude 73°7′30″E) and Vastan South (latitude 21°23′51″N, longitude 73°4′47″E). Vastan North Pit, the most productive site in the Cambay Shale, is about 3.5 km across and was closed in June 2012 (and is now inaccessible), whereas Vastan South Pit is still operational but on the verge of closure. Mangrol Mine (latitude 21°26′58″N, longitude 73°7′60″E) is situated a little to the northeast of Vastan North Pit, more or less adjacent to it. This mine has been nonoperational and inaccessible since 2015, although it may reopen in the future. Valia Mine (latitude 21°31′05″N, longitude 73°12′21″E) is the
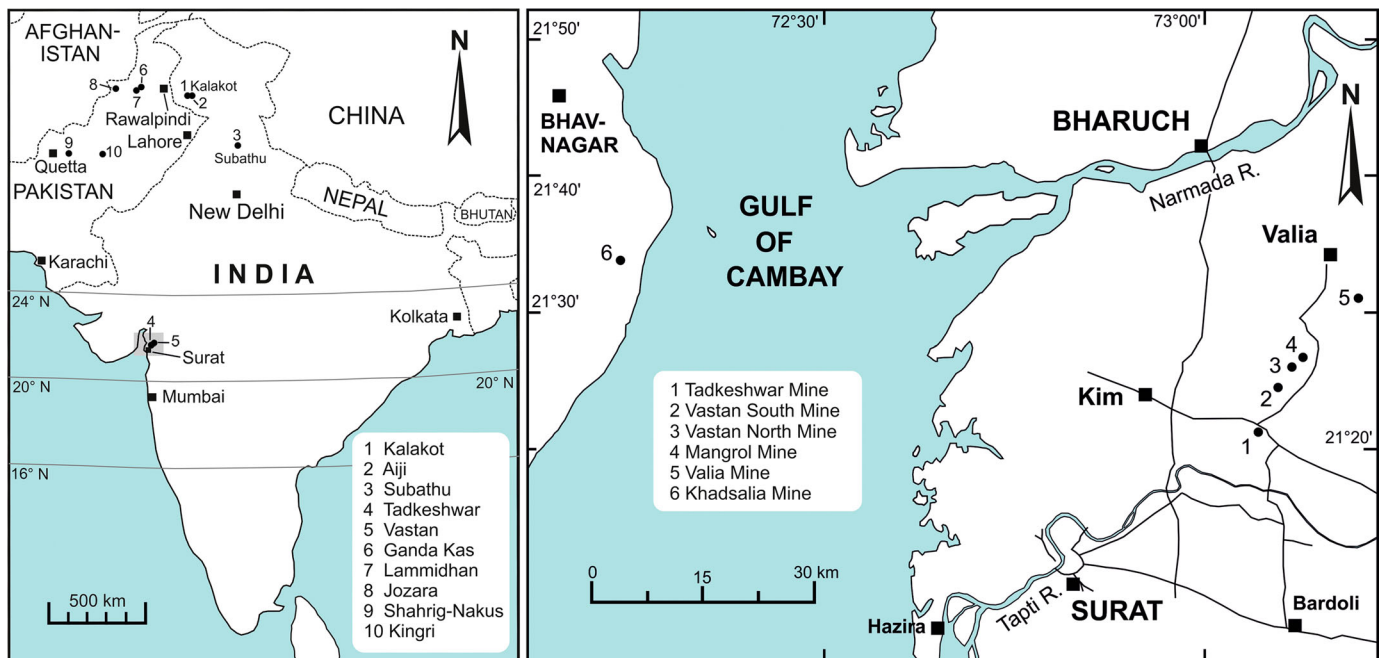

FIGURE 1. Location maps of mines in Gujarat that have produced *Cambaytherium*. Left, location of lignite mines near Surat, as well as localities in northern India and Pakistan that have yielded anthracobunid fossils. Right, enlargement of the small shaded area near Surat, showing location of Gujarat lignite mines. Modified after Smith et al. (2016).

FIGURE 2. Vastan Lignite Mine in 2006; our field team near the water.

northernmost in the series and lies to the northeast of Mangrol. It differs from the other mines in having multiple lignite seams and in generally lacking shelly mudstone beds. Tadkeshwar Mine (latitude 21°20′47″N, longitude 73°04′08″E), located about 10 km southwest of Vastan Mine, is the southernmost mine and is currently fully operational.

Sediments of the Cambay Shale in Vastan, Mangrol, and Tadkeshwar mines are generally similar, comprising two major lignite seams (the higher Lignite 1, and lower Lignite 2 at the floor of the mines). The intervening beds consist of a few minor and often impersistent lignite seams interbedded with shelly and nonshelly mudstones, some of them sandy or carbonaceous, that vary from greenish gray to dark brown or black (Figs. 3–6; e.g., Sahni et al., 2006; McCann, 2010; Prasad et al., 2013). The nonshelly mudstones between the two main lignites contain fish and plant remains (Rana et al., 2004; Singh et al., 2015), whereas fossil mammals are largely restricted to the lowest mudstones just above the lower lignite (see below). The thicknesses of the major lignite seams and the mudstone beds, as well as the number and thickness of minor lignite seams, vary within each mine and between mines, making precise correlation of fossiliferous beds challenging because most beds other than Lignites 1 and 2 are difficult or impossible to trace between sections. As a result of this variation, the two main lignites range from ~15 to 36 m apart in different sections (Sahni et al., 2006; McCann, 2010; Adatte et al., 2014; Smith et al., 2016); nevertheless, each of these two major lignites is believed to have been deposited essentially synchronously across these local mines. The lignites,

especially Lignite 1, contain abundant amber, which has yielded an extensive arthropod fauna (Alimohammadian et al., 2005; Rust et al., 2010). Much of the sequence, including the main mammal-bearing layer at Vastan Mine, contains pyrite or pyritized organic remains (both plants and vertebrates), as well as minor amounts of amber, possibly reworked from the underlying lignite.

The Cambay Shale Formation in Vastan, Mangrol, and Tadkeshwar mines has produced abundant and diverse fossils of continental and marine vertebrates, invertebrates, and plants, as well as dinoflagellate cysts, pollen, and other microfossils. *Cambaytherium* has been found in all three mines, although the majority of specimens were recovered from Vastan Mine (Vastan North). Discovery of fossil material from these mines is possible only because of the ongoing mechanized excavation for lignite coal, which continually exposes fresh surfaces of fossiliferous layers. However, because of mine operations and safety issues, only very small areas of exposure have been accessible to our research team for fossil excavation. Vastan and Mangrol mines, being nearly adjacent to each other, have very similar beds, and the position of the principal vertebrate-yielding layer is nearly the same in the two mines: about 1–3 m above the top of Lignite 2 (Fig. 3C; Sahni et al., 2006). At Vastan Mine, most mammal fossils are concentrated in the lowest part of this interval, but some fossils (including specimens of *Cambaytherium*) have been found in clays 1–2 m higher (at the top of the interval). Almost all *Cambaytherium* specimens from these two mines come from this narrow interval, but at least two specimens, an isolated

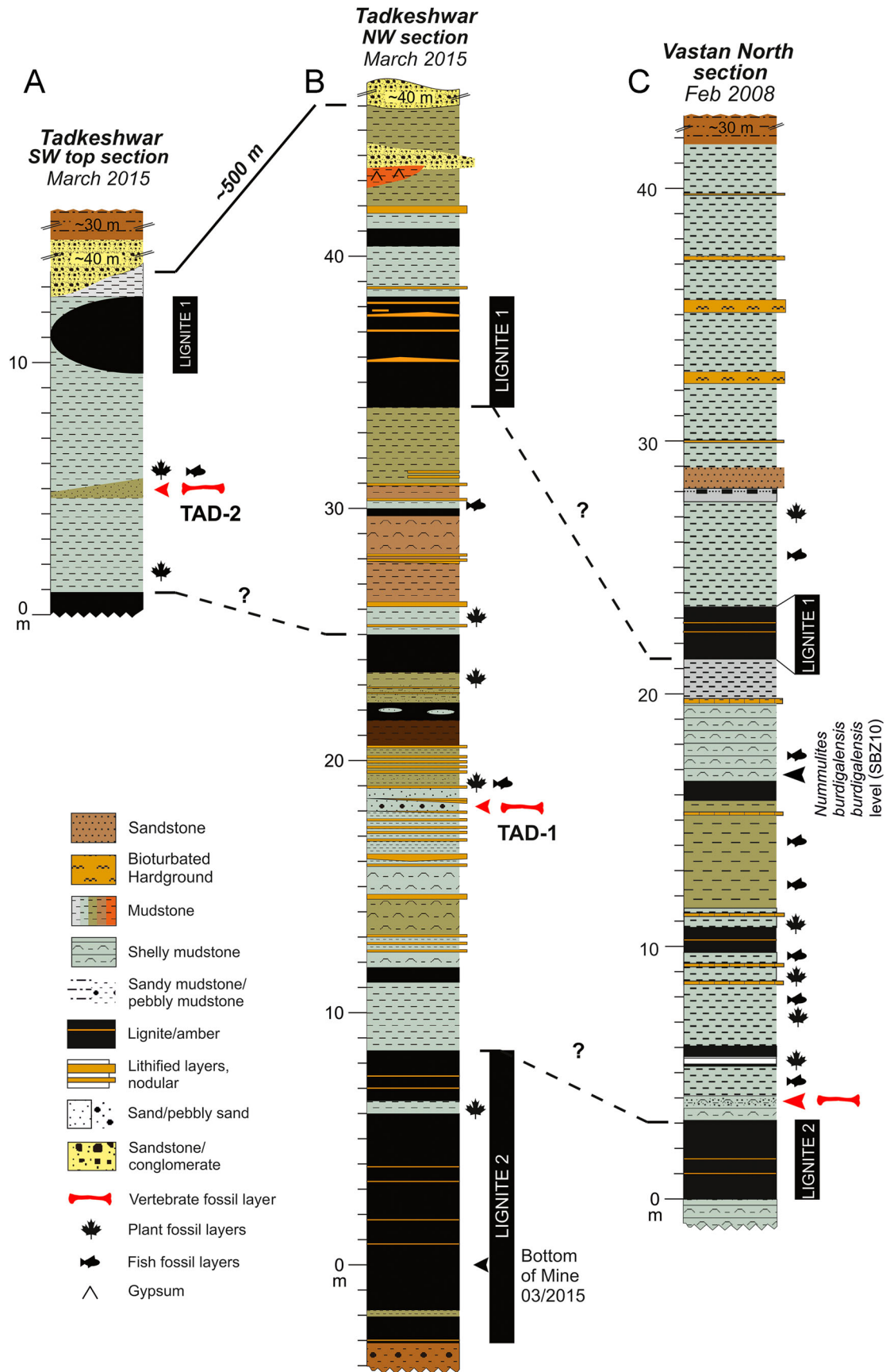FIGURE 3. Stratigraphic sections in Tadkeshwar and Vastan mines showing the location of vertebrate-bearing beds (red arrows) that have produced *Cambaytherium*. Localities TAD-2 (column **A**) and TAD-1 (column **B**) have produced both *C. thewissi* and *C. gracilis*, whereas the bone bed just above Lignite 2 at Vastan (column **C**) has yielded *C. thewissi* and *C. marinus*. Note the variable nature of the sections and thickness.
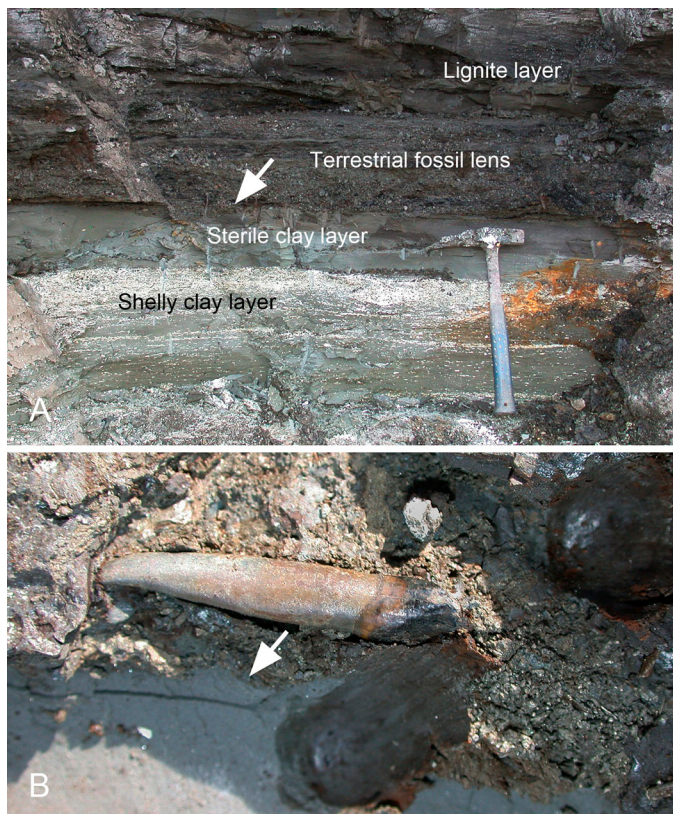
FIGURE 4. **A**, detailed cross-section of the first terrestrial bone-bearing lens found at Vastan Mine on November 17, 2004. **B**, first mammal tooth (*Cambaytherium* incisor, GU 8022) discovered in situ just above the contact between the terrestrial bone-bearing lens and the clay layer below. Arrows in **A** and **B** indicate the contact between the bone-bearing lens and underlying sterile clay layer, which contained no macrofossils.

molar (GU 8013) and a phalanx (GU 8006), were found just below Lignite 1 at Vastan Mine, and it is possible that some of the specimens provided by miners came from above the main layer. In addition, a small number of indeterminate bone fragments were found during our early field work a few meters above Lignite 1, but no other remains were found at this level. Tadkeshwar Mine (Fig. 7) is somewhat different sedimentologically: it has sandier, less carbonaceous channel beds with fewer plant remains, and the fossiliferous layers are stratigraphically higher relative to Lignite 2 (Fig. 3B). Two levels have produced vertebrates at Tadkeshwar (Fig. 3A, B): the lower TAD-1 (channels situated about 5–10 m above Lignite 2 in various sections) and the higher TAD-2 (~12–15 m above TAD-1 and 3–4 m below Lignite 1) (Smith et al., 2016). Both of these levels have produced *Cambaytherium* (Fig. 8). TAD-1 is a sandy channel (or multiple channels) that is up to 60 cm thick, variably conglomeratic at the base, and extends laterally for almost 100 m. It is lighter in color and has less clay and less organic matter than the mammal-bearing bed at Vastan Mine but is thought to be close to the latter in age. TAD-2 was a dark, lenticular, organic sandy clay pocket (worked out) about 30 cm thick and only a few meters wide. It was much richer in organic matter than TAD-1 and was sedimentologically comparable to the lenses at Vastan. TAD-2 lies at the top of another channel, which cuts into the underlying layers. Both TAD-1 and TAD-2 were deposited in a nearshore fluviatile environment (Smith et al., 2016).

Paleoenvironmental Interpretation—The palynofacies, sediments, and sequence stratigraphy of the Cambay Shale in

Vastan, Mangrol, and Tadkeshwar mines indicate that the formation was deposited in a low-energy, coastal marsh-bay environment that received only fine-grained muddy sediment from the weathered Deccan Traps (Sahni et al., 2006; McCann, 2010; Prasad et al., 2013). The sequence contains diverse invertebrate, vertebrate, and plant fossils, as well as microfossils, indicating both continental and marine origins. Lignites formed in coastal marshes, with amber (now known to come largely from dipterocarps; see below) probably washing into lagoons from nearby coastal forests (McCann, 2010; Prasad et al., 2013). Freshwater channels also carried fine-grained sediment, as well as other continental organic matter (leaves, seeds, fruits, bones, and teeth), into the marshland; whereas estuarine sediments and marine mollusk shells, ostracods, foraminiferans, bony fish, and elasmobranch remains washed into the marsh from the shallow bay. In general, however, layers with these assemblages alternate, and there is little mixing of their elements except for occasional shark and ray teeth in the continental lenses. The exceptional preservation of many of the continental vertebrates suggests that they were not transported far from their source.

The flora of the Cambay Shale provides additional information about the paleoenvironment in which *Cambaytherium* lived. Angiosperm pollen, pteridophyte spores, and macrofossils including leaf and fruit impressions, seeds, fruits, wood fragments, and root casts (mangrove) have been found throughout the sequence preserved at Vastan Mine. Singh et al. (2015) reported leaves attributed to the Calophyllaceae (carnation family), Rutaceae (citrus family), Anacardiaceae (cashew-sumac family), Rubiaceae (coffee family), Combretaceae, and Lythraceae (crape myrtle), as well as wood representing Sapindaceae (horse chestnut, maple, lychee), Malvaceae (mallows, hybiscus), and Ebenaceae (ebony, persimmon). Seeds tentatively identified as belonging to the olive family Oleaceae (Sahni et al., 2006:pl. 1) are abundant in and near the mammal layer. These seeds also resemble those of extant Dipterocarpaceae, which have been documented at Vastan from amber found in the lignites and from pollen from strata just above Lignite 2 (Mallick et al., 2009; Prasad et al., 2009; Rust et al., 2010; Dutta et al., 2011; Rao et al., 2013; Paul et al., 2015). Although the seeds cannot be confirmed as deriving from dipterocarps, fossil pollen and the geochemistry of the amber confirm the presence of dipterocarps from Vastan Mine. This is the oldest occurrence of dipterocarps in Southeast Asia and extends their geological range by 20 million years (Dutta et al., 2011). Dipterocarps predominate in present-day rain forests of Southeast Asia. Their abundance in the lower part of the Vastan sequence (Dutta et al., 2011; Rao et al., 2013), together with pollen representing Arecaceae (palms) and Bombaceae (kapok and baobab family), and other tropical angiosperms, provides strong evidence that a coastal tropical rain forest existed in this area in the early Eocene (Paul et al., 2015; Singh et al., 2015).

Vertebrate Fauna of the Cambay Shale

The Cambay Shale Formation at Vastan, Mangrol, and Tadkeshwar lignite mines has produced a diverse fauna of over 100 species of vertebrates: more than 40 species of fishes (including at least 12 sharks and rays), four or five frogs, about 19 species of reptiles (including at least nine snakes and five lizards, but only one rare crocodilian and three turtles), three or four birds, and at least 38 mammal species (Tables 1, 2). This is the most diverse Eocene vertebrate fauna known from an equatorial/tropical region. Although the fauna is overwhelmingly a continental fauna, the sharks and rays and many of the bony fishes indicate estuarine or nearshore marine conditions, and a significant number of the nonmammalian taxa besides fishes were aquatic (frogs, turtles, snakes, and crocodilian). The fishes also include brackish and freshwater taxa (Rana et al., 2004).

FIGURE 5. Excavation at Vastan Mine, 2008. **A**, fossil vertebrate layer (arrows) 1–2 m above the top of the lower lignite (Lignite 2). Sediment is dried on tarps for screen-washing. Prominent white layers higher up are nearshore marine mollusk beds. **B**, excavating the vertebrate-bearing layer and sacking matrix for screen-washing.
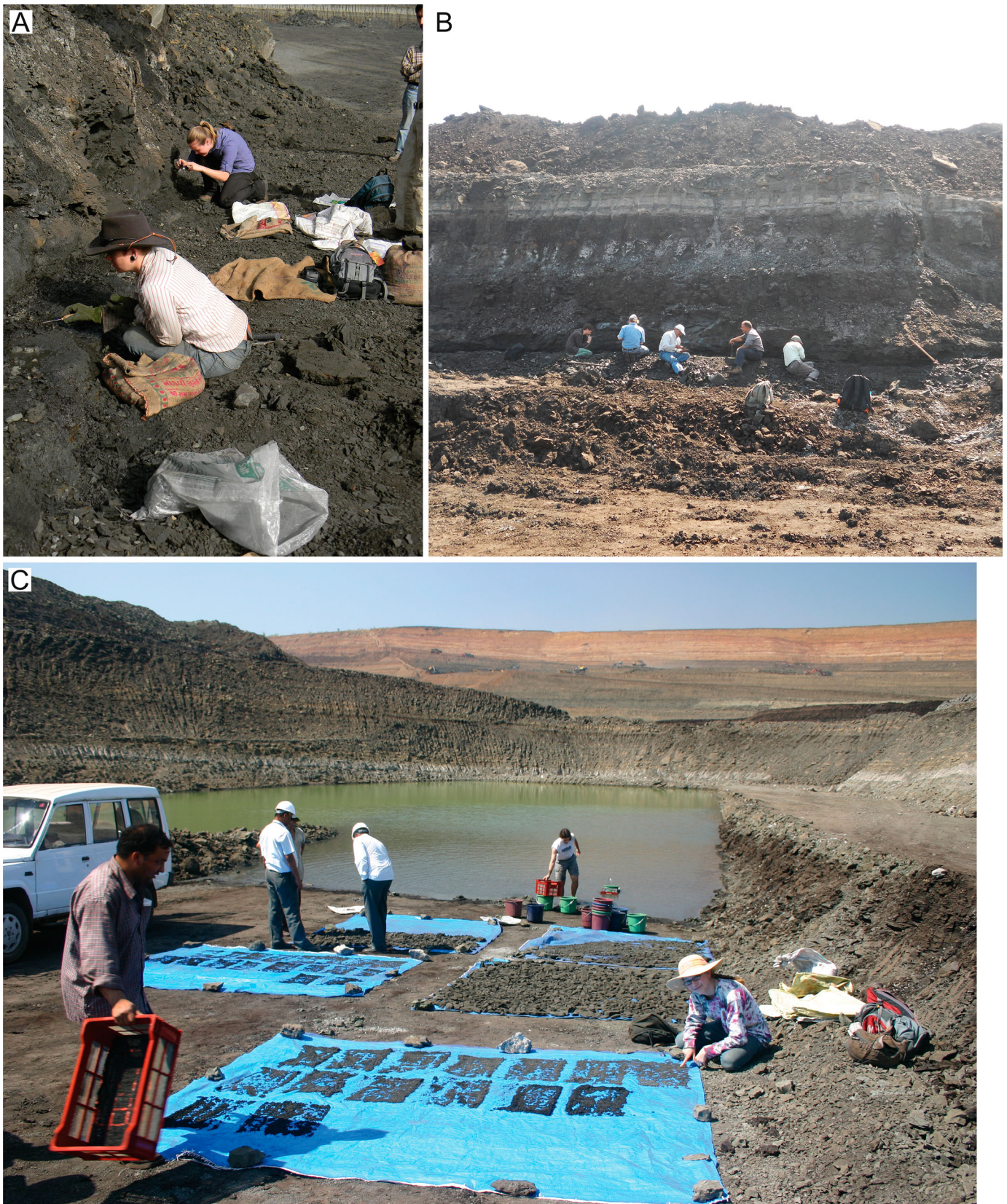
FIGURE 6. **A**, excavation at Vastan Mine, 2011. **B**, excavation at Mangrol Mine, 2013. Note white nearshore marine shell beds above vertebrate layer. **C**, screen-washing at Vastan Mine in 2006.

FIGURE 7. Excavation at Tadkeshwar Mine, 2015. **A**, TAD-1. **B**, TAD-2.

Age of the Cambay Shale Vertebrate Fauna—Most specimens of *Cambaytherium* come from the principal vertebrate-bearing interval at Vastan and Mangrol mines, situated 1–3 m above Lignite 2 (Fig. 3). This bed has been estimated to date from ca. 54.5 Ma, based on combined evidence from foraminiferans, dinoflagellate cysts, and isotope records. Despite the multiple independent age assessments, however, the precise age of the Cambay Shale vertebrate fauna remains uncertain, because the ages of the foraminiferans and dinoflagellate cysts are themselves approximations and the various isotope studies are in conflict.

Initial estimates of the age of the Vastan vertebrate fauna were based on the occurrence of the foraminiferans *Nummulites* *burdigalensis burdigalensis* and *Nummulites burdigalensis kuepperi* in a layer about 14 m above the vertebrate-bearing lenses (Fig. 3C; Sahni et al., 2006; Punekar and Saraswati, 2010). These foraminiferans are considered to be markers of Shallow Benthic Zone (SBZ) 10 (early Cuisian), indicating an age of ca. 53 Ma. However, the Foraminifera provide only a minimum age for the vertebrates. Moreover, the species identification of these foraminiferans is controversial: Garg et al. (2008) suggested that it could be *N. globulus*, which would indicate a slightly older minimum age (SBZ 8 or 9; Serra Kiel et al., 1998). The dinoflagellates were sampled throughout the lower part of the Vastan section, i.e., between Lignites 1 and 2 (Garg

FIGURE 8. **A**, *Cambaytherium thewissi*, WIF/A 4207, femur in situ at TAD-1. **B**, *C. gracilis*, part of holotype mandible in situ at TAD-2.

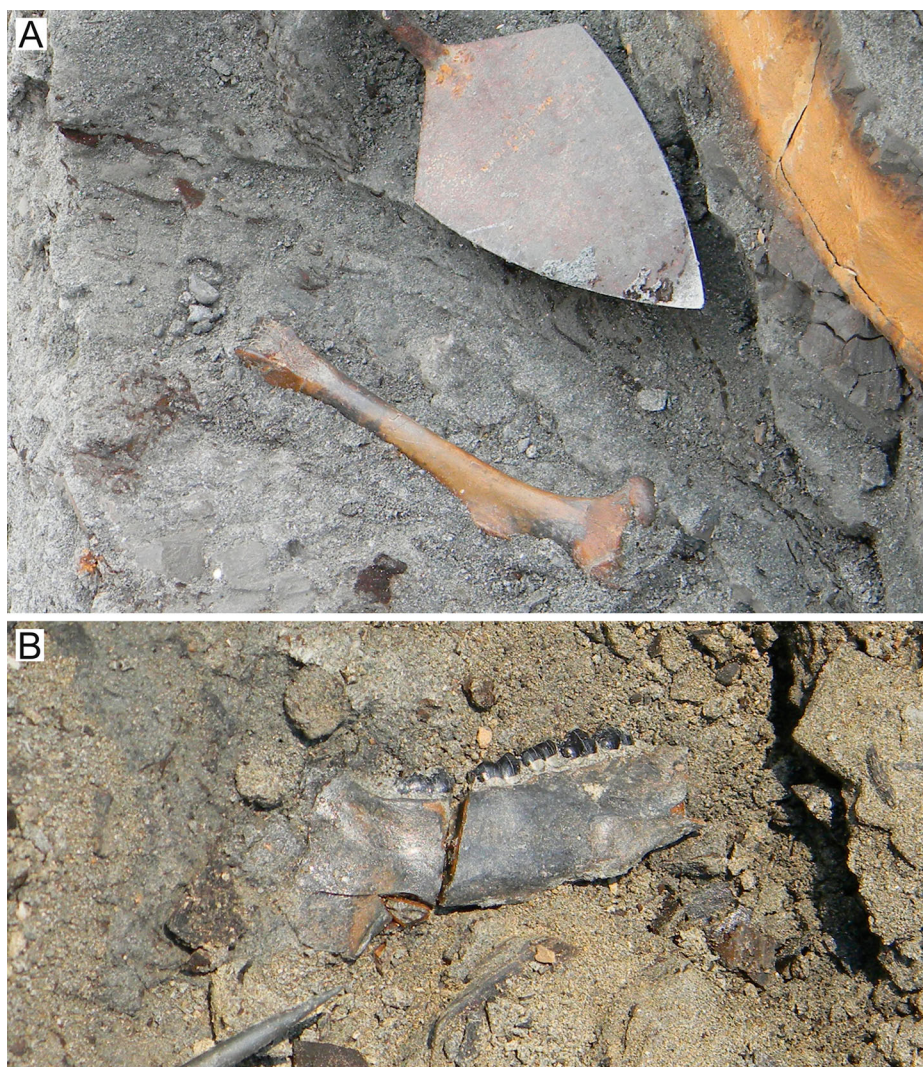et al., 2008). Because the lowest samples came from the top of Lignite 2 and the base of the vertebrate-bearing layer, they should provide a much closer age assessment, which should be the maximum age. According to Garg et al. (2008), marker taxa from these lower samples indicate an age of ~55 Ma ("late Paleocene–early Eocene"), but some of these same dinoflagellate taxa also occur much higher in the Vastan section (Garg et al., 2008:fig 2), raising the question of whether they are truly age-diagnostic. Garg et al. (2008) considered the main vertebrate-layer to be of early Ypresian (= Sparnacian) age, 54–55 Ma.

Isotope analyses provide an independent age estimate. Strontium isotope dating of marine fossils from the bed overlying the vertebrate layer suggests an age of 54.0 Ma (Clementz et al., 2011; see also Samanta et al., 2013), consistent with estimates based on dinoflagellate cysts. In addition, Clementz et al. (2011) analyzed organic carbon isotopes ($\delta^{13}C$) in the sediments through the Vastan section and detected a single, sharp carbon isotope excursion (CIE) about 25 m above the vertebrate layer, which they interpreted to reflect hyperthermal Eocene Thermal Maximum 2 (ETM2), dated at ca. 53.7 Ma. Based on Clementz et al. (2011:fig. 3) and Garg et al. (2008), who depicted a thicker section between Lignites 1 and 2 than shown in Figure 3 herein, the position of this CIE is just below Lignite 1 and presumably just above the *Nummulites b. burdigalensis* zone.

Curiously, the carbon isotope analyses of Clementz et al. (2011) failed to detect any other carbon isotope excursions (including the Paleocene-Eocene Thermal Maximum [PETM]) in the Vastan section. A subsequent isotope study of the Vastan section by Samanta et al. (2013), however, found evidence for multiple carbon isotope excursions, which they correlated with the PETM, ETM2, H2, I1, and I2 hyperthermals. They confirmed the position of ETM2 above the *Nummulites b. burdigalensis* zone but placed ETM2 at the top of Lignite 1 (Samanta et al., 2013), somewhat higher than by Clementz et al. (2011). Despite their discrepancies, these isotope studies indicate that the vertebrates from the main productive layer at Vastan Mine are more than 54 Ma old and probably at least 54.5 Ma. The carbon isotope record documented by Samanta et al. (2013:figs. 5, 6) suggests that the section between Lignites 1 and 2 spans ca. 1–1.5 Ma.

Tadkeshwar Mine has two lignite seams identified as the same ones (Lignite 1 and Lignite 2) as at Vastan. As noted above, the two vertebrate-bearing layers at Tadkeshwar are somewhat higher than the productive layer at Vastan: TAD-1 is 5–10 m above Lignite 2, whereas TAD-2 is 4–5 m below Lignite 1 (and about 12–14 m above TAD-1; see Fig. 3). Whereas each level contains some unique elements, the two assemblages also share several species in common, suggesting that they are not appreciably different in age. However, Adatte et al. (2014) recently

TABLE 1. Mammals from the Cambay Shale Formation in Gujarat.

Taxon	Vastan	Mangrol	TAD-1	TAD-2	Reference(s)
Mammalia, incertae sedis					
Indodelphis luoi	x				Bajpai et al., 2005b
Bharatlestes kalamensis[1]	x				Kapur et al., 2017a, 2017b
Pahelia mysteriosa			x	x	Zack et al., 2019
Cimolesta					
?Palaeoryctidae					
Anthraryctes vastanensis	x				Bajpai et al., 2005a
?Cimolestidae					
Suratilestes gingerichi	x				Bajpai et al., 2005a
Pantodonta					
cf. Coryphodontidae indet.			x	x	Smith et al., 2016
Tillodontia					
Esthonychidae					
cf. *Esthonyx* sp.	x				Rose et al., 2009b
Anthraconyx hypsomylus	x				Rose et al., 2013
Indoesthonyx suratensis			x		Smith et al., 2016
cf. *Indoesthonyx suratensis*				x	Smith et al., 2016
Apatotheria					
Apatemyidae					
Frugivastodon cristatus	x				Bajpai et al., 2005a; Solé et al., in press
Rodentia					
Ischyromyidae					
Meldimys musak[2]	x				Rana et al., 2008
cf. *Meldimys* sp.			x		Smith et al., 2016
cf. Chapattimyidae					
Gen. et sp. indet.[3]	x				Bajpai et al., 2007
Lagomorpha					
Lagomorpha indet.	x				Rose et al., 2008
Primates					
Asiadapidae					
Marcgodinotius indicus[4]	x		x	x	Bajpai et al., 2005c; Rose et al., 2009a; Dunn et al., 2016; Smith et al., 2016
Marcgodinotius sp.[5]	x				Rose et al., 2009a
Asiadapis cambayensis[6]	x				Rose et al., 2007, 2009a; Dunn et al., 2016
Asiadapis tapiensis				x	Rose et al., 2018b
cf. *Asiadapis* unnamed sp. nov.			x		Smith et al., 2016; Rose et al., 2018b
Omomyidae					
Vastanomys gracilis	x				Bajpai et al., 2005c
Vastanomys major	x				Rose et al., 2009a; Dunn et al., 2016
Hyaenodonta					
Hyaenodontidae					
Indohyaenodon raoi	x			x	Bajpai et al., 2009; Rana et al., 2015; Smith et al., 2016
Insectivora					
?Erinaceomorpha					
Vastania sahnia	x				Bajpai et al., 2005a
Chiroptera					
Icaronycteris sigei	x				Smith et al., 2007
Protonycteris gunnelli	x				Smith et al., 2007
Archaeonycteris storchi	x				Smith et al., 2007
Hassianycteris kumari	x				Smith et al., 2007
Cambaya complexus[7]	x				Bajpai et al., 2005a
Microchiropteryx folieae	x				Smith et al., 2007
Jaegeria cambayensis[8]	x				Bajpai et al., 2005b
Undescribed larger bat[9]	x				Smith et al., unpublished
'Eochiroptera' indet. 1		x			Smith et al., 2016
'Eochiroptera' indet. 2		x			Smith et al., 2016
Condylarthra?					
?Arctocyonidae					
?Arctocyonid indet.	x				Bajpai et al., 2009
Anthracobunia					
Cambaytheriidae					
Cambaytherium thewissi[10]	x	x	x	x	Bajpai et al., 2005a, 2006; Rose et al., 2006, 2014b; Smith et al., 2016; this paper
Cambaytherium marinus[11]	x	x			Bajpai et al., 2006; this paper

(*Continued*)

TABLE 1.   Continued.

Taxon	Vastan	Mangrol	TAD-1	TAD-2	Reference(s)
Cambaytherium gracilis			x	x	Smith et al., 2016; this paper
Perissodactyla					
Tapiroidea					
Vastanolophus holbrooki	x				Smith et al., 2015
Cambaylophus vastanensis	x				Kapur and Bajpai, 2015
Artiodactyla					
Artiodactyla indet.[12]	x				Kumar et al., 2010
Diacodexeidae					
Diacodexis indicus[13]	x				Kumar et al., 2010
Diacodexis parvus	x				Kumar et al., 2010
Diacodexeidae indet.[14]	x				Kumar et al., 2010

Occurrences in each of four localities reported here are shown.
[1] = *Indolestes kalamensis* Kapur et al., 2017a; = *Bharatlestes kalami* (Kapur et al., 2017b), which was an 'unjustified emendation' according to Article 33.2.3 of the International Code of Zoological Nomenclature (ICZN) (International Commission on Zoological Nomenclature 2012). The original ending of the species name ('-ensis') connotes a place name and, although inappropriate, does not constitute a misspelling (see also ICZN Articles 32.3 and 32.5.1).
[2] ? = *Anthramys vastani* Bajpai et al., 2007.
[3] Based on one upper molar that is much smaller than *Meldimys musak*.
[4] Includes most or all specimens allocated to *Anthrasimias gujaratensis* Bajpai et al., 2008, including the holotype.
[5] Smaller than *M. indicus*.
[6] Includes *Suratius robustus* Bajpai et al., 2007, which was initially described as an omomyid.
[7] Described as a nyctitheriid insectivoran by Bajpai et al. (2005a).
[8] Described as a marsupial by Bajpai et al. (2005b).
[9] Possibly *Hassianycteris* sp., known only from upper teeth.
[10] Includes *C. bidens* Bajpai et al., 2005a, and *C. minor* Bajpai et al., 2005a.
[11] Originally described as *Kalitherium marinus* Bajpai et al., 2006.
[12] Three isolated teeth apparently different from *Diacodexis*.
[13] = *Gujaratia indica* Bajpai et al., 2005a.
[14] Two isolated teeth slightly smaller than *Diacodexis indicus*.

detected three carbon isotope excursions in a 10-m-thick section at Tadkeshwar, extending from within Lignite 2 to several meters below Lignite 1. They identified these excursions as the PETM, ETM2, and ETM3, purportedly spanning 3 million years. They placed ETM2 midway between the two lignites, much lower than the Vastan isotope records. If correct, this would suggest that the vertebrates from the two levels at Tadkeshwar could span as much as 2 million years. These results are inconsistent with both the fossil vertebrate evidence and the isotope records from Vastan Mine, which place ETM2 either near the base or the top of Lignite 1.

The uncertain age of the Cambay Shale vertebrate fauna, together with the imprecision of the timing of India's collision with Asia, makes it difficult to determine whether the Cambay Shale fauna dates from before, during, or just after the collision.

MATERIALS AND METHODS

Samples

We report here more than 300 specimens of *Cambaytherium* from the Vastan, Mangrol, and Tadkeshwar mines, housed in the collections of H. N. B. Garhwal University and the Wadia Institute of Himalayan Geology. Holotypes and referred specimens are listed under each species below in Systematic Paleontology. Illustrations of most specimens (unless otherwise noted) have been prepared from digital surface models created from ultra-high-resolution micro-computed tomography (micro-CT) scans of the fossils, performed at the Duke University Shared Materials Instrumentation Facility (SMIF) using a Nikon XT H 225 ST micro-CT scanner, and at the Royal Belgian Institute of Natural Sciences using an RX Solutions Easy Tom. Most images were captured in orthographic mode, but some articular views, in particular, were better shown in perspective mode. Consequently, for measurement data, readers should rely on measurements in tables rather than scales in figures, which should be used only as close approximations. A list of digital

object identifiers (DOIs) for three-dimensional (3D) models and micro-CT scan data for figured specimens is provided in Appendix 1. Some larger specimens were imaged by conventional digital photography (using the stacking utility in Photoshop), in most cases after whitening with ammonium chloride to highlight surface detail, or by low-resolution laser scanning using a Next-Engine Ultra 3D laser surface scanner with a rotating plate and ScanStudio software. Measurements have been made with Fowler digital calipers to the nearest 0.05 mm.

Cambaytherium has been compared with many fossil and extant taxa, particularly anthracobunids, perissodactyls, and phenacodontids, all of which have been considered close relatives. Other condylarths, including quettacyonids, have also been compared. In the course of our comparisons, the following specimens have been especially useful: Anthracobunidae (casts): *Anthracobune aijiensis*: WIF/A 1101 (holotype; mandible), WIF/A 616 (paratype; maxilla), tentatively H-GSP 1000; *A. wardi* (= *Pilgrimella pilgrimi*, *Lammidhania wardi*): LUVP 15006, GSP-UM 1615; *A. pinfoldi*: NHMUK 15792 (holotype), NHMUK M32169, NHMUK 15793, NHMUK M15795, GSP-UM 1860; '*Anthracobune* sp.': GSP-UM 1745; *Nakusia shahrigensis*: MNHN M5310 (holotype); *Obergfellia occidentalis*: H-GSP 1981 (holotype), H-GSP 538 (an isolated tooth listed by Cooper et al., 2014, as both a left M3 of *A. wardi* and a left M2 of *O. occidentalis*), H-GSP 568 (questionably *Obergfellia*); *Jozaria palustris*: GSP-UM 738 (holotype); *Perissobune intizarkhani*: GSP-UM 4656 (holotype), GSP-UM 4046, GSP-UM 4345. Perissodactyla (original specimens): '*Hyracotherium*' spp.: USGS 5901, USGS 6097, USGS 6110, USGS 25105, USGS 25157, USGS 25234, USGS 25308, USGS 38039, USGS 38472, USNM 487930, USNM 493831, USNM 527497; *Homogalax protapirinus*: USGS 25032; cf. *Heptodon* sp.: USGS 25325, USGS 25333; unidentified early Eocene perissodactyls: USGS 25308, USGS 25341. Tapiridae: *Tapirus terrestris* (Recent): USNM-M 218778. Phenacodontidae (original specimens): *Phenacodus trilobatus*: USGS 7146, USGS 25169, USNM 487923, USNM 527728; *Phenacodus vortmani*: USGS 7159, USGS 21878; *Phenacodus*

TABLE 2. Nonmammalian vertebrates from the Cambay Shale Formation in Gujarat.

Taxon	Vastan	Mangrol	TAD-1	TAD-2	Reference(s)
CHONDRICHTHYES					
Carchariniformes					
Carcharhinidae					
Physogaleus sp.	x		x		Rana et al., 2004; Smith et al., 2016
Abdounia sp.	x				Rana et al., 2004
Galeocerdo latidens	x				Rana et al., 2004
Eogaleus sp.	x				Rana et al., 2004
Rhizoprionodon sp.	x				Rana et al., 2004
Triakidae					
Triakis sp.	x				Rana et al., 2004
Galeorhinus sp.	x				Rana et al., 2004; Rose et al., 2006
Myliobatiformes					
Myliobatidae					
Myliobatis spp.	x		x		Rana et al., 2004; Rose et al., 2006; Smith et al., 2016
Rhinopteridae					
Rhinopteridae indet.	x				Rana et al., 2004
Dasyatoidea					
Heterotorpedo sp.	x				Rana et al., 2004
Dasyatidae					
Dasyatis spp.	x				Rana et al., 2004; Rose et al., 2006
Rajiformes					
Rhinobatidae					
Rhinobatos sp.	x				Rana et al., 2004
OSTEICHTHYES					
Amiiformes					
Amiidae indet.	x				Rose et al., 2006
Elopiformes					
Phyllodontidae					
Egertonia sp.	x				Rana et al., 2004
Osteoglossiformes					
Osteoglossiformes indet.	x				Rana et al., 2004; Rose et al., 2006
Siluriformes					
Siluriformes indet.	x				Rose et al., 2006
Aulopiformes					
Enchodontidae					
Enchodus sp.	x				Rana et al., 2004
Acanthopterygii					
Acanthopterygii indet.	x				Rose et al., 2006
Pristigasteridae					
?*Pellona* sp.	x				Nolf et al., 2006
Pristigasteridae indet.	x				Nolf et al., 2006
Atherinidae					
Atherinidarum rhomboides	x				Nolf et al., 2006
Atherinidarum spinifer	x				Nolf et al., 2006
Perciformes					
Sphyraena sp.	x				Rana et al., 2004; Rose et al., 2006
Eutrichiurides sp.	x				Rana et al., 2004; Rose et al., 2006
Percoidei					
Percoideorum thierrysmithi	x				Nolf et al., 2006
Centropomidae					
Centropomidarum obesum	x				Nolf et al., 2006
Acropomatidae					
Acropoma massiva	x				Nolf et al., 2006
Acropomatidorum angulosum	x				Nolf et al., 2006
Ambassidae					
Ambassidarum dominans	x				Nolf et al., 2006
Ambassidarum celatum	x				Nolf et al., 2006
Ambassis sp.	x				Nolf et al., 2006
Apogonidae					
Apogon sp.	x				Nolf et al., 2006
Apogonidarum robertwesti	x				Nolf et al., 2006
Menidae					
Menidarum inflatum	x				Nolf et al., 2006
Cepolidae					
Cepolidarum sp.	x				Nolf et al., 2006

(*Continued*)

TABLE 2. Continued.

Taxon	Vastan	Mangrol	TAD-1	TAD-2	Reference(s)
Percophidae					
?*Bembrops* sp.	x				Nolf et al., 2006
Gobioidei					
Gobioideorum nolfi	x				Bajpai and Kapur, 2004; Nolf et al., 2006
Gobioidei indet.	x				Nolf et al., 2006
Gobiidae					
Gobiidarum vastani	x				Bajpai and Kapur, 2004; Nolf et al., 2006
Brachypleuridae					
Brachypleura sp.	x				Nolf et al., 2006
Tetraodontiformes					
Eotrigonodontidae					
Eotrigonodon indicus	x				Rana et al., 2004
Diodontidae					
Diodon sp.	x				Rana et al., 2004; Rose et al., 2006
Trigonodontoidae					
Stephanodus lybicus	x				Rana et al., 2004
Avitoplectidae					
Avitoplectus molaris[1]			x		Bemis et al., 2017
AMPHIBIA					
Anura					
Bombinatoridae					
Eobarbourula delfinoi[2]	x				Bajpai and Kapur, 2008; Folie et al., 2013
Pelobatidae					
Eopelobates sp.	x				Folie et al., 2013
cf. *Eopelobates* sp.			x		Smith et al., 2016
'Ranidae'					
'Ranidae' indet.	x		x		Bajpai and Kapur, 2008; Folie et al., 2013; Smith et al., 2016
Rhacophoridae					
Indorana prasadi	x				Folie et al., 2013
REPTILIA					
Testudinata					
Pleurodira					
Pelomedusoides indet.			x		Smith et al., 2016
Cryptodira					
Carettochelyidae indet.			x		Smith et al., 2016
Trionychidae indet.			x		Smith et al., 2016
Squamata					
Lacertilia					
Acrodonta					
Priscagamidae					
Heterodontogama borsukae	x				Rana et al., 2013
Agamidae					
Suratagama neeraae	x				Rana et al., 2013
Vastanagama susanae	x				Prasad and Bajpai, 2008; Rana et al., 2013
Indiagama gujarata	x				Rana et al., 2013
Tinosaurus indicus	x		x		Prasad and Bajpai, 2008; Rana et al., 2013; Smith et al., 2016
Serpentes					
Madtsoiidae					
Madtsoiidae indet.	x		x		Rage et al., 2008; Smith et al., 2016
Platyspondylophis tadkeshwarensis			x		Smith et al., 2016
Boidae					
Boidae indet.	x		x		Rage et al., 2008; Smith et al., 2016
Palaeophiidae					
Palaeophis vastaniensis[3]	x		x	x	Bajpai and Head, 2007; Smith et al., 2016
Pterosphenus sp.	x				Rage et al., 2008
Russellophiidae					
Russellophis crassus	x				Rage et al., 2008
Russellophiidae indet.	x				Rage et al., 2008
Colubroidea					
Procerophis sahnii	x		x		Rage et al., 2008; Smith et al., 2016

TABLE 2.   Continued.

Taxon	Vastan	Mangrol	TAD-1	TAD-2	Reference(s)
Cenophidia incertae sedis					
Taumastophis missiaeni	x		x		Rage et al., 2008; Smith et al., 2016
Cenophidia indet. A	x				Rage et al., 2008
Cenophidia indet. B	x				Rage et al., 2008
Crocodilia					
Crocodylomorpha					
Dyrosauridae					
cf. *Congosaurus* sp.			x		Smith et al., 2016
AVES					
Aves indet.	x		x		Mayr et al., 2010; Smith et al., 2016
?Psittaciformes					
Vastanavidae					
Vastanavis eocaena	x				Mayr et al., 2007
Vastanavis cambayensis	x				Mayr et al., 2010
Vastanavis sp.	x		x		Mayr et al., 2013; Smith et al., 2016

[1]Reported as Tetraodontiformes indet. by Smith et al., 2016.
[2]Includes Discoglossidae indet. and Leptodactylidae indet. in Bajpai and Kapur (2008).
[3]Reported as *Palaeophis* sp. by Rage et al. (2008).

vortmani or *Copecion brachypternus*: USGS 25302. Phenacolophidae (casts): *Phenacolophus*: AMNH 20411, IVPP V4084, IVPP V4086, IVPP V5041; *Minchenella grandis*: IVPP V5600 (holotype). Quettacyonidae (casts): *Quettacyon parachai*: GSP-UM 4000 (holotype); *Machocyon abbasi*: GSP-UM 4208 (holotype); *Sororocyon usmanii*: GSP-UM 4007 (holotype).

We make frequent comparisons with phenacodontids, especially *Phenacodus*, which is well known anatomically, because the family has been considered to be among the closest relatives of Perissodactyla (e.g., Radinsky, 1966; Thewissen and Domning, 1992; Cooper et al., 2014), and because its anatomy more closely approaches that of primitive perissodactyls than most other forms. Some recent phylogenetic analyses, including those presented here, do not place Phenacodontidae as close to the source of Perissodactyla as Radinsky (1966, 1969) imagined, but they remain arguably the best model of a primitive mesaxonic ungulate progenitor to compare with more derived modern ungulates.

Anatomical Terminology—We have generally followed the Nomina Anatomica Veterinaria (NAV; International Committee on Veterinary Gross Anatomical Nomenclature, 2012), although we have employed the widely used Anglicized versions of these terms. In a few cases, anatomical terms not listed in the NAV were used for precision, with appropriate citations (e.g., Davis, 1964; Getty, 1975; Evans and Christensen, 1979). We relied heavily on the latter references and several others (including Murie, 1872; Campbell, 1936; Kneepkens et al., 1989; Macdonald and Kneepkens, 1995; Williams, 1995; Fisher et al., 2007, 2009), particularly for myology of perissodactyls, artiodactyls, and other laurasiatheres, to make inferences of muscle attachment sites and size in *Cambaytherium*. Dental terminology follows conventional usage as illustrated by Van Valen (1966), Szalay (1969), Hooker (2005), and Rose et al. (2018a).

Statistical Methods

About half of the sample consists of teeth and jaws. Descriptive statistics of teeth at each dental position from each locality (N, minimum, maximum, mean, standard deviation) were generated in MYSTAT (version 12.02; SYSTAT Software). The Shapiro-Wilk statistic was used to test for deviations from normality that could indicate the presence of multiple species. This statistic compares the distribution of the sample with the null hypothesis of normality; therefore, $P < 0.05$ indicates significant departure

from a normal distribution. Differences among *Cambaytherium* teeth from each locality and species were examined using a multivariate analysis of variance (MANOVA) in IBM SPSS Statistics for Windows (IBM Corp, 2017). For these analyses, we selected teeth represented by samples of more than two in each locality (p4, m2, m3, and M3). For each tooth, all measurements were included as dependent variables in the MANOVA with group as a factor. Between-group differences were examined using a post hoc Tukey's honestly significant difference (HSD) test.

Phylogenetic Methods

In order to investigate the phylogenetic position of cambaytheres (see Phylogenetic Position of *Cambaytherium*, below), we constructed a matrix of 321 characters in 72 taxa, based in part on the matrix from Rose et al. (2014b). Descriptions of characters and their states, and other notes on characters, can be found in Appendix 2. The matrix is available on MorphoBank (morphobank.org) under project number P2607. Taxa chosen for the analyses included Paleogene representatives of cambaytheres, anthracobunids, perissodactyls, hyracoids, proboscideans, and cetartiodactyls, as well as a number of archaic ungulates. *Cambaytherium thewissi* and *C. gracilis* were included, but *C. marinus* was not, because it is too poorly known. Three primitive anthracobunid species were scored: two species of *Anthracobune*, and *Obergfellia occidentalis*. For purposes of the analyses, we grouped *A. aijiensis* with *A. wardi*, following Cooper et al. (2014), but as noted below (Nomenclatural Comments) we regard *A. aijiensis* as a valid species. Archaic ungulates included the phenacodontids *Phenacodus*, *Tetraclaenodon*, *Ectocion*, and *Meniscotherium*, as well as the phenacolophid *Phenacolophus* and the possible phenacolophid *Radinskya*. The latter two taxa are rare (*Radinskya* is unique) and represented by only very fragmentary remains, which for *Phenacolophus* are often poorly preserved. Both are somewhat bilophodont Paleocene ungulates from Asia whose relationships are enigmatic; nevertheless, we included them in the analyses because of their potential relevance to *Cambaytherium*. Both *Radinskya* and phenacolophids are characterized by upper molars with conules situated on the protoloph and metaloph (i.e., in line with the paracone-protocone and metacone-hypocone), unlike the more mesially shifted conules of *Cambaytherium* and perissodactyls (McKenna et al., 1989; Hooker and Dashzeveg, 2003; Hooker, 2005; Mao et al., 2016). In addition, we included the

Recent tubulidentate *Orycteropus*; the Recent macroscelideans *Elephantulus*, *Petrodromus*, and *Rhynchocyon*; the Eocene carnivoran *Vulpavus*; the Eocene euprimate *Notharctus*; the Eocene rodent *Paramys*; and the Eocene eurymylid *Rhombomylus*. These taxa provide additional non-'ungulate' representation of three of the major clades of placental mammals supported by results based on molecular sequences, namely, Afrotheria, Euarchontoglires, and Laurasiatheria. The Eocene desmostylian *Behemotops proteus* was included for two reasons. First, there are interesting similarities between the teeth of this taxon and those of cambaytheres and anthracobunids (Ray et al., 1994). Second, the analysis of Cooper et al. (2014) placed Desmostylia in a polytomy that included most perissodactyls and anthracobunids (but not cambaytheres). Historically, paleontologists have considered Desmostylia (like anthracobunids) to be closely related to tethytheres (Domning et al., 1986; Ray et al., 1994). The didelphid marsupial *Didelphis* and the Cretaceous eutherian *Asioryctes* were also included for the purposes of rooting the tree.

Two other poorly known taxa, *Minchenella* and Quettacyonidae, were included in an additional analysis, along with the other taxa listed above. *Minchenella* is an archaic ungulate from the Paleocene of China. Originally classified as a phenacolophid by Zhang (1978), it has sometimes been considered to be a possible ancestor of anthracobunids (Wells and Gingerich, 1983), but like phenacolophids it is lophodont. It is known only from a poorly preserved pair of lower jaws, and our scores are based on casts of the type material and the published figures from Zhang (1978). Quettacyonids are a group of archaic ungulates endemic to the early Eocene of the Indian Plate that exhibit some similarities to arctocyonids (Gingerich et al., 1997, 1998, 1999). They have low, bunodont dentitions with simple premolars that wear in a manner very similar to those of cambaytheres, but they differ from cambaytheres in a number of ways, including shape of the dentary. Quettacyonids are known mainly from lower dentitions and a small number of upper teeth. For purposes of this analysis, we included Quettacyonidae as a composite taxon based on information from *Quettacyon parachai*, *Machocyon abbasi*, and *Sorocyon usmani*, derived from casts and published figures from Gingerich et al. (1997, 1998, 1999).

Some recent ancient protein and DNA studies (Buckley, 2015; Welker et al., 2015; Westbury et al., 2015) have provided evidence for perissodactyls as the closest living relatives of notoungulates and litopterns, two major groups of South American native 'ungulates' (SANUs) whose relationships have been enigmatic. We did not include any SANUs in our analyses for several reasons. The aforementioned studies were based on molecules extracted from specimens of two Pleistocene members of these groups, specifically the notoungulate *Toxodon* and the litoptern *Macrauchenia*. These taxa are highly derived compared with the Paleogene taxa that constitute most of our taxonomic set, and specimens were not readily available at the time of our analyses. Furthermore, these two genera are members of much more diverse groups, and dealing appropriately with this diversity for inclusion in our analyses was beyond the scope of this study.

We conducted maximum parsimony analyses using heuristic searches in PAUP* 4.0 (Swofford, 2003) and New Technology searches in TNT (Goloboff et al., 2008). Heuristic searches in PAUP* used random stepwise addition for 10,000 replications. Searches in TNT used tree fusion and sectorial search set to find the shortest tree 1,000 times. Trees were rooted using *Didelphis* as the outgroup.

Because the unconstrained results differ in the placement of extant lineages from results of analyses using molecular data, we performed additional analyses in PAUP* with constraints to keep the relationships among the extant lineages congruent with results of molecular studies. Specifically, the constraint tree required that the living taxa be arranged to form a clade of

perissodactyls, cetartiodactyls, and the carnivoran *Vulpavus* (i.e., Laurasiatheria); a clade of *Orycteropus*, macroscelideans, proboscideans, and hyracoids (i.e., Afrotheria); and a clade of *Notharctus*, *Rhombomylus*, and *Paramys* (i.e., Euarchontoglires). This 'backbone' constraint tree did not constrain how fossils were placed among or within these clades, nor did it constrain the relationships among extant taxa within each clade.

The analyses described above were run excluding *Minchenella* and Quettacyonidae, given the limited data on these taxa. We ran an additional analysis that included these taxa and otherwise conformed to the parameters of the unconstrained analysis described above.

Bootstrap support was calculated using 1,000 pseudoreplicates in PAUP*. Bremer support was calculated using the AutoDecay 5.0 script of Eriksson (2001) in PAUP*.

Methods for Estimating Body Size

The body mass of *Cambaytherium* was estimated based on limb and tooth dimensions, using regressions developed from extant ungulates (see Paleobiology of *Cambaytherium*/Body Size, below). For limb dimensions, body mass was calculated from relationships based on two samples (Scott, 1990): 'all extant ungulate taxa' (a diverse sample of ~1,000 individuals representing 160 species of extant artiodactyls and equids) and suoids-only (20 species), because the latter share a more similar overall body form to *Cambaytherium*. Measures from the humerus, ulna, radius, femur, and tibia (Scott, 1983:fig. 1) were selected based on availability of the fossil material (Table 3). For dental measures, body mass was calculated from relationships based on a sample of non-selenodont artiodactyls (Damuth, 1990; number of species not specified), which was found to provide a reliable estimate for archaic ungulates with more primitive tooth morphology. We focus on the molars and fourth premolar, which are best represented in our sample. Measures from third

TABLE 3. Measures used for body mass estimation (see Scott, 1983: fig. 1).

Element	Measure	Description	Source
Humerus	H3	Breadth of the humeral head	Scott, 1990
Humerus	H4	Width of distal articular surface	Scott, 1990
Humerus	H5	Width of the distal humerus	Scott, 1990
Humerus	H7/H8	Transverse/anteroposterior diameter at midshaft of humerus	Scott, 1990
Radius	R2	Breadth of proximal radius	Scott, 1990
Radius	R3	Width of the proximal radius	Scott, 1990
Radius	R6	Transverse diameter at midshaft of radius	Scott, 1990
Femur	F2	Height of greater trochanter	Scott, 1990
Femur	F3	Projection of femoral head	Scott, 1990
Femur	F5	Width of the distal femur	Scott, 1990
Femur	F6/F7	Mediolateral/anteroposterior diameter at midshaft of femur	Scott, 1990
Tibia	T2/T3	Width/height of proximal tibia	Scott, 1990
Tibia	T4/T5	Width/height of distal tibia	Scott, 1990
Tibia	T6/T7	Transverse/anteroposterior diameter at midshaft of tibia	Scott, 1990
Upper teeth	2UM	M2 length	Damuth, 1990
Upper teeth	1UM	M1 length	Damuth, 1990
Upper teeth	4UP	P4 length	Damuth, 1990
Lower teeth	2LM	m2 length	Damuth, 1990
Lower teeth	1LM	m1 length	Damuth, 1990
Lower teeth	4LP	p4 length	Damuth, 1990

molars were excluded due to the elongate morphology of these teeth in *Cambaytherium*, which may overestimate body mass. Estimates are based on tooth length because molar width-based measures (including tooth area) tend to overestimate body mass in Paleogene ungulates (Damuth, 1990).

All measurements were taken directly from specimens using digital calipers and, where appropriate, were averaged across left and right sides for these estimates. Body mass estimates were calculated for each measure separately then averaged across elements (Fig. A4). Grand means for *C. thewissi* and *C. gracilis* were calculated from element averages. A tentative body mass estimate for *C. marinus* was made based on published measurements of three upper teeth (P4, M1, and M2) in the holotype (Bajpai et al., 2006), as well as the widths of the proximal femur and distal tibia referred here tentatively to *C. marinus*.

Nomenclatural Comments

Condylarths—We use the common name condylarths without quotation marks, for convenience, as an informal name to designate the broad paraphyletic group of archaic ungulates and ungulate antecedents, including such presumed clades as Phenacodontidae, Arctocyonidae, Hyopsodontidae, Periptychidae, and Mioclaenidae, which generally display plesiomorphic placental anatomical traits compared with those of the basal members of the modern orders. Among these, Phenacodontidae provide particularly useful comparisons with *Cambaytherium* because of their bunodont dentition, subcursorial skeletal adaptations, and mesaxonic foot symmetry. We accept Thewissen's (1990) arguments for using the species name *Phenacodus trilobatus* for large specimens of early Eocene *Phenacodus* that were long assigned to *P. primaevus*.

Anthracobunidae—The appropriate names of several anthracobunids remain unstable, largely because the earlier holotypes (*Anthracobune pinfoldi*, *A. wardi*, *A.*(?) *daviesi*, and *Pilgrimella pilgrimi*) are either isolated or fragmentary teeth or are so poorly preserved that critical details are ambiguous. This is highlighted by the mercurial position of *A. wardi* (variously assigned to aff. *Anthracobune* [Pilgrim, 1940], *Pilgrimella* [Dehm and Oettingen-Spielberg, 1958], *Lammidhania* [Gingerich, 1977], and back to *Anthracobune* [Cooper et al., 2014]), which likely results from the fact that the holotype of *A. wardi* consists of a molar talonid that may prove to be nondiagnostic. Because revision of Anthracobunidae is beyond the scope of this work, we follow most assignments of Cooper et al. (2014). However, we regard *A. aijiensis* Kumar, 1991, which Cooper et al. (2014) considered a junior synonym of *A. wardi*, as a valid species because of apparent differences from other specimens allocated to *A. wardi* by Cooper et al. (2014:figs. 1, 2: H-GSP 96258, H-GSP 96434). *Anthracobune aijiensis* (e.g., WIF/A 1101) appears to have relatively wider lower cheek teeth and less molarized premolars than *A. wardi*. In particular, the premolar metaconids are lower and less developed than in *A. wardi*, and that of p3 is posteromedial to the protoconid rather than medial to it. In addition, premolars of *A. aijiensis* lack an entoconid, whereas *A. wardi* has a distinct entoconid on p4 (H-GSP 96258 and H-GSP 96434) and also on p3 of H-GSP 96258. H-GSP 1000 (referred to *Lammidhania wardi* by West, 1980, but not listed by Cooper et al., 2014) consists of two casts of NHMUK M41896a (a right p2–4) and NHMUK M41896b (a right dp3–4–m1); they are the same size and morphology as the holotype of *A. aijiensis* and appear to belong to that species if it is distinct. Based on these and other specimens of anthracobunids and cambaytheriids, increasing molarization of premolars was an important trend in anthracobunians.

Perissodactyla—Throughout this work, we make comparisons with the North American early Eocene equids that have long been known as *Hyracotherium*. We continue to use the name

'*Hyracotherium*' sensu lato (henceforth without quotation marks, for simplicity) for reasons explained below, notwithstanding that the holotype of *H. leporinum* (Owen's type species of the genus) has been considered to be a palaeotheriid equoid (Hooker, 1989, 1994), and that North American species conventionally included in *Hyracotherium* have subsequently been assigned to multiple other genera (Froehlich, 1999, 2002). It may seem ironic that one of the two most abundant early Eocene mammals still lacks a consistent, widely accepted taxonomy. Unfortunately, the appropriate taxonomic assignments of the majority of specimens of Wasatchian equids (including most of those used for comparison here) remain elusive, partly because many genus and species distinctions were based on subtle characters of premolars and m3 (Froehlich, 2002), which are missing in many specimens, or on differences in average size or subjective characters (Gingerich, 1991) that overlap substantially in large samples, making consistent taxonomic separation difficult or impossible. (The ambiguity even extends to some basal tapiromorphs, the dental morphology of which may closely approach that of basal equids.) Comprehensive studies of intraspecific variation that might clarify the situation have not been conducted. Furthermore, postcranial specimens are often associated with fragmentary dentitions or may lack associated teeth, preventing species identification, while possessing characters that allow confident assignment to either Equidae or Tapiromorpha. Fortunately, the taxonomic intricacies of Wasatchian equids do not impact our broader comparisons with *Cambaytherium*; consequently, we follow Wood et al. (2011) in using the name *Hyracotherium* for North American Wasatchian equids compared here. In the phylogenetic analyses, however, we include several early Eocene North American taxa using the nomenclature of Froehlich (2002), namely, *Protorohippus*, *Arenahippus*, *Sifrhippus*, *Eohippus*, and *Xenicohippus*.

This publication and the nomenclatural acts it contains have been registered with Zoobank: zoobank.org:pub:92D48EBC-9626-49BF-A5E7-D657F543E601.

SYSTEMATIC PALEONTOLOGY

Superorder PERISSODACTYLAMORPHA, new

We propose this new higher taxon to include conventional Perissodactyla + Anthracobunia, the latter composed of Anthracobunidae and Cambaytheriidae (and possibly Desmostylia and *Radinskya*; see Phylogenetic Position of *Cambaytherium*, below), and we define it as the common ancestor of Anthracobunia and Perissodactyla, and all of its descendants, with the caveat that the intent is that Perissodactylamorpha should simply be a more inclusive taxon containing all taxa more closely related to Perissodactyla than to any other extant order. Defining Perissodactylamorpha in such a fashion, however, would make it synonymous with the definition of Panperissodactyla, which Welker et al. (2015) established to accommodate their results uniting litopterns and notoungulates with perissodactyls, based on collagen amino acid sequences. Assuming, as we think is likely, that anthracobunians are more closely related to perissodactyls than are litopterns and notoungulates, our provisional definition of Perissodactylamorpha would make it a subdivision of Panperissodactyla.

Despite the length of the name, there are sound reasons to prefer Perissodactylamorpha over the shorter existing name Mesaxonia. Mesaxonia Marsh, 1884, was initially used for what is now considered conventional Perissodactyla. Earlier, Owen (1848) had proposed Perissodactyla for a group including conventional Perissodactyla + Hyracoidea (as well as *Coryphodon* and *Macrauchenia*). In an effort to avoid confusion, Fischer (1989) resurrected Marsh's name Mesaxonia, applied in the same

sense as Marsh did, despite the fact that Perissodactyla had long been widely used for the same concept. Because Mesaxonia is now considered synonymous with Perissodactyla (Simpson, 1945; McKenna and Bell, 1997) and has never been used for a broader concept, we prefer to avoid the ambiguity that could result by employing it with yet another meaning. Therefore, we propose the unambiguous, if cumbersome, name Perissodactylamorpha to encompass Perissodactyla and its sister taxon Anthracobunia.

The name Perissodactylamorpha follows a convention adopted by other studies recognizing clades that include extant orders and some number of their respective extinct sister taxa, and it is used in analogy with mammalian higher taxa such as Primatomorpha (Beard, 1993), Carnivoramorpha (Wyss and Flynn, 1993), and Rodentiamorpha (Wyss and Meng, 1996) to encompass crown clades and their stem taxa. As far as we are aware, Perissodactylamorpha has not been formally adopted previously, but there are informal references online to 'Perissodactylomorpha' (note difference in spelling), presumably inspired by this convention. We deem the spelling that we have adopted for this taxon preferable, because it conforms to the convention used with ordinal taxa that share the '-a' ending of Perissodactyla, such as Carnivora and Rodentia.

Order ANTHRACOBUNIA Ginsburg, Durrani, Kassi, and Welcomme, 1999

Anthracobunia was proposed as an infraorder of Tethytheria, to include the Anthracobunidae Wells and Gingerich, 1983, an Eocene family endemic to the Indian subcontinent then thought to be allied with tethytheres or Proboscidea (West, 1980; Wells and Gingerich, 1983; Domning et al., 1986; Kumar, 1991; Ray et al., 1994), based on a hypothesis credited to E. Manning (Domning et al., 1986). Association with proboscideans was based primarily on perceived dental resemblances to moeritheriids. Previously, *Anthracobune* (including *Pilgrimella*) had been allied with Artiodactyla (e.g., Pilgrim, 1940; Dehm and Oettingen-Spielberg, 1958), but Coombs and Coombs (1979), in a particularly insightful article, provided strong evidence for perissodactyl affinities. Despite this, anthracobunids were for several decades assigned to Proboscidea before new evidence and two independent phylogenetic analyses corroborated a much closer relationship to Perissodactyla than to Proboscidea (Cooper et al., 2014; Rose et al., 2014b).

An additional justification for allocating Anthracobunidae to Proboscidea was an isolated astragalus from the Eocene Subathu Fornation of Pakistan that was attributed to *Anthracobune* and interpreted to share significant traits with that of *Moeritherium*, including an enlarged medial tubercle (Gingerich et al., 1990). This astragalus contrasts markedly with that of cambaytheres, however, and is therefore very unlikely to represent an anthracobunid. Its large size suggests that it belongs to a taxon otherwise unknown from the Subathu Formation. The morphology is more consistent with that of primitive placentals such as hyaenodontans, arctocyonids, and tillodonts. (See further discussion below in Comparison with '*Anthracobune*' Astragalus, under Postcranial Comparisons of *Cambaytherium*.)

As shown below, detailed dental and gnathic resemblances indicate that anthracobunids are closely allied with

TABLE 4. Stratigraphic and geographic distribution of Eocene anthracobunians.

Genus and species	Stratigraphic horizon	Geographic locality	References
Anthracobunidae			
Anthracobune aijiensis Kumar, 1991	Subathu Formation (middle Eocene)	Aiji, Kalakot, Rajauri District, Jammu and Kashmir, India	Kumar, 1991
Anthracobune pinfoldi Pilgrim, 1940	Kuldana Formation (middle Eocene)	Lammidhan, west of Ganda Kas, Attock District, Punjab, Pakistan	Pilgrim, 1940; Dehm and Oettingen-Spielberg, 1958; Sahni and Khare, 1973; Gingerich, 1977; West, 1980, 1983; Kumar, 1991; Cooper et al., 2014
Anthracobune wardi (Dehm and Oettingen-Spielberg 1958)	Kuldana Formation (middle Eocene)	Lammidhan, west of Ganda Kas, Attock District, Punjab, Pakistan	Pilgrim, 1940; Dehm and Oettingen-Spielberg, 1958; Gingerich, 1977; Cooper et al., 2014
Ishatherium subathuensis Sahni and Kumar, 1980	Subathu Formation (lower Eocene)	Subathu, Solan District, Himachal Pradesh, India	Sahni and Kumar, 1980; Wells and Gingerich, 1983
Jozaria palustris Wells and Gingerich, 1983	Kuldana Formation (middle Eocene)	Jozara, Kohat District, North West Frontier, Pakistan	Wells and Gingerich, 1983
Obergfellia occidentalis Cooper et al., 2014	Kuldana Formation (middle Eocene)	Ganda Kas, Attock District, Punjab, Pakistan	Cooper et al., 2014
Cambaytheriidae			
Cambaytherium gracilis Smith et al., 2016	Cambay Shale Formation (lower Eocene)	Tadkeshwar Lignite Mine, Surat District, Gujarat, India	Smith et al., 2016; this report
Cambaytherium marinus (Bajpai et al., 2006)	Cambay Shale Formation (lower Eocene)	Vastan and Mangrol lignite mines, Surat District, Gujarat, India	Bajpai et al., 2006; this report
Cambaytherium thewissi Bajpai et al., 2005a	Cambay Shale Formation (lower Eocene)	Vastan, Mangrol, and Tadkeshwar lignite mines, Surat District, Gujarat, India	Bajpai et al., 2005a, 2006; Rose et al., 2006, 2014b; this report
Nakusia shahrigensis Ginsburg et al., 1999	Ghazij Formation (lower Eocene)	Shahrig-Nakus, Kach-Harnai, Quetta, Pakistan	Ginsburg et al., 1999; Cooper et al., 2014; this report
Perissobune intizarkhani Missiaen and Gingerich, 2014	Ghazij Formation (lower Eocene)	Kingri, Balochistan, Pakistan	Missiaen and Gingerich, 2014; this report
Perissobune munirulhaqi Missiaen and Gingerich, 2014	Ghazij Formation (lower Eocene)	Kingri, Balochistan, Pakistan	Missiaen and Gingerich, 2014; this report

Records of anthracobunids are presented as reported in the literature. *Ishatherium* is based on a fragmentary tooth, and its anthracobunid status is questionable. *Hsanotherium* Ducrocq et al., 2000 (middle Eocene of Myanmar), is excluded from Anthracobunidae following Tsubamoto et al. (2003), Rose et al. (2006), and Cooper et al. (2014); it may be an artiodactyl. Records for cambaytheriids reflect the systematics presented in this report.

cambaytheriids, and that Anthracobunidae + Cambaytheriidae compose a clade that is sister to Perissodactyla, for which the name Anthracobunia is available and appropriate. The stratigraphic and geographic distribution of anthracobunians is summarized in Table 4.

The following combination of dental characters is diagnostic of Anthracobunia: bunodont cheek teeth with little or no loph development (when present, crests are low and weak); canines with enlarged roots; molar paraconids lost and paracristid (= paralophid) low and usually arcuate; molar metaconids twinned, and lingual cusps of lower molars posterior to the corresponding buccal cusps; molar hypoconulids posterior to (not on) the hypolophid; m3 with an expanded hypoconulid lobe bearing a twinned or multiple hypoconulid; upper molar parastyles small or absent, and paracones distinctly larger than metacones; conules prominent on upper molars and mesially shifted (anterior to lines joining paracone-protocone and metacone-hypocone), paraconules typically also well developed on P3–4; and cheek tooth enamel rugose. In addition to this suite of dental characters, anthracobunians have a markedly postero-ventrally expanded mandibular angle, a high condyle, and dentaries coossified to form a strong and extensive mandibular symphysis that typically extends posteriorly to p2. Most of these characters are either certainly or arguably derived, and many are shared with Perissodactyla, but in combination they are found only in Anthracobunia. Bunodonty, lophs absent or weakly developed, and prominent canines with large roots are probably plesiomorphic relative to Perissodactyla. Anatomical characters uniting anthracobunians are currently restricted to the dentition and mandible, because the cranium is inadequately known and the postcranial skeleton is known only in *Cambaytherium*. However, the limb skeleton of *Cambaytherium* shows a similar combination of synapomorphies with perissodactyls and plesiomorphic features not found in perissodactyls.

<div style="text-align:center">

Family CAMBAYTHERIIDAE Bajpai, Kapur, Das, Tiwari,
Saravanan, and Sharma, 2005a

</div>

Revised Diagnosis—Bunodont anthracobunian perissodactyla-morphs with very weakly developed or absent lophodonty, perikymata coarse and conspicuous, upper molar paraconule and metaconule prominent, lower molar paraconid reduced or absent. Accessory cusps common, especially on third molars; m3 hypoconulid usually multiple; M3 hypocone often twinned or multiple. Lower permanent premolars simple except p4, which is sometimes molarized but never fully molariform. Upper molars with a crest or accessory cusp buccal to hypocone (twinned hypocone or metaconule). Cheek teeth exhibit a steep wear gradient (differential wear, with early eruption of permanent premolars and delayed eruption of third molars). Mandibular symphysis fused. Astragalar canal variably present, in contrast to Perissodactyla. Differ from Anthracobunidae in lacking lophodonty and in having simpler premolars, accessory cusps, relatively larger upper molar conules, and salient perikymata.

Included Genera—*Cambaytherium, Nakusia, Perissobune.*

Discussion—Cambaytheriidae are highly distinctive perissodactylamorphs, more bunodont than all others including anthracobunids. As detailed below, they also retain many plesiomorphic features in the postcranial skeleton. Anthracobunidae differ from cambaytheriids in having taller molar cusps, weak lophodonty (distinct but low crests), and more molarized premolars (uppers with paracone-metacone almost equal, conules stronger; lowers with trigonids more developed: metaconids distinct on p3–4, incipient on p2, paraconid distinct on p2–3). Some of these characters have been modified in *Behemotops*, whose relationship to anthracobunids remains tentative (see further discussion under Phylogenetic Position of *Cambaytherium*, below).

<div style="text-align:center">

CAMBAYTHERIUM Bajpai, Kapur, Das, Tiwari, Saravanan,
and Sharma, 2005a

</div>

Synonyms—*Indobune* Rose, Smith, Rana, Sahni, Singh, Missiaen, and Folie, 2006; *Kalitherium* Bajpai, Kapur, Thewissen, Das, and Tiwari, 2006.

Included Species—*C. thewissi* Bajpai, Kapur, Das, Tiwari, Saravanan, and Sharma, 2005 (type species); *C. gracilis* Smith, Kumar, Rana, Folie, Solé, Noiret, Steeman, Sahni, and Rose, 2016; *C. marinus* (Bajpai, Kapur, Thewissen, Das, and Tiwari, 2006).

Revised Diagnosis—Bunodont cambaytheriids lacking lophodonty. Differs from *Nakusia* in having less buccolingually wide P4–M2 and relatively smaller P4. Differs from *Perissobune* in lacking even incipient crest development and in having less molariform P4 and p4.

Remarks—As noted in the Introduction, the description of *Cambaytherium* was initially based primarily on lower dentitions, whereas that of *Indobune* was based on upper teeth. With increasing sample size, which included probably associated upper and lower dentitions, it became clear that these two taxa represented the same genus (Missiaen et al., 2011b). Similarly, with better understanding of dental anatomy in *Cambaytherium*, it is now evident that *Kalitherium* is also congeneric with *Cambaytherium* (see below).

Nakusia shahrigensis Ginsburg, Durrani, Kassi, and Welcomme, 1999, and *Perissobune intizarkhani* Missiaen and Gingerich, 2014, are cambaytheres closely related to *Cambaytherium*. The larger and slightly younger *P. munirulhaqi* has wider and somewhat more lophodont lower molars and thus appears to be somewhat more derived. All three species come from the early Eocene Ghazij Formation of Pakistan and are probably somewhat younger than at least the Vastan and Mangrol samples of *Cambaytherium* (Missiaen and Gingerich, 2014). Further study and more complete specimens are needed to determine whether *Nakusia* and *Perissobune* should be synonymized with *Cambaytherium*. *Nakusia* is known from only a single maxillary fragment with P4–M2. It has more transverse upper teeth than *Cambaytherium* and *Perissobune* but otherwise appears to be similar as far as can be determined, although some details are obscured by heavy wear. Without a larger sample and more complete specimens, it may not be possible to determine whether *Nakusia* and *Cambaytherium* are congeneric (in which case *Nakusia* would have priority unless the species is designated a nomen dubium). For this reason, and the fact that *Cambaytherium* is so much better known, we maintain its use here.

Perissobune intizarkhani has very similar molars to *Cambaytherium*, although they are incipiently lophodont, with weak cristid obliqua, hypolophid, and protocristid on p4 and the lower molars and rudimentary cross-lophs on the upper molars. They also have a strong buccally directed metaconid buttress (Hooker, 1994) that bears a low but distinct cuspule on m2 and m3, a similar accessory cuspule is present in *C. gracilis*. *Perissobune* further differs from *Cambaytherium* in having more molarized posterior premolars than in most *Cambaytherium*, as well as longer diastemata around p1 (= dp1, especially the diastema posterior to dp1), but diastemata are now known to vary in *Cambaytherium*. Inasmuch as these are almost surely derived states in *Perissobune*, as in perissodactyls, it is quite likely that *Perissobune* evolved from *Cambaytherium*.

Anthracobunidae (in particular, *Anthracobune, Pilgrimella, Lammidhania,* and *Obergfellia*) are also very similar to *Cambaytherium*. Cooper et al. (2014) synonymized the first three under the genus *Anthracobune* and proposed the name *Obergfellia* for a specimen that had been published earlier as *Anthracobune pinfoldi* (West, 1980) and *Pilgrimella pilgrimi* (Wells and Gingerich, 1983). *Obergfellia* was distinguished from *Anthracobune* by having relatively wider molars, a short m3,

and a long angular process on the mandible (but shorter than in *Anthracobune*). It also appears to have more molarized premolars than *Anthracobune* (including *A. aijiensis*). Comparison of dental morphology strongly suggests that anthracobunids also evolved from a cambaytheriid, although our phylogenetic analyses do not corroborate this, instead indicating that the two families are sister taxa. Discovery of anthracobunid postcrania might provide the data to test this relationship.

CAMBAYTHERIUM THEWISSI Bajpai, Kapur, Das, Tiwari, Saravanan, and Sharma, 2005a

Synonyms—*C. bidens* Bajpai, Kapur, Das, Tiwari, Saravanan, and Sharma, 2005; *C. minor* Bajpai, Kapur, Das, Tiwari, Saravanan, and Sharma, 2005; *Indobune vastanensis* Rose, Smith, Rana, Sahni, Singh, Missiaen, and Folie, 2006.

Holotype—IITR 505, dentaries with left and right p4–m3, from just above Lignite 2, Vastan Lignite Mine, Gujarat, India.

Referred Specimens—From Vastan Mine: GU 1, LM3; GU 2, Ldp2; GU 3, Ldp2; GU 4, Rdp4 talonid; GU 5, L maxilla, LdP3–4, P4–M1, holotype of *Indobune vastanensis*; GU 10, canine; GU 12, R maxilla, M2; GU 18, RM1; GU 198, R femoral head and distal end; GU 201, LM2; GU 202, LM1; GU 203, Lm1; GU 204, RP4; GU 206, LM2?; GU 209, RM1 or M2; GU 213, RdP4; GU 221, Lp2; GU 222, Ldp1; GU 223–224, canines; GU 225, incisor; GU 270, distal R humerus; GU 274, R radius; GU 275, R Mt IV; GU 278, distal R tibia; GU 280, proximal phalanx; GU 281, proximal phalanx; GU 282, intermediate phalanx; GU 292, R Mc II; GU 293–295, R lunars; GU 296, R cuneiform; GU 297, R navicular; GU 298, proximal phalanx; GU 299, intermediate phalanx; GU 300, distal R fibula; GU 304, L astragalus; GU 333, L pisiform; GU 401, L dentary, m2–3; GU 402, cranium with almost complete dentition, M3s erupting; GU 403, mandible with almost complete dentition, m3s erupting; GU 404, maxillae, LdP1–M3, RP2–M3; GU 405–407, canines; GU 409, Ldp1; GU 412, RP4; GU 413, LM1; GU 414,

Rp4; GU 415, RP4; GU 417, RM2; GU 418, RM3; GU 424, LM1; GU 425, LM3; GU 426, LP3; GU 427, Rp2; GU 428, LP2?; GU 430, LP4; GU 432, canine; GU 433, incisor; GU 626, incisors; GU 659, Ldp2; GU 660, Lp2?; GU 661, RP3–4; GU 662, RP4; GU 663, RP4; GU 664, Rdp3; GU 665, LM2; GU 674, Lm3; GU 730, juvenile skull with LdP2–4–M1, RdP2, dP4–M1; GU 731, LM1; GU 732, RP4; GU 733, Rdp3?; GU 734, Ldp4; GU 735, L Mt III; GU 736, R dentary, dp3–4; GU 737, R humerus; GU 738, distal R humerus; GU 739, L tibia; GU 768, L cuboid; GU 769–770, L astragali; GU 771, proximal R radius; GU 772, distal L calcaneus; GU 773, vertebra C1; GU 774, vertebra C2; GU 775, cervical vertebra; GU 776, R dentary, p3–m3, associated canines; GU 777, distal R radius; GU 778, R humerus; GU 779, R tibia; GU 780, R astragalus; GU 782, vertebra C1; 783, vertebra T1?; GU 784, LM1; GU 785, LM3; GU 786–787, lumbar vertebrae; GU 788, thoracic vertebra; GU 789, lumbar vertebra; GU 790–791, thoracic vertebrae; GU 792, canine; GU 809, proximal R humerus; GU 814, R astragalus; GU 815, L Mc II; GU 816, L Mt IV; GU 817, R Mc II; GU 818, R Mc IV; GU 819, R Mt IV; GU 820, R scapula; GU 821, R Mt III; GU 822, L Mc IV; GU 823, Rm3; GU 824–825, caudal vertebrae; GU 828–830, proximal phalanges; GU 831, R Mt IV; GU 832, L Mc II?; GU 833, canine; GU 834, R humerus; GU 835, R scaphoid; GU 842, proximal L radius; GU 843, proximal phalanx; GU 844–845, intermediate phalanges; GU 846, L Mt III; GU 847, R Mc V; GU 848, L proximal Mc IV; GU 1211, distal L humerus; GU 1213, R scapula; GU 1214, proximal L humerus; GU 1215–1216, proximal L ulnae; GU 1217, R Mc III; GU 1218, distal R femur; GU 1219, distal L femur; GU 1220, distal L tibia; GU 1221, LM3; GU 1222–1223, RM1s; GU 1515, Lm3; GU 1516, RM3; GU 1588, R dentary, p2 or p3 and m2; GU 1592, canine; GU 1593, Rdp2; GU 1594, Rdp1; GU 1595, R dentary, m2–3; GU 1596, R dentary, m2–3; GU 1597, Lm3; GU 1598, Lm2; GU 1610, R proximal Mc IV; GU 1615, LM1; GU 1616, LM2; GU 1671, Rp4; GU 1672, RM3; GU 1675–1676, incisors; GU 1678, Ldp1; GU 1679, Rp4; GU 1682,
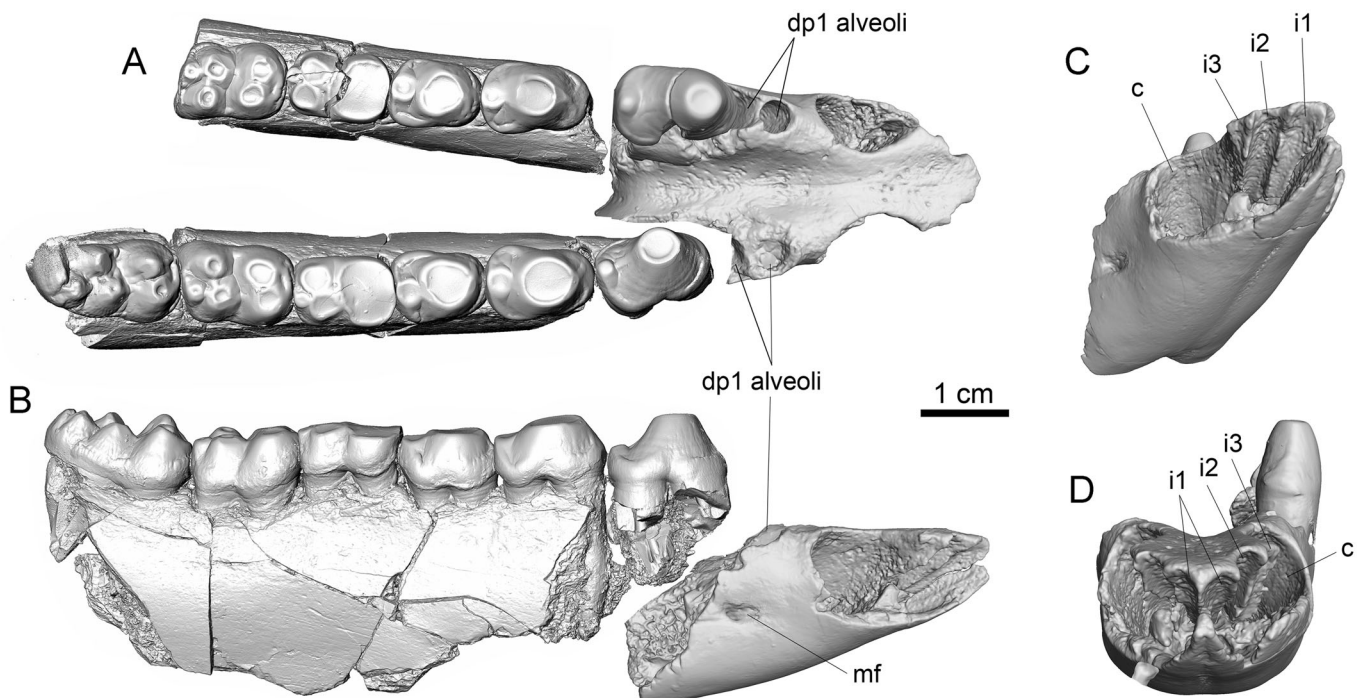

FIGURE 9. *Cambaytherium thewissi* mandible with right p2–m3, left p2–m2, and symphysis preserving anterior alveoli, GU 7004, from Mangrol Mine. **A**, occlusal, **B**, lateral, **C**, oblique anterior, and **D**, anterior views. **Abbreviation**: **mf**, mental foramen.
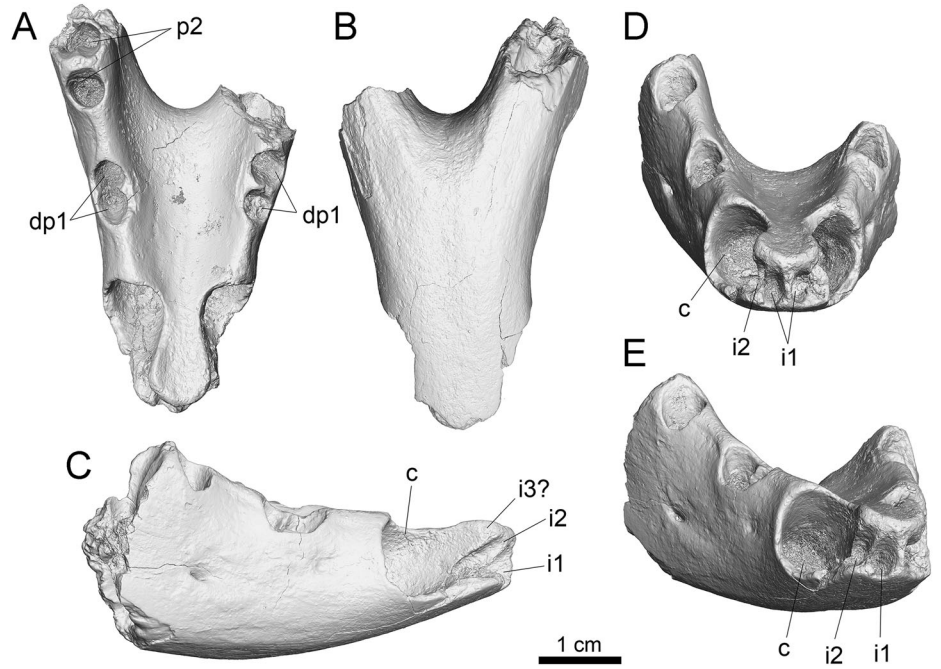
FIGURE 10. *Cambaytherium thewissi* mandibular symphysis showing anterior alveoli, GU 9002, from TAD-2. This is the only specimen in our sample that may have had only two lower incisors on each side, although it is possible that i3 was rooted in the same alveolus as the canine. **A**, superior (dorsal), **B**, inferior, **C**, right lateral, **D**, anterior, and **E**, oblique anterior views.
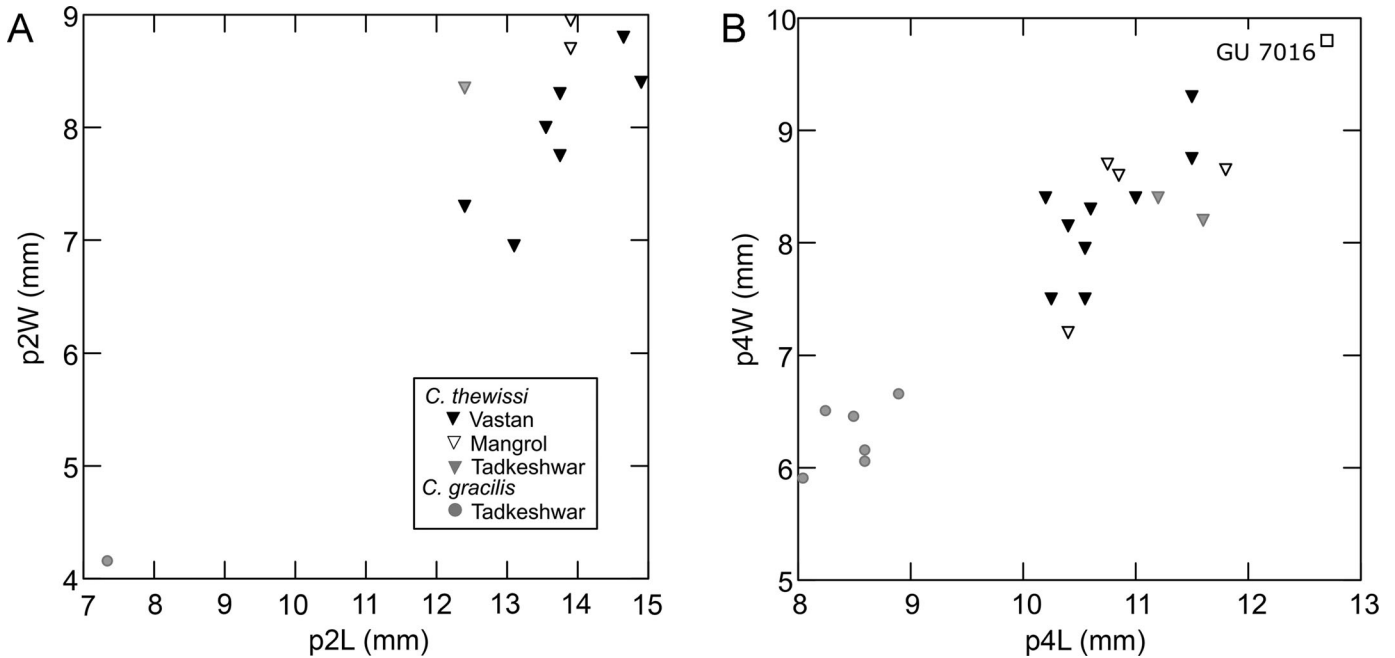

FIGURE 11. Lower premolar size distribution in *Cambaytherium*. **A**, p2 length vs. width. **B**, p4 length vs. width. Note overlap of *C. thewissi* samples from the three mines, whereas *C. gracilis* is distinctly smaller. GU 7016 is an outlier and might represent a small *C. marinus* or an unusually large *C. thewissi*. **Abbreviations**: **L**, length; **W**, width.

Ldp3; GU 1683, RP2; GU 1700, R dentary, m2–3; GU 1701, R dentary, dp2–3; GU 1702a–d, multiple specimens, upper teeth; GU 1704, R Mc V; GU 1708, RP4; GU 1709, Rp2?; GU 1710, mandible, Lp2–m2 and symphysis; GU 1711, L dentary, m1–3; GU 1727, C, LP2–4, M2, RM3; GU 1728, maxillae, L and R M2–3s; GU 8003, RM1; GU 8004, Lm2; GU 8005, Ldp3; GU 8006, proximal phalanx; GU 8007, Ldp3; GU 8008, Rp2; GU 8009, Lp4; GU 8010–8011, Rm3s; GU 8012, LM3; GU 8013, Lm2; GU 8014, L and R m2s; GU 8015, RdP1; GU 8016, incisor; GU 8017, caudal vertebra; GU 8018, patella; GU 8019, RP2; GU 8020, LdP1; GU 8021, Rdp4; GU 8022–8028, incisors; GU 8029, intermediate phalanx; GU 8030, incisor; GU 8031, Ldp1; GU 8032, Ldp2; GU 8033–8034, incisors; GU 8039, Ldp3; GU 8041, Lp2; GU 8042, lumbar vertebra; GU 8043, cervical vertebra; GU 8044, R scaphoid; GU 8045, sternal segment; GU 8046, proximal L Mc II; GU 8047, proximal phalanx; GU
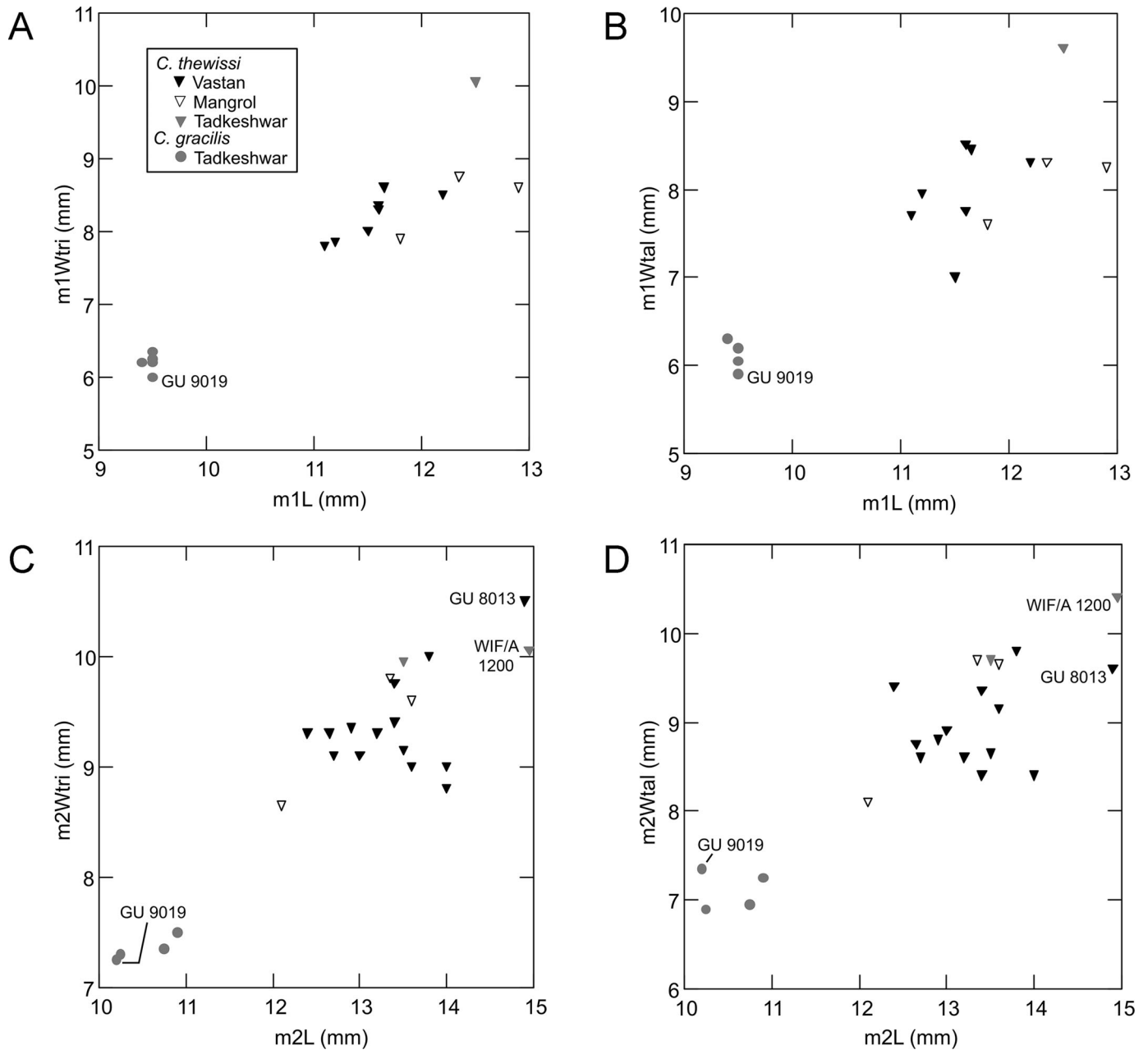
FIGURE 12. Lower molar size distribution in *Cambaytherium*. **A**, m1 length vs. width of trigonid. **B**, m1 length vs. width of talonid. **C**, m2 length vs. width of trigonid. **D**, m2 length vs. width of talonid. GU 8013 is a large individual of *C. thewissi* from a layer just below Lignite 1 at Vastan Mine which is believed to be roughly the same age as TAD-2. WIF/A 1200 is a large individual from TAD-2. GU 9019 is the only dental specimen referred to *C. gracilis* from TAD-1. **Abbreviations**: **L**, length; **Wtal**, width of talonid; **Wtri**, width of trigonid.

8048, proximal R Mc IV; GU 8049, proximal R pisiform; GU 8051, distal L radius, listed as GU 280 by Rose et al. (2014b); WIF/A 1193, RM2; WIF/A 1194, LM3; WIF/A 1195, RM2; WIF/A 1196, LM2; WIF/A 1197, LM2; WIF/A 1198, Rm1; WIF/A 1199, LdP3.

Also from Vastan Mine, based on Bajpai et al. (2005a, 2006): IITR 503, holotype of *C. bidens*, R dentary with c–m3, L dentary with dp1–m3; IITR 505, holotype of *C. thewissi*, L and R dentaries with p4–m3; and IITR 539, holotype of *C. minor*, Rdp4 part; the following specimens referred to *C. bidens*: IITR 502, mandible with most postcanine teeth and some upper teeth; IITR 521, L dentary, m3, LM1; IITR 535, R astragalus;

IITR 791, R dentary, m1–2; IITR 792, L dentary, p2–m3; and probably IITR 520, IITR 532, IITR 541–547, IITR 558, IITR 786, IITR 795, IITR 811, and IITR 957; the following specimens referred to *C. thewissi*: IITR 764, RM1 or M2; IITR 765, LM1 or M2; IITR 894, miscellaneous teeth; and probably IITR 548, IITR 551, IITR 726, IITR 767, and IITR 830; and the following specimens referred to *C. minor*: IITR 540, Ldp4 part; IITR 761, R dentary, dp4–m2; and probably IITR 830, IITR 841, and IITR 895. Specimens illustrated by Bajpai et al. (2005a, 2006) can be referred with confidence and are indicated above; those listed in their hypodigms but not figured (which we could not verify) are indicated as 'probably' referred to *C. thewissi*. Note that
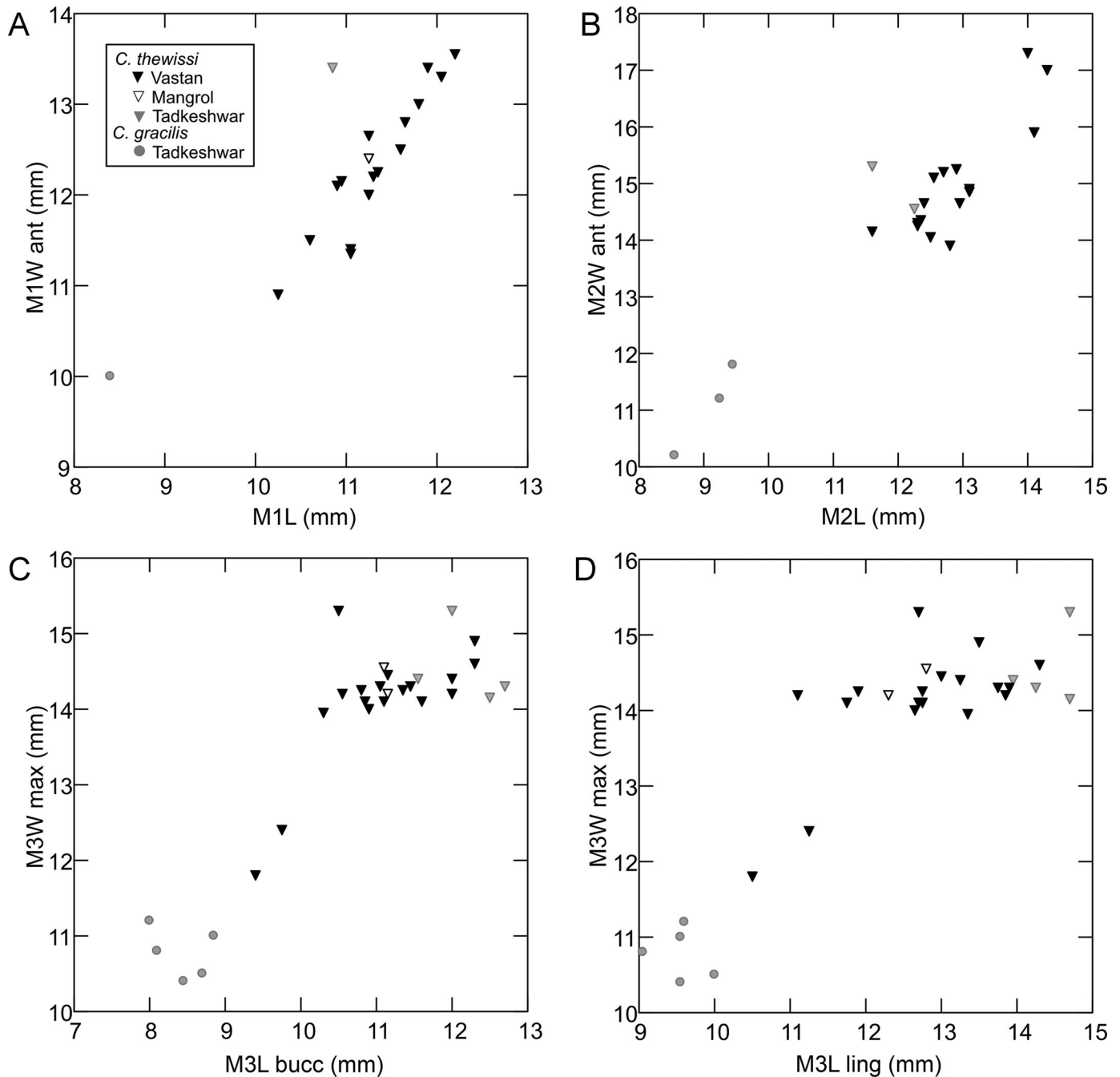
FIGURE 13. Upper molar size distribution in *Cambaytherium*. **A**, M1 length vs. anterior width. **B**, M2 length vs. anterior width. **C**, M3 buccal length vs. maximum width. **D**, M3 lingual length vs. maximum width. **Abbreviations**: **L**, mesiodistal length; **Lbucc**, length measured buccally; **Lling**, length measured lingually; **Want**, anterior width; **Wmax**, maximum width.

Bajpai et al. (2006) listed IITR 764 and IITR 765 under both *C. bidens* and *C. thewissi* but identified them as *C. thewissi* in their illustrations.

From Mangrol Mine: GU 7001, R dentary, p3–m3; GU 7002, RP4, M2; GU 7003, vertebra C2; GU 7004, mandible, Rp2–m3, Lp2–m2; GU 7005, R ulna; GU 7006, distal L humerus; GU 7007, L Mc II; GU 7008, proximal phalanx; GU 7009, intermediate phalanx; GU 7010, sternal segment; GU 7011–7012, LM3s; GU 7013, RP4, questionably referred; GU 7014, canine; GU 7015, Rdp1; GU 7016, Lp4?, questionably referred; GU 7017, Rp3; GU 7018, Rp4; GU 7019, distal R

radius; GU 7020, intermediate? phalanx; GU 7021, terminal phalanx; GU 7022, RP4, LM1; GU 7023, RdP3–4; WIF/A 1190, L calcaneus; WIF/A 1192, L magnum; WIF/A 4408, R magnum.

From Tadkeshwar Mine, TAD-1: WIF/A 2262, L femur; WIF/A 4207, L femur; WIF/A 4253, canine; TAD-2: GU 9002, mandibular symphysis; GU 9006, Lp4; GU 9016, R innominate; GU 9202, L maxilla, P4–M3; GU 9207, L tibia; GU 9211, proximal L tibia; GU 9214, L scapula; GU 9237, femoral shaft; WIF/A 1200, mandible, Lp3–4, m2 and symphysis; WIF/A 4216, L astragalus; WIF/A 4217, R maxilla, P4–M2; WIF/A 4218, L radius; WIF/A 4219,

TABLE 5. Summary measurements (in mm) and statistics for upper and lower teeth of *Cambaytherium thewissi* (combined sample from Mangrol, Vastan, and Tadkeshwar mines).

Statistic	P1L	P1W	P2L	P2W	P3L	P3W	P4L	P4W	M1L	M1Want	M1Wpost
N of cases	2	2	6	6	8	8	19	19	19	18	17
Minimum	8.65	5.70	11.35	8.20	10.55	11.55	8.90	11.20	10.25	10.90	10.60
Maximum	9.80	6.00	13.35	9.70	12.85	12.95	11.20	14.40	12.20	13.55	13.10
Arithmetic mean	9.23	5.85	12.50	8.74	11.42	12.16	10.04	12.55	11.28	12.38	11.92
Standard deviation	0.813	0.212	0.915	0.520	0.701	0.429	0.609	0.770	0.499	0.777	0.787
Coefficient of variation	8.8	3.6	7.3	5.9	6.1	3.5	6.1	6.1	4.4	6.3	6.6
Shapiro-Wilk statistic	—	—	0.808	0.865	0.900	0.968	0.982	0.963	0.978	0.960	0.951
Shapiro-Wilk P-value	—	—	0.070	0.205	0.290	0.886	0.964	0.634	0.917	0.607	0.471

Statistic	M2L	M2Want	M2Wpost	M3Lbucc	M3Lling	M3Wmax	dP3L	dP3W	dP4L	dP4Want	dP4Wpost
N of cases	19	19	18	24	24	24	5	5	4	4	4
Minimum	11.60	13.90	12.70	9.40	10.50	11.80	9.10	7.90	8.85	9.40	8.75
Maximum	14.30	17.30	15.40	12.70	14.70	15.30	10.00	8.45	10.00	10.05	9.30
Arithmetic mean	12.77	15.00	13.95	11.27	12.99	14.19	9.59	8.14	9.58	9.64	9.05
Standard deviation	0.738	0.918	0.604	0.835	1.125	0.737	0.344	0.216	0.504	0.287	0.227
Coefficient of variation	5.8	6.1	4.3	7.4	8.7	5.2	3.6	2.7	5.3	3.0	2.5
Shapiro-Wilk statistic	0.922	0.864	0.958	0.975	0.964	0.748	0.987	0.970	0.872	0.870	0.963
Shapiro-Wilk P-value	0.123	0.012	0.563	0.801	0.526	0.000	0.969	0.875	0.305	0.296	0.797

Statistic	p1L	p1W	p2L	p2W	p3L	p3W	p4L	p4W	m1L	m1Wtri	m1Wtal
N of cases	6	6	10	10	6	6	15	15	11	11	11
Minimum	6.80	4.25	12.40	6.95	12.00	7.60	10.20	7.00	11.10	7.80	7.00
Maximum	8.80	5.15	14.90	8.95	13.30	9.00	11.80	8.80	12.90	10.05	9.60
Arithmetic mean	7.64	4.60	13.63	8.15	12.88	8.53	10.88	8.11	11.86	8.43	8.13
Standard deviation	0.732	0.324	0.826	0.653	0.462	0.516	0.527	0.560	0.563	0.633	0.663
Coefficient of variation	9.6	7.0	6.1	8.0	3.6	.60	4.8	6.9	4.8	7.5	8.2
Shapiro-Wilk statistic	0.938	0.909	0.929	0.937	0.808	0.866	0.919	0.912	0.945	0.823	0.936
Shapiro-Wilk P-value	0.645	0.432	0.441	0.520	0.069	0.213	0.189	0.144	0.576	0.019	0.471

Statistic	m2L	m2Wtri	m2Wtal	m3L	m3Wtri	m3Wtal	dp2L	dp2W	dp3L	dp3W	
N of cases	19	19	18	15	15	15	6	6	8	8	
Minimum	12.10	8.65	8.10	14.70	8.50	7.40	9.30	4.40	10.25	4.35	
Maximum	14.95	10.50	10.40	19.00	10.90	10.60	10.45	5.40	11.60	6.10	
Arithmetic mean	13.42	9.43	9.11	16.67	9.68	8.73	9.90	4.84	11.19	5.19	
Standard deviation	0.739	0.479	0.620	1.211	0.671	0.745	0.406	0.340	0.528	0.576	
Coefficient of variation	5.5	5.1	6.8	7.3	6.9	8.5	4.1	7.0	4.7	11.1	
Shapiro-Wilk statistic	0.957	0.963	0.956	0.950	0.963	0.939	0.986	0.975	0.707	0.972	
Shapiro-Wilk P-value	0.511	0.630	0.518	0.531	0.737	0.367	0.977	0.923	0.003	0.915	

Statistic	dp4L	dp4Wtri	dp4Wtal	MD at p3tal	MD at m2tri	Dent ML at m1
N of cases	2	2	2	5	7	7
Minimum	10.70	6.25	6.15	18.80	27.70	10.40
Maximum	11.05	7.15	7.00	30.85	40.00	17.50
Arithmetic mean	10.88	6.70	6.58	24.06	33.06	14.09
Standard deviation	0.247	0.636	0.601	4.736	3.940	2.447
Coefficient of variation	2.3	9.5	9.1	19.7	11.9	17.4
Shapiro-Wilk statistic	—	—	—	0.971	0.969	0.971
Shapiro-Wilk P-value	—	—	—	0.884	0.894	0.906

Abbreviations: **ant**, anterior; **bucc**, buccal; **d**, deciduous; **Dent ML**, mediolateral thickness of dentary; **L**, length; **ling**, lingual; **max**, maximum; **MD**, mandibular depth; **post**, posterior; **tal**, talonid; **tri**, trigonid; **W**, width.

Rose et al.—*Cambaytherium* from the lower Eocene of India

TABLE 6. Multivariate comparisons of teeth from each locality.

Group	Species	Locality	p4		m2			m3			M3		
			p4L	p4W	m2L	m2Wtri	m2Wtal	m3L	m3Wtri	m3Wtal	M3Lbucc	M3Lling	M3Wmax
A	*C. thewissi*	Vastan	10.73	7.99	13.21	9.31	8.90	16.69	9.57	8.55	11.08	12.72	14.09
B	*C. thewissi*	Mangrol	10.95	8.29	13.02	9.35	9.15	16.65	9.45	8.55	11.13	12.55	14.38
C	*C. thewissi*	TAD	11.40	8.30	14.45	10.17	9.90	16.58	10.50	9.88	12.19	14.40	14.54
D	*C. gracilis*	TAD	8.48	6.28	10.53	7.35	7.11	12.70	7.63	7.00	8.42	9.55	10.78
Group difference			D < A – C		D < A + B < C			D < A – C	D < A + B < C	D < A + B < C	D < A – C	D < A + B < C	D < A – C
Multivariate P-value			0.001		0.005			<0.001			<0.001		

Values indicate group means for each measure. Group difference indicates significant pairwise differences between the groups from post hoc Tukey HSD test, indicated by designated group. Multivariate P-value calculated from Pillai's Trace statistic. **Abbreviations: bucc**, buccal; **L**, length; **ling**, lingual; **max**, maximum; **tal**, talonid; **tri**, trigonid; **W**, width.

RM3; WIF/A 4220, RM3; WIF/A 4221, RM3; WIF/A 4222, Rm3; WIF/A 4223, Lm3; WIF/A 4224, Rm2; WIF/A 4232, Rp2; WIF/A 4233, Lm1; WIF/A 4234, Ldp3; WIF/A 4251–4252, canines; WIF/A 4255, Lp4; WIF/A 4258, R femur; WIF/A 4259, L femur; WIF/A 4260, proximal R ulna; WIF/A 4261, L radius; WIF/A 4262, L humeral shaft; WIF/A 4264, Lp4.

Revised Diagnosis—Medium-sized species of *Cambaytherium*, larger than *C. gracilis*, smaller than *C. marinus*. Further differs from *C. gracilis* in typically having less molarized fourth premolars, and p2 longer than other lower premolars.

Discussion

Bajpai et al. (2005a) designated *Cambaytherium thewissi* as the type species of the genus, though they described *C. bidens* as the first species of their new genus in the same publication. *Cambaytherium thewissi* was diagnosed as a "medium-sized species of *Cambaytherium*, lacking diastema between p1 and p2; three lower incisors" (Bajpai et al., 2005a:110). *Cambaytherium bidens* was distinguished as a "large species of *Cambaytherium* with diastema between p1 and p2; two lower incisors" (Bajpai et al., 2005a:109). It was described as "approximately 118% as large as the type species" (Bajpai et al., 2005a:110). Both species are from continental lenses situated about 1–2 m above the lower lignite (Lignite 2) at Vastan Mine. The larger samples now available show the supposed diagnostic features to vary (or to be suspect: incisor number), as discussed below, casting doubt on the validity of two species. For example, GU 7004 (Fig. 9) is well within the size range of *C. bidens* but has three incisor alveoli on each side and lacks a diastema behind dp1. (The anterior-most premolar is identified here as the unreplaced dp1 rather than p1, following Luckett, 1993.) The only specimen in our sample that might be interpreted to have had two incisors and a distinct diastema behind dp1—GU 9002 (Fig. 10), from the higher level at Tadkeshwar Mine (see discussion below)—is among the smaller individuals. With larger samples, Bajpai et al. (2006) found the molar pattern of *C. bidens* and *C. thewissi* to be the same, and we concur. Consequently, *C. bidens* is here considered a synonym of *C. thewissi* (see further discussion below, following tooth descriptions).

Bajpai et al. (2005a) recognized a third species of *Cambaytherium* from the same stratum at Vastan Mine, *C. minor*, based on two incomplete, worn 'molars,' described as "smaller than other *Cambaytherium*, approximately 75% as large as *C. thewissi*" (Bajpai et al., 2005a:111). Subsequently, Bajpai et al. (2006) identified these teeth as m1. The two teeth in question, which are relatively narrower than molars of *C. thewissi*, are in fact dp4s, and the dentary illustrated by Bajpai et al. (2006:pl. 3) and identified as having m1–3 contains dp4–m2. The apparent absence of a third lobe on m3 of *C. minor* observed by Bajpai et al. (2006) is therefore easily explained because the tooth is m2, not m3. Once the correct homologies are recognized, it is obvious that *C. minor* is not different from *C. thewissi*. For these reasons, *C. minor* is also a junior synonym of *C. thewissi*.

The principal sample of *C. thewissi* comes from Vastan Mine. Several additional specimens were found in a similar level at the neighboring Mangrol Mine. The size distribution of cheek teeth of *Cambaytherium* from these samples as well as Tadkeshwar Mine is shown in Figures 11–13 and A1–A3, and summary measurements and statistics for the combined sample are presented in Table 5. Measurements for all individual specimens in our sample are provided in Appendices 3 and 4, and summary measurements and statistics for the Vastan-Mangrol sample vs. the Tadkeshwar sample are presented in Appendices 5 and 6. Except for GU 7013 (an isolated P4) and GU 7016 (an isolated p4), the Mangrol specimens plot within or on the periphery of the range of Vastan *C. thewissi*, and nearly all mean dimensions

TABLE 7. Summary measurements (in mm) and statistics for upper and lower teeth of *Cambaytherium gracilis* (Tadkeshwar Mine).

Statistic	P2L	P2W	P3L	P3W	P4L	P4W	M1L	M1Want	M1Wpost
N of cases	3	3	3	3	4	4	1	1	1
Minimum	7.10	5.40	7.60	8.20	7.60	9.60	8.40	10.00	9.55
Maximum	7.35	5.70	8.15	9.00	8.20	9.90	8.40	10.00	9.55
Arithmetic mean	7.18	5.55	7.90	8.50	7.89	9.74	8.40	10.00	9.55
Standard deviation	0.144	0.150	0.278	0.436	0.307	0.125	—	—	—
Coefficient of variation	2.0	2.7	3.5	5.1	3.9	1.3	—	—	—
Shapiro-Wilk statistic	0.750	1.000	0.976	0.842	0.842	0.982	—	—	—
Shapiro-Wilk P-value	0.000	1.000	0.702	0.220	0.202	0.911	—	—	—

Statistic	M2L	M2Want	M2Wpost	M3Lbucc	M3Lling	M3Wmax	dP4L		
N of cases	3	3	3	5	5	5	1		
Minimum	8.55	10.20	9.60	8.00	9.05	10.40	8.30		
Maximum	9.45	11.80	10.75	8.85	10.00	11.20	8.30		
Arithmetic mean	9.08	11.07	10.22	8.42	9.55	10.78	8.30		
Standard deviation	0.473	0.808	0.580	0.368	0.337	0.335	—		
Coefficient of variation	5.2	7.3	5.7	4.4	3.5	3.1	—		
Shapiro-Wilk statistic	0.907	0.980	0.984	0.928	0.910	0.950	—		
Shapiro-Wilk P-value	0.407	0.726	0.762	0.581	0.468	0.737	—		

Statistic	p2L	p2W	p3L	p3W	p4L	p4W	m1L	m1Wtri	m1Wtal
N of cases	1	1	2	2	6	6	5	5	5
Minimum	7.35	4.15	8.25	5.40	8.05	5.90	9.40	6.00	5.90
Maximum	7.35	4.15	8.90	5.70	8.90	6.65	9.50	6.35	6.30
Arithmetic mean	7.35	4.15	8.58	5.55	8.48	6.28	9.48	6.20	6.13
Standard deviation	—	—	0.460	0.212	0.298	0.293	0.045	0.127	0.157
Coefficient of variation	—	—	5.4	3.8	3.5	4.7	.5	2.1	2.6
Shapiro-Wilk statistic	—	—	—	—	0.964	0.941	0.552	0.921	0.931
Shapiro-Wilk P-value	—	—	—	—	0.847	0.671	0.000	0.537	0.603

Statistic	m2L	m2Wtri	m2Wtal	m3L	m3Wtri	m3Wtal	MD at p3tal	MD at m2tri	Dent ML at m1
N of cases	4	4	4	5	5	5	1	2	2
Minimum	10.20	7.25	6.90	12.10	7.35	6.65	18.5	19.7	9.05
Maximum	10.90	7.50	7.35	13.30	8.20	7.20	18.5	22.0	10.5
Arithmetic mean	10.53	7.35	7.11	12.70	7.63	7.00	18.5	20.85	9.78
Standard deviation	0.352	0.108	0.221	0.476	0.355	0.276	—	1.626	1.025
Coefficient of variation	3.3	1.5	3.1	3.7	4.6	3.9	—	7.8	10.5
Shapiro-Wilk statistic	0.855	0.927	0.878	0.956	0.838	0.737	—	—	—
Shapiro-Wilk P-value	0.242	0.577	0.332	0.782	0.161	0.023	—	—	—

Abbreviations: **ant**, anterior; **bucc**, buccal; **d**, deciduous; **Dent ML**, mediolateral thickness of dentary; **L**, length; **ling**, lingual; **max**, maximum; **MD**, mandibular depth; **post**, posterior; **tal**, talonid; **tri**, trigonid; **W**, width.

fall within the 95% confidence intervals for the Vastan sample. Multivariate analysis of variance (MANOVA) on the most abundant teeth found no support for significant differences between the Vastan and Mangrol samples (p4, m2, m3, M3; Table 6, groups A and B). Furthermore, of 44 dental and gnathic measurements that could be tested for the combined Vastan + Mangrol samples, 41 were not significantly distinguishable from a normal distribution. Of the 22 among these that are represented by sample sizes of ≥10 specimens, 20 were indistinguishable from normality. The null hypothesis of normality could only be rejected for three measures (anterior width of M2, maximum width of M3, and length of dp3; see Appendix 5). Notably, the first two of these dimensions proved challenging to measure consistently. Because the Mangrol specimens are also similar morphologically to those from Vastan, they are accordingly referred to *C. thewissi*, with the two aforementioned exceptions. GU 7013 and GU 7016 are larger and lie well outside the range and confidence interval for these teeth in *C. thewissi*. Consequently, they may represent exceptionally large individuals of that species, or possibly a distinct, larger species, which is otherwise unrepresented in our sample; hence, they were excluded from statistical comparisons between groups.

The large cambaytheres from Tadkeshwar Mine, which are from a higher stratum and therefore somewhat younger than the Vastan sample (although how much younger is uncertain), tend to occupy the larger end of the size range of *C. thewissi* or to be slightly larger, except for M2, which is slightly smaller. Despite some significant differences in dimensions of M2, M3, and m2 from those of the Vastan-Mangrol sample, the means for many other measurements are indistinguishable between the two groups, based on current sampling (Table 6). The only other consistent morphological difference observed is the relatively larger and posterolingually more elaborate M3 (n = 4) of the Tadkeshwar sample.

Thus, statistical analyses provide little support for subdividing the Vastan and Mangrol samples we have assigned to *Cambaytherium thewissi*, and the only other criterion for recognizing more than one species in this sample is the unconfirmed variation in incisor number. Somewhat more evidence, including statistical differences in some molar dimensions and the morphology of M3 (a notoriously variable tooth), could be cited to justify separating the larger *Cambaytherium* specimens from Tadkeshwar. However, the Tadkeshwar sample is too small to allow a reasonable assessment of intraspecific variation, although a comparison of the few tooth loci for which multiple specimens are known suggests that it was substantial. Therefore, we opt at present for the more conservative interpretation that these Tadkeshwar specimens (mainly from TAD-2) represent a slightly more derived population attributable to *C. thewissi*. If larger samples become available, it may become necessary to reevaluate this interpretation.

Cambaytherium thewissi is clearly significantly larger than *C. gracilis* in most dental dimensions (Table 6); for example, it
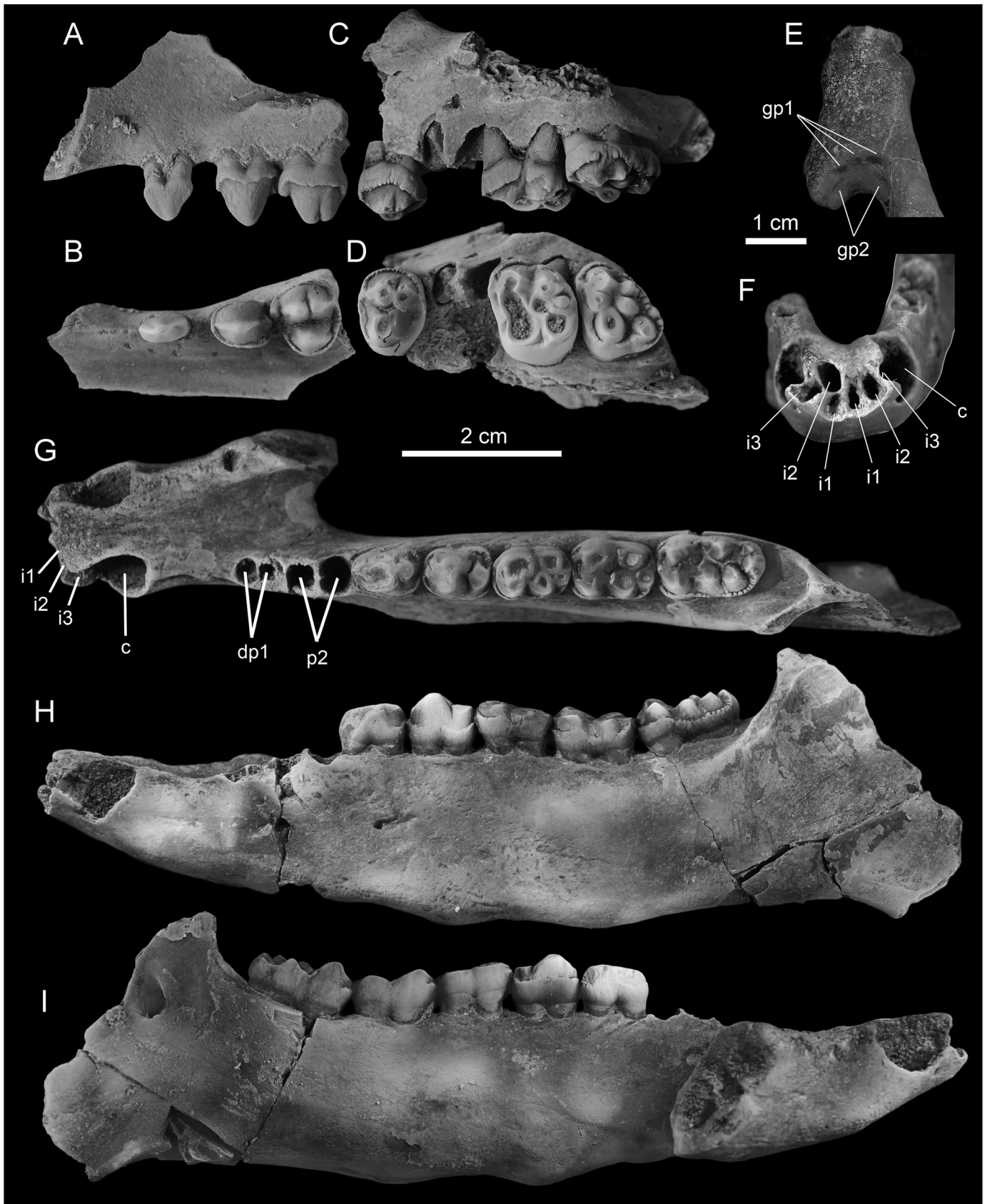
FIGURE 14. *Cambaytherium gracilis* from TAD-2. **A**, **B**, WIF/A 4213, right maxilla (reversed) with dP1, P2–3, in **A**, buccal and **B**, occlusal views. **C**, **D**, WIF/A 4214, left maxilla with P4, M2–3, in **C**, buccal and **D**, occlusal views. **E–I**, GU 9001, holotype, mandible with symphysis and left p3–m3: **E**, **F**, symphysis in **E**, ventral and **F**, anterior views; **G–I**, mandible in **G**, occlusal, **H**, buccal, and **I**, lingual views. Digital photographs modified from Smith et al. (2016). **Abbreviations**: **gp1**, genial pits, probably marking attachment of digastric and geniohyoid muscles; **gp2**, genial pits marking attachment of m. genioglossus. Scale bars equal 2 cm (**A–D**, **F–I**) and 1 cm (**E**).
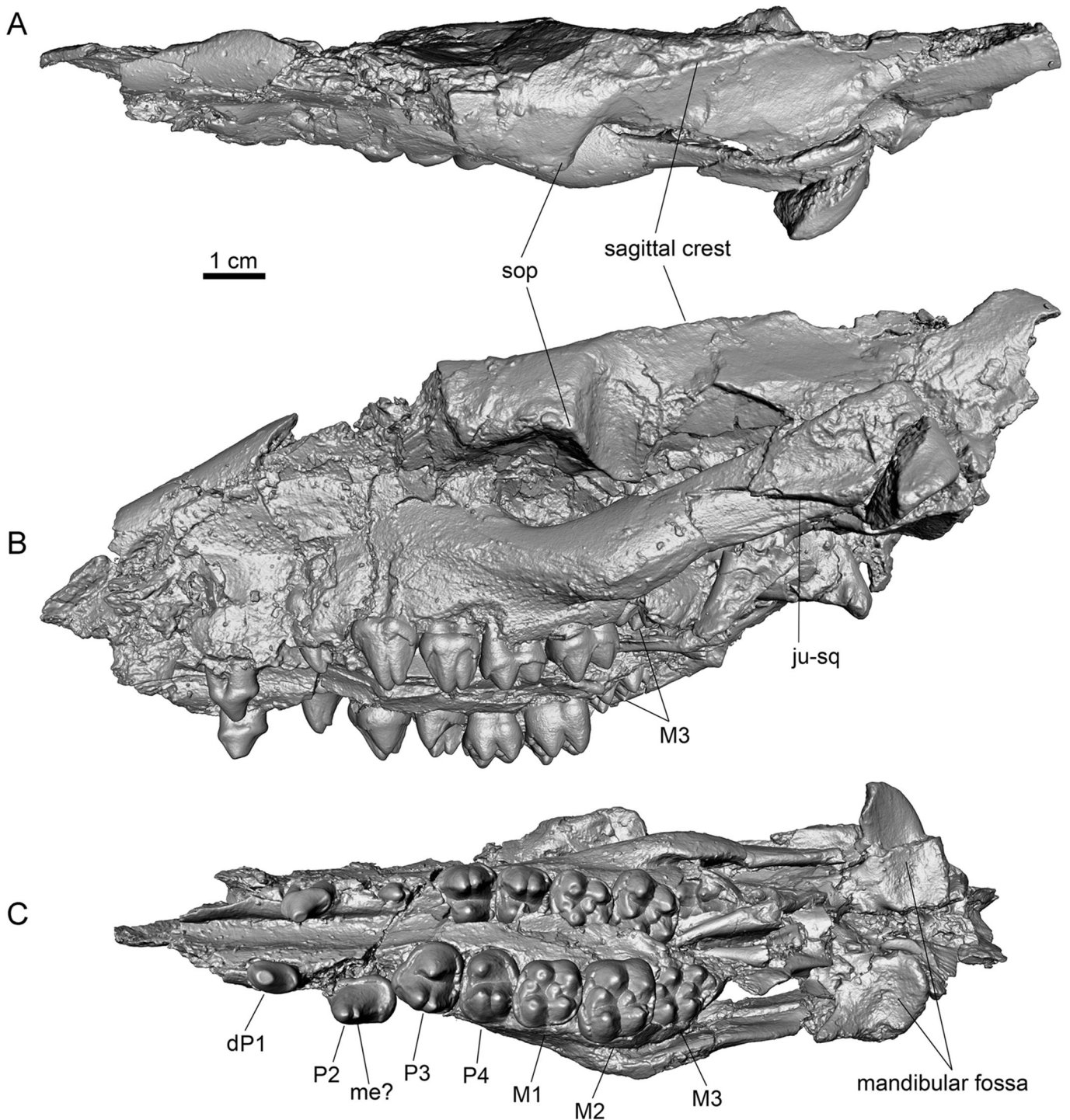
FIGURE 15. *Cambaytherium thewissi*. **A–E**, GU 402, skull, in **A**, dorsal, **B**, left lateral, **C**, ventral (palatal), **D**, ventral (palatal), and **E**, right lateral views. **F**, GU 403, probably associated mandible in right lateral view, to the same scale. **Abbreviations**: **ju-sq**, jugal-squamosal suture; **me**, metaconid; **pgp**, postglenoid process; **sop**, supraorbital process.

is 25–35% larger in linear dimensions of first molars, and postcranial bones assigned to *C. gracilis* are markedly smaller. *Cambaytherium thewissi* is also clearly distinct from *C. marinus*. Compared with the only known dental specimen of *C. marinus*, *C. thewissi* is about 25–35% smaller in linear dimensions of M1–2, and the few skeletal elements allocated to *C. marinus* are substantially larger than their counterparts in *C. thewissi*.

CAMBAYTHERIUM MARINUS (Bajpai, Kapur, Thewissen, Das, and Tiwari, 2006)

Synonym—*Kalitherium marinus* Bajpai, Kapur, Thewissen, Das, and Tiwari, 2006.

Holotype—IITR 931, rostrum with right P3–M3 and damaged dP1–P2, from Vastan Lignite Mine, level uncertain.
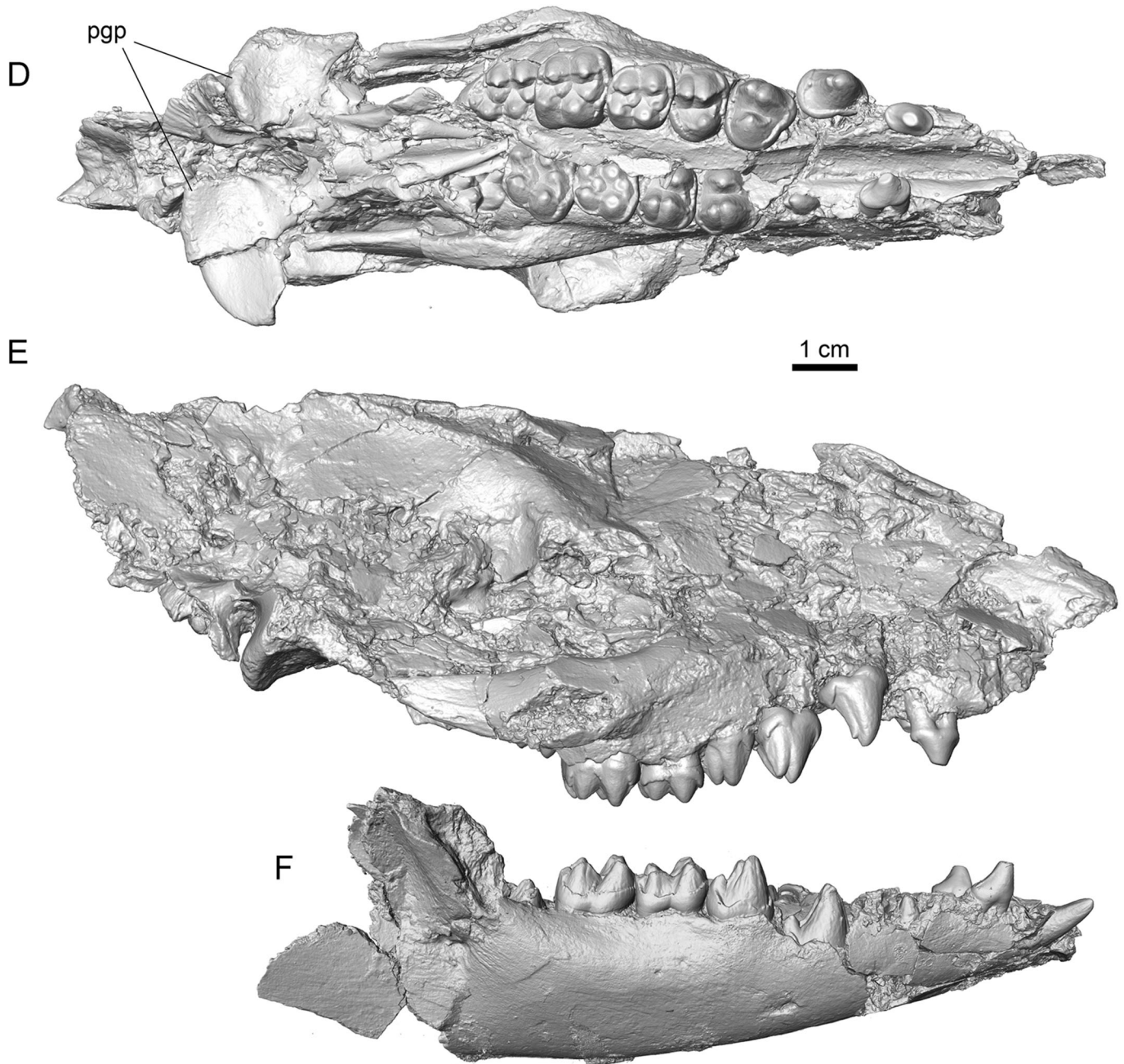
FIGURE 15. Continued.

Bajpai et al. (2006:101) reported the locality as "about 55 m above the lower mammal horizon," which would place it well above Lignite 1, in the 'overburden' depicted by Bajpai et al. (2005a:fig. 1). Later in the description of the species, however, they reported the horizon as "*N. burdigalensis* Zone (SBZ 10)" (Bajpai et al., 2006:106), which is below Lignite 1 and only about 14 m above the lower mammal horizon. They further noted that the holotype "was provided to one of us by a miner at the Vastan Lignite Mine" (Bajpai et al., 2006:106). Together these comments suggest that the exact horizon of the holotype is unknown.

Tentatively Referred Specimens—Vastan Mine: GU 841, L Mt II, level unknown; GU 8001, sacrum, level unknown; GU 8052, distal L tibia. Mangrol Mine: GU 7026, proximal R femur. The latter two specimens come from the principal vertebrate layer just above Lignite 2.

Discussion

This species was originally described as *Kalitherium marinus* and was differentiated from *Cambaytherium* primarily by its larger size. Bajpai et al. (2006) reported that P4 (length = 15.0 mm) was about 30% longer, M1 50% longer, and M2 100% longer than in *C. thewissi* and '*C. bidens*.' However, they provided length measurements only for P4 of '*C. bidens*' (reported as 12.8 mm by Bajpai et al., 2005a, but corrected to 9.6 mm in Bajpai

et al., 2006) and three molars unassigned to locus (length ranging from 10.4 to 11.4 mm). Based on their own measurements, P4 is 56% longer in *Kalitherium* than in 'C. bidens,' whereas the molars range from 44% to 97% larger depending on locus. Compared with means for our Vastan sample of *C. thewissi*, the published lengths of P4–M2 in the unique specimen of 'K.' *marinus* are 46%, 33%, and 62% larger, respectively. M1 in the holotype is clearly damaged and was probably larger than it appears now (or than its published measurements). The diagnosis distinguished '*Kalitherium*' as having "P2 longer than other premolars; M1 much smaller than M2 and M3; M2 wider than M1; M3 with reduced and relatively anteriorly positioned metacone, enlarged metaconule and paracone and distinct accessory cusps on the anterior and posterior aspects of hypocone" (Bajpai et al., 2006:104). None of these features distinguishes it from *Cambaytherium*, and except for size we can find no differences from *C. thewissi*. Accordingly, we regard *Kalitherium* as a synonym of *Cambaytherium* and transfer '*Kalitherium*' *marinus* to *Cambaytherium*.

The four postcranial specimens tentatively referred to *C. marinus* are all conspicuously larger than their counterparts allocated to *C. thewissi* but are very similar in most other respects. The metatarsal and sacrum were found in dumped sediment at Vastan Mine (level unknown) by mine workers, whereas the proximal femur and distal tibia were found in situ by our field team, the tibia from the productive layer just above Lignite 2 at Vastan Mine, and the proximal femur from the comparable layer at Mangrol Mine.

CAMBAYTHERIUM GRACILIS Smith, Kumar, Rana, Folie, Solé, Noiret, Steeman, Sahni, and Rose, 2016

Holotype—GU 9001, mandible with left p3–m3, symphysis, and anterior alveoli, from Tadkeshwar Lignite Mine (TAD-2).

Referred Specimens—TAD-1: GU 9019, R dentary, m1–3, erroneously reported as GU 9555 in Smith et al. (2016); WIF/A 4208, R ulna; WIF/A 4256, L Mc III; WIF/A 4263, L astragalus. TAD-2: GU 9007, LP3; GU 9008, LM3; GU 9009, Lm1; GU 9010, Rp4; GU 9017, L Mt III; GU 9018, L humeral shaft; GU 9206, R ulna; GU 9208, L femur; GU 9209, femoral shaft; GU 9210, proximal R femur; GU 9213, distal L femur; WIF/A 4210, L dentary, p2–m3; WIF/A 4211, R dentary, p4–m1, m3; WIF/A 4212, R dentary, m3; WIF/A 4213, R maxilla, dP1–P3; WIF/A 4214, L maxilla, P4, M2–3; WIF/A 4215, LP2; WIF/A 4235, Rp4; WIF/A 4236, Lp4; WIF/A 4237, Rm2; WIF/A 4238 RdP4; WIF/A 4239, RP4; WIF/A 4240, LP4; WIF/A 4241, LM2; WIF/A 4242, LM3; WIF/A 4243, RM3; WIF/A 4244, L radius; WIF/A 4245, R ulna; WIF/A 4246, R ulna; WIF/A 4257, L femur; WIF/A 4265, L maxilla, P2–M3.

Discussion

Cambaytherium gracilis, recorded only from somewhat younger strata at Tadkeshwar Mine (mostly TAD-2) than the Vastan sample of *Cambaytherium thewissi*, is decidedly smaller (at least 20%) in linear dental dimensions than *C. thewissi* (Figs. 11–13 and A1–A3; Table 7; Appendices 3, 4); and it has a longer diastema between the canine and dp1, less robust lower premolars, and a well-developed metaconid on p4 (Fig. 14). Nearly all means for dental dimensions of *C. gracilis* are significantly different from those of *C. thewissi* from TAD-2, and they lie well outside the 95% confidence intervals for Vastan *C. thewissi*. Furthermore, MANOVAs on the most abundant teeth revealed significant differences compared with both Vastan and Tadkeshwar *C. thewissi* (p4, m2, m3, M3; P < 0.01; Table 6). Postcranial elements also indicate a substantially smaller, less robust animal than *C. thewissi* (see Paleobiology,

Body Mass, below). These differences justify its specific distinction from *C. thewissi*. In most other details, however, *C. gracilis* closely resembles *C. thewissi*. Where differences occur, they are mentioned in the following description.

CRANIODENTAL ANATOMY OF *CAMBAYTHERIUM*

Skull

Two specimens of *C. thewissi*, GU 402 and GU 730 (Figs. 15, 16), provide the best representation of the skull. Both specimens are subadult, but GU 730 is clearly younger, retaining dP2–4 and having only M1 erupted. M3 is erupting in GU 402 (as is m3 in an associated lower jaw, GU 403), but otherwise the adult dentition is in place in this specimen. Both skulls are missing the tip of the rostrum and much of the basicranial and occipital regions, and there is significant distortion due to crushing. As preserved, approximately from the front of the rostrum to the occiput, GU 402 is 181 mm long and GU 730 is 132 mm long. The orbits of these specimens are also damaged to the extent that little can be gleaned of the extent of orbital bones and the positions of orbital foramina. Some skull features can also be recognized in more fragmentary material, and WIF/A 4265 is a maxillary fragment assigned to *C. gracilis* that preserves some cranial features.

General Morphology and Proportions—Overall, the known skulls of *Cambaytherium* have a shape and proportions similar to those of early perissodactyls. The preorbital and postorbital portions of the skull appear to be similar in length, and the anterior edge of the orbit is situated over M1 or P4. There is a low but distinct sagittal crest formed by paired converging ridges extending posteriorly from the supraorbital processes. There is little to no preservation of the narial incision, from which it can at least be inferred that the incision was not deep.

Premaxilla—The premaxilla is either not preserved or represented by fragments damaged beyond recognition. Given the extent of the maxilla, which is preserved as far rostral as the canine alveolus in GU 730, the premaxilla clearly did not extend caudally as it does in tethytheres. Considering the overall shape of the rostrum and its similarity to that of early perissodactyls, it is likely that the premaxilla was relatively small and may have contacted the nasal.

Maxilla—The maxilla dominates the lateral aspect of the rostrum. Damage obscures the position of the rostral opening of the infraorbital foramen in the two skulls of *C. thewissi* (GU 402 and GU 730), but in WIF/A 4265 (*C. gracilis*) this foramen is positioned over the posterior end of P2. In all three specimens, there is a prominent tuber maxillae forming the floor of the anterior half of the orbit and housing the posterior molars. Poor preservation prevents any further interpretation of the extent of the maxilla in the orbit. Short diastemata separate dP1 from the canine and from P2 in GU 402 and WIF/A 4265; the anterior diastema is slightly longer. In GU 730, which represents a younger ontogenetic stage, the diastema between dP1 and dP2 (judging from roots of dP1) is barely developed.

Nasal—The nasals are damaged and are missing their rostral tips in both skulls, but it is clear that the nasal extended rostrally probably to the tip of the snout, based on the extent and degree of tapering of the preserved portions. The caudal ends of the nasals form a broad table in GU 730, similar to what is observed in perissodactyls, and there appears to be a transverse suture with the frontal.

Lacrimal—The lacrimal is preserved to some extent on both sides of GU 730, although its extent is clearer on the left side. The lacrimal has a moderate facial exposure but does not seem to contact the nasal, as it typically does in early perissodactyls.
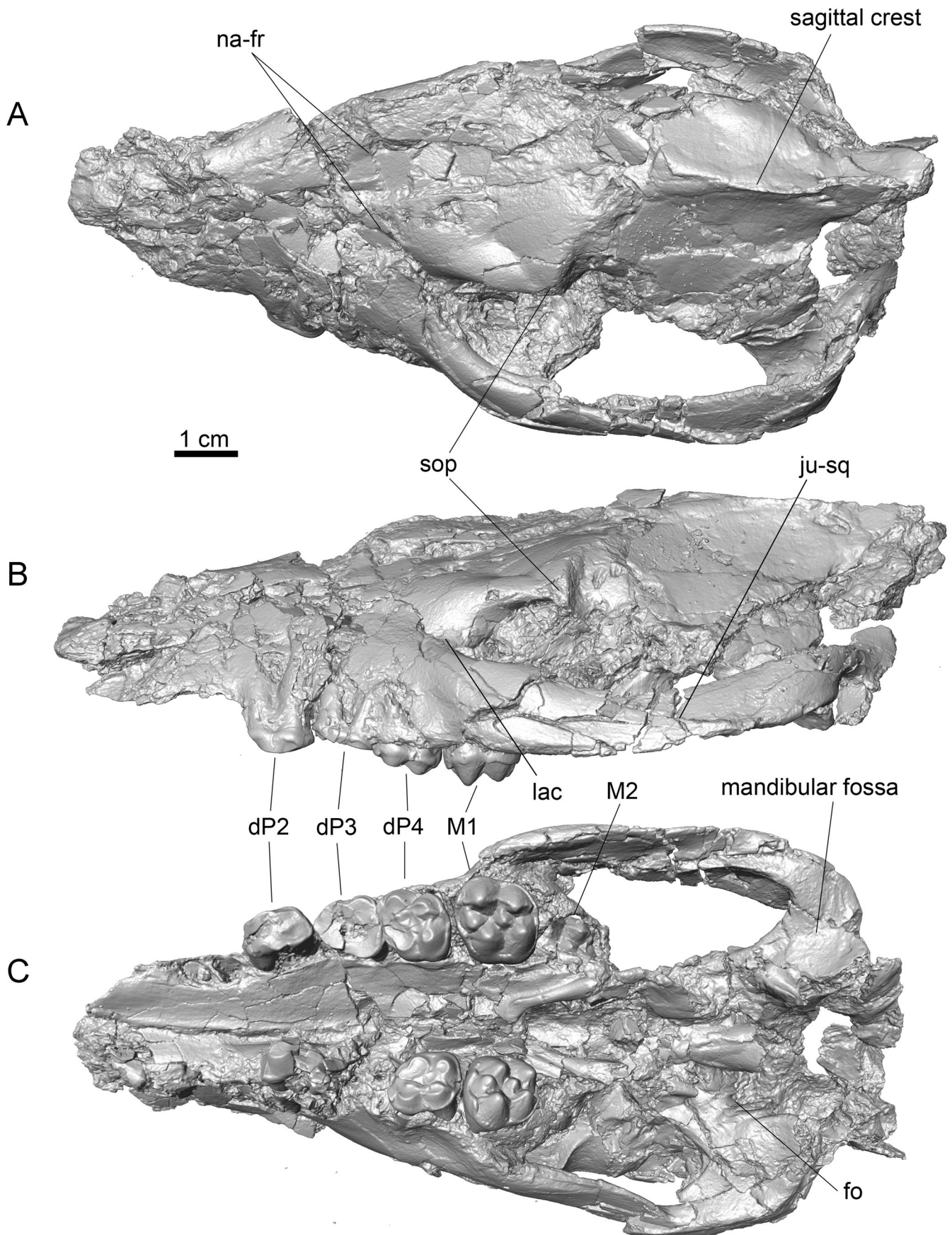
FIGURE 16. *Cambaytherium thewissi*, GU 730, cranium of juvenile with left dP2–4, M1, M2 in crypt, right dP4–M1, in **A**, dorsal, **B**, left lateral, and **C**, palatal views. **Abbreviations**: **fo**, foramen ovale; **ju-sq**, jugal-squamosal suture; **lac**, lacrimal; **na-fr**, nasofrontal suture; **sop**, supraorbital process.

Displacement of the bone makes it unclear whether it possesses a tubercle.

Palatine—The palatine is only visible in the palate, and even there its suture with the maxilla is indistinct. The posterior edge is thickened as a torus and forms a deep notch extending anteriorly to the anterior edge of M2. The young ontogenetic age of both skulls means that this notch might ultimately lie farther back relative to the tooth row once all molars are erupted. The torus bounds a broad gutter between it and the molars.

Frontal—The frontals and the nasals, and perhaps part of the parietals, form a diamond-shaped table covering most of the dorsal surface of the skull. The supraorbital processes are blunt and show no supraorbital foramina or notches.

Parietal—The suture between the frontal and the parietal is indistinct. Ridges extend posteriorly from the supraorbital processes of the frontal and eventually meet, presumably on the parietal, to form a low but distinct sagittal crest.

Jugal—The general form and extent of the jugal is similar to that of early perissodactyls. Anteriorly, the jugal forms the anteroventral border of the orbit, contacting the lacrimal and forming an oblique suture with the maxilla. There is a small, blunt postorbital process about halfway along the dorsal edge of the jugal marking the posterior edge of the orbit. Posteriorly,
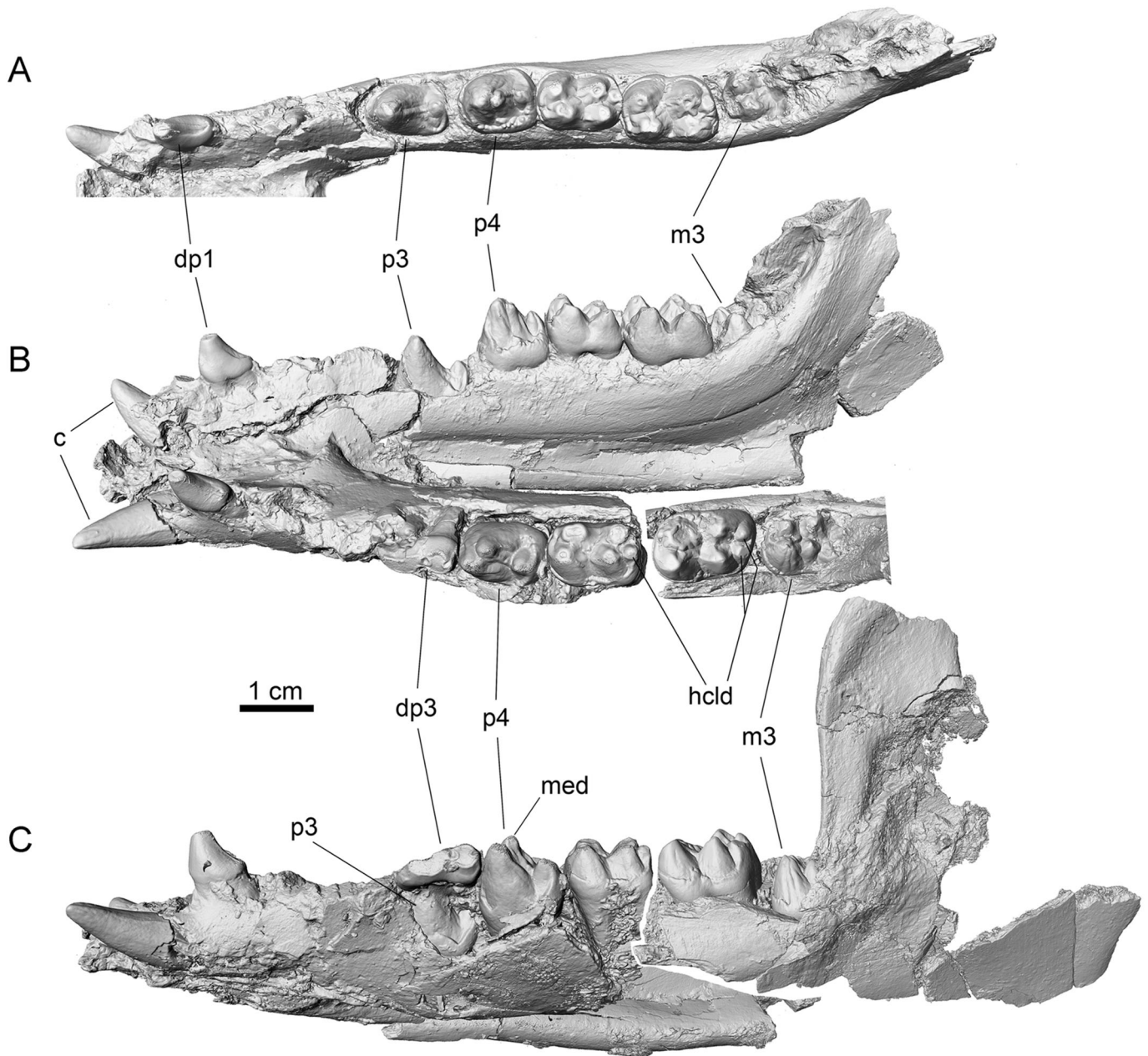

FIGURE 17. *Cambaytherium thewissi*, GU 403, mandible with right c, dp1, p2 erupting, p3–4, m1–3, left c, dp1, dp3, p3 erupting, p4, m1–3, m3s erupting. **A**, occlusal view of right dentary; **B**, oblique superior view of mandible with lingual view of right dentary and occlusal view of left dentary; **C**, lateral view of left dentary.

the jugal thickens and then tapers as it forms a horizontal suture with the squamosal, which contacts it dorsally. The posterior end of the jugal terminates short of the glenoid fossa and therefore does not contribute to the jaw joint.

Sphenoid Complex—The best-preserved parts of the sphenoid complex are parts of the alisphenoid visible in ventral view, and even these are damaged. The most notable feature is a pair of notches, separated by a narrow ridge of bone, that lie medial to the groove that is medial to the glenoid fossa. The lateral notch is presumably the foramen ovale, which appears to be confluent with the opening posterior to it that corresponds to the cranial hiatus (Mead and Fordyce, 2009). However, it is not clear whether this confluence is an artifact of damage. The medial

notch is presumably the medial lacerate foramen, which would also be confluent with the cranial hiatus.

Squamosal—The squamosals are damaged to a considerable extent in both GU 402 and GU 730. The best-preserved parts include the glenoid fossa and the contact with the jugal. The glenoid fossa consists mainly of a flat, horizontal surface whose posterior end sweeps ventrally as a slightly concave surface onto the broad postglenoid process. Deformation makes it difficult to determine the exact orientation of the postglenoid process, but it appears to face anteriorly or slightly anterolaterally. Damage prevents determining whether or not a postglenoid foramen is present. A distinct groove is present medial to the glenoid fossa. The zygomatic process extends anteriorly as a
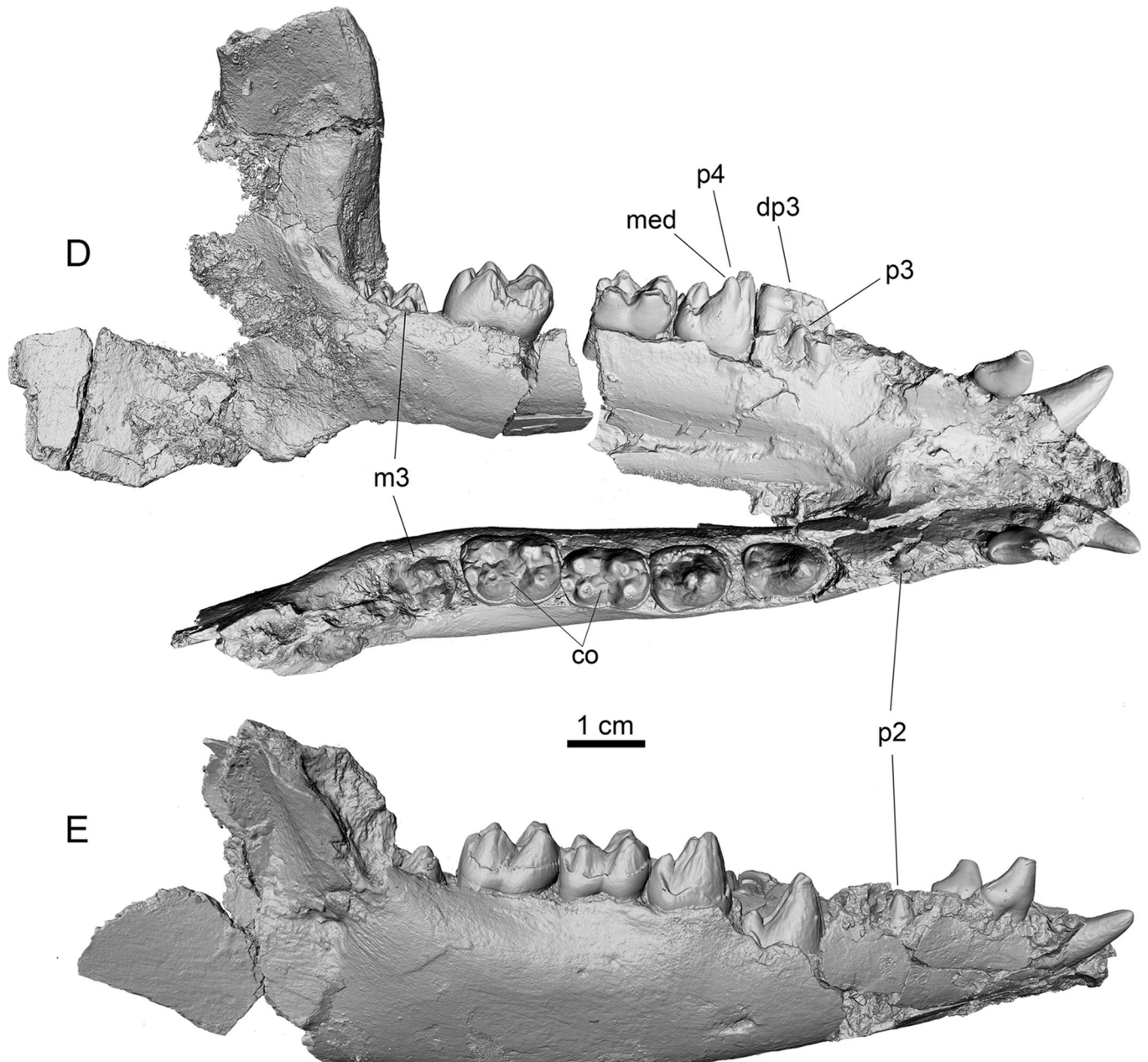

FIGURE 17. Continued. **D**, oblique superior view showing lingual side of left dentary and occlusal view of right dentary; **E**, lateral view of right dentary. See Figure 15 for probably associated cranium, GU 402. **Abbreviations**: **co**, cristid obliqua; **hcld**, hypoconulid (double on m2); **med**, metaconid.
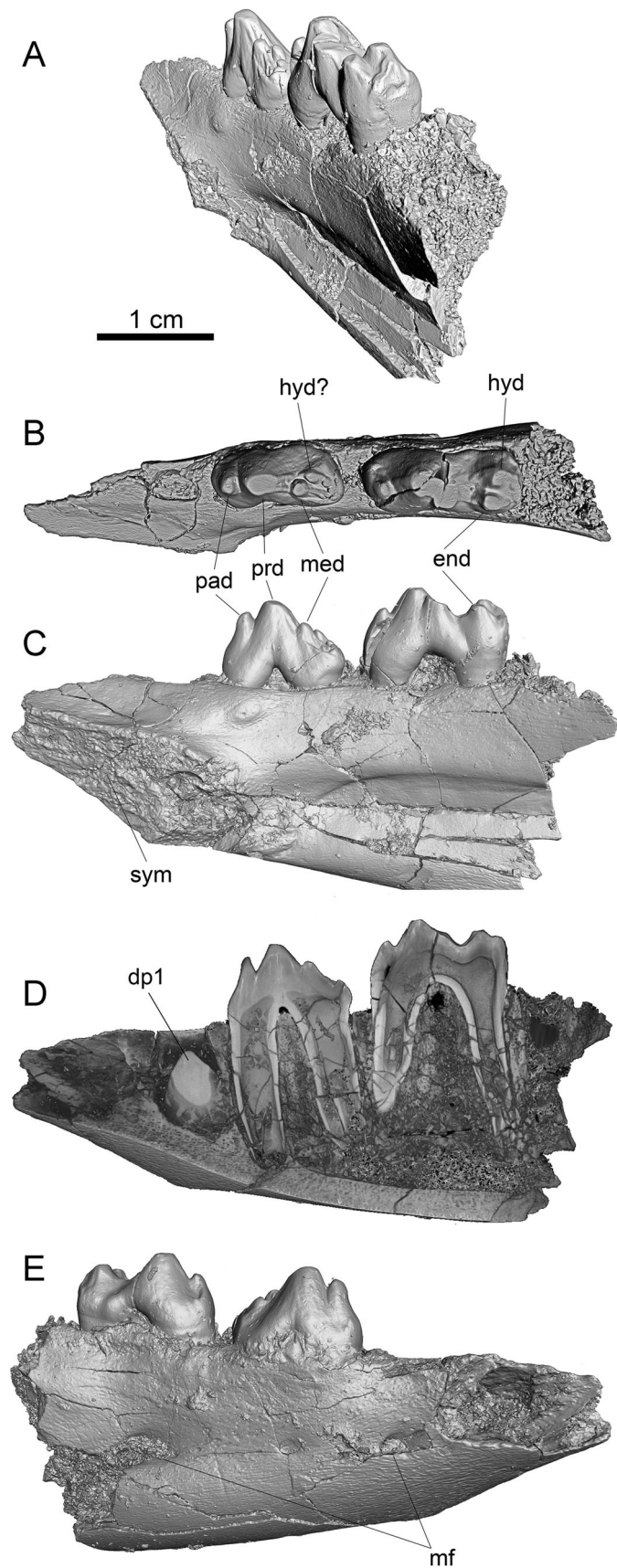
FIGURE 18. *Cambaytherium thewissi*, GU 1701, right dentary with dp2–3. **A**, oblique posterior view; **B**, occlusal view; **C**, lingual view; **D**, micro-CT sagittal section through dentary showing roots of dp2–3, and dp1 crown in the crypt; **E**, buccal view. **Abbreviations**: **end**, entoconid; **hyd**, hypoconid; **med**, metaconid; **mf**, mental foramen; **pad**, paraconid; **prd**, protoconid; **sym**, unfused symphysis.

mediolaterally narrow bar that tapers anteriorly to form the horizontal contact with the jugal ventral to it.

Occipital and Petrosal—The occipitals and the petrosals are not preserved in any specimen.

Mandible—Nineteen specimens in our sample include part of the lower jaw, and 10 of them preserve details of either the mandibular symphysis or the back of the jaw. Adult *Cambaytherium* had a true mandible, i.e., consisting of dentaries joined by a solidly fused symphysis that extends posteriorly as far as p2 (GU 403, GU 1710, GU 7004, GU 9002, WIF/A 1200, *C. thewissi*; GU 9001, *C. gracilis*; Figs. 9, 10, 14, 17), a length that is increased by diastemata and a two-rooted dp1. The symphysis thus appears to be as long as in primitive equids and *Homogalax*, if not more extensive. All of the specimens noted above have a diastema between the canine and dp1, but it varies in length from short (GU 403, GU 1710, GU 7004) to medium (GU 9002) in *C. thewissi* to long in the holotype of *C. gracilis*. The diastema between dp1 and p2 is also variable (see below). A strongly coossified symphysis is shared with primitive perissodactyls but contrasts with most phenacodontids, in which the symphysis was typically unfused (e.g., *Phenacodus primaevus*, USGS 7158, USNM 527625; *P. wortmani*, USGS 813; *Ectocion osbornianus*, USNM 487874, USNM 487875; see also Thewissen, 1990). However, according to Thewissen (1990), fusion of the symphysis is variable in *Ectocion* and *Copecion* and otherwise occurs only in European *P. lemoinei*. A fused symphysis is also present in the possible phenacodontid *Meniscotherium* (Gazin, 1965; Williamson and Lucas, 1992). The primitive proboscidean *Phosphatherium* has an unfused symphysis (Gheerbrant et al., 2005a) (symphyses are unknown in *Eritherium* and *Daouitherium*). Shallow pits, for attachment of the anterior digastric and/or geniohyoid muscles, are present on both sides of the midline at the most ventral part of the symphysis in the holotype of *C. gracilis* (Fig. 14E). Just above these pits are a pair of larger but shallower fossae marking the attachment of the m. genioglossus. No pits are evident in *C. thewissi* (GU 1710, GU 9002), and in other specimens none can be detected owing to poor preservation.

Two juvenile specimens of *C. thewissi* (GU 736, GU 1701; Fig. 18) appear to show unfused symphyses. They contain slightly worn dp3–4 and dp2–3, respectively, and both show juvenile surface texture and are much shallower than other dentaries. The subadult GU 403, with left dp3 still in place and erupting p3s and m3s, has a fused symphysis, so it appears that fusion occurred at a fairly young age. Both specimens have two mental foramina, one below dp3 and the other below the short dp2–dp1 diastema.

The tooth-bearing part of the dentary is approximately uniform in depth below the molars and posterior premolars but shallows toward the symphysis, despite large canine alveoli (which are inclined; Figs. 9, 14G–I, 17). Most jaws of *C. thewissi* are relatively deep, but there is some variation in depth (the subadult GU 403 and the adult GU 7001 are shallower than others), although the available evidence is insufficient to determine whether this relates to sexual dimorphism. The juveniles GU 736 and GU 1701 have the shallowest jaws, as would be expected, and the mandibular canal, transmitting the inferior alveolar nerve and vessels, is exposed (by breakage) near the base of the lateral side of GU 736. All specimens that are adequately preserved have two or more mental foramina, typically one each below p3 and p4, with some variation in the exact position (under p2 in GU 7001, under p3–p4 junction in GU 776). Another one or two foramina are present below dp1 in GU 1710, GU 7004, GU 9001, and WIF/A 1200.

The mandibular angle in *C. thewissi* is greatly expanded posteroinferiorly to accommodate large masseter and medial pterygoid muscles (GU 776, GU 1710, GU 1711; Figs. 19, 20). The angle of the smaller *C. gracilis* (GU 9001, GU 9019; Figs. 14, 21) is
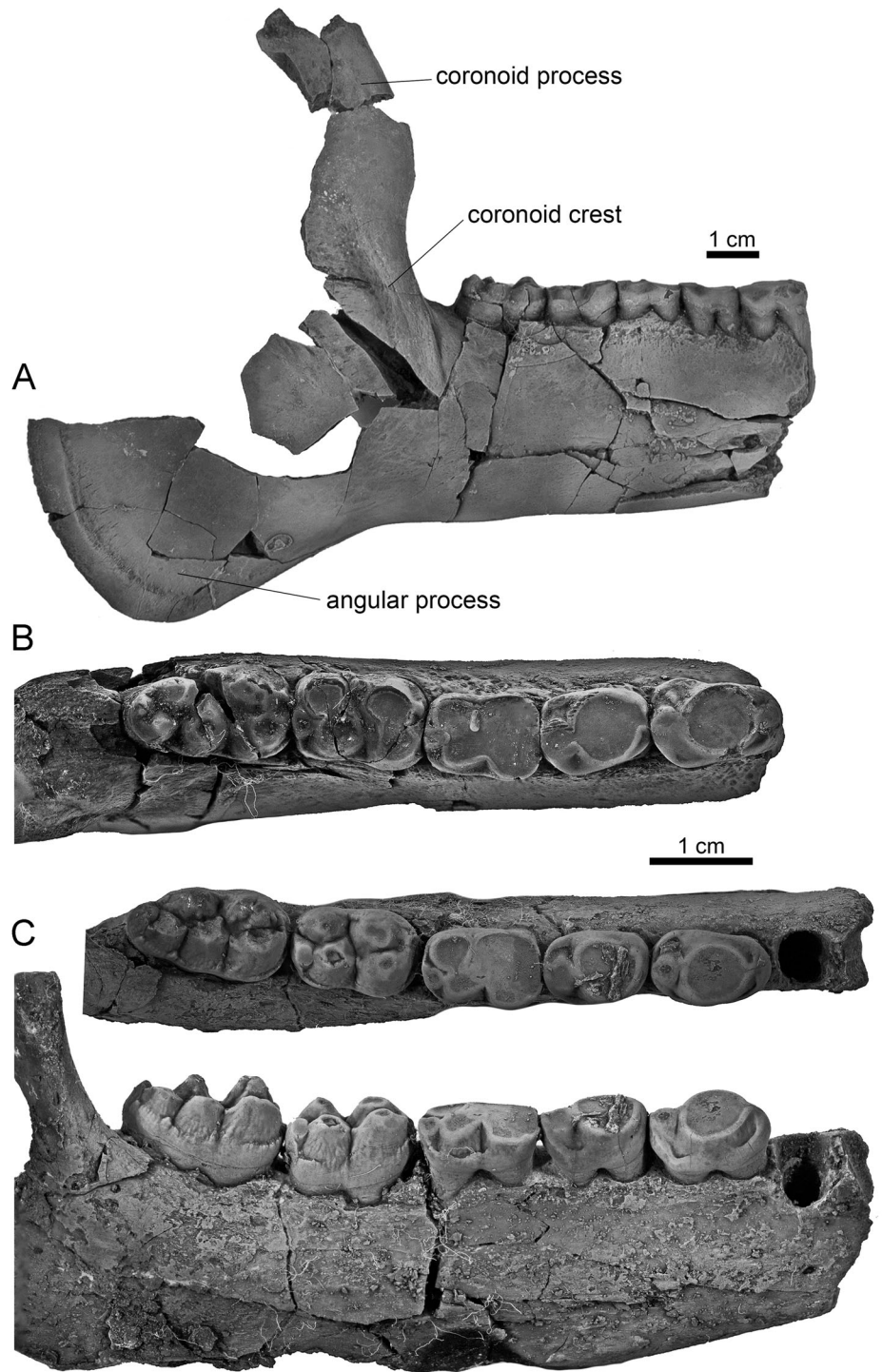
FIGURE 19. *Cambaytherium thewissi*, right dentaries with p3–m3, digital photographs. **A**, GU 776 in lateral view, to show expanded angular process and tall coronoid process; **B**, GU 776 in occlusal view; **C**, GU 7001 in occlusal and buccal views. Lower scale bar applies to **B** and **C**.

somewhat less expanded, resembling the condition in *Meniscotherium* (Gazin, 1965:pl. 3; Williamson and Lucas, 1992: fig. 45). The expansion is greater than that in basal equids and *Phenacodus* except in GU 9019, from TAD-1, which projects ventrally less than the others. The posteroinferior edge is smoothly rounded and medially inflected on its ventral border, forming a fossa for the medial pterygoid muscle. The posterior margin is thickened on its lateral aspect, forming a distinct ridge that demarcates the back of the masseteric fossa (Fig. 19A). The ascending ramus is essentially vertical, and the coronoid process is recurved and reduced (though less so than in early equids),

but there is usually a well-developed coronoid crest (Evans and Christensen, 1979) anterolaterally; and the mandibular condyle is subcylindrical and very high, well above the tooth row (GU 1710, GU 1711, GU 9019; Figs. 20, 21), as in equids and *Phosphatherium*.

Dentition

The most striking characteristics of the dentition of *Cambaytherium*, compared with primitive perissodactyls, are the marked bunodonty of the molars and posterior premolars,
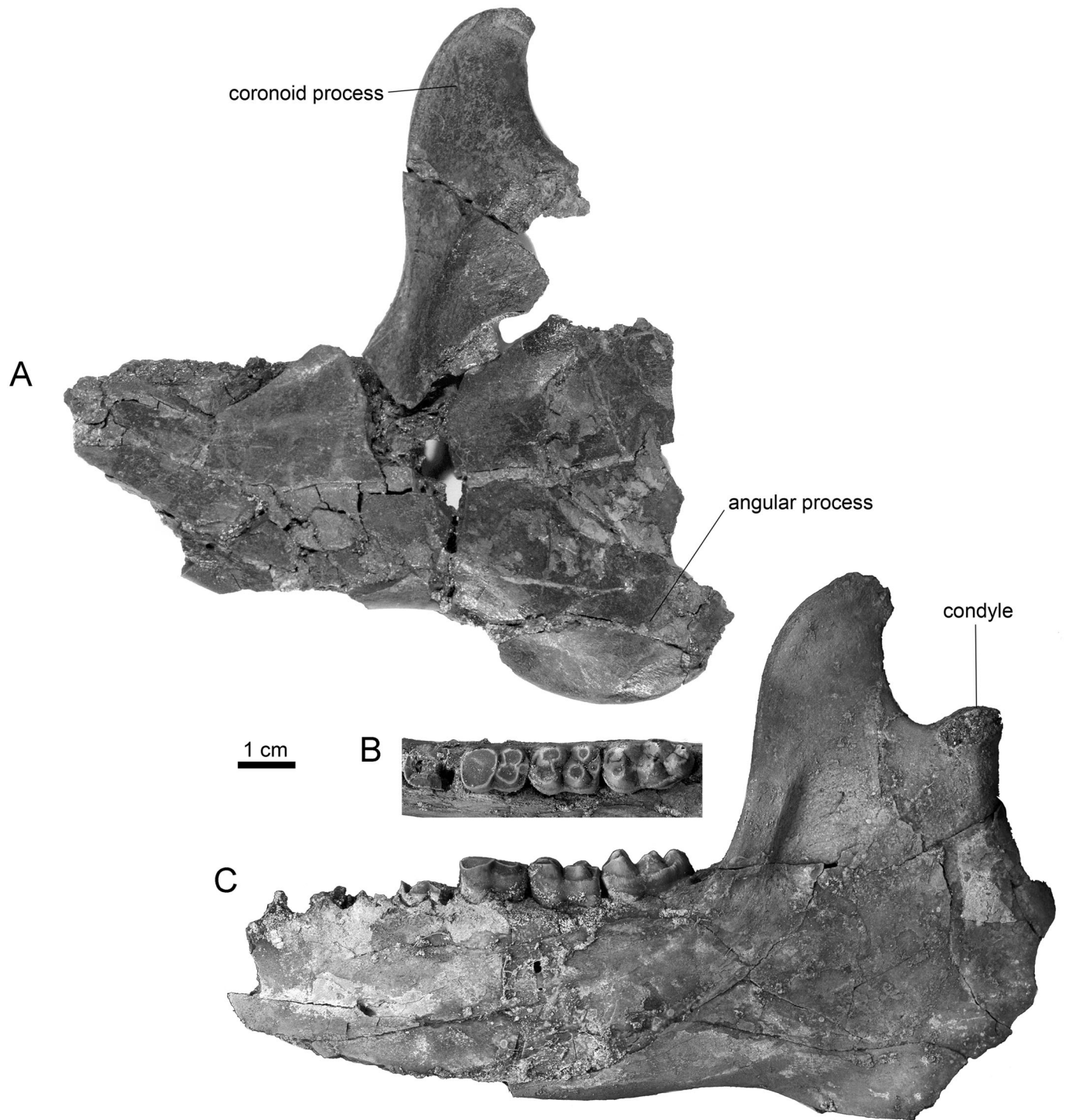
FIGURE 20. *Cambaytherium thewissi*, left dentaries, digital photographs. **A**, GU 1710, back of dentary with coronoid and angular processes; **B**, **C**, GU 1711, left dentary with m1–3, in **B**, occlusal and **C**, buccal views.

coupled with little or no crest development, and the simpler premolars. In addition, all teeth of *Cambaytherium* typically exhibit distinct, coarse perikymata (Fig. 22), the surface manifestation of striae of Retzius, 'long-period lines' that are caused by interruption in enamel deposition usually over periods of days (approximately weekly, or circaseptan) during tooth formation (Dean, 1987). Teeth with taller crowns such as canines tend to show more perikymata. Because of their known periodicity in humans and some other primates, the number of perikymata has been used to estimate the time it took for crown formation, as a tool for estimating age in fossil hominids (Dean, 1987; Ungar, 2010). Dirks et al. (2009) used striae periodicity (the number of days between striae of Retzius), together with other histological data, to estimate that it took a little less than a year for molar crowns to form in *Phenacodus*. This may provide a rough approximation of molar crown formation time in
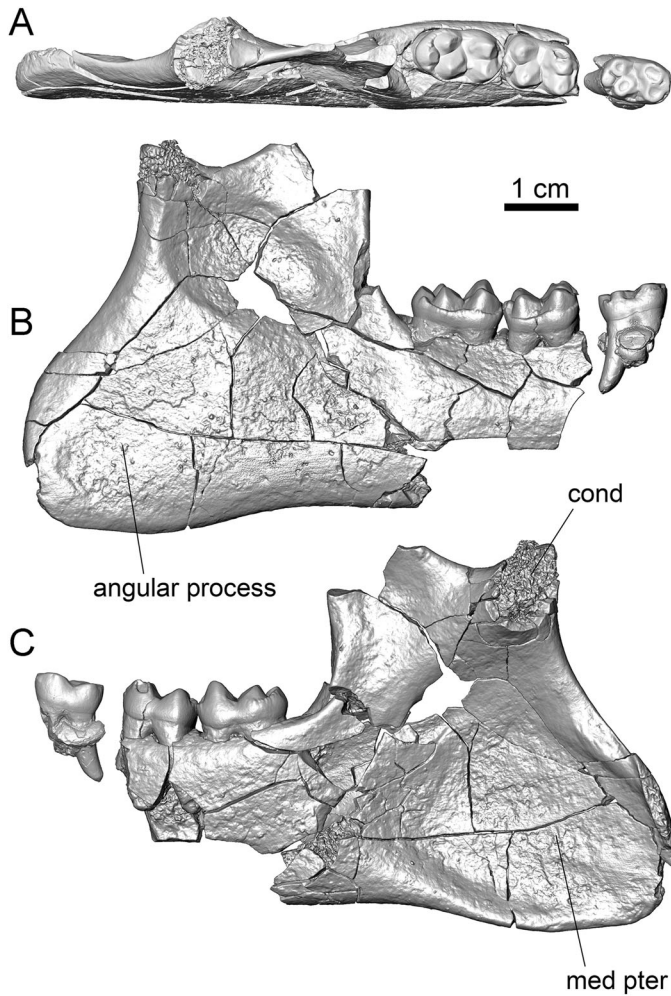
FIGURE 21. *Cambaytherium gracilis*, GU 9019, right dentary with m2–3 and associated m1, from TAD-1, in **A**, occlusal, **B**, buccal, and **C**, lingual views. **Abbreviations**: **cond**, mandibular condyle (broken); **med pter**, fossa for medial pterygoid muscle.
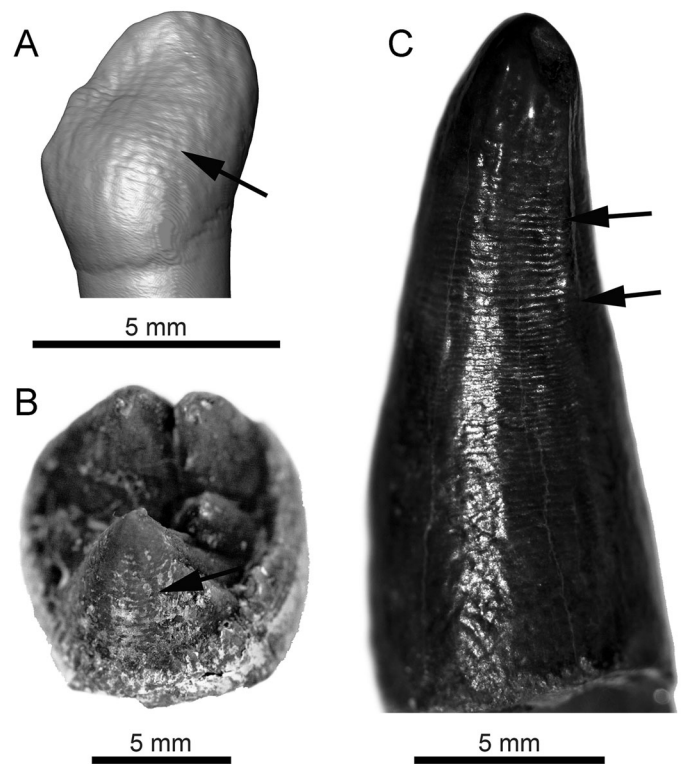

FIGURE 22. Teeth of *Cambaytherium thewissi* showing perikymata, digital photographs. **A**, incisor, GU 8034; **B**, unerupted P4, GU 5 (holotype of *Indobune vastanensis*); **C**, canine, GU 407. Arrows are approximately aligned with parallel, horizontal perikymata.

Cambaytherium. The perikymata of *Cambaytherium* are spaced at more or less regular intervals (~0.10 mm apart) and in unworn teeth can be seen to extend along the entire crown (not just at the base). They are straight or slightly wavy near the base of the crown and may become distinctly wavier toward the cusp apices. In addition, the enamel of *Cambaytherium*, when not worn or eroded, typically has a wrinkled or corrugated surface, with ridges and valleys that intersect the perikymata and are sometimes quite conspicuous.

The description of the teeth presented here is based primarily on our large sample from Vastan and Mangrol mines, referred to *Cambaytherium thewissi*. Unless otherwise noted, *C. gracilis* and *C. thewissi* from Tadkeshwar Mine are similar (where known).

Incisors—A reconsideration of the incisor number in *Cambaytherium* is important, because this was one of the principal criteria used to distinguish *Cambaytherium bidens* from *C. thewissi*. Based on our sample, the number of lower incisors on each side of the mandible is probably three, but there is some ambiguity among the few specimens that preserve the symphysis. No specimens preserve incisors in place. Lower incisor alveoli are preserved to various extents in four specimens, which represent both species: GU 1710 (Vastan), GU 7004

(Mangrol Mine), and GU 9002 (TAD-2), representing *C. thewissi*, and GU 9001 (TAD-2), holotype of *C. gracilis*, but they are not all easy to interpret. The symphysis is also present in WIF/A 1200 and GU 403, but the incisor region is damaged in these specimens and does not preserve the incisor configuration; however, three isolated incisors are associated with GU 403 and may be lower incisors. Except for GU 403, a subadult with erupting canines, premolars, and m3s, these jaws are fully adult with strongly fused symphyses and moderate (GU 7004, GU 9001) to heavy (GU 1710, WIF/A 1200) wear on cheek teeth (except GU 9002, which is edentulous).

GU 1710 appears to have two incisor alveoli on the left side, with i2? larger than i1, but the labial part of the symphysial region is damaged and largely missing, making the specimen difficult to interpret. On the right side of this specimen, three incisor alveoli are clearly present, although the lingual border of the alveoli resembles that on the left side—i.e., two apparent alveoli, for i1–2. What is clear on the right side is that the alveoli of i1 and i3 extend toward the labial margin, with i2 wedged lingually between them. On the left side, with the labial portion missing, evidence of i3 has been lost, but it seems likely that three incisors were present on the left as well. This suggests that the number and arrangement of incisors could be misinterpreted in specimens in which the symphysis is incomplete either labially or lingually. GU 7004 (Fig. 9) preserves three clear alveoli arranged mesiodistally on the left; i3 is less obvious on the right because the labial margin is damaged, but close comparison with the left side suggests that it is the same. Thus, the position of the three incisors varies in these two specimens (either aligned or offset due to crowding of the incisors). GU 9002 (Fig. 10), however, is a relatively narrow, edentulous
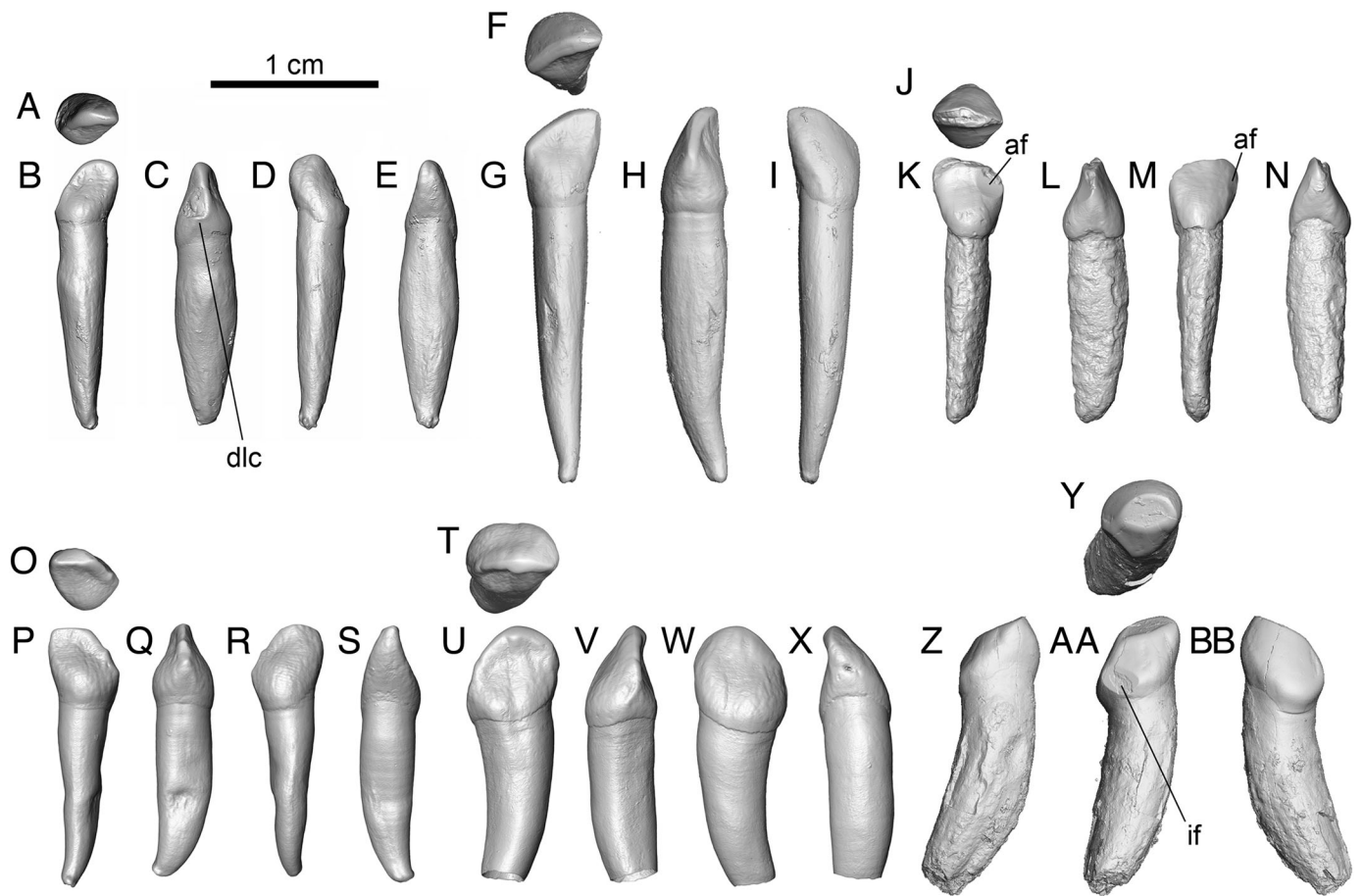
FIGURE 23. Incisors of *Cambaytherium thewissi*, loci uncertain. **A–E**, GU 1676 in **A**, occlusal, **B**, lingual, **C**, distal, **D**, labial, and **E**, mesial views. **F–I**, GU 8033 in **F**, occlusal, **G**, lingual, **H**, distal, and **I**, labial views. **J–N**, GU 8023 in **J**, occlusal, **K**, lingual, **L**, distal, **M**, labial, and **N**, mesial views. **O–S**, GU 8034 in **O**, occlusal, **P**, lingual, **Q**, distal, and **R**, labial, and **S**, mesial views. **T–X**, GU 8026 in **T**, occlusal, **U**, lingual, **V**, distal, **W**, labial, and **X**, mesial views. **Y–BB**, GU 8030 in **Y**, occlusal, **Z**, lingual, **AA**, distolingual, and **BB**, labial views. **Abbreviations**: **af**, attritional facet; **dlc**, distolabial cingulid; **if**, interstitial facet.
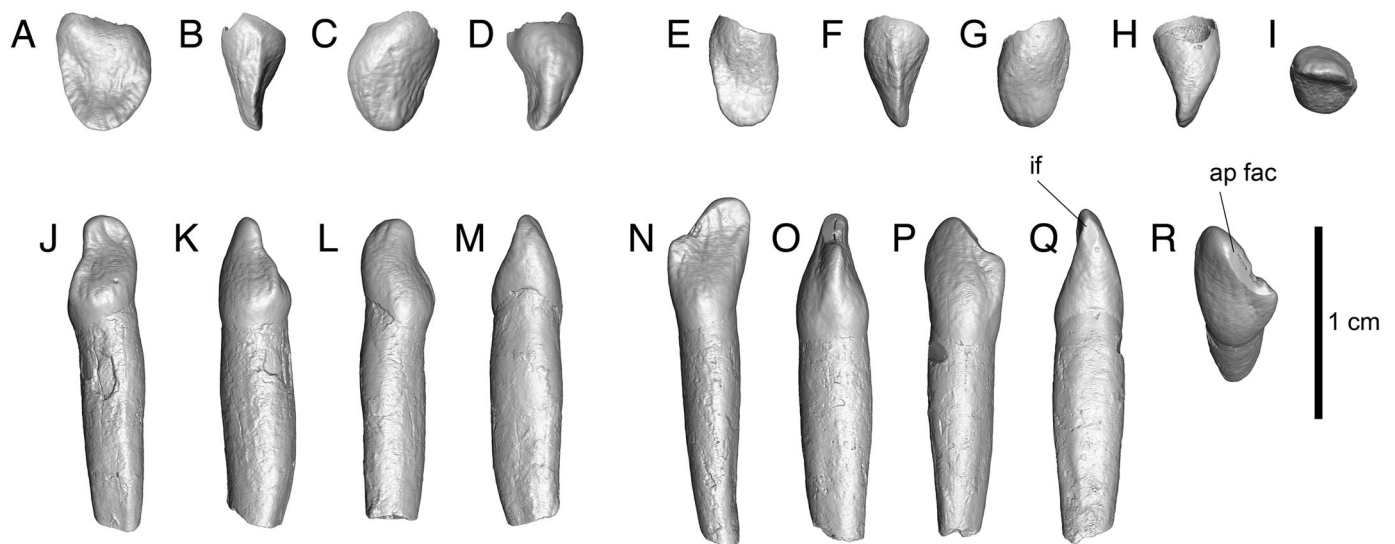

FIGURE 24. Incisors of *Cambaytherium thewissi*, possibly associated with cranium and mandible (GU 402 and GU 403; Figs. 15, 17). **A–D**, GU 626-1, possible I1 in **A**, lingual, **B**, distal (posterior), **C**, labial, and **D**, mesial views. **E–I**, GU 626-2, possible upper lateral incisor in **E**, lingual, **F**, distal (posterior), **G**, labial, **H**, mesial, and **I**, occlusal views. **J–M**, GU 403-1, possible left i1 or i2 in **J**, lingual, **K**, distal (posterior), **L**, labial, and **M**, mesial views. **N–R**, GU 403-2, possible left i3 in **N**, lingual, **O**, distal (posterior), **P**, labial, **Q**, mesial, and **R**, oblique occlusal views. Strong roots on supposed lower incisors and lack of roots on the uppers raise doubt of the association of both sets with the subadult skull. **Abbreviations**: **ap fac**, apical facet; **if**, interstitial facet.

symphysis, which appears to have only two incisors on each side. It is the only specimen in our sample showing this condition, but it must be noted that the labial margin as well as the alveolar septa and medial margin of the canine alveoli are damaged, leaving the incisor count ambiguous. It is possible that both i2 and i3 occupied the lateral alveolus, one lingually and the other labially, or that i3 was situated on the medial side of the canine alveolus.

GU 9001 (Fig. 14), representing *C. gracilis*, has three right incisor alveoli: i1 and i3 labially and i2 slightly larger and situated on the lingual margin (presumably owing to crowding of the incisors, similar to the configuration in GU 1710). Concomitantly, there are two clear alveoli (i1–2) on the left side and a medial indentation at the front of the left canine alveolus that probably held i3—again, an asymmetrical arrangement in left and right quadrants. In all of these specimens, the alveoli indicate that the incisors were small and approximately equal in size, although the root of i1 seems to be slightly smaller than the others. Thus, based on the few available specimens, we consider it most probable that *Cambaytherium* normally had three relatively small lower incisors on each side, but we cannot exclude the possibility that some individuals had only two incisors on one or both sides. Nevertheless, any such variation is unlikely to have taxonomic significance, considering that the rest of the dentition appears to be within the bounds of a single species. There are no diastemata between incisor alveoli (on the contrary, all are quite compacted) and no diastema between i3 and c, in contrast to early perissodactyls in which at least a short gap separates these two teeth.

At least 20 isolated incisors are tentatively attributed to *Cambaytherium thewissi* (Fig. 23) based on their size, crown morphology, and the presence of conspicuous, coarse perikymata as in other teeth of *Cambaytherium*; incisors of *C. gracilis* have not been identified. The precise loci represented, and which ones are upper vs. lower incisors, are not obvious, although some inferences can be made. As noted above, three unworn isolated incisors were found associated with GU 403 (Fig. 24J–R) and are tentatively identified as lower incisors, based on their long, straight roots and crown morphology. Two are probably left and right i1s or i2s (Fig. 24J–M). These teeth have a robust, cylindrical root, tapering at the base, about twice as long as the crown height. The crown is almost round at the base (about 10% longer mesiodistally than labiolingually), strongly convex labially, and weakly convex lingually at the base of the crown; toward the apex, the lingual surface is concave. The crown tilts slightly mesially and bears a tall cusp on the mesial half that is gently rounded mesiodistally; a marked crest, concave in profile and weakly sinuous viewed from behind, descends from the distal end of the cusp. The enamel is weakly crenulated. No interstitial facets are present, suggesting that these teeth had not finished erupting; however, a small apical facet is visible on the left incisor. The third incisor associated with GU 403 is tentatively identified as left i3 (Fig. 24N–R) based on its mesiodistally longer crown with a tall mesial cusp (like i2) and a lower distal cusp, similar to i3 in *Homogalax* (USGS 25032). The labial surface is strongly convex as in i2, the lingual surface flat to slightly concave. This tooth has a distinct apical wear facet on the posterior half of the crown, as well as a small mesial interstitial facet, but there is no distal interstitial facet. The root is mesiodistally compressed (wider labiolingually).

Based on comparison with the incisors associated with GU 403, GU 8034 (Fig. 23O–S) is tentatively identified as a right i2 but differs in displaying clear apical wear. GU 1676 (Fig. 23A–E) closely resembles i2 in GU 403 but differs in having a distinct distolabial cingulid. It is also slightly smaller and mesiodistally shorter than the i2s in GU 403 and therefore could be i1. Several other isolated incisors are tentatively identified as I3: GU 8016, GU 8022, GU 8023, GU 8024, GU 8027, and GU 8033 (Fig. 23F–N). Most are rather heavily worn (having lost about 25–30% of crown height), becoming spatulate, as we believe the i3 of GU 403

would look if heavily worn. GU 8022 and GU 8033, however, have conspicuous mesial interstitial facets, as would be expected if these teeth met on the midline; consequently, they may be I1. GU 8023 differs from the others in having a small attritional facet mesiolabially and a larger one distolingually near the apex.

Various isolated incisors, most of which are worn and have more or less spatulate crowns, are tentatively interpreted as upper incisors: GU 225, GU 433, GU 8025, GU 8028, and GU 8030 (Fig. 23Y–BB). These teeth tend to have more robust and curved roots than those identified as lowers. GU 433 and GU 8030 have similar crowns with a prominent basal distolingual interstitial facet, and their robust roots are slightly curved; they appear to represent right and left incisors of the same locus. Three isolated incisor crowns (GU 626; Fig. 24A–I), unworn, rootless, and evidently unerupted, are also tentatively identified as uppers (left I1–2 and right I2), and they may have been associated with the subadult skull GU 402. The tooth identified as I1 is almost 50% longer (mesiodistally) than it is in labiolingual width and is similarly longer than I2. Both I1 and I2 are convex labially, swollen at the base lingually, and flatter (labiolingually) apically. The enamel is wrinkled with irregular vertical ridges that radiate at the margin of the apex. The unworn apices are smoothly rounded mesiodistally, but we expect that they would have worn to flat, spatulate crowns. By comparison, GU 8026 (Fig. 23T–X) is a slightly worn right I1 and GU 225 and GU 8028 are more heavily worn I1s. Primitive perissodactyls typically have small, spatulate incisors, but the primitive chalicothere *Litolophus* had similar rounded I2 and i2 (Bai et al., 2010).

In contrast to *Cambaytherium*, the basal proboscideans *Eritherium* and *Phosphatherium* have somewhat to distinctly enlarged and procumbent i1, with i2 (and i3 in *Eritherium*) successively smaller (Gheerbrant et al., 2005a, 2012). The canine was reduced (no larger than the most anterior premolar; p1 [= dp1] in *Eritherium* or p2 in *Phosphatherium*; Gheerbrant et al., 2012). The incisors of *Cambaytherium* are apparently somewhat more vertical, and small, with i1 no larger than i2 and possibly smaller, to judge from alveoli. The canine in *Cambaytherium* is moderately enlarged and substantially larger than the incisors. Primitive perissodactyls have three incisors per quadrant that are nearly equal in size or may show slight increase posteriorly (i1 < i2 < i3); they have spatulate crowns and are moderately procumbent (e.g., *Cardiolophus*, USGS 22408; *Homogalax*, USGS 6085, USGS 25032; *Hyracotherium*, USGS 19944).

Canines—Our sample includes 16 isolated canines, all tentatively attributed to *Cambaytherium thewissi* (Fig. 25), which show considerable size variation (primarily in the roots; crown size is relatively similar in all), suggesting a marked difference in upper and lower canine root size, sexual dimorphism, or intraspecific variation. However, in most cases, it is difficult to identify confidently whether they are upper or lower, left or right. Nevertheless, all specimens, including those from TAD-2, appear to be too large (based on root size) to represent *C. gracilis*. A less likely possibility is that not all represent *Cambaytherium*; however, as has been noted, no other mammal of comparable size has been found in the Cambay Shale.

In all canines that are adequately preserved, the root is much larger than the crown—at least twice as long, and greater, or much greater, in caliber. In relatively unworn teeth (e.g., GU 405, GU 407, GU 1592, WIF/A 4253), coarse perikymata are evident in the enamel extending from the base to the apex (Fig. 22C). Five specimens (GU 10, GU 432, GU 792, WIF/A 4251, WIF/A 4252) have much larger and more swollen roots than the others; two others (GU 406, GU 833) have moderately swollen roots. Based on canine root size in some specimens, such as GU 7004, these could be lower canines and may represent males, but these specimens are heavily worn and do not preserve obvious attritional facets (e.g., Sperber, 2017) formed by opposing canines, making determination as upper vs. lower difficult.
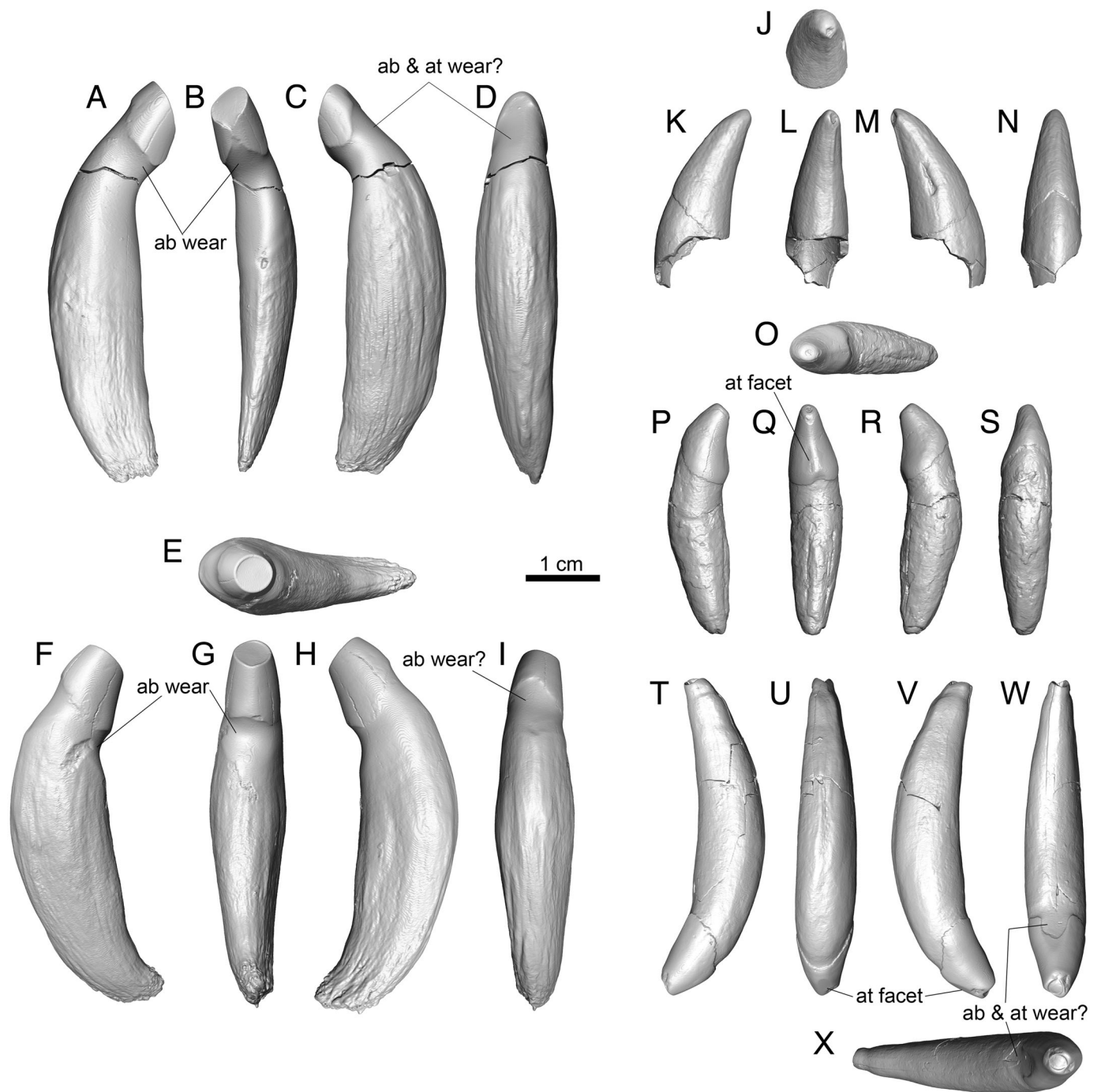
FIGURE 25. Isolated canines of *Cambaytherium thewissi*, all to the same scale. Loci unknown: whether upper or lower, and therefore which side is represented, are uncertain. **A–D**, GU 792 in **A**, side, **B**, distal (posterior), **C**, side, and **D**, mesial (anterior) views. **E–I**, GU 10 in **E**, occlusal, **F**, side, **G**, distal (posterior), **H**, side, and **I**, mesial (anterior) views. **J–N**, GU 407 in **J**, occlusal, **K**, side, **L**, distal (posterior), **M**, side, and **N**, mesial (anterior) views. **O–S**, GU 224, left c1?, in **O**, occlusal, **P**, labial (lateral), **Q**, distal (posterior), **R**, lingual (medial), and **S**, mesial (anterior) views. **T–X**, GU 833, right C1?, in **T**, labial (lateral), **U**, mesial (anterior), **V**, lingual (medial), **W**, distal (posterior), and **X**, occlusal views. **Abbreviations**: **ab**, abrasive; **at**, attritional.

GU 776 (two canines; Fig. 26), GU 833 (Fig. 25T–X), WIF/A 4251, and GU 223 (less evident) have an attritional wear facet on the anteromedial surface, presumably caused by occlusion with the lower canine and consistent with being upper canines; however, GU 833 also appears to have an attritional wear facet on its posterobasal aspect. GU 792 (Fig. 25A–D) has a less developed anterior wear facet. In addition, most of the more worn canines show very heavy abrasive wear (with transverse micro-striations) at their bases, especially posteriorly but also anteriorly, resulting in a conspicuous groove, which suggests that tough vegetation was stripped through the teeth at the base of the canines. A similar condition and functional interpretation have been reported in cave bear canines (Frischauf et al., 2016). The remaining canines are smaller, with shorter roots (GU 223, GU 224, GU
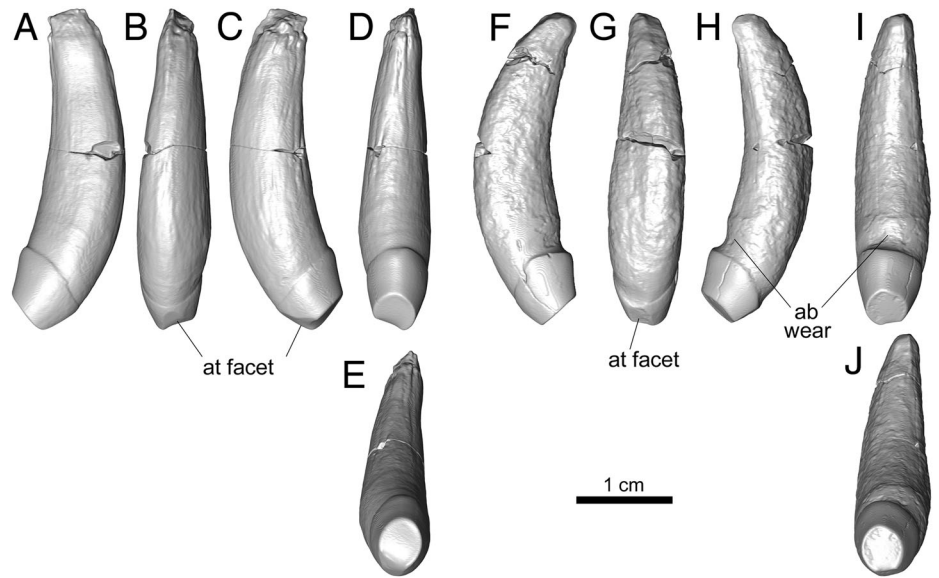
FIGURE 26. *Cambaytherium thewissi*, upper (?) canines associated with GU 776. **A–E**, right C1 in **A**, labial (lateral), **B**, mesial (anterior), **C**, lingual (medial), **D**, distal (posterior), and **E**, occlusal views. **F–J**, left C1 in **F**, labial (lateral), **G**, mesial (anterior), **H**, lingual (medial), **I**, distal (posterior), and **J**, occlusal views. **Abbreviations**: **ab**, abrasive; **at**, attritional.
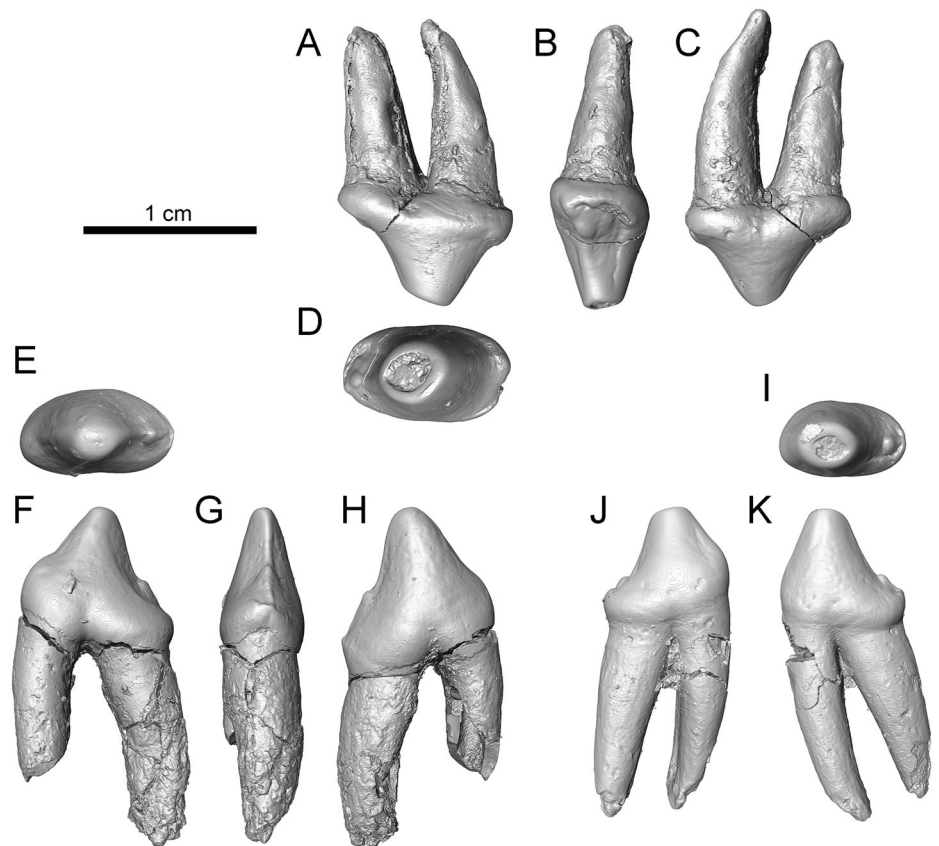

FIGURE 27. First premolars of *Cambaytherium thewissi* (quadrants uncertain). **A–D**, GU 8020, ?left dP1, in **A**, lingual, **B**, distal (posterior), **C**, buccal, and **D**, occlusal views. **E–H**, GU 7015, ?right dp1, in **E**, occlusal, **F**, lingual, **G**, distal, and **H**, buccal views. **I–K**, GU 409, ?left dp1, in **I**, occlusal, **J**, lingual, and **K**, buccal views.

405, GU 407, GU 776, GU 1592, GU 7014, WIF/A 4253), in several cases because the root is open and not fully formed. However, the smallest canines (GU 223, GU 224, GU 405) have tapered, closed roots. Based on their small size, it is possible that these canines represent *C. gracilis*, but this seems unlikely inasmuch as no other remains of *C. gracilis* are known from Vastan Mine. Assuming that they belong to *C. thewissi*, they provide some of the strongest evidence for extreme intraspecific variation or sexual dimorphism. GU 224 has a large, obliquely striated attritional wear facet on its posterolateral surface, as expected if it were a left lower canine; it also bears a small anterior attritional facet.

Only one specimen in our sample preserves canines in situ: GU 403, a subadult in which the canines are neither fully erupted nor fully formed (radiographs show open roots similar in diameter to the base of the crown); hence, their adult size is difficult to judge. To the extent that they can be compared, the isolated canines are similar to those in GU 403. GU 776 is a right dentary with two associated relatively small canines (Fig. 26). Although it would be reasonable to assume that they are lower canines, both have bluntly worn crowns and prominent attritional facets on the anterior surface, consistent with being upper canines. The presumed left upper canine also shows marked posterobasal abrasive wear.

Canine alveoli are preserved in four other specimens, in which the alveolar diameter and symphysis depth varies. From smallest to largest, the specimens are GU 9001 (*C. gracilis*), GU 9002, GU 7004, and GU 1710 (all *C. thewissi*). Because of the small sample size and taxonomic diversity, sexual dimorphism cannot be demonstrated unequivocally, but as has been noted, the variation in canine size is suggestive of that possibility.

dp1—This tooth is represented in situ in GU 403, in the crypt in GU 1701, and by six isolated teeth—GU 222, GU 409, GU 1594, GU 1678, GU 7015, GU 8031—all representing *C. thewissi* (Figs. 17, 18, 27). There is no evidence of tooth replacement at the first premolar position in either the mandible or the maxilla; consequently, we follow Luckett (1993; see also Rose et al., 2018a) in regarding the first premolars as unreplaced dp1 and dP1. It should be noted, however, that the perissodactyls *Tapirus* (extant) and Eocene–Oligocene *Hyracodon* (see discussion in Luckett, 1993, and Rose et al., 2018a) are among the very few eutherians in which there is evidence of replacement at the P1/p1 locus, so the possibility that *Cambaytherium* also replaced dP1/dp1 cannot be ruled out. Therefore, it is possible that some or all of the isolated teeth included here could be p1 or P1.

The dp1 is typically a simple tooth with two long roots and a conical crown. All isolated first premolars are biradicular, as is dp1 in GU 403 and in several specimens illustrated by Bajpai et al. (2005a, 2006). The posterior root is larger in caliber than the anterior root, and variations do occur. As observed by Bajpai et al. (2005a), dp1 may have two well-separated roots (as on the left side of GU 9002; Fig. 10) or two fused roots (as appears to be the case on the right side of GU 9002). The right side of the holotype of *C. gracilis* has only one alveolus, comparable to the anterior alveolus of left dp1 (Fig. 14), but the more posterior alveolus seems to have been obliterated through bone remodeling after in vivo loss of the tooth. At first glance, GU 7004 also seems to show a possible single-rooted dp1 (Fig. 9), but the jaw is damaged near the dp1–p2 junction, and the broken edges suggest that a posterior dp1 root was present.

A juvenile dentary of *Cambatherium thewissi*, GU 1701, also appears to have a single, matrix-filled alveolus for dp1 (Fig. 18B), but close inspection of the micro-CT slices indicates that the crown of a developing tooth is in the crypt (Fig. 18D) and that the root or roots have not yet formed. The apparent alveolus may reflect resorption of bone as the tooth began to erupt. This tooth could potentially be dp1 or p1, but as noted above, the likelihood that it is dp1 is more consistent with the known eruption sequence in placentals (i.e., late eruption of dp1) and the current hypothesis that dp1 is unreplaced in nearly all placentals. Furthermore, wear on dp3 is moderate and that on dp2 is slight, and there is no evidence of developing crowns of permanent p2 and p3 below the deciduous premolars, all of which suggest that this jaw belonged to a very immature individual in which dp2–3 were relatively newly erupted. Thus, it seems highly improbable that dp1 had already been lost in GU 1701 and that the tooth in the crypt is a permanent p1. If we accept that the developing tooth is dp1, GU 1701 would provide direct evidence that dp1
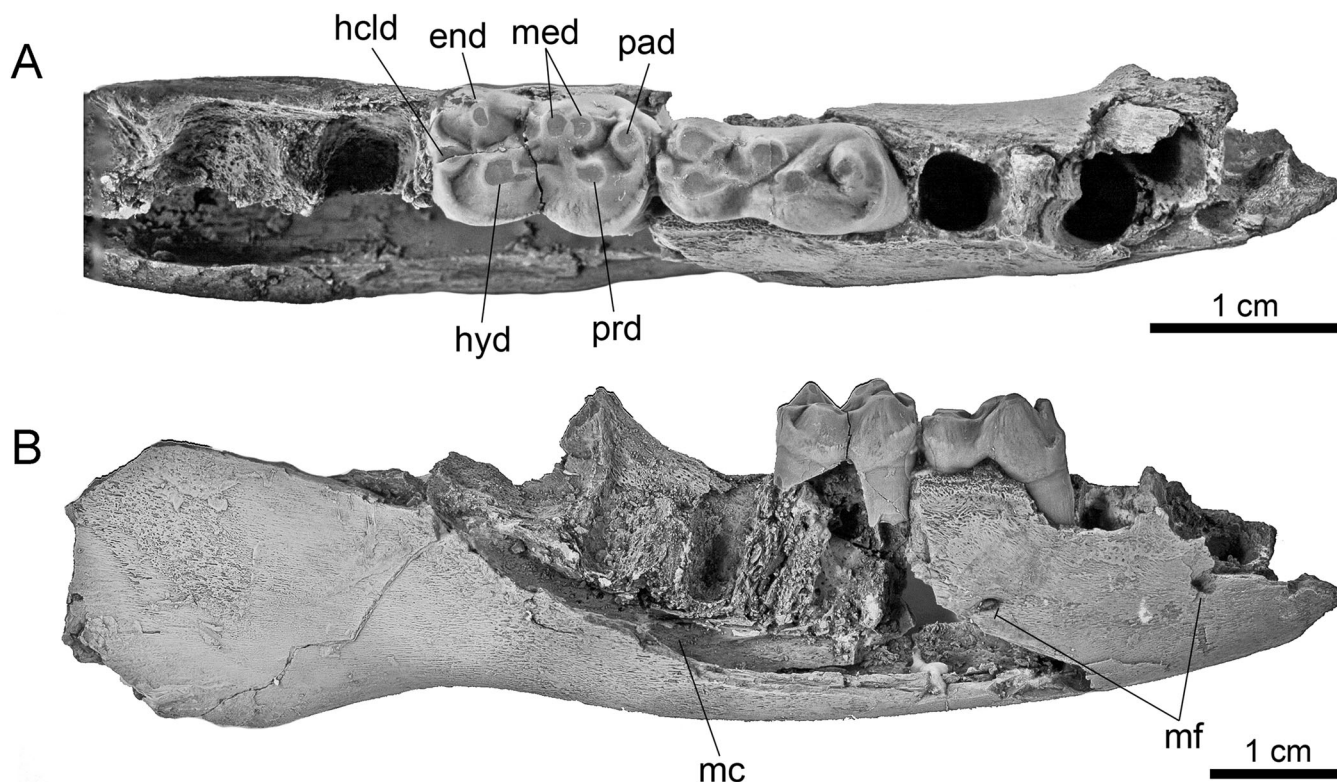

FIGURE 28. *Cambaytherium thewissi*, GU 736, right dentary with dp3–4. Digital photographs of **A**, occlusal and **B**, buccal views. **Abbreviations**: **end**, entoconid; **hcld**, hypoconulid; **hyd**, hypoconid; **mc**, mandibular canal; **med**, metaconid; **mf**, mental foramen; **pad**, paraconid; **prd**, protoconid.

erupts after dp2 and dp3 are in place in *Cambaytherium*, a pattern that seems to be typical in perissodactyls; indeed, dp1 is the last deciduous premolar to erupt in eutherians (Luckett, 1993; see review in Rose et al., 2018a). In phenacodontids, dp1 appears to be single-rooted, and in basal perissodactyls it has one root or two closely appressed roots.

The main cusp of dp1 is situated on the anterior part of the crown, with a steep anterior aspect and more gradual straight or concave posterior aspect; weak crests extend anteriorly and posteriorly from the cusp. Most specimens have no distinct heel, but a small posterobasal cusp is present in GU 409 (Fig. 27I–K), and a tiny cuspule is developed a little higher on the posterior crest in GU 7015 from Mangrol Mine (Fig. 27E–H). A weak posterolingual cingulid is evident in GU 403 (right dp1) and GU 1678. The isolated teeth here identified as dp1 are either narrower or smaller overall than those identified as dP1. The dP1s in GU 402 (cranium) are slightly larger than the dp1s in GU 403 (presumably associated mandible). Nevertheless, as only three specimens have either dp1 or dP1 in association with other teeth, we cannot be certain that the various isolated dP1s are correctly identified as either lower or upper.

Bajpai et al. (2005a) distinguished *Cambaytherium bidens* from *C. thewissi* based partly on the presence of a diastema between (d)p1 and p2 in the former (based on heavily worn specimens) compared with no diastema in *C. thewissi* (based on a single specimen with unworn teeth). Radinsky (1963a:11), referring to the basal perissodactyl *Homogalax*, concluded that "development of anterior diastemata seems too variable and inconsistent to be of taxonomic value." The presence of diastemata between anterior premolars may also be related to ontogeny (e.g., Rose et al., 2014a) and is variable in our sample of *Cambaytherium thewissi*: the diastema between dp1 and p2 is moderate in length in GU 9002, short in GU 403, very short in GU 1710, and short or absent in GU 7004 (damage at the back of the symphysis may conceal a short diastema). There is no diastema between dp1 and p2 in the holotype of *C. gracilis*, the only specimen of the smaller species that preserves the dp1 locus.
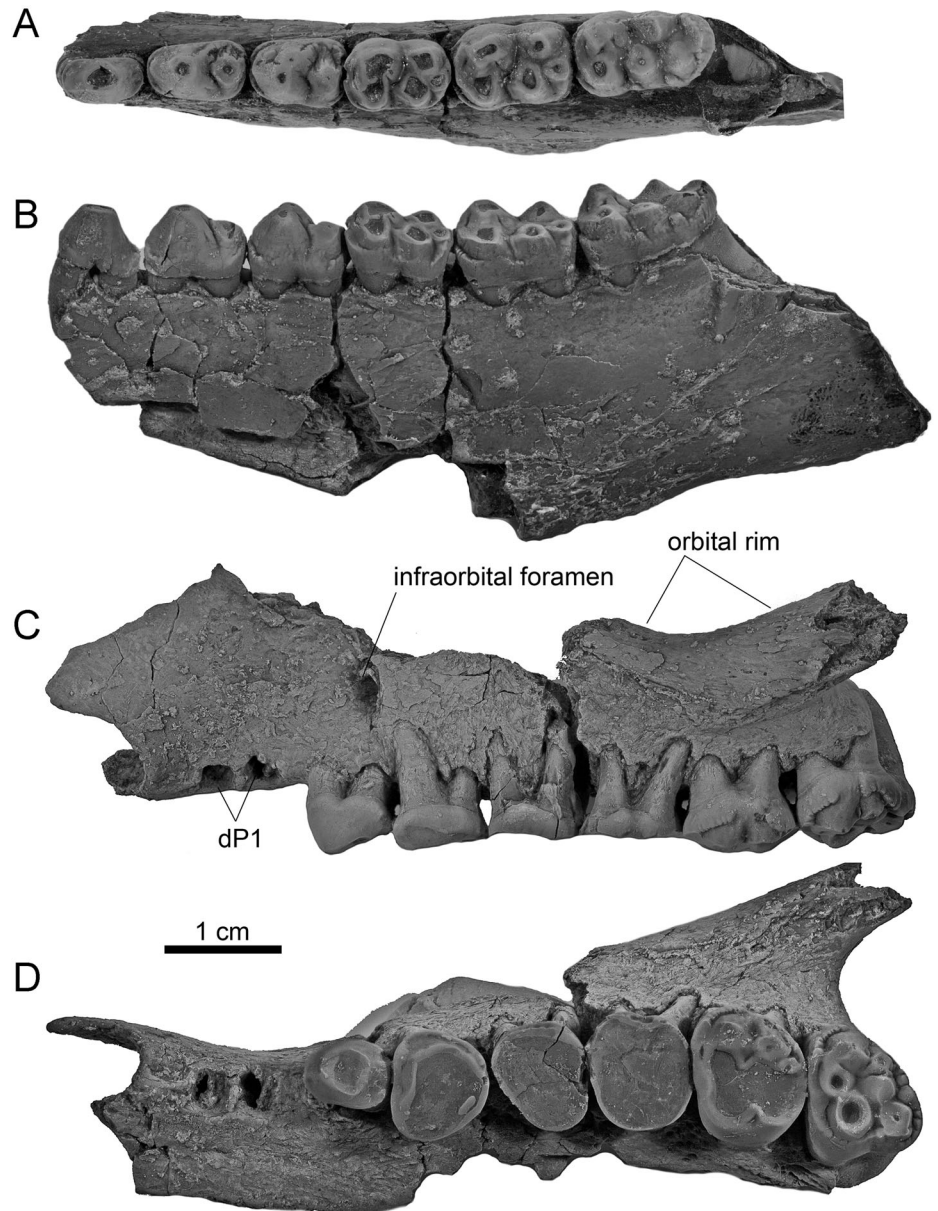

FIGURE 29. *Cambaytherium gracilis* from TAD-2, digital photographs. **A**, **B**, WIF/A 4210, left dentary with p2–m3, in **A**, occlusal and **B**, buccal views. **C**, **D**, WIF/A 4265, left maxilla with P2–M3, in **C**, buccal and **D**, occlusal views.

dp2—The deciduous lower premolars, known only for *C. thewissi*, are considerably more complex than the permanent ones (except dp1); all three are semimolariform (sensu Szalay, 1969) or nearly so (dp2). Deciduous p2, best seen in GU 3 (Rose et al., 2006:fig. 3N) and GU 1701 (Fig. 18), is elongate and narrow and has a mediolaterally compressed trigonid with the three cusps nearly aligned mesiodistally, or with the paraconid and metaconid set slightly lingual to the protoconid in some specimens. The metaconid is distinctly lower than the paraconid, on the distal slope of the protoconid. Posterobuccal to the metaconid, a small, low talonid cusp (incipient hypoconid?) is usually present, from which crests descend lingually and buccally. The lingual crest forms a short postcingulid, which variably continues as a posterolingual cingulid, whereas the buccal one may run to

the base of a short, incipient posterobuccal cingulid. The talonid cusp is joined to the metaconid by a very short crest; a longer distinct crest extends from the metaconid to the postcingulid. These crests are not developed in GU 1701. Instead, the hypoconid is more or less isolated, with a short, low crest to the postprotocristid and two tiny cuspules posterolingual to the cusp. The talonid cusp is indistinct in GU 1593.

dp3—The dp3 (Figs. 17, 18, 28) is elongate and narrow and slightly more molariform than dp2: the paraconid and metaconid are rotated a little more lingually, and the talonid includes equal-sized hypoconid and entoconid cusps, the entoconid directly lingual to the hypoconid. A much smaller hypoconulid, best developed in GU 736, is joined to the hypoconid but separated from the entoconid by a valley. A shallow furrow lingually on the metaconid (e.g., GU 733, GU 1682) foreshadows the twinned metaconid of dp4 and the molars. A weak, low cristid obliqua extends from the hypoconid to the buccal side of the metaconid, and a low entocristid runs from the entoconid to the talonid notch, these crests bounding a small and shallow talonid basin. Weak anterior and posterior cingulids are present at the extremities of the buccal side.

dp4—Deciduous p4, best preserved in GU 734 and GU 736 (Fig. 28), is fully molariform but narrower than m1. Its trigonid is more extended mesiodistally than on the molars and has a distinct paraconid. As in the molars, the metaconid is twinned and the entoconid is posterolingual to the hypoconid (unlike dp3). Very weak crests extend from the hypoconid anteriorly toward the protoconid and toward the metaconid. There is a weak ectocingulid. As noted earlier, dp4 is also represented in *Cambaytherium* 'minor' (IITR 539 [holotype] and IITR 761; =*C. thewissi*), in which it was misidentified as m1 (Bajpai et al., 2005a, 2006).

p2—The p2 is present in situ in GU 1710, GU 7004 (both sides), *C. thewissi*, and in WIF/A 4210, *C. gracilis*. Isolated p2s of *C. thewissi* include GU 221, GU 427, GU 660, GU 1709, GU 8008, and WIF/A 4232. The p2 of *C. thewissi* (Fig. 9) is premolariform and is the longest premolar. It is much larger than dp1 and slightly longer than p3 but similar in morphology; hence, the length relationships of the lower premolars in *C. thewissi* are p2 > p3 > p4 > dp1. The p2 has two roots that are robust and roughly twice as long as crown height. It is dominated by the tall protoconid, from which a crest descends posteriorly, sometimes to a much lower, small, rounded central talonid cusp. The latter cusp is well developed in GU 427, GU 7004, and GU 8008, but indistinct in GU 221, GU 660, GU 1709, and GU 1710. The enamel on the lower posterior wall of the trigonid and sides of the talonid cusp is variably crenulated. Crests extend anteriorly from the talonid cusp on the lingual and buccal aspects of the tooth, becoming short posterolingual and posterobuccal cingulids, which fade out along the base of the posterior slope of the protoconid. A short anterobuccal cingulid is usually present, and in one specimen (GU 8008) there is an anterolingual cingulid as well. In most specimens, the protoconid is truncated and worn flat, leaving a large dentine window. WIF/A 4232, from TAD-2, is slightly higher crowned and has a higher basal cingulum than the others.

The p2 in *C. gracilis*, in contrast to *C. thewissi*, is smaller and simpler than p3 (WIF/A 4210, the only specimen preserving p2; Fig. 29A, B), though markedly larger than dp1; consequently, relative lengths are p3 > p4 > p2. The posterior aspect of the protoconid is steeper and the tooth is shorter posteriorly than in *C. thewissi*, and both the posterior crest and the talonid cusp are indistinct. In other respects, it resembles p2 of *C. thewissi*.

Although most specimens of *Cambaytherium* have very dark enamel, GU 8008 has somewhat lighter, clearer enamel that reveals the presence of zigzag Hunter-Schreger bands (Koenigswald et al., 2018:fig. 4d). This phenomenon has been observed in various carnivores and herbivores (e.g., pantodonts,

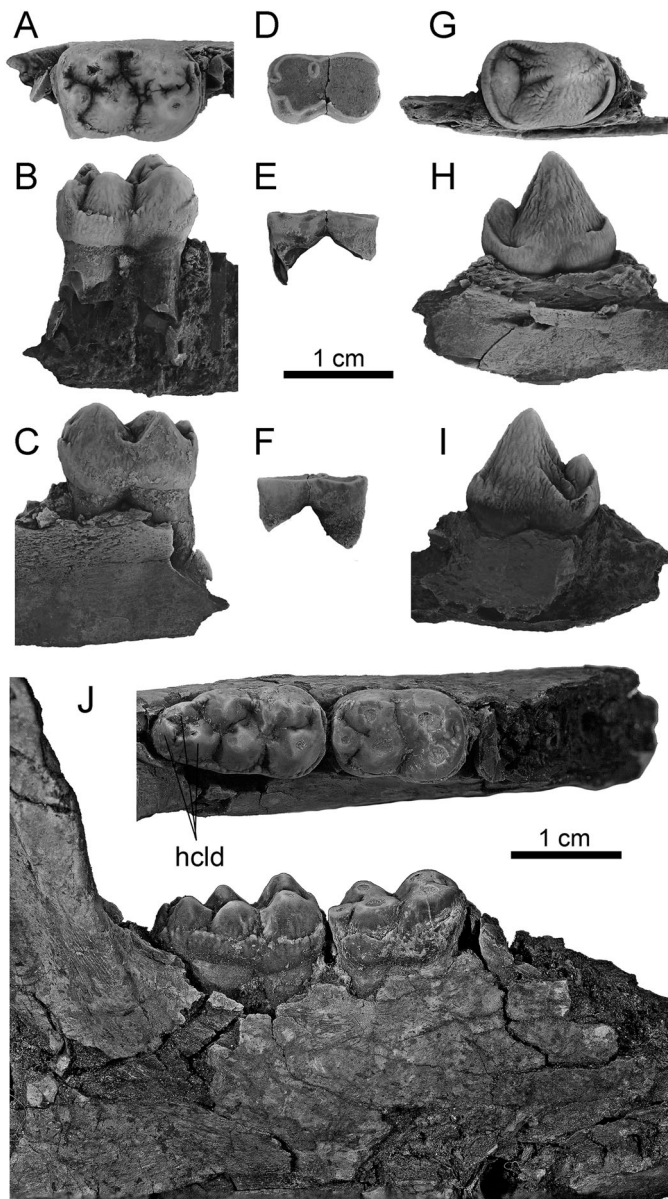FIGURE 30. *Cambaytherium thewissi* from Vastan Mine, digital photographs. **A–I**, GU 1588, associated right lower dentition: **A–C**, m2 in occlusal, buccal, and lingual views; **D–F**, heavily worn dp4 in occlusal, buccal, and lingual views; **G–I**, newly erupted unworn p3? in occlusal, buccal, and lingual views. **J**, GU 1596, right m2–3, in occlusal and buccal views. **Abbreviation**: hcld, multiple hypoconulids.
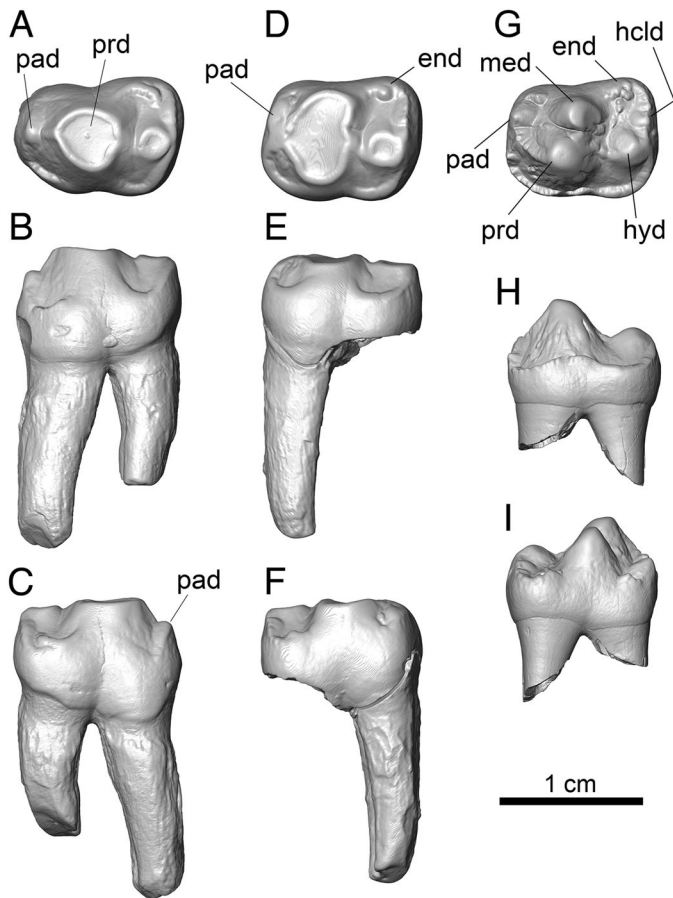
FIGURE 31. Left p4s of *Cambaytherium thewissi* from TAD-2, showing variable extent of molarization. **A–C**, GU 9006 in **A**, occlusal, **B**, buccal, and **C**, lingual views. **D–F**, WIF/A 4255 in **D**, occlusal, **E**, buccal, and **F**, lingual views. **G–I**, WIF/A 4264, unworn p4, in **G**, occlusal, **H**, buccal, and **I**, lingual views. **Abbreviations**: **end**, incipient entoconid; **hcld**, incipient hypoconulid; **hyd**, hypoconid; **med**, metaconid; **pad**, paraconid; **prd**, protoconid.

uintatheres, and artiodactyls) and is thought to be an adaptation to strengthen enamel for especially tough or hard food items (e.g., Stefen, 1997; Koenigswald and Rose, 2005).

p3—Like p2, p3 in *C. thewissi* is dominated by the tall protoconid followed by a low but distinct single talonid cusp (Figs. 9, 17, 19, 30G–I). The talonid is wider than the trigonid. A crest runs down the back of the trigonid to the notch separating trigonid and talonid, and low cingulids extend anteriorly both lingually and buccally from the base of the talonid cusp to below the notch (best seen in GU 1588; Fig. 30G–I). A crest typically also descends anteriorly from the protoconid and gives rise to a well-developed anterobuccal cingulid. A small cuspule is present at the base of the crest in GU 776 (Fig. 19B), whereas GU 7017 lacks any distinct features anterior to the protoconid. Where premolars are serially preserved, p3 is longer than p4 but shorter than p2.

The p3 of *C. gracilis* (Fig. 29A, B) is generally similar to that of *C. thewissi*, but its talonid cusp is larger and taller, and a distinct crease in the enamel separates the trigonid from the talonid buccally. The anterobuccal cingulid is very weak (WIF/A 4210).

p4—In *C. thewissi*, p4 is typically similar to p3; it is a simple premolariform tooth, but shorter than p3 and with a slightly stronger talonid cusp and more prominent posterolingual cingulid (Figs. 9, 19). The cingulids and the teeth themselves are quite variable in the sample, however, as illustrated by GU 403 (Fig. 17), a

subadult in which the p4s are not quite fully erupted. In this unworn specimen, both p4s have a metaconid. It is prominent, posterolingual to the protoconid, and almost as tall as the protoconid on the left p4, but smaller, lower, and just posterior to the protoconid on the right p4. The right P4 has a very prominent, complete, beaded lingual cingulid, but there is no discernible lingual cingulid on the left p4. The enamel of the trigonid of the right p4 is strongly wrinkled, whereas that on the left p4 is much less so. Most of the other specimens show heavy apical wear, making it difficult to discern whether or not a metaconid was present, but the appearance of the worn protoconid suggests that it would have been small and close to the protoconid if present in those specimens. However, a few specimens described below diverge markedly from this morphology. GU 7016 is unusually large but is identified as p4 by its morphology and proportions (Fig. 11). It may represent an exceptionally large individual or possibly a different species, or perhaps it is an abnormally wide p3.

Five less worn, isolated p4s display a morphocline of increasing complexity, which could indicate that p4 in *C. thewissi* was even more variable than indicated in GU 403. However, it is not certain that all of them belong to *Cambaytherium*. Because this sample suggests a wider spectrum of morphological variation than is normally seen or expected in a single species—which, had they been found in stratigraphic succession, could be interpreted as progressive evolutionary change through time—we have excluded them from the statistics on the sample but include them in the plot of p4 size (Fig. 11). Three of these specimens (GU 1671, GU 1679, GU 8009) are from the same horizon at Vastan Mine that has produced the largest sample of *C. thewissi*. The other two (WIF/A 4255, WIF/A 4264; Fig. 31) come from TAD-2, which produced *C. thewissi* and *C. gracilis*, and they are of appropriate size for *C. thewissi*. All five have a distinct metaconid, but it varies in size and position relative to the protoconid, being smaller and posterolingual to the protoconid in GU 1671 and GU 8009, and larger and more directly lingual to the protoconid in the others. The three Vastan specimens lack a paraconid, whereas the Tadkeshwar specimens have a small paraconid, closer to the protoconid and more centrally positioned in WIF/A 4255 and situated more anterolingually in WIF/A 4264. A small paraconid is also present on GU 9006 (also from Tadkeshwar), which is otherwise premolariform (Fig. 31A–C). All five p4s have a well-developed talonid cusp placed just buccal of the midline. There is considerable variation in cingulids. GU 8009 has short, weak posterolingual and posterobuccal cingulids, each bearing a couple of tiny enamel beads. In GU 1671, the cingulids are better developed, especially posterolingually, and a small, low cusp appears twinned with the main talonid cusp on its lingual face. GU 1679 has similar development of the posterior cingulids but no twinned cusp, and it also has a distinct anterobuccal cingulum. WIF/A 4255 is characterized by an anterobuccal cingulid and a posterolingual cingulid bearing two tiny cuspules posteriorly and a larger lingual cuspule (incipient entoconid?). Despite their apparent differences from other specimens, close comparison shows that GU 8009 is virtually identical to GU 414 (a premolariform p4) except for the presence of a small metaconid; both are from Vastan. Similarly, GU 1671 (Vastan) closely resembles GU 9006 (TAD-2) except for having a metaconid, which is lacking in GU 9006. WIF/A 4264 (Fig. 31G–I) is semimolariform, with an open trigonid bearing a prominent metaconid and a broad talonid with a small cuspule lingual to the talonid cusp and a wide lingual expansion bearing several small, beadlike cuspules. It further differs from the others in having a well-developed, crenulated complete buccal cingulid. If any of these teeth represents a different taxon, WIF/A 4264 is the best candidate. Nevertheless, comparison with the other teeth described here suggests that this is a slightly more ornate unworn p4 of the same taxon. The close resemblance in size and other details
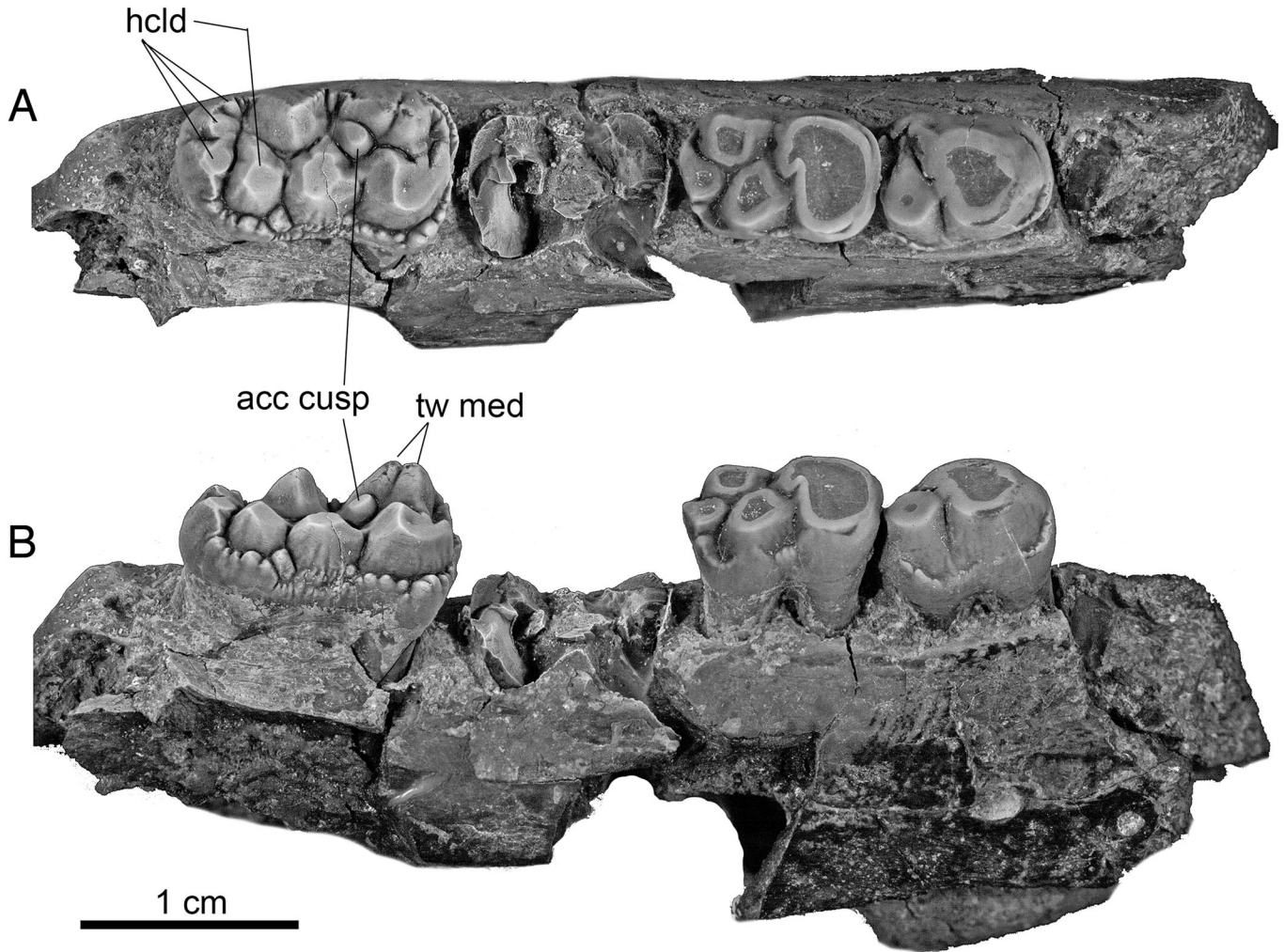
FIGURE 32. *Cambaytherium gracilis*, WIF/A 4211, right p4, m1, m3, in **A**, occlusal and **B**, buccal views (digital photographs). **Abbreviations**: **acc cusp**, accessory cusp; **hcld**, multiple hypoconulids; **tw med**, twinned metaconid.

to undoubted individuals of *C. thewissi*, which show variation in metaconid expression, together with the absence of any other similar-sized taxa to which these teeth could be referred, leads us to conclude that they must belong to *C. thewissi*, illustrating a remarkable extent of variation in p4. They further suggest that the metaconid was a highly mutable feature in p4 of *Cambaytherium*, and that it may not be possible to determine whether a metaconid was present in heavily worn specimens. Radinsky (1963a) described somewhat similar variation in p4 morphology in *Homogalax protapirinus*.

The p4 of *C. gracilis* (Figs. 14, 29, 32) is semimolariform in all six known specimens (from TAD-2), with a well-developed metaconid situated more lingual to the protoconid than posterolingual and a relatively longer talonid than in *C. thewissi*. An incipient paraconid is barely discernible in worn specimens but is distinct in WIF/A 4235 (Fig. 33A–C), an unerupted or newly erupted crown, in which the metaconid is incipiently twinned. The talonid is dominated by a prominent hypoconid; no entoconid or hypoconulid is developed. The p4 of *C. gracilis* and the five molarized p4s of *C. thewissi* described above are quite similar to p4 of *Perissobune intizarkhani* (GSP-UM 6553 and GSP-UM 4656; Missiaen and Gingerich, 2014). The latter differs subtly in lacking a distinct paraconid and having a relatively slightly larger talonid (roughly equal-sized trigonid and talonid), slightly

stronger crests, and a taller, twinned metaconid, almost equal in height to the protoconid. Thus, there is essentially a continuum in p4 morphology from *Cambaytherium* to *Perissobune*, leaving little but slightly stronger lophodonty to separate the two genera. *Perissobune* is certainly a cambaythere, very closely related to if not synonymous with *Cambaytherium*.

m1—The m1 is present in many specimens of both *C. thewissi* and *C. gracilis*, but most are moderately to heavily worn, obscuring details (e.g., Figs. 9, 19). Crown details in *C. thewissi* are best seen in two relatively unworn specimens, GU 203 and GU 403 (Fig. 17). All three molars are bunodont, with moderately tall cusps separated by relatively deep valleys; crests are very short, low, and weakly developed; hence, the molars contrast with those of primitive perissodactyls in lacking lophodonty. Nevertheless, the cusps are somewhat more acute than in *Phenacodus*. The m1 is elongate and often narrower than p4, although WIF/A 4233 from TAD-2 is relatively wider than m1 in the Vastan and Mangrol samples. The trigonid consists of the protoconid and slightly taller twinned metaconid. GU 403 lacks any trace of a paraconid but has an arcuate paracristid, notched anteriorly, joining the protoconid to the metaconid. In GU 203, the paracristid is continuous and a tiny remnant of a paraconid attaches to it anterolingual to the protoconid. All other specimens are too worn to assess whether a vestigial paraconid was present. A very weak
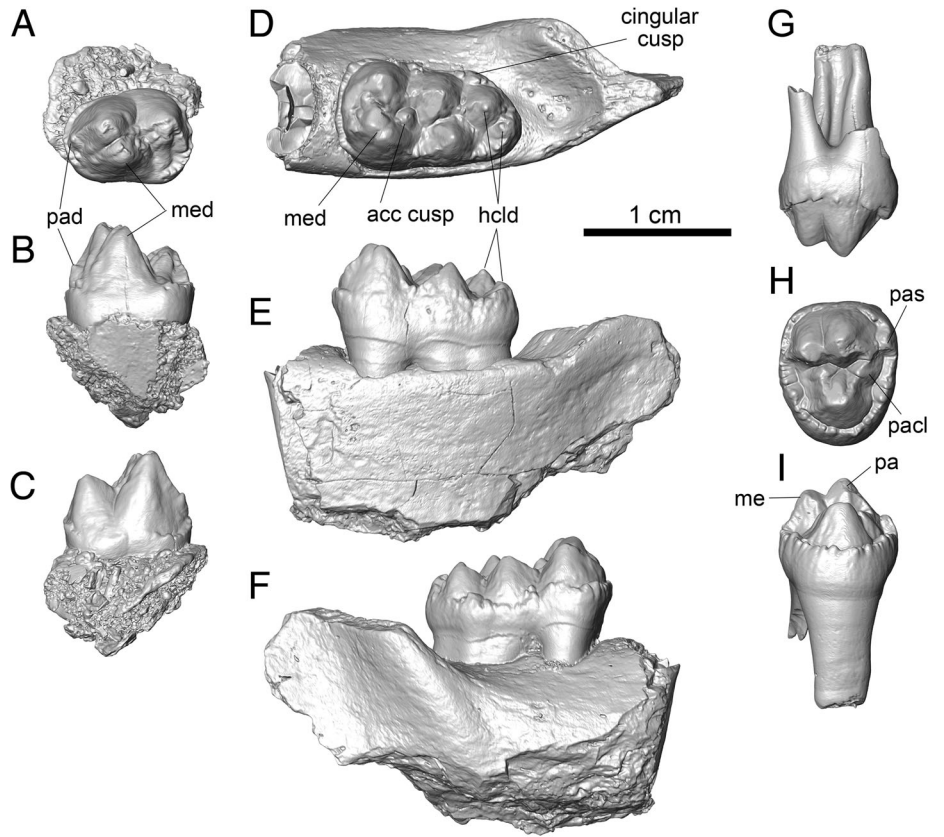
FIGURE 33. Isolated teeth of *Cambaytherium gracilis* from TAD-2. **A–C**, right p4, WIF/A 4235, in **A**, occlusal, **B**, lingual, and **C**, buccal views. **D–F**, right dentary fragment with m3, WIF/A 4212, in **D**, occlusal, **E**, lingual, and **F**, buccal views. **G–I**, right P4, WIF/A 4239, in **G**, buccal, **H**, occlusal, and **I**, lingual views. **Abbreviations**: **acc cusp**, accessory cusp; **hcld**, hypoconulids; **hyd**, hypoconid; **me**, metacone; **med**, twinned metaconid; **pa**, paracone; **pacl**, paraconule; **pas**, parastyle.
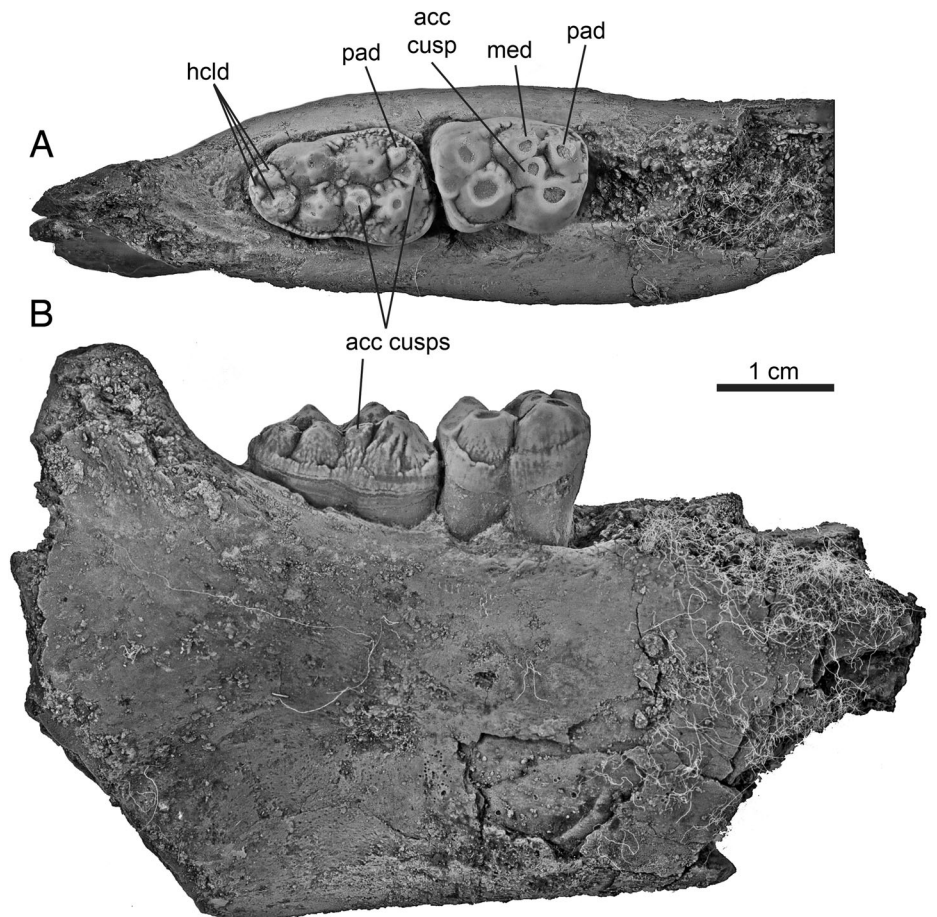
FIGURE 34. *Cambaytherium thewissi*, GU 1700, right dentary with m2–3, in **A**, occlusal and **B**, lateral views (digital photographs). **Abbreviations**: **acc**, accessory; **hcld**, hypoconulids; **med**, metaconid; **pad**, paraconid.

and deeply notched protolophid connects the posterior side of the protoconid and the metaconid. The metaconid is twinned, as in primitive perissodactyls (Hooker, 2005). Phenacodontids have a lower metastylid cusp that is in approximately the same position as the more posterior metaconid and appears somewhat similar, but, based on occlusal relationships, it is probably not homologous with the twinned metaconid cusp (Hooker, 1994). In the *Cambaytherium* m1, the transverse valley separating trigonid and talonid is sinuous and deep (although less well defined in *C. gracilis* than in *C. thewissi*), open both lingually and buccally. The rudimentary, low cristid obliqua ends in this valley and does not meet the postvallid. This condition differs from both phenacodontids and basal perissodactyls, in which a well-developed cristid obliqua crosses the valley to meet or ascend the postvallid, forming a wall that divides the valley into lingual and buccal parts. The talonid notch is deep. The entoconid is slightly higher than and posterolingual to the hypoconid, the two barely linked by a very weak and short hypolophid. The hypoconulid is lower and essentially isolated almost directly posterior to the hypoconid (buccally shifted); the two cusps are joined by a weak crest in GU 403, but not in GU 203. A moderately expressed ectocingulid is best developed just posterior to the hypoflexid and continues onto the anterior and posterior ends of the tooth. All known specimens of m1 of *C. gracilis* show significant wear (Figs. 14, 29, 32), but they appear to be essentially identical to *C. thewissi* except for being smaller and having a small accessory cuspule posterobuccal to the metaconid (better developed on m2 and m3).

The m1 is similar overall to that of *Hyracotherium* but more bunodont. The trigonid is more like that of *Phenacodus* and *Copecion* in shape of the paracristid (arcuate and low, joining the protoconid and the metaconid). The talonid, however, is more perissodactyl-like (narrower, with the hypoconid and entoconid closer to each other, and the hypoconulid distal to and completely separate from the hypoconid and entoconid); there is virtually no hint of bilophodonty in *Cambaytherium* except for the parallelogram arrangement of the four main cusps. *Cambaytherium* further differs from *Hyracotherium* in having a much weaker cristid obliqua, which, when discernible at all, is a short, low crest that ends in the valley between trigonid and talonid, rather than crossing the talonid to reach the buccal side of the metaconid as in *Hyracotherium*. The m1 of *Perissobune intizarkhani* has a distinct metaconid buttress extending to the accessory cuspule and a slightly better developed cristid obliqua but is otherwise essentially identical to that of *C. thewissi*.

m2—The m2 of *C. thewissi* is almost identical to m1 but is, on average, roughly 10–15% larger in linear dimensions (e.g., Figs. 9, 17, 20, 30). In this tooth, the cristid obliqua, though still weak, is slightly better developed than on m1, and in unworn specimens (e.g., GU 403, GU 8013, GU 8014) it can be seen continuing onto the postvallid toward the protoconid. The condition in GU 8014 mirrors that in *Perissobune intizarkhani*. The ectocingulid is variable, from indistinct or faintly developed (GU 401, GU 7001), to moderate in most specimens, to prominent and beaded (GU 8013, WIF/A 4224). When distinct, it is more or less complete buccally, extending around the entire anterior border of the tooth and to the base of the hypoconulid posteriorly. The left m2 of GU 403 also has a rugose lingual cingulid extending from below the talonid notch anteriorly; a slightly weaker lingual cingulid is present on m2 of GU 1700 (Fig. 34). Furthermore, left m2 of GU 403 (Fig. 17) is unique in our sample in having a double hypoconulid, the two cusps almost directly posterior to the hypoconid and entoconid, but both hypoconulids shifted slightly toward the center of the tooth. The two cusps are separated from each other and from the other two talonid cusps by deep notches. These features are not present on the right m2 of GU 403, which is typical in having a single hypoconulid posterior to the hypoconid. Like m1, m2 is not bilophodont,
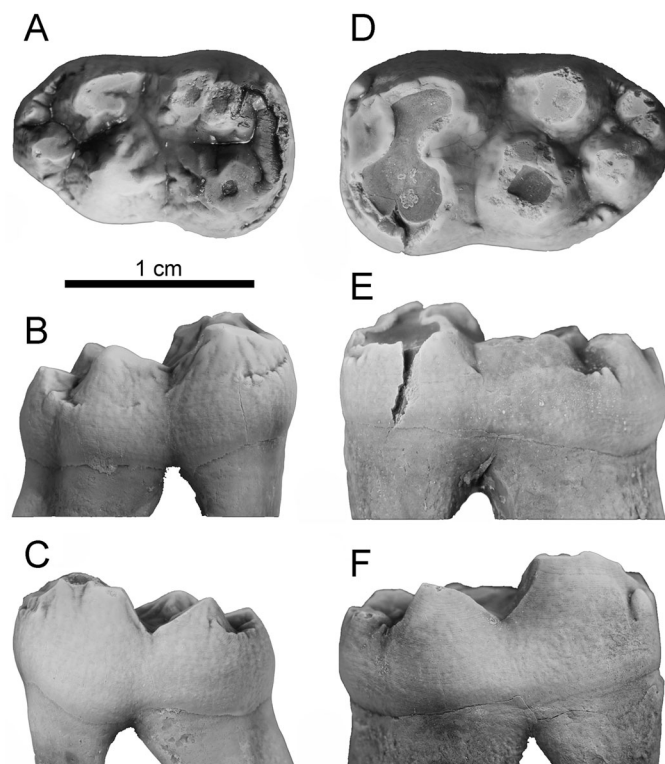

FIGURE 35. Lower third molars of *Cambaytherium thewissi* from TAD-2. **A–C**, WIF/A 4222, right m3, in **A**, occlusal, **B**, buccal, and **C**, lingual views. **D–F**, WIF/A 4223, left m3, in **D**, occlusal, **E**, buccal, and **F**, lingual views. Digital photographs from Smith et al. (2016).

although with heavy wear (e.g., GU 776; Fig. 19B); the crown may appear weakly bilophodont. The m2 in *C. thewissi* shows other variations as well. GU 1598 is somewhat more bunodont than other specimens and has a vestigial paraconid. A prominent paraconid (typically absent in molars of *Cambaytherium*), equal in size and height to the metaconid, is present on m2 of GU 1700 (Fig. 34). This tooth also has an accessory cusp midway between the protoconid and the metaconid. GU 8013 has two small cuspules in the floor of the valley between trigonid and talonid.

Except for being smaller, m2 of *C. gracilis* (Figs. 14, 21, 29) is anatomically very similar to that of *C. thewissi*. It differs from the latter in usually having a distinct, low accessory cuspule posterobuccal to the posterior metaconid (e.g., WIF/A 4237), just as in *Perissobune intizarkhani*; but unlike the latter, there is no distinct metaconid buttress. The cusp is worn and therefore less distinct in GU 9001 and WIF/A 4210 (the three specimens of *C. gracilis* from TAD-2), but it is poorly defined in GU 9019 (from TAD-1).

m3—This is a highly variable tooth in *C. thewissi*, with morphology similar to m1 and m2 except that the hypoconulid extends posteriorly forming a third lobe, as is characteristic of perissodactyls and anthracobunids but not phenacodontids; hence, m3 is always longer than the other molars (e.g., Figs. 9, 19, 20). In relatively unworn teeth, the two trigonid cusps (protoconid and metaconid) and the two more anterior talonid cusps are separated from each other by valleys, and the internal cusp of each pair is somewhat taller and set posterolingual to the buccal cusp. Rarely (e.g., GU 1595, GU 1711), a very weak, incipient low crest joins each pair of cusps; nevertheless, the teeth are not lophodont. The metaconid is twinned in unworn specimens (e.g., GU 401, GU 403, GU 8010, GU 8011), but this is difficult

to detect in heavily worn specimens. The paraconid is typically absent and the paracristid low and variable. A weakly developed ectocingulid is mostly continuous along the buccal aspect and may extend onto the anterior surface, but in some specimens the cingulid is quite discontinuous. The posterior lobe bears multiple hypoconulids: two (GU 823, GU 1711, GU 7001, GU 7004, GU 8011), three (GU 401, GU 1596, GU 1700), three or four (GU 1515; one cusp twinned), or four (GU 674, GU 1595, GU 1597, GU 8010). In tethytheres, the posterobuccal cusp of m3 has been identified as the hypoconulid, whereas the more lingual cusp has been designated variously as 'entoconid II' (Domning et al., 1986) or the postentoconulid (e.g., Tassy and Shoshani, 1988; Fischer and Tassy, 1993). In *Cambaytherium*, we have considered these accessory cusps on m3 to be proliferations of the hypoconulid, although it is likely that one of them is the equivalent of the postentoconulid.

As on its m2, GU 1700 (Fig. 34) has additional cusps on m3: a small, low and rounded paraconid; a larger but lower paracristid cusp between the paraconid and the protoconid; a large, low accessory cuspule between the protoconid and the hypoconid; and a tiny, rounded bead of enamel in the center of the talonid basin. The hypoconulid is doubled, with a third, tiny posterocentral cuspule.

The m3s of *C. thewissi* from the upper level at Tadkeshwar (TAD-2)—WIF/A 4222, WIF/A 4223 (Fig. 35)—are relatively broader and have a shorter third lobe than those from Vastan and Mangrol. The metaconid of WIF/A 4222 is more clearly twinned than in the Vastan-Mangrol sample. The hypoconulids are doubled in both specimens, and the primary hypoconulid (behind the hypoconid) in WIF/A 4223 is almost as large as the hypoconid.

Like *C. thewissi*, *C. gracilis* from TAD-2 has two to four hypoconulids on the third lobe of m3. The four available specimens differ slightly from each other: WIF/A 4212 (Fig. 33D–F) has two hypoconulids, the buccal one distinctly larger, with two tiny cuspules lingually; WIF/A 4210 (Fig. 29) has two roughly equal cusps; GU 9001 (the holotype; Fig. 14) has three cusps (a main buccal cusp, a smaller secondary central cusp, and a much smaller lingual cusp); and WIF/A 4211 (Fig. 32) has four successively smaller cusps from buccal to lingual. The latter specimen has a strongly beaded ectocingulid with a small cuspule at the base of the furrow between the hypoconid and the main hypoconulid; this cingular cusp is also present in WIF/A 4210 and WIF/A 4212. All show a small accessory cusp posterobuccal to and at the base of the metaconid (similar to but better developed than that in *Perissobune intizarkhani*).

GU 9019, a right dentary with m1–3 from TAD-1, tentatively referred to *C. gracilis*, is essentially identical in size and most aspects of morphology to the TAD-2 sample of *C. gracilis* but differs in having a somewhat simpler m3 (Fig. 21). It lacks the cusp on the postvallid posterobuccal to the metaconid and has a less expanded third lobe with a single, centrally positioned main hypoconulid, flanked by a tiny cuspule on each side. Additional specimens are needed to determine whether these differences signal specific difference or intraspecific variation.

dP1—This tooth is preserved in series in two specimens of *C. thewissi*: GU 402 (Fig. 15; the subadult cranium described above) and GU 404 (Fig. 36; an adult with moderately worn dP1–M3). Two isolated teeth (GU 8015, GU 8020; Fig. 27A–D) are similar and appear to represent dP1. Like dp1, they are two-rooted. The dP1 is similar to dp1 but slightly larger and more robust (especially wider), with a slightly stronger posterolingual cingulum. It is elongate, about 50% longer than wide, with a single primary cusp near the center of the tooth and weak crests running anteriorly and posteriorly from it. The anterior crest divides partway down the anterior slope, merging into weak anterolingual and anterobuccal cingula. The posterior crest bears a tiny cuspule near its distal end, before joining with a distinct

posterolingual cingulum. The enamel is weakly crenulated. As noted earlier, based on the close similarity of dP1 and dp1 in the three specimens in which these teeth are preserved in situ, it is possible that some isolated uppers and lowers have been confused.

The dP1 of *C. gracilis* (WIF/A 4213; Fig. 14A, B) is relatively narrower (width/length = 3.0/5.4 = 0.56) than in *C. thewissi* and of similar morphology, except that the crests and cingula are very weak and the enamel is smooth. As in *C. thewissi* (GU 402), there is a short diastema separating dP1 and P2.

dP2—The dP2 is present only in the juvenile cranium of *C. thewissi*, GU 730 (Fig. 16), where it is heavily worn, making the morphology somewhat ambiguous. It is almost twice as long as wide, and it seems to have had a large anterobuccal cusp (paracone) and, judging from a weak indentation in the buccal enamel, a smaller, connate metacone. A low worn area lingual to the paracone (on the right dP2) suggests an incipient protocone. These details are similar to dP2 in *Hyracotherium* (Rose et al., 2018a). The structure of the posterior moiety is less clear.

dP3—This tooth is preserved in GU 5 (the holotype of *Indobune vastanensis* = *Cambaytherium thewissi*) and in four other specimens (GU 730, GU 7023, GU 8039, WIF/A 1199). It is triangular to trapezoidal, longer than wide, narrow anteriorly, and wider posteriorly. Although both GU 5 (Rose et al., 2006: fig. 3) and GU 730 (Fig. 16) are very young individuals in which only M1 of the molars has erupted (and is almost unworn), dP3 is already very heavily worn, obscuring nearly all details. Three other specimens, however, reveal the surface structure of this tooth. GU 8039 is somewhat worn but still retains crown morphology, WIF/A 1199 is an unworn isolated dP3, and GU 7023 contains virtually unworn dP3–4 (Fig. 37). In these three specimens, dP3 has four main cusps: equal-sized paracone and metacone, slightly lower but large hypocone, and a small and low protocone. The latter is slightly closer to the paracone than the hypocone is to the metacone except in WIF/A 1199, in which the two pairs are the same distance apart. The paracone and metacone are joined by a weak, deeply notched centrocrista, and a pair of short, weaker crests extends from the hypocone to the base of the metacone anterior and posterior to the cusp apex. A prominent, low parastyle is present, but no mesostyle or metastyle. A variably developed cingulum is present around much of the tooth but is discontinuous on parts of the lingual and buccal sides; it is best developed posterobuccally, anterolingually, and posteriorly. The overall anatomy of dP3 is very similar to that in the basal equids conventionally referred to *Hyracotherium*, including the oldest equid *Sifrhippus sandrae* (USNM 525626), but in the equids the lingual cusps are more widely separated from the buccal cusps and weak protoloph and metaloph may be present (Rose et al., 2018a). The cambaythere dP3 is less similar to that of *Ectocion osbornianum* (USNM 494922), in which the same four cusps are present but the posterior part of the tooth is more expanded transversely and the hypocone is shifted more lingually. It further differs from dP3 of *Phenacodus trilobatus* (USNM 527702), which has accessory buccal cusps and in which the protocone may be very small or absent.

dP4—The dP4 is known in four specimens of *C. thewissi*: GU 5, GU 213, GU 730, and GU 7023 (Figs. 16, 37). It is fully molariform but is more transversely compressed (narrower) than M1. The four main cusps are approximately equal in size, the lingual cusps slightly posterior to their buccal counterparts. In GU 7023 (the unworn specimen), the paracone and metacone are more widely separated from each other than either is from its corresponding lingual cusp. The hypocone is twinned in GU 5: a slightly smaller cusp is present directly buccal to the hypocone proper and posterior to the metaconule (Rose et al., 2006:fig. 3E). This cusp is not present in the other two specimens, suggesting that twinning of this cusp varied intraspecifically. The condition in GU 5, also seen in its M1, is reminiscent of that in
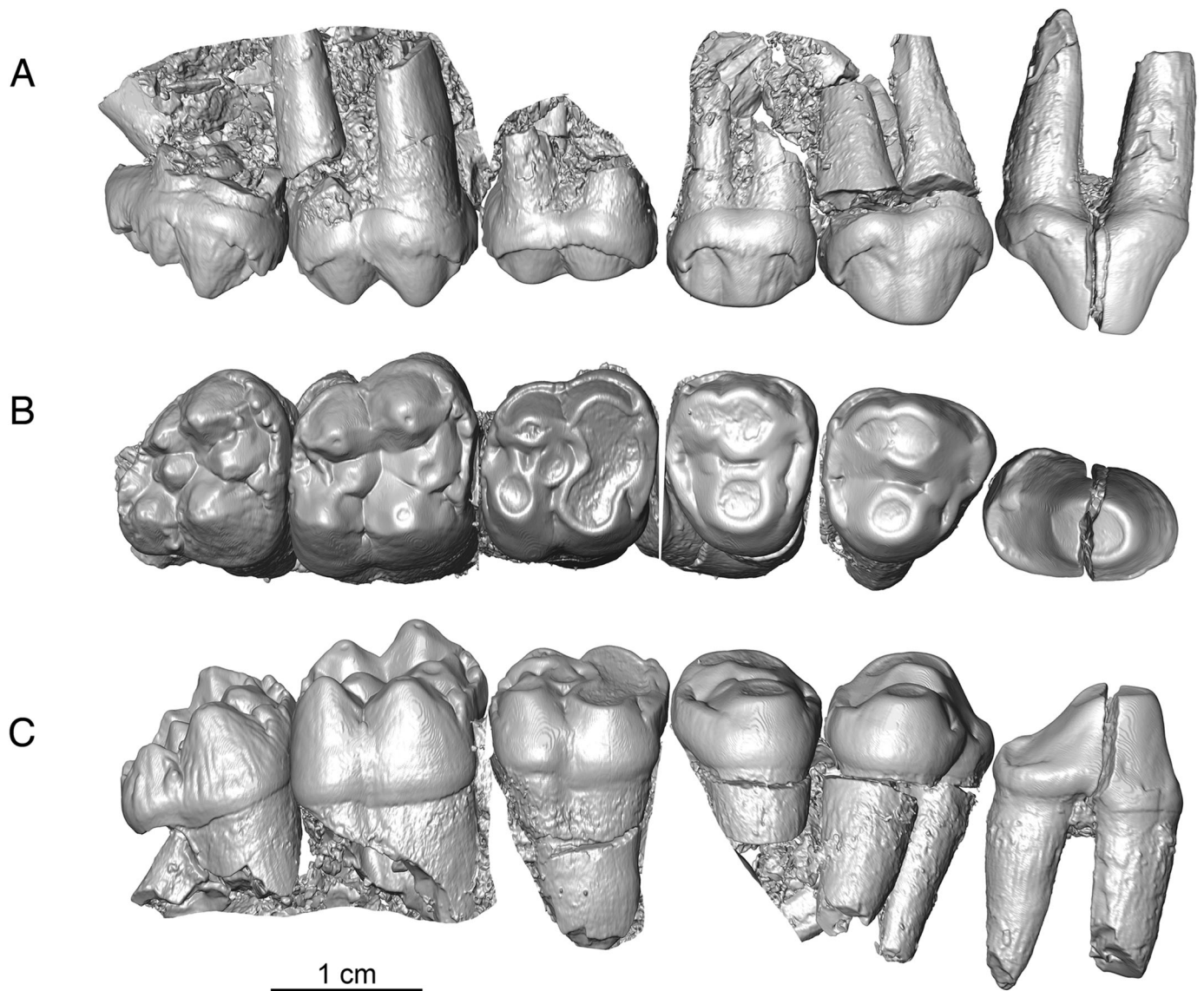
FIGURE 36. Maxillary dentition of *Cambaytherium thewissi*, GU 404. **A–C**, right P2–M3 in **A**, buccal, **B**, occlusal, and **C**, lingual views. **D–F**, left dP1–M3 in **D**, buccal, **E**, occlusal, and **F**, lingual views. **Abbreviation**: **pec**, pericone.

M1–2 of *Cambaytherium thewissi* (WIF/A 4217; see description below) from TAD-2. Large para- and metaconules are anteriorly shifted relative to the main cusps. A distinct parastyle and a tiny cingular mesostyle (not joined to the centrocrista) are present. In the unworn specimen (GU 7023), a low, deeply notched centrocrista is evident, as well as very low, incipient crests between protocone and hypocone, protocone and paraconule, paraconule and paracone, hypocone and metaconule, and hypocone and metacone, but there is no crest between metaconule and metacone. Most of these crests are obliterated by even moderate wear (e.g., GU 730). The crest connecting the protocone and the hypocone matches the description of the endoprotocrista identified in the premolars of perissodactyls by Holbrook (2015). A low cuspule is also present on the anterior cingulum near the base of the paraconule. Cingula encircle the tooth except on parts of the lingual margin.

A single dP4 of *C. gracilis* is known (WIF/A 4238). It is fully molariform but differs from that of *C. thewissi* in being smaller and in having the paracone and metacone closer to each other than either is to its corresponding lingual cusp. Like GU 5, it has a twinned hypocone. The incipient crests seen joining some cusps in GU 7023 are even weaker in WIF/A 4238, the most evident being between paraconule and paracone, metaconule and metacone, and the more buccal hypocone and the metacone.

The dP4 in *Cambaytherium* is narrower buccolingually than that of *Hyracotherium* (*Sifrhippus*) *sandrae*, in this regard being more like dP4 in phenacodontids (West, 1971).

P2—P2 of *Cambaytherium thewissi* is similar morphologically to dP1 and about one-third larger in linear dimensions. It is preserved in place and unworn in GU 402 (right side; erupting on the left; Fig. 15), in series and worn in GU 404 (Fig. 36) and GU 1727, and associated with other upper teeth in GU 1702. In addition, three isolated teeth of somewhat different morphology are also tentatively identified as P2 of *C. thewissi* (GU 428, GU 1683, GU 8019). In GU 402, GU 404, and GU 1702, P2 is a simple, elongate tooth, about 1.5 times longer than wide and only slightly wider posteriorly than anteriorly. It has two robust roots. The tooth is dominated by a single main cusp, presumably homologous with the
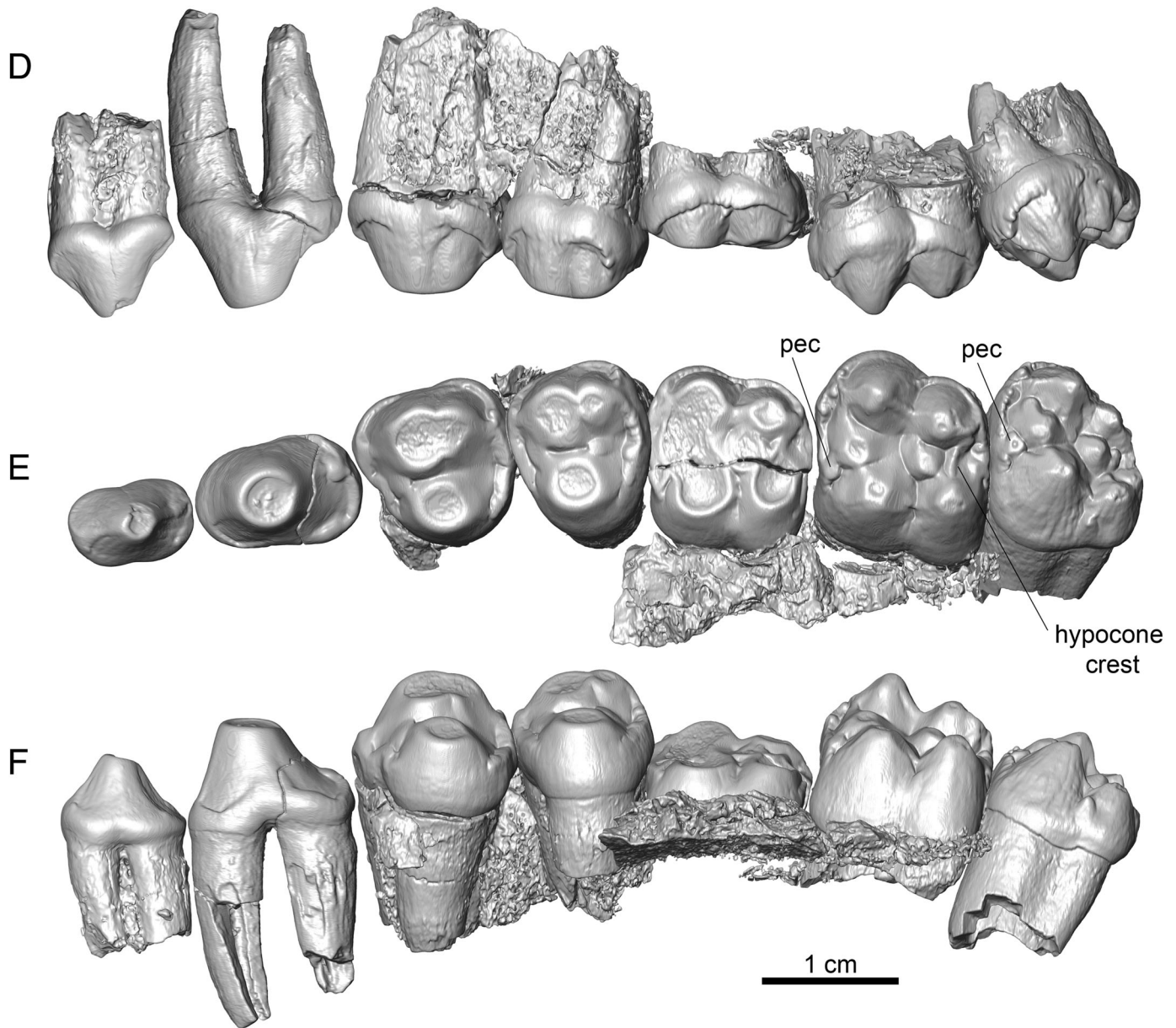
FIGURE 36. Continued

paracone, slightly anterior to the center of the tooth. The cusp is tall and conical, with a very steep anterior face. Immediately behind the paracone and connate with it in the newly erupted P2 of GU 402 is a much smaller and lower cusp (metacone?); this cusp, if present in GU 404, was obliterated by wear, making it appear that only a single cusp was present. A low crest descends steeply from the metacone to a very small posterior cusp, from which short posterolingual and posterobuccal cingula extend. The posterolingual cingulum is wider and more prominent than the posterobuccal one and makes a 90° turn at the posterolingual angle of the tooth, suggesting an incipient basin.

GU 428 is an unworn tooth similar in size and shape to P2 in GU 404. It differs from GU 402 and GU 404 in having a larger posterior cusp (adjoining the cingulum) and from GU 402 in lacking a metacone. GU 8019 has a prominent paracone connate with a smaller and lower metacone. It differs from other specimens in having a more expanded posterolingual lobe with a small but distinct

basin bounded posteriorly and lingually by a thick crest that is continuous anteriorly with the lingual cingulum. The crest bears two small, rounded cusps, one on the posterior crest and one on the lingual crest. GU 1683 is a triangular tooth with a large posterolingual lobe bounded by a complete lingual cingulum. There is no distinct basin, but a small protocone occupies the anterolingual part of the lobe. As in GU 402 and GU 8019, the tooth is dominated by a large conical paracone connate with a much smaller metacone. All three of these teeth have weakly crenulated enamel and coarse perikymata, as in other specimens of *C. thewissi*, and, despite their differences from more 'typical' specimens, they are best interpreted as P2s of *C. thewissi*. They exhibit intraspecific variation comparable to that described above in p4. Similar variation in P2 has been reported in *Homogalax protapirinus* (Radinsky, 1963a) and in *Litolophus gobiensis* (Bai et al., 2010:fig. 9).

P2 of *C. gracilis* (WIF/A 4213, WIF/A 4215, WIF/A 4265; Fig. 14A–B) is noticeably larger and relatively wider than dP1
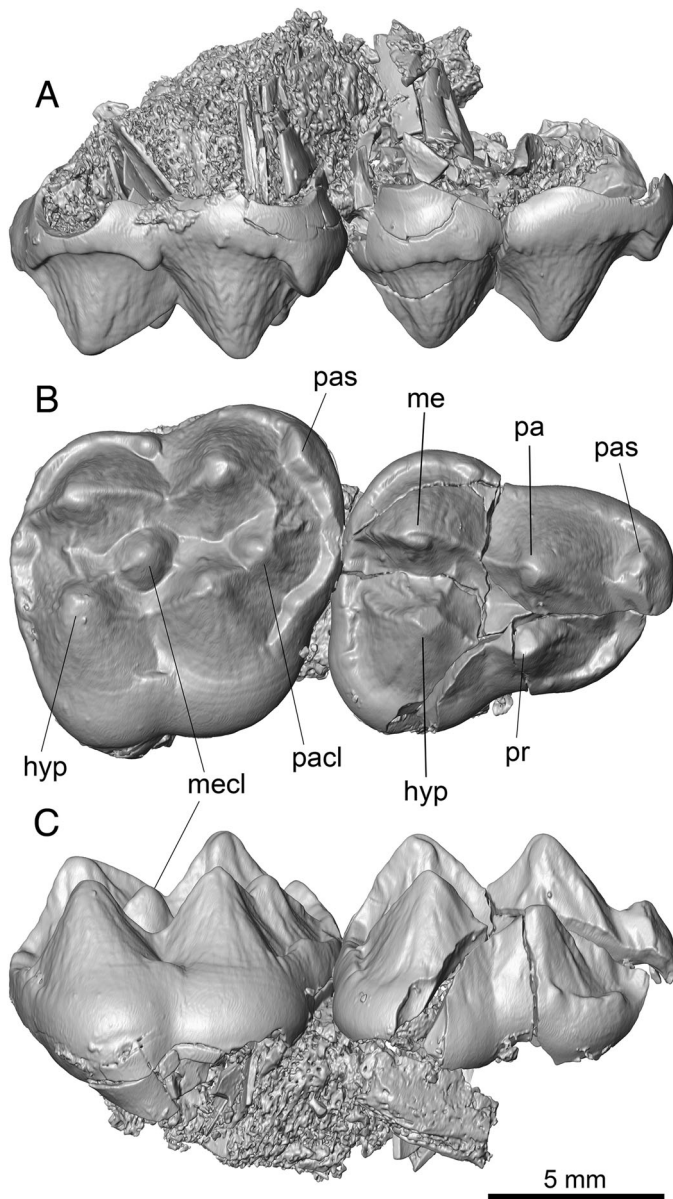
FIGURE 37. *Cambaytherium thewissi*, GU 7023, right dP3–4, in **A**, buccal, **B**, occlusal, and **C**, lingual views. **Abbreviations**: **hyp**, hypocone; **me**, metacone; **mecl**, metaconule; **pa**, paracone; **pacl**, paraconule; **pas**, parastyle; **pr**, protocone.

FIGURE 38. Comparison of upper teeth (left P4–M3) of *Cambaytherium thewissi* from Vastan and Tadkeshwar (TAD-2) mines, to the same scale. **A**, GU 404 (part, micro-CT image from Figure 36), in occlusal view; from Vastan. **B**, **C**, GU 9202, digital photographs in **B**, occlusal and **C**, lingual views; from TAD-2. **D**, WIF/A 4217, right P4–M2 (digital photograph, reversed), occlusal view; from TAD-2. **E**, WIF/A 4219, right M3 (digital photograph, reversed), occlusal view; from TAD-2. Note variation in M3 hypocone expansion and M1–2 metaconule. **Abbreviations**: **acc**, accessory; **mecl**, metaconule; **pas**, parastyle; **pec**, incipient pericone.

(mean width/length of P2 = 0.77) and is slightly wider posteriorly than anteriorly. It is dominated by a central cusp, followed by a small, low posterior cusp, but there is no trace of a metacone. The small posterior cusp is more prominent and slightly higher in WIF/A 4215, making this tooth closely resemble GU 428. P2 of *C. gracilis* is completely surrounded by a cingulum, which is best developed lingually.

P2s of the anthracobunids *Anthracobune wardi* (LUVP 15006, formerly *Pilgrimella pilgrimi*) and *A. aijiensis* (WIF/A 616) are elongate and wider posteriorly than anteriorly. The latter is very similar to GU 8019, with a prominent lingual cingulum, thickened posteriorly and bearing a couple of rounded cusp-like swellings. In *A. aijiensis*, these cuspules and the metacone are more distinct than in GU 8019. P2 of LUVP 15006 has a small posterolingual cusp just inside the cingulum, possibly homologous with that in GU 1683.

P3—P3 and P4 are very similar triangular teeth in *Cambaytherium* (Figs. 15, 36), each with three roots, two buccal roots, and one robust lingual root, which is sometimes bifid (GU 1702a). The buccal roots of P3 may be separate (GU 404, GU 1727, WIF/A 4213) or so closely appressed that they appear fused (GU 426). P3 is typically longer anteroposteriorly and narrower transversely than P4 (L/W ≥ 0.90 in all specimens except GU 1727, in which it is slightly shorter), and the anterobuccal margin of the tooth is slightly expanded compared with that of P4 (e.g., GU 402, GU 404). These distinguishing features enable confident identification of most isolated teeth. The cusp patterns of P3 and P4 are

otherwise essentially identical: the three principal cusps consist of the tall paracone, which is connate with a slightly lower and smaller metacone (the two cusps being separate only at their apices), and a large but somewhat lower protocone. There are well-developed pre- and postcingula (clearly crenulated in the unworn GU 402), which are discontinuous lingually and on the middle of the buccal border in *C. thewissi*. GU 404 has rudimentary parastyle and metastyle on both P3 and P4, but GU 402 has no trace of these cusps. GU 404 has a small, rounded paraconule, anteriorly displaced relative to the paracone and protocone, but conules are absent in GU 402. GU 426 has weak pre- and postprotocristae but no conules.

P3 of *C. gracilis* (WIF/A 4213 and GU 9007; Fig. 14) is almost identical to that of *C. thewissi* but smaller and has a nearly complete cingulum encircling the tooth. Both teeth have a small parastyle but lack a metastyle and conules.

P4—P4 is shorter anteroposteriorly and wider than P3 (L/W ≤ 0.83) in all but three specimens of *C. thewissi* (GU 412, GU 7013, and GU 9202). GU 412 (L/W = 0.86) is a heavily worn isolated tooth that has the outline shape of P4 (no anterobuccal expansion), but it is possibly a P3. GU 7013 (L/W = 0.91), from Mangrol Mine, is an unusually large and unworn (unerupted?) tooth discussed below. GU 9202 (L/W = 0.87) is from TAD-2 and is likely to be slightly derived compared with the Vastan sample. Among the sample of P4s of *C. thewissi*, there is considerable variability in development of conules and protocristae. The newly erupted and unworn P4s in GU 402 lack evidence of either conules or protocristae. A tiny, rounded metaconule is discernible in the worn P4s of GU 404; a tiny metaconule and distinct preprotocrista are present in GU 1708; a larger metaconule and preprotocrista are seen in GU 5; pre- and postprotocristae and a small metaconule are present in GU 430 and GU 662; tiny para- and metaconules occur in GU 204; distinct paraconule and preprotocrista and a small, twinned metaconule are present in WIF/A 4217 (TAD-2; Fig. 38D); and strong pre- and postprotocristae are evident in GU 732 (heavy wear prevents determination of presence of conules). The few P4s of *C. gracilis* (WIF/A 4214, WIF/A 4239, and WIF/A 4240; Fig. 33G–I) have a small parastyle and also show variation in conule expression. WIF/A 4214 (Fig. 14) has a small metaconule and a worn, thick preprotocrista but no distinct paraconule, whereas the other two have distinct paraconules and very tiny metaconules.

As noted earlier, GU 7013, from Mangrol Mine, is outside the range of other P4s allocated to *C. thewissi*. It bears strongly crenulated pre- and postcingula as in GU 204, and a rudimentary paraconule and an even tinier metaconule, both smaller than in GU 204. It may represent an exceptionally large individual of *C. thewissi* or perhaps *C. marinus*, although it is about 25% narrower than the holotype P4 of *C. marinus* based on measurements provided by Bajpai et al. (2006).

M1—M1 is a nearly square tooth, slightly wider anteriorly than posteriorly (Figs. 15, 36, 38). It is distinctly bunodont, showing a hint of lophodonty only when the cusps are worn flat (e.g., GU 404, GU 7022). Paracone, metacone, and protocone are inflated and conical, the paracone slightly taller than the other cusps. A large hypocone, slightly taller than the protocone when unworn, is situated posterior to and even with or slightly buccal to the protocone. As in some dP4s, the hypocone is often twinned, with a smaller cusp seemingly budding off the buccal side of the hypocone (GU 5, GU 18, GU 202, GU 731, GU 1615, GU 8003), but other specimens have only a single hypocone (GU 209, GU 402, GU 424, GU 730), whereas a slight thickening of enamel (GU 730) or a crest (GU 404; Fig. 38A) is present in place of a twinned cusp in others. The lingual cusps are slightly more separated from the buccal cusps than on dP4, but the metacone and the hypocone are much closer together than are the paracone and the protocone. Large conules are present, situated anterior to imaginary lines joining paracone-protocone and metacone-hypocone;

the metaconule tends to be more anteriorly offset than the paraconule. In GU 402, a distinct but low crest joins the hypocone and the metaconule and a weaker crest joins the metaconule with the metacone. One or both of these crests are present in some other specimens as well (GU 424, GU 731). GU 209 and GU 404 have a low crest extending buccally from the hypocone and bending back to meet the postmetacrista, not seen in other specimens, whereas GU 18 and GU 202 have only faint crests between conules and the corresponding buccal cusps. The cingulum is usually elevated just anterior to the paracone and posterior to the metacone, often creating a small but distinct parastyle and a weaker metastyle, but some specimens lack distinct styles (including mesostyle). The parastyle is incipient in GU 730, GU 784, and GU 1615, more distinct in GU 18, GU 202, GU 424, and GU 8003, and well developed in WIF/A 4217 (Fig. 38D). GU 7022 has a small parastyle and an incipient cingular mesostyle. A cuspule on the precingulum anterior to the protocone (incipient pericone) is somewhat better developed than on dP4 (also in WIF/A 4217). The cingulum tends to be mostly complete around much of the tooth but is usually absent lingually.

WIF/A 4217 (Fig. 38D), from TAD-2, differs from other specimens of *C. thewissi* in having a large accessory cusp on M1 just buccal to the hypocone and posterior to the metaconule, which is probably homologous with the twinned hypocone of some individuals (alternatively interpreted as a twinned metaconule). In this specimen, however, the accessory cusp is larger than the metaconule and as large as the primary hypocone, although slightly lower and more separated from it than in specimens such as GU 5. Short crests link the accessory cusp to both the hypocone and the metaconule. WIF/A 4217 also has a small cingular cusp on the lingual border between the protocone and the hypocone (also on M2). In size and in all other crown details, however, M1 of WIF/A 4217 is essentially identical to the Vastan-Mangrol sample of *C. thewissi*.

The M1 is preserved in only a single specimen of *C. gracilis* (WIF/A 4265; Fig. 29C–D), in which it is so heavily worn as to obscure all crown details.

M2—This tooth in *C. thewissi* is very similar to M1 but generally larger and relatively wider (Figs. 15, 36, 38). The paracone is slightly more buccally expanded than on M1, but the difference is not great, so it can be difficult to distinguish isolated M1s and M2s. In contrast to some M1s, no specimen of M2 in the Vastan-Mangrol sample has a twinned hypocone, although a slight enamel thickening (WIF/A 1193) or crest extending toward the metacone (WIF/A 1195) can be seen in some specimens. Other specimens (e.g., GU 404, GU 1616, GU 1727; Fig. 36D–F) have a low crest from the hypocone to the postmetacone crista; in all others, including unworn specimens (GU 402), the crest is absent. Two specimens (GU 785 from Vastan and GU 7012 from Mangrol) have an accessory cusp posterior to the metacone. Otherwise, the morphology is virtually identical to M1. In unworn teeth, the metacone is lower than the paracone, and the protocone is typically lower than the hypocone.

M2 of WIF/A 4217 (TAD-2; Fig. 38D) differs from other M2s of *C. thewissi* in having a large accessory cusp buccal to the hypocone (probably a twinned hypocone), of identical morphology to its M1. Two specimens of *C. gracilis* (WIF/A 4214 and WIF/A 4265) from TAD-2 also have a twinned hypocone, but they otherwise differ from *C. thewissi* primarily in being smaller (both specimens are heavily worn). A third specimen (WIF/A 4241) has a low crest joining the hypocone and the metacone but lacks a twinned hypocone.

M3—The M3 (Figs. 36, 38) differs in shape from the other two molars; in particular, the buccal portion is anteroposteriorly compressed and the lingual portion expanded, making it difficult to compare their sizes, but M3 in the Vastan sample is approximately the same size as M2 or slightly smaller (Fig. 13; Appendix 3). The cingula are mainly confined to the anterior and posterior margins.
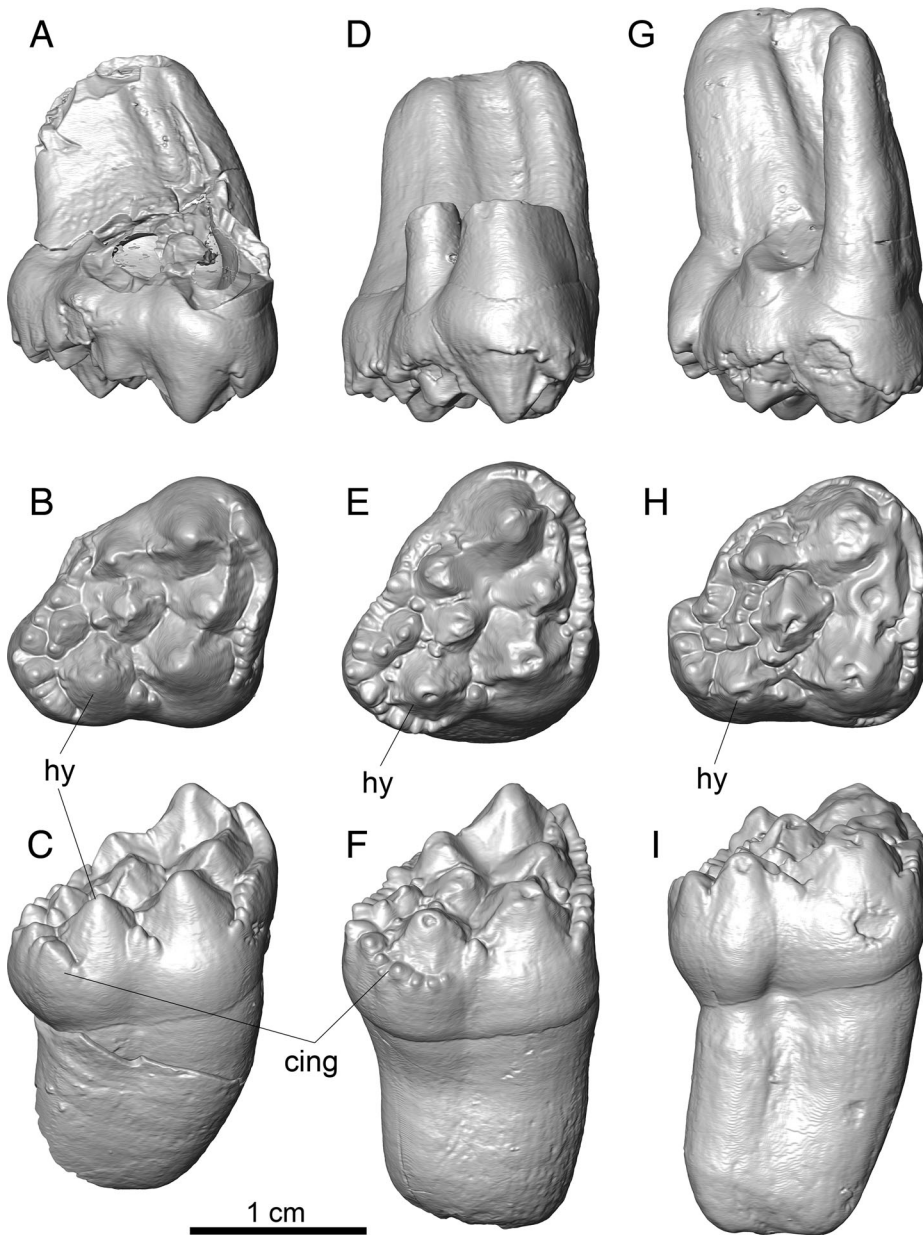
FIGURE 39. Variation in right M3 of *C. thewissi* from TAD-2, to the same scale. **A–C**, WIF/A 4221 in **A**, buccal, **B**, occlusal, and **C**, lingual views. **D–F**, WIF/A 4220 in **D**, buccal, **E**, occlusal, and **F**, lingual views. **G–I**, WIF/A 4219 in **G**, buccal, **H**, occlusal, and **I**, lingual views. **Abbreviations**: **cing**, cingulum; **hy**, hypocone.

M3 always has three roots: two buccal roots and a massive, elongate bilobed lingual root.

The cusp pattern is generally similar to that of M2: the same principal cusps and conules in more or less the same positions, except that the metacone is reduced and closer to the paracone, the hypocone is reduced and lower (about the size of the metacone or slightly larger) but the hypocone lobe is usually expanded, and the conules are very prominent, almost as large as the metacone and the hypocone. A tiny parastyle is typically present, as is a small cingular cusp (pericone) just anterolingual to the paraconule (but not in GU 418 and GU 425). The most obvious difference from M1–2 is a posterolingual expansion of the tooth consisting of the hypocone and accessory cuspules that vary in number and size. In the Vastan sample of *C. thewissi*, a prominent cingular cusp, often accompanied by additional cuspules, is situated posterobuccal to the hypocone, and a small basal cuspule is often present on the anterolingual base of the hypocone. GU 404 (Fig. 36) has two accessory cuspules behind the hypocone, although they differ in expression on the two sides. GU 1702a has three distinct cuspules on the postcingulum behind the hypocone, as well as an additional accessory cuspule between the metaconule and the postcingulum, and GU 1702b has six discrete cuspules on the postcingulum.

The four known large M3s from Tadkeshwar (Fig. 39) differ from the Vastan-Mangrol sample in being more expanded posterolingually and having more elaborate cusp development, although each one is slightly different. Each has numerous accessory cuspules between the hypocone-metaconule and the posterior margin of the tooth. This ranges from a large accessory cusp between the metaconule and an arc of four cuspules on the postcingulum (GU 9202, reminiscent of GU 1702a; Fig. 38B, C) to a series of three buccolingually arranged crests posterior to the metaconule, each bearing at least three cuspules (WIF/A 4219; Fig. 39G–I). The two others (WIF/A 4220 and WIF/A 4221) have intermediate conditions, each with postcingula bearing at least five cuspules. Because this is the only consistent morphological difference

from the Vastan-Mangrol sample, and third molars are notoriously variable, these specimens are here considered to represent a derived population of *C. thewissi* from TAD-2.

Also from TAD-2 is the much smaller and less elaborate *C. gracilis*. Its M3 (WIF/A 4214, WIF/A 4242, WIF/A 4243, WIF/A 4265, GU 9008), also roughly the size of M2 (Fig. 14), is less expanded posterolingually and has only a broad 'beaded' postcingulum bearing three to five rounded cuspules, the central one (posterobuccal to the hypocone) largest.

Although *Cambaytherium marinus* is known from a skull, its upper teeth are poorly preserved except for M3 (Bajpai et al., 2006). The M3 is slightly more expanded than in *C. thewissi* from Vastan Mine, and the postcingulum bears three well-developed cuspules, features that are reminiscent of the TAD-2 sample of *C. thewissi*.

Dental Variation and Sexual Dimorphism in *Cambaytherium*

In the foregoing descriptions, we have indicated the substantial size range and morphological variability in crown morphology among the Vastan sample referred here to *Cambaytherium thewissi*. This raises the question of whether this can be explained by sexual dimorphism or other intraspecific variation, or whether it indicates the presence of more than one species. Although some tooth loci display a remarkable range of morphological variability, the variation between left and right teeth in the same individuals and the more or less continuous gradation in size and morphology (especially in p4, m3, P2) within the sample, despite its restricted geographic and stratigraphic range, lead us to conclude that it is best interpreted as one species with unusually extensive intraspecific variation rather than more than one species. It is true that some of the most extreme variants (M3s from TAD-2) are likely to be geologically somewhat younger than the Vastan sample, but we prefer to recognize these as a different, somewhat more derived population of *C. thewissi*, rather than as a new taxon. Nevertheless, the bulk of the *C. thewissi* sample (exhibiting most of the observed variation) comes from a narrow stratigraphic interval of no more than a few meters, across a very limited geographic area of only a few hundred meters to a few kilometers (Vastan and Mangrol mines). To interpret the sample as multiple species would thus require that coexisting species of similar body size differed only in mutable features of one or two teeth (e.g., p4, P2, or M3) but apparently were indistinguishable in other aspects of their anatomy.

Some of the variation might be attributable to sexual dimorphism, as suggested by Bajpai et al. (2005a). For example, depth and thickness measurements of the dentaries of several specimens are consistent with this interpretation; however, variation in these dimensions is increased by two juvenile dentaries and a subadult jaw, all of which are distinctly shallower than the other measurable jaws. The wide range of dental measurements might also be considered evidence of sexual dimorphism, but no evidence of a bimodal size distribution in tooth dimensions was detected in the Vastan sample. Substantial differences in canine size are also suggestive of sexual dimorphism, and Bajpai et al. (2005a) mentioned two specimens that had markedly different sized canines despite molars of the same size. However, because nearly all canines in our sample are isolated, the available evidence does not allow positive determination whether the size difference reflects jaw location (i.e., upper vs. lower), individual variation, or sexual dimorphism. Thus, although sexual dimorphism seems a reasonable explanation for some of the size variation in the sample of *C. thewissi*, it is not conclusive.

Let us suppose that the observed variation in the sample we attribute to *Cambaytherium thewissi* reflects two species that overlap substantially in size and morphology. In that case, it might be expected that the sample would display at least a hint
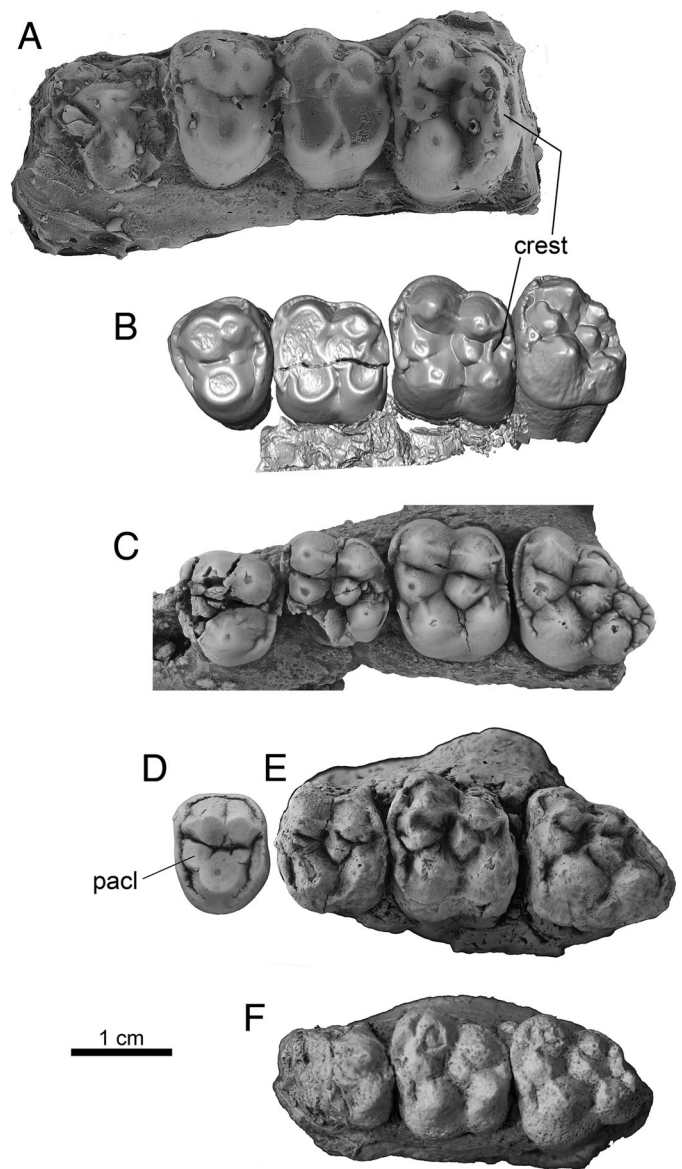
FIGURE 40. Upper left cheek teeth of *Nakusia shahrigensis* and *Perissobune intizarkhani* compared with those of *Cambaytherium thewissi*, occlusal views. **A**, *N. shahrigensis*, cast of holotype, left P4–M2. **B**, *C. thewissi*, GU 404, left P4–M3, micro-CT image from Figure 36 (Vastan). **C**, *C. thewissi*, GU 9202, left P4–M3 (TAD-2) digital photograph. **D–F**, casts of *P. intizarkhani*: **D**, GSP-UM 4046, left P4; **E**, GSP-UM 4345, left M1–3; **F**, GSP-UM 4466, left M1–3. Note expanded hypocone lobe on M3 in *C. thewissi* (GU 9202) and *P. intizarkhani*. **Abbreviation**: **pacl**, paraconule.

of bimodality in size, as well as greater levels of variation than are typical for a single species. Yet it is notable that nearly all tooth dimensions show normal distributions and coefficients of variation consistent with a single population (Table 5; see discussion in Systematic Paleontology). Coefficients of variation (CVs) for tooth dimensions (where n > 2) in the Vastan and combined samples range from 2.3 to 9.6, values usually considered within the range of a single species (Simpson et al., 1960; Gingerich, 1974). All dimensions with exceptionally low CVs (<4.0) pertain to adult or deciduous premolars with small sample sizes (n ≤ 8), whereas those with the highest values (CV ≥ 9.0) also
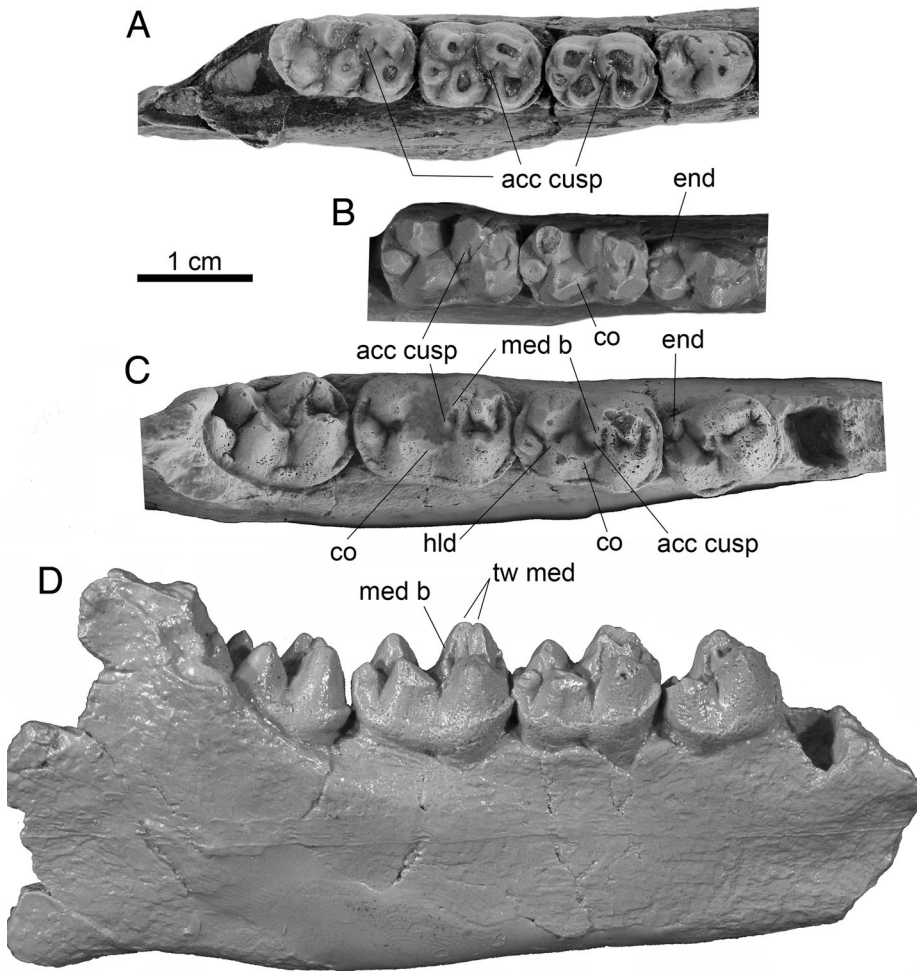
FIGURE 41. Lower right cheek teeth of *Perissobune intizarkhani* compared with those of *Cambaytherium gracilis*, to the same scale. **A**, *C. gracilis*, p4–m3 of WIF/A 4210 (digital photograph, reversed), in occlusal view. **B**, *P. intizarkhani*, cast of GSP-UM 6553, p4–m2, in occlusal view. **C**, **D**, *P. intizarkhani*, cast of GSP-UM 4656 (holotype), p4–m3, in **C**, occlusal and **D**, buccal views. **Abbreviations**: **acc cusp**, accessory cuspule; **co**, cristid obliqua; **end**, entoconid; **hld**, hypolophid; **med b**, metaconid buttress; **tw med**, twinned metaconid.

pertained to premolars. Even those teeth that are the most difficult to measure consistently (M2, M3) had normal CV values.

Furthermore, if the sample represented two or more species, it would also be expected that at least some dental characters would separate more or less consistently between species, but we have not found this to be the case. For example, we are unable to confirm a bimodal distribution in incisor number or diastemata around dp1 that was initially proposed as a distinction between *C. bidens* and *C. thewissi* (Bajpai et al., 2005a), in part because the sample preserving anterior dentition is inadequate. The few specimens at hand that preserve the symphysis suggest that incisor number might have been variable, even between left and right sides of the same individual, and that incisors were commonly misaligned. Equally important, these specimens demonstrate that less than well-preserved symphyses can be misleading in the number of incisors present as inferred from alveoli. Indeed, we may simply not be able to assess incisor number accurately from the alveoli in these specimens. We suspect that three incisors were probably present in each quadrant, even in those individuals that appear to have only two alveoli (three incisors may have been compressed into what appears in the fossil to be two alveoli). Thus, we find no compelling evidence that sympatric species of *Cambaytherium* differed in incisor count. In addition to incisor count, Bajpai et al. (2005a:109–110) distinguished *C. bidens* from *C. thewissi* by size (*C. bidens* described as "large species" and *C. thewissi* as "medium-sized") and by the presence of a diastema between (d)p1 and p2 in *C. bidens*, absent in *C. thewissi*. The number of

specimens upon which this was initially based was very small, as is the number of specimens in our sample that preserve the anterior part of the dentary, and there is no correlation between dental size and diastema in our sample. The dp1–p2 diastema varies from apparently absent (GU 7004, a large specimen the size of the holotype of *C. bidens*, with three incisor alveoli per quadrant), to short (GU 1710, a large specimen with three right incisors, and possibly two left incisors), to moderate (GU 403, an intermediate-sized subadult, incisor number uncertain; GU 9002, a small individual with apparently two incisors on each side). Thus, each of our specimens has characters that overlap with both *C. bidens* and *C. thewissi*. It should be noted that the symphysial portion of GU 7004 is damaged posteriorly at the back of the dp1 alveoli, so the presence of a short diastema cannot be ruled out. Finally, based on a larger sample, Bajpai et al. (2006:104) concluded that "the molar cusp morphology described for *Cambaytherium*, and based on a specimen of *C. thewissi*, also occurs in *C. bidens*." With no convincing characters by which to separate the principal Vastan and Mangrol samples into two species, we recognize the type species, *C. thewissi*, as the valid species and consider *C. bidens* and *C. minor* to be junior synonyms.

Additional variation in the larger specimens from TAD-2 has been described above. Features such as the very prominent conules, large twinned metaconule (present only in one specimen, WIF/A 4217), and expanded posterolingual lobe of M3 with multiple accessory cusps appear to be outside the range of variation of the Vastan-Mangrol sample, and some statistically significant
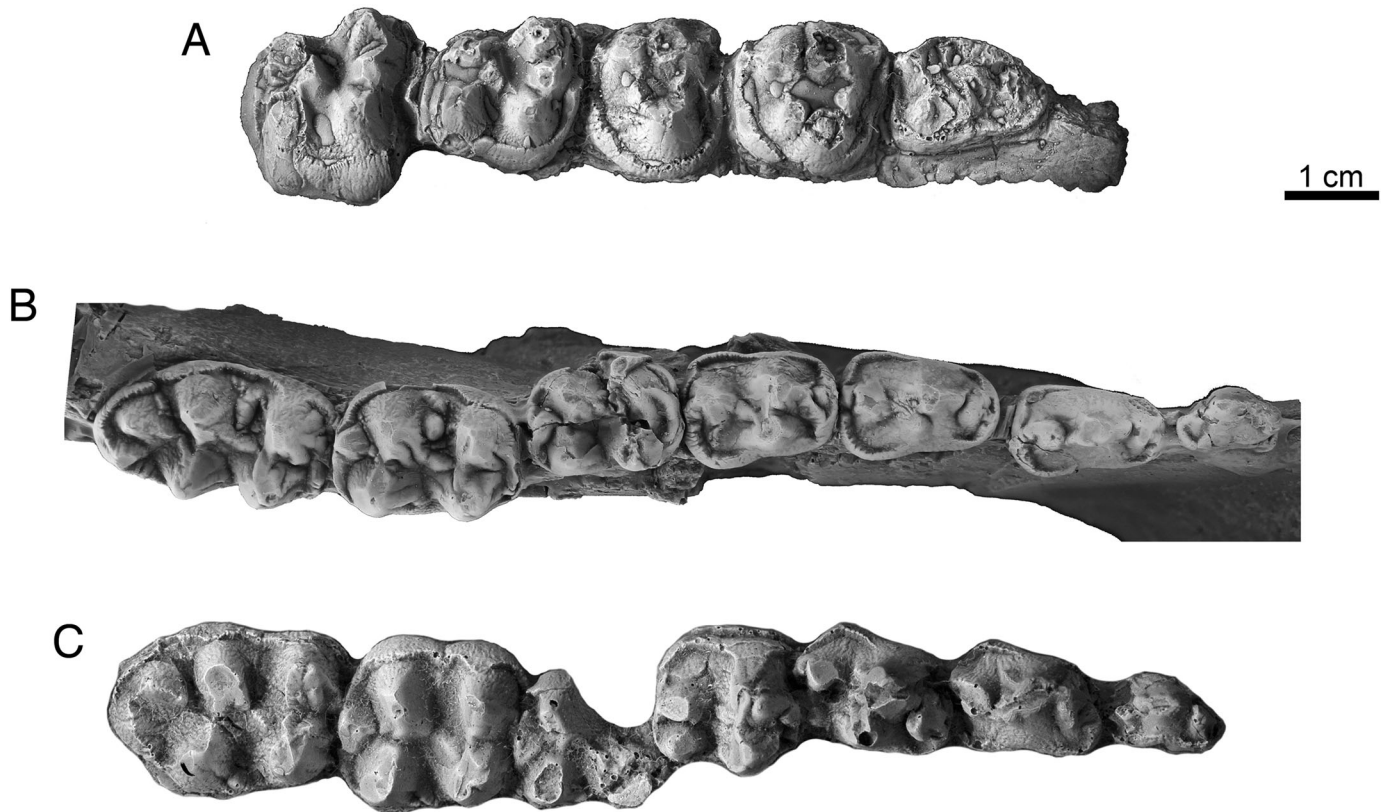
FIGURE 42. Cheek teeth of anthracobunids in occlusal view. **A**, *Anthracobune wardi*, cast of LUVP 15006, right P2–M2. **B**, *A. aijiensis*, cast of WIF/A 1101, left dp1–m3. **C**, *Obergfellia occidentalis*, cast of H-GSP 1981, left dp1–m3.

size differences were observed (Table 6). However, Vastan specimens are now known that approach these conditions, and a second maxilla from TAD-2, GU 9202, has only a single metaconule on M2 (the area is damaged on M1), resembling the Vastan sample in this regard. Rather than recognizing a distinct species for these TAD-2 specimens based primarily on M3 morphology, we regard them as a later, more derived population of *C. thewissi*.

Significant size differences indicating that there are additional species of *Cambaytherium* do exist, of course. *Cambaytherium gracilis* (from Tadkeshwar Mine) is readily distinguished from *C. thewissi* by its smaller size, as well as its more molariform p4 and relatively less enlarged p2 and M3. *Cambaytherium marinus* is distinguished by its much larger size.

Craniodental Comparisons of *Cambaytherium*

Other Cambaytheriids—As noted above, the single specimen of *Nakusia*, a fragmentary maxilla, is similar to that of *Cambaytherium thewissi* to the extent that they can be compared, except for having transversely wider upper teeth (Fig. 40A). Similarities include the presence of a crest extending buccally from the hypocone toward the metacone on M2. *Perissobune intizarkhani* Missiaen and Gingerich, 2014, is also very similar to *Cambaytherium* but slightly larger (generally less than 10%) in most dimensions (Fig. 40D–F). Close comparison of the dentitions shows near identity in most details, but *Perissobune* tends to have slightly higher and more acute main cusps, has slightly more molarized posterior premolars, and shows incipient lophodonty (rudimentary hypolophid and cristid obliqua; Fig. 41), which is completely missing in *C. thewissi* and *C. gracilis*. P4 of *P. intizarkhani* has more equal-sized paracone and metacone, and larger conules

(especially the paraconule). *Perissobune* has a rudimentary entoconid on p4, which is typically not present in *Cambaytherium* (but see Fig. 31D–I). Unlike in some *C. thewissi*, there is neither a twinned metaconule nor a low crest between the hypocone and the metacone (in the position of a twinned metaconule); thus, the upper molars of *P. intizarkhani* are quite similar to those of GU 402 (Fig. 15). The upper molars of *P. intizarkhani* increase in size posteriorly (only M3 is known for *P. munirulhaqi*; Missiaen and Gingerich, 2014), whereas M3 of *Cambaytherium* tends to be about the same size as M2 or slightly smaller. Lower molars of *Perissobune* also have a slightly more anterior twinned metaconid, and a prominent metaconid buttress that is not present in *Cambaytherium*. As in *Cambaytherium*, the lower molars increase in size, especially length, posteriorly.

These three genera are clearly closely related and might equally well be considered congeneric. However, because we have observed minor distinctions, and the names exist, we retain these names here as closely allied cambaytheres.

Anthracobunids—For this comparison, we follow Cooper et al. (2014) in recognizing three genera of Anthracobunidae: *Anthracobune*, *Obergfellia*, and *Jozaria*. According to these authors, *Anthracobune* includes most specimens formerly referred to *Pilgrimella* and *Lammidhania*. Their new genus *Obergfellia* was based on a specimen that had been placed in *Anthracobune* or *Pilgrimella* by previous authors, which underscores the similarity of these genera. Both *Obergfellia* and *Jozaria* are monotypic, but the number of valid species of *Anthracobune* requires further study. The challenge in determining the proper generic and specific attribution of many anthracobunid specimens stems from the fact that the holotypes of most of the early named species were badly preserved and very

fragmentary, in some cases not even a complete tooth. Consequently, it has been difficult to demonstrate that new and much better preserved specimens belong to one or another of the original taxa. It could be argued that these names are nomina dubia or nomina vana (Mones, 1989) and therefore invalid, but this issue is outside the scope of the present study.

All three genera of anthracobunids are larger than *Cambaytherium thewissi* and *C. gracilis*; however, based on published measurements (Bajpai et al., 2006), *C. marinus* has teeth comparable in size to those of the largest known anthracobunids. Like *Cambaytherium*, anthracobunids, so far as known, have a primitive placental dental formula of 3 small incisors, 1 large canine, 4 premolars, and 3 molars in each quadrant. Cusps of the cheek teeth are more acute and less bunodont than in *Cambaytherium*, but the cusp pattern is strikingly similar (Fig. 42). The premolars are unreduced, even dP1 and dp1 almost always retaining two roots, and there is no compression of antemolar teeth; they show increasing molarization from dP1/dp1 to P4/p4. The molars increase in size from M1/m1 to M3/m3 and are more lophodont than in *Cambaytherium*, although the lophodonty is not very strong. *Obergfellia* and *Jozaria* appear to be derived relative to *Anthracobune*. *Obergfellia* has broader lower molars and a relatively shorter m3 than in *Anthracobune* (though still longer than m2). *Jozaria* is more lophodont than the other two genera and has a relatively larger p3 and further reduced molar paraconid region (Wells and Gingerich, 1983); it resembles *Cambaytherium thewissi* in having p3 larger than either p4 or m1. Both *Obergfellia* and *Jozaria* have more molarized premolars than in *Anthracobune*. In view of the more primitive conditions in *Anthracobune*, we focus our remaining comparisons on this genus.

The upper dentition of anthracobunids is poorly known. The few specimens of *Anthracobune* preserving upper premolars reveal that they are slightly more molarized than in *Cambaytherium* (Fig. 42A). The paracone and metacone of P2–4 are tall and connate, but their apices are separate and both cusps of P3–4 are almost equal in size and height; the metacone of P2 is only slightly smaller than the paracone. Thus, the metacone is relatively a little larger than in *Cambaytherium*. P2 is expanded posterolingually and bears a small protocone (WIF/A 616, *A. aijiensis*; Kumar, 1991). P2 of *A. pinfoldi* is similar in having a small protocone but evidently differs in lacking a metacone, instead having "two cuspules on the posterior crest of the paracone" (Cooper et al., 2014:5–6). P2 in *Cambaytherium* is usually simpler, but a few specimens have an incipient metacone or protocone. P3 of *Anthracobune*, as in *Cambaytherium*, is slightly longer but narrower than P4 and has a slightly taller crown. Incipient parastyle and metastyle are present on both P3 and P4. In *A. wardi* (LUVP 15006; Sahni and Khare, 1973), P3 has prominent conules but weak crests, whereas P4 has smaller conules and stronger pre- and postprotocristae extending to the bases of the paracone and metacone and defining a clear trigon basin. The paraconules are well developed on both P3 and P4 of *A. aijiensis* (WIF/A 616), but crests are not evident. Only P4 seems to have had a metaconule, but this part of the crown is damaged on P3. Buccal cingula are weak on P3–4, but pre- and postcingula are well developed on both teeth and join lingually on P4 (LUVP 15006). Although the upper premolars of *Anthracobune* are derived and more complex than those of *Cambaytherium*, the basic pattern is very similar and some outliers among *Cambaytherium* approach the morphology of *Anthracobune*, suggesting that only minor modifications could transform the crown pattern of *Cambaytherium* into that of *Anthracobune*.

The same is true for the upper molars. M2 is larger and relatively broader buccolingually than M1 in both *Anthracobune* and *Cambaytherium*. M1 and M2 of *Anthracobune* have the same cusp configuration and the same relative height of the main cusps as in *Cambaytherium*. For example, the paracone is taller than the metacone and the hypocone is taller than the protocone. In particular, the conules are prominent and low crests join hypocone-metaconule-metacone, and protocone-paraconule-paracone, creating weak bilophodonty. M3 is similar to M1–2 but is expanded posterolingually. However, illustrated specimens and casts available to us show no indication of the accessory cuspules characteristic of M3 of *Cambaytherium* or of a twinned hypocone in any of the molars.

The lower premolars of *Anthracobune aijiensis* (WIF/A 1101, H-GSP 1000) increase in size from dp1 to p4; in contrast to *Cambaytherium thewissi*, but similar to *C. gracilis*, p2 is not longer and taller than the other premolars (Fig. 42B). The permanent premolars are markedly more complex than those of *Cambaytherium*. The dp1 has a tall main cusp flanked by small, low mesial and distal cusps, whereas p2, although dominated by the protoconid, has a distinct, low paraconid, an incipient metaconid twinned with the protoconid, and a talonid cusp (hypoconid). The p3 and p4 accentuate the features of p2: the metaconids and hypoconids are better developed, the talonids wider, and the incipient crests (paracristid, cristid obliqua) stronger; however, the paraconid is lost on p4, and there is no distinct entoconid cusp on any premolar of *A. aijiensis*. As aforementioned, *A. wardi* has a distinct entoconid on p4 in both H-GSP 96258 and H-GSP 96434, as well as on p3 of H-GSP 96258. The more molarized premolars of *Anthracobune* differ from the simple premolars that characterize most *C. thewissi*, but the cusp pattern of p2–4 (except for the reduced paraconid and the absent entoconid) resembles to a remarkable degree the relatively longer and narrower dp2–4 of *C. thewissi*. The dp3–4 of *Anthracobune* (H-GSP 1000; West, 1980:pl. 4) are even more similar to those of *C. thewissi*, differing only in loss of the paraconid on dp4, and in being larger, relatively wider, and having noticeable crests (cristid obliqua and postcristid). *Obergfellia* shows further molarization of premolars, with tighter p3–4 trigonids and the addition of an entoconid on these teeth.

The lower molars of anthracobunids, like those of *Cambaytherium*, lack a paraconid, although *Anthracobune* retains a distinct, low paracristid. The metaconid is weakly twinned, but less obviously than in *Cambaytherium* or *Perissobune*. The talonids of *Anthracobune* are relatively more elongate than those of *Cambaytherium*, with a distinct, low cristid obliqua and weak hypolophid and entocristid surrounding a talonid basin that is open lingually. The hypoflexid is deep. Otherwise, the molar cusps are very similar in position and relative size to those of *Cambaytherium* (and basal perissodactyls). The lingual cusps are posterior (rather than directly lingual) to their corresponding buccal cusps. The trigonids are barely higher than the talonids, and the hypoconulid is isolated behind the hypolophid notch, to which it is joined by a weak crest. On m3, the third lobe is elongate, the hypoconulid is twinned, and in *A. aijiensis* a tiny accessory cuspule is present anterior to the lingual hypoconulid. *Obergfellia* and *Jozaria* also have elongate m3s with twinned hypoconulids. Despite the deeply notched protocristid and hypolophid, the crowns of *Anthracobune* appear incipiently bilophodont, a condition accentuated in *Obergfellia* and *Jozaria*. Overall, anthracobunids exhibit dental morphology that could have evolved from a basic cambaythere morphology by selection for progressive molarization of premolars and bilophodonty of the molars.

The mandible of *Anthracobune* also shares several features with *Cambaytherium*. The symphysis is solidly fused in adults but unfused in juveniles (Cooper et al., 2014). Like *Cambaytherium*, *Anthracobune* has an expanded mandibular angle, a reduced and vertically oriented coronoid process, and a relatively high condyle (Cooper at al., 2014:fig. 1). Compared with *Cambaytherium*, however, the coronoid process is further reduced and the angular process projects more posteriorly (well behind the condyle and coronoid) than inferiorly.
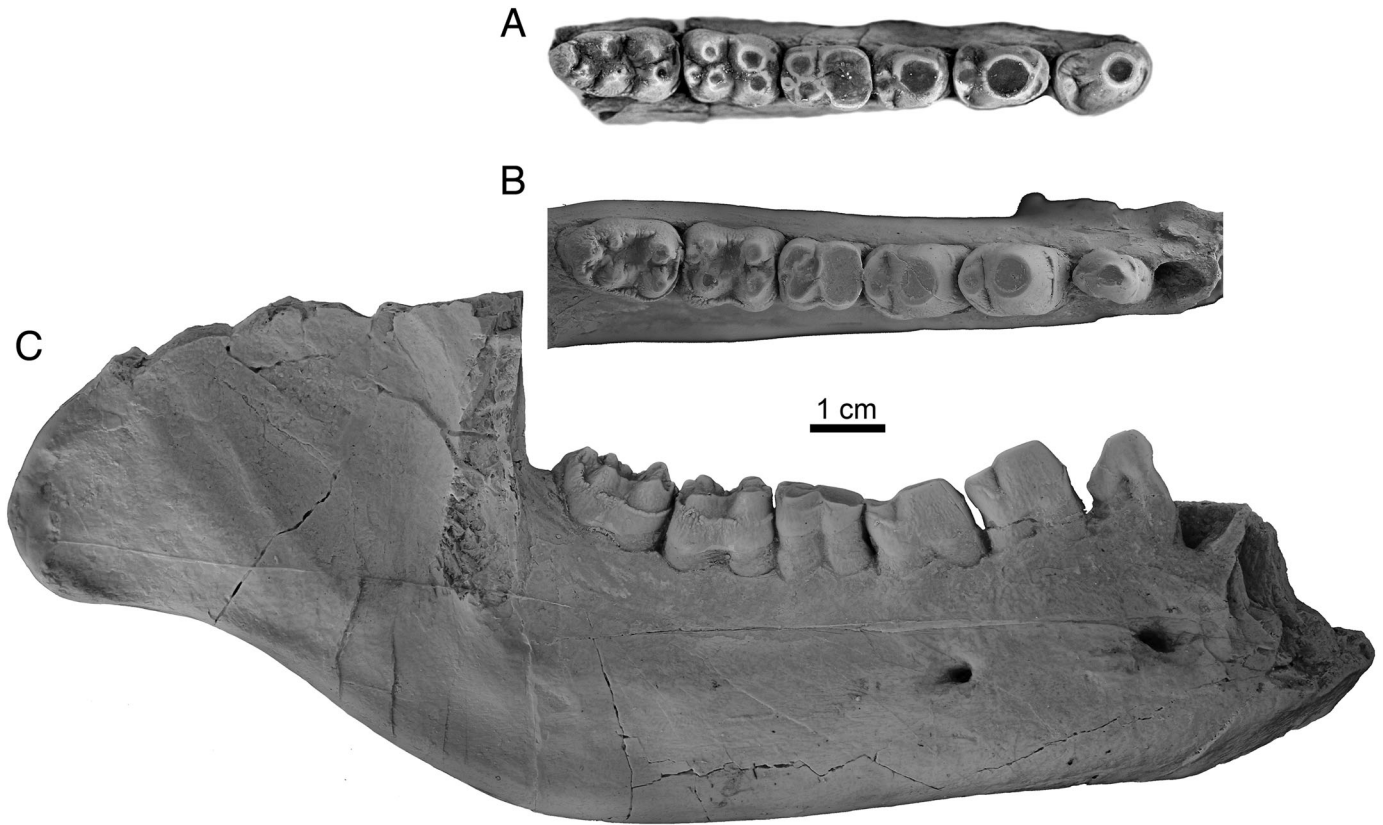
FIGURE 43. Comparison of *Cambaytherium thewissi* with the quettacyonid *Machocyon abbasi* from the lower Eocene of Pakistan. **A**, right p2–m3 of *C. thewissi*, GU 7004, in occlusal view, digital photograph. **B**, **C**, right dentary with p2–m3 of *M. abbasi*, GSP-UM 4208 (digital photographs of cast), in **B**, occlusal and **C**, buccal views, showing general similarity of crown morphology and wear pattern of cheek teeth to *C. thewissi*. Note smaller p2, shorter m3, and different jaw morphology (compare Fig. 19A) in *Machocyon*.

Basal Perissodactyls—The cheek teeth of basal perissodactyls differ from those of *Cambaytherium* primarily in being more lophodont, having smaller (although still distinct) upper molar paraconules and (with some exceptions) metaconules, and having more complex premolars, particularly the posterior premolars (although the complexity of P4/p4 in *C. gracilis* approaches that of basal perissodactyls). Even the more bunodont perissodactyls, such as the European early Eocene *Hallensia* and *Propachynolophus*, exhibit rudimentary lophodonty that is absent in *Cambaytherium*. *Cambaytherium* resembles perissodactyls in the possession of twinned lower molar metaconids, an unusual feature also observed in anthracobunids. The dp2 of *Hyracotherium sandrae* (USNM 525626) is similar to that of *Cambaytherium* but has a weaker paraconid, a tiny metaconid twinned with the protoconid, two small talonid cusps, and an incipient basin. The dp3 of *Hyracotherium sandrae*, compared with that of phenacodontids, is much more like that of *Cambaytherium*, with slightly lower and less acute cusps, stronger talonid crests, and a better-developed ectocingulid; cusps are identically placed and expressed. *Hyracotherium sandrae* dp4 is very similar to that of *Cambaytherium*, differing in having no distinct paraconid, a less distinctly twinned metaconid, a slightly wider talonid, a stronger ectocingulid, and a cristid obliqua that extends up the middle of the postvallid. In general, the features observed in the dentition of *Cambaytherium* are those that would be expected in the ancestry of perissodactyls. The main exceptions to this are the possibly derived bulbous, bunodont cusps; the complex of connections between upper molar hypocones and metacones variously consisting of twinned metaconules, twinned hypocones, or a crest extending buccally from the hypocone to the metacone; and the variable number of cusps in the region of the m3 hypoconulid and M3 hypocone. None of these features is suggestive of a relationship to any non-perissodactyl lineage, however, with the exception of anthracobunids.

The general shape of the known skulls of *Cambaytherium* is not unlike those of early perissodactyls. As in perissodactyls, the preorbital and postorbital regions appear to be roughly equal in length, there is a low sagittal crest, and the nasals are posteriorly broad and form a long transverse suture with the frontals. Unfortunately, the posterior portions of the base of the skull are not known, so there is no information at present on whether the mastoid is exposed laterally rather than posteriorly or whether there are arterial grooves on the surface of the petrosal.

Radinskya—This enigmatic Paleocene taxon from Asia is known from a single skull preserving most of the cheek teeth and has been considered to be possibly a close relative of perissodactyls (McKenna et al., 1989; Holbrook, 2014). It is smaller than known cambaytheres or basal perissodactyls. The most interesting features it shares with perissodactyls are broad nasals that meet the frontal at a wide transverse suture and a laterally facing exposure of the mastoid. The former is also shared by *Cambaytherium*, but the disposition of the latter is unknown in *Cambaytherium*. The cusps of the cheek teeth of *Radinskya* are bunodont but incipiently lophodont, about as in *Hallensia*. The conules lie along lines connecting their respective lingual and buccal cusps, whereas in *Cambaytherium* and perissodactyls the conules are more mesially (anteriorly) positioned.

Phenacodontids—The molars of *Cambaytherium* are reminiscent of those of *Phenacodus* in their greater bunodonty and simpler premolars compared with perissodactyls, but *Cambaytherium* differs from *Phenacodus* in possessing larger upper molar conules, lacking upper molar mesostyles, and having lower molars with twinned metaconids. Lower molars of *Phenacodus* differ from those of *Cambaytherium* in having distinct metastylids rather than twinned metaconids, hypoconulids that are incorporated into the hypolophid, and greater development of crests. The third molars of phenacodontids are generally not larger than the second molars. The m3 of phenacodontids lacks an extended hypoconulid (third) lobe, which is characteristic of *Cambaytherium* and basal perissodactyls, and the hypocone of M3 tends to be reduced or absent in phenacodontids (Thewissen, 1990), rather than large and complex as in *Cambaytherium*. The dp3 of phenacodontids (*Ectocion*, USNM 494919, USNM 494920; *Phenacodus* [West, 1971]) is much simpler than that of *Cambaytherium*. Its tall protoconid is flanked by a tiny paraconid and a variable metaconid (either present or absent intraspecifically), and there is a single low talonid cusp; consequently, the tooth is even less molariform than dp2 of *Cambaytherium*. The dp4s of *Ectocion* and *Phenacodus* are molariform (USNM 494919, USNM 494920, USGS 7158), with a more mesiodistally extended trigonid and a wider talonid than in *Cambaytherium*, as well as accessory cusps.

The main differences in cranial anatomy between phenacodontids and *Cambaytherium* are the shape of the nasal and the nature of the nasofrontal suture. In phenacodontids, the nasals are narrow, splint-like bones and their posterior ends are embraced by the frontals, forming sutures that are curved and more longitudinal in orientation. This condition is common among placental mammals, whereas in *Cambaytherium* and perissodactyls the nasals are posteriorly broad and form a transverse suture with the frontal.

Quettacyonidae—*Cambaytherium*, particularly *C. thewissi*, bears a striking superficial similarity in cheek tooth morphology and heavy apical wear patterns to quettacyonids (Gingerich et al., 1997, 1998, 1999), an enigmatic group of condylarths from the early Eocene of Pakistan (Fig. 43). This suggests either that cambaytheres and quettacyonids are closely related or that a similar diet led to dental convergence. Shared features include robust and simple p3–4, low-crowned lower molars with bunodont cusps and trigonid and talonid approximately equal in height, loss of molar paraconids, and wrinkled enamel. In addition, like *Cambaytherium*, *Machocyon abbasi* (Fig. 43B, C) shows increasing molar size posteriorly, including a slightly extended hypoconulid lobe on m3. But this size relationship is less evident in *Quettacyon* and *Sororocyon*, in which m3 is slightly smaller than m2 (Gingerich et al., 1998, 1999). Like *Cambaytherium*, *Machocyon* also had large canine teeth with very large roots, which show similar posterobasal wear (Gingerich et al., 1999:fig. 8a).

However, we believe these resemblances are more likely the result of homoplasy than indicative of close relationship, for the following reasons. Quettacyonids differ from *Cambaytherium* in mandible shape (especially the angular process) and in having an apparently unfused, though extensive, mandibular symphysis. Quettacyonid molars are incipiently lophodont (in particular, having distinct cristid obliqua and paracristid), and they are relatively wider, with well-developed talonid basins. The molar cusps are less inflated than in *Cambaytherium*, the metaconid and entoconid are lingual to the buccal cusps rather than posterolingual, and the hypoconulids are lingually situated. The hypoconulid of m3 is much less expanded than in *Cambaytherium* and is not multiple. Importantly, the metaconid is not twinned, nor is there a metastylid. In addition, the few postcranial bits tentatively attributed to quettacyonids differ markedly from those of *Cambaytherium*. The humeri are robust, with flaring lateral supracondylar ridge, prominent deltopectoral crest, and an entepicondylar foramen, resembling the humerus of *Arctocyon*, whereas the proximal radius is ovoid and implies substantial capability for supination (Gingerich et al., 1999:figs. 9o, 10). These contrasts are sufficient to suggest that cambaytheres and quettacyonids are not closely related, and that their similarities evolved independently (see Results of Phylogenetic Analyses below). It is more likely that they inhabited similar environments and had a similar abrasive diet.

Proboscidea—Although anthracobunids were previously considered basal Proboscidea, the most primitive known proboscideans (*Eritherium*, *Phosphatherium*; Gheerbrant et al., 1996; Gheerbrant, 2009) differ from both anthracobunids and cambaytheriids in having quadritubercular upper molars that lack any trace of conules (unless the cusp in the position of the hypocone is actually a displaced metaconule; Gheerbrant et al., 2016) and that have small mesostyles joined to the centrocrista. *Phosphatherium* is already markedly bilophodont, although *Eritherium* is not. One pair of incisors is enlarged, and the canines are reduced (Gheerbrant et al., 2005a), the reverse of the condition in *Cambaytherium*. The orbit is shifted anteriorly to be above P4–M1. Where known, these characters conflict with those of anthracobunids and *Cambaytherium*, and there is no longer any compelling evidence for a relationship between anthracobunids and Proboscidea.

Other Taxa—The unusual bunodont dentition of *Cambaytherium* merits comparison with certain other bunodont archaic ungulates, which, together with phenacodontids, can provide a frame of reference for establishing plesiomorphic characters. *Arctocyon* is similar in having simple premolars and bunodont molars with well-developed conules, but the molar cusps are lower and less distinct and the premolar cusps are sharper and more trenchant. The p4 is the largest and tallest lower premolar, rather than p2 as in *C. thewissi*. The lower molar hypoconulids of *Arctocyon*, like those of other condylarths (and arctocyonids generally), are small and incorporated into the postcristid (Matthew, 1937; Russell, 1964), rather than being situated posterior to the hypoconid (*Cambaytherium*) or hypolophid (early perissodactyls). M3 of *Arctocyon*, unlike that of *Cambaytherium*, is much smaller than the other upper molars and has less well-developed cusps.

Like cambaytheriids, periptychids also have bunodont cheek teeth with simple premolars. Unlike *Cambaytherium*, however, the posterior upper and lower premolars of periptychids are larger than the corresponding molars and the upper molar conules and hypocones are smaller. Periptychid molars have a protostyle or pericone (Shelley et al., 2018), a cusp mesiolingual to the protocone on the anterior cingulum, which is also present in *Meniscotherium* and is similar to a cuspule seen on the anterior cingulum of some upper molars of *Cambaytherium* (e.g., Figs. 15C, D, 36E). However, the pericone in *Cambaytherium* is more buccally situated, closer to the paraconule than to the protocone; consequently, it probably arose independently. The lower molars of periptychids have a distinct, although mesiodistally compressed, triangular trigonid with a strong, mesiolingually placed paraconid. It should also be noted that *Meniscotherium* differs markedly from *Cambaytherium* in having selenodont molars.

POSTCRANIAL SKELETAL ANATOMY OF
CAMBAYTHERIUM

Because *Cambaytherium thewissi* is the largest and most abundant mammal from Vastan Mine, except for the much larger and very rare *C. marinus*, and is the only perissodactyl-like mammal of its size, we can have high confidence in the accurate allocation of most isolated postcranial elements here referred to this species. This is also true for fossils from Mangrol Mine. Tadkeshwar Mine, however, has produced two sizes of *Cambaytherium*—

C. thewissi and the smaller *C. gracilis*—both of roughly equal relative abundance, as well as a few undescribed isolated teeth of a very diminutive tapiroid somewhat smaller than *C. gracilis*. The presence of two small perissodactylamorphs with similar anatomy could lead to some ambiguity in assignment of isolated postcrania. However, the tapiroid teeth are similar in morphology and size to those of *Cambaylophus vastanensis* Kapur and Bajpai, 2015, which are approximately 20–50% smaller in linear dimensions than cheek teeth of *Cambaytherium gracilis*. Consequently, postcrania representing *Cambaylophus* would be expected to be noticeably smaller than those of *Cambaytherium gracilis*. A few such elements believed to represent tapiroids have been identified from Tadkeshwar and will be described elsewhere. Nevertheless, postcranial sample sizes are very small, and whereas some elements from Tadkeshwar are readily attributable to *C. gracilis* based on particular, usually plesiomorphic, traits described below, others are less certainly allocated. Therefore, we cannot rule out the possibility that some isolated elements here referred to *C. gracilis* actually represent a small tapiroid.

Vertebrae

We attribute 19 isolated vertebrae from Vastan mine to *Cambaytherium thewissi*: C1 (atlas; GU 773, GU 782), C2 (axis; GU 774, GU 7003), cervical (probably C5; GU 775), undetermined cervical centrum (GU 8043), C7 or T1 (GU 783), undetermined thoracics (GU 788, GU 790, GU 791), lumbars (GU 786, GU 787, GU 789, GU 8042), and intermediate or distal caudals (GU 824, GU 825, GU 8017). GU 825 consists of three unassociated distal caudals. The sacrum of *C. thewissi* is unknown, but a sacrum of a larger taxon is tentatively allocated to *C. marinus* (GU 8001).

C1—Two atlas vertebrae are preserved, both from Vastan Mine. GU 773 is a complete C1, whereas GU 782 is incomplete (Fig. 44). The vertebral foramen is roughly pyriform, about 50% wider dorsally than ventrally and slightly wider mediolaterally than dorsoventrally. It is close to the shape in *Hyracotherium grangeri* (Wood et al., 2011). The cranial end of GU 773, including the shape of the occipital facets and position of the lateral vertebral foramen (which transmits the vertebral vessels and the first cervical nerve through the craniodorsal aspect of the arch and into the vertebral canal just dorsal and posterior to the occipital facet; Richards and Watson, 1991), is similar to that of *Canis* (Evans and Christensen, 1979) and bears a strong resemblance to that of *H. grangeri*. The facets for the occipital condyles are deeply concave and differ in shape between the two Vastan specimens. In GU 773, the dorsoventral dimension of each facet is about 1.5 times the transverse dimension and the lateral margin is smoothly curved and approximately semicircular. The facets are taller (twice the transverse width) and more vertical, with an angular margin, in GU 782. These differences may be partly attributable to postmortem deformation, but we lack sufficient data to assess their significance. A brief examination of intraspecific variation in occipital facet shape in extant suids (n = 9) suggests that subtle variations in facet depth and orientation are common. However, the strong variation in height and depth proportions between the two Vastan specimens suggests that deformation may also be a contributing factor. Other aspects of the anatomy, including size, are similar in the two specimens, and with no other taxa of comparable size known from Vastan, it seems probable that both represent *C. thewissi* rather than one belonging to an otherwise unknown taxon. At the distal or caudal end, the axial facets are flat, slightly wider than high, and obliquely oriented (facing posteromedially, but much closer to the transverse plane than in *Canis*). The transverse foramen in the ventral aspect of the ala is directed caudally and opens posteriorly just

lateral to the axial facet, as in *Hyracotherium* (Wood et al., 2011), rather than dorsomedially on the ala as in *Canis*. The dorsal and ventral arches are relatively short craniocaudally, and there is a small ventral tubercle similar to that in *Canis*. The transverse processes (alae) are robust and craniocaudally longer than the arches, but less elongate than in *Canis*. C1 is twice as wide as deep (dorsoventrally), perhaps relatively wider transversely than that of *Hyracotherium* (Wood et al., 2011), but not as wide as in *Canis*. Overall, C1 also resembles that of the tapiroid *Heptodon* (Radinsky, 1965a:fig. 5), but C1 of *Cambaytherium* is shorter and wider.

C2—Two axis vertebrae are known, one from Vastan Mine (GU 774), the other from Mangrol Mine (GU 7003). GU 774 is smaller than GU 7003 (33.3 mm wide × 30.0 mm long vs. 37.85 mm wide × 43.8 mm long) and has a shorter centrum that appears to be incomplete posteriorly (possibly missing its anular epiphysis). Besides this size difference, GU 774 (Fig. 45) has more transversely oriented atlantal facets that are more obviously transversely concave, a relatively shorter odontoid process, and a flatter centrum. The posterior centrum of GU 7003 (Fig. 46B) is only about 25% wider than tall (20.7 mm × 16.4 mm), but it shows a marked ventral expansion at the posterior end, which may be missing from GU 774. In other respects, the anatomy of the two vertebrae is very similar; hence, it is likely that they represent the same species. The minor differences could reflect sexual dimorphism, intraspecific variation, or an earlier ontogenetic stage of GU 774. The posterior half of the centrum in both specimens bears a ventral keel that broadens into a tubercle at the caudal end, as in *Hyracotherium* and *Hyrachyus* (Wood et al., 2011:fig. 4; Bai et al., 2017:fig. 6). On the posterior half of the dorsal side of the centrum, GU 7003 bears a distinct deep fossa (Fig. 46I), the significance of which is unknown. The most conspicuous feature of GU 7003 is the salient spinous process, extending cranially over the back of the odontoid process and high above the vertebral arch (Fig. 46C, F); it is distinctly thickened and elevated at the caudal end, where it projects over C3. The posterior zygapophyses are nearly flat transversely and weakly convex craniocaudally and face mostly ventrally and slightly laterally. Compared with *Hyracotherium grangeri*, the odontoid process is larger in both Vastan specimens (also longer in GU 7003) and the spinous process projects farther cranially. The spinous process also appears to be taller dorsally in GU 7003, perhaps reflecting larger body size and a stronger nuchal ligament, but possibly due to the less complete process in *H. grangeri* (Wood et al., 2011:fig. 4). C2 of *Cambaytherium* is also very similar to that of *Heptodon* (Radinsky, 1965a:fig. 5), differing in having a somewhat longer centrum, which is less ventrally expanded at the distal end than in *Heptodon*.

C5—The presence of transverse foramina and a very large vertebral foramen indicate that GU 775 (Fig. 47A–F) is a cervical vertebra. It is tentatively identified as C5 because of its relatively small, cranially directed inferior transverse process (or inferior lamella) coupled with a bell-shaped vertebral foramen that is slightly narrower but still rounded at the apex. This differs from more caudal cervicals that either exhibit a broad, plate-like expansion of the inferior lamella (C6) or lack it altogether (C7), whereas more cranial cervicals have a relatively rounder vertebral foramen and more dorsally positioned transverse foramina (Radinsky, 1965a; Bai et al., 2017). The prezygapophyses of GU 775 are flat and oriented dorsally and slightly medially; the preserved (left) postzygapophysis is ovoid, longer than wide, very slightly concave, and directed almost fully ventrally. The transverse processes are damaged but consist of a hook-like, cranially directed inferior lamella (preserved on the left side), with a laterally projecting transverse process (broken off) caudal and superior to the inferior lamella. The centrum is relatively short (length = 16.4 mm at the center), weakly opisthocoelous, and wider than tall (17.8 × 13.6 mm cranially, 18.5 × 14.7 mm

FIGURE 44. Atlas (C1 vertebra) of *Cambaytherium thewissi*, dorsal or cranial at top. **A–F**, GU 773 in **A**, cranial, **B**, right lateral, **C**, caudal, **D**, ventral, **E**, left lateral, and **F**, dorsal views. **G–K**, GU 782 in **G**, cranial, **H**, right lateral, **I**, caudal, **J**, ventral, and **K**, dorsal views. **Abbreviations**: **lat v for**, lateral vertebral foramen; **occip**, occipital; **tr for**, transverse foramen; **vent tub**, ventral tubercle; **vert for**, vertebral foramen.

caudally), unlike the nearly round centrum in *Heptodon* and *Hyrachyus* (Radinsky, 1965a:fig. 5; Bai et al., 2017:fig. 8), and its dorsal aspect slants craniad. There is a low ventral keel, less pronounced than that in *Hyracotherium*, but otherwise it generally resembles cervical vertebrae of the latter. There is no ventral tubercle, as occurs in C3–4 of *Hyrachyus*. The spinous process is broken, making its size and orientation ambiguous, but it seems to have been short anteroposteriorly and tilted slightly cranially. C5 of *Cambaytherium* is wider overall than the illustrated cervicals of *Heptodon* and *Hyrachyus*.

C7 or T1—GU 783 (Fig. 47G–L) has a mix of cervical and thoracic vertebral traits, including absence of transverse foramina, which indicates that it is either C7 or T1. It is characterized by distinct demifacets for ribs on the caudal end of the centrum, more widely spaced and ventrally placed prezygapophyseal facets (low on the arch) than on C5 (GU 775), a mediolaterally wide and dorsoventrally compressed centrum, and craniocaudally short length. It appears to be missing at least its caudal epiphysis and probably the cranial epiphysis as well; therefore, we are unable to confirm the presence of anterior demifacets, which
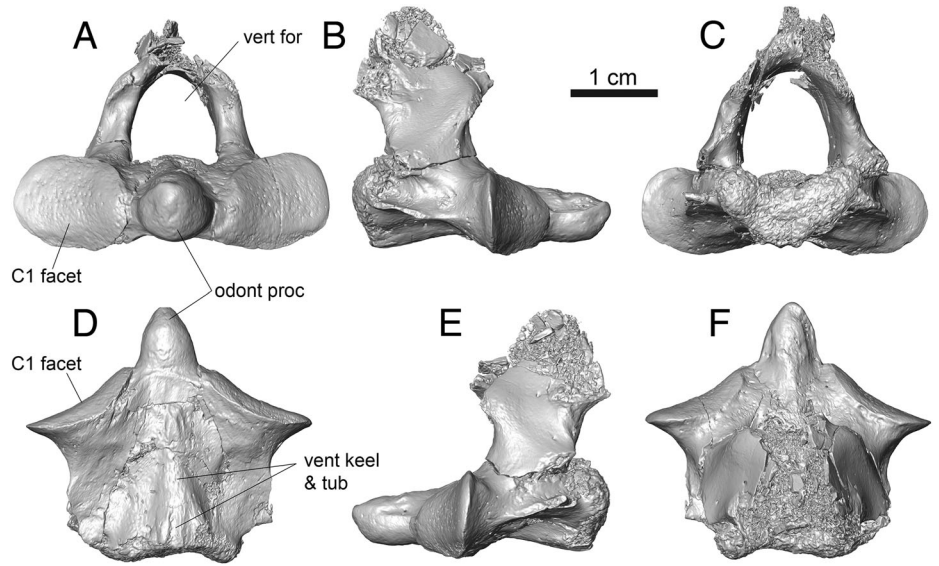
FIGURE 45. Axis (C2 vertebra) of *Cambaytherium thewissi*, GU 774, in **A**, cranial, **B**, right lateral, **C**, caudal, **D**, ventral, **E**, left lateral, and **F**, dorsal views. Dorsal (**A–C**, **E**) or cranial (**D**, **F**) to top. **Abbreviations**: **odont proc**, odontoid process; **vent keel & tub**, ventral keel and tubercle; **vert for**, vertebral foramen.
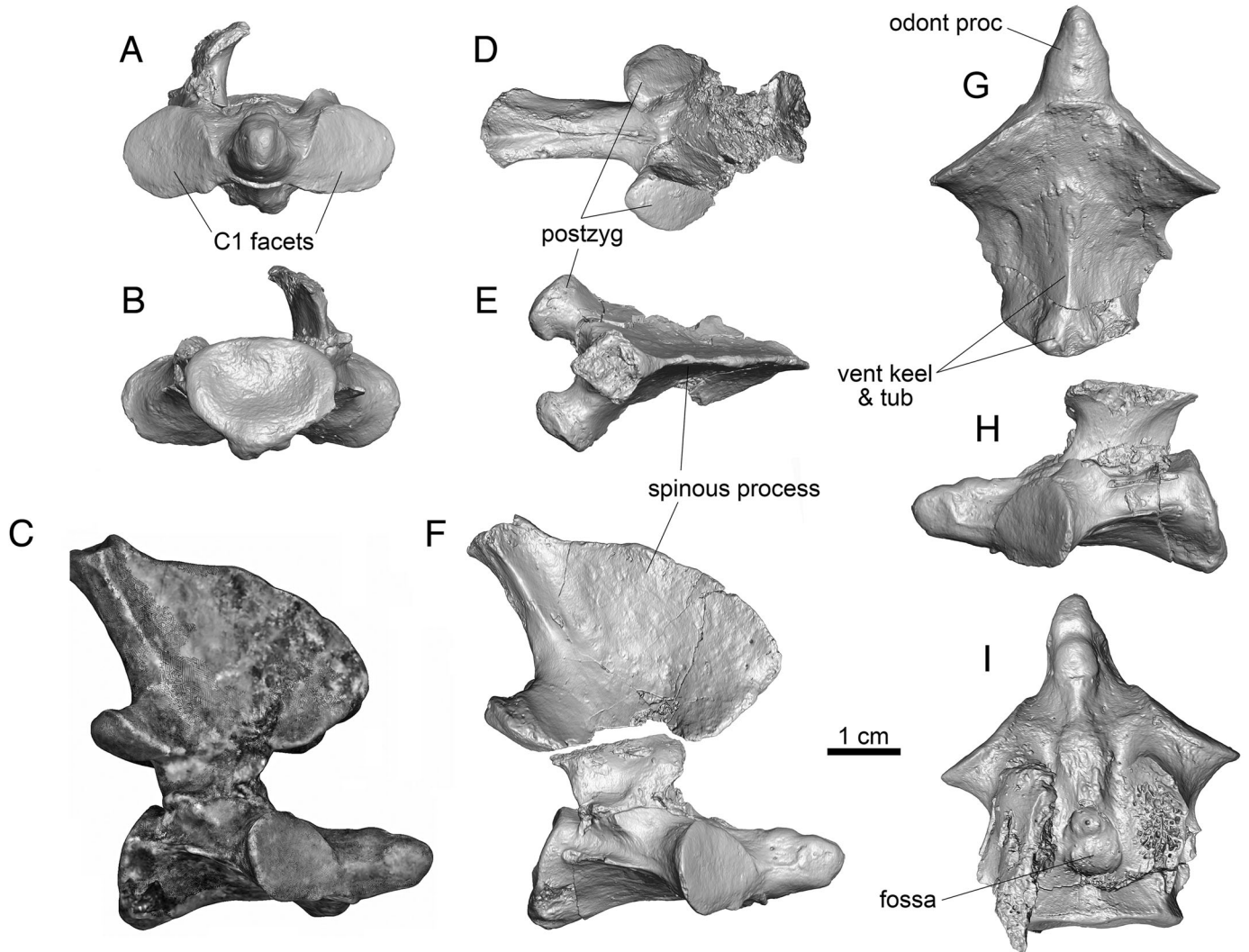
FIGURE 46. Axis (C2 vertebra) of *Cambaytherium thewissi*, GU 7003, micro-CT images except **C**. **A**, cranial and **B**, caudal views of centrum. **C**, laser scan of complete axis before damage. **D**, ventral and **E**, dorsocaudal views of arch. **F**, right lateral and **G**, ventral views. **H**, left lateral and **I**, dorsal views of centrum. **Abbreviations**: **odont proc**, odontoid process; **postzyg**, postzygapophysis; **vent keel & tub**, ventral keel and tubercle.
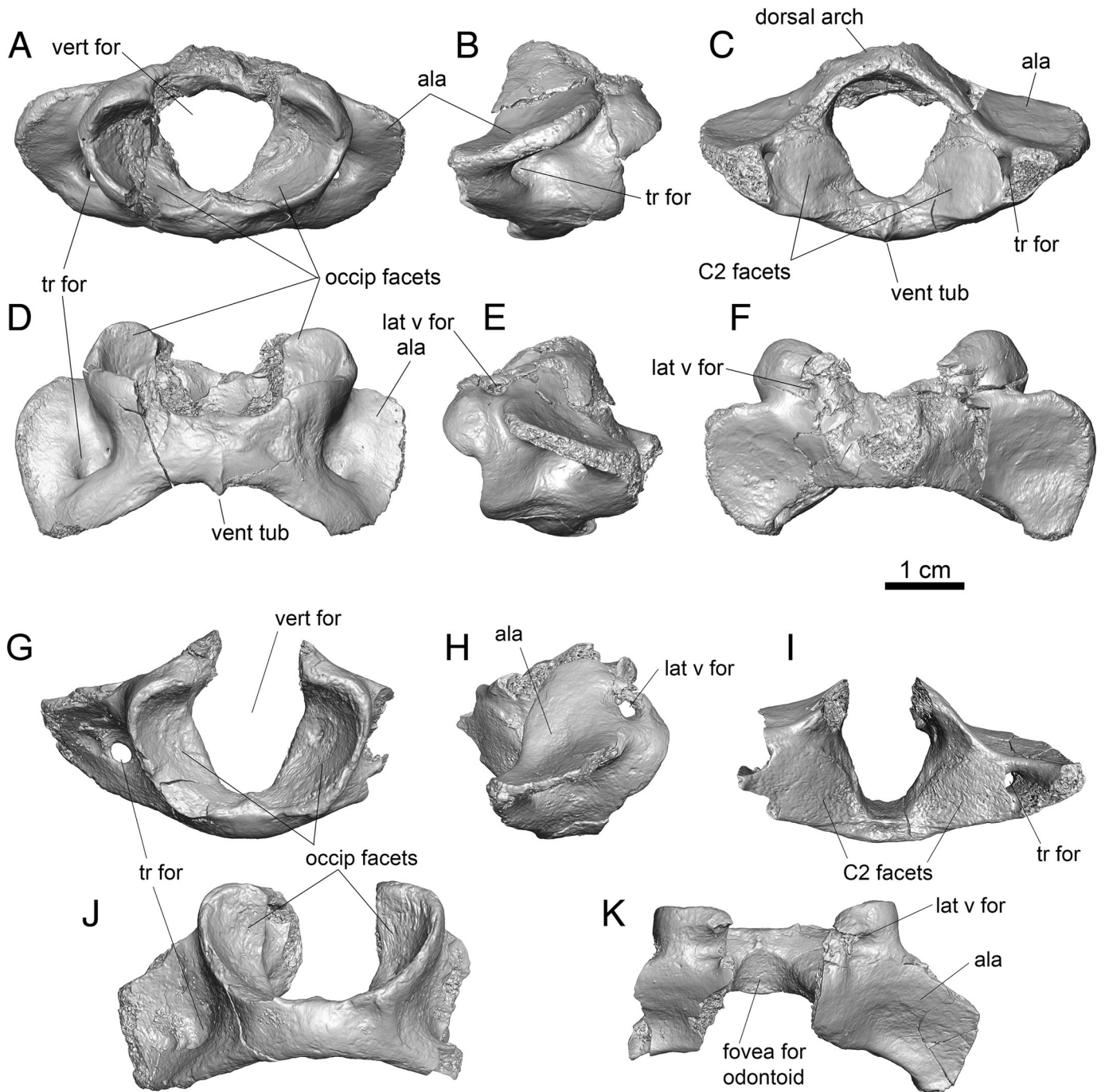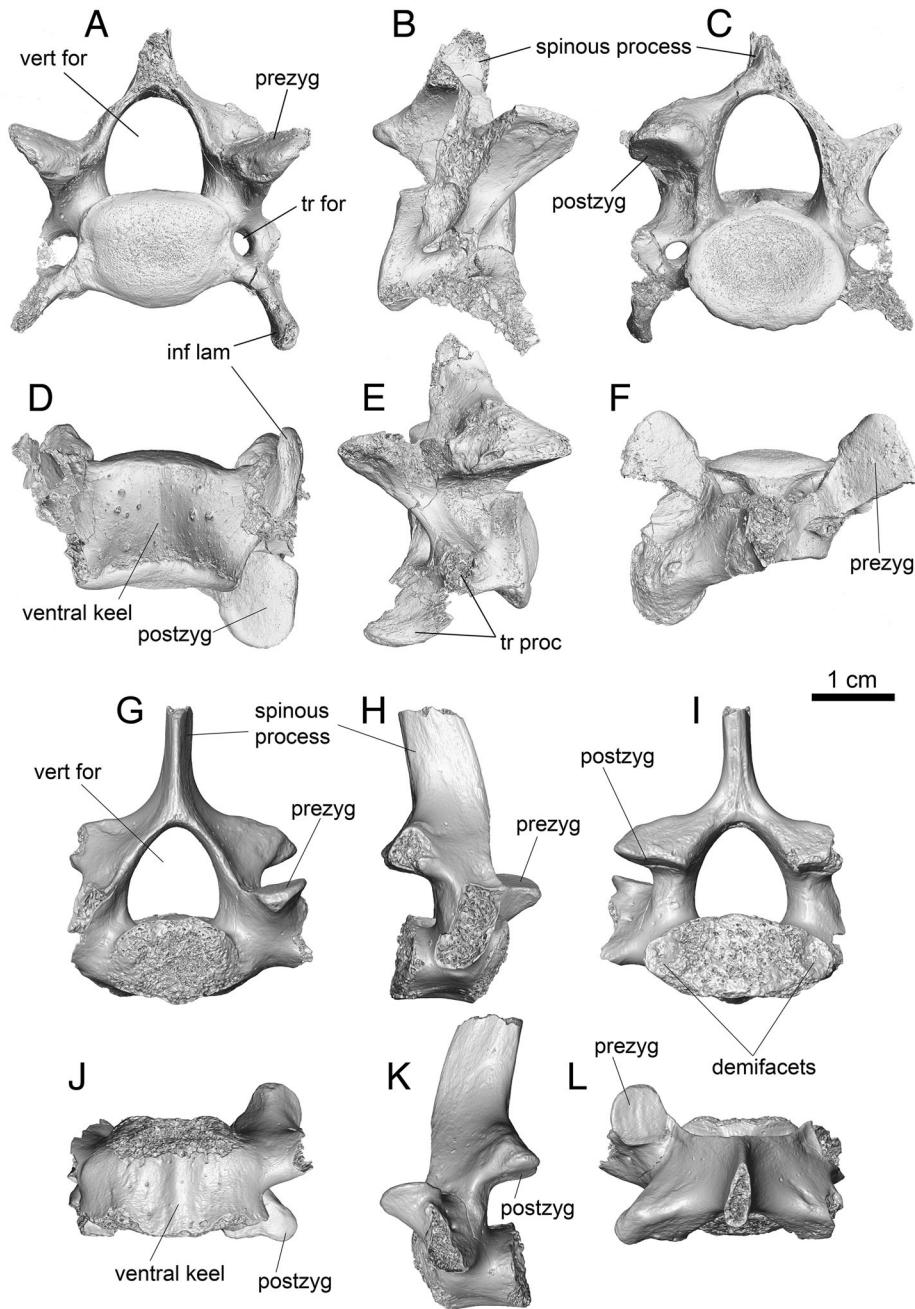
FIGURE 47. Cervical vertebrae of *Cambaytherium thewissi*, dorsal or cranial at top. **A–F**, C5, GU 775, in **A**, cranial, **B**, right lateral, **C**, caudal, **D**, ventral, **E**, left lateral, and **F**, dorsal views. **G–L**, C7/T1, GU 783, in **G**, cranial, **H**, right lateral, **I**, caudal, **J**, ventral, **K**, left lateral, and **L**, dorsal views. **Abbreviations**: **inf lam**, inferior lamella of transverse process; **postzyg**, postzygapophysis; **prezyg**, prezygapophysis; **tr for**, transverse foramen; **tr proc**, transverse process; **vert for**, vertebral foramen.

would verify that this is T1. The vertebral foramen is slightly smaller than in C5 and of similar shape. The centrum is larger cranially than caudally (cranial end measures 16.1 × 11.1 mm; caudal end ~13.2 × 10.3 mm; width = 22.7 mm including demifacets; length = 12.7 mm). The ventral keel is even weaker than on C5. The prezygapophyseal facet is flat, almost round, and faces dorsally and very slightly medially, the orientation being somewhat more like that of T1 than C7 in *Tapirus*. The postzygapophyseal facet is flat, much wider than long, and faces ventrally and slightly laterally. Both pre- and postzygapophyses resemble those of cervicals more than thoracics, which is also typical of T1 in *Equus*. The spinous process is prominent, anteroposteriorly longer than on C5, and tilts caudally.

Functional Morphology of Cervical Vertebrae—The cervical vertebrae of *Cambaytherium* are less craniocaudally elongate than those of *Equus*, indicating that *Cambaytherium* had a

relatively shorter neck. The vertebrae are more similar in proportions to those of *Hyracotherium* (Wood et al., 2011:fig. 1) and *Tapirus*. The well-developed and dorsally expanded axial neural spine suggests a strong and broad nuchal ligament for supporting the head. The centra are much flatter than in *Equus*, which has strongly opisthocoelous cervicals, and that of C5 is less trapezoidal in lateral view.

Thoracic Vertebrae—GU 790 and GU 791 can be identified as thoracics by their relatively short, stout, and spool-shaped centra, as well as the presence of demifacets for articulation with the rib heads. The articular ends of the centrum in GU 790 are weakly heart-shaped, and the narrower end (presumably anterior) preserves a demifacet, whereas no demifacets are evident caudally; hence, this appears to be the last thoracic vertebra. Its centrum is 17.8 mm long and measures 15.15 mm wide (16.6 mm including demifacet) × 13.2 mm high anteriorly and 17.4 mm wide × 12.7
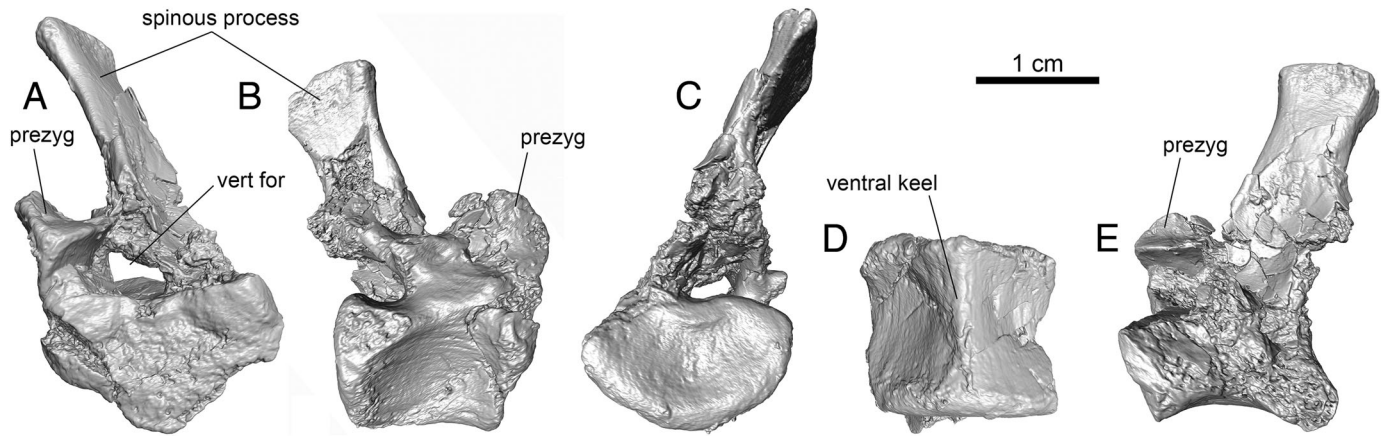
FIGURE 48. Thoracic vertebra of *Cambaytherium thewissi*, GU 788, in **A**, anterior, **B**, right lateral, **C**, posterior, **D**, ventral, and **E**, left lateral views. **Abbreviations**: **prezyg**, prezygapophysis; **vert for**, vertebral foramen.

mm high posteriorly. GU 791 preserves demifacets at both ends and is therefore a more proximal thoracic; its centrum measures approximately 16 mm long and 18 mm wide (including demifacets) × 14 mm high at the more complete end. Both centra have a ventral keel, slightly stronger in GU 790.

The only more complete thoracic is GU 788 (Fig. 48), although it is somewhat damaged and distorted. Like GU 790 and GU 791, its centrum is wider than high (the damaged anterior end measures approximately 13.9 mm wide × 10.7 mm high, length = 14.5 mm). The margins of the centrum are damaged, making it difficult to discern demifacets. The posterior endplate is reniform and measures 18.2 mm wide × 10.7 mm high. The zygapophyses are broken except for the right prezygapophysis, which is concave transversely (although less than in the lumbars) and faces dorsomedially. The spinous process is tall and thickened

dorsally but relatively short craniocaudally (craniocaudal length at midheight = 9.0 mm, at apex = 11.4 mm; height from roof of vertebral canal ~24 mm), and it does not taper toward the apex. Although it now inclines caudally, its orientation has clearly been altered by postmortem deformation. The morphology of the process (nontapering) most closely resembles vertebrae of *Hyracotherium*, particularly T16 (Wood et al., 2011:fig. 6), that are caudal to the anticlinal (i.e., with cranial inclination). As in the other two centra, there is a ventral keel. The orientation of the prezygapophyses, together with the absence of a transverse process and the near-vertical orientation of the neural spine, suggests that GU 788 is from the most posterior portion of the thoracic series, caudal to the diaphragmatic vertebra.

Lumbar Vertebrae—GU 789 and GU 8042 are isolated lumbar centra, but they add nothing that is not better preserved in GU

FIGURE 49. Lumbar vertebrae of *Cambaytherium thewissi*. **A–E**, GU 787 in **A**, cranial, **B**, left lateral, **C**, oblique caudal, **D**, caudal, and **E**, dorsocaudal views. **F–J**, GU 786 in **F**, cranial, **G**, oblique cranial, **H**, right lateral, **I**, caudal, and **J**, oblique craniodorsal views. **Abbreviations**: **prezyg**, prezygapophysis; **rev postzyg**, revolute postzygapophysis; **tr proc**, transverse process; **vent keel**, ventral keel; **vert for**, vertebral foramen.
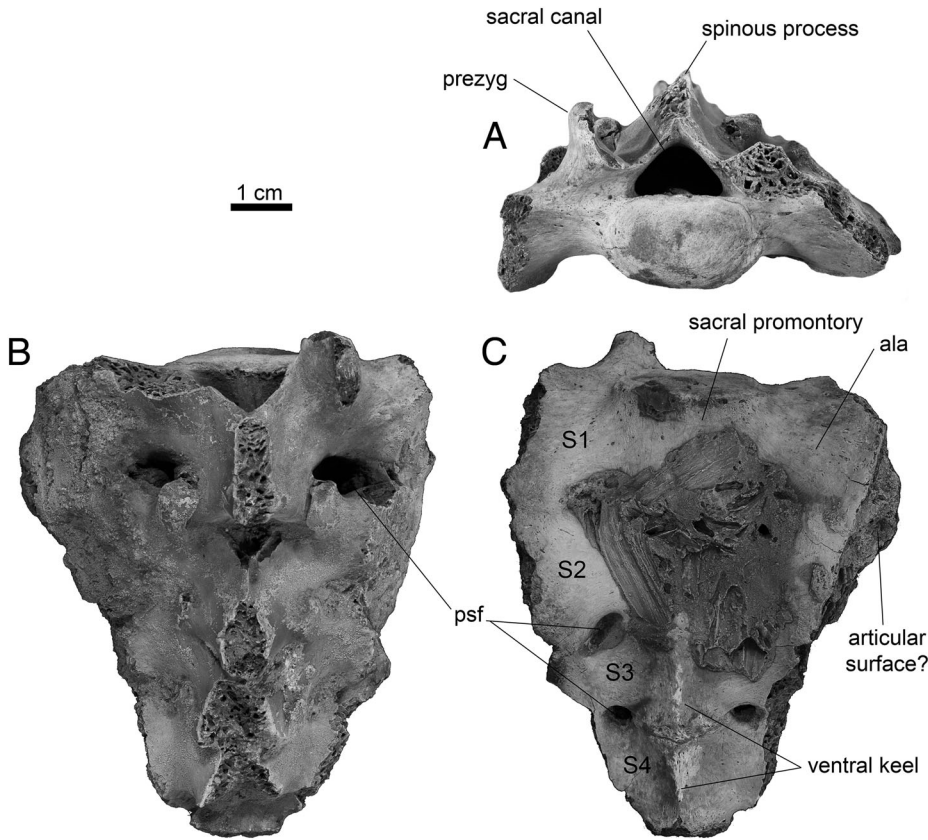
FIGURE 50. Sacrum tentatively referred to *Cambaytherium marinus*, GU 8001, in **A**, cranial, **B**, dorsal, and **C**, ventral views; digital photographs. **Abbreviations**: **prezyg**, prezygapophysis; **psf**, pelvic sacral foramina; **S1–S4**, sacral vertebrae 1–4.

786 and GU 787 (Fig. 49); hence, the following description is based on the latter two vertebrae. The centra of these two vertebrae are longer than those of the thoracics, about 10–30% wider than high. They are heart-shaped at the ends, and they bear a strong ventral keel. Neither vertebra has anapophyses.

GU 787 (Fig. 49A–E) preserves the neural arch, one prezygapophysis, and both postzygapophyses intact, but the spinous process is missing. Measurements of its centrum are: length = 18.6 mm; anterior 18.0 mm wide × 16.1 mm high; posterior 19 mm wide × 15.1 mm high. The prezygapophysis is transversely concave and relatively elongate. The postzygapophyses are cylindrical in posterior perspective and strongly revolute (i.e., the articular surface is sinuous in coronal section and is also described as 'embracing' or interlocking; Slipjer, 1946; Halpert et al., 1987; Zhou et al., 1992; Jones, 2015a), as in extant ruminants and *Hyracotherium* (Wood et al., 2011), but unlike the relatively flat or slightly convex postzygapophyses of *Phenacodus* and *Meniscotherium* (Otts, 1991; Williamson and Lucas, 1992). The spinous process is relatively long at the base but is broken away. Only stems of the transverse processes remain. They are about 60% as long (craniocaudally) at the base as the centrum and appear to have been essentially horizontal.

GU 786 (Fig. 49F–J) is interpreted as a more posterior lumbar. Its centrum dimensions are: length = 19.55 mm; anterior 16.1 mm wide × 13.3 mm high; posterior 16.6 mm wide × 13.1 mm high; spinous process ~12.3 mm long (craniocaudally) at the base, height 22.9 mm from the roof of the vertebral canal. It is similar to GU 787 but has a slightly longer centrum that is smaller in diameter (presumably because it represents a smaller individual). The left prezygapophysis is nearly complete, showing the strongly concave, embracing articular surface. The postzygapophyses are similar to those of GU 787—strongly revolute and interlocking

but more widely spaced, implying a position near the caudal end of the lumbar series. The transverse processes are nearly horizontal and craniocaudally elongate, and they project laterally and perhaps very slightly caudally rather than cranially. The spinous process is moderately long (craniocaudally) at its base, slightly longer than in the thoracic vertebra (GU 788), but it expands substantially toward the apex, which is transversely thickened along its length and somewhat swollen anteriorly, for attachment of the supraspinous ligament. The process inclines very slightly craniad. It is more elongate and more nearly vertical than in *Hyracotherium* or *Phenacodus* and in shape resembles that of *Tapirus*.

Functional Morphology of Posterior Thoracic and Lumbar Vertebrae—The postdiaphragmatic zygapophyseal joints in *Cambaytherium* resemble neither the buttressed morphology of *Equus* and *Tapirus* (i.e., inclined but nearly flat and tightly interlocking) nor the planar morphology of *Phenacodus*. Instead, they most closely resemble the embracing morphology of modern artiodactyls, which is shared with *Hyracotherium* (Wood et al., 2011) and several other archaic ungulate groups (e.g., mesonychids, creodonts, arctocyonids; Wortman, 1894; Slipjer, 1946; Zhou et al., 1992; Argot, 2012). The chalicothere *Moropus elatus* displays an intermediate condition, exhibiting mostly planar joints but with slight curvature toward the posterior lumbars (Holland and Peterson, 1914). Thus, the evolution of zygapophyseal morphology in perissodactyls is complex, but the strong development of sigmoid-revolute joints in *Cambaytherium* and *Hyracotherium* suggests that this may be the ancestral condition for perissodactylamorphs, which was subsequently lost in more derived taxa. Interlocking joints of this nature have been suggested to restrict both sagittal motion and torsion in the posterior spine (Halpert et al., 1987; Boszczyk et al., 2001; Jones, 2015a) and imply the origin of lumbar stability very early in the

FIGURE 51. Caudal vertebra of *Cambaytherium thewissi*, GU 824, in **A**, cranial, **B**, right lateral, **C**, caudal, **D**, ventral, **E**, left lateral, and **F**, dorsal views. Cranial to top in **D** and **F**. **Abbreviations**: **hem proc**, hemal processes; **postzyg**, postzygapophysis (broken); **prezyg**, prezygapophysis (broken); **tr proc ant**, anterior transverse process; **tr proc post**, posterior transverse process; **vert canal**, vertebral canal.

evolution of perissodactyls. Interestingly, in comparison with *Cambaytherium*, the muscular processes (transverse, spinous) of *Hyracotherium* seem to be longer, slenderer, and more inclined and the zygapophyseal curvature less pronounced (not forming a full sigmoid shape), suggesting perhaps relatively more mobility in this taxon. In contrast, the robust, craniocaudally long, and mediolaterally thickened neural spine tip on the posterior lumbar vertebra of *Cambaytherium* suggests well-developed interspinous and supraspinous ligaments, which would presumably strongly restrict ventroflexion, whereas the distinct ventral keel on the centra implies a well-developed ventral longitudinal ligament to limit dorsiflexion (Koob and Long, 2000; Jones, 2015b). Thus, the morphology of the postdiaphragmatic vertebrae of *Cambaytherium* suggests a relatively stabilized lumbar region, typical of species that utilize transverse footfall patterns during asymmetrical gaits (Hildebrand, 1959; Bertram and Gutmann, 2009; Jones, 2016).

Sacrum—A relatively large sacrum (GU 8001; Fig. 50) from Vastan Mine is too large to represent *C. thewissi* and may belong to *C. marinus*. No other mammal larger than *C. thewissi* has been found at Vastan Mine. Maximum dimensions of the sacrum as preserved are: about 70 mm wide across the alae, 84 mm long; S1 centrum 27.0 mm wide × 16.2 mm high; S4 centrum ~15.6 mm wide × 9.6 mm high. It consists of four solidly fused vertebrae. In comparison, the sacrum of *Phenacodus* has three (*P. vortmani*) or four (*P. trilobatus*) vertebrae (Osborn, 1898; Otts, 1991), that of *Meniscotherium* has four (Gazin, 1965), and that of *Hyracotherium* has five (Wood et al., 2011).

The cranial end of S1 in GU 8001 lacks lateral accessory articulations (lateral joints) between the transverse processes. These joints are present at the last one or two presacral joints in extant perissodactyls (Jones and Holbrook, 2016), but they are absent from several extinct perissodactyls (*Hyracotherium*, brontotheres, and chalicotheres), as well as *Phenacodus*. Their absence in *Cambaytherium* and *Hyracotherium* supports the hypothesis that lateral joints are not ancestral for Perissodactyla, instead arising multiple times within the group, possibly linked to increasing thoracolumbar count.

The centrum of S1 is more strongly elliptical (width/height = 1.67) than that of the preserved lumbar vertebrae. Dorsal to the centrum is the triangular sacral canal, and extending from its

apex is the spinous process. Although only its base remains, it is separate from the successive sacral spines (again represented only by their bases), which appear to have fused into a median sacral crest. Lateral to the sacral canal on the right side is a prominent concave prezygapophysis (broken on the left). Successive zygapophyses are much smaller and fused, and they do not form an obvious crest. The transverse processes (alae) of S1 are broad and transversely concave on the ventral face. The auricular surface is poorly preserved and partly covered by iron deposit, but it appears to occupy the lateral side of both S1 and S2 and is apparently larger than in *Hyracotherium* in which it is largely restricted to S1. Three paired pelvic sacral foramina are evident, as well as small paired notches at the caudal end of S4. Dorsally, only the first pair of sacral foramina is obvious, the others obscured by ironstone. The ventral surface of S3 and S4 has a distinct ventral keel.

Caudal Vertebrae—Five caudal vertebrae are tentatively referred to *C. thewissi* based on their size and overall similar morphology. All consist of relatively simple, elongate, cylindrical centra. Based on their length and greatly reduced processes, all appear to be distal caudals, although GU 824 may be from the transitional region (Youlatos, 2003). GU 824, GU 825a, and GU 8017 preserve remnants of a minimally developed neural arch enclosing a very small vertebral canal (≤1.0 mm in diameter); the other two caudals have no neural arch or canal. The centrum in all five is either round or slightly elliptical at the ends.

GU 824 (Fig. 51) has the largest diameter and largest zygapophyses (although they are broken at both ends); therefore, it is the most proximal caudal of those preserved. The neural arch bears a low median spine along its entire length. Small, knoblike anterior transverse processes are present lateral to the broken prezygapophyses. They are connected by a low, longitudinal crest to wing-like posterior transverse processes that widen caudally and end in a small, posteriorly projecting tubercle. The central constriction between the anterior and posterior transverse processes gives the vertebra a waisted appearance. Parallel to the longitudinal crest is a weaker crest extending posteriorly from the prezygapophyses. At the anterior base of the centrum are a pair of small hemal processes, from which extend crests (keels) that run the length of the ventral surface of the centrum but are stronger and thicker posteriorly. GU 8017 (Fig. 52A–F) has a slightly
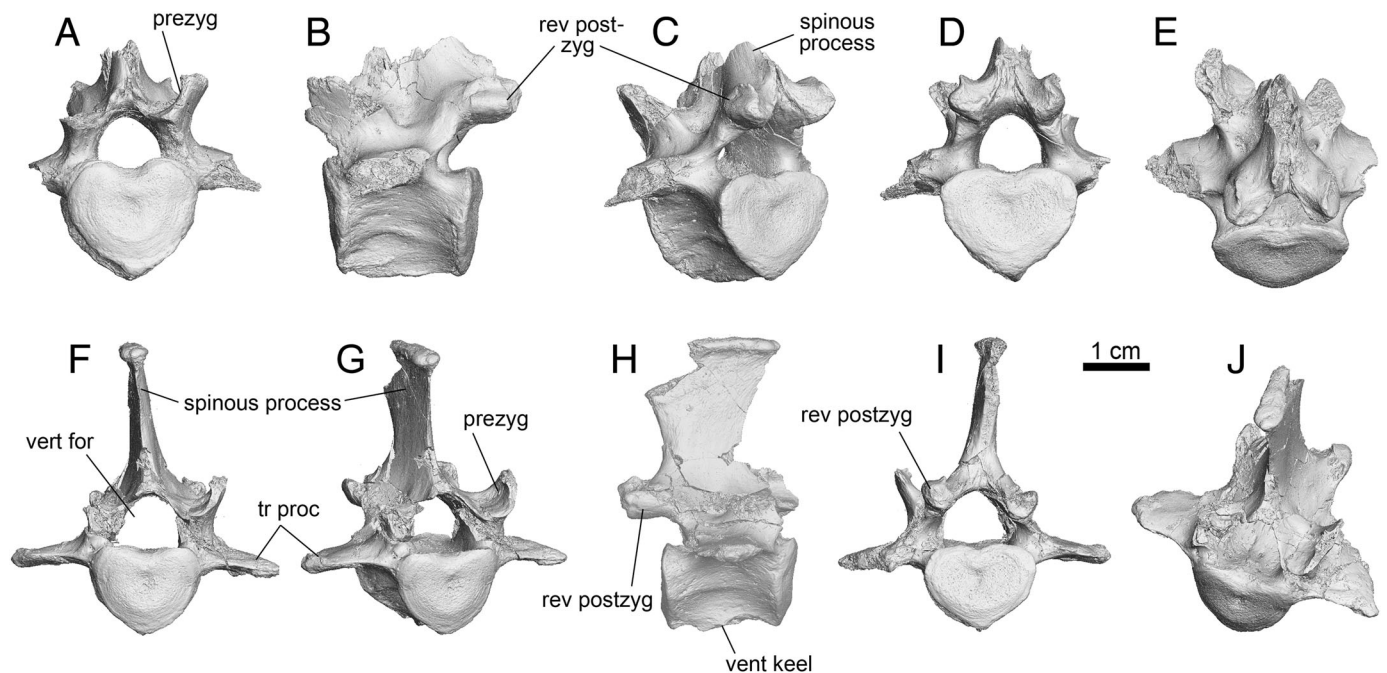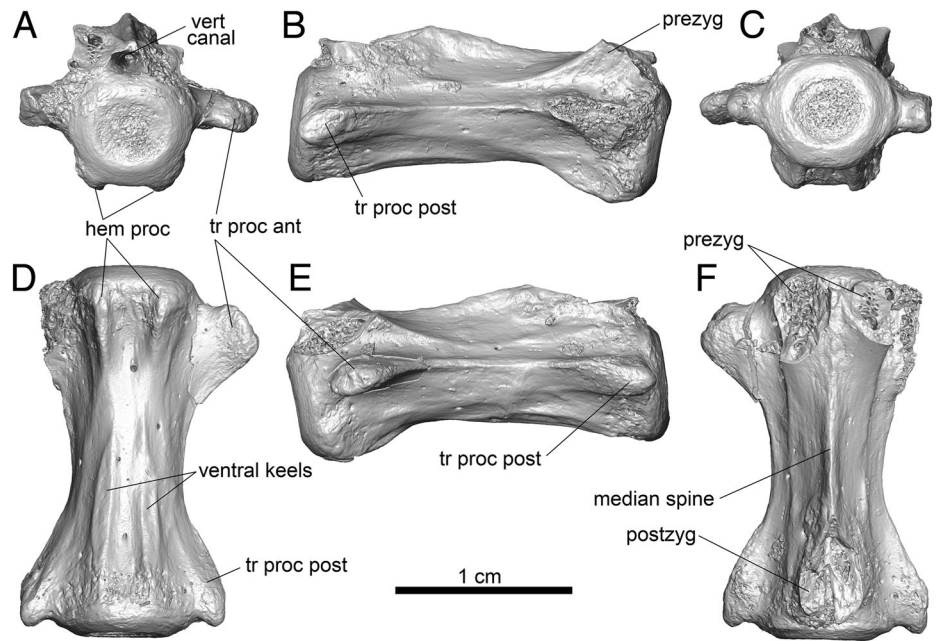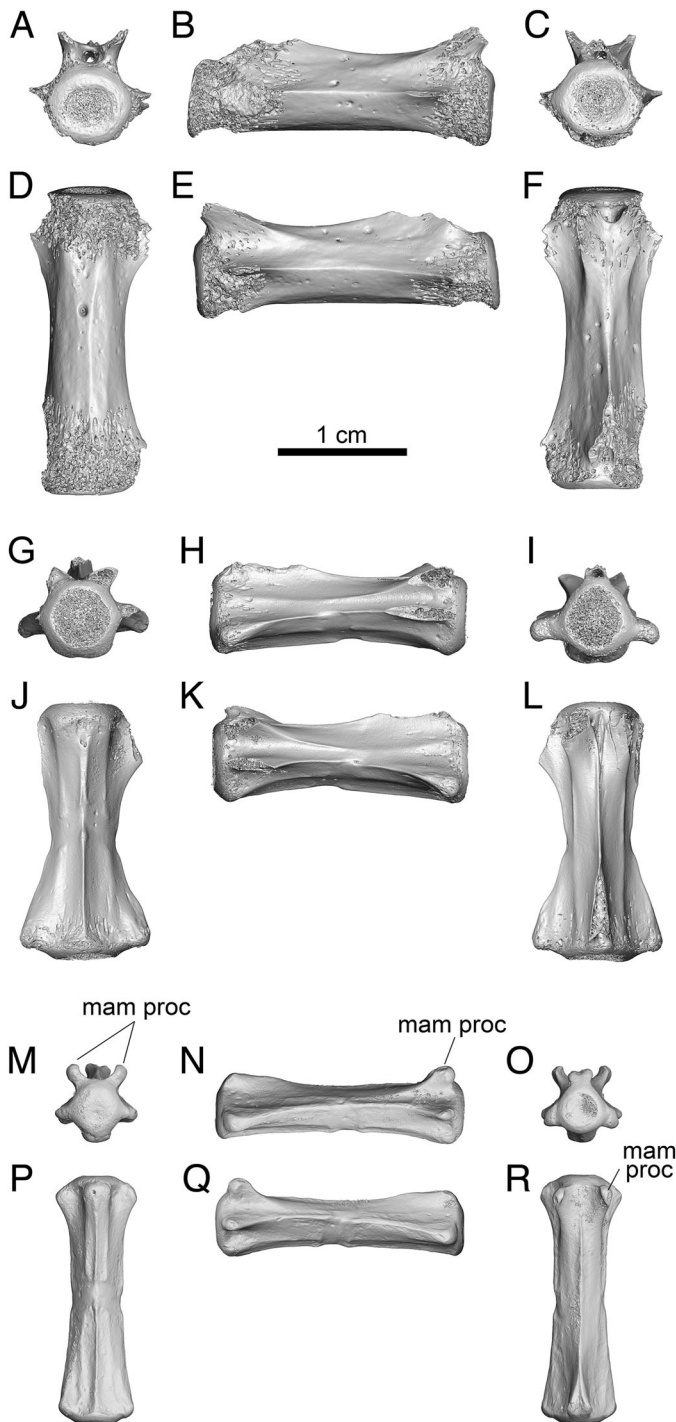
FIGURE 52. Caudal vertebrae of *Cambaytherium thewissi*. **A–F**, GU 8017 in **A**, cranial, **B**, right lateral, **C**, caudal, **D**, ventral, **E**, left lateral, and **F**, dorsal views. **G–L**, GU 825a in **G**, cranial, **H**, right lateral, **I**, caudal, **J**, ventral, **K**, left lateral, and **L**, dorsal views. **M–R**, GU 825b in **M**, cranial, **N**, right lateral, **O**, caudal, **P**, ventral, **Q**, left lateral, and **R**, dorsal views. **Abbreviation**: **mam proc**, mammillary process.

those of GU 824 except on the ventral aspect, where the hemal processes are further reduced and only a single median keel is present. On each side, midway between the keel and the crest joining the transverse processes is a low but distinct longitudinal crest (very weakly developed in GU 824), broken bilaterally by a faint groove that also crosses the ventral keel. This groove is also present on GU 825b (Fig. 52M–R) and GU 825c and is very faintly developed in GU 824. GU 825b and GU 825c are slightly smaller versions of GU 825a, in which the anterior articular processes are further reduced.

From the few preserved caudals, it is not possible to make a definitive statement regarding length or robustness of the tail in *Cambaytherium*, but these specimens allow some tentative remarks. The known caudals seem to be relatively less robust than those of *Phenacodus trilobatus* (Osborn, 1898) and more robust than the tail as conventionally restored in *Hyracotherium* (e.g., Wood et al., 2011:fig. 1), suggesting a tail of intermediate length.

Dimensions of the caudal vertebrae are provided in Table 8.

Sternum and Ribs

Two rectangular sternal segments (GU 7010 from Mangrol, GU 8045 from Vastan) are tentatively assigned to *Cambaytherium thewissi* based on size. Both are elongate and mediolaterally narrow, but wider dorsally than ventrally. They are consequently trapezoidal in cross-section and therefore are probably posterior sternebrae. GU 7010 is dorsoventrally deeper than it is wide at midlength, whereas GU 8045 (abraded at the ends) is wider than deep. Measurements (in mm) of the two bones: GU 7010 length = 20.35, depth = 10.1, width = 9.4, both measured at midlength; GU 8045 length = 18.9, depth = 9.0, width = 10.8.

Several rib fragments from Vastan and Tadkeshwar mines might belong to *Cambaytherium* based on their size. The most complete specimen (GU 9515; Smith et al., 2016:fig. 17) measures about 25 cm long and is somewhat flattened but otherwise not distinctive. This rib appears to be too small and gracile to go with the possible pantodont reported from Tadkeshwar Mine, which is the only other large mammal known from that assemblage.

Forelimb

Scapula—Three fragments of the distal (glenoid) portion are known: GU 820 (Fig. 53), GU 1213, and GU 9214. GU 820 is about 13% larger than GU 1213, whereas GU 9214 (TAD-2) is slightly larger than GU 1213; these minor size differences are considered to represent intraspecific variation or sexual dimorphism. The glenoid cavity is pyriform, shallow, and about 30% longer than wide (diameters [mm] of GU 820 = 25.4 × 19.4; GU 1213 = 22.5 × 17.1; GU 9214 = 23.8 × 17.2), its lateral border expanding out slightly more than the medial border. Thus, the glenoid is relatively narrower than in *Hyracotherium grangeri* (~24% longer than wide based on measurements in Wood et al., 2011).

The superior (cranial) margin of the glenoid cavity in GU 820 forms a slightly projecting, beak-like process approximating that in *Canis* and more pronounced than that in *Homo*. In some mammals, including *Canis* and *Homo*, this process is considered the supraglenoid tubercle, from which the long head of m. biceps brachii originates (Evans and Christensen, 1979; Williams, 1995). The shoulder joint is modified in *Equus*, in which the biceps brachii has only a single belly and has become part of a 'passive stay-apparatus' associated with habitual standing (Hermanson and MacFadden, 1992). Related to this specialization, the supraglenoid tubercle in *Equus* is enlarged, craniodorsally shifted compared with that in *Canis*, and separated from the glenoid rim. This shoulder modification evolved relatively late in equid evolution, but an enlarged supraglenoid tubercle that may have promoted the adaptation is present in *Mesohippus* and

smaller but longer centrum. The prezygapophyses are largely intact but greatly reduced, and articular facets are not evident. Other details, as far as they are preserved, appear to be similar to GU 824. GU 825a (Fig. 52G–L) is smaller in diameter than GU 824 but only slightly shorter. Its features are very similar to

TABLE 8. Dimensions (in mm) of caudal vertebrae of *Cambaytherium thewissi*.

Specimen no.	Length	Ant cent m-l diameter	Ant cent dv diameter	Post cent m-l diameter	Post cent dv diameter	Ant max m-l breadth	Post max m-l breadth
GU 824	20.7	6.5	6.3	7.0	6.3	~14.8	11.3
GU 825a	19.5	6.2	5.9	5.0	5.6	—	9.7
GU 825b	18.9	3.5	3.8	3.4	3.5	6.1	5.7
GU 825c	—	4.5	4.7	—	—	9.4	—
GU 8017	23.8	6.2	5.9	6.5	6.1	—	—

Abbreviations: **ant**, anterior; **cent**, centrum; **dv**, dorsoventral; **max**, maximum; **m-l**, mediolateral; **post**, posterior.
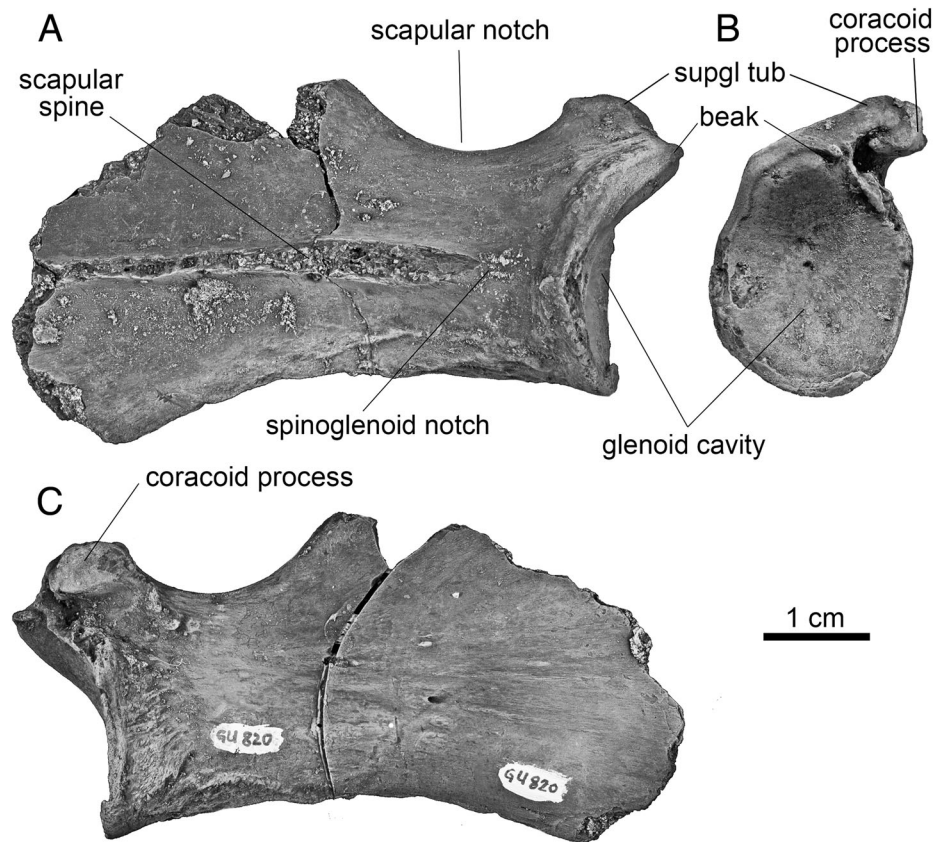
FIGURE 53. Right scapular fragment of *Cambaytherium thewissi*, GU 820, in **A**, lateral, **B**, distal, and **C**, medial views, digital photographs. **Abbreviations**: **beak**, beak-like process of glenoid rim; **supgl tub**, supraglenoid tubercle.

Tapirus (Hermanson and MacFadden, 1992), suggesting that it could be plesiomorphic for perissodactyls. A rugose surface on the lateral side of the coracoid process, extending to the beak-like process on the glenoid margin in GU 820, suggests similar expansion of the supraglenoid tubercle in *Cambaytherium* and reflects a well-developed biceps brachii muscle.

A prominent, blunt coracoid process is present on GU 820 and GU 9214 but is best preserved on GU 820. Both the tubercle and the process are evidently larger than in *Hyracotherium* (Kitts, 1956; Wood et al., 2011) but slightly smaller and less projecting than in *Phenacodus* (USGS 7146, USGS 38504), which is otherwise similar. The coracoid is separated from the cranial border of the scapula by a conspicuous scapular notch. The scapular spine and acromion are broken in all three specimens, but the preserved portion indicates a relatively thin, moderately elevated spine with a distinct spinoglenoid (great scapular) notch (see Williams, 1995), well separated from the glenoid cavity. Although incomplete, what is preserved in GU 820 suggests that the supraspinous fossa was slightly wider than the infraspinous fossa. If accurate, this would be a resemblance to *Hyracotherium* but not to *Equus*.

Humerus—We assign 11 incomplete humeri to *Cambaytherium*: GU 270, GU 737, GU 738, GU 778, GU 809, GU 834, GU 1211, GU 1214, GU 7006, GU 9018, and WIF/A 4262 (Fig. 54). All except the last three are from Vastan Mine and represent *C. thewissi*. GU 7006, from Mangrol Mine, is essentially identical to specimens from Vastan and also belongs to *C. thewissi*. The other two incomplete specimens are from the higher level at Tadkeshwar (TAD-2). Both of these specimens consist of the shaft without the articular ends, and both differ in some features from the Vastan humeri, as indicated below. Nevertheless, no other ungulate species of appropriate size are known from Tadkeshwar, so they are tentatively referred to *Cambaytherium*. Based on size differences, WIF/A 4262 is questionably assigned to *C. thewissi*, and GU 9018 is tentatively assigned to *C. gracilis*.

The humerus of *C. thewissi* shows a mosaic of primitive and derived traits that are more or less intermediate between those of archaic ungulates such as *Phenacodus* and basal perissodactyls. It is relatively more robust than humeri of *Hyracotherium* and *Homogalax*, as judged by relatively larger articular ends and shafts with greater caliber, although it was probably similar in
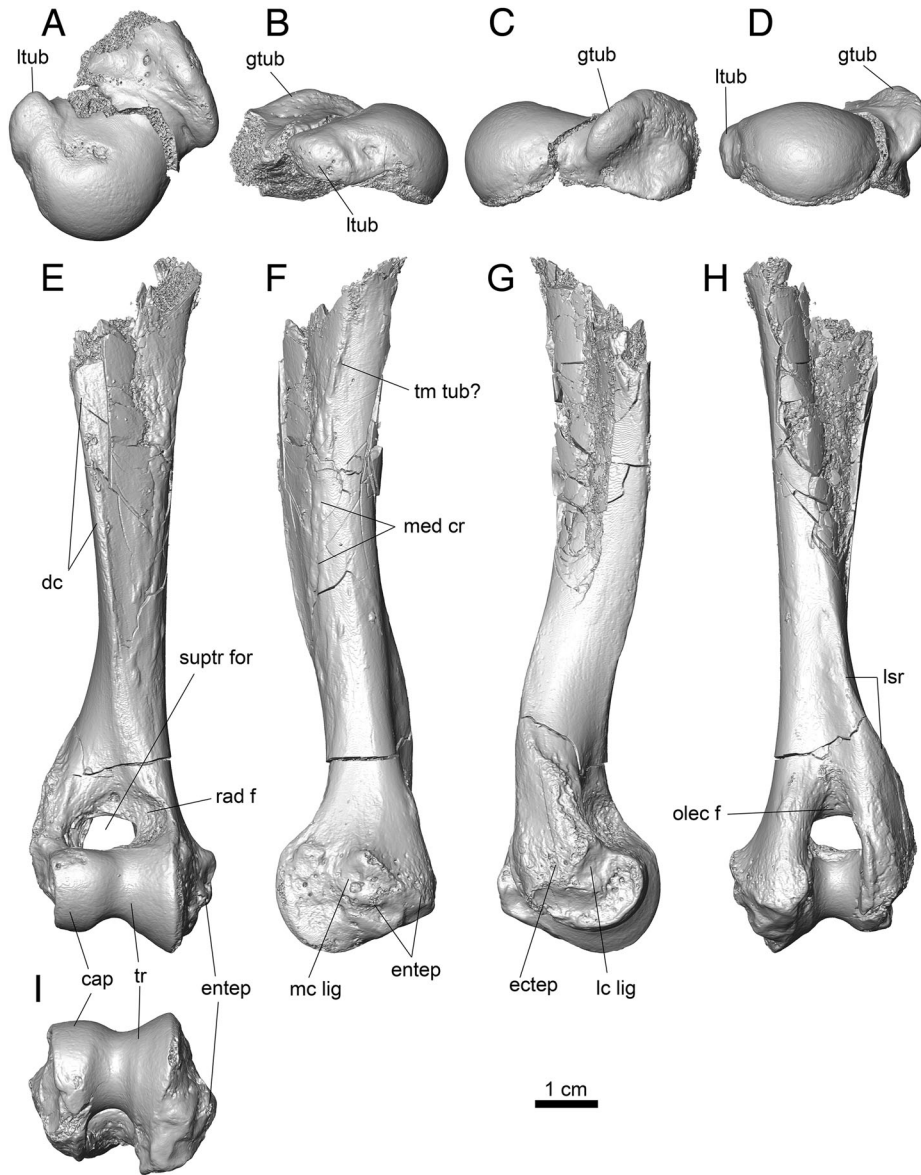
FIGURE 54. Right humerus of *Cambaytherium thewissi*. **A–D**, proximal epiphysis, GU 809, in **A**, proximal (superior), **B**, medial, **C**, lateral, and **D**, posterior (caudal) views. **E–I**, distal humerus, GU 834, in **E**, anterior (cranial), **F**, medial, **G**, lateral, **H**, posterior (caudal), and **I**, distal views. Approximate humeral length is indicated by position of proximal epiphysis in **B–D** relative to distal portion (**F–H**), based on damaged proximal end of GU 834. **Abbreviations**: **cap**, capitulum; **dc**, deltoid crest; **ectep**, ectepicondyle; **entep**, entepicondyle; **gtub**, greater tubercle; **lc lig**, fossa for lateral collateral ligament; **lsr**, lateral supracondylar ridge; **ltub**, lesser tubercle; **mc lig**, fossa for medial collateral ligament; **med cr**, medial crest; **ol f**, olecranon fossa; **rad f**, radial fossa; **suptr for**, supratrochlear foramen; **tm tub**, teres major tubercle; **tr**, trochlea.

TABLE 9. Humerus dimensions (in mm) in *Cambaytherium* and comparative taxa.

Specimen no.	Taxon	A	B	C	D	E	F	G	H
GU 270	*C. thewissi*			31.20	20.00	24.00	13.10	11.10	9.00
GU 737	*C. thewissi*	23.00	18.35	31.35	21.60	24.20	13.00	11.25	10.10
GU 738	*C. thewissi*				19.45		12.50	9.15	9.00
GU 778	*C. thewissi*	22.30	18.00		21.50	21.80	12.0e	10.40	10.60
GU 809	*C. thewissi*	22.50	17.25e						
GU 834	*C. thewissi*	25.60	17.0e	29.75	20.80	25.70	12.20	9.90	10.00
GU 1211	*C. thewissi*			33.20	23.40	26.55	14.15	11.00	11.50
GU 1214	*C. thewissi*	23.20	18.40						
GU 7006	*C. thewissi*			28.20	21.20	25.95	12.20	10.50	9.90
USGS 25032	*Homogalax*	18.30	16.80	26.10	14.4/17.6[1]	16.15	9.45	10.25/7.3[2]	6.80
USGS 7159	*Phen. vortmani*	17.50	18.0e	24.45	15.80	15.70	10.05	9.30	6.60
USGS 25169	*Phen. trilobatus*	33.00	30.00						
USNM 510890	*Phen. trilobatus*	36.00	30.00						
USNM 527728	*Phen. trilobatus*			58.60	35.50	33.25	22.25	21.30	14.70

A: head width; **B**: greatest head length measured proximodistally; **C**: maximum distal width; **D**: distal articular width measured anteriorly; **E**: maximum distal depth; **F**: trochlear groove anteroposterior dimension; **G**: capitular width measured anteriorly, to the depth of the trochlear groove; **H**: trochlear width measured anteriorly, to the depth of the trochlear groove. **Abbreviations**: **e**, estimated; ***Phen***, *Phenacodus*.
[1]Includes capitular tail.
[2]Capitular width with/without capitular tail.

length to that of *Homogalax* (see below). Moreover, it has a distinct deltopectoral crest that extends distally almost to the radial fossa, as in *Phenacodus* (e.g., USGS 7159, *P. vortmani*; USNM 527728, *P. trilobatus*) and in contrast to the greatly reduced crest in basal perissodactyls. This morphology is corroborated in all seven Vastan and Mangrol specimens that preserve the distal end, whereas the two Tadkeshwar specimens have shorter deltopectoral crests that extend just beyond midshaft. The crests in the Tadkeshwar bones are otherwise similar in expression to those of Vastan *C. thewissi* and are conspicuously better developed than in basal perissodactyls. The lateral supracondylar ridge of *C. thewissi* is more prominent and rugose than in basal perissodactyls, and the distal articulation is wider than in perissodactyls.

Although no complete humeri are known, a close estimate of humeral length can be attained by comparing the available partial humeri. GU 834 includes both ends of the bone that almost join at a break near the proximal end. The shaft is crushed at that point, but preserved matching edges suggest that little of the bone is missing and indicate a total articular length of ~130 mm (and almost certainly not more than 10% longer), which is slightly longer than the humerus of *Homogalax protapirinus* and about 15% longer than that of *Phenacodus vortmani* (Rose, 1996). Approximate midshaft maximum diameter (oriented obliquely anterolateral to posteromedial owing to the orientation of the deltopectoral crest) and minimum diameter in GU 834 are 17.2 and 9.5 mm, respectively, indicating a distinctly greater anteroposterior than mediolateral dimension, as in *Phenacodus* and basal perissodactyls. Although distortion of GU 834 probably exaggerates the difference in diameters, other specimens confirm a proportional difference similar to that of *Phenacodus* and *Homogalax* (see below). Midshaft area compared with length provides an estimate of robustness: area/length in GU 834 is ~1.26 and in GU 738 ~1.04. The humeral shaft referred to *C. gracilis* measures just under 80 mm and suggests a complete element approximately 100 mm in length. Its maximum and minimum midshaft diameters are 9.95 and 8.65 mm, and a rough estimate of its midshaft area/length is ~0.86, relatively more gracile than *C. thewissi*. Direct comparison between *Homogalax protapirinus* (USGS 25032) and *Phenacodus vortmani* (USGS 7159) (Rose et al., 2014b:fig. 4), in which the articular ends are very close in size, reveals that the humerus of *Homogalax* is longer and more slender: length = 132 mm, midshaft diameters = 11.4 mm (anteroposterior) × 7.4 mm (mediolateral), midshaft area/length = 0.64 in *Homogalax*, vs. length = 115 mm, midshaft diameters = 14.0 mm (anteroposterior) × 10.2 mm (mediolateral), midshaft area/length = 1.24 in *Phenacodus*. *Hyracotherium grangeri* (Wood et al., 2011) is more robust than *Homogalax* but more gracile than *Phenacodus*: length = 99 mm, midshaft diameters = 11.3 mm (anteroposterior) × 8.9 mm (mediolateral), midshaft area/length = 1.02. Thus, the limited evidence at hand suggests that *C. thewissi* had a relatively more robust humeral shaft than in basal perissodactyls, whereas the single humeral shaft attributed to *C. gracilis* (GU 9018) was closer in length and robustness to that of *Hyracotherium grangeri* (Wood et al., 2011).

The proximal end of the humerus is preserved in five specimens but is damaged in all of them. Most nearly complete is GU 809 (Fig. 54A–D), a proximal epiphysis preserving the complete articular head and both tubercles almost intact. The head is subspherical, about 30% wider mediolaterally than long (Table 9). The humeral head of phenacodontids (except *P. vortmani*, USGS 7159, which is possibly distorted) and basal perissodactyls is also relatively wider than long. The greater tubercle in *C. thewissi* is a prominent, elevated ridge, mediolaterally compressed and anteroposteriorly elongate with a convex superior margin. It projects superiorly above the head (although not appreciably), as in both *Phenacodus* and basal perissodactyls. Muscle scars are not well defined on the greater tubercle, GU

737 and GU 809 showing only a shallow depression where the infraspinatus and/or teres minor muscles would have inserted, in contrast to the distinct fossa present in both *Phenacodus* (USGS 7159) and *Hyracotherium* (Wood et al., 2011). The lesser tubercle, for insertion of the subscapularis muscle, is a low rugosity on the medial side of the head, its long axis a little more horizontal than in *Phenacodus* and *Homogalax* and more like *Hyracotherium* in this regard. Because of damage to all specimens, the width of the bicipital groove cannot be accurately judged, although it seems to have been rather wide.

The principal surface feature of the humeral shaft is the deltopectoral crest, a slightly elevated, narrow ridge that extends most of the length of the shaft. In GU 9018 (*C. gracilis*), the crest is weaker and less elevated than that of *C. thewissi*. No discrete deltoid tubercle is evident in the Vastan and Mangrol specimens of *C. thewissi*, although there is a slight thickening of the crest near the distal end. Along much of the medial border of GU 834 (Fig. 54F), apparently extending from below the lesser tubercle (posteromedially) anteriorly almost to the end of the deltoid crest, is a low medial crest for muscle attachment (probably at least partly associated with pectoral muscles). A slight thickening proximal to midshaft may indicate attachment of the teres major and latissimus dorsi muscles. WIF/A 4262, from TAD-2, differs from other specimens in having a sharp, weakly sinuous deltoid crest with a more prominent, slightly laterally deflected portion estimated to be about one-third of total humeral length from the proximal end (missing in this specimen), which resembles the deltoid tubercle in *Canis* (Evans and Christensen, 1979). On the medial border, opposite this tubercle, is a similar, posteriorly deflected crest, stronger than in GU 834, that probably marks the insertion of m. teres major. This part of the shaft is not preserved on any other *C. thewissi* humerus. A similar but less prominent feature is present in *Phenacodus vortmani* (USGS 7159), but a distinct teres tubercle is not evident on any early perissodactyl humeri available to us.

The distal end of the humerus of *C. thewissi* is derived, as in perissodactyls, in lacking an entepicondylar foramen (retained in condylarths, including *Phenacodus*) and in having a more posteriorly and less medially projecting entepicondyle, a relatively narrower capitulum and wider trochlea, and a craniocaudally longer (deeper) distal articulation. The capitulum is more mediolaterally compressed than in *Phenacodus* but less so than in *Hyracotherium*, *Homogalax*, and *Heptodon* (Radinsky, 1965a; Rose, 1996:pl. 1; Wood et al., 2011). In most specimens, it is more cylindrical (i.e., rounded anteroposteriorly but mediolaterally nearly flat; Fig. 54E, I) than spherical, but GU 737 has a more rounded mediolateral profile approaching that of *Phenacodus*. In contrast to early perissodactyls, there is no capitular tail (i.e., lateral articular surface); hence, in anterior view, the capitulum and trochlea are about equal in width (comparable to capitular width in early perissodactyls if the capitular tail is excluded). In *Phenacodus*, however, the capitulum is wider than the trochlea, even though there is no capitular tail or only the most rudimentary expression of this feature. In *Cambaytherium*, a deep trochlear groove separates the capitulum from the conical trochlea with its prominent, steep, distally projecting medial rim. The extent of distal projection beyond the capitulum approximates that in *Phenacodus* and exceeds that in early perissodactyls, although *Homogalax* comes close. Proximal to the distal articulation, as in cursorial ungulates generally, the coronoid fossa (proximal to the trochlea) and the radial fossa (proximal to the capitulum) have coalesced to form a moderately deep radial fossa (Getty, 1975; Evans and Christensen, 1979) pierced by a large supratrochlear foramen that opens posteriorly into the deep olecranon fossa. This anatomy enhanced antebrachial extension. The ectepicondyle, which provides origin for the manual and digital extensor muscles, is comparable in size to that in *Phenacodus* and basal perissodactyls, and muscle and
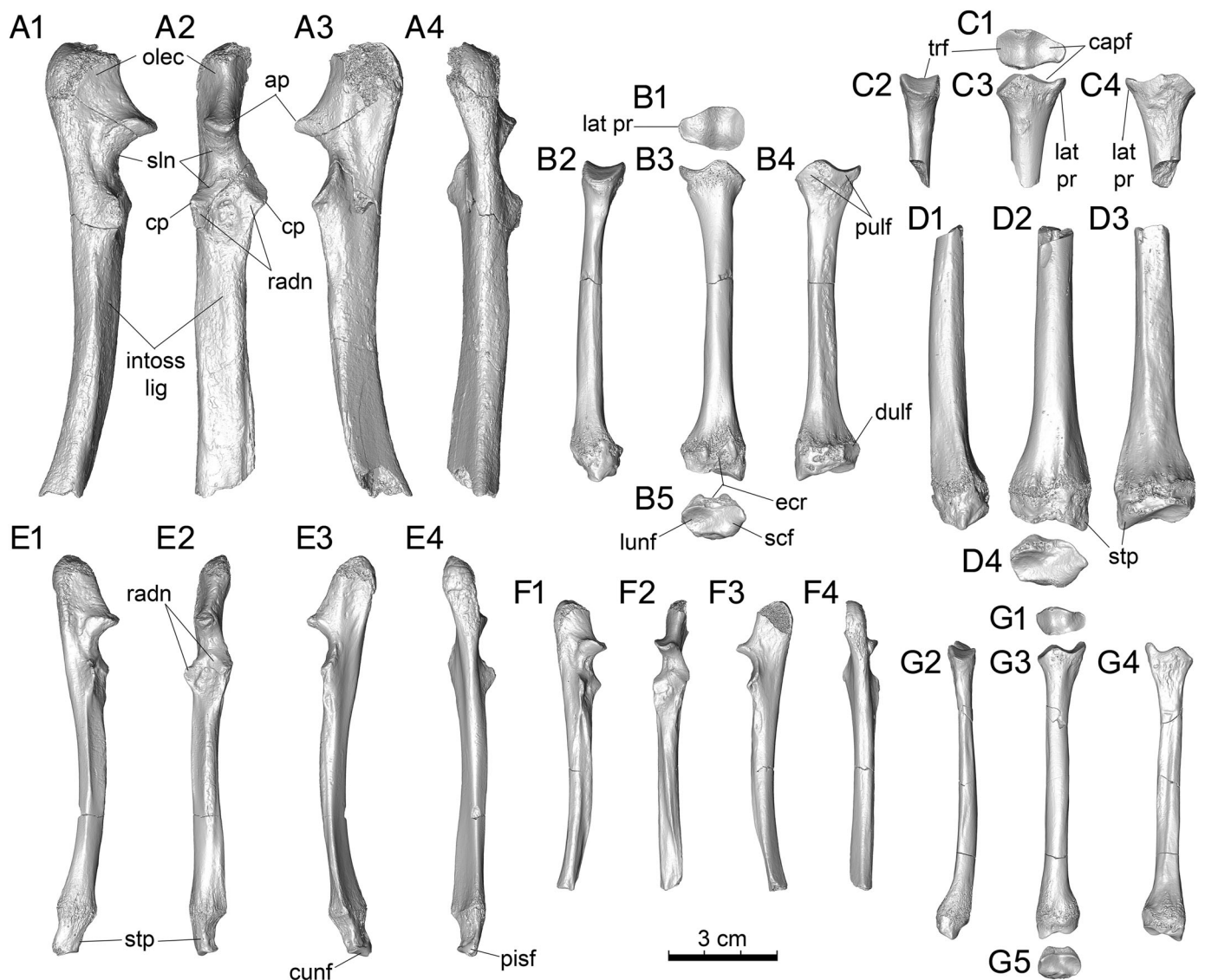
FIGURE 55. Ulna and radius of *Cambaytherium*, all to the same scale. **A–D**, *C. thewissi*: **A**, proximal right ulna, GU 7005, in **A1**, lateral, **A2**, anterior, **A3**, medial, and **A4**, posterior views; **B**, right radius, GU 274, in **B1**, proximal, **B2**, medial, **B3**, anterior, **B4**, posterior, and **B5**, distal views; **C**, proximal left radius, GU 842, in **C1**, proximal, **C2**, medial, **C3**, anterior, and **C4**, posterior views; **D**, distal right radius, GU 7019, in **D1**, medial, **D2**, anterior, **D3**, posterior, and **D4**, distal views. **E–G**, *C. gracilis*: **E**, right ulna, WIF/A 4208, in **E1**, lateral, **E2**, anterior, **E3**, medial, and **E4**, posterior views; **F**, proximal right ulna, GU 9206, in **F1**, lateral, **F2**, anterior, **F3**, medial, and **F4**, posterior views; **G**, left radius, WIF/A 4244, in **G1**, proximal, **G2**, medial, **G3**, anterior, **G4**, posterior, and **G5**, distal views. **Abbreviations**: **ap**, anconeal process; **capf**, capitular facet; **cp**, coronoid process; **cunf**, cuneiform facet; **dulf**, distal ulnar facet; **ecr**, sulcus for m. extensor carpi radialis; **intoss lig**, rugosity or crest for interosseous ligaments; **lat pr**, lateral process of proximal radius; **lun f**, lunar facet; **olec**, olecranon process; **pisf**, pisiform facet; **pulf**, proximal ulnar facet; **radn**, radial notch; **sln**, semilunar notch; **scf**, scaphoid facet; **stp**, styloid process; **trf**, trochlear facet.

ligament scars (including for the lateral collateral ligament) resemble those of perissodactyls, especially *Heptodon*. The entepicondyle, although appearing smaller in anterior view compared with that of *Phenacodus*, is reoriented to project farther posteriorly than medially, a resemblance to early perissodactyls. The more posterior origin may confer mechanical advantage on the flexors that originate there.

Ulna—Eight ulnar specimens have been identified. Four are allocated to *C. thewissi* (GU 1215 and GU 1216 from Vastan, GU 7005 from Mangrol, and WIF/A 4260 from TAD-2; Fig. 55A), and four are referred to *C. gracilis* (WIF/A 4208 from TAD-1 and GU 9206, WIF/A 4245, and WIF/A 4246 from TAD-2; Fig. 55E, F). Although all show essentially the same morphology, there is size variation even within these two small

samples. This may reflect sexual dimorphism, individual variation, or in the case of the smaller *C. gracilis* ulnae, that they represent immature individuals. GU 7005 is slightly larger than other *C. thewissi* ulnae, and WIF/A 4208 is larger and more robust than the other three *C. gracilis* ulnae. There are also slight differences in olecranon size, muscle scars, shaft curvature, and shaft cross-sectional shape among the ulnae assigned to each species, but some of this variation is probably attributable to postmortem deformation of the shaft. Nevertheless, it is possible that one or more of the smallest ulnae referred to *C. gracilis* could pertain to the small tapiroid recorded from TAD-1. WIF/A 4208 is the only complete ulna, measuring 112 mm in length. It is relatively elongate and slender—more gracile than in *Phenacodus* (Otts, 1991) but more robust than the ulna of

TABLE 10. Ulna dimensions (in mm) in *Cambaytherium*.

Specimen no.	Species	A	B	C	D	E	F	G
GU 1215	*C. thewissi*		25.0	13.0	16.0		11.6	7.7
GU 1216	*C. thewissi*					20.7	13.7	7.7
GU 7005	*C. thewissi*		34.0	15.15	21.4	21.8	15.0	9.6
WIF/A 4260	*C. thewissi*		32.0	12.2 est	20.1	18.7	11.2	7.7
WIF/A 4208	*C. gracilis*	112.0	24.0	9.4	12.8	13.5 est	7.8	5.35
WIF/A 4245	*C. gracilis*					10.3 est	5.5	4.55
WIF/A 4246	*C. gracilis*					9.8 est	6.7	4.7
GU 9206	*C. gracilis*		18.0 est		10.7	10.6	6.5	4.7

A: total length (= U1 in Scott, 1983:fig. 1); **B**: olecranon length (= U2); **C**: olecranon maximum width; **D**: olecranon anteroposterior depth at midpoint; **E**: semilunar notch maximum width; **F**: midshaft maximum width; **G**: midshaft minimum width. **Abbreviation**: **est**, estimated.

TABLE 11. Radius dimensions (in mm) in *Cambaytherium*.

Specimen no.	Species	A	B	C	D	E	F	G
GU 274	*C. thewissi*	91.60	19.10	11.60	8.10	6.15	18.55	13.25
GU 771	*C. thewissi*		17.55	11.00				
GU 842	*C. thewissi*		19.85	11.50				
GU 7019	*C. thewissi*				10.20	8.65	23.35	15.20
GU 8051	*C. thewissi*				8.85	7.80	21.80	14.20
WIF/A 4218	*C. thewissi*	101.1 est			9.50	6.95		
WIF/A 4261	*C. thewissi*	>92.0			8.10	5.55		
WIF/A 4244	*C. gracilis*	83.90	13.85	7.90	6.75	4.50	12.50	8.90

A: length (= R1 in Scott, 1983:fig. 1); **B**: head width (= R4); **C**: head anteroposterior depth (= R3); **D**: midshaft mediolateral width (= R6); **E**: midshaft anteroposterior depth; **F**: distal width (= R5); **G**: distal anteroposterior depth.

Hyracotherium grangeri (Wood et al., 2011:fig. 12), to which it is closer in length.

The olecranon process in both *C. thewissi* and *C. gracilis* is prominent, somewhat posteriorly directed and slightly medially inflected, and relatively a little longer than in perissodactyls. In WIF/A 4208, the olecranon, measured from the anconeal process to the tip, is about 21% of total ulnar length (Table 10). No complete ulna is known for *C. thewissi*, but the olecranon preserved in several specimens is more robust than that of *C. gracilis*, so it is probable that it was relatively at least as long compared with total ulnar length. In *Hyracotherium* and *Heptodon*, the olecranon is roughly 17% of ulnar length (based on illustrations in Radinsky, 1965a; Wood et al., 2011), whereas the olecranon of *Phenacodus vortmani* is the same relative length as in *C. gracilis*, and that of *P. trilobatus* is longer, about 25% of ulnar length (based on photographs in Otts, 1991). Only in GU 1215 is the end of the olecranon intact and well preserved, showing the proximomedial eminence and longitudinal groove lateral to it, similar to olecranon morphology in basal perissodactyls (Radinsky, 1965a; Wood et al., 2011; USGS 21913). As in *Heptodon*, the eminence merges posteriorly with a broad tuberosity for insertion of the long head of m. triceps brachii, the other two heads presumably attaching medially and laterally into shallow fossae on the olecranon (Radinsky, 1965a). The olecranon in *Phenacodus* lacks the deep groove lateral to the proximomedial eminence (e.g., *P. vortmani*, USGS 7159; *P. trilobatus*, USGS 7146; Otts, 1991:figs. 69, 70).

The semilunar notch is sharply curved proximally and, when articulated with the radius, formed a tight semicircular joint for the distal humeral articulation, restricting forearm movement largely or entirely to the sagittal plane. The articular surface of the notch is strongly concave in the sagittal plane and convex transversely, with a prominent, beak-like anconeal process that projected into the deep olecranon fossa during extension. The coronoid process (which projects both medially and laterally; Fig. 55A) is much less prominent than the anconeal process;

nevertheless, the lateral coronoid process seems to project more than that in *Phenacodus* (e.g., *P. vortmani*, USGS 7159; *P. trilobatus*, USGS 38504). Immediately distal to the semilunar humeral surface on the coronoid processes, and offset from it, are the paired facets of the radial notch (Fig. 55A, E), which angle slightly toward each other, reflecting the weak convexity of the proximal ulnar facet of the radius. In our specimens of *C. thewissi*, the two radial facets have, at best, a narrow connection, or none at all, but in *C. gracilis* the two ends of the radial notch are joined, forming an arched, crescent-shaped facet. It is possible that the morphology was the same in *C. thewissi*, but that the specimens at hand are eroded in this area, or perhaps the area was bridged only by articular cartilage. On the anteromedial part of the ulnar shaft just distal to the radial facet is a muscular scar that appears to correspond to the ulnar insertion of the brachialis and biceps muscles in *Tapirus* and *Heptodon* (Campbell, 1936; Radinsky, 1965a); both muscles also insert proximomedially on the radius in those genera.

The ulnar shaft is concave posteriorly and convex anteriorly in most specimens (Fig. 55), as in early perissodactyls (Radinsky, 1965a; Wood et al., 2011) and to a lesser extent in some other early cursorial and subcursorial mammals such as *Phenacodus* and *Pachyaena* (Kitts, 1956; Otts, 1991; O'Leary and Rose, 1995); but the curvature is not as great as in *Hyracotherium* (Kitts, 1956: pl. 3; Wood et al., 2011:fig. 12). One ulna of each species—WIF/A 4260, assigned to *C. thewissi*, and WIF/A 4245, referred to *C. gracilis*—shows less curvature than the others, the latter specimen being nearly straight. In contrast to *Heptodon*, the shaft is not mediolaterally compressed, but rather is flattened obliquely so that its maximum diameter runs anteromedially to posterolaterally and its minimum diameter runs anterolaterally to posteromedially. The shaft distal to the semilunar notch therefore has two wide surfaces, facing anterolaterally and posteromedially, which are flat or slightly concave mediolaterally. The anterolateral surface probably provided origin for some of the digital extensors (e.g., m. extensor pollicis longus and possibly m. extensor digitorum
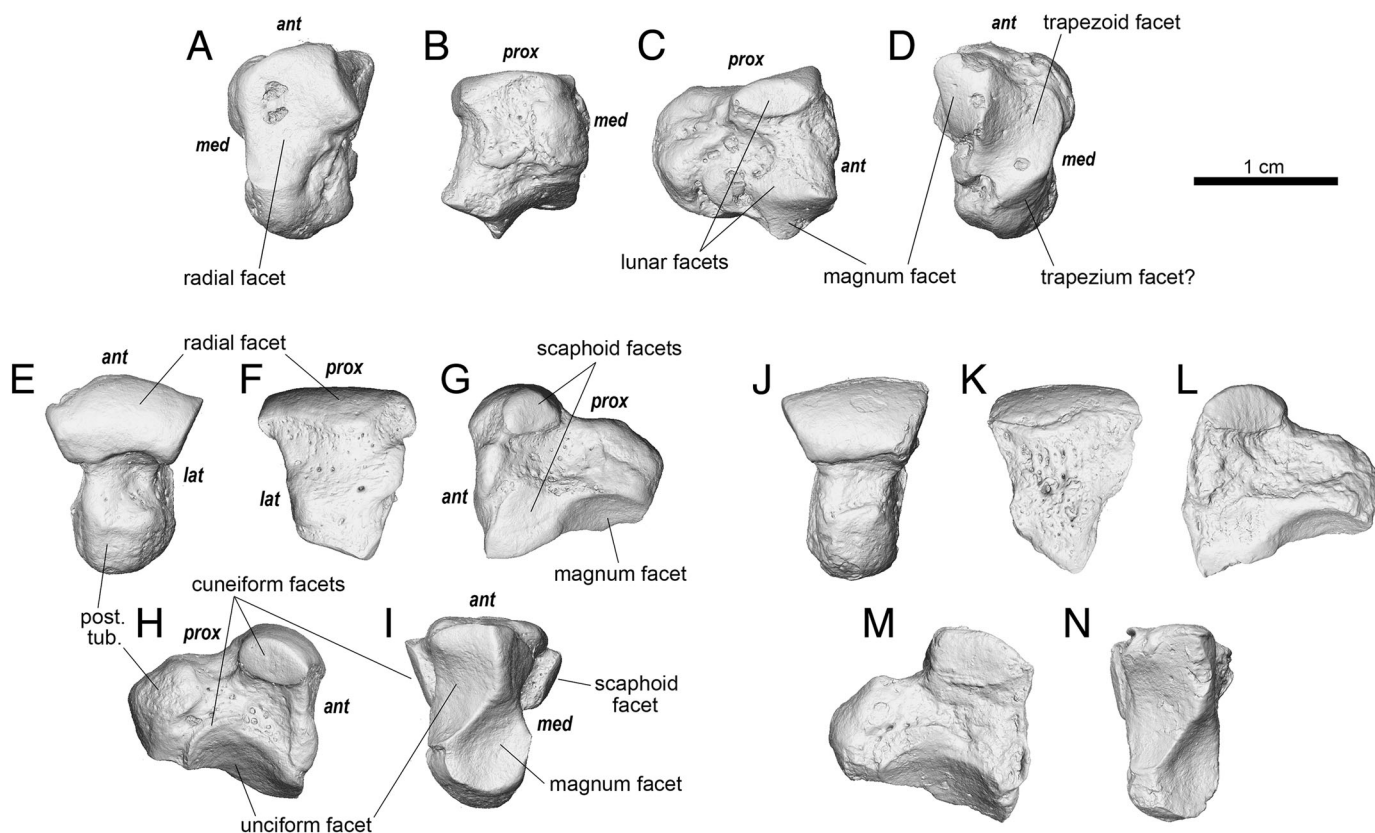
FIGURE 56. Scaphoid and lunar of *Cambaytherium thewissi*. **A–D**, right scaphoid, GU 835, in **A**, proximal, **B**, anterior, **C**, lateral, and **D**, distal views. **E–I**, right lunar, GU 295, in **E**, proximal, **F**, anterior, **G**, medial, **H**, lateral, and **I**, distal views. **J–N**, right lunar, GU 294, in **J**, proximal, **K**, anterior; **L**, medial, **M**, lateral, and **N**, distal views. **Abbreviations**: **ant**, anterior; **lat**, lateral; **med**, medial; **post tub**, posterior tubercle; **prox**, proximal.

lateralis) and, more anteriorly, m. abductor pollicis longus, as in *Tapirus* (Campbell, 1936), various carnivorans (Davis, 1964; Getty, 1975), and many other mammals. The medial border of this surface is a rugose crest to which the interosseous ligament likely attached. The ligament, together with the configuration of the elbow and radioulnar joints, presumably restricted rotatory (supinatory) mobility to a considerable extent, although radius and ulna do not appear to have been as closely appressed as in basal perissodactyls. The lateral border of the ulnar shaft is a sharp crest extending distally from the lateral coronoid process; this crest may mark the boundary between m. extensor indicis posteriorly and the more anterior digital extensors. The posteromedial surface of the shaft, which widens distally in WIF/A 4208, probably served (together with the medial side of the olecranon) for origin of the m. flexor digitorum profundus and, more distally, for attachment of m. pronator teres. The distal half of the medial (radial) border is sharp.

A prominent styloid process is preserved in WIF/A 4208 (*C. gracilis*; Fig. 55E), which displays two articular facets: a quadrate sellar surface facing distally, and a smaller, roughly triangular, convex joint facing mostly posteriorly. Radinsky (1965) described similar joint surfaces in *Heptodon* and identified them as cuneiform and pisiform joints, respectively. The distal radial facet is not evident on WIF/A 4208, the only ulna with the distal end intact.

Radius—Nine radii are known, eight representing *C. thewissi* (GU 274, GU 771, GU 777, GU 842, and GU 8051 [= GU 280 in Rose et al., 2014b:suppl. note 1] from Vastan, GU 7019 from Mangrol, and WIF/A 4218 and WIF/A 4261 from TAD-2; Fig. 55B–D) and one belonging to *C. gracilis* (WIF/A 4244, from

TAD-2; Fig. 55G). Of these specimens, one of each species (GU 274, WIF/A 4244) is complete, two are nearly complete but have damaged ends (WIF/A 4218, WIF/A 4261), two are proximal ends (GU 771, GU 842), and three are distal ends (GU 777, GU 7019, GU 8051). The radius of *C. thewissi* (Table 11) is relatively more robust and shorter than that of *Hyracotherium*, with considerably larger articular ends than in *H. grangeri* (Wood et al., 2011:table 2). Without associated elements or a complete humerus, an accurate brachial index ([radius length/humerus length] × 100) cannot be calculated; however, a rough estimate can be proposed based on the estimate of humeral length and the lengths of the three complete or nearly complete radii of *C. thewissi* (which, compared with other radial and ulnar specimens, appear to represent the middle to small end of the size range). These elements suggest that the radius of *C. thewissi* was almost certainly relatively shorter compared with humeral length than in *Hyracotherium* and suggest a brachial index of ~80, compared with >90 in *H. grangeri* (Wood et al., 2011:table 2, articular lengths). The estimated brachial index in *C. thewissi* approximates that in the comparably sized smaller phenacodontids *Tetraclaenodon puercensis* (79) and *Phenacodus vortmani* (82) (Otts, 1991). The antebrachium of *C. thewissi* might have been relatively longer than in *Tetraclaenodon* if Kondrashov and Lucas's (2012) estimate of ~70, based on a broken radius and nearly complete ulna, is correct. The radius of *C. gracilis* is much closer in proportions to that of *H. grangeri* but is still slightly shorter with more robust articulations. In contrast to *Hyracotherium*, in which both radius and ulna are distinctly arched anteriorly (Kitts, 1956; Wood et al., 2011), the radii of both *C. thewissi* and *C. gracilis* are only weakly bowed anteriorly.

As in ungulates generally, the radius is positioned anterior to the ulna and articulates across the entire width of the distal humeral joint surface. Therefore, the proximal (humeral) articulation of the radius is ovoid and 1.6–1.75 times wider mediolaterally than anteroposteriorly (Table 11). As in both *Phenacodus* and *Hyracotherium*, this articular surface is uneven, with a moderately wide and deep fossa for the capitulum and a narrower, medially inclined surface for the trochlea. The two parts of the articular surface are separated by an elevated ridge, higher on anterior and posterior borders, that fits in the trochlear groove. Viewed proximally, the trochlear surface is semicircular and anteroposteriorly concave (viewed medially), matching the conical humeral trochlea. The concave capitular surface projects laterally (homologous with the lateral process in perissodactyls) and proximally and is narrower laterally but has a rounded margin. Along almost the entire posterior surface of the proximal end is a broad, slightly convex facet for the ulna, best developed adjacent to the capitular facet but also extending along the trochlear facet. It is very similar to the homologous facet in *Phenacodus trilobatus* (USGS 7146).

The radial shaft is mostly relatively smooth and featureless, making it difficult to identify attachment sites of muscles such as biceps brachii, abductor pollicis longus, and supinator. It is somewhat flattened anteroposteriorly (Table 11). The anterior surface is mediolaterally convex, whereas the posterior (ulnar) surface is flat or slightly concave and marked by a rugose surface extending most of its length, which is bounded medially by a low interosseous crest to which the interosseous ligament attached. The posterior surface (probably more distally) also typically serves for attachment of m. pronator quadratus (e.g., Davis, 1964; Evans and Christensen, 1979), but in *Tapirus*, perhaps the closest extant analogue for *Cambaytherium*, this surface provides origin for m. abductor pollicis longus (Campbell, 1936). Posterolaterally at the distal end is a shallow oval facet marking the distal radioulnar articulation. On the anterodistal surface, a wide sulcus bounded by prominent ridges guided what must have been a relatively large tendon of m. extensor carpi radialis. This is the largest of the extensors in *Tapirus* (Campbell, 1936).

The distal articulation is broad and concave laterally, weakly concavoconvex, for articulation with the scaphoid and lunar; however, the facets for these two elements are less well defined than in basal perissodactyls.

Carpals—Ten elements representing five bones of the carpus are referred here to *Cambaytherium*: two right scaphoids (GU 835, GU 8044), three right lunars (GU 293, GU 294, GU 295), a right cuneiform (= triquetrum; GU 296), a left pisiform (GU 333), the articular end of a right pisiform (GU 8049), a left magnum (WIF/A 1192), and a right magnum (WIF/A 4408). Thus, the complete proximal carpal row is represented, but only a single element is known from the distal row. For ease of comparison, we describe and illustrate the bones following Radinsky (1965a).

The scaphoid (Fig. 56A–D) resembles that of many early perissodactyls. The radial facet dominates the proximal face (Fig. 56A). This facet is anteroposteriorly (i.e., dorsoventrally) convex at its anterior end and extends slightly onto the anterior face. The rest of the facet is gently concave. The outline of the radial facet is much broader anteriorly than posteriorly. The medial edge is rounded, whereas the lateral edge has two distinct segments. The anterior segment is distinctly shorter than the
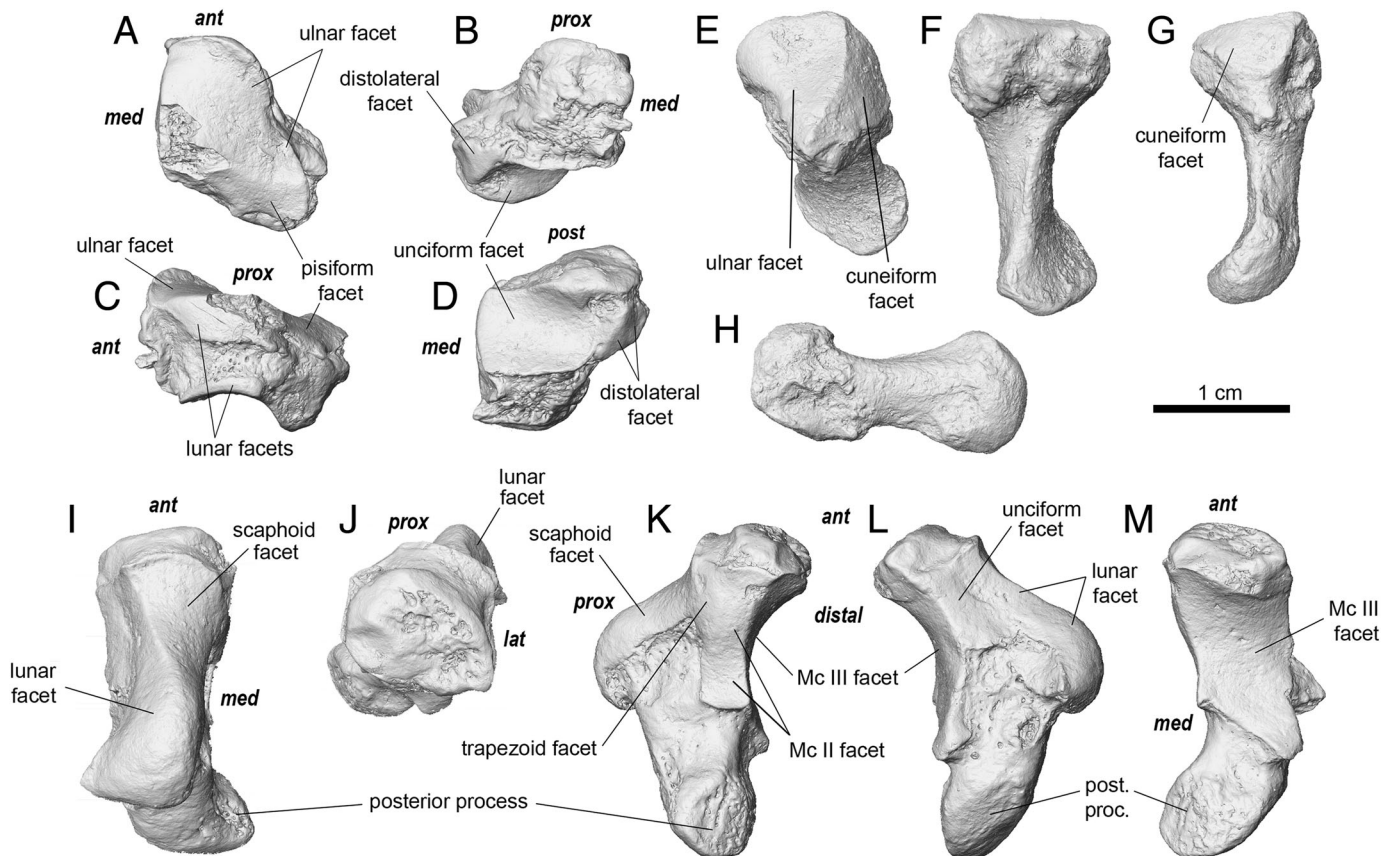
FIGURE 57. Cuneiform, pisiform, and magnum of *Cambaytherium thewissi*. **A–D**, right cuneiform, GU 296, in **A**, proximal, **B**, anterior, **C**, medial, and **D**, distal views. **E–H**, left pisiform, GU 333, in **E**, articular or anteromedial, **F**, proximal, **G**, distal, and **H**, lateral views. **I–M**, left magnum, WIF/A 1192, in **I**, proximal, **J**, anterior, **K**, medial, **L**, lateral, and **M**, distal views. **Abbreviations**: ant, anterior; **distolat**, distolateral; **lat**, lateral; **med**, medial; **post**, posterior; **post proc**, posterior process; **prox**, proximal.

posterior segment, as is typical for early perissodactyls (Holbrook, 2001; Bai et al., 2017). The anterior segment is oblique and runs posterolaterally, forming the contact with the radial facet of the lunar. The posterior segment of the lateral edge forms a rounded, shallow concavity, and the radial facet in this region descends slightly onto the lateral face of the scaphoid.

The anterior face of the scaphoid is rough and nondescript (Fig. 56B). Its outline in anterior view is a rough polygon whose sides are the medial edge and the edges of the facets for the radius, lunar, magnum, and trapezoid.

Like the anterior face, the medial face of the scaphoid is relatively nondescript, bearing no facets and having a rough texture. The anterior half of the medial face bulges out more than the posterior half and has a smoother, convex surface. The posterior half merges with the prominent posterior tubercle that dominates the posterior face. The posterior tubercle also occupies much of the posterior part of the lateral face.

Three facets are visible on the lateral aspect of the scaphoid (Fig. 56C). The proximal and distal facets for the medial surface of the lunar are both somewhat elongate and positioned at the anterior end of the lateral face. The proximal facet faces laterally, and the distal facet faces posterolaterally. The elliptical proximal facet meets the scaphoid radial facet at a right angle, whereas the distal facet meets the facet for the magnum at an obtuse angle. The magnum facet, while most obvious in distal view, is angled distolaterally to such a degree that it is also visible in lateral view.

In distal view, the magnum facet of the scaphoid is concavoconvex (saddle-shaped) and has a posterior extension that bends more proximally (Fig. 56D). A well-developed ridge on the medial edge of the anterior part of the magnum facet separates it from the large, saddle-shaped trapezoid facet, which takes up most of the distal face and is angled distomedially. The posteromedial corner of the trapezoid facet folds back onto the distomedial part of the posterior tubercle, forming what is presumably the facet for the trapezium. A distinct trough delineates the posterior edges of the magnum and trapezoid facets from the posterior tubercle.

Measurements (in mm) of the scaphoids: maximum anteroposterior dimension in proximal view (Fig. 56A) = 13.85 (GU 835), 13.65 (GU 8044); maximum proximodistal length (Fig. 56B) = 11.60 (GU 835), 12.0 (GU 8044).

The anatomy of the lunar is best seen in GU 294 and GU 295, right lunars that show minor differences in their anatomy (Fig. 56E–N). The proximal face of the lunar consists of the mediolaterally wide and anteroposteriorly convex radial facet, the posterior tubercle, and a trough separating the facet from the tubercle. The trough is shallower at the medial edge, where a low, rounded ridge connects the base of the medial edge of the facet to the tubercle. The radial facet does not extend posteriorly into this trough as it does in *Heptodon* (Radinsky, 1965a:fig. 10).

The anterior face of the lunar is roughly wedge-shaped. The proximal edge is the widest and consists of the anterior aspect of the radial articular surface, which is visible in this view due to its convex shape. The medial and lateral edges of the anterior surface are slightly oblique and converge distally toward the distal edge. The distal edge is distinctly oblique, oriented at an angle a little less than 30° relative to the proximal edge. As a result, the lateral edge is shorter than the medial edge. The oblique distal edge represents the contact with the unciform.

The medial face of the lunar has proximal and distal facets for the scaphoid at its anteroproximal and anterodistal corners, respectively. The distal facet extends posteriorly along the distal edge, curving strongly with the edge of the distal facet for the magnum 'hump.' Unlike in *Heptodon* and *Tapirus*, there is no separate posterior facet for the scaphoid (Radinsky, 1965a:fig. 10), although the posterior facet of *Heptodon* is elongate and on the distal edge it nearly contacts the anterior distal facet. The

condition in *Cambaytherium* could simply be interpreted as having the anterior and posterior distal facets confluent. A facet for the anterior magnum extends slightly laterodistally from the distal scaphoid facet, forming a faint angle between the two facets. As a result, in anterior view, the contact with the magnum is almost indiscernible as a distinct part of the medial edge, similar to the case in some perissodactyls, such as *Heptodon* (Radinsky, 1965a:fig. 10), but different from what is observed in other perissodactyls, such as *Lophiodon* (Holbrook, 2009:fig. 10a). The proximal and distal scaphoid facets are separated by a pit whose posterior rim is formed by the medial face of the posterior tubercle. Visible in medial view is the angled facet for the 'hump' of the magnum on the distal face of the posterior tubercle.

The lateral face of the lunar has two facets for the cuneiform, one proximal and one distal. The proximal facet for the cuneiform is roughly oval and placed in the anteroproximal corner of the lateral face. The distal facet is long and thin and runs along the curved distal edge formed by the concavity of the distal unciform facet. The anterior extent of the distal facet does not reach the anterior edge of this face. The unciform facet is visible on the lateral aspect because of the way it is angled.

The distal aspect of the lunar is dominated by two concave facets, the aforementioned facet for the 'hump' of the magnum and the unciform facet. The unciform facet is larger and more anterior and lateral than the magnum facet. The unciform facet is concave in the anteroposterior plane, whereas the magnum facet is concave in both anteroposterior and transverse planes. The two facets have a long, continuous, posterolaterally oblique contact. The contact is similar to what is observed in *Heptodon*, although even more extensive, and differs from *Tapirus*, in which the two facets are separated by a trough (Radinsky, 1965a:fig. 10). Both the unciform and magnum facets are strongly angled and are visible in lateral and medial views, respectively.

Measurements (in mm) of the lunars: maximum anteroposterior dimension in proximal view = 14.10 (GU 294), 13.80 (GU 295); maximum proximodistal length = 13.45 (GU 294), 12.50 (GU 295); maximum mediolateral width (proximally) = 10.50 (GU 294), 11.0 (GU 295). GU 293 is abraded; consequently, measurements were not taken.

The cuneiform (Fig. 57A–D) is remarkable for being so short proximodistally relative to its mediolateral width. The proximal face is formed by an articular surface, broken at its posteromedial corner in the one specimen, and angled at the posterolateral corner. The ulnar and pisiform facets have little to distinguish them from each other, but the pisiform facet appears to be much smaller than the ulnar facet.

The anterior face of the cuneiform consists mostly of the rugose surface of the bone and is oriented more anterolaterally than anteriorly. The distal facet for the unciform is angled so as to be visible in this view. More notable is the presence of a small but distinct convex facet at the distolateral corner of this face, touching but offset from the edge of the unciform facet by roughly 90° and completely separate from the pisiform facet. This facet is absent in perissodactyls (e.g., Radinsky, 1965a:fig. 11), and its function in *Cambaytherium* is unknown.

The medial face of the cuneiform has separate proximal and distal facets for the lunar, separated by a trough. The proximal facet is larger, oval, and placed at the proximal edge where it contacts the ulnar facet at a right angle. The distal facet is very thin, concave distally, and runs along the distal edge, in contact with the unciform facet and roughly perpendicular to it. A medial extension of the anterior face forms an irregular ridge anterior to the two lunar facets.

The lateral and posterior surfaces of the cuneiform are rough and have no facets, with the lateral being the smallest face, due to the convergence of the anterior and posterior surfaces. The distal surface consists entirely of the anteroposteriorly concave and mediolaterally wide unciform facet.

TABLE 12. Metapodial dimensions (in mm) of *Cambaytherium*.

Specimen no.	Species	Position	Locality	Length	W prox	D prox	W mid	D mid	W distal	D distal
GU 292	*C. thewissi*	R Mc II	Vastan	41.85	9.50	9.85	7.85	4.90	11.05	9.55
GU 815	*C. thewissi*	L Mc II	Vastan	39.80	8.40		7.80	4.35	11.45	10.00
GU 817	*C. thewissi*	R Mc II	Vastan	40.40	8.90	~9.0	6.85	4.00	9.90	8.75
GU 832	*C. thewissi*	R Mc II?	Vastan				6.85	4.40	9.80	8.80
GU 7007	*C. thewissi*	L Mc II	Mangrol	42.00	8.80	9.55	7.40	4.55	10.90	8.50
GU 8046	*C. thewissi*	L Mc II	Vastan		10.00					
GU 1217	*C. thewissi*	R Mc III	Vastan	~50.0	11.80	10.70	9.75	4.60	13.35	
WIF/A 4256	*C. gracilis*	L Mc III	TAD-1	41.90	~8.1		6.70	3.20	9.05	5.15
GU 818	*C. thewissi*	R Mc IV	Vastan	42.20	8.75	9.35	7.90	4.10	10.80	~7.4
GU 822	*C. thewissi*	L Mc IV	Vastan	40.60	9.05	9.85	6.85	4.10	11.40	9.50
GU 848	*C. thewissi*	L Mc IV	Vastan		8.65		8.45	4.55		
GU 1610	*C. thewissi*	R Mc IV	Vastan		8.60	10.15	7.45	4.30		
GU 8048	*C. thewissi*	R Mc IV	Vastan		8.50	9.65	7.25	4.05		
GU 847	*C. thewissi*	R Mc V	Vastan	36.70	8.85	8.80	7.25	4.80	11.10	9.50
GU 1704	*C. thewissi*	R Mc V	Vastan	31.80	8.05	7.80	5.90	4.10	8.75	8.80
GU 841	cf. *C. marinus*	L Mt II	Vastan	73.15	13.00	17.70	13.20	10.00	18.40	17.15
GU 735	*C. thewissi*	L Mt II	Vastan	48.70	10.05	11.00	9.50	4.80	11.50	8.20
GU 821	*C. thewissi*	R Mt III	Vastan		11.90					
GU 846	*C. thewissi*	L Mt III	Vastan		11.90	12.60	10.05	4.70		
GU 9017	*C. gracilis*	L Mt III	TAD-2	47.05	7.35	7.70	6.30	2.95	8.80	5.10
GU 275	*C. thewissi*	R Mt IV	Vastan	54.00	12.20	11.10	7.00	5.65	10.80	10.25
GU 816	*C. thewissi*	L Mt IV	Vastan	51.00			6.05	4.80	9.80	9.50
GU 819	*C. thewissi*	R Mt IV	Vastan	50.35	12.30	10.75	7.05	5.35	10.90	10.60
GU 831	*C. thewissi*	R Mt IV	Vastan	51.85	12.20	10.10	6.65	5.20	10.30	10.35

Abbreviations: **D**, depth; **mid**, midshaft; **prox**, proximal; **W**, width.

Measurements (in mm) of the cuneiform (GU 296): maximum dimension in proximal view (Fig. 57A; taken diagonally) = 16.25; mediolateral width at mid-facet = 9.90; minimum proximodistal length between proximal and distal facets = 7.00; width of unciform facet = 8.75.

Two pisiforms are known. GU 333 (Fig. 57E–H) preserves the entire bone but is somewhat weathered, whereas GU 8049 preserves only the articular end but is otherwise undamaged. The pisiform is sizable and elongate, longer than the other proximal carpals. Its shape is similar to the pisiform of *Hyracotherium* (Wood et al., 2011:fig. 14d), but it is relatively larger than in *Hyracotherium* and *Heptodon*. It has a well-developed articular head and posterior tubercle. The lateral face of GU 333 is gently convex and the medial face is distinctly concave, giving the posterior tubercle a hook-like appearance. The shaft connecting the head and the tubercle is narrower than what is observed in *Heptodon* and *Tapirus* (Radinsky, 1965a:fig. 11). For reasons given below, we provisionally identify GU 333 as a left pisiform and GU 8049 as a right pisiform. The directional terminology used in the following description reflects these identifications. This interpretation is supported by the presence of what appear to be two roughly triangular facets on the articular heads of both specimens, one essentially flat and corresponding well to the pisiform facet on the cuneiform (GU 296) and one shallowly concave and at a right angle to the other facet, presumably for the ulna. Based on these identifications for the facets, we can infer which sides these specimens represent. The facets are unusual in comparison with perissodactyls in terms of their arrangement relative to the long axis of the bone. In perissodactyls, both facets are typically oblique to the long axis, whereas in both *Cambaytherium* pisiforms the cuneiform facet is parallel to the long axis and the ulnar facet is nearly perpendicular to the long axis. This arrangement appears to reflect the proximodistal compression of the cuneiform, which results in its proximal facets lying closer to the transverse plane.

There are additional swellings at various corners of the facets, giving the articular head a robust appearance relative to the narrow shaft. These are more prominent in GU 333 than in GU 8049.

Measurements (in mm) of GU 333: length = 21.50; dimensions of articular end = 10.20 × 7.45; GU 8049: dimensions of articular end = 8.95 × 6.25.

The magnum is the only distal carpal represented in our sample. It is a distinctive element, highly irregular in shape compared with the other carpals (Fig. 57I–M) and generally similar to that of *Hyracotherium* and *Heptodon*. It essentially consists of an anterior 'head,' a proximal 'hump' extending posterior to the head, and a posterior process that hooks medially. The posterior process accounts for more than a third of the anteroposterior length.

In proximal view, facets for the scaphoid and lunar extend from the anterior head posteriorly onto the hump. The scaphoid facet is medial to the lunar facet, but their contact is oblique and runs anterolateral to posteromedial, such that the scaphoid facet dominates the proximal aspect of the head and the lunar facet dominates the proximal aspect of the hump. The ridge separating the two facets is more distinct anteriorly than posteriorly. The lunar facet extends onto the lateral aspect of the magnum, where it is confluent with the more distal unciform facet; the two facets dominate the lateral face of the magnum.

In anterior view, the head of the magnum is shaped like an irregular hexagon, with a proximal edge for contact with the scaphoid, the edge for the lunar and unciform contact lateral to that, and a small facet for the trapezoid medial to the scaphoid contact. The two most distal edges of the hexagon reflect the contacts with the second and third metacarpals (Mc II and III).

In medial view, the scaphoid facet is concave and large, occupying the proximal half of this side and extending from the head posteriorly and proximally to cover the hump. Distal to the anterior portion of the scaphoid facet are smaller facets for the trapezoid and, more distally, Mc II. These two relatively flat facets are differentiated from each other and from the scaphoid facet by faint ridges.

As noted above, a large articular surface dominates the lateral aspect, its anterior portion quadrate and flat and extending from the proximal face to the distal edge, and its posterior, hook-shaped portion extending posteriorly and proximally onto the hump. The elongate proximal part of the facet accommodates the lunar, whereas the anterodistal portion articulates with the unciform, the two facets being demarcated by a faint trough. The arrangement of these facets is very similar to that of *Heptodon* (Radinsky, 1965a:fig. 12).
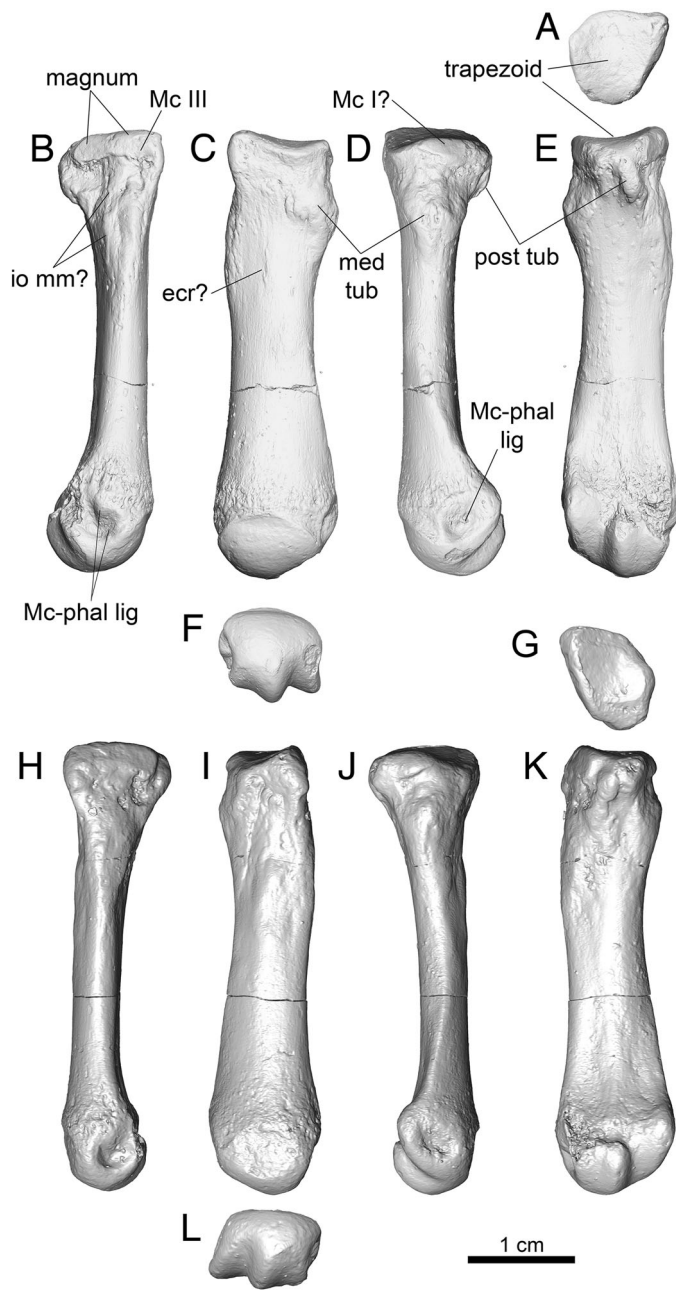
FIGURE 58. Second metacarpal of *Cambaytherium thewissi*. **A–F**, right Mc II, GU 292, in **A**, proximal, **B**, lateral, **C**, anterior, **D**, medial, **E**, posterior, and **F**, distal views. **G–L**, left Mc II, GU 7007, in **G**, proximal, **H**, lateral, **I**, anterior, **J**, medial, **K**, posterior, and **L**, distal views. **Abbreviations**: ecr, insertion of extensor carpi radialis; io mm, attachment of interosseous muscles; **magnum**, facet for magnum; **MC I**, facet for first metacarpal; **MC III**, facet for third metacarpal; **Mc-phal lig**, attachment site of metacarpophalangeal ligaments; **med tub**, medial tubercle; **post tub**, posterior tuberosity; **trapezoid**, facet for trapezoid.

The facet for Mc III and the posterior process occupy the distal face, with the Mc III facet constituting more than half the length of this side. The facet for Mc III is saddle-shaped, strongly concave anteroposteriorly and gently convex mediolaterally.

Measurements (mm) of the magna: maximum anteroposterior dimension = 23.45 (WIF/A 1192), 21.20 (WIF/A 4408); maximum proximodistal length at hump = 13.0 (WIF/A 1192), 12.65 (WIF/A

4408); maximum width of Mc III facet = 8.70 (WIF/A 1192), 7.70 (WIF/A 4408).

Metacarpals—Fifteen metacarpals have been identified, all except one representing *Cambaytherium thewissi* (five or six Mc IIs, one Mc III, five Mc IVs, two Mc Vs). A single Mc III is the only metacarpal known for *C. gracilis*. Dimensions are presented in Table 12. All are relatively short and stout in comparison with those of early Eocene perissodactyls (*Hyracotherium*, *Homogalax*, and *Heptodon*) and more closely approximate those of *Phenacodus* in proportions. The shafts of the metacarpals are distinctly flattened (in most specimens they are 50–100% wider than deep); this appears to be the original condition rather than distortion. The distal articulations are asymmetrical and slightly wider than deep, with a prominent median keel and a weaker lateral ridge. The latter ridges are developed on the posterior half of the articulation; the anterior part of the articulation is smooth and roughly cylindrical. Medial and lateral sides of the distal articulation are marked by a pit and more proximal tubercle, for attachment of the metacarpophalangeal collateral ligaments.

Metacarpal II (GU 292, GU 815, GU 817, GU 7007, GU 8046, and tentatively GU 832; Fig. 58) is short and robust, much shorter and stouter than in *Hyracotherium* (Kitts, 1956; Wood et al., 2011), and more robust than in *Homogalax*, in which Mc II is about the same length but more slender (Rose, 1996). Mc II of the basal tapiroid *Heptodon posticus* is much longer but approximately the same distal width (Radinsky, 1965a). The trapezoid facet is saddle-shaped and roughly triangular, wider anteriorly than posteriorly, transversely concave and anteroposteriorly weakly convex. The narrow posterior part of the facet projects posteriorly, supported by a prominent posterior tuberosity. Radinsky (1965a) described a similar feature in *Heptodon*, which he postulated to serve as an attachment site for the m. flexor carpi radialis or a carpal ligament. This seems likely for *Cambaytherium* as well, because the m. flexor carpi radialis in *Tapirus* inserts on the palmar (posterior) side of the bases of Mc II and III (Campbell, 1936). The narrow facet proximolaterally is mostly for the magnum, because Mc II extends proximally farther than Mc III, but the distal part of the articular surface (mostly anteriorly) is slightly offset and articulates with Mc III. This is best seen in GU 292 and GU 7007, and the configuration of facets is similar to that in *Tapirus*. Proximally on the dorsum (anterior) of the shaft (most evident in GU 7007) is a subtle rugosity that may mark the insertion of the extensor carpi radialis muscle (Fig. 58C); however, the attachment site of this muscle is uncertain (see further discussion below). The proximal third of the shaft on the lateral side bears a rugose scar, probably for attachment of interosseous muscles or possibly intermetacarpal ligaments (Fig. 58B). Proximomedially (and facing medially) is a narrow facet, not present in *Tapirus*, possibly indicating the presence of a small Mc I. Alternatively, this facet may have articulated with the trapezium or a sesamoid bone. Distal to the facet is a prominent, rugose (medial) tubercle extending onto the anterior surface, perhaps an alternative insertion point for the m. extensor carpi radialis, which is large in perissodactyls (Campbell, 1936; Getty, 1975). A similar tubercle is present on Mc II in *Tapirus* (USNM-M 218778), and Davis (1964:100) observed "a conspicuous scar on the radial side of the second metacarpal" in *Ailuropoda*, where m. extensor carpi radialis longus inserted. These observations would seem to support the same site of insertion in *Cambaytherium*. However, Campbell (1936) reported that the extensor carpi radialis in *Tapirus* inserts mainly on Mc III with a small attachment on Mc IV, whereas the m. abductor pollicis longus inserts on "the base of the second metacarpal" (Campbell, 1936:226). The same arrangement for both muscles obtains in *Sus*, except that extensor carpi radialis inserts only on Mc III (Getty, 1975), whereas both muscles insert proximally on Mc II in *Babyrousa* (Kneepkens et al., 1989). It is also possible that a ligament attached to this tubercle in *Cambaytherium*.
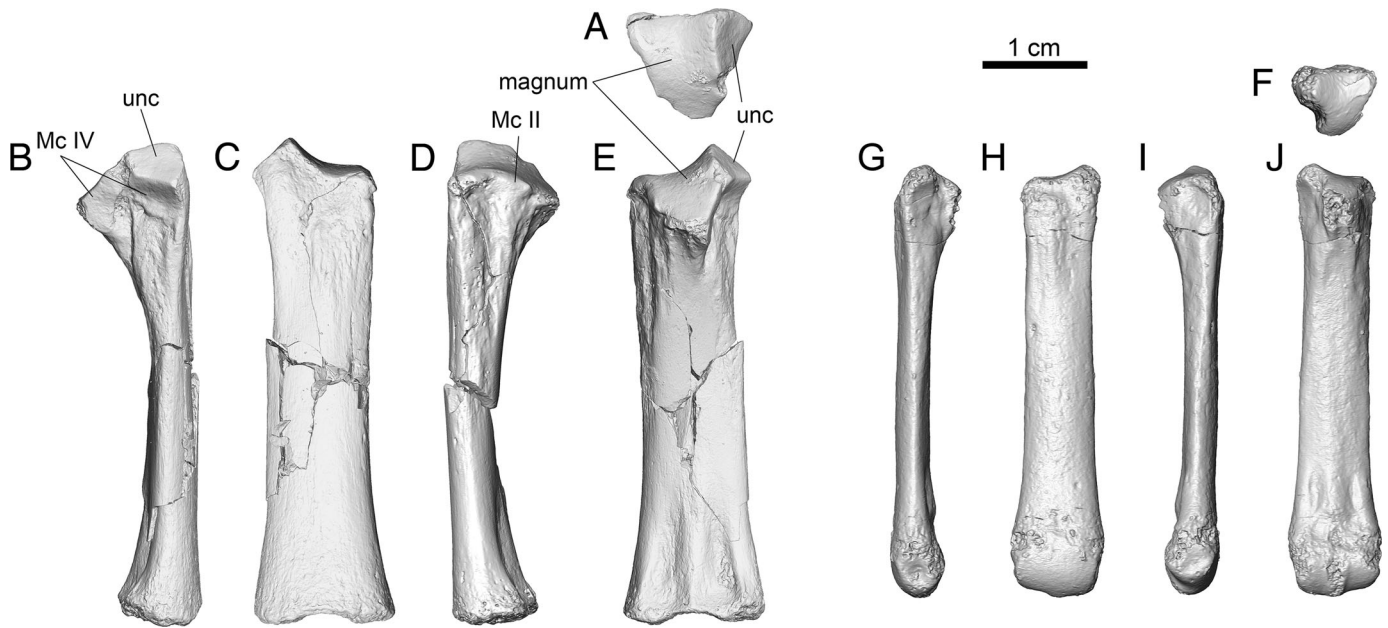
FIGURE 59. Third metacarpals of *Cambaytherium*, to the same scale. **A–E**, right Mc III of *C. thewissi*, GU 1217 (Vastan), distal epiphysis missing, in **A**, proximal, **B**, lateral, **C**, anterior, **D**, medial, and **E**, posterior views. **F–J**, left Mc III of *C. gracilis*, WIF/A 4256 (TAD-1), in **F**, proximal, **G**, lateral, **H**, anterior, **I**, medial, and **J**, posterior views. **Abbreviations**: **magnum**, facet for magnum; **MC II**, facet for second metacarpal; **MC IV**, facet for fourth metacarpal; **unc**, facet for unciform.

GU 1217 is a well-preserved right Mc III of *C. thewissi* missing its distal epiphysis (Fig. 59). This fact and the bone surface suggest that GU 1217 represents a subadult. The shaft is straight and slightly bowed anteriorly. The shaft is wider than that of the other metacarpals; the width is more than twice the depth, although the latter is comparable to the other metacarpals (Table 12). The proximal articulation bears two facets—a large, triangular saddle-shaped facet for the magnum (transversely concave, anteroposteriorly convex, with a prominent posterior projection) and a flat, roughly triangular facet (slightly crescentic, wider anteriorly than posteriorly), facing proximolaterally, for the unciform. The unciform facet is set at a right angle to the magnum facet. The posterior projection may have served for attachment of m. flexor carpi radialis, which inserts at the "bases of the second and third metacarpals" in *Tapirus* (Campbell, 1936:228) or perhaps somewhat more distally, as in *Canis* (Evans and Christensen, 1979). It is also likely that these posterior projections provided origin for the mm. interossei, as in *Canis* and *Tapirus*. There is a narrow, arcuate facet proximomedially for Mc II. Proximolaterally are three nearly flat facets. Anteriorly, and facing anteriorly and laterally, is the aforementioned unciform facet. Immediately distal to the unciform facet is a quadrate facet set at a right angle to it, and therefore facing distally and slightly posteriorly. A third, irregular-shaped facet lies posterior to the quadrate facet and faces laterally; it is separated from the two anterior facets by a notch in the lateral margin of the magnum facet. These last two facets articulate with Mc IV. The anterior of the shaft of Mc III shows no evident scar for attachment of m. extensor carpi radialis, although this may be due to the subadult age of the individual or to postmortem damage to the shaft. As noted by Campbell (1936), this muscle attaches primarily on Mc III in *Tapirus*, and it typically leaves a rugose scar in many mammals, including *Tapirus* and *Heptodon* (Radinsky 1965a). Toward the distal end of the bone the posterior surface is marked by a pair of distinct shallow fossae separated by a median ridge that would have been aligned with the median keel of the articular surface. These fossae may be related to sesamoid bones or to attachment of interosseous muscles. WIF/A 4256 (Fig. 59F–J) is a somewhat eroded Mc III from TAD-1, a little shorter and much more gracile than GU 1217, but otherwise similar as far as can be determined. It is referred to *C. gracilis*.

FIGURE 60. Left metacarpal IV of *Cambaytherium thewissi*, GU 822, in **A**, proximal, **B**, lateral, **C**, anterior, **D**, medial, **E**, posterior, and **F**, distal views. **Abbreviations**: **MC III**, facet for third metacarpal; **MC V**, facet for fifth metacarpal; **Mc-phal lig**, attachment site of metacarpophalangeal ligaments; **post tub**, posterior tubercle; **unc**, facet for unciform.

FIGURE 61. Fifth metacarpal of *Cambaytherium thewissi*, to the same scale. **A–F**, right Mc V, GU 847, in **A**, proximal, **B**, lateral, **C**, anterior, **D**, medial, **E**, posterior, and **F**, distal views. **G–L**, right Mc V, GU 1704, in **G**, proximal, **H**, lateral, **I**, anterior, **J**, medial, **K**, posterior, and **L**, distal views. **Abbreviations**: **lat tub**, lateral tubercle; **MC IV**, facet for fourth metacarpal; **Mc-phal lig**, attachment site of metacarpophalangeal ligaments; **io mm**, attachment of interosseous muscles; **unciform**, facet for unciform.

Mc IV (Fig. 60) is represented by five specimens: GU 818, GU 822, GU 848, GU 1610, and GU 8048. The first two are complete elements, whereas GU 848, GU 1610, and GU 8048 are proximal ends broken near midshaft. The important features are best preserved on GU 822 and GU 1610; the others are somewhat eroded. The shaft of Mc IV is not bowed anteriorly, but it is distinctly bent laterad about one-third the distance from the proximal end, resulting in a slight concavity laterally. The proximal articulation, for the unciform, is triangular, convex anteroposteriorly and slightly concave mediolaterally, and it projects proximally more on the medial side. As in Mc II and Mc III, the posterior projection of the articular surface forms a prominent posterior tubercle. In proximal view, the medial border of the unciform facet appears straight, whereas the lateral border is concave laterally; both borders viewed from the side are convex proximally. A narrow

curved facet facing laterally meets a matching facet on Mc V. The proximomedial face has a pair of flat facets, slightly offset (the more anterior one slightly oblique, facing proximally as well as medially), for Mc III.
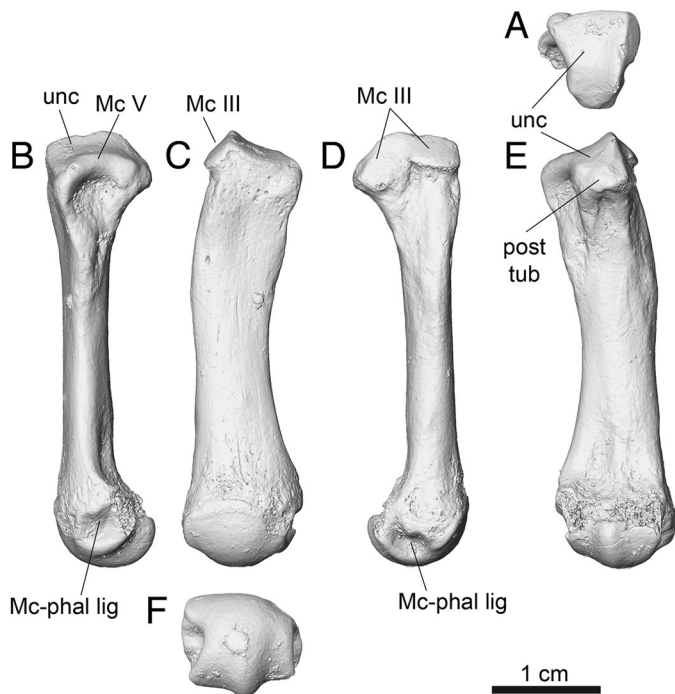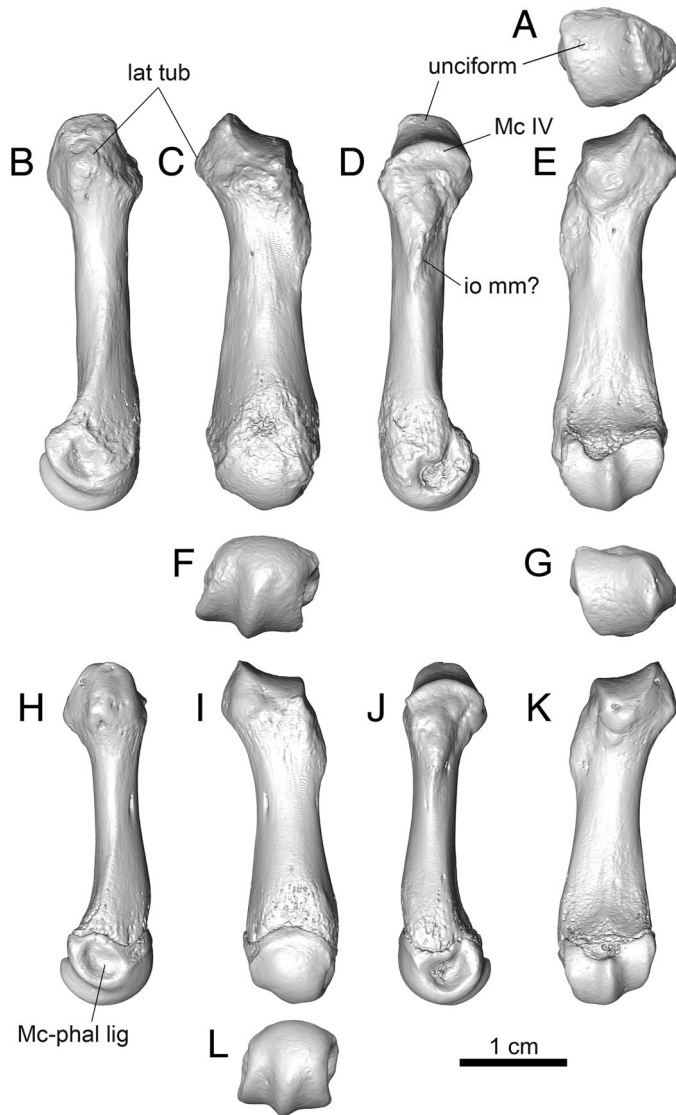
Mc V (GU 847, GU 1704; Fig. 61) is shorter than other metacarpals but otherwise is not reduced: the base and head are as large as those of Mc II and IV. The shaft is straight, with little or no bowing. Unlike the other metacarpals, the shaft is not narrowest at midshaft but rather at a point about one-third the distance from the proximal end. The proximal articulation is a distinctive saddle-shaped facet for the unciform. It is strongly convex anteroposteriorly and concave mediolaterally. The lateral margin of the facet is anteroposteriorly constricted and projects proximally much more than the longer medial margin. Both margins, viewed from the side, are markedly convex proximally. A very narrow facet along the arched medial margin is for Mc IV. A prominent lateral tubercle is present just distal to the lateral margin of the unciform facet; it probably served for insertion of the extensor carpi ulnaris, as in *Tapirus* (Campbell, 1936).

Phalanges—Eighteen phalanges have been identified from Vastan Mine, all pertaining to *C. thewissi*. Because all are isolated and show only small differences in size or morphology, we assume that manual and pedal phalanges are very similar. Consequently, any of the bones described here could pertain to either the manus or the pes, and it is not possible to assign them confidently to particular digits. Ten specimens are proximal phalanges, seven are intermediate, and one is a terminal (ungual) phalanx (Table 13). All are short and stout (broad and relatively flattened dorsoventrally), much more so than in *Hyracotherium* or *Homogalax*, and more closely approximating those of *Phenacodus trilobatus* and *Heptodon posticus* in proportions. In most respects, they conform closely to Radinsky's (1965a) description of the phalanges of *Heptodon*.

Ten specimens can be identified as proximal phalanges (Fig. 62) by their proportions (about 30–50% longer than they are wide at the proximal end), the shape of the proximal articulation (narrower and dorsoventrally taller than the intermediate phalanges, with a faint notch at the center of the ventral [i.e., volar] margin for the distal metapodial keel), and the lack of extension of the distal articulation onto the dorsal surface. Nevertheless, the proximal ends are wider than they are high ([mean proximal depth/mean proximal width] × 100 = 74, n = 8, range: 63–81; Table 13). The shape of the distal articulation would have limited the range of extension at the proximal interphalangeal joint. Slight proximal and/or distal asymmetry suggests that some of these phalanges represent lateral digits II or IV (GU 829, GU 830, GU 8006, GU 8047; Fig. 62L–P) or, based on their smaller size, digits I or V (GU 281, GU 298, GU 843), with appropriate reservations given the uncertainty surrounding the expression of digit I and pedal digit V (see Metatarsals, below). Two phalanges are relatively symmetrical (GU 280, GU 7008; Fig. 62A–G) and probably belong to digit III. In the best preserved specimens (GU 280, GU 829, GU 830, GU 8006), the lateral borders of the phalangeal shafts are buttressed ventrally; these low marginal ridges may have served for attachment of the fibrous digital sheaths that formed part of the osseofibrous tunnels enclosing the digital flexor tendons, as well as for attachment of interphalangeal collateral ligaments. The ventral surface of the shaft is very slightly concave mediolaterally, and shallow fossae are present just proximal to the distal articulation (GU 280, GU 8006). In *Equus*, m. flexor digitorum superficialis inserts partly to this area of the proximal phalanx (Getty, 1975).

Seven bones, identified as intermediate phalanges (Fig. 63), are even shorter (lengths are less than 20% more than width at the proximal end). The proximal articulation is flatter than that of the proximal phalanges ([mean proximal depth/mean proximal width] × 100 = 63, n = 6, range: 55–81), and its ventral margin projects proximally. The sides are slightly swollen at the sites of

TABLE 13. Phalangeal dimensions (in mm) of *Cambaytherium thewissi*.

Specimen no.	Position	Locality	L	W prox	D prox	W mid	D mid	W dist max	W dist art	D dist
GU 280	proximal	Vastan	19.4	12.9	8.15	10.75	4.4	11.1	8.8	4.3
GU 281	proximal	Vastan	13.95	10.7	7.5	8.8	4.35	8.65	7.4	4.7
GU 298	proximal	Vastan	12.2	9.35	7.6	8.1	4.15	9.45	8.2	4.5
GU 828	proximal	Vastan		11.15	8.4	9.65	6.0			
GU 829	proximal	Vastan	17.45	12.45	9.35	9.75	5.7	10.3	9.1	5.9
GU 830	proximal	Vastan	18.1	12.4	9.7	10.1	5.95	10.15	9.2	5.85
GU 843	proximal	Vastan	14.05	10.9	7.65	9.9	5.6	~9.7	~7.8	4.6
GU 7008	proximal	Mangrol				10.4	4.3	11.45	9.0	4.65
GU 8006	proximal	Vastan-upper	17.9	12.6	9.8	10.65	6.05	10.4	8.85	5.9
GU 8047	proximal	Vastan	15.9	11.7	9.2	9.8	5.4	9.8	7.95	5.45
GU 282	intermed	Vastan	14.8	13.3	7.3	10.4	4.1		10.5	4.75
GU 299	intermed	Vastan	11.2	9.05	7.3	8.0	3.8	9.1	7.8	4.8
GU 844	intermed	Vastan	10.0	9.85	6.25	8.2	4.0		8.3	4.5
GU 845	intermed	Vastan	11.65	11.35	6.25	9.1	3.25		8.7	4.25
GU 7009	intermed	Mangrol	12.6	10.9	6.1	8.5	3.6		8.5	4.0
GU 7020	intermed?	Mangrol	12.45	10.7	7.75	9.1	5.15		7.1	5.1
GU 8029	intermed	Vastan	12.9	11.55	7.0	8.8	4.0		9.05	4.75
GU 7021	terminal	Mangrol	16.25	14.7/11.5*	7.85					

Abbreviations: **art**, articulation; **D**, depth; **dist**, distal; **L**, length; **max**, maximum; **prox**, proximal; **W**, width; *maximum/articular.
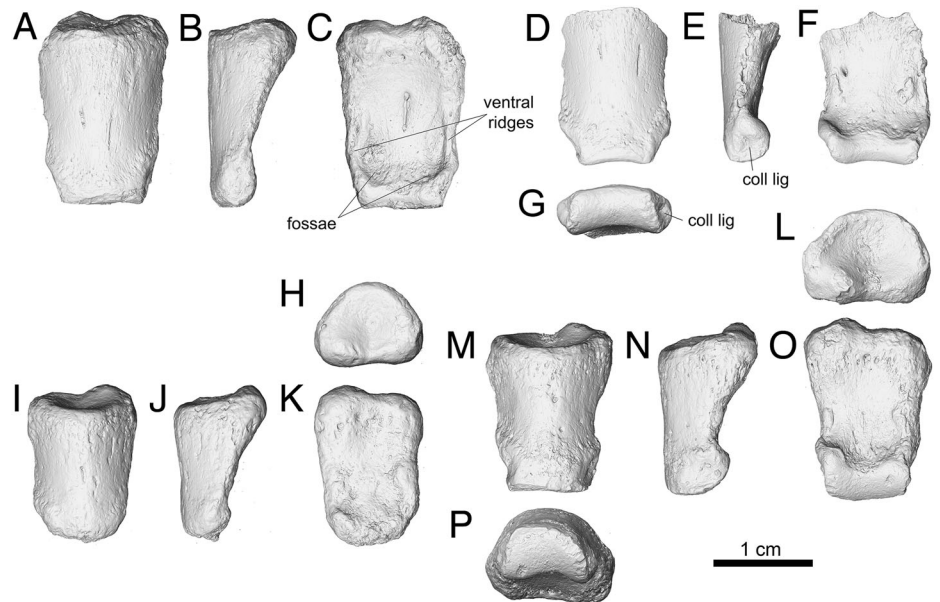
FIGURE 62. Proximal phalanges of *Cambaytherium thewissi*, to the same scale. Digit and side uncertain. **A–C**, GU 280 (Vastan) in **A**, dorsal, **B**, side, and **C**, ventral views. **D–G**, GU 7008 (Mangrol) in **D**, dorsal, **E**, side, **F**, ventral, and **G**, distal views. **H–K**, GU 828 (Vastan) in **H**, proximal, **I**, dorsal, **J**, side, and **K**, ventral views. **L–P**, GU 829 (Vastan) in **L**, proximal, **M**, dorsal, **N**, side, **O**, ventral, and **P**, distal views. **Abbreviation**: **coll lig**, pit for collateral ligament.

insertion of the superficial digital flexor. As with the proximal phalanges, weak asymmetry of the proximal end suggests that some of these phalanges come from lateral digits (e.g., GU 844; Fig. 63F–J), whereas more symmetrical elements may belong to the central digit (GU 8029; Fig. 63P–T), but the asymmetry is more subtle than for the proximal phalanges. The distal articulation extends onto the dorsal surface, indicating the possibility of hyperextension at the more distal interphalangeal joint. Notably, the proximal articulation of both the proximal and intermediate phalanges is slightly distally (anteriorly) inclined, in contrast to this articulation in *Phenacodus trilobatus* (e.g., USGS 7146), which is vertical. The morphology of the intermediate phalanges is consistent with that of mammals with digitigrade to sub-unguligrade posture.

A single terminal phalanx (GU 7021; Fig. 64C–F) has been identified. It is broad and flattened, as in *Phenacodus* (Fig. 64A, B) and basal perissodactyls, but is relatively broader than in basal perissodactyls (although not as short and wide as in *Tapirus*) and more like *Phenacodus* in this respect. It is relatively shorter than in both *Phenacodus* and *Hyracotherium* and lacks the distinctive constriction between the base and the distal part of the ungual seen in both *Phenacodus* and basal perissodactyls. It is only 10% longer than the proximal width and tapers toward the end, which appears to have been rounded with a shallow fissure, although it is now damaged. The volar (ventral) surface is relatively flat but ornamented with low ribs that radiate out from a broad, low flexor tubercle, on which the tendon of the m. flexor digitorum profundus inserted. The dorsal surface is gently convex in both directions, with a rugged surface on its distal half. The dorsal slope is relatively shallow (≤30°), similar to that in *Phenacodus trilobatus*, and about as in *Tapirus* or slightly shallower. More proximally, the dorsal surface in *C. thewissi* is essentially parallel to the volar surface, then rises slightly to form an extensor process at the proximal end, for insertion of m. extensor digitorum communis. The proximal articulation is essentially perpendicular to the volar surface,
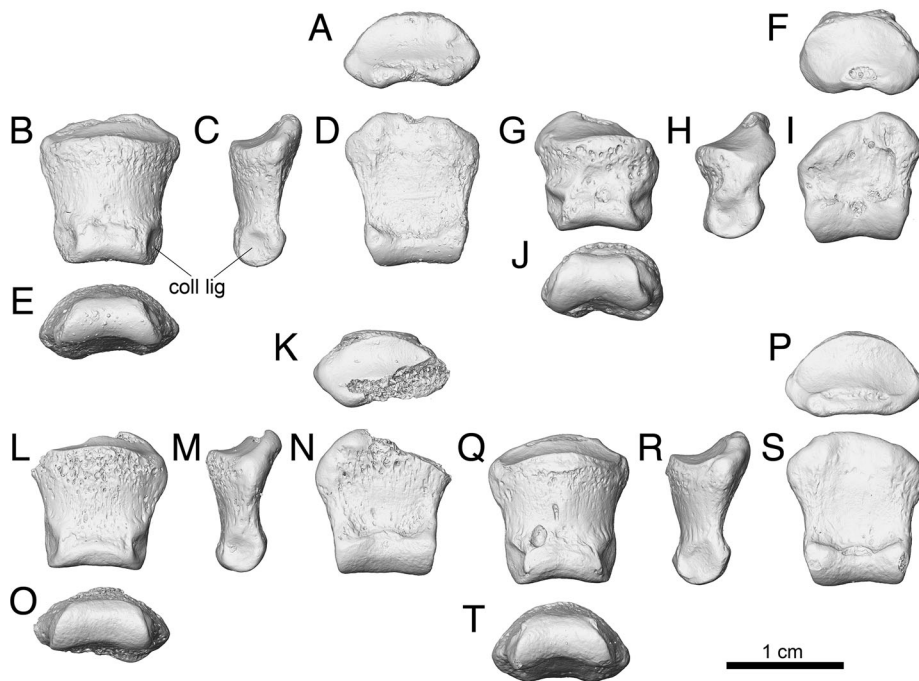
FIGURE 63. Intermediate phalanges of *Cambaytherium thewissi*, to the same scale. Digit and side uncertain. **A–E**, GU 7009 (Mangrol) in **A**, proximal, **B**, dorsal, **C**, side, **D**, ventral, and **E**, distal views. **F–J**, GU 844 (Vastan) in **F**, proximal, **G**, dorsal, **H**, side, **I**, ventral, and **J**, distal views. **K–O**, GU 845 (Vastan) in **K**, proximal, **L**, dorsal, **M**, side, **N**, ventral, and **O**, distal views. **P–T**, GU 8029 (Vastan) in **P**, proximal, **Q**, dorsal, **R**, side, **S**, ventral, and **T**, distal views. **Abbreviation**: **coll lig**, pit for collateral ligament.
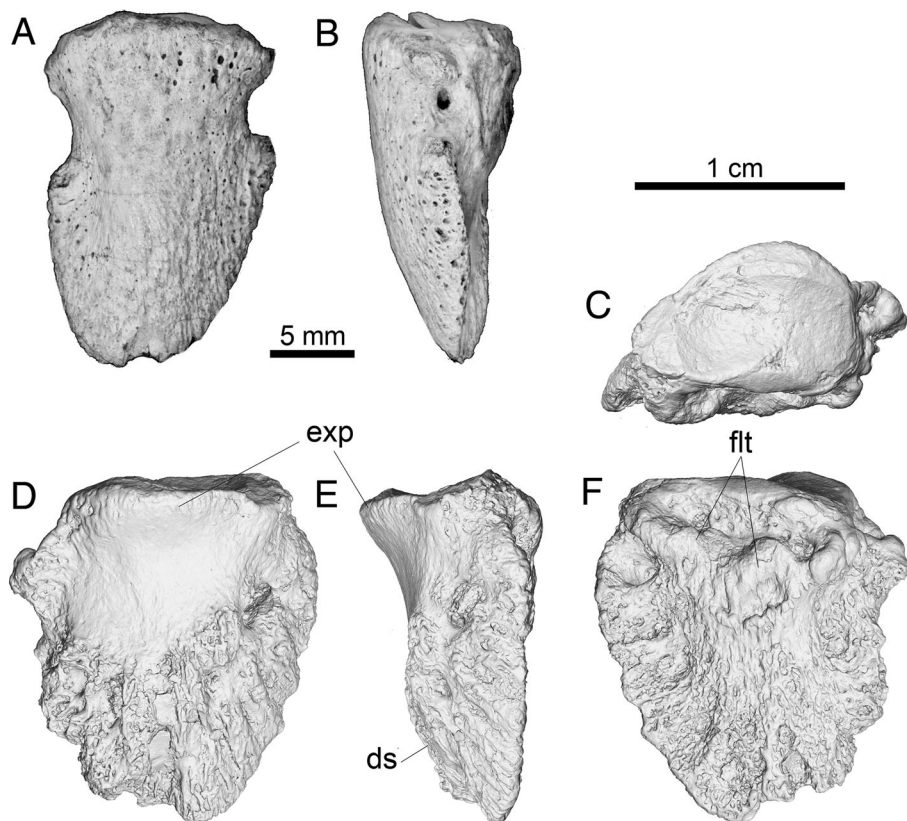
FIGURE 64. Lateral terminal phalanges of *Phenacodus trilobatus* (USGS 7146, Willwood Formation; digital photographs) and *Cambaytherium thewissi* (GU 7021, Mangrol Mine), to the same length. **A**, **B**, *P. trilobatus* in dorsal and side views. **C–F**, *C. thewissi*, in **C**, proximal, **D**, dorsal, **E**, side, and **F**, volar (ventral) views. **Abbreviations**: **ds**, dorsal slope; **exp**, extensor process; **flt**, flexor tubercle. Scale bars equal 5 mm (**A**, **B**) and 1 cm (**C–F**).

compared with the slightly posteriorly inclined proximal articulation of the terminal phalanx of *Phenacodus* (USGS 7146). The orientation of this articulation is very similar to that in *Tapirus* and *Hyracotherium* (e.g., USGS 25119), and unlike the progressively inclined proximal articulations in fossil horses and the eventually almost dorsally facing joint surfaces of extant horses and ruminants (Sondaar, 1968; Getty, 1975; Hussain, 1975). Asymmetry of the proximal articulation indicates that

FIGURE 65. Reconstructed composite right manus of *Cambaytherium thewissi*, using only preserved elements, to provide an approximation of structure and proportions. Carpus above, digits below. All elements were found isolated and represent multiple individuals. Carpus was reassembled from micro-CT scans (in Figs. 56 and 57), and some images were reversed or resized here to achieve the best fit, so scale is accurate only for digits. The phalanges are not certainly from the manus, and their digital positions are hypothetical. Metacarpals: Mc II, GU 292; Mc III, GU 1217; Mc IV, GU 818; Mc V, GU 847. Proximal phalanges (from digits II to V): GU 829, GU 280, GU 7008 (Mangrol Mine), GU 828. Intermediate phalanges (from digits II to V): GU 7009 (Mangrol), GU 8029, GU 845, GU 844. Terminal phalanx, GU 7021 (Mangrol). Except for the three specimens indicated from Mangrol Mine, and the magnum (WIF/A-1192, Mangrol), all others are from Vastan Mine. Digital photograph of digits II–V modified from Rose et al. (2014b).

this ungual pertains to digit II or IV, but whether it is from the manus or pes is unknown.

Figure 65 shows a reconstructed manus based on isolated elements now available, to provide an approximation of its proportions. The shorter and broader manus contrasts dramatically with that of the early perissodactyls *Hyracotherium* (Radinsky, 1966:fig. 3; Wood et al., 2011:fig. 13), *Homogalax* (Rose, 1996:

fig. 1), and *Heptodon* (Radinsky, 1965a:fig. 13) and more closely conforms with that of *Phenacodus* (Radinsky, 1966:fig. 3; Otts, 1991). *Cambaytherium* also seems to have relatively shorter and more robust metacarpals and phalanges than in the Torrejonian phenacodontid *Tetraclaenodon puercensis* (Kondrashov and Lucas, 2012:fig. 4). We caution that the elements shown in Figure 65 are not from one individual. Moreover, whereas the metacarpals can be definitively identified to digit, this is not true of the phalanges, which may come from a different digit than shown or may even derive from the pes. As indicated above, however, phalanges can be confidently identified as proximal, intermediate, or terminal.

Functional Morphology of the Forelimb

The forelimb of *Cambaytherium* possesses many features in common with phenacodontids and early perissodactyls, which are typically associated with cursorial adaptation—features such as a prominent greater tubercle, a deep olecranon fossa with a supratrochlear foramen, a wide and uneven radial head that is positioned anterior to the ulna rather than laterally, and anteriorly bowed antebrachial elements (e.g., Osborn, 1898; Rose, 1990; Otts, 1991; Wood et al., 2011). These features generally enhance speed, increase stride, and limit motion to a parasagittal plane. Little or no supination would have been possible at the elbow, and the manus would have been limited more or less to a pronated position. While primitively maintaining a long (but low) deltopectoral crest, lacking a capitular tail, and having less bowed and less reduced antebrachial bones, *Cambaytherium* is more derived than phenacodontids and resembles early perissodactyls in having a narrower capitulum and reduced entepicondyle, lacking an entepicondylar foramen, and having a more distinct lateral coronoid process on the ulna, which probably contributed to stability at the elbow.

The known carpal bones are generally similar to those of basal perissodactyls, with minor differences noted above. In particular, the pisiform is relatively larger than in perissodactyls, presumably a primitive resemblance to archaic ungulates such as *Arctocyon* (Argot, 2012). As in the latter, the relatively large pisiform may reflect that, compared with early perissodactyls, *Cambaytherium* had more powerful mm. flexor carpi ulnaris, abductor digiti quinti, and flexor digiti quinti brevis, which attach to the pisiform (e.g., Davis, 1964).

Cambaytherium had four well-developed and fully functional manual digits and may have retained the pollex as well, as in archaic ungulates. The manus of *Cambaytherium* was mesaxonic (Mc III longer and broader than adjacent metacarpals), but the relative difference in size from the other metacarpals is not great and is comparable to that in *Phenacodus* and *Homogalax*, and slightly less than in *Tapirus*. The metacarpals and phalanges are relatively short and robust, as in *Phenacodus*, and show no evidence of the elongation that characterizes *Hyracotherium* and *Heptodon*; however, they are relatively only slightly shorter than in *Homogalax*. The phalangeal articular anatomy suggests digitigrade to subunguligrade (with a digital pad as in *Tapirus*; Sondaar, 1968) stance, somewhat more advanced than *Phenacodus* and probably similar to *Hyracotherium*, based on the shape of the terminal phalanx and orientation of its proximal articulation. In equids, the angle between the dorsal slope and the ground (or volar surface) increased during evolution, as they became progressively unguligrade, from ~ 25° in *Mesohippus*, to 31° in *Merychippus*, and eventually to 47° in *Equus* (Hussain, 1975).

The combination of plesiomorphic and derived traits in the forelimb suggests that *Cambaytherium* was somewhat better adapted for running than was *Phenacodus*, but less cursorially specialized than basal perissodactyls. *Cambaytherium* may be best characterized as subcursorial.
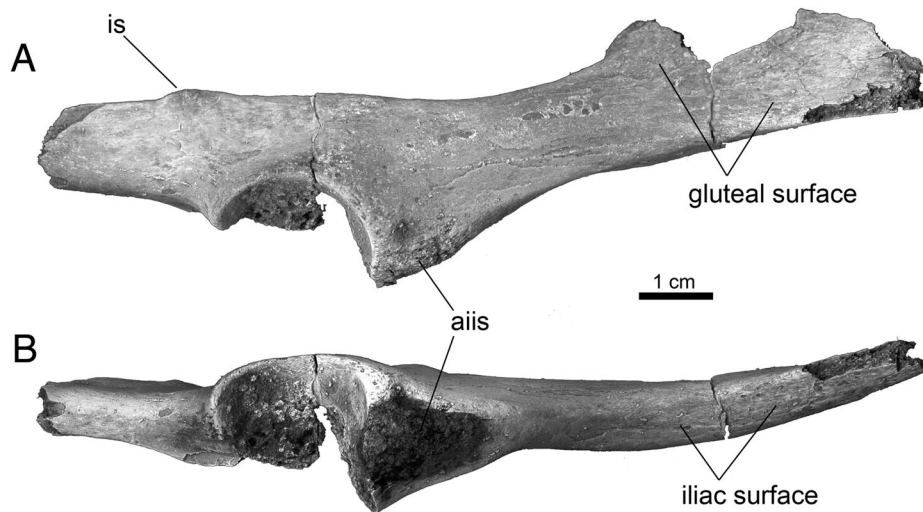
FIGURE 66. Right innominate of *Cambaytherium thewissi*, GU 9016, in **A**, lateral and **B**, ventral views; digital photographs. **Abbreviations**: **aiis**, anterior inferior iliac spine (for rectus femoris attachment); **is**, ischial spine.

Hind Limb

Pelvis—A fragmentary innominate from TAD-2 (GU 9016; Fig. 66) is allocated to *C. thewissi*. It consists of an incomplete ilium and ischium with a partial acetabulum. Notwithstanding its fragmentary condition, GU 9016 (TAD-2) is adequate to show that the ilium was longer than the ischium, with a flaring expansion craniomedially, as in both *Phenacodus* (Osborn, 1898) and *Hyracotherium* (Hussain, 1975; Wood et al., 2011). The dorsolateral-facing surface, for origin of deep gluteal muscles, is extensive (more so cranially) and flat or slightly concave; the ventrally facing iliac surface is narrow. The anterior inferior iliac spine (for origin of m. rectus femoris), anterior to the acetabulum, seems poorly defined, but its surface is eroded and it may originally have been larger. The ischial spine is weakly developed and slightly posterior to the acetabulum, as in *Hyracotherium* and *Heptodon*. The acetabulum, although incomplete, measures approximately 21 mm in craniocaudal diameter, an appropriate size for *C. thewissi* and too large for *C. gracilis*.

Femur—Fourteen femoral specimens belong to *Cambaytherium* (GU 198, GU 1218, and GU 1219 from Vastan; GU 7026 from Mangrol; GU 9208, GU 9209, GU 9210, GU 9213, GU 9237, WIF/A 2262, WIF/A 4207, and WIF/A 4257–4259 from Tadkeshwar). There is considerable size variation among these femora, making species identification challenging; however, most of the larger specimens probably represent *C. thewissi*, including the three specimens from Vastan Mine (which consist of only articular ends), two specimens from TAD-1 (WIF/A 2262 and WIF/A 4207; Fig. 67), and three specimens from TAD-2 (GU 9237, WIF/A 4258, and WIF/A 4259). Five smaller specimens from TAD-2 (GU 9208, GU 9209, GU 9210, and GU 9213, and tentatively WIF/A 4257) are referred to *C. gracilis* (Fig. 68), whereas the large proximal femur from Mangrol Mine (GU 7026) is tentatively referred to *C. marinus* (Fig. 69). GU 9210 and WIF/A 4257 differ from the others in having a flattened shaft; however, this may reflect postmortem deformation. The anatomy of these two specimens is otherwise perissodactyl-like and resembles that of the other *Cambaytherium* femora.

Only two specimens are complete (WIF/A 4207) or nearly so (GU 9208), preserving intact proximal and distal articulations and trochanters. The former, representing *C. thewissi*, measures approximately 138 mm in articular length (head to condyles) and is a little more than 20% longer than GU 9208, belonging to *C. gracilis* (Table 14). Width of the proximal end in *C. thewissi* (WIF/A 4207) is also roughly 20% greater than in *C. gracilis*, whereas the width of the proximal femur referred to *C. marinus* is twice the dimension in *C. gracilis*. The other specimens consist of either proximal or distal ends, or shafts with articular ends and greater trochanter missing. Nevertheless, the better-preserved specimens show anatomy closely similar to that of basal perissodactyls as well as *Phenacodus*.

In all three species, the head is hemispherical, with a prominent, deep fovea capitis for the ligamentum capitis (Figs. 67C, K, 69), located in the posteroproximal quadrant (Jenkins and Camazine, 1977). In two specimens, GU 198 (*C. thewissi*) and GU 9208 (*C. gracilis*), the fovea is a circular pit that does not appear to interrupt the distal margin of the articular surface, although damage to the margin renders this ambiguous in GU 9208. In the other three specimens (WIF/A 4207, *C. thewissi*; GU 7026, *C. marinus*; and GU 9210, *C. gracilis*), a shallow trough extends from the pit toward the posterior margin of the head and probably interrupted the margin, as in basal perissodactyls, but this cannot be established with certainty because the margin is slightly damaged in these three specimens. Maximum head diameter (approximately mediolateral) measures 11.3–12.4 mm in *C. gracilis*, 16.1–19.7 mm in *C. thewissi*, and 24.0 mm in *C. marinus*. The three trochanters are well developed as in early perissodactyls and phenacodontids. The greater trochanter projects above the head in all three species. In WIF/A 4207 (Fig. 67A–C), this projection is comparable in height to that in *Homogalax* (Rose, 1996) but relatively not as high as in *Hyracotherium* (Kitts, 1956; Wood et al., 2011). Although it is intact only in WIF/A 4207 (*C. thewissi*) and GU 7026 (*C. marinus*), the broken base of the trochanter is even with the head in GU 9208 and GU 9210 (*C. gracilis*), indicating that it extended above the head in these as well. In WIF/A 4207 and GU 7026, there is a salient superior projection on the posterior half of the greater trochanter, probably associated with the insertion of a large gluteus medius muscle, as in *Equus* (Getty, 1975), *Tapirus* (Murie, 1872), and many other mammals. The trochanteric fossa is elongate and deep and is bounded caudally by the prominent intertrochanteric crest, which extends distally to the level of the top of the lesser trochanter. The lesser trochanter is an elongate crest on the posteromedial border extending from the base of the neck along the proximal third of the shaft. Opposite the distal end of the lesser trochanter is the prominent third trochanter, marked by an elongate tubercle with an anteriorly deflected lip, on which the superficial gluteal muscle inserts (Getty, 1975). As in *Homogalax* and *Hyracotherium*, the third trochanter is positioned slightly more proximally than in
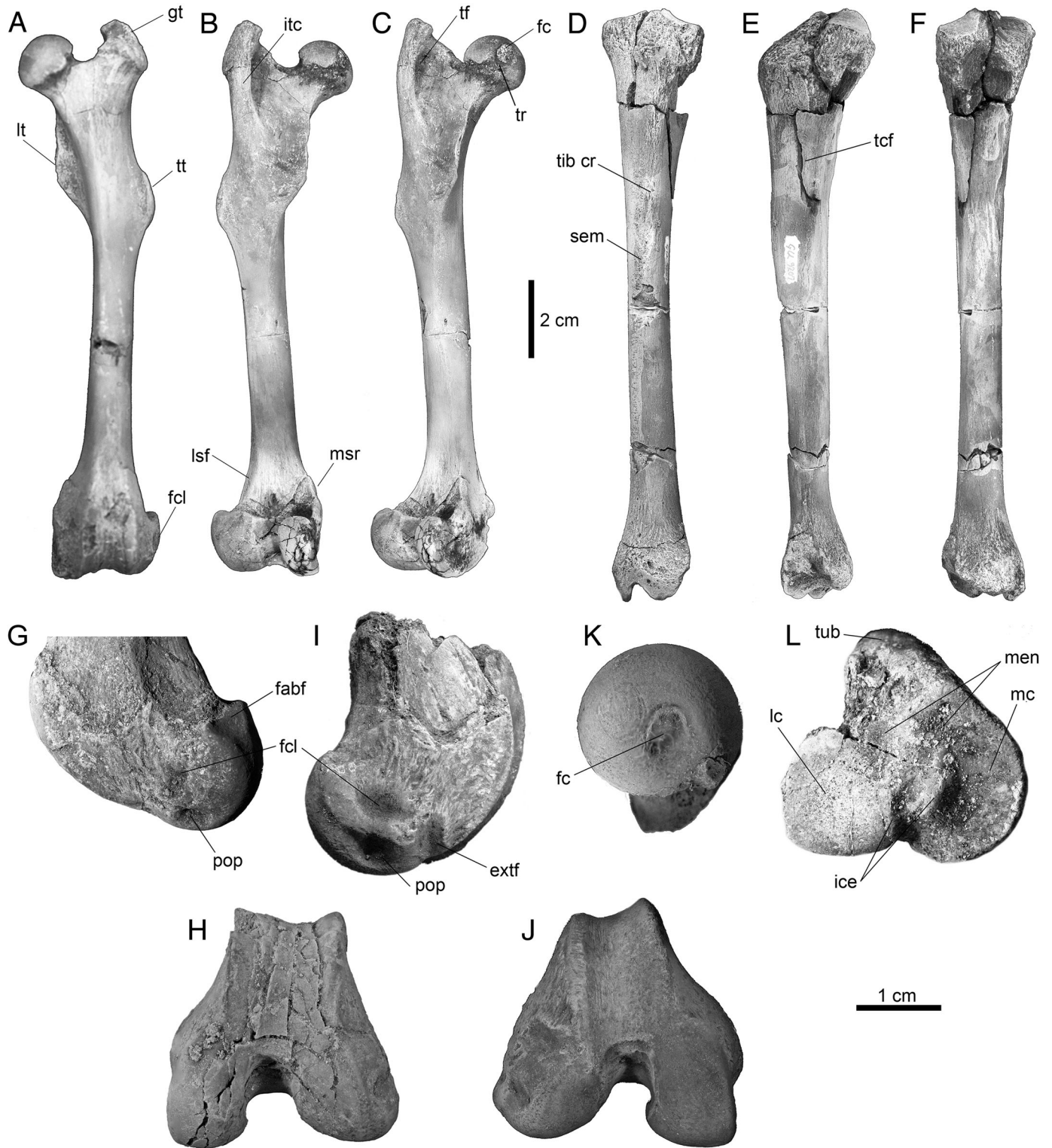
FIGURE 67. Femur and tibia of *Cambaytherium thewissi*, digital photographs. **A–C**, left femur, WIF/A 4207, in **A**, anterior, **B**, posterior, and **C**, posteromedial views. **D–F**, left tibia, GU 9207, in **D**, anterior, **E**, lateral, and **F**, posterior views. **G, H**, distal end of WIF/A 4207 in **G**, lateral and **H**, distal views. **I, J**, distal end of right femur, GU 198, in **I**, lateral and **J**, distal views. **K**, posteromedial view of right femoral head, GU 198. **L**, proximal end of left tibia, GU 9211. **A–F** to the same scale; **G–L** to the same scale. **Abbreviations**: **extf**, extensor fossa for origin of m. extensor digitorum longus; **fabf**, fabellar facet; **fc**, fovea capitis; **fcl**, fossa for fibular collateral ligament; **gt**, greater trochanter; **ice**, intercondylar eminence; **itc**, intertrochanteric crest; **lc**, lateral condyle of tibia; **lsf**, lateral supracondylar fossa; **lt**, lesser trochanter; **mc**, medial condyle of tibia; **men**, fossae for attachment of menisci; **msr**, medial supracondylar ridge; **pop**, fossa for tendon of m. popliteus; **sem**, tubercle for insertion of m. semitendinosis; **tcf**, fossa for m. tibialis cranialis; **tf**, trochanteric fossa; **tib cr**, tibial crest; **tr**, trough from fovea; **tt**, third trochanter; **tub**, tibial tuberosity.
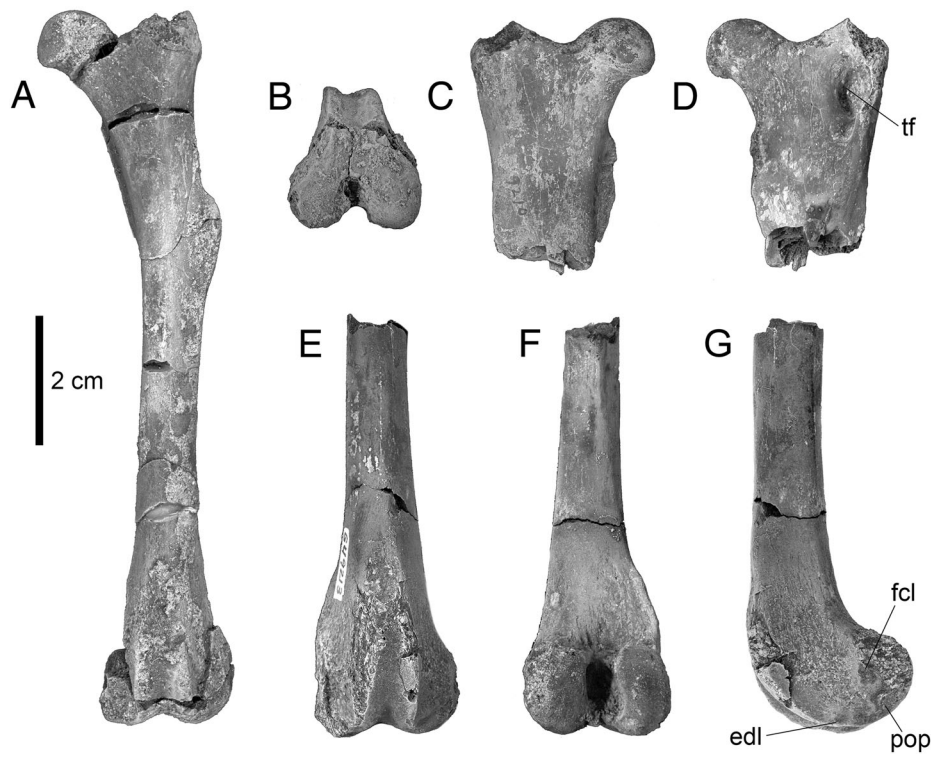
FIGURE 68. Femora of *Cambaytherium gracilis*, digital photographs. **A**, **B**, left femur, GU 9208, in **A**, anterior and **B**, distal views. **C**, **D**, proximal right femur, GU 9210, in **C**, anterior and **D**, posterior views. **E–G**, distal left femur, GU 9213, in **E**, anterior, **F**, posterior, and **G**, lateral views. **Abbreviations**: **edl**, fossa for origin of m. extensor digitorum longus; **fcl**, fossa for attachment of fibular collateral ligament; **pop**, fossa for attachment of m. popliteus tendon; **tf**, trochanteric fossa.
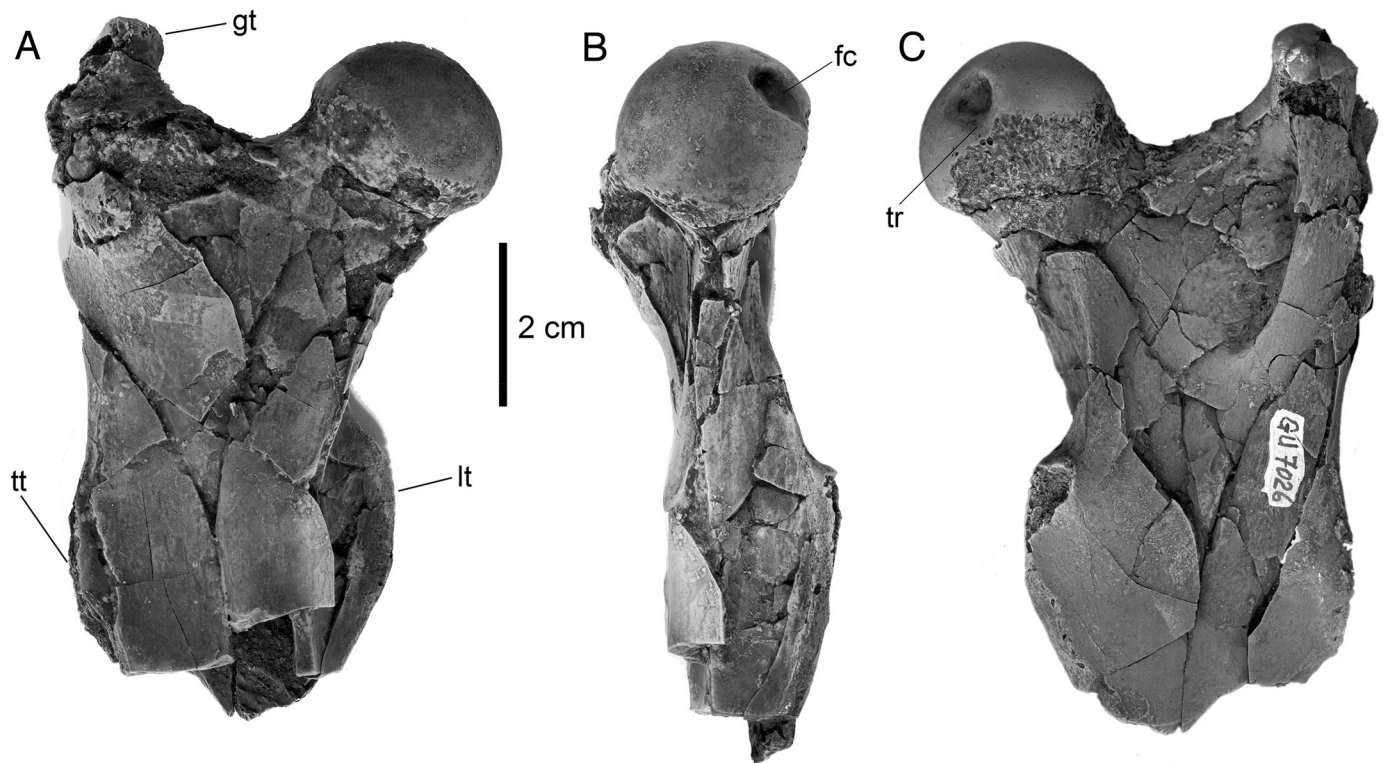
FIGURE 69. Proximal right femur of *Cambaytherium marinus*, GU 7026, digital photographs in **A**, anterior, **B**, medial, and **C**, posterior views. **Abbreviations**: **fc**, fovea capitis; **gt**, greater trochanter; **lt**, lesser trochanter; **tr**, trough from fovea; **tt**, third trochanter.

TABLE 14. Femur dimensions (in mm) of *Cambaytherium*.

Specimen no.	Species	A	B	C	D	E	F	G	H	I	J	K	L
GU 198	*C. thewissi*?			19.0 × 19.7					32.4	34.0	13.35		
GU 1218	*C. thewissi*?								>30.0		13.8		
GU 7026	*C. marinus*			21.7 × 24.0	54.5	23.8 est							
GU 9208	*C. gracilis*		112.7	12.4 × —	26.1		9.0	10.0	21.3 est	23.2	9.1		
GU 9210	*C. gracilis*			11.3 × 11.2	29.2								
GU 9213	*C. gracilis*						9.25	11.05	22.7	25.3	9.0		
WIF/A 2262	*C. thewissi*						11.6	12.3					
WIF/A 4207	*C. thewissi*	142.0	138.0	16.1 × 15.1	33.5	17.5	10.3	11.6	27.1	29.6	13.95	37.0	46.0
WIF/A 4257	*C. gracilis*?						11.4	9.8					
WIF/A 4258	*C. thewissi*						11.9	13.1					
WIF/A 4259	*C. thewissi*						13.6	13.8					

A: maximum length; **B**: articular length (= F1 in Scott, 1983:fig.1); **C**: head diameters; **D**: proximal width; **E**: greater trochanter anteroposterior dimension; **F**: midshaft mediolateral diameter; **G**: midshaft anteroposterior diameter; **H**: distal mediolateral width; **I**: distal anteroposterior depth; **J**: width of patellar groove; **K**: distance from top of greater trochanter to middle of lesser trochanter; **L**: distance from top of greater trochanter to middle of third trochanter. **Abbreviation**: **est**, estimated.

phenacodontids, in which it is distal to the lesser trochanter (e.g., Kitts, 1956:pl. 4; USGS 25094). The cross-section of the midshaft is ovoid, its long axis oblique (anteromedial-posterolateral, in most specimens about 10–20% greater than the lesser diameter); farther distally, the shaft becomes more nearly round in cross-section. Apart from the trochanters, the shaft generally displays no distinctive surface features. Distally, however, a narrow and shallow lateral supracondylar fossa is present proximal to the lateral condyle. In *Equus*, this marks the origin of m. flexor digitorum superficialis and the lateral head of m. gastrocnemius (Getty, 1975). Medially, a short, sharp supracondylar ridge arises proximal to the medial condyle (Fig. 67B), as in *Hyracotherium* (Wood et al., 2011). This is the site of insertion of the largest head of the m. semimembranosus in *Tapirus*, *Equus*, *Babyrousa*, and many other mammals, and also the adductor muscle in *Equus* (Murie, 1872; Getty, 1975; Macdonald and Kneepkens, 1995). The medial head of the gastrocnemius muscle also originates here.

The distal articulation is slightly deeper (5–10%) in the anteroposterior plane than mediolaterally, with a moderately wide and deep patellar trochlea (Figs. 67H, J). The trochlea is about half or less than half the distal femoral width and is relatively slightly narrower in *C. gracilis* (Fig. 68B). Both the distal end and the patellar trochlea are relatively wider than in *Hyracotherium*. The medial condyle is narrower and projects farther distally than the lateral condyle, as in early perissodactyls. The lateral condyle is wider than the medial condyle and extends slightly farther proximally. In WIF/A 4207, the lateral condyle bears a slightly concave, semilunar facet on its proximal-facing posterior surface, indicating a sesamoid bone (fabella) in the tendon of the lateral head of the gastrocnemius muscle (Fig. 67G). Wood et al. (2011) reported such a fabella in *Hyracotherium grangeri*. There is no evidence of a fabellar facet on the medial condyle of WIF/A 4207, nor were facets detected in other specimens of *Cambaytherium* owing to damage in this area. Several features are clearly visible on the well-preserved epicondyles of WIF/A 4207 and GU 198 (Fig. 67G, I). An extensor fossa (for origin of the extensor digitorum longus) is evident as a notch where the lateral ridge of the patellar trochlea meets the lateral condyle. Posterior to this fossa on the margin of the lateral condyle is a pit for the popliteal tendon, and proximal to this on the lateral epicondyle is another pit for the fibular collateral ligament. A less well-defined fossa for the tibial collateral ligament is present on the medial epicondyle.

Patella—A single left(?) patella, GU 8018, is assigned to *C. thewissi* (Fig. 70A–C). It is moderately elongate and tapers distally, with the apex broken off; even so, it is nearly 50% longer than wide (length = 19.3 mm, width = 13.2 mm). The posterior (articular) surface consists of the large femoral facet, gently concave proximodistally with a central, rounded, vertical ridge, and more strongly convex mediolaterally but flattened at the margins. The femoral surface is relatively symmetrical, making it difficult to be certain of the side; however, if it is a left side, the medial femoral surface is slightly larger, as in *Equus* (Getty, 1975). The anterior surface is convex in both directions and rugose, for insertion of some fibers of m. quadriceps femoris. There is a rectangular, concavoconvex surface proximally for attachment of the central part of the quadriceps tendon and an elongate, slightly concave surface proximomedially (assuming it is a left patella) for the m. vastus medialis component of the quadriceps.

Tibia—Seven tibial specimens are known, six representing *Cambaytherium thewissi* (GU 278, GU 739, GU 779, and GU 1220 from Vastan; GU 9207 and GU 9211 from TAD-2; Figs. 67D–F, 71A–E) and one tentatively allocated to *C. marinus* (GU 8052 from Vastan; Fig. 71F–J); no tibiae referable to *C. gracilis* have been found. Only one specimen (GU 9207) is complete, although the proximal end is somewhat damaged. GU 9211, however, preserves the proximal end more or less intact, and the distal end is well preserved in several other specimens. Because no individuals with associated femur and tibia are known, it is impossible to be certain of the relative proportions of the long bones; however, GU 9207 is about 10% longer (Table 15) than the only complete femur (WIF/A 4207), so it is reasonable to conclude that the tibia was at least as long as the femur and probably slightly longer. If this is an accurate inference, the crural index ([tibia length/femur articular length] × 100) of *C. thewissi* may have been more comparable to that of the small phenacodontids *Tetraclaenodon puercensis* and *Phenacodus vortmani* (crural indices [CIs] of 106 and 112, respectively; Otts, 1991) than to that of *Hyracotherium grangeri* (CI = 96, from measurements in Wood et al., 2011).

The proximal end (Fig. 67L) is triangular (viewed from above), the apex formed anteriorly by the tibial tuberosity, for attachment of the patellar ligament; mediolateral and anteroposterior dimensions of the proximal end are roughly equal. The medial and lateral condyles, tubercles of the intercondylar eminence, and tibial tuberosity are essentially the same as in *Hyracotherium*. The condyles are mediolaterally concave and anteroposteriorly slightly convex (the lateral one more clearly so). Anterior to the intercondylar tubercles in GU 9211 are two shallow depressions to which the medial and lateral menisci attached (Getty, 1975). Neither the proximal fibular facet nor the extensor groove (for the tendon of m. extensor digitorum longus) is preserved in either of the proximal tibiae.

The tibial crest (= cranial border) is low and rounded and ends in a weak tubercle a little less than halfway down the shaft. This
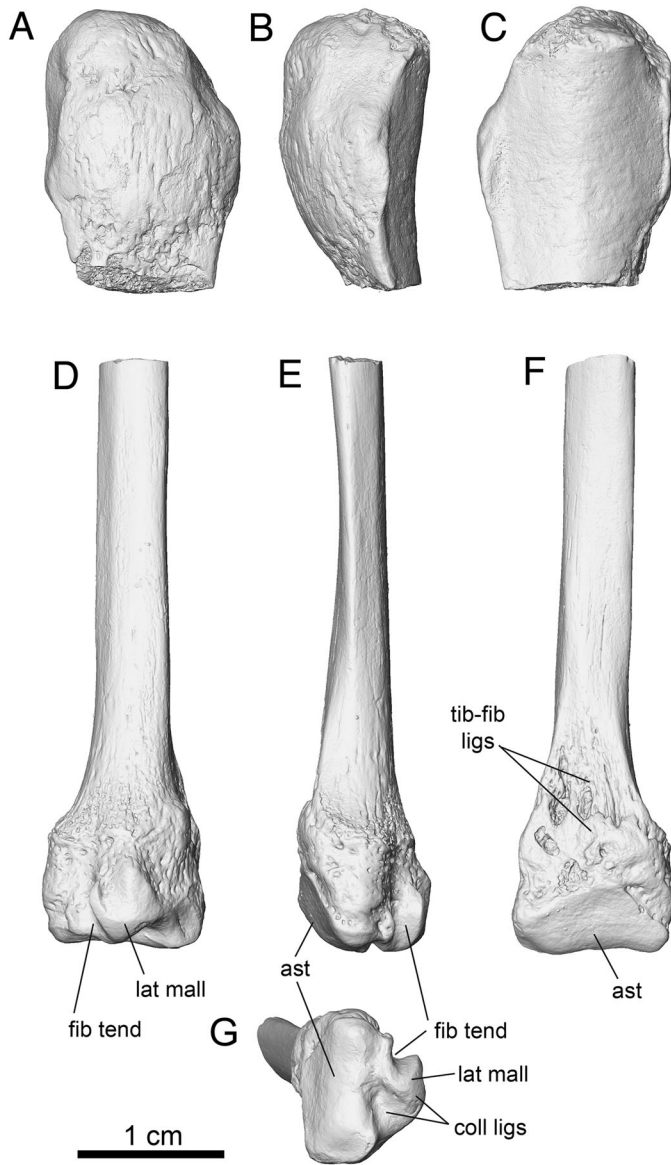
FIGURE 70. Patella and fibula of *Cambaytherium thewissi*. **A–C**, left(?) patella, GU 8018, in **A**, anterior, **B**, lateral, and **C**, posterior views. **D–G**, distal right fibula, GU 300, in **D**, lateral, **E**, posterior, **F**, medial, and **G**, distal views. **Abbreviations**: **ast**, astragalar facet; **coll ligs**, lateral collateral ligaments; **fib tend**, sulcus for tendon of fibularis muscle; **lat mall**, lateral (fibular) malleolus; **tib-fib ligs**, tibiofibular ligaments.

FIGURE 71. Distal left tibiae of *Cambaytherium*, to the same scale. **A–E**, *C. thewissi*, GU 739, in **A**, anterior, **B**, lateral, **C**, posterior, **D**, medial, and **E**, distal views. **F–J**, *C. marinus*, GU 8052, in **F**, anterior, **G**, lateral, **H**, posterior, **I**, medial, and **J**, distal views. **Abbreviations**: **ant pr**, anterior process; **ast f**, astragalar facet; **f dig long**, sulcus for tendon of flexor digitorum longus; **f hall long**, sulcus for tendon of flexor hallucis longus; **fib**, distal fibular syndesmosis; **intoss cr**, crest for attachment of interosseous ligament; **m mall**, medial malleolus; **mall f**, malleolar facet (anterior extension); **med coll lig**, attachment site of medial (tibial) collateral ligament; **musc line**, muscular line; **pop line**, popliteal line; **post pr**, posterior process; **sem**, insertion of m. semitendinosus; **tib cr**, tibial crest; **?**, posteromedial rugosity of unknown function.

tubercle, marking the insertion of the semitendinosus muscle (Figs. 67D, 71A), is more distal than in *Hyracotherium* (e.g., USGS 21858; see also Wood et al., 2011) and *Homogalax* (Rose, 1996) but appears to be slightly more proximal than in *Phenacodus trilobatus* (e.g., USNM 487923) and similar in position to that in *P. vortmani* (Otts, 1991:fig. 102). The

TABLE 15. Tibia dimensions (in mm) of *Cambaytherium*.

Specimen no.	Species	A	B	C	D	E	F	G
GU 278	*C. thewissi*						22.2	15.9
GU 739	*C. thewissi*				9.4	12.0	20.5	15.2
GU 9207	*C. thewissi*	155.0	26.8 est	29.0 est	10.6	13.1	21.2	15.85
GU 9211	*C. thewissi*		30.5 est	29.0 est	13.2	11.75		
GU 8052	*C. marinus*						28.5	23.6

A: maximum length; **B**: proximal width; **C**: proximal anteroposterior depth; **D**: midshaft mediolateral diameter; **E**: midshaft anteroposterior diameter; **F**: distal width; **G**: distal anteroposterior depth. **Abbreviation**: **est**, estimated.

semitendinosus is a hamstring muscle that extends the hip and flexes the knee (e.g., Getty, 1975), and a more distal insertion confers power, whereas speed would be increased by a more proximal insertion. The moderately deep fossa for m. tibialis cranialis (= tibialis anterior) on the anterolateral surface of the proximal shaft (Fig. 67E) is similar to that in basal perissodactyls and *Phenacodus*. The posterior (caudal) surface of the proximal shaft is flat to slightly mediolaterally concave, and in GU 9211 it preserves an oblique popliteal line that extends toward the middle of the medial edge (less evident in GU 739; Fig. 71C). In *Equus*, this line marks the boundary between the popliteus muscle proximomedially and the flexor digitorum profundus distolaterally (Getty, 1975). Other muscular lines lateral to the popliteal line in GU 9211 are probably related to the origin of m. flexor digitorum profundus. On the lateral side of the shaft, running from the posterolateral border proximally to the anterior margin of the fibular facet distally, is a low sharp interosseous crest (GU 739, GU 779, GU 9207, GU 9211), which is slightly rugose near midshaft in GU 739 (Fig. 71B). This interosseous crest is barely detectable in GU 8052 (*C. marinus*). On the posteromedial aspect of the shaft, about 2 cm proximal to the distal end, is a short rugosity (GU 278, GU 739) of unknown significance; notably it is also present in GU 8052 (Fig. 71D, I).

The distal end of the tibia, wider mediolaterally than it is deep anteroposteriorly, consists of the astragalar facet flanked by sizable anterior and posterior processes and the salient tibial malleolus medially (Fig. 71E, J). The astragalar articulation is formed by a pair of obliquely oriented grooves to accommodate the astragalar ridges—a deep, narrow groove medially and a wider, steeply inclined lateral surface (which forms a groove with the distal fibula). The two grooves are separated by an oblique ridge that articulates with the trochlear groove of the astragalus and gives rise to anterior and posterior processes at the margin of the joint surface.

The malleolus projects distally slightly farther than the processes, and slightly more so at its anterior end. The laterally facing facet on the malleolus articulates with the crescentic facet on the medial side of the astragalar trochlea (Fig. 72K). This malleolar facet extends onto the anterior surface of the malleolus (best seen in GU 278 but also evident in GU 739; Fig. 71A) and contacts a shallow fossa on the medial side of the neck of the astragalus during dorsiflexion (Fig. 72B; see Tarsals, below). Neither the fossa nor the articulation was observed in *Phenacodus* (e.g., *P. trilobatus*, USGS 7146; *P. vortmani*, USGS 21878, USGS 25302), but both are clearly seen in *Hyracotherium* (e.g., USGS 25157, USNM 527497). At the anterior end of the medial face of the malleolus is a prominent, shallow fossa, probably marking attachment of the medial collateral ligament (Fig. 71D, I), as inferred in *Heptodon* and *Hyracotherium* (Radinsky, 1965a; Wood et al., 2011). Just posterior to this fossa is a deep, narrow sulcus for the tendon of the flexor digitorum longus muscle (Radinsky, 1965a); posterior to the latter, a less well-defined groove may be associated with the tendon of m. flexor hallucis longus. The anterior and posterior processes at the distal end of the tibia arise at the ends of the trochlear ridge, the posterior process almost as prominent as the malleolus and mainly bordering the medial groove, and the anterior process somewhat smaller and bordering the lateral groove. These processes further restricted any mediolat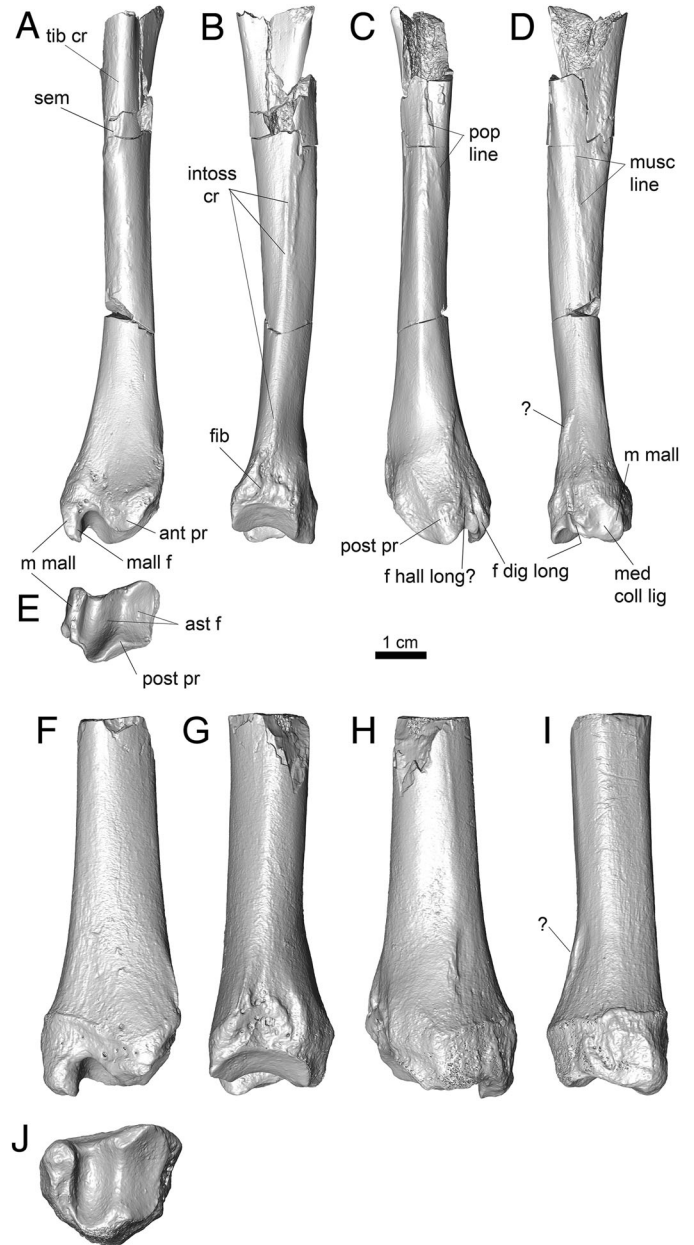eral movement at the ankle joint. On the lateral aspect of the distal tibia, just proximal to the astragalar facet, a triangular rugose surface facing laterally and somewhat posteriorly marks the syndesmotic distal tibiofibular joint (Fig. 71B). The configuration of the cruroastragalar joint in *Cambaytherium* closely resembles that of perissodactyls and effectively restricted motion at the joint to parasagittal flexion-extension.

GU 8052 (Fig. 71F–J) is much larger than the other tibiae and is tentatively referred to *C. marinus*. It is deeper anteroposteriorly

than the distal tibiae of *C. thewissi* (depth/width = 0.83 compared with 0.72–0.75 in *C. thewissi*; see Table 15) and has a less defined sulcus for m. flexor digitorum longus, but in other respects it is essentially identical to the tibia of *C. thewissi*.

Fibula—The fibula is represented by a single specimen, a distal right fibula (GU 300; Fig. 70D–G). It is a slender, gracile bone, substantially smaller in caliber than the tibia. The preserved fragment is about 4 cm long, and the shaft is flattened in a plane slightly oblique to a transverse (coronal) plane. Its mediolateral dimension is 60% as wide (~3 mm) as the anteroposterior dimension (~5 mm) at a distance 3 cm from the distal end. It expands markedly at the distal end (anteroposterior length = 11.0 mm, anteroposterior width = 9.0 mm).

The medial surface bears a long, triangular facet, for the lateral side and flange of the astragalus, which wraps smoothly onto the distal face. The facet extends from the anterior to the posterior border of the bone. Proximal to this articular surface medially, the shaft is rugose for about 1 cm, the rugosity marking the attachment of tibiofibular and interosseous ligaments of the tibiofibular syndesmosis. Lateral to the astragalar facet is the fibular (lateral) malleolus, with a distinct groove posterior to it to guide the tendons of the fibularis longus and brevis muscles, evertors of the foot. Various collateral ligaments (astragalofibular, calcaneofibular, and posterior tibiofibular) generally attach to the lateral malleolus and the fossa just posterior to it, but it is difficult to be certain of the precise attachment sites on GU 300. Nevertheless, these ligaments and the well-developed syndesmosis helped to stabilize the distal crural joint and limit mobility largely to a parasagittal plane.

Tarsals—The tarsus of *Cambaytherium* has an alternating or interlocking (diplarthral) arrangement, like that of perissodactyls but unlike that of paenungulates and some phenacodontids (Rasmussen et al., 1990): i.e., the astragalus articulates with both the navicular and the cuboid. In most other respects, however, the known elements (astragalus, calcaneus, cuboid, and navicular) show a mosaic of perissodactyl and more primitive phenacodontid-like features. All known tarsals represent *C. thewissi* except for one astragalus, referred to *C. gracilis*.

Six astragali are known from Vastan Mine: GU 304, GU 769, GU 770, GU 780 (Fig. 72A–L), GU 814, and IITR 535 (Bajpai et al., 2006). The trochlea is wider and proximodistally shorter than in basal perissodactyls (Table 16), and the neck is relatively slightly longer. All Vastan specimens have either a dorsal astragalar foramen and canal (GU 780, IITR 535) or an open canal (notch) in the same position (Fig. 72E, J). The canal was traced through successive micro-CT slices in GU 780 and was observed to extend from the dorsal astragalar foramen to the astragalar sulcus on the ventral surface (Fig. 72L). These astragalar characters are more like those of *Phenacodus* and other condylarths than they are like basal perissodactyls such as *Hyracotherium* and *Homogalax* (Fig. 73A–F). Notably, the astragalar canal and foramen have been lost in all perissodactyls.

As in basal perissodactyls, the astragalar trochlea is deeply grooved and oriented obliquely to the long axis of the pes (to about the same degree as in *Hyracotherium*), but it is asymmetrical (the lateral part wider than the medial part), more as in phenacodontids. Consequently, the deepest part of the tibial articulation is medial to the midline of the trochlea. The medial part of the trochlear tibial facet is steeply inclined, forming a sharply acute angle with the medial wall, whereas the lateral part is more gently sloping; the two parts of the facet meet at the trochlear groove at a right or slightly obtuse angle. The medial trochlear rim is somewhat rounded and longer than the lateral rim (because of its greater posterior extension), whereas the lateral rim is sharper. The medial and lateral walls of the trochlea (except for the distolateral flange, which articulated with the distal face of the fibular malleolus), with their tibial and fibular malleolar facets, respectively, are essentially vertical
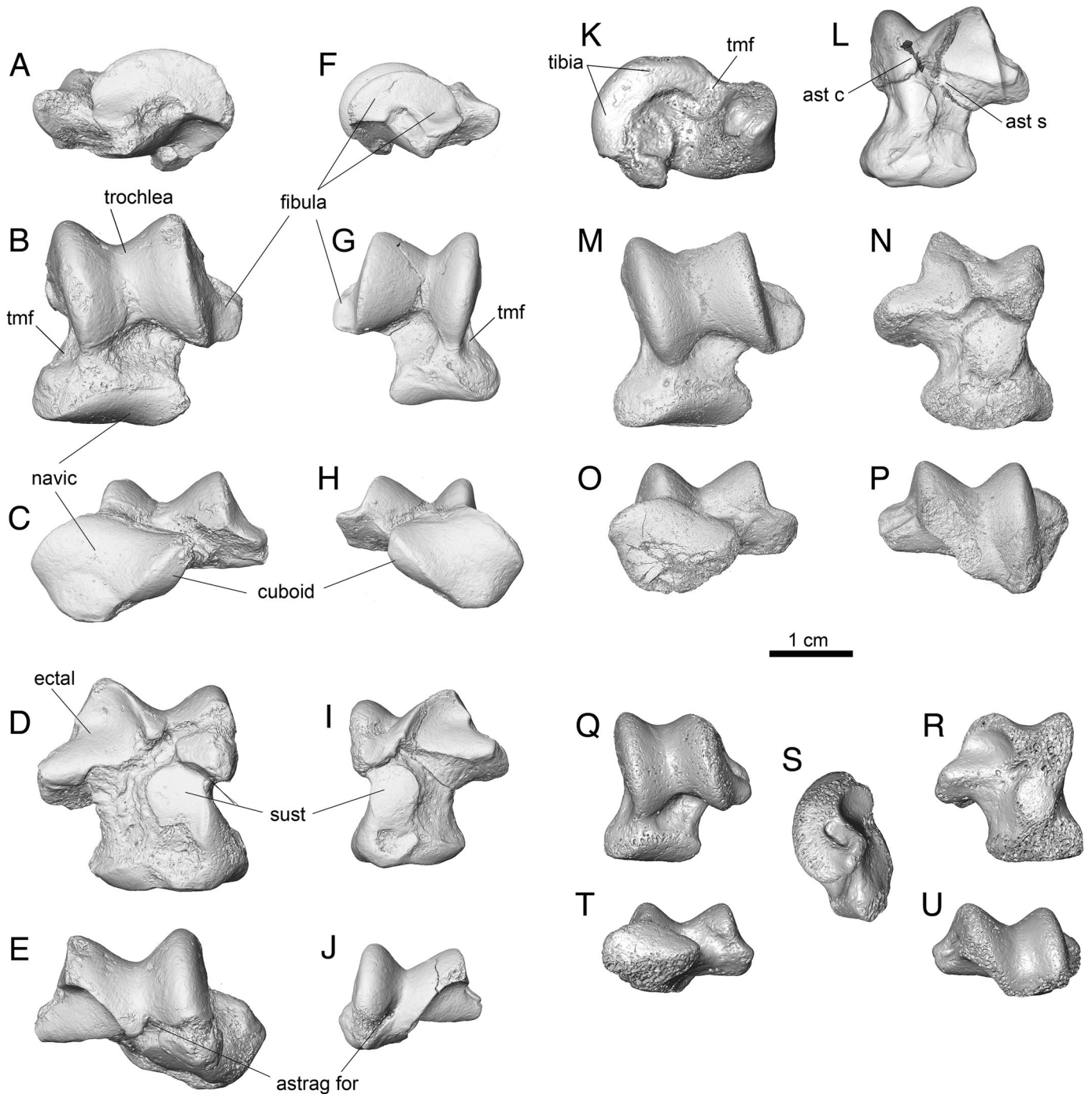
FIGURE 72. Astragali of *Cambaytherium*. **A–E, K,** *C. thewissi*, left astragalus, GU 770, from Vastan Mine, in **A,** lateral, **B,** anterior (= dorsal), **C,** distal, **D,** posterior (= ventral), **E,** proximal, and **K,** medial views. **F–J, L,** *C. thewissi*, right astragalus, GU 780, from Vastan Mine, in **F,** lateral, **G,** anterior (= dorsal), **H,** distal, **I,** posterior (= ventral), and **J,** proximal views. **L,** transparent posterior view showing digitally filled astragalar canal (dark gray) passing from dorsal astragalar foramen to the astragalar sulcus. **M–P,** *C. thewissi*, left astragalus, WIF/A 4216, from TAD-2, in **M,** anterior, **N,** posterior, **O,** distal, and **P,** proximal views. **Q–U,** *C. gracilis*, left astragalus, WIF/A 4263, from TAD-1, in **Q,** anterior, **R,** posterior, **S,** lateral, **T,** distal, and **U,** proximal views. Joint surfaces indicated. **Abbreviations: ast c,** astragalar canal; **ast s,** astragalar sulcus; **astrag for,** astragalar foramen; **ectal,** ectal or posterior calcaneal facet; **navic,** navicular facet; **sust,** sustentacular facet; **tmf,** tibial malleolar fossa.

relative to the trochlear articulation. Distally, the tibial malleolar facet continues onto the medial side of the neck, forming a shallow fossa (Fig. 72B, G) that articulated with the anterior face of the malleolus in full dorsiflexion. This fossa appears to be homologous with the cotylar fossa of afrotheres and some

other mammals (e.g., tillodonts), although it is much less conspicuous.

The navicular articulation is saddle-shaped, as in perissodactyls and in contrast to the convex astragalar head of phenacodontids, but the concavity is shallower than in *Hyracotherium* and most

TABLE 16. Astragalar dimensions (in mm) in *Cambaytherium* and comparative taxa.

Specimen no.	Taxon	Locality	L med	L lat	D med keel	L med keel	L lat keel	L neck	W troch max	W troch mid
GU 304	*C. thewissi*	Vastan	21.1		14.6	15.35		9.35 est		
GU 769	*C. thewissi*	Vastan	24.1+	23.5+	15.3	17.4	16.2	11.0	22.0 est	15.8
GU 770	*C. thewissi*	Vastan	24.25	25.0	17.2	18.5	17.05	10.7	24.6	16.25
GU 780	*C. thewissi*	Vastan	20.75	22.0	13.25	15.9	12.65	10.2	19.3	12.65
GU 814	*C. thewissi*	Vastan	20.5	22.5	15.25	16.3	14 est	9.3	22.3	14.25
WIFA 4216	*C. thewissi*	TAD-2	23.15		15.3	17.95		11.1	21.5	14.5
WIFA 4263	*C. gracilis*	TAD-1	18.4+	17.8+		13.95+	12.35+	8.7		12.1
USGS 6097	*Hyracotherium* sp.	Willwood	15.05	16.8	10.15	12.0	11.9	5.5	11.95	9.0
USGS 25157	*Hyracotherium* sp.	Willwood	16.7	18.9		13.5	13.2	5.45	13.3	9.6
USGS 38039	*Hyracotherium* sp.	Willwood	15.7	16.35	9.35	12.5	11.05		12.0	8.65
USNM 487930	*Hyracotherium* sp.	Willwood	16.95	18.0		14.1	13.0	6.4	14.5	10.15
USNM 527497	*Hyracotherium* sp.	Willwood	12.05	12.5	7.4	9.1	8.8	5.4	9.5	6.7
DMNS 125130	*Hyracotherium* sp.	Willwood	15.7	16.55		12.7	11.35+	6.1	12.0	8.4
DMNS 125131	*Hyracotherium* sp.	Willwood	14.4	15.3	9.05	12.3	10.55	5.95	12.0	9.25
USGS 25308	Perissodactyla	Willwood	18.3	19.6	10.15	13.9+	14.9	7.7	15.9	11.6
USGS 25325	*Heptodon* or *Lambdotherium*	Willwood	28.5	31.9	18.6+	23.4	23.65	11.2	24.45	18.2
USGS 7146	*Phenacodus trilobatus*	Willwood	40.5	41.85	21.1	27.9	31.7	17.55	33.1	24.3

Specimen no.	Taxon	Locality	W lat troch	W med troch	Head W max	Head D max	W nav facet	W cub facet
GU 304	*C. thewissi*	Vastan		6.4	15.3	9.7	9.55	4.1
GU 769	*C. thewissi*	Vastan	8.2	7.0				
GU 770	*C. thewissi*	Vastan	8.55	7.6	19.0	11.8	12.2	6.15
GU 780	*C. thewissi*	Vastan	7.1	5.85	13.9	10.4	9.5	4.1
GU 814	*C. thewissi*	Vastan	8.0	6.0	15.9	11.4	10.15	4.7
WIFA 4216	*C. thewissi*	TAD-2	7.7	6.9	16.9	12.35	11.6	
WIFA 4263	*C. gracilis*	TAD-1	6.2	5.8	12+			
USGS 6097	*Hyracotherium* sp.	Willwood	4.65	4.0	9.95	7.9	7.15	
USGS 25157	*Hyracotherium* sp.	Willwood	5.1	4.4	11.55	8.65	8.2	2.7
USGS 38039	*Hyracotherium* sp.	Willwood			10.15	7.8	6.9 est	3.0
USNM 487930	*Hyracotherium* sp.	Willwood	5.25	4.2	12.0	8.8	7.95	2.15
USNM 527497	*Hyracotherium* sp.	Willwood	3.5	3.2	8.9	6.5	5.1	1.95
DMNS 125130	*Hyracotherium* sp.	Willwood	4.7	3.7		7.85		
DMNS 125131	*Hyracotherium* sp.	Willwood	4.8	4.1	10.65	7.75	6.5	
USGS 25308	Perissodactyla	Willwood	6.0	5.3	12.8	9.5	9.25	3.9 est
USGS 25325	*Heptodon* or *Lambdotherium*	Willwood	10.35	8.8	21.0	15.5	13 est	
USGS 7146	*Phenacodus trilobatus*	Willwood	13.0	10.45	25.0	18.3	25.0	

Abbreviations: **D med keel**, anteroposterior depth of medial keel; **est**, estimated; **Head D max**, maximum anteroposterior depth of head; **Head W max**, maximum width of head; **L lat**, length measured laterally; **L lat keel**, length of lateral keel; **L med**, length measured medially; **L med keel**, length of medial keel; **L neck**, length of neck from base of trochlear groove to middle of navicular facet; **W cub facet**, width of cuboid facet; **W lat troch**, width of lateral part of trochlea from keel to depth of groove; **W med troch**, width of medial part of trochlea from keel to depth of groove; **W nav facet**, width of navicular facet; **W troch max**, maximum width of trochlea including flanges measured parallel to navicular facet; **W troch mid**, width of trochlea at the middle between outsides of keels.

other basal perissodactyls. However, it appears to be comparable in this feature to *Pliolophus barnesi* from the early Ypresian at Abbey Wood (Hooker 2010:fig. 54). On the lateral side of the head is a narrow facet for the cuboid, gently convex for most of its length but becoming slightly concave at the posterior end. The cuboid facet is relatively a little larger than in *Hyracotherium*. In this respect, *Cambaytherium* is more like perissodactyls, because phenacodontids have a serial tarsus and lack a cuboid facet.

On the posterior (calcaneal) surface of the astragalus, the posterior calcaneal (ectal) facet is relatively wider and less strongly convex than in *Hyracotherium*. The shallower ectal facet is a resemblance to *Phenacodus*, but the facet is more triangular in *Cambaytherium*. The sustentacular facet is ovoid and wider

than that of *Hyracotherium* and is nearly flat, except at the proximal end where it is abruptly reflected onto the ventrodistal surface of the medial trochlear rim, as in *Phenacodus* and most *Hyracotherium* examined.

Astragali of *C. thewissi* (WIF/A 4216, from TAD-2; Fig. 72M–P) and *C. gracilis* (WIF/A 4263, from TAD-1; Fig. 72Q–U) from Tadkeshwar Mine, each represented by a single specimen, lack an astragalar foramen; hence, the trochlear articular surface extends farther posteroventrally. In other respects, they closely resemble the astragali from Vastan Mine.

Two calcanei are allocated to *Cambaytherium thewissi* (Fig. 74). WIF/A 1190 from Mangrol Mine is a complete left calcaneus, although somewhat eroded. GU 772 is a damaged distal left
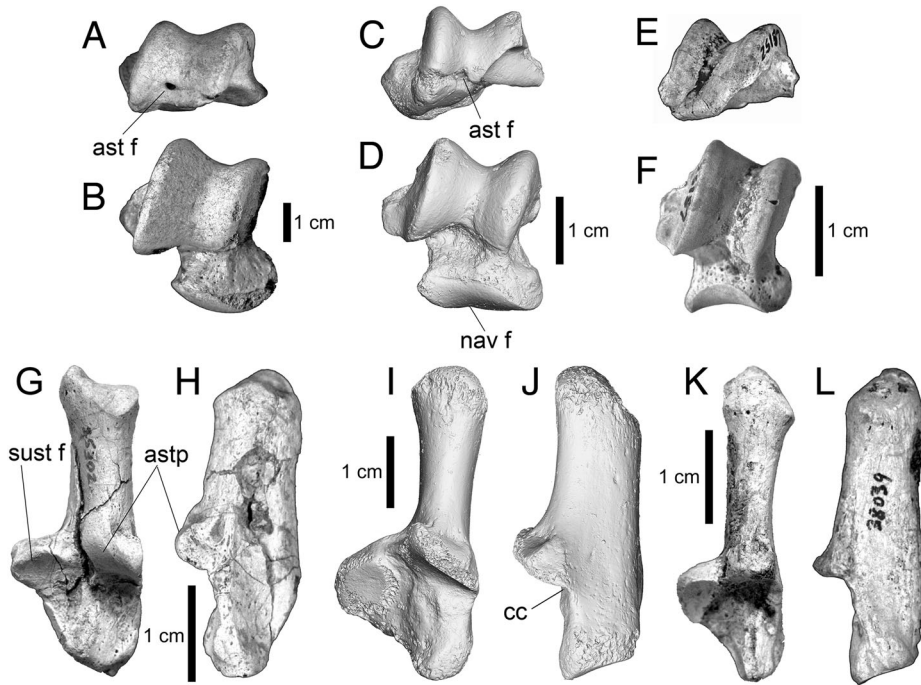
FIGURE 73. Comparative right astragali (**A**–**F**) and left calcanei (**G**–**L**). **A**, **B**, *Phenacodus primaevus*, USGS 7146, digital photographs, in **A**, proximal and **B**, anterior views. **C**, **D**, *Cambaytherium thewissi*, GU 770, left astragalus, micro-CT images (reversed), in **C**, proximal and **D**, anterior views. **E**, **F**, *Hyracotherium* sp., USGS 25157, digital photographs, in **E**, proximal and **F**, anterior views. **A**–**F** are scaled to the same length. **G**, **H**, phenacodontid *Copecion brachypternus*, USGS 25302, digital photographs in **G**, anterior and **H**, lateral views. **I**, **J**, *Cambaytherium thewissi*, WIF/A 1190, micro-CT images, in **I**, anterior and **J**, lateral views. **K**, **L**, *Hyracotherium* sp., USGS 38039, digital photographs in **K**, anterior and **L**, lateral views. **G**–**L** are scaled to the same length. **Abbreviations**: **ast f**, astragalar foramen; **astp**, posterior astragalar (ectal) facet; **cc**, strong concavity; **nav f**, navicular facet; **sust f**, sustentacular facet.

calcaneus from Vastan, but what remains is better preserved and articulates well with the astragali described above. The two specimens are close enough in size and morphology to instill confidence that they represent the same species, but their condition leaves some details inadequately known. Nevertheless, several features are clear. The calcaneus of *C. thewissi* is markedly more robust than that of *Hyracotherium*. Not only are the proximal arm and tuber calcanei wider than in the latter, the sustentaculum tali projects medially much more, and the posterior astragalar (ectal) facet is more rounded on its anterodistal margin and strongly angled (~60°) relative to the long axis, extending across the calcaneal shaft. Thus, the two main parts of the ectal facet meet at a rounded obtuse angle rather than the sharp right angle typical of *Hyracotherium* and *Heptodon*. In all these features, *Cambaytherium* is morphologically either intermediate between a phenacodontid-like condition and that of basal perissodactyls or more similar to *Phenacodus* than to basal perissodactyls. Among the latter, it is most like *Homogalax*. A more rounded ectal facet would have allowed some proximodistal translation (rotation) of the astragalus on the calcaneus. As perissodactyls became better adapted for cursorial locomotion, this mobility was progressively restricted by the sharply angular lateral profile of the ectal facet (as seen, for example, in *Hyracotherium*; Fig. 73K, L). In other ways, the ectal facet in *Cambaytherium* is perissodactyl-like: its diagonal distal part is strongly concave proximodistally (in a vertical plane) on the lateral side ('cc' in Fig. 73I, J) where it extends onto the anterodistal surface (as in *Hyracotherium*), and is very slightly concave mediolaterally on its distal-facing surface, and convex anteroproximally. On the proximal side of the process are two small, flat articular facets that face proximally: one for the fibula laterally and one for the tibia medially (Fig. 74F, G). Both facets would have functioned when the pes was maximally plantar-flexed at the crurotarsal joint (Radinsky, 1965a); the more medial facet is perpendicular to the medial convexity of the ectal facet and forms an extension of the lateral trochlear facet of the astragalus. Wood et al. (2011) reported the same facet in *Hyracotherium*.

Distally, the cuboid facet is not well preserved in either calcaneal specimen, but it was certainly taller anteroposteriorly than wide and inclines slightly posteriorly in side view (Fig. 74B, C). It appears to be wider than in *Hyracotherium* but narrower than in *Phenacodus*. On the distolateral face of GU 772 is a prominent triangular rugosity, the peroneal tubercle (Fig. 74E, G). It is smaller than that of *Phenacodus trilobatus*, more prominent than that of *Hyracotherium*, and comparable in size to that of *Homogalax*. The peroneal tubercle is missing from WIF/A 1190 as a result of abrasion.

When the calcaneus and the astragalus are articulated, the medial and lateral parts of the transverse tarsal joint (i.e., astragalonavicular and calcaneocuboid joints) are essentially aligned, as in *Phenacodus* and *Homogalax*, not offset (with the calcaneus extending farther distally than the astragalus) as in *Hyracotherium* (Rose, 1990:fig. 8, 1996; Wood et al., 2011). In this respect, *Cambaytherium* retains a more primitive condition, similar to that shown in the mesonychids *Pachyaena* and *Mesonyx* (Scott, 1888; Matthew, 1915; O'Leary and Rose, 1995).

A single navicular is known. GU 297 (Fig. 75A–D) is a well-preserved, complete right navicular of *Cambaytherium thewissi* (measurements [in mm]: proximodistal length = 6.15 anteriorly, 8.8 posteriorly at tubercle; mediolateral width = 13.5; anteroposterior depth = 17.4). It is proximodistally very short, less than half as long in anterior view as it is wide (anterior length/width = 0.46). The relative length is comparable to that in *Phenacodus trilobatus* (USGS 7146: anterior length = 11.6 mm, width = 25.4 mm, length/width = 0.46) and is markedly shorter than in basal perissodactyls (e.g., *Homogalax*, USGS 25032: length/width = 5.65 mm/10.5 mm = 0.54; *Hyracotherium*, USGS 38472: length/width = 6.2 mm/8.8 mm = 0.70). However, as in perissodactyls, the navicular is much deeper compared with its width (depth/width = 1.29) than in *Phenacodus* (depth/width = 25.4 mm/25.4 mm = 1.0), closely approximating *Homogalax* (depth/width = 13.7 mm/10.5 mm = 1.30).

The proximal surface of the navicular consists of a large saddle-shaped facet for the astragalus. The medial half is smoothly
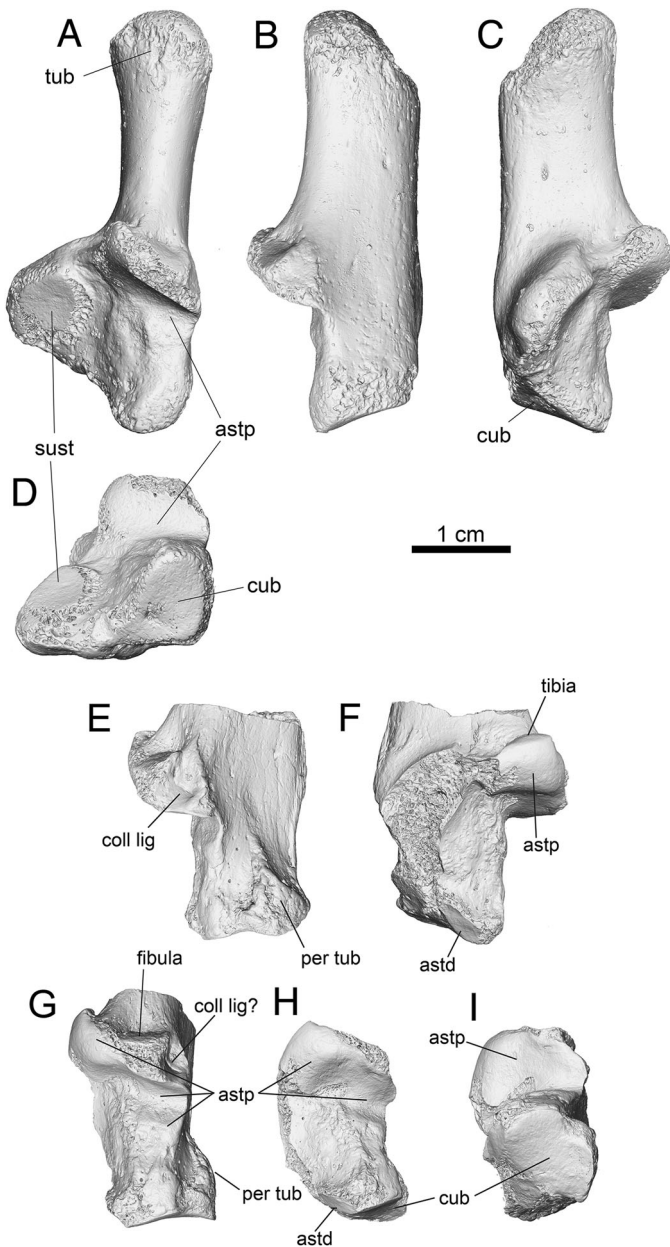
FIGURE 74. Left calcanei of *Cambaytherium thewissi*. **A–D**, WIF/A 1190 in **A**, dorsal, **B**, lateral, **C**, medial, and **D**, distal views. **E–I**, distal calcaneus, GU 772, in **E**, lateral, **F**, medial, **G**, dorsal, **H**, dorsodistal, and **I**, distal views. **Abbreviations**: **astd**, distal astragalar facet; **astp**, proximal astragalar (= ectal) facet; **coll lig**, attachment site for collateral ligament; **cub**, cuboid facet; **per tub**, peroneal tubercle; **sust**, sustentacular facet; **tibia**, facet for tibia; **tub**, tuber calcanei.

concave anteroposteriorly, and the main part of the astragalar facet covers the entire depth of the bone. The lateral half is concave on the anterior half, where it joins a shallow, conical concavity on the posterolateral part of the facet; this concavity seems to articulate with a low eminence near the posterior margin of the astragalar head. At the posterolateral margin of the proximal surface is a notch enclosing a nonarticular fossa, and its border forms a short tubercle on the lateral side of the posterior surface. The lateral surface bears a facet for articulation with the cuboid.

The distal surface of the navicular bears several nearly flat facets. Most of the surface is occupied by an extensive triangular facet for the ectocuneiform laterally (gently convex anteroposteriorly) and the adjacent smaller, roughly ovoid facet for the mesocuneiform anteromedially. Contiguous with the latter but offset and facing posterodistally is a small, triangular facet for the entocuneiform. The entocuneiform facet is weakly convex, as in *Phenacodus* (e.g., USGS 7146) but is relatively a little smaller; however, it appears to be slightly larger and to face a little more posteriorly than in *Hyracotherium* (USGS 38472).

GU 768 (Fig. 75E–I) is the only known cuboid. It is a left cuboid significant for its similar morphology to that of basal perissodactyls such as *Hyracotherium*, *Homogalax*, and *Heptodon*, although it is relatively shorter and wider, resembling *Phenacodus* in these proportions. The proximal surface is a broad, trapezoid-shaped articulation with two facets: a larger triangular facet for the calcaneus laterally and a narrower, roughly elliptical facet medially for the head of the astragalus; thus, the tarsus has an alternating (interlocking) arrangement, as in basal perissodactyls. The calcaneal facet is saddle-shaped—slightly concave anteroposteriorly and slightly convex mediolaterally; the astragalar facet is concave in both planes. The astragalar facet is larger than that in the basal perissodactyls mentioned. In comparison, *Phenacodus* has a serial (taxeopode) tarsus and lacks contact between astragalus and cuboid; the proximal facet of the cuboid is anteroposteriorly convex and mediolaterally flat and articulates only with the calcaneus. The medial surface of GU 768 has two facets for the ectocuneiform (anterodistally and more proximally and posteriorly on the medial surface) and two smaller facets for the navicular on the anterior (cranial) end of the medial surface. The distal surface consists mainly of a roughly triangular, anteroposteriorly concave articular facet that matches the proximal articulation of Mt IV. No distinct articular surface for Mt V is evident, but it is possible that there was some contact between the two elements (the joint surface in *Phenacodus* is also difficult to differentiate from that for Mt IV). Lateral to the articular surface is a prominent sulcus (for the tendon of fibularis longus), which separates the articulation from the lateral tubercle. The tubercle, although prominent as in basal perissodactyls, is smaller and less posterior in position compared with that of *Phenacodus* (USGS 7146).

Measurements (in mm) of the cuboid are: maximum length (anteriorly) = 12.35, maximum width (anteriorly) = 12.5, proximal depth = 11.0. The comparable dimensions in *Homogalax* (USGS 25032) are: length = 11.55, width = 8.4, depth = 10.65; *Hyracotherium* (USGS 25157), length = 11.0, width = 7.0, depth = 8.55; *Phenacodus trilobatus* (USGS 7146), length = 22.3, width = 19.0, depth ~ 18.

Metatarsals—Seven metatarsals are preserved for *C. thewissi*, but they represent only Mt III and Mt IV. A single Mt III is known for *C. gracilis*. In addition, a single metapodial, probably Mt II, represents a much larger animal and is tentatively allocated to *C. marinus*. Although only two metatarsal positions are known for *C. thewissi*, articular facets on these two elements allow the conclusion that all five pedal digits were probably present to some extent in *Cambaytherium*. Without additional evidence, however, it is difficult to predict the size of Mt I and V, or whether these digits had phalanges.

The metatarsals of *Cambaytherium* are shorter and generally more robust than those of early perissodactyls, closely approximating phenacodontids in this regard. Mt III length/width at midshaft in *C. thewissi* is 5.1 (Table 12), compared with 5.4 in *Phenacodus trilobatus* (USGS 7146), 9.3 in *Homogalax* (Rose, 1996), and about 8.6–10 in *Hyracotherium* (Wood et al., 2011; Kitts, 1956:table 1). Not surprisingly, Mt III of the smaller *C. gracilis* (GU 9017; Fig. 76K–P) is relatively more slender and elongate than that of *C. thewissi*, but still less so than in basal perissodactyls (length/width at midshaft = 7.5; Table 12). Mt IV of
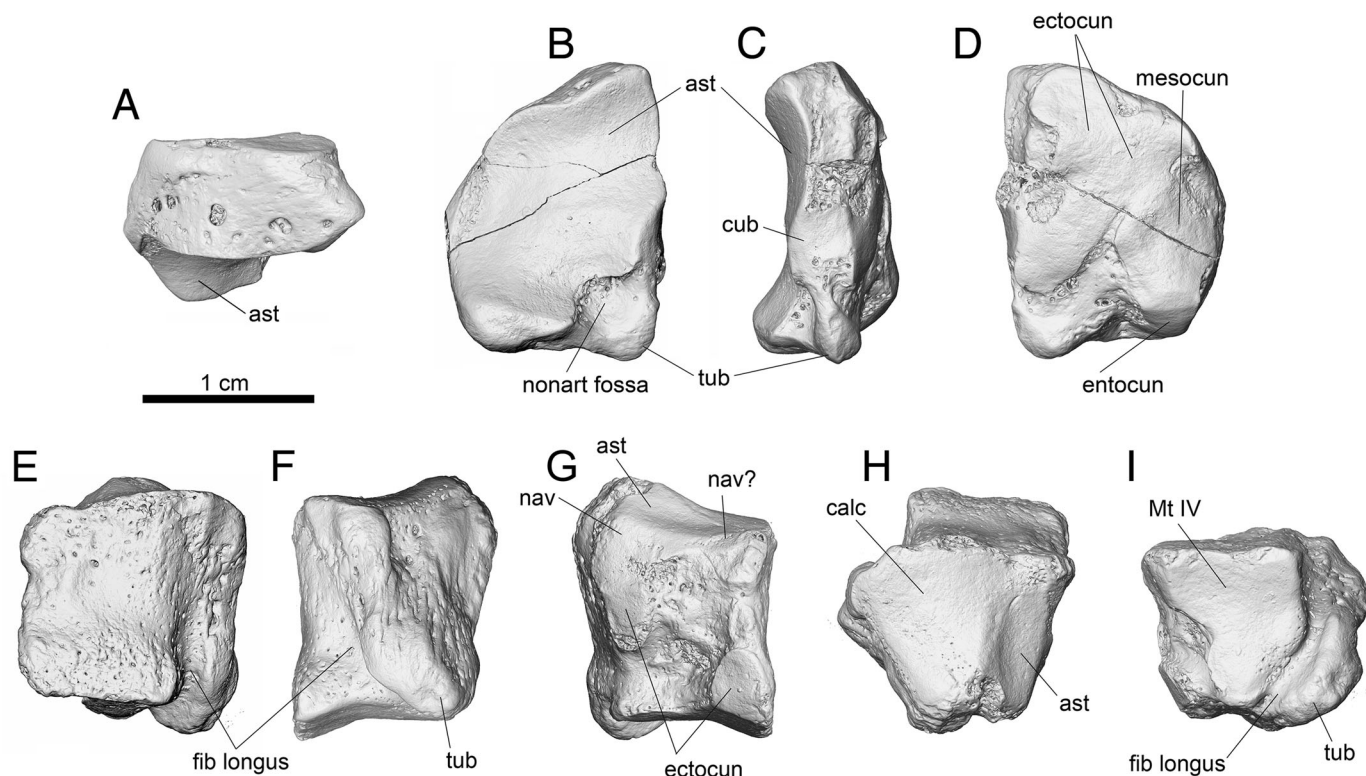
FIGURE 75. Navicular and cuboid of *Cambaytherium thewissi*. **A–D**, right navicular, GU 297, in **A**, anterior (distal to top), **B**, proximal, **C**, lateral, and **D**, distal views. **E–I**, left cuboid, GU 768, in **E**, anterior, **F**, lateral, **G**, medial, **H**, proximal, and **I**, distal views. **Abbreviations**: **ast**, astragalar facet; **calc**, calcaneal facet; **cub**, cuboid facet; **ectocun**, ectocuneiform facets; **entocun**, entocuneiform facet; **fib longus**, sulcus for fibularis longus tendon; **mesocun**, mesocuneiform facet; **Mt IV**, facet for fourth metatarsal; **nav**, navicular facet; **nonart fossa**, nonarticular fossa; **tub**, lateral tubercle.
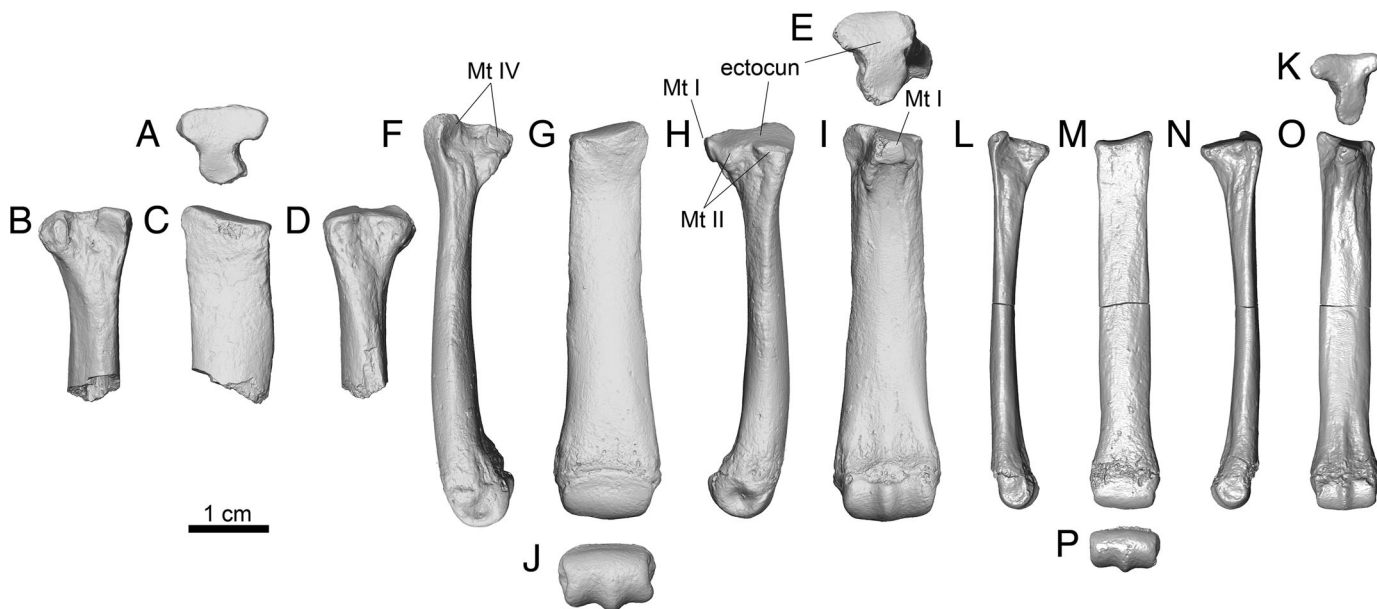
FIGURE 76. Third metatarsals of *Cambaytherium*, all to the same scale. **A–D**, proximal end of right Mt III of *C. thewissi*, GU 821, in **A**, proximal, **B**, lateral, **C**, anterior, and **D**, medial views. **E–J**, left Mt III of *C. thewissi*, GU 735, in **E**, proximal, **F**, lateral, **G**, anterior, **H**, medial, **I**, posterior, and **J**, distal views. **K–P**, left Mt III of *C. gracilis*, GU 9017, in **K**, proximal, **L**, lateral, **M**, anterior, **N**, medial, **O**, posterior, and **P**, distal views. **Abbreviations**: **ectocun**, ectocuneiform facet; **Mt I**, facet for first metatarsal; **Mt II**, facet for second metatarsal; **Mt IV**, facet for fourth metatarsal.
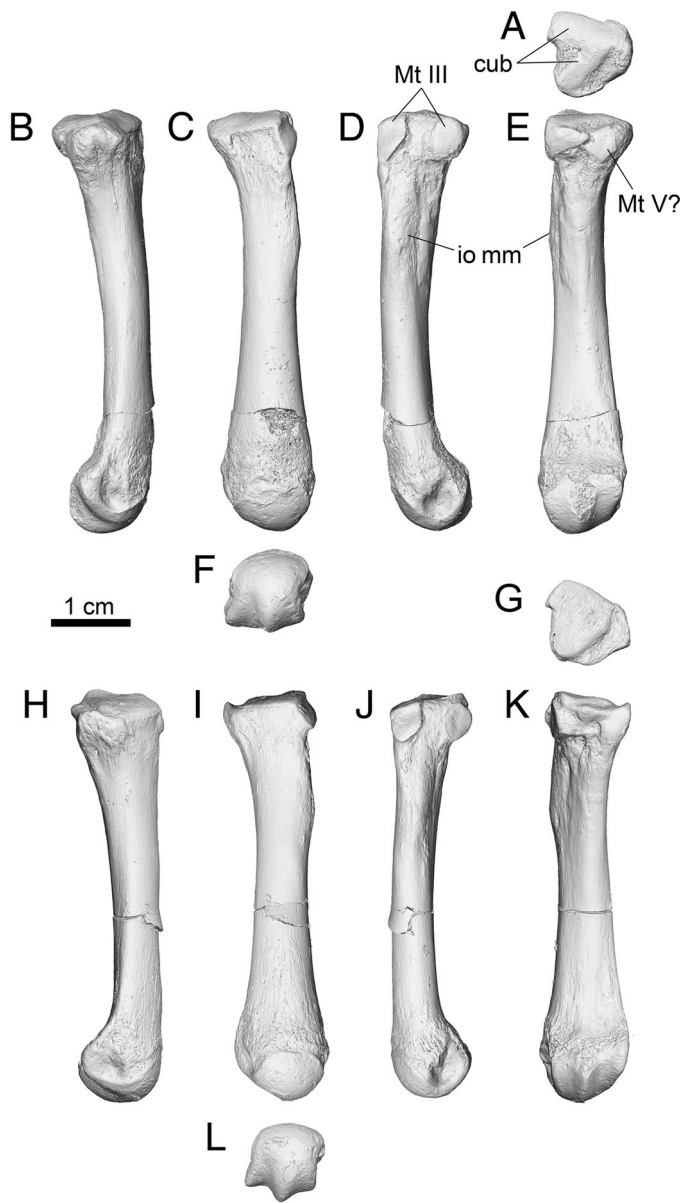
FIGURE 77. Right metatarsal IV of *Cambaytherium thewissi*. **A–F**, GU 275 in **A**, proximal, **B**, lateral, **C**, anterior, **D**, medial, **E**, posterior, and **F**, distal views. **G–L**, GU 831 in **G**, proximal, **H**, lateral, **I**, anterior, **J**, medial, **K**, posterior, and **L**, distal views. **Abbreviations**: **cub**, cuboid facet; **io mm**, attachment site of interosseous muscles; **Mt III**, facet for third metatarsal; **Mt V**, facet for fifth metatarsal.

C. thewissi is noticeably narrower than Mt III; it is also a little narrower than Mt IV in *Phenacodus*, but even so it is more robust than in perissodactyls. The mean length/width at midshaft is 7.7 (Table 12), compared with 5.5 in *Phenacodus trilobatus*, 9.4 in *Homogalax*, and about 11–12 in *Hyracotherium*. The Mt II referred to *C. marinus* (GU 841) is slightly larger than Mt II of *Phenacodus trilobatus* and closely approximates the latter in robustness: its length/width at midshaft = 5.55, compared with 5.1 in *P. trilobatus*.

Three specimens allocated to *C. thewissi* represent Mt III (GU 735, GU 821, GU 846; Fig. 76A–J), but only GU 735 is complete; GU 821 is the proximal half of Mt III, and GU 846 is missing the distal articulation. The shaft of Mt III in both *C. thewissi* and

C. gracilis is distinctly flattened anteroposteriorly (= dorsoventrally), being about twice as wide mediolaterally as anteroposteriorly—relatively flatter than in *Phenacodus*, *Homogalax*, and apparently *Hyracotherium*. The bone is distally symmetrical, reflecting the mesaxonic symmetry of the pes. The proximal articulation (for the ectocuneiform) is roughly triangular, wider dorsally and waisted, with a salient notch laterally and a weak indentation on the medial border. The articular surface is gently concave mediolaterally on its anterior (= dorsal) half and slightly convex dorsoventrally. The lateral notch separates a pair of articular facets (for Mt IV): the anterior one facing posterolaterally, the posterior one more nearly lateral. The proximomedial articular surface for Mt II is much less evident.

Of particular importance on the proximal end of Mt III is a prominent posterior process bearing the posterior facet for Mt IV on its lateral aspect and a distinctive convex facet directed posteriorly. These facets—particularly the posteriorly directed facet—closely resemble those in *Tapirus*. In the latter, this more posterior-facing facet articulates with a vestigial Mt I (Radinsky, 1963b), and the presence of this facet in *Cambaytherium* implies that Mt I (and therefore Mt II as well) was present and articulated in a similar manner. According to Radinsky (1963b:4), "a vestigial first metatarsal is rarely found in fossil specimens, but its presence may be deduced from articular facets on the back of metatarsal III and on the laterodistal edge of the entocuneiform."

The shaft of Mt IV (GU 275, GU 816, GU 819, GU 831; Fig. 77) is slightly bowed in the anteroposterior plane, and the distal half is slightly bowed laterally; at midshaft, it is about 25% wider than deep. The medial side of the proximal third of the shaft is marked by a poorly defined, rugose ridge terminating in a weak tubercle, which mirrors a similar rugosity on the proximolateral side of Mt III. These ridges presumably mark attachment sites of strong interosseous muscles and/or intermetatarsal ligaments. The proximal articular surface for the cuboid is wider, flatter, and more triangular than in *Tapirus*. Rather than being transversely concave as in *Tapirus*, it is almost flat transversely and very gently convex anteroposteriorly, in this respect resembling Mt IV of *Phenacodus*. The cuboid facet is triangular (widest anteriorly) and notched medially; lateral to the facet is a narrow, nonarticular shelf. Proximomedially, there are two distinct facets, which angle away from each other, for Mt III. The facets are of roughly equal size (the anterior facet is not proximodistally extended as in *Phenacodus*). In *Tapirus*, these facets are quadrate, roughly equal in size, and approximately in the same plane. In *C. thewissi*, the anterior facet for Mt III is very slightly sinuous proximodistally, not convex as in *Phenacodus* or nearly flat as in *Tapirus*. When articulated, the proximal end of Mt IV is essentially even with that of Mt III and no significant contact between Mt IV and the ectocuneiform is evident. This conformation is similar to that in *Hyracotherium* (Wood et al., 2011) and *Tapirus* but differs from that in *Heptodon* (Radinsky, 1965a:fig. 18), in which Mt IV extends proximally more than Mt III and also articulates proximomedially with the ectocuneiform. A small, smooth surface on the posterolateral aspect of the proximal end of Mt IV may be an articular surface for a presumably vestigial Mt V; this articular surface is not present in perissodactyls. This possible facet for Mt V is situated in approximately the same location as the concave crescentic facet for Mt V in *Phenacodus trilobatus* (USGS 7146). However, in *Phenacodus*, the cuboid has a facet for Mt V, whereas such a facet is not evident on the cuboid in *Cambaytherium*. If a vestigial Mt V was present in *Cambaytherium*, it evidently contacted Mt IV but did not articulate directly with the cuboid. *Pachyaena* exhibits an intermediate condition, whereby Mt V is reduced and articulates mainly with Mt IV (in a proximolateral concavity) but has a small contact with the cuboid (O'Leary and Rose, 1995). Alternatively, the facet on Mt IV of *Cambaytherium*
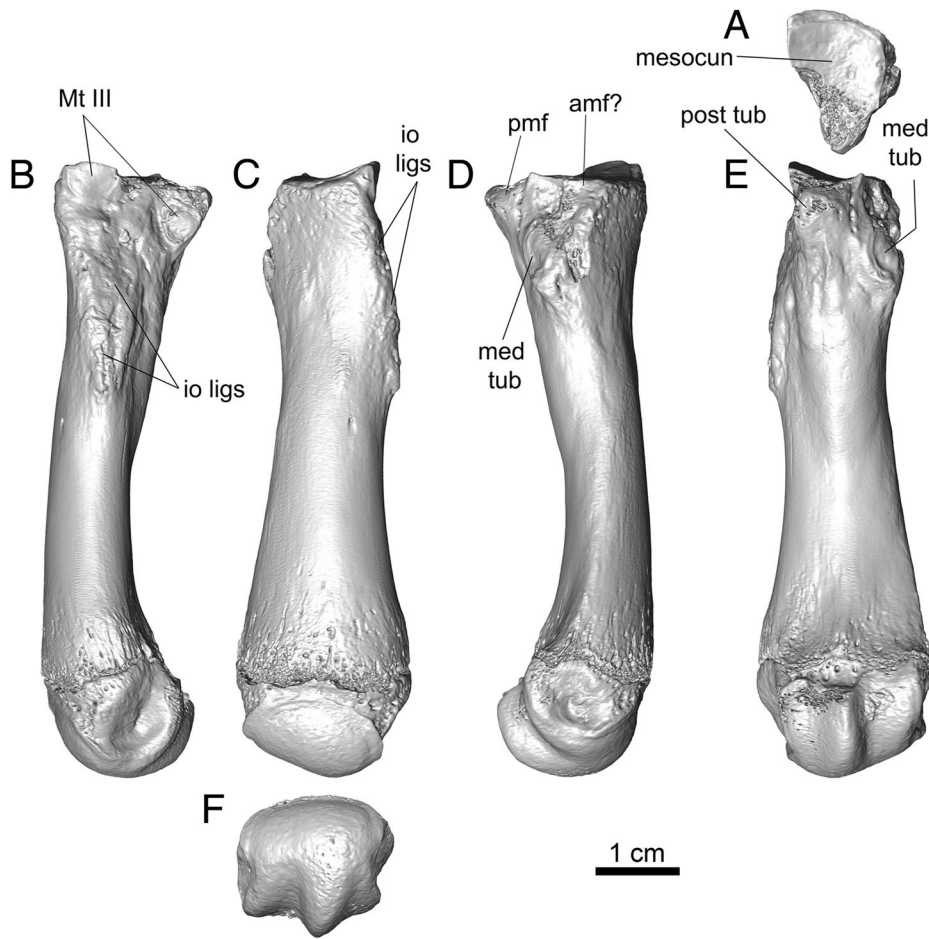
FIGURE 78. Left second metatarsal(?) of *C. marinus*, GU 841, in **A**, proximal, **B**, lateral, **C**, anterior, **D**, medial, **E**, posterior, and **F**, distal views. **Abbreviations**: **amf**, anteromedial facet; **io ligs**, attachment site of interosseous ligaments; **med tub**, medial tubercle; **mesocun**, mesocuneiform facet; **pmf**, posteromedial facet; **post tub**, posterior tubercle.

might be for a sesamoid in the m. fibularis longus tendon as it wraps around the lateral side of the cuboid, but we are not aware of a comparable situation in any perissodactyl. The distal articulation of Mt IV is asymmetrical, the medial part narrower and extending farther distally. The articular surface is roughly semicylindrical, with a marked keel on the posterior half; it is barely 10% wider than deep.

Two metatarsals pertaining to other *Cambaytherium* species have been identified. GU 9017 is a complete Mt III of *C. gracilis* from TAD-2 (Fig. 76K–P). It is morphologically similar to that of *C. thewissi* but much more gracile; midshaft width/length is 0.13, and the bone is almost as long as that of *C. thewissi* (GU 735). Unfortunately, the ventral margin of the proximal articulation is eroded, so the presence of the Mt I facet posteriorly cannot be confirmed. The second specimen is an isolated metapodial (GU 841 from Vastan Mine; Fig. 78), tentatively identified as left Mt II of *C. marinus*, that is substantially larger and more robust than those attributed to *C. thewissi*. Although some aspects of the articular facets differ, it is most similar to Mt II in *Phenacodus trilobatus* (USGS 7146) and *Tapirus* (USNM-M 218778); the proximal articulation is also similar to that of *Homogalax* (USGS 25032). However, it also bears some resemblance to Mc II and Mt IV of *Tapirus*; it is possible that it represents one of those positions. Unfortunately, Mt II of *C. thewissi*, which would provide the best comparison, is unknown. GU 841 is roughly 50% longer than Mt III or Mt IV of *C. thewissi*, smaller than Mt II of *Tapirus*, but slightly larger than that of *P. trilobatus*. As noted above, its robustness is comparable to that of Mt II of *Phenacodus trilobatus*, and in both of

them the shaft is somewhat flattened anteroposteriorly. Early perissodactyls had a relatively longer and less robust Mt II: in *Homogalax* (USGS 25032), the length/width at midshaft = 8.04, and this ratio is higher in *Hyracotherium grangeri* (Wood et al., 2011). GU 841 bears a pair of relatively flat articular facets proximolaterally for Mt III, and the lateral side of the proximal shaft is marked by a rugose scar that extends from just below these facets for more than a third the length of the shaft. A similar but weaker scar is present in *Phenacodus*, whereas *Tapirus* has a longer, more prominent scar. These scars presumably mark attachment of strong interosseous metatarsal ligaments. The proximomedial surface of GU 841 is beveled, much as in *P. trilobatus*, and bears a triangular rugose area half the length of the lateral one but equally prominent, which is marked by two ovoid scars more anteriorly (Fig. 78; anteromedial facet and medial tubercle) and a short, wide, smooth, apparently articular, surface posterolaterally (posteromedial facet), contiguous with the proximal articular surface. The function of these features is unknown, but it is likely that they relate to either the entocuneiform or a vestigial Mt I (or the fused element), or both as in *Phenacodus* (in which Mt I is reduced but functional). The proximal articular facet, for the mesocuneiform, is triangular, much deeper than wide and tapers to a posteriorly projecting tubercle. The articular surface is mediolaterally concave and very slightly convex anteroposteriorly, as in *Phenacodus*. The distal articulation is similar to that in second and fourth metapodials of *C. thewissi* and not as narrow as in *Tapirus*. The distal epiphyseal line is still evident in GU 841, suggesting that the individual represented was not skeletally fully mature.

Functional Morphology of the Hind Limb

Like the forelimb, the bones of the hind limb have many features in common with phenacodontids and early perissodactyls that are commonly associated with cursorial or subcursorial locomotion (e.g., Howell, 1944). These features—including a high greater trochanter, posteromedially directed lesser trochanter, anteroposteriorly deep distal femur with a well-defined and elevated patellar trochlea, and a tibia with a deeply grooved distal astragalar articulation—increase the mechanical advantage of muscles that move the hip and knee joints (gluteal and quadriceps muscles), or help to restrict motion to the sagittal plane. The femur and tibia are quite similar in these three groups, but *Cambaytherium* is more like early perissodactyls in having slightly more proximal insertions of the superficial gluteal (third trochanter) and semitendinosus muscles (distal tibial tuberosity). Some of these features would have enhanced parasagittal movement, and the minor differences from phenacodontids suggest that *Cambaytherium* was slightly better adapted for speed. At the same time, however, the tibioastragalar joint is not quite as deep as in perissodactyls, and the astragalar trochlea is wider and shorter, as in phenacodontids. The tarsus is wider and shorter than in early perissodactyls but relatively not as wide as in *Phenacodus*. The alternating tarsal arrangement, with its astragalocuboid articulation, probably added stability to the foot. At the same time, however, the aligned transverse tarsal joint may have allowed limited rotation within the foot, thus suggesting a more flexible tarsus that was less well adapted for running than in *Hyracotherium*. The metatarsals and phalanges are relatively short and robust, and there is evidence suggesting a pentadactyl pes, but one in which the hallux had rotated posteriorly to articulate with Mt III and Mt V was vestigial. The preserved parts of the pes are reassembled and compared with the pedes of *Phenacodus* and basal perissodactyls in Figure 79. What seems apparent is that the tarsus is more or less intermediate in proportions and morphology between a more primitive phenacodontid-like condition and the more derived state in basal perissodactyls, whereas the metapodials and phalanges are perhaps somewhat closer to the phenacodontid condition. Overall, the anatomy of the hind limb, like that of the forelimb, suggests a subcursorial animal more specialized for running than phenacodontids but one that had not yet achieved the level of cursorial specialization seen in earliest perissodactyls.

Postcranial Comparisons of *Cambaytherium*

Among the fossil taxa we have compared with *Cambaytherium*, early perissodactyls and phenacodontids are the best known from the postcranial skeleton. Little of the postcranial skeleton is known for anthracobunids, the most significant specimen being an astragalus referred to *Anthracobune* sp. by Gingerich et al. (1990), which we discuss below.

Comparisons of Vertebrae—The vertebrae of *Cambaytherium* are similar in most features to those of *Hyracotherium* (Wood et al., 2011) but show proportional differences and are generally
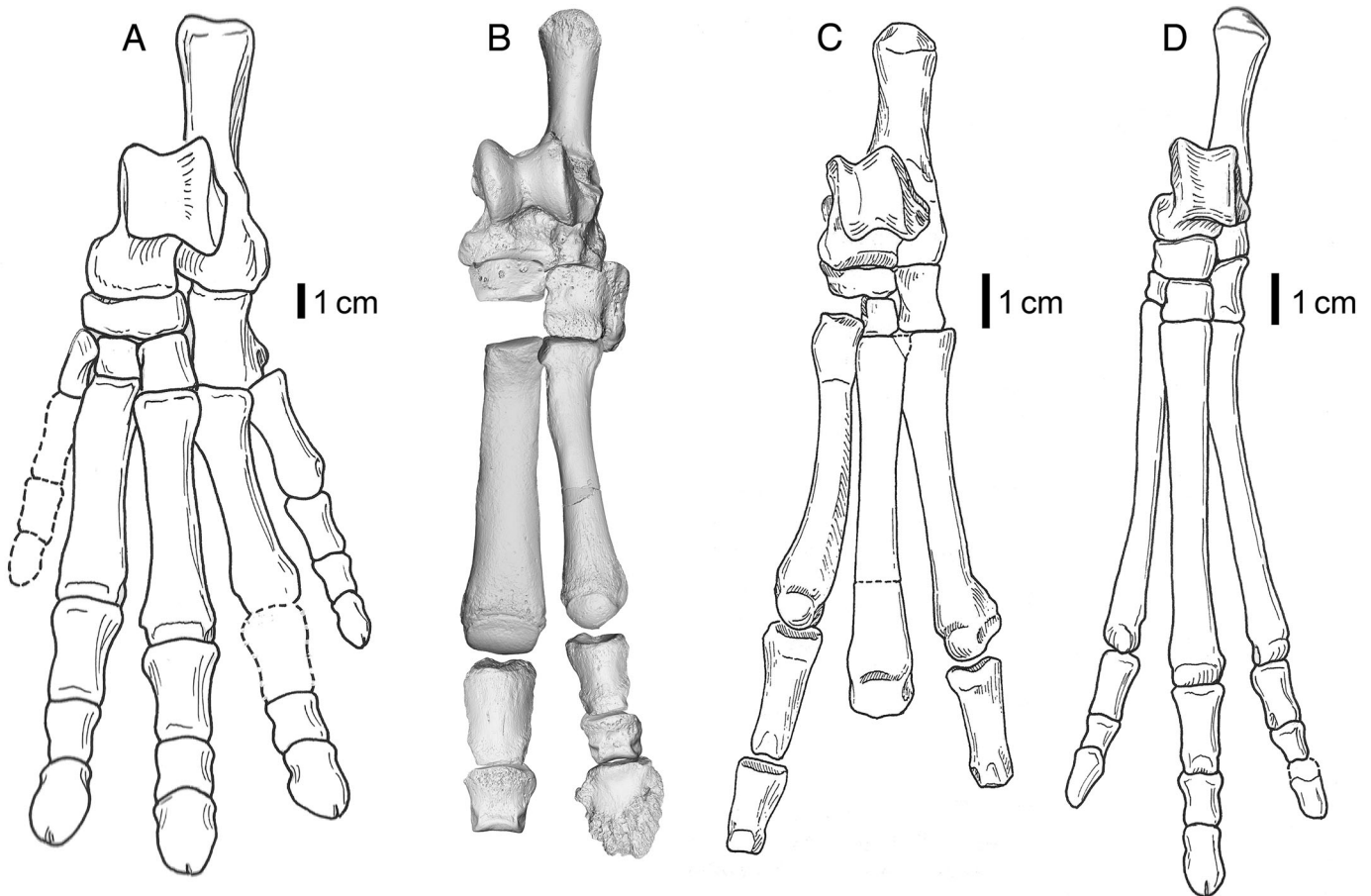
FIGURE 79. Reconstructed composite left pes of *Cambaytherium thewissi*, based only on known elements from multiple individuals, compared with those of *Phenacodus* and basal perissodactyls. **A**, *Phenacodus trilobatus*; **B**, *Cambaytherium thewissi*; **C**, *Homogalax protapirinus*; **D**, *Hyracotherium* sp. Micro-CT images of some *C. thewissi* bones have been reversed or resized to achieve the most probable approximation, so no scale is shown for **B**. **A** and **D** from Rose (1990), **C** from Rose (1996).

slightly more robust. The atlas (C1) is wider and has larger alae. The spinous and odontoid processes of C2 are relatively larger than in *Hyracotherium*, and the odontoid is comparable in size to that in *Heptodon* (Radinsky, 1965a). The contour of the spinous process, however, is very similar to that in *Hyracotherium*, unlike the steeply sloping anterior margin seen in *Heptodon* and *Arctocyon* (Argot, 2012). Perhaps most interesting is the zygapophyseal anatomy of the lumbar vertebrae, which have strongly revolute, interlocking articulations. This morphology (presumably a derived state despite its presence in several archaic placentals) is shared with *Hyracotherium*, *Arctocyon*, mesonychians, and extant ruminants, as well as extant Pholidota, but it is not present in phenacodontids, which have planar zygapophyseal joints. The distribution of this character is not well understood, but its presence in *Cambaytherium* and *Hyracotherium* suggests that such interlocking zygapophyses could be the ancestral state for perissodactylamorphs. The conditions of the sacrum and the few caudals known also suggest more plesiomorphic states than in basal perissodactyls. If GU 8001 is correctly referred to *Cambaytherium marinus* and accurately represents sacral anatomy in *Cambaytherium*, then the latter (with four sacrals) is more like phenacodontids (three or four sacrals) or is intermediate in number of sacrals between them and *Hyracotherium* (five sacrals). As noted above, the few known caudals are more gracile than those of phenacodontids but appear to be more robust than those of *Hyracotherium*.

Comparisons of Forelimb—The forelimb of *Cambaytherium* is similar to that of early perissodactyls in most respects. The main difference is in proportions, with *Cambaytherium* generally having relatively shorter, more robust long bones than those of early perissodactyls, resembling condylarths such as phenacodontids in this regard. For example, *Cambaytherium* has stronger humeral crests, a relatively longer ulnar olecranon process, and a less bowed antebrachium than in basal perissodactyls. However, the humerus of *Cambaytherium* resembles that of perissodactyls and differs from that of phenacodontids in lacking an entepicondylar foramen and in having a generally reduced medial epicondyle, as well as in having a narrow or even gently keeled capitulum, rather than a more spherical one as in *Phenacodus*. Unlike that of early perissodactyls and like that of phenacodontids, however, the humerus of *Cambaytherium* lacks a capitular tail (i.e., lateral articular shelf), and the deltopectoral crest extends distally almost to the radial fossa. The radius and ulna of *Cambaytherium* are very similar to those of early perissodactyls except in proportions and the features noted above.

The known carpals of *Cambaytherium* are very similar to those of early perissodactyls, including displaying the alternating (rather than serial) pattern of articulation between the proximal and distal carpal rows (Holbrook, 2001; Bai et al., 2017). The carpals of cambaytheres differ from those of perissodactyls in the following ways. The radial facet of the lunar does not extend posteriorly from the anterior half-cylinder. There is no posterior scaphoid facet on the lunar separate from the anterior distal facet (although the two might be confluent). The cuneiform is proximodistally far shorter than that of any early perissodactyl and unlike any perissodactyl except perhaps some rhinocerotids. The cuneiform also possesses a small facet of unknown function in the laterodistal corner of the anterior face. The ulnar and cuneiform facets of the pisiform are parallel and orthogonal, respectively, to the long axis of the pisiform, whereas each is at roughly a 45° angle to the long axis in perissodactyls.

The presence of any vestige of the first digit of the manus would be especially interesting in any perissodactyl relative. Solounias et al. (2018) have argued that vestiges of Mc I and V are fused into the proximal ends of the reduced Mc II and IV in *Equus*, and that the terminal phalanx of digit III has incorporated vestiges of the other digits. However, a separate element representing even a reduced Mc I has not been unequivocally identified in any living

or extinct perissodactyl (Matthew, 1917). Presence of digits II to V is the most ancestral condition observed in any perissodactyl, including the earliest perissodactyls that preserve this region (*Hyracotherium grangeri*, *Homogalax protapirinus*), and this condition is retained in extant *Tapirus*. Several lineages, including rhinocerotoids and multiple equoid lineages, have reduced the number of manual digits by losing digit V and, in the case of horses, reducing digits II and IV to splints of the metacarpals. It is of course expected that the ancestors of perissodactyls had a pentadactyl manus including a distinct digit I, which is known to be present in *Phenacodus* (Matthew, 1917; Radinsky, 1966). The facet on the medial side of the Mc II of *Cambaytherium* at least indicates that the trapezium is well developed, and it is possible that this facet was instead for the proximal end of Mc I. However, Matthew (1917) argued convincingly that the facet observed on the proximomedial side of Mc II in some fossil equids (but not Eocene forms) actually accommodated the trapezium during flexion. Franzen (2007) identified a possible vestige of Mc I in *Propalaeotherium*, and Franzen and Habersetzer (2017) identified a similar element as Mc I in *Eurohippus* (both specimens from the middle Eocene of Messel); however, it seems more likely that the bone in these equids is actually the trapezium.

The postcranial skeletons of other archaic ungulates, such as Paleocene *Arctocyon* (Russell, 1964; Argot, 2012) and *Periptychus* (Matthew, 1937; Shelley et al., 2018), when compared with the skeleton of *Cambaytherium*, further highlight plesiomorphic features of *Cambaytherium*. They also underscore a greater degree of cursorial specialization shared by cambaytheres, perissodactyls, and phenacodontids, which is absent in these other archaic groups. The humeri of both *Arctocyon* and *Periptychus* are quite stout and have strong deltopectoral crests, broad lateral flanges (variously called lateral supracondylar or epicondylar crests, or supinator crests) that extend nearly halfway up the humeral shaft, and prominent medially projecting medial epicondyles. All of these features contrast strongly with the corresponding anatomy of the humeri in early perissodactyls and *Cambaytherium*, and to a lesser extent with that of phenacodontids. The humeri of these three groups are more gracile relative to those of *Arctocyon* and *Periptychus* and have relatively weak lateral crests and less projecting or greatly reduced medial epicondyles. Whereas early perissodactyls have lost a distinct deltopectoral crest, phenacodontids and *Cambaytherium* retain a low crest, much reduced compared with those of *Arctocyon* and *Periptychus*. *Arctocyon*, *Periptychus*, and phenacodontids retain an entepicondylar foramen, which is absent in *Cambaytherium* and perissodactyls.

The radius and the ulna of Paleocene archaic ungulates are relatively shorter and more robust than those of *Cambaytherium* (brachial index ~74 in *Arctocyon* [Russell, 1964]; ~70 in *Ectoconus* [Shelley et al., 2018]; <70 in *Periptychus* [S. Shelley, pers. comm.]), early perissodactyls, and phenacodontids, whose longer and more slender antebrachial elements suggest a greater degree of cursoriality. A single coronoid process of the proximal ulna projects medially in *Arctocyon* and *Periptychus*, unlike the symmetrical medial and lateral coronoid processes of *Cambaytherium* and perissodactyls. The radial notch is laterally placed in *Arctocyon* and *Periptychus*, rather than situated centrally between the two coronoid processes as in *Cambaytherium* and perissodactyls, or almost fully centrally as in *Phenacodus*.

The most notable features of the manus of *Arctocyon* and *Periptychus* are the presence of five unreduced functional digits, the presence of a free centrale in *Periptychus* (but not in *Arctocyon*), and the claw-like distal phalanges of *Arctocyon* but hoof-like distal phalanges of *Periptychus*. The first three of these are considered plesiomorphic placental traits.

Comparisons of Hind Limb—As with the forelimb, the long bones of the hind limb of *Cambaytherium* are similar to those of early perissodactyls, differing mainly in their proportions,

which are more gracile in perissodactyls. Again, the more robust proportions of *Cambaytherium* are generally similar to those of phenacodontids. The most significant comparisons pertain to the astragalus. The saddle-shaped navicular facet of the astragalus is a classic derived feature of perissodactyls (Radinsky 1966, 1969), and the presence of a strikingly similar facet in *Cambaytherium* is the clearest indication of a close relationship between cambaytheres and perissodactyls. Overall, the astragalus of *Cambaytherium* is very similar to that of early perissodactyls, but the trochlear proportions and neck length are more similar to those of *Phenacodus* (Fig. 73). It further differs from the astragalus of *Hyracotherium* in having the trochlea more 'offset' laterally in relation to the head, but this feature is observed in some perissodactyls, especially rhinocerotoids (Holbrook, 2001; Bai et al., 2017), and might simply be a by-product of having a relatively wider tarsus. The presence of an astragalar foramen on the astragalus of *Cambaytherium* distinguishes it from astragali of all perissodactyls, which lack this feature. The astragalar foramen is widely distributed across placental mammals, and absence of the foramen is likely a derived feature of perissodactyls.

Although there is some doubt regarding the presence of Mc I in *Cambaytherium*, there is stronger evidence for the presence, in some form, of all five pedal digits. No perissodactyl is known to have more than three functional pedal digits, representing digits II, III, and IV. Mt I, however, is retained in a reduced form in many taxa, as part of a complex with the entocuneiform that is rotated posteriorly (Radinsky, 1963b). In this configuration, Mt I articulates with the posterior aspect of the proximal Mt III. This is a distinctive feature of perissodactyls. The presence of a facet for Mt I on the posterior aspect of the proximal Mt III in *Cambaytherium* indicates that it shares this unusual positioning of the entocuneiform and Mt I, further supporting a close relationship with perissodactyls. At the same time, the medial side of Mt II (*C. marinus*) is beveled in a manner that is similar to what is observed in *Phenacodus*, which in that taxon accommodates the entocuneiform and functional Mt I (Fig. 79A). This suggests that the condition in *Cambaytherium* is intermediate between those in pentadactyl taxa and perissodactyls, i.e., a more robust Mt I is retained, but it has adopted the position observed in perissodactyls.

The facet on the lateral side of proximal Mt IV in *Cambaytherium* is a strong indication of some development of Mt V. No such facet is present on Mt IV of any perissodactyl. Presence of a vestigial Mt V has been reported in *Homogalax* (Wortman, 1896), *Hyracotherium* (Kitts, 1956; Wood et al., 2011), and the European Eocene equoid *Eurohippus* (Franzen, 2007; Franzen and Habersetzer, 2017). Wortman's (1896) claim for Mt V in *Homogalax* appears to be incorrect (Holbrook, 2001). The reports of Mt V in *Hyracotherium* and in *Eurohippus* are based on the presence of a small, irregularly shaped bone situated on the posterolateral aspect of the proximal pes (Mt IV). It appears from the illustration in Wood et al. (2011:fig. 17) that the vestigial Mt V had little or no contact with the cuboid. An alternative interpretation of this morphology is that this is the vestigial Mt I, which has been displaced slightly laterally. Thus, the evidence for at least a vestigial Mt V in *Cambaytherium* appears to be marginally stronger.

In many respects, the metatarsals display features intermediate between those of a morphology like that of *Phenacodus* and that of more generalized perissodactyls such as *Tapirus*. Mt III is very similar to that of *Tapirus*, in the shape of the proximal articulation, including a deep lateral notch and prominent posterior process with an articular surface for Mt I. It also resembles *Phenacodus trilobatus* in overall proportions and in the outline of the proximal articulation, although the articular surface in *Phenacodus* is very gently convex in both directions, not mediolaterally concave as in *Cambaytherium*, and the medial notch is

deeper than the lateral notch in *Phenacodus*. The articular facets for Mt II and IV are morphologically intermediate between those of *Phenacodus* (Mt II facets smaller, Mt IV anterior facet distinctly concave) and those of *Tapirus*; in particular, the Mt II facets are smaller than in *Tapirus*, whereas the anterior Mt IV facet is more concave than that of *Tapirus*, but much less so than in *Phenacodus*.

As was shown above for the forelimb, the main differences between the hind limbs of archaic ungulates such as *Arctocyon* (Argot, 2012) and *Periptychus* (Shelley et al., 2018) on the one hand and *Cambaytherium*, perissodactyls, and phenacodontids on the other concern the greater degree of cursorial specialization in the latter set of taxa. The long bones of the hind limb of both *Arctocyon* and *Periptychus* are much more robust than those of more cursorial taxa. The femoral head of *Arctocyon* has a fovea that does not interrupt the distal margin of the articular surface, and the proximal extent of the greater trochanter is well below the head. The femur of *Periptychus* is more like cursorial taxa in these respects, with a fovea that interrupts the distal margin of the articular surface of the head and a greater trochanter whose proximal tip is about even with the proximal margin of the femoral head. The greater trochanter of *Cambaytherium* clearly projects above the head, but not to the extent seen in most perissodactyls (Hussain, 1975:fig. 3). The anatomy of the fovea capitis in *Cambaytherium* appears to be intermediate between that in less cursorial mammals such as *Arctocyon* and that in cursorial basal perissodactyls, some specimens having an isolated pit as in *Arctocyon* and others with a trough extending from the pit to interrupt the posterior margin of the head as in perissodactyls. The third trochanter of the femur in *Periptychus* differs from that of cursorial taxa in being positioned about halfway toward the distal end of the shaft, whereas the third trochanter of the femur of *Arctocyon* is more proximally placed, as in more cursorial ungulates. The tibial crest is longer in *Arctocyon* and *Periptychus* than in early perissodactyls, with the semitendinosus tubercle just proximal to midshaft. *Cambaytherium* is more or less intermediate, with a more proximal tubercle than in those Paleocene taxa, but not as proximal as in early perissodactyls. Both *Arctocyon* and *Periptychus* differ from cursorial taxa in having a distal tibia with a strong medial malleolus and weakly developed grooves for the astragalar trochlea. In *Cambaytherium*, perissodactyls, and phenacodontids, the medial malleolus is less prominent and similar in size to the prominent posterior process, and the articular surface for the astragalar trochlea is deeply grooved.

As the distal tibiae indicate, the astragali of *Arctocyon* and *Periptychus* have trochleae with blunt medial and lateral crests joined by a shallow groove, in contrast to the deep groove separating the sharper trochlear ridges in cambaytheres and especially in perissodactyls. As mentioned above, the astragali of *Arctocyon* and *Periptychus* share with those of phenacodontids and *Cambaytherium* the presence of an astragalar canal, and they share with the astragali of phenacodontids a hemispherical distal facet for the navicular.

Like phenacodontids, *Arctocyon* and *Periptychus* possess five pedal digits with complete sets of phalanges, and the entocuneiform of these taxa is positioned on the medial side of the foot, rather than rotated posteriorly as in perissodactyls and as inferred for *Cambaytherium*. As with the manus, the pedal terminal phalanges of *Arctocyon* differ from those of other taxa discussed here in being mediolaterally compressed claws, rather than dorsoplantarly compressed hooves.

Comparison with 'Anthracobune' Astragalus—Because anthracobunids are the closest relatives of cambaytheriids, a comparison of their anatomy is of interest. Unfortunately, only a single postcranial element has been published. Gingerich et al. (1990) reported a large astragalus (GSP-UM 1745, maximum length = 47 mm, maximum width = 49 mm) from the

middle Eocene Subathu Formation (Kihman A locality) of Pakistan Kashmir, which they allocated to *Anthracobune* (Fig. 80). Because there were no associated teeth or bones, this attribution was based primarily on size and the apparent resemblance to an astragalus of the proboscidean *Moeritherium*, and was probably influenced by the hypothesis at that time that anthracobunids were basal proboscideans (West, 1980; Wells and Gingerich, 1983). The Kihman astragalus is much larger than those of *Cambaytherium thewissi* (about twice the linear dimensions), as would be expected for *Anthracobune* considering its much larger teeth. However, in view of the evidence for a close relationship of anthracobunids and cambaytheres (see Phylogenetic Position of *Cambaytherium*, below), and their relationship to Perissodactyla, we now anticipate that anthracobunid astragali would possess a similar anatomy, with certain hallmarks shared by *Cambaytherium* and basal perissodactyls—in particular, a deeply grooved trochlea and a saddle-shaped navicular facet. Our study of a cast of the Kihman astragalus indicates a few similarities to *Cambaytherium*—a wide trochlea and a dorsal astragalar foramen (both plesiomorphic traits) and a tibial malleolar facet (better developed as a shallow cotylar fossa[?] in the Kihman astragalus, and probably derived)—but otherwise shows a strikingly different morphology. Unlike *Cambaytherium*, it has a prominent medial tubercle proximally (a feature present in *Moeritherium*, which Gingerich et al. [1990] considered to be an important synapomorphy with early proboscideans) and appears to lack a lateral flange for the distal fibular malleolus. The trochlear groove is much shallower than in *Cambaytherium* (forming a widely obtuse angle between medial and lateral components), and the lateral side is distinctly elevated compared with the medial side, more closely approximating the shape in *Arctocyon* (Argot, 2012:fig. 15). Unlike both *Cambaytherium* and perissodactyls, the navicular facet is strongly convex (hemispherical), much more like that of *Arctocyon* and *Phenacodus*.

The anatomy of the Kihman astragalus conflicts with the astragalar morphology of *Cambaytherium* and with the expected anatomy of anthracobunids, which, based on dental evidence, are perissodactylamorphs. Its general resemblance to the astragali of archaic ungulates such as *Arctocyon* and *Periptychus* (Argot, 2012; Shelley et al., 2018) indicates that it represents a large, primitive, ambulatory (not cursorial) placental whose craniodental remains have not yet been found in the Subathu Formation—perhaps a quettacyonid or a tillodont. The astragali of North American tillodonts, although relatively not as wide, have interesting similarities to the Kihman astragalus. Like the latter, the astragalus of Bridgerian *Trogosus* is relatively flattened and has a shallowly grooved trochlea, a short neck, and a wide, convex navicular facet (Gazin, 1953). Although much smaller, *Esthonyx* (USGS 5649, USNM 527667) has a similar shallow trochlea with a posteriorly extended medial trochlear ridge, a medial flange, and a cotylar fossa. Because tillodonts are present in the early Eocene Cambay Shale and Ghazij formations (Gingerich et al., 2001; Rose et al., 2009a, 2013; Smith et al., 2016), their presence in the Subathu Formation would not be unexpected.

PHYLOGENETIC POSITION OF *CAMBAYTHERIUM*

Results of Phylogenetic Analyses

Unconstrained analyses (excluding *Minchenella* and quettacyonids) produced 16 shortest trees of 1,970 steps in both PAUP* and TNT. The strict consensus of these results is given in Figure 81. Bremer values (indicated in Fig. 81 as a number preceded by 'd') range from 1 to 15, depending on the node. In all 16 trees, there is a cambaythere clade that includes *Nakusia*, *Perissobune*, and the two species of *Cambaytherium*. *Perissobune* is sister taxon to the others, but *Nakusia* is nested between the two species of *Cambaytherium*.

The cambaythere clade is the sister taxon to a clade including anthracobunids and *Behemotops*, and *Radinskya* is the sister taxon to the cambaythere-anthracobunid-*Behemotops* clade. This clade of cambaytheres, anthracobunids, *Behemotops*, and *Radinskya* is in turn the sister taxon of perissodactyls.

The successive sister taxa of the clade including perissodactyls, cambaytheres, anthracobunids, *Behemotops*, and *Radinskya* are, from most closely related to most distantly related: cetartiodactyls; a clade of proboscideans and hyracoids; a clade of phenacodontids plus *Phenacolophus*; macroscelideans; a clade of *Paramys*, *Rhombomylus*, *Notharctus*, and *Orycteropus*; *Vulpavus*; and *Asioryctes*.

The constrained analyses (see Materials and Methods) produced 18 shortest trees (tree length [TL] = 1,982); the strict consensus of these results is given in Figure 82. The consensus trees of both constrained and unconstrained analyses are identical in terms of how they relate perissodactyls, cambaytheres, anthracobunids, and *Behemotops* to each other, and how these groups plus *Radinskya* form a clade exclusive of other taxa. The main differences between the results of the constrained and unconstrained analyses, apart from those imposed by the constraint tree, concern the relationships among perissodactyls, which are less resolved in the constrained consensus, and the relationship of the phenacodontid-*Phenacolophus* clade to other groups, where this clade is part of Afrotheria in the constrained results.

When *Minchenella* and Quettacyonidae were included in the unconstrained analysis, the result was 408 shortest trees of 1,997 steps. The consensus of these trees is shown in Figure 83. As the much larger number of shortest trees would indicate, there is far less resolution in the consensus of these results, although they do not unequivocally conflict with the results of the
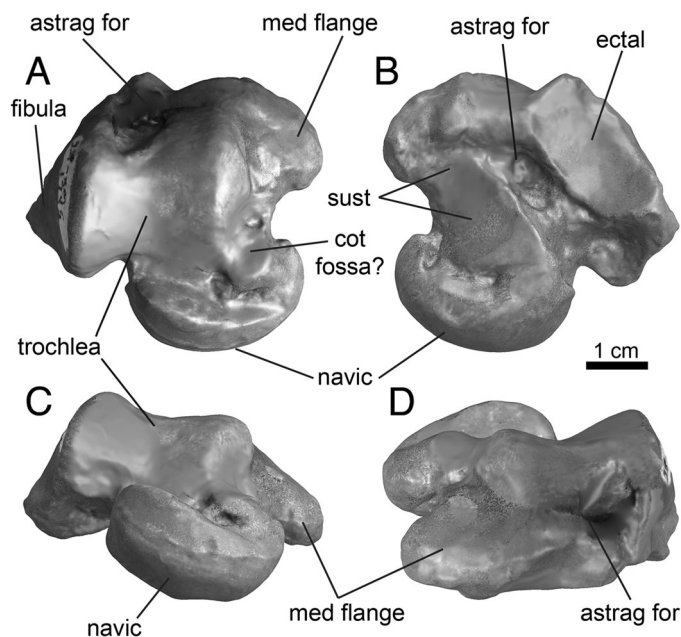
FIGURE 80. Right astragalus, GSP-UM 1745, from the middle Eocene Subathu Formation of Pakistan, attributed to *Anthracobune* sp. by Gingerich et al. (1990), in **A**, anterior (= dorsal), **B**, posterior (= ventral), **C**, distal, and **D**, proximal views. Laser scan of epoxy cast. **Abbreviations**: **astrag for**, astragalar foramen; **cot fossa**, cotylar fossa; **med flange**, medial flange (= medial tubercle); **navic**, navicular facet; **sust**, sustentacular facet.
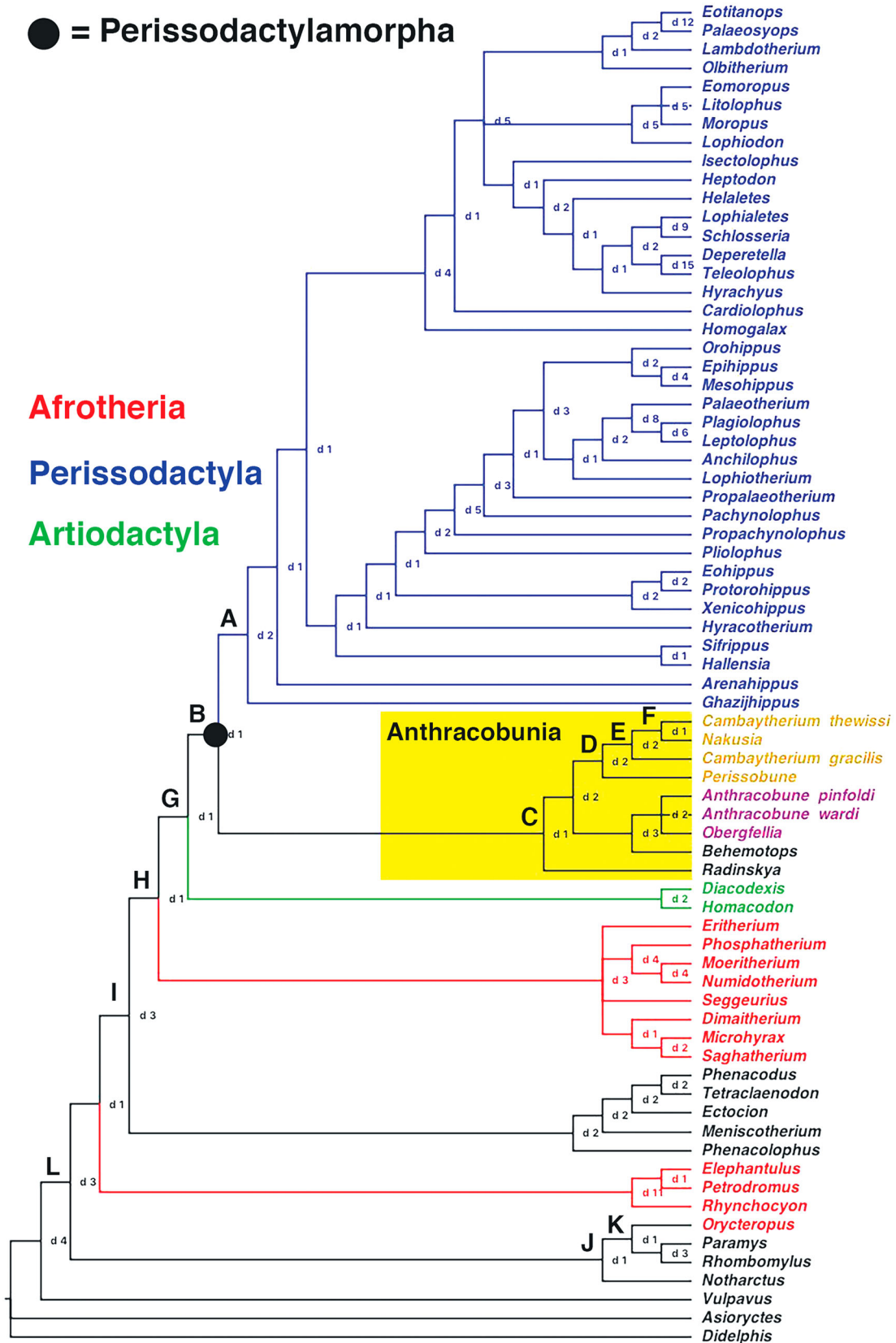
FIGURE 81. Strict consensus of 16 shortest trees of 1,970 steps based on unconstrained parsimony analysis. Afrotheres (red), artiodactyls (green), and perissodactyls (blue) are indicated by colored branches and terminal taxa. Gold names represent Cambaytheriidae and purple names represent Anthracobunidae. Yellow box indicates Anthracobunia. Black dot indicates node corresponding to Perissodactylamorpha. Uppercase letters refer to nodes listed in Table 17. Numbers preceded by 'd' represent Bremer (decay) values for the associated node.
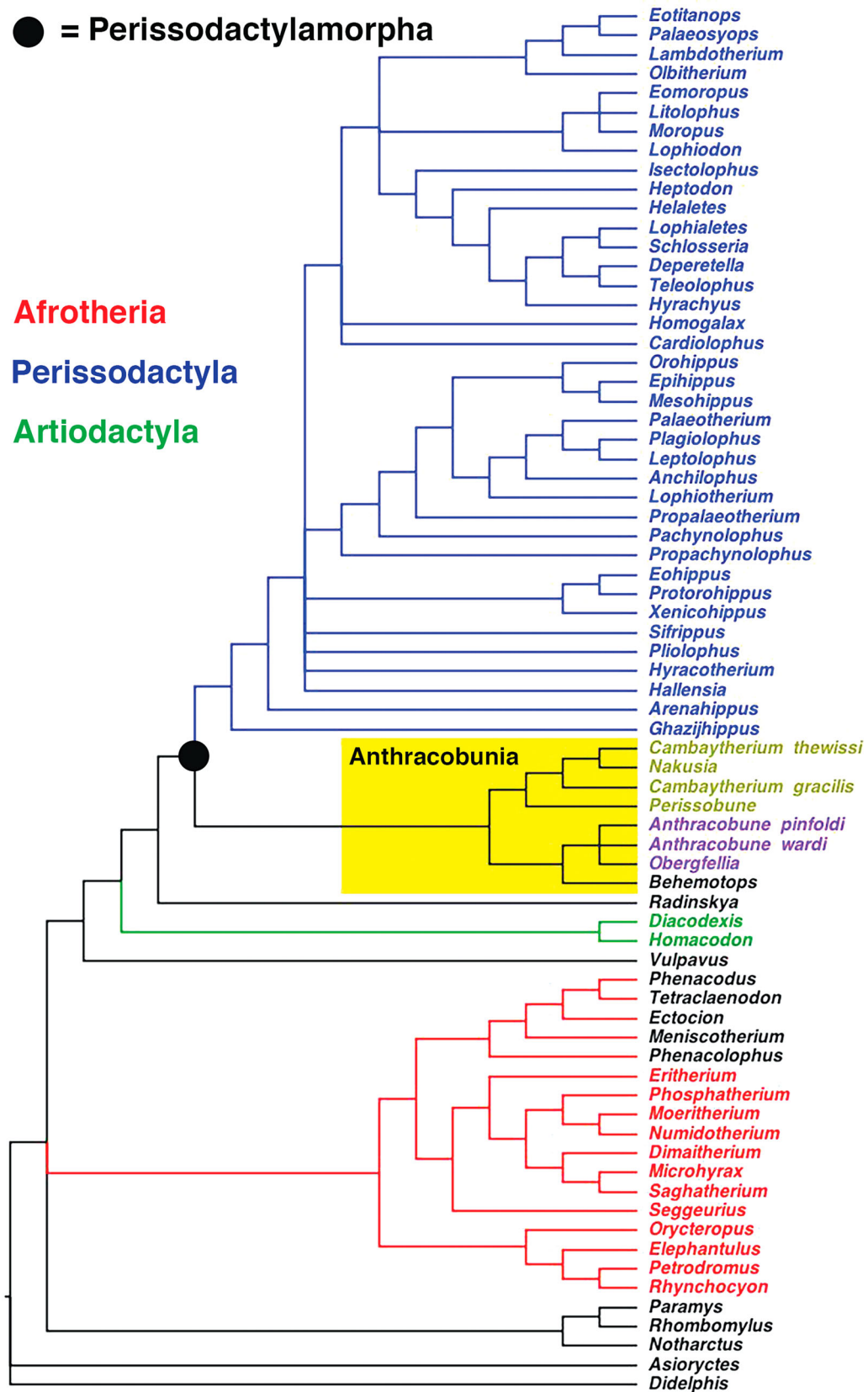
FIGURE 82. Strict consensus of 18 shortest trees of 1,982 steps based on parsimony analysis where results are constrained to accord with results of analyses of placental mammal phylogeny using molecular data. Afrotheres (red), artiodactyls (green), and perissodactyls (blue) are indicated by colored branches and terminal taxa. Gold names represent Cambaytheriidae and purple names represent Anthracobunidae. Yellow box indicates Anthracobunia. Black dot indicates node corresponding to Perissodactylamorpha.

FIGURE 83. Strict consensus of 408 shortest trees of 1,997 steps based on unconstrained parsimony analysis including *Minchenella* and Quettacyonidae. Black dots indicate positions of *Minchenella* and Quettacyonidae.

TABLE 17. Character-state changes at selected nodes from results of unconstrained parsimony analysis.

Node A: traditional Perissodactyla
18 (facial exposure of lacrimal): 0 → 1
57 (sulcus for internal carotid artery): 0 → 1
65 (foramen for ramus superior of stapedial artery): 0 → 2
77 (number of sacral vertebrae): 1 → 2
82 (shape of scapular glenoid fossa): 0 → 1
98 (capitulum of humerus): 1 → 2
117 (first metacarpal): 0 → 1
123 (fovea capitis of femur): 0 → 1
125 (height of greater trochanter): 1 → 2
162 (plantar process of navicular): 0 → 1
225 (upper molar centrocrista): 0 → 2
231 (M1–2 postmetacrista): 0 ⇒ 1
232 (M3 postmetacrista): 0 ⇒ 1
245 (upper molar preparaconule crista): 0 ⇒ 2
250 (M2 lingual cingulum): 0 ⇒ 1
264 (diastema between last lower incisor and lower canine): 0 → 1
265 (diastema between lower canine and adjacent premolar): 1 → 2
281 (p4 paraconid and paralophid): 1 → 3

Node B: Perissodactyla + Anthracobunia (Perissodactylamorpha):
1 (posterior nasal): 0 ⇒ 1
9 (tuber maxillae): 0 ⇒ 1
10 (orbital portion of maxilla): 1 → 0
12 (common recess for sphenopalatine foramen and dorsal palatine foramen): 0 → 1
17 (position of caudal border of palatines): 1 → 0
29 (contact of frontal and alisphenoid in orbit): 0 → 1
42 (postglenoid process): 1 → 2
63 (tympanic aperture of hiatus Fallopii): 0 → 1
77 (number of sacral vertebrae): 0 → 1
107 (articular surface of distal radius): 0 → 1
119 (anterior iliac crest): 0 → 2
126 (orientation of lesser trochanter of femur): 1 ⇒ 0
127 (size of third trochanter of femur): 0 ⇒ 1
132 (posterior process and median ridge of distal articulation of tibia): 0 ⇒ 1
137 (orientation of trochlear ridges of astragalus): 0 ⇒ 1
143 (lateral process of astragalus): 0 → 1
148 (posterior tubercle of medial trochlear facet): 0 ⇒ 1
149 (proximal calcaneal facet of astragalus): 0 ⇒ 1
152 (lateral groove on calcaneum): 0 ⇒ 1
161 (anterior contact between navicular and calcaneum): 0 → 1
168 (first metatarsal): 1 → 2
197 (P3 parastyle): 0 → 1
198 (P3 paraconule): 0 → 1
209 (P4 paraconule): 2 ⇒ 0
238 (M metaconules or corresponding part of metalophs): 0 → 1
276 (p3 metaconid): 0 ⇒ 1
286 (p4 hypoconid position): 1 → 2
288 (ratio of p4 length to m1 length): 1 → 2
293 (lower molar protolophid notch): 1 → 0
294 (lower molar twinned metaconids): 0 ⇒ 1

Node C: Anthracobunia
56 (fossa for tensor tympani): 1 → 0
58 (sulcus for proximal stapedial artery): 1 → 0
87 (proximal projection of greater tuberosity of humerus): 1 → 2
89 (ridge from deltopectoral crest extending onto distal anterior shaft of humerus): 1→ 0
90 (supinator crest of humerus): 2 → 1
91 (lateral articular shelf (capitular tail):): 1 → 0
96 (medial epicondyle): 2 → 1
104 (shape of lateral process of proximal radius): 1 → 0
105 (styloid process of distal radius): 1 → 0
131 (medial malleolus of tibia): 1 → 0
136 (astragalar canal): 1 → 0
158 (orientation of distal edge of calcaneum between sustentaculum and cuboid): 1 → 0
169 (fifth metatarsal): 2 → 1
182 (diastema between last upper incisor and upper canine): 0 → 1
212 (P4 metaconule): 2 ⇒ 0
213 (P4 metaconule position): 1 → 0
239 (upper molar parastyles): 1 ⇒ 0
262 (distal cusp on i3): 0 → 1
291 (m1 paraconid or paralophid): 2 → 5
298 (height of lower molar metaconids): 2 → 1

unconstrained analysis excluding these taxa. Whereas Quettacyonidae is part of the largest polytomy, *Minchenella* consistently groups with post-Wasatchian equids. The results did not support a close relationship between Quettacyonidae or *Minchenella* and either cambaytheres or anthracobunians.

319 (m3 hypoconulid connection): 2 → 0

Node D: Cambaytheriidae
197 (P3 parastyle): 1 → 0
198 (P3 paraconule): 1 → 0
212 (P4 metaconule): 0 ⇒ 1
213 (P4 metaconule position): 0 → 1
251 (labial crest of M hypocone): 0 ⇒ 1
280 (p3 paraconid or paralophid): 1 ⇒ 0
281 (p4 paraconid and paralophid): 1 → 0
285 (p4 hypoconid): 1 ⇒ 2
292 (m3 protolophid shape): 0 → 1
296 (lower molar metaconid buttress): 0 → 2

Node E: *Cambaytherium* (two species): + *Nakusia*
72 (lateral coronoid crest): 0 → 1
209 (P4 paraconule): 0 ⇒ 2
211 (P4 metacone): 1 ⇒ 0
254 (M3 metacone): 0 ⇒ 1
266 (p1 presence): 0 → 1
276 (p3 metaconid): 1 ⇒ 0
286 (p4 hypoconid position): 2 ⇒ 1
288 (ratio of p4 length to m1 length): 2 → 0
320 (lower molar entoconulid): 1 ⇒ 0

Node F: *C. thewissi* + *Nakusia*
100 (proportions of head of radius): 1 → 0
103 (extent of proximal ulnar facet on posterior aspect of proximal radius): 1 → 0
231 (M1–2 postmetacrista): 0 ⇒ 1
232 (M3 postmetacrista): 0 → 1
253 (M3 size): 1 → 0
255 (M3 hypocone): 2 → 1
256 (M3 hypocone position): 1 → 2
257 (M3 hypostyle): 2 → 1
274 (p2 talonid): 0 → 1
284 (p4 metaconid position): 0 → 1
296 (lower molar metaconid buttress): 2 → 0
303 (height of cristid obliqua within valley between trigonid and talonid): 1 → 0
315 (m1 and m2 hypoconulid position): 1 → 0

Node G: Artiodactyla + Perissodactylamorpha (Euungulata):
20 (lacrimal tubercle): 0 → 1
24 (crista orbitotemporalis): 0 → 1
52 (subarcuate fossa): 1 → 2
68 (bones enclosing foramen magnum): 0 → 1
72 (lateral coronoid crest): 1 → 0
75 (number of lumbar vertebrae): 1 → 4
79 (fusion of spines on caudal-most two sacral vertebrae): 0 → 1
82 (shape of scapular glenoid fossa): 1 → 0
96 (medial epicondyle): 1 → 2
98 (capitulum of humerus): 0 → 1
102 (articular surface of lateral process of proximal radius): 0 ⇒ 1
104 (shape of lateral process of proximal radius): 0 → 1
113 (centrale): 0 ⇒ 1
133 ('beaked' distal tibia articulation): 0 ⇒ 1
138 (depth of trochlear groove of astragalus): 1 → 2
142 (cotylar fossa): 1 → 0
150 (navicular facet of astragalus): 0 → 1
151 (contact between astragalus and cuboid): 0 ⇒ 1
155 (orientation of astragalar facet of calcaneum in lateral view): 0 → 1
164 (entocuneiform): 0 → 1
177 (first or central upper incisor size): 0 ⇒ 1
265 (diastema between lower canine and adjacent premolar): 0 → 1
275 (p3 paraconid): 3 → 0
285 (p4 hypoconid): 2 ⇒ 1

Node H: Paenungulata + Euungulata
10 (Orbital portion of maxilla): 0 → 1
42 (postglenoid process): 2 → 1
46 (exposure of mastoid): 0 → 1
56 (fossa for tensor tympani): 0 → 1
62 (tympanic process or medial section of caudal tympanic process of petrosal): 1 → 2
64 (lateral section of caudal tympanic process of petrosal): 0 → 1
74 (number of thoracic vertebrae): 1 → 3
75 (number of lumbar vertebrae): 5 → 1
90 (supinator crest of humerus): 1 → 0
92 (placement of lateral articular shelf): 0 → 1
94 (entepicondylar foramen): 0 ⇒ 1

131 (medial malleolus of tibia): 0 → 1
159 (shape of cuboid facet of calcaneum): 0 ⇒ 1
166 (mesocuneiform and navicular facets of entocuneiform): 1 → 0
168 (first metatarsal): 0 → 1
169 (fifth metatarsal): 0 → 2
225 (upper molar centrocrista): 2 → 0
253 (M3 size): 0 → 1
286 (p4 hypoconid position): 2 → 1
300 (lower molar cristid obliqua): 1 ⇒ 0
313 (m3 postentoconulid): 0 → 2
319 (m3 hypoconulid connection): 0 → 2

Node I: Phenacodonta + (Paenungulata + Euungulata):
23 (sinus canal and cranio-orbital foramen): 1 → 0
28 (sphenorbital fissure): 1 → 0
31 (posterior opening of alisphenoid canal): 1 ⇒ 0
49 (tympanic roof): 0 ⇒ 1
52 (subarcuate fossa): 0 → 1
58 (sulcus for proximal stapedial artery): 0 → 1
73 (ventral border of mandibular angle): 1 ⇒ 2
74 (number of thoracic vertebrae): 0 → 1
80 (clavicle): 0 → 1
83 (coracoid process of scapula): 1 → 0
84 (metacromion process of scapula): 0 → 1
99 (proximal radius): 0 → 1
120 (anterior inferior iliac spine): 1 → 0
143 (lateral process of astragalus): 1 → 0
152 (lateral groove on calcaneum): 1 → 0
170 (distal phalanges): 0 ⇒ 1
237 (upper molar metaconules): 2 → 0
275 (p3 paraconid): 1 → 3
278 (p3 hypoconid): 2 → 0
314 (m1 and m2 hypoconulids): 2 ⇒ 0

Node J: *Notharctus* + (*Orycteropus* + Glires):
2 (length of postorbital portion of skull): 1 ⇒ 2
5 (orientation of caudal border of premaxilla): 1 ⇒ 0
30 (alisphenoid canal (posterior opening):): 0 ⇒ 1
33 (foramen ovale position): 1 → 0
82 (shape of scapular glenoid fossa): 1 → 0
90 (supinator crest of humerus): 1 → 0
100 (proportions of head of radius): 1 → 0
101 (lateral process of radius): 1 → 0
172 (postcanine diastema): 0 → 1
179 (third upper incisor): 0 ⇒ 1
182 (diastema between last upper incisor and upper canine): 0 → 1
185 (P1): 0 → 1
197 (P3 parastyle): 0 ⇒ 1
214 (P4 endoprotocrista): 0 → 1
234 (upper molar paraconules): 0 ⇒ 1
246 (upper molar ectoloph-metaloph junction): 0 → 2
261 (third lower incisor): 0 ⇒ 1
264 (diastema between last lower incisor and lower canine): 0 → 1
266 (p1 presence): 0 → 1
310 (lower molar posthypocristid): 1 ⇒ 0
316 (m2 hypoconulid): 0 → 1
319 (m3 hypoconulid connection): 0 ⇒ 1

Node K: *Orycteropus* + Glires
17 (position of caudal border of palatines): 1 → 0
42 (postglenoid process): 2 → 0
43 (postglenoid process orientation): 0 → 1
91 (lateral articular shelf (capitular tail):): 1 → 0
108 (orientation of olecranon process): 0 → 2
121 (ileopectineal tubercle): 0 → 1
132 (posterior process and median ridge of distal articulation of tibia): 0 → 1
158 (orientation of distal edge of calcaneum between sustentaculum and cuboid): 1 → 0
171 (canine size): 0 ⇒ 2
178 (second upper incisor): 0 ⇒ 1
185 (P1): 1 → 2
189 (P2): 0 → 1
190 (diastema posterior to P2): 0 → 1
215 (P4 metaloph): 0 → 2
223 (M1 ectocingulum): 2 → 0
224 (M2 ectocingulum): 2 → 0
245 (upper molar preparaconule crista): 0 → 1
260 (second lower incisor): 0 ⇒ 2
265 (diastema between lower canine and adjacent premolar): 0 → 2

266 (p1 presence): 1 → 2
270 (p2 presence): 0 ⇒ 1
278 (p3 hypoconid): 2 → 0
279 (p3 entoconid): 0 → 2
287 (p4 entoconid): 0 → 1
300 (lower molar cristid obliqua): 1 → 3
311 (lower molar postentocristid): 0 → 1
318 (m3 hypoconulid position): 0 → 1

Node L: All taxa except *Vulpavus*, *Asioryctes*, and *Didelphis*
55 (tegmen tympani): 0 ⇒ 1
70 (height of mandibular condyle): 1 ⇒ 2
75 (number of lumbar vertebrae): 3 ⇒ 5
116 (contact between unciform and third metacarpal): 1 → 0
136 (astragalar canal): 0 → 1
140 (height of lateral ridge of trochlea of astragalus): 0 → 1
143 (lateral process of astragalus): 0 → 1
177 (first or central upper incisor size): 1 → 0
240 (main mass of M parastyle): 1 → 0
244 (M1–2 paracone and metacone sizes): 0 → 1
248 (M1–2 hypocone): 0 ⇒ 1
257 (M3 hypostyle): 0 ⇒ 2
258 (M1–2): 1 → 0
281 (p4 paraconid and paralophid): 0 ⇒ 1
282 (p4 width): 0 ⇒ 1
283 (p4 metaconid): 1 → 2
289 (m1 and m2 occlusal areas): 1 → 2
290 (m3 size): 2 → 0
298 (height of lower molar metaconids): 0 ⇒ 2
304 (lower molar talonid height): 0 ⇒ 1

Arrows indicate unambiguous (double-lined) and ambiguous (single-lined) direction of change. Letters refer to nodes labeled in Figure 81.

Discussion

The present analysis generally reinforces the close relationship between cambaytheres and perissodactyls. The main difference between these results and those of Rose et al. (2014b) with regard to cambaytheres is that cambaytheriids and anthracobunids are sister taxa, whereas in our previous analysis (Rose et al., 2014b; see also Cooper et al., 2014) cambaytheriids were a sister taxon to perissodactyls, and anthracobunids nested within Perissodactyla. The current results seem more plausible, given the strong similarities in tooth morphology of cambaytheres and anthracobunids and the considerable dissimilarities between anthracobunids and the perissodactyls with which they were united (*Sifrhippus* and *Hallensia*) in Rose et al. (2014b). To reflect the close relationship between cambaytheriids and anthracobunids, we refer them to the order Anthracobunia, and we place Anthracobunia and Perissodactyla in a superordinal taxon, Perissodactylamorpha.

The relationships among *Perissobune*, *Nakusia*, and the two species of *Cambaytherium*, based on their close dental similarity, suggest that these taxa could all be referred to a single family, Cambaytheriidae. The nesting of *Nakusia* between the two species of *Cambaytherium* could support synonymizing *Cambaytherium* as a junior synonym of *Nakusia*. However, of the 13 character-state changes occurring at the node uniting *Nakusia* and *C. thewissi* (see Table 17), only one (presence of a postmetacrista on M1–2 that is in line with the paracone and metacone) is found in both taxa. This is because *Nakusia* is known only from one specimen with P4–M2, which is heavily worn, obscuring some critical details. An argument could also be made that *Nakusia shahrigensis* is based on an inadequate holotype and the name therefore should be rejected. For these reasons, we elect not to make any taxonomic changes based on this part of the topology. *Perissobune*, at least *P. intizarkhani*, might also be congeneric with *Cambaytherium*, but until it is better known, we maintain its distinction based on the differences enumerated above (see Systematic Paleontology).

The placement of the supposed basal desmostylian *Behemotops* with anthracobunids (represented by two species of *Anthracobune* and the genus *Obergfellia* in our analysis) is consistent with the results of Cooper et al. (2014), at least in terms of placing these taxa closer to perissodactyls than to tethytheres, as was previously proposed (West, 1980; Wells and Gingerich, 1983; Domning et al., 1986; Ray et al., 1994). If correct, this perhaps clarifies the biogeographic origin of Desmostylia, which otherwise would have to reconcile their northern trans-Pacific distribution with the largely African origins of tethytheres. Further investigations of the phylogenetic position of *Behemotops*, and whether Desmostylia are highly modified perissodactylamorphs rather than tethytheres, will require including additional desmostylian taxa in an analysis like this one.

The relationship of *Radinskya* to the clade including cambaytheres, anthracobunids, and *Behemotops* is somewhat unexpected, because *Radinskya* had previously been allied with either perissodactyls or phenacolophids (McKenna et al., 1989; Holbrook, 2014), and the results of Rose et al. (2014b) placed *Radinskya* either close to perissodactyls or nested within Afrotheria with phenacodontids. While *Radinskya* would be part of Anthracobunia based on the unconstrained results, its placement outside of the Anthracobunia-Perissodactyla clade in the constrained results renders this only a tentative suggestion at present.

Of the groups that constitute Anthracobunia, cambaytheriids —and *Cambaytherium* specifically—are the best known, including fairly good representation of the cranium and the postcranial skeleton. *Cambaytherium* provides the best opportunity for direct comparisons with perissodactyls; therefore, it is the best candidate to serve as an outgroup for morphological studies of perissodactyl phylogeny.

In contrast to the results of most prior morphological analyses, which supported the paenungulate-perissodactyl clade called Altungulata or Pantomesaxonia (Thewissen and Domning, 1992; Kondrashov and Lucas, 2012; Rose et al., 2014b), and in accord with results from molecular studies (e.g., Meredith et al., 2011) and from Cooper et al. (2014) and O'Leary et al. (2013), the unconstrained tree from the present study places perissodactyls closer to cetartiodactyls, rather than to paenungulates. Unlike molecular studies, the unconstrained results did not recover a monophyletic Afrotheria, nor did they place the carnivoran *Vulpavus* with other laurasiatheres.

Phenacodontids—represented in the present study by *Phenacodus*, *Ectocion*, *Tetraclaenodon*, and possibly *Meniscotherium*—have been considered to be close relatives of perissodactyls by previous workers (Radinsky, 1966, 1969; Hooker, 1994) and are frequently employed as outgroups in analyses of perissodactyl phylogeny and evolution (Hooker, 1994; Froehlich, 1999, 2002; Holbrook, 1999, 2001, 2009; Holbrook and LaPergola, 2011; Koenigswald et al., 2011). Other studies have placed phenacodontids either as basal members of Altungulata (Prothero et al., 1988; Thewissen and Domning, 1992; Fischer and Tassy, 1993; Ladevèze et al., 2010; Kondrashov and Lucas, 2012; Holbrook, 2014), or as basal laurasiatheres (O'Leary et al., 2013) or afrotheres (Asher et al., 2003). Our results place all phenacodontids in a monophyletic group, along with *Phenacolophus*, which is similar to Phenacodonta of Thewissen and Domning (1992). We thus refer here to these taxa as phenacodontans, with the caveat that our study was not necessarily testing the monophyly of Phenacodonta. The results of the unconstrained analysis place phenacodontans essentially at the base of a modified version of what was historically called Ungulata, including Perissodactyla, Artiodactyla, and Paenungulata. In the constrained analysis, phenacodontans are placed within Afrotheria as the sister taxon to Paenungulata. In both cases, Perissodactyla shares a more recent common ancestry with Anthracobunia and Artiodactyla than with phenacodontans. The consistent placement of

TABLE 18. Body mass estimates (kg) for *Cambaytherium* from teeth and postcrania, using relationships between tooth size or postcranial dimensions and body mass in various extant ungulates.

Element	n	BM (NSA)	BM (Suoid)	BM (All)	n	BM (NSA)	BM (Suoid)	BM (All)	n	BM (NSA)	BM (Suoid)	BM (All)
		C. thewissi				*C. gracilis*				*C. marinus*		
M2	19	23.4	—	—	3	8.5	—	—	1	93.9*	—	—
M1	18	24.4	—	—	1	9.7	—	—	1	58.6*	—	—
P4	19	19.9	—	—	4	9.3	—	—	1	69.4*	—	—
m2	19	29.8	—	—	2	14.6	—	—	—	—	—	—
m1	11	28.0	—	—	4	13.7	—	—	—	—	—	—
p4	16	24.7	—	—	6	10.9	—	—	—	—	—	—
Femur	5	—	19.5	16.2	3	—	11.5	9.9	1	—	158.0	115.3
Humerus	7	—	24.7	22.3	1	—	7.1	7.7	—	—	—	—
Radius	6	—	20.0	11.9	1	—	7.9	5.3	—	—	—	—
Tibia	5	—	21.7	15.6	—	—	—	—	1	—	90.7	57.6

See Table 3 for measurement definitions. **Abbreviations**: **All**, all ungulates; **BM**, body mass in kg; **NSA**, nonselenodont artiodactyls. *Measurements from Bajpai et al. (2006).

Phenacolophus as sister taxon to Phenacodontidae is a novel result but is mainly supported by a small number of characters of the lower dentition, such as distinct lower molar metastylids and a small m3 hypoconulid. Although phenacodontans might not be especially closely related to perissodactyls, the many plesiomorphic features they retain still provide informative comparisons with *Cambaytherium* and perissodactyls, as we have employed in our discussion of cambaythere morphology.

The results of the analysis that included *Minchenella* and Quettacyonidae highlight our poor knowledge of the anatomy of these intriguing taxa. Placement of *Minchenella* with post-Wasatchian equids is certainly due to superficial similarities, including a more lophodont and dilambdodont dentition in all of these taxa. This outcome, however, emphasizes that the dentition of *Minchenella* is unusually advanced for a Paleocene archaic ungulate, exhibiting greater lophodonty and premolar molarization than are typical in archaic ungulates. These features distinguish it from anthracobunians, which occur later but are more bunodont and have premolars that are no more molarized (anthracobunids) or much less molarized (cambaytheriids). Similarities between quettacyonids and anthracobunians are likewise superficial and mostly reflect shared plesiomorphies, such as simple premolars that show little or no molarization (shared with cambaytheriids).

The precise relationships of quettacyonids, phenacolophids, *Minchenella*, and *Radinskya* are likely to remain uncertain and controversial until more complete and/or better-preserved fossils are available.

PALEOBIOLOGY OF *CAMBAYTHERIUM*

The anatomy of *Cambaytherium* is now well enough known to enable a reconstruction of the living animal, which should provide insight to the paleobiology of the common ancestor of perissodactylamorphs. Here, we consider what the fossils imply about body size, diet, and locomotion of *Cambaytherium*.

TABLE 19. Grand mean body mass estimates (kg) for *Cambaytherium thewissi*, *C. gracilis*, and *C. marinus*.

Taxon	PC-suoid	Teeth	Grand mean
C. thewissi	21.4	25.0	23.2
SD	2.35	3.49	2.92
C. gracilis	8.8	11.1	10.0
SD	2.34	2.49	2.42
C. marinus	124.4	74.0	99.2

Abbreviations: **PC**, postcrania; **SD**, standard deviation.

Body Size

Body mass estimates based on the postcranial and dental measures are generally in good agreement with each other and suggest that *Cambaytherium thewissi* weighed about 23 kg, whereas the smaller *C. gracilis* weighed only 10 kg (Tables 18, 19). These estimates put these two species of *Cambaytherium* roughly in the size range of the peccary, *Pecari tajacu* (Silva and Downing, 1995). Estimates vary among measures. Tooth regressions generally result in slightly higher estimates than postcranial regressions, except in *C. marinus*. In *C. thewissi*, for which sampling was most comprehensive, larger estimates are obtained from the molars than from the premolars, and from the lower teeth than from the upper teeth, perhaps reflecting relative elongation of the dentition posteriorly. Similarly, larger estimates are obtained from the humerus than from the radius, suggesting a relatively robust proximal forelimb in *Cambaytherium*, compared with extant suoids (Table 18; Appendix 7). Estimates based on suoid postcrania are almost always higher than those based on 'all ungulates' but probably yield more reliable estimates for cambaytheres.

Data for *Cambaytherium marinus* are very limited but indicate that it was considerably larger than *C. thewissi*. The mean body mass estimate based on three upper teeth in the holotype is 74 kg, whereas the estimate based on two postcranial elements (proximal femur and distal tibia) is much higher: 86 kg based on the 'all-ungulate' regression, 124 kg based on suoids, which are probably a better model for *C. marinus*. The average of estimates based on teeth and suoid postcrania gives an estimate of 99 kg (Table 19), about the size of *Babyrousa*. Although *Tapirus* probably provides the best living analogue for *Cambaytherium*, cambaytheres were generally much smaller than extant tapirs.

Compared with early Eocene perissodactyls, bones of *Cambaytherium thewissi* are roughly comparable to or slightly larger than those of *Homogalax protapirinus* (Rose, 1996) and markedly more robust. *Cambaytherium gracilis* was roughly the size of a medium-sized *Hyracotherium* (*H. grangeri* to *H. aemulor*). Compared with *Phenacodus*, *C. thewissi* was intermediate in size between *P. vortmani* and the much larger *P. trilobatus*, although *C. marinus* was about the size of the latter, or larger, based on the few available elements. *Cambaytherium gracilis* was distinctly smaller than *P. vortmani*. These body size comparisons are generally consistent with body mass estimates based on teeth by Damuth (1990).

Dental Function and Diet

Judging from their relatively low-crowned, bunodont cheek teeth, cambaytheres were probably generalized herbivores.

Most *Cambaytherium thewissi* dentitions (except for newly erupted teeth) show unusually heavy abrasive wear that resulted in flattened cusps with broad dentine exposures (Figs. 9, 19). This is even the case in some deciduous dentitions (e.g., Fig. 16; Rose at al., 2006:fig. 3e). Closer inspection reveals that not all teeth are heavily worn. Instead, *C. thewissi* is characterized by a steep wear gradient, whereby posterior premolars and first molars may have cusps worn flat, exposing broad areas of dentine, while at the same time second molars show only modest wear and third molars may be newly erupted and virtually unworn (Figs. 19, 20B; Koenigswald et al., 2018). The same wear pattern occurs in the holotype of *Nakusia shahrigensis* (Fig. 40A). The wear gradient in *C. gracilis* is less extreme (e.g., Figs. 14, 29A); nevertheless, abrasive wear of the cusp apices of the posterior premolars and anterior molars is evident, and very heavily worn specimens are known (e.g., Fig. 29C, D).

The significant wear gradient in the dentition of *Cambaytherium thewissi*, together with the presence of robust premolars and zigzag Hunter-Schreger bands in the enamel of some specimens (an enamel structure typical of durophagous feeders such as bone crushers; Stefen, 1997), supports the inference that *Cambaytherium* had a durophagous diet of tough vegetation, probably including hard fruits, nuts, and abrasive stems and leaves (Koenigswald et al., 2018). The lesser wear gradient (and relatively smaller premolars) in *C. gracilis* suggests a somewhat less harsh diet. Based on the subadult skull and mandible (GU 402 and GU 403), the permanent premolars of *Cambaytherium thewissi* were either erupting or fully erupted (P3–4, p4) before the third molars were in place (Koenigswald et al., 2018). Late eruption of third molars may be a derived condition and appears to contrast with both Phenacodontidae and basal Equidae, in which the third molars apparently erupted before the premolars were replaced (West, 1971; Rose et al., 2018a). The delayed eruption of third molars, and the posterior elaboration of these teeth, may have been adaptations for durophagy, because they would have extended the duration during which at least one of the molars retained cuspate crowns. It is also possible that heavy abrasive wear, which occurs before the crowns are worn down, is itself adaptive for a durophagous diet.

Early Eocene quettacyonids, which have been found in similar depositional environments in Pakistan, also show heavy abrasive wear on the cheek teeth, with a steep wear gradient (Fig. 43B, C), as well as a deep jaw, features suggesting durophagy or exposure to abrasive substances during feeding. It is possible that something in the lagoonal environment of quettacyonids and cambaytheres led to heavy tooth wear.

As described above, many canine teeth of *Cambaytherium* also show unusual heavy wear. The apex may be truncated and worn flat, and transverse grooves are often formed at the base of the crown of canine teeth, probably indicating that coarse vegetation was pulled through the teeth. This is further evidence of an abrasive diet.

The mandibular anatomy of *Cambaytherium*, including the fused symphysis, high condyle, and expanded angular process and reduced coronoid process (reflecting enlargement of the masseter and medial pterygoid muscles and reduction of the temporalis), is typical of herbivorous mammals. These traits reinforce the conclusions drawn from dental wear.

Skeletal Anatomy and Locomotion

Most skeletal elements of *Cambaytherium* are now known, enabling us to reconstruct the skeleton of *Cambaytherium thewissi* with reasonable confidence (Fig. 84). The known
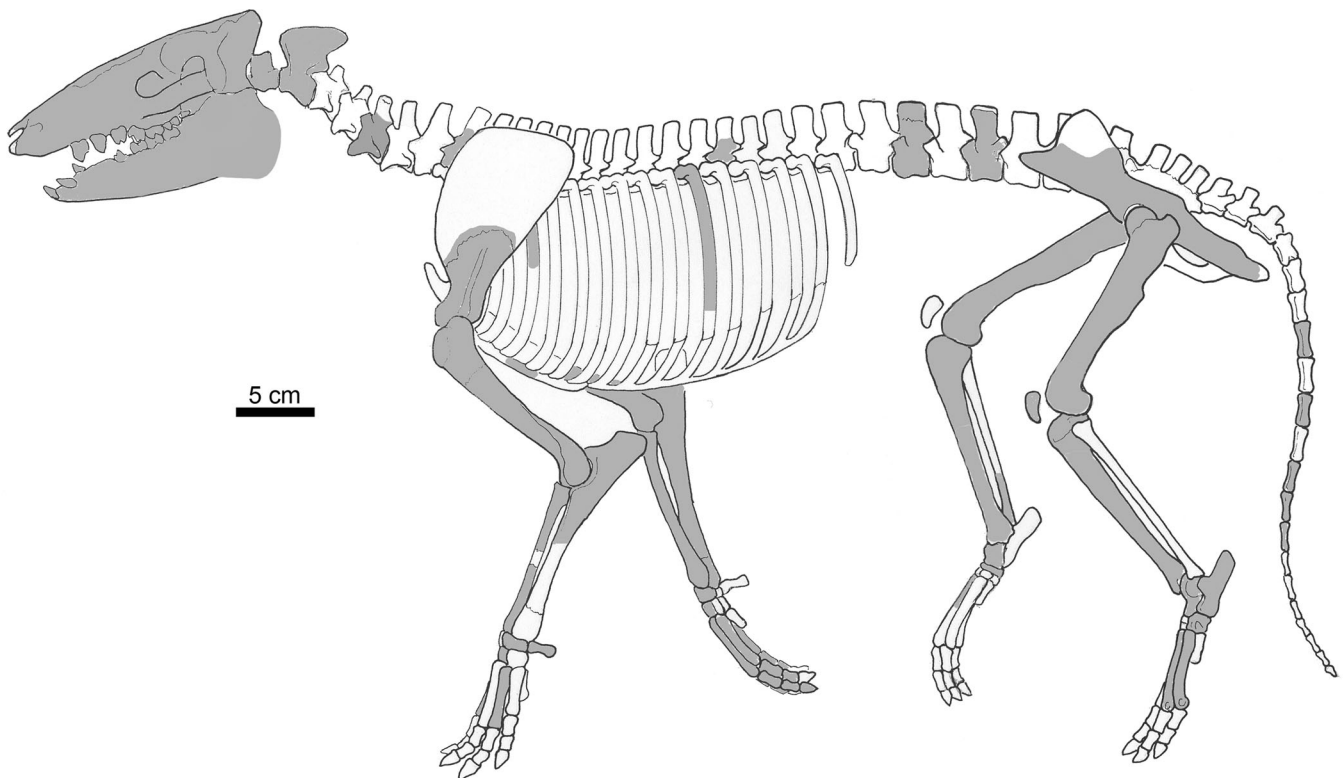
FIGURE 84. Skeletal reconstruction of *Cambaytherium thewissi*, with preserved elements shown in gray. Although much of the skeleton is represented, proportions should be regarded as approximate because elements were found isolated and represent multiple individuals. Because phalanges cannot be assigned definitively to digit or limb, representative phalanges are shown only in one manus but likely represent both manus and pes.

elements of *C. gracilis* suggest that, aside from being smaller and more slender, it was similar.

Cambaytherium exhibits a number of features related to cursoriality that are shared with early perissodactyls and, to a lesser extent, phenacodontids. In the axial skeleton, the robust muscular processes and strongly revolute zygapophyses of the postdiaphragmatic vertebrae of *Cambaytherium* (not shared with *Phenacodus*) suggest relative stability in its posterior spinal column compared with that of *Hyracotherium*. This may relate to size and/or locomotor differences between these taxa. Extant horses, which employ transverse (contralateral) footfall patterns during galloping, experience limited vertebral bending compared with cheetahs, which use rotary (ipsilateral) footfall patterns and emphasize spinal flexion/extension; other mammals utilize both patterns depending on their speed (Bertram and Gutmann, 2009). Although vertebral kinematics are poorly understood in mammals more broadly, Bertram and Gutmann (2009) provided a mechanistic link between center of mass transitions during rapid locomotion and 'flexed back' versus 'stiff back' running gaits. These gaits exemplify extremes of a continuum between species specialized for rotary versus transverse galloping gaits (Bertram and Gutmann, 2009). The relative stability of the lumbar region in *Cambaytherium*, combined with the subcursorial adaptation suggested by its appendicular skeleton, indicates that use of 'flexed back' galloping gaits, in which center of mass transitions are initiated by the forelimb, was probably more limited than in *Hyracotherium*. The transition away from 'flexed back' running toward specialization for transverse galloping gaits has been linked to increasing body size in fossil horses (Jones, 2016).

A number of features of the elbow joint also are usually associated with cursorial locomotion, including a relatively narrow distal humerus with a reduced entepicondyle, a narrow and non-spherical capitulum of the humerus, a radial head with an uneven surface and a more rectangular outline in proximal view, and medial and lateral coronoid processes of the ulna that articulate with the anteriorly placed radial head in a way that greatly restricts rotation. Like both phenacodontids and early perissodactyls, *Cambaytherium* has a deep, perforated olecranon fossa, a cursorial trait that increases the range of extension at the elbow.

The femur and the tibia are quite similar in *Cambaytherium*, phenacodontids, and early perissodactyls and also display cursorial features. All of them have a deep distal femur with an elevated patellar trochlea. In many cases, *Cambaytherium* and perissodactyls share slightly more specialized conditions than in phenacodontids. Like early perissodactyls, *Cambaytherium* has a more elevated greater trochanter and a more proximal third trochanter than in phenacodontids. The tibial crest is slightly shorter than in phenacodontids. In the ankle, the astragalar articulation of the tibia covers the entire distal surface and has deep grooves for the narrow trochlear ridges of the astragalus. Together with the distal fibula, this forms a tight mortise-and-tenon joint that restricted movement to the parasagittal plane. Although the astragalar trochlea resembles that of phenacodontids in being wider and shorter than in early perissodactyls, the saddle-

FIGURE 85. Restoration of *Cambaytherium thewissi*, by Elaine Kasmer.

shaped navicular facet and alternating tarsus (cuboid articulating with both the calcaneus and the astragalus) probably helped to restrict the foot to parasagittal motion. The articulations of the manual and pedal digits of *Cambaytherium* suggest a digitigrade to subunguligrade stance, comparable to that in *Tapirus* and *Hyracotherium*. The shape of the terminal phalanx and the orientation of its proximal articulation are closer to those of *Hyracotherium* than to those of *Phenacodus*.

Although *Cambaytherium* exhibits these cursorial features, several of them are expressed to a lesser degree than in more specialized cursors such as early perissodactyls, whereas other cursorial traits seen in specialized cursors are lacking altogether. The long bones of the limbs of *Cambaytherium* are somewhat more robust than those of *Hyracotherium*, *Homogalax*, and *Heptodon*, and the radius and the ulna are less bowed than in early perissodactyls. To the extent that it can be ascertained from the isolated elements in our sample, there is no evidence in *Cambaytherium* of the elongation of distal limb segments (i.e., metapodials and phalanges) that characterizes early perissodactyls. Instead, these distal elements are similar in proportions to those of *Phenacodus*. The short, robust metacarpals, together with the less arched antebrachium, would have reduced stride length and elbow extension in comparison with early perissodactyls. The evidence at hand suggests that both manus and pes were pentadactyl at least to some extent, indicating less reduction of lateral digits than in more cursorial early perissodactyls.

In the hind limb of *Cambaytherium*, compared with that of *Hyracotherium*, the greater trochanter is not as elevated, the patellar groove is relatively wider, and the astragalar facet of the tibia is slightly wider and shallower, suggesting slightly less cursorial specialization, but these features in *Cambaytherium* approximate those of *Homogalax* (Rose, 1996). In the ankle, the shape and orientation of the articulations between the astragalus and the calcaneus are more like those described for *Homogalax* than the more interlocking articulations observed in most *Hyracotherium* (Rose, 1996), and the saddle-shaped navicular facet of the astragalus is shallower than in most early perissodactyls. Cuboid and navicular are relatively shorter than in early perissodactyls, again resembling those of *Phenacodus*.

On the whole, the anatomical evidence indicates that *Cambaytherium* (Fig. 85) was specialized for a degree of cursoriality that was greater than that of *Phenacodus* but less than that in the oldest and most primitive perissodactyls for which skeletons are known (e.g., *Homogalax*, *Hyracotherium*, *Heptodon*), although it approached *Homogalax* in some respects more than other early perissodactyls. It was more robust and generalized than basal perissodactyls.

DISCUSSION

Phylogenetic Implications

We initially interpreted *Cambaytherium* as the sister taxon of Perissodactyla (Rose et al., 2014b), a phylogenetic position supported by all of our analyses at that time. Our current analyses also support this interpretation, with the alteration that cambaytheriids + anthracobunids (and possibly *Radinskya* and Desmostylia) constitute the sister taxon to perissodactyls. The fact that cambaytheriids lie outside of all unequivocal perissodactyls supports this interpretation. As shown above, *Cambaytherium* possesses a mosaic of anatomical traits, some more plesiomorphic than in basal perissodactyls and suggestive of condylarth (specifically phenacodontid) ancestry, and others more derived and synapomorphic with basal perissodactyls. Plesiomorphic traits include bunodont cheek teeth lacking lophodonty and with well-developed conules on the upper molars, shorter and more robust long bones and metapodials, humerus with a long deltopectoral crest and lacking a capitular tail (i.e., a lateral articular shelf), probable

presence of five digits on both manus and pes, a wider and shorter tarsus, and an astragalus with a dorsal foramen and astragalar canal (or a notch) and a shallower navicular facet than in early perissodactyls. Derived traits that link *Cambaytherium* with Perissodactyla include features of the skull (transverse nasofrontal suture), mandible (fused symphysis, expanded angle), dentition (twinned lower molar metaconids), tarsus (alternating, with contact between astragalus and both navicular and cuboid; astragalus with deep trochlea and saddle-shaped navicular contact), and metatarsus (mesaxonic with similar articular surfaces including a facet on Mt III for Mt 1). These diagnostic perissodactyl traits demonstrate conclusively that *Cambaytherium* is closer to Perissodactyla than to any other extant clade, and they could be cited in a stem-based definition to place cambaytheres as the most basal members of Perissodactyla. The phylogenetic position, whether considered basal perissodactyls or the sister taxon of Perissodactyla, is topologically identical. However, the phylogenetic analysis presented here, more comprehensive than the one we published in 2014, now demonstrates that cambaytheriids form a clade with anthracobunids, a clade that lies outside all other perissodactyls and is their sister taxon. This phylogenetic position is supported by a suite of anatomical features more plesiomorphic than in any known perissodactyl (Table 17), which argues for separation of Anthracobunia from Perissodactyla. It is possible that the prominence of the conules and the tendency toward accessory cusps, especially multiple hypoconulids on m3, are autapomorphous for Anthracobunia.

The polarity of bunodonty versus lophodonty in perissodactyl evolution has been a topic of debate. Although it was long assumed that the stem perissodactyl must have been bunodont, discoveries of very ancient perissodactyls from near the base of the radiation led to the hypothesis that the most primitive perissodactyls more likely were lophodont (Hooker, 1984; Ting, 1993). But *Cambaytherium* revives the debate: its long list of plesiomorphic traits, coupled with bunodont, nonlophodont cheek teeth, strongly suggests that bunodonty was the primitive state for perissodactylamorphs.

The probable phylogenetic relationship between condylarth antecedents and Perissodactyla does not, however, mean that *Cambaytherium* itself was ancestral to any perissodactyl. At present, the only close phylogenetic link seems to be with anthracobunids. The age of *Cambaytherium*—early Eocene but younger than the demonstrably oldest perissodactyls on Laurasian continents (Gingerich, 1989; Hooker, 2010; Hooker and Collinson, 2012; Rose et al., 2012, 2014b; Bai et al., 2018)—eliminates it from direct ancestry. Nevertheless, as the earliest anthracobunian and the most primitive known perissodactylamorph, it provides the best current anatomical model for the last common ancestor of Perissodactyla.

Paleobiogeographic Implications

Although the vertebrate assemblage of the Cambay Shale Formation represents a mixed fauna of Laurasian and Gondwanan affinities, it is mainly composed of taxa with European affinities and, to a lesser degree, North American affinities (Figs. 86, 87; see Smith et al., 2016, for an overview). Taxa with European affinities include at least pelobatid frogs (Folie et al., 2013), russellophiid snakes (Rage et al., 2008), vastanavid psittaciform birds (Mayr et al., 2013), hassianycterid, icaronycterid, and archaeonycterid bats (Smith et al., 2007), ailuravine rodents (Rana et al., 2008), esthonychine tillodonts (Rose et al., 2009a, 2013; Smith et al., 2016), adapoid primates (Rose et al., 2007, 2009b), and diacodexeid artiodactyls (Kumar et al., 2010). The two latter groups are especially interesting because they constitute two of the three 'modern' orders (the other being Perissodactyla) that make their first appearance across Laurasia at the beginning of the Eocene (e.g., Gingerich, 2010). Cambay Shale primates
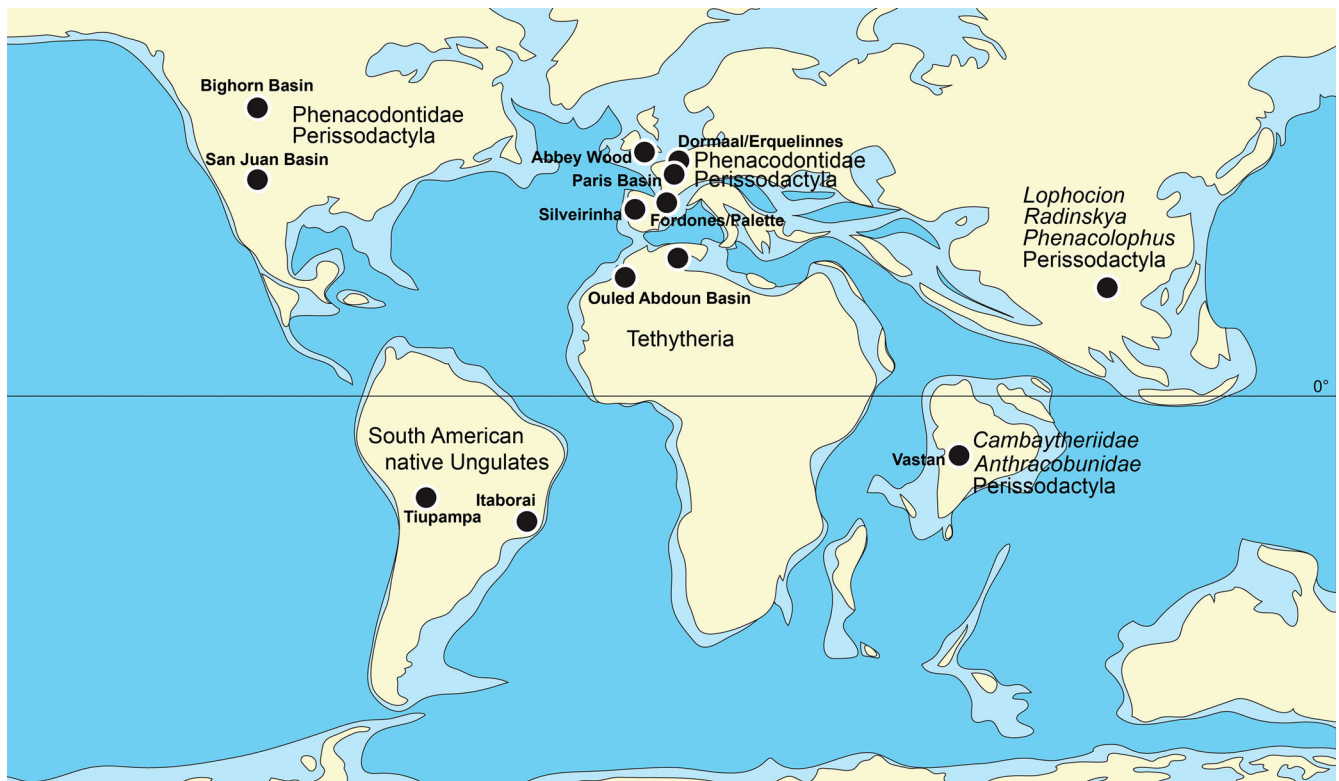
FIGURE 86. Late Paleocene–early Eocene map showing distribution of cambaytheres and their possible relatives. Modified after Scotese (2006) and Smith et al. (2012).

such as *Marcgodinotius indicus* are seemingly as primitive as the most primitive known euprimates (*Donrussellia*, *Teilhardina*), whereas *Diacodexis indicus* and *D. parvus* from Vastan (as well as *D. pakistanensis* from northern Pakistan) are as primitive as *Diacodexis* species known from the very early Eocene in North America and Europe. Taxa with Gondwanan affinities include a giant madtsoid snake, a turtle of the Pelomedusoides group, and a dyrosaurid crocodyliform (Smith et al., 2016), but no mammals. Taxa with Asian ties are few, the most significant being one of the oldest known lagomorphs (Rose et al., 2008). Only a few Indian taxa discovered are considered endemic to the Indian subcontinent, among which the most remarkable are *Cambaytherium* and *Pahelia mysteriosa* (Rose et al., 2014b; Zack et al., 2019).

Perissodactyla, like Artiodactyla and Primates, appeared almost simultaneously in Europe, Asia, and North America at the beginning of the Eocene, ca. 56 Ma, with no clear source area. Recent discoveries have expanded the Asian record of early perissodactyls to the Indian subcontinent (Missiaen et al., 2011a; Missiaen and Gingerich, 2012, 2014), but the oldest Indian perissodactyl fossils are those from the Cambay Shale Formation (Kapur and Bajpai, 2015; Smith et al., 2015), which are younger than those from the northern continents by about a million years. Early perissodactyls or obvious close relatives are absent from Africa and South America. On the northern continents, perissodactyls appear suddenly, just after the beginning of the PETM (e.g., Gingerich, 1989; Bowen et al., 2002; Rose et al., 2012; Missiaen et al., 2013; Bronnert et al., 2017). Bai et al. (2018) recently argued that all four earliest perissodactyl lineages (equids, brontotheres, chalicotheres, and ceratomorphs) were already present in the earliest Eocene of China and thereby suggested that all diverged near the Paleocene–Eocene boundary, the last three originating in non-Indian Asia. This proposal,

however, was based not on new discoveries but on reinterpretation of fragmentary fossils previously allocated to two species: the basal ceratomorph *Orientolophus hengdongensis* and the early equoid '*Propachynolophus*' *hengyangensis*. The fossils in question differ in only minor ways, and these taxonomic reassignments are debatable.

Hooker (2015) postulated that the PE I biozone (Hooker, 1996), which contains the oldest European perissodactyls, actually predates the PETM; hence, he regarded these perissodactyls to be of latest Paleocene age. He related their dispersal (presumably from Asia) to lower sea level prior to the carbon isotope excursion and global warming event that define the beginning of the Eocene. If correct, this would be consistent with the apparent high perissodactyl diversity in the earliest Eocene of Asia. However, although Hooker (2015) has demonstrated that PE I faunas are older than PE II faunas, a latest Paleocene age for PE I localities remains to be corroborated by independent dating methods.

Consequently, the place of origin of Perissodactyla has long been disputed, with various authors postulating the origin of the order in North America, Central America, Africa, India, or Asia, often with little or no fossil evidence. In the case of North America and Asia, however, this has been based on potential perissodactyl relatives. The condylarth family Phenacodontidae, abundant in the Paleocene and early Eocene of North America, has often been associated with perissodactyl origins (Radinsky, 1966, 1969; Hooker, 1994), and *Radinskya yupingae* from the Paleocene of China has been considered to be a possible early sister taxon to Perissodactyla (McKenna et al., 1989; Holbrook, 2014). But recent phylogenetic analyses have failed to provide strong support for close affinities between perissodactyls and either phenacodontids or *Radinskya* (Kondrashov and Lucas, 2012; Holbrook, 2014), with the exception that Cooper et al.
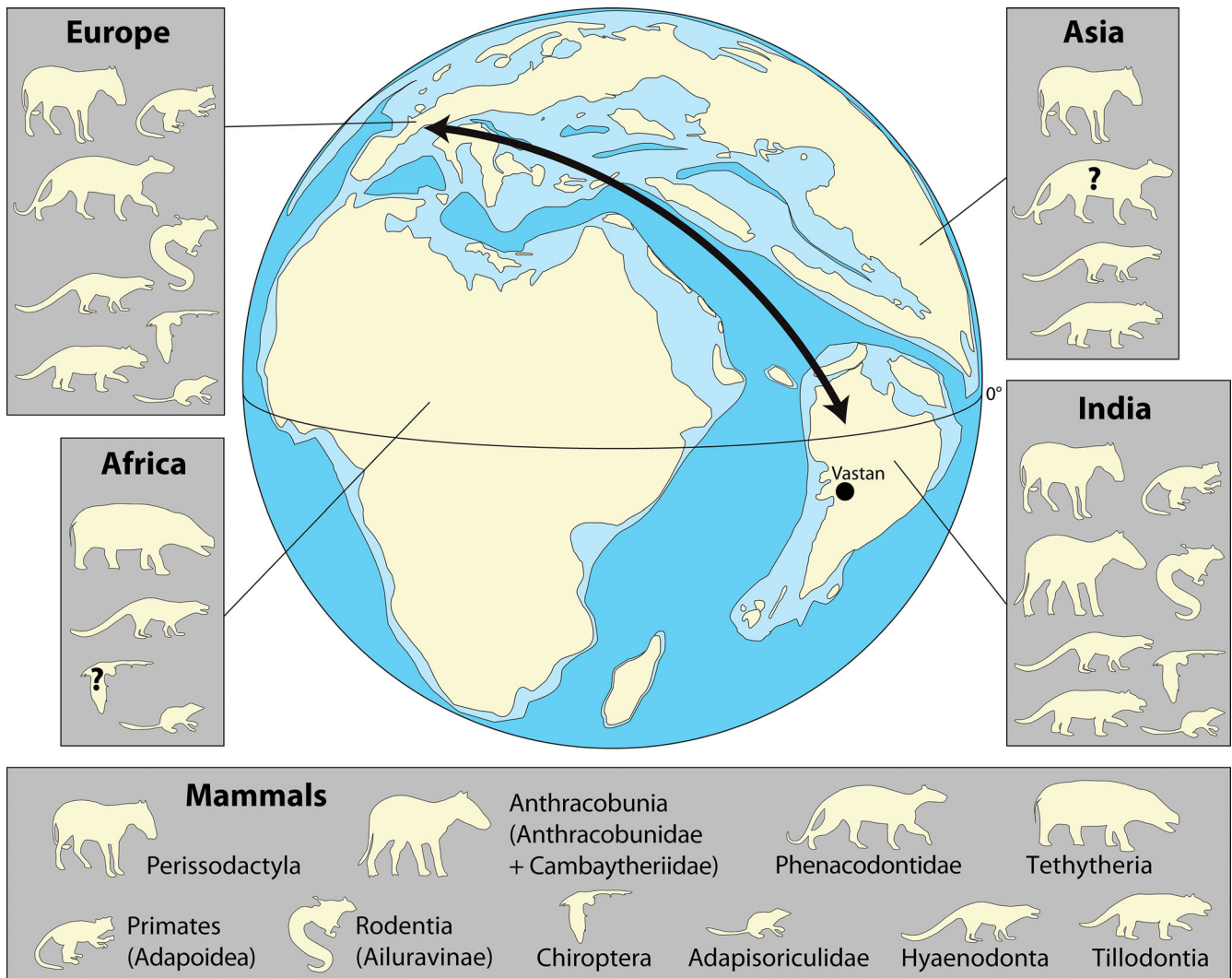
FIGURE 87. Paleogeographic reconstruction showing position of Vastan Mine in the early Eocene, and possible migration route of *Cambaytherium* and its associated mammalian fauna. Modified after Smith et al. (2016).

(2014) recovered *Phenacodus* and *Meniscotherium* as part of several 'stem Perissodactyla' closer to perissodactyls than to any other extant order. Results of both the unconstrained and constrained analyses presented herein place *Radinskya* closer to Perissodactyla than to any other extant order, but not as the sister taxon of Perissodactyla. Our results also place phenacodontids outside the clade that includes perissodactyls, artiodactyls, and afrotheres, or else closer to afrotheres than to perissodactyls. Thus, the case for an Asian rather than a North American origin of Perissodactyla is somewhat stronger.

The proposal that anthracobunids were early tethytheres, specifically proboscideans (e.g., West, 1980; Wells and Gingerich, 1983; Domning et al., 1986; Gingerich et al., 1990; Kumar, 1991; Fischer and Tassy, 1993), presented a biogeographic problem, because the earliest proboscideans and sirenians were known from Africa and the Caribbean, whereas anthracobunids, like cambaytheres, are known exclusively from Indo-Pakistan. A close relationship between anthracobunids and perissodactyls (as well as cambaytheres) to the exclusion of tethytheres remedies this problem.

Hooker (2005) summarized various proposals for the geographic origin of perissodactyls. Below we provide a brief

review of these hypotheses, updated for new findings including those of this study, as a convenient framework for reevaluating the source area of Perissodactyla.

Central and North America—The early appearance of perissodactyls in North America (Gingerich, 1989; Rose et al., 2012) and the historical association of perissodactyls with North American phenacodontids (Cope, 1884; Radinsky, 1966, 1969) long suggested a North American origin before early perissodactyls were better known from other Holarctic faunas. Because perissodactyls appear suddenly at the beginning of the Eocene, Sloan (1969) and Gingerich (1976) suggested that perissodactyls originated in Central America in the late Paleocene, and their sudden appearance is due to migration northward during or after what is now called the PETM. As noted above, the oldest North American perissodactyls are now known to date from the beginning of the PETM (Rose et al., 2012), but no plausible immediate perissodactyl predecessor has been found in the Paleocene of North America. Perhaps the clearest biogeographic conclusion that comes from the present study is that a Central or North American origin is unlikely. The sister-taxon relationship of cambaytheres and perissodactyls effectively places perissodactyl origins in the Eastern Hemisphere.

Asia Exclusive of India—Hooker and Dashzeveg (2003) and Hooker (2005) considered an origin for perissodactyls in non-Indian Asia to be the best supported hypothesis. They based this largely on a close relationship between perissodactyls and the putative Asian phenacodontid *Lophocion*, as well as the presence and phylogenetic position of early Eocene perissodactyls in Asia, particularly *Danjiangia* and *Orientolophus*. Beard (1998) came to a similar conclusion, based mainly on the supposed perissodactyl affinities of *Radinskya* and the report of *Lambdotherium*-like fossils—now considered to belong to *Olbitherium* (Tong et al., 2004), a possible perissodactyl or perissodactyl-like taxon—from Bayan Ulan, which was interpreted by Meng et al. (1998) as late Paleocene in age. Although he came to the same conclusion regarding perissodactyl origins, Hooker (2005) rejected close perissodactyl affinities for *Radinskya* and questioned the reliability of the stratigraphic information on the Bayan Ulan perissodactyls.

Hooker and Dashzeveg (2003) further speculated that equoids evolved in Europe in the latest Paleocene (see also Hooker, 2015; Bai et al., 2018), following dispersal of a basal perissodactyl from Asia across the Turgai Straits during an episode of lower sea level (Iakovleva et al., 2001). Their hypothesis included "dispersal to the Indian subcontinent sometime in the early Eocene" (Hooker and Dashzeveg, 2003:491).

Subsequent studies raised questions regarding the evidence used to support perissodactyl origins in non-Indian Asia. The position of *Radinskya* relative to perissodactyls is still equivocal, despite the fact that it does display some derived features of perissodactyls (Holbrook, 2014; Rose et al., 2014b). In our unconstrained phylogenetic analysis, *Radinskya* allies with Anthracobunia, which would support an Asian origin for Perissodactylamorpha, but in the constrained analysis the position of *Radinskya* as sister taxon to Perissodactylamorpha is more ambiguous. *Olbitherium* is now considered to be of early Eocene age (Tong et al., 2004), and it and other early Eocene Asian taxa seem to indicate the same pattern of sudden appearance observed in North America. The position of *Lophocion*, known only from three upper molars, is also uncertain and does not show any clear affinity with perissodactyls (Holbrook, 2014).

As mentioned above, Bai et al. (2018) recently reinterpreted some specimens previously attributed to the tapiromorph *Orientolophus* as a new basal equid, and others assigned to the equoid '*Propachynolophus*' *hengyangensis* as a chalicothere and a brontothere, thus arguing that a diversity of perissodactyls was already present in China at the beginning of the Eocene and that the divergence of these groups occurred in Asia around the PETM. If correct, this could be seen as support for the timing of Hooker and Dashzeveg's (2003) dispersal scenario to Europe, as well as additional evidence that Asia was the geographic center of origin for the order. But it does not demonstrate that the origin was in *central* Asia. Bowen et al. (2002:2064) highlighted this uncertainty: "Perissodactyls, documented in the upper Lingcha fauna, were present in Asia at the P/E boundary, and their Asian first appearance is at least synchronous with their appearance in North America. This result does not offer direct support for the hypothesized Asian origin of this group, but neither does it falsify the hypothesis."

Notably, the hypotheses of Hooker and Dashzeveg (2003), Hooker (2005), Beard (1998), and Bai et al. (2018) were based on the presence of early perissodactyls in Asia that exhibit varying degrees of lophodonty. But the evidence we present in this report suggests that the stem perissodactyl was more likely bunodont, like *Cambaytherium*.

Restriction of Anthracobunia, the sister taxon of perissodactyls, to the Indian Plate does not preclude perissodactyl origins in non-Indian Asia, but it does render this scenario less likely. It could imply that the common ancestor of perissodactyls and anthracobunians lived on or adjacent to the Indian Plate, or in both areas, prior to its collision with Asia. Perissodactyls might then have evolved either in India or in southern or southwestern non-Indian Asia during the Paleocene and shortly thereafter dispersed to other parts of the Eurasian landmass and to Indo-Pakistan in the form of perissodactyls known from the Cambay Shale and Ghazij faunas. This scenario remains speculative, however, because of the lack of a fossil record from peripheral areas of southern and southwestern Asia that could test this hypothesis.

Africa—Previous proposals for an African origin (Gingerich, 1986, 1989; Franzen, 1989) were based on arguments for a close relationship between perissodactyls and hyracoids (Fischer, 1986, 1989; Fischer and Tassy, 1993). This relationship has found no support from molecular data (Murphy et al., 2001; Meredith et al., 2011), and early African 'ungulates' have more recently been allied with Afrotheria (Gheerbrant et al., 2005b, 2016). It is possible, though, that the ancestors of perissodactyls and anthracobunians reached India from Afro-Arabia, which would further explain the European affinities of other elements of the Cambay Shale fauna (Rana et al., 2008; Rose et al., 2009a, 2009b; Kumar et al., 2010; Smith et al., 2016). However, no perissodactyl-like forms have yet been found in the Paleogene of Africa or the Arabian Peninsula.

India (and Other Gondwanan Areas)—Because anthracobunians appear to have been restricted to the Indian Plate, we hypothesize that the earliest perissodactylamorphs either evolved in India or reached the subcontinent from nearby areas of southern or southwestern Asia in the Paleocene. In the latter case, dispersal to India could have occurred across the Tethyan seaway (by 'sweepstakes routes'; Simpson, 1940); but because much of the mammalian fauna has European ties, such a mechanism presumably would have required multiple independent dispersal events across a water barrier (direction uncertain), lowering the probability of this scenario. More likely, dispersal took place across ephemeral land connections between southwest Asia (including Arabia or island arcs) and western India. Exactly where these bridges were or when dispersal took place is unknown, but various possibilities have been proposed (e.g., Ali and Aitchison, 2008; Clementz et al., 2011; Chatterjee et al., 2017). Some mammalian taxa, including the ancestor of *Cambay therium*, could have immigrated to India during the PETM, but Perissodactylamorpha clearly evolved prior to the Eocene, because unequivocal Perissodactyla are present in North America, Europe, and Asia at the beginning of the PETM.

The timing of the origin of Perissodactyla does not alter the hypothesis presented here, that they probably evolved in or near India. This hypothesis is not based on age of the Indian fossils, which are almost certainly younger than the oldest perissodactyls known from northern continents; rather, it is based on the phylogenetic position and stage of evolution of cambaytheres. The first arrival of unequivocal perissodactyls across the Laurasian continents near the start of the PETM is evidence that the order originated earlier than the Cambay Shale fossils, most likely in the Paleocene, but exactly where is still a mystery. The fact that *Cambaytherium* is more plesiomorphic than any known perissodactyl, yet probably at least a million years younger than the oldest perissodactyls known from basal Eocene strata of western North America, Europe, or Asia, strongly suggests that it is a relict of a lineage that originated much earlier, which had changed little from the common ancestor of anthracobunians and perissodactyls.

Krause and Maas (1990) proposed that India might have harbored ancestors of several mammalian orders, including perissodactyls, which spread into Asia and other Holarctic continents after India's contact with the rest of Asia. The presence of perissodactylamorphs in the early Eocene of the Indian subcontinent provides some of the first possible support for the Krause and Maas (1990) hypothesis. This hypothesis would further predict

the presence of perissodactylamorphs (or panperissodactylans) in the Paleocene fossil record of India, which is as yet unknown. In addition to *Cambaytherium*, the occurrence of the basal tapiroids *Vastanolophus* and *Cambaylophus* in the Cambay Shale Formation attests to the early presence of true perissodactyls on the Indian subcontinent. In view of the clear relationship of cambaytheres to other placental mammals, it is highly probable that cambaytheres or a perissodactylamorph ancestor reached India after its separation from Madagascar, and during its northward drift.

The timing of India's collision with Asia has obvious importance for the dispersal of *Cambaytherium* or its ancestor, as well as other animals including perissodactyls, to and from India. Chatterjee et al. (2017) estimated that the initial collision with Asia began ca. 55 Ma, coincident with the PETM, but they acknowledged that the timing of the collision "remains highly controversial" (p. 77). In fact, they previously suggested that the collision began somewhat later, ca. 50 Ma (Chatterjee et al., 2013), which was in accord with the estimate of Meng et al. (2012) based on paleomagnetic data from Tibet. However, several more recent works date the initial collision earlier, at ca. 55 Ma, based on geochronological and geochemical data on magmatic activity (Zhu et al., 2015) and detrital zircon U-Pb geochronology (Ding et al., 2016), or even ca. 59 ± 1 Ma, based on a combination of radiolarian and nannofossil biostratigraphy and detrital zircon geochronology (Hu et al., 2015, 2016). The discrepancies partly reflect different definitions of the collision onset (Hu et al., 2016). Furthermore, initial collision was not necessarily coincident with subaerial contact with Asia (which would have promoted faunal exchange), because the Neotethys persisted for some time between India and south Asia, presumably creating a barrier to dispersal. Thus, it is difficult to ascertain whether the Vastan fauna documents the Indian biota prior to, during, or slightly after the initial collision with Asia. Chatterjee et al. (2017) hypothesized that the Vastan fauna reflects faunal exchange with North Africa and Europe (via Spain-Morocco contact) through the Oman/Kohistan/Ladakh arc, which, they propose, would have served as a 'mobile gangplank' for more or less continual dispersal to or from Europe as well as Asia during the Paleocene and early Eocene (direction uncertain).

The possibility of perissodactyl ancestry on the Indian plate is made more intriguing by recent studies of ancient amino acid and mitochondrial DNA sequences obtained from fossils of South American native ungulates (SANUs), specifically a litoptern and a notoungulate (Buckley, 2015; Welker et al., 2015; Westbury et al., 2015). The phylogenetic position of SANUs has been enigmatic. The analysis of O'Leary et al. (2013) placed some SANUs with Afrotheria and others with Laurasiatheria. All the ancient protein and DNA studies have placed the two sampled SANUs closer to perissodactyls than to any other extant taxon. If this is correct, then the split of perissodactylamorphs from SANUs likely occurred before the Paleocene, because SANUs are known from the late Paleocene and possibly from a specimen from the early Paleocene Tiupampa fauna of Bolivia (Muizon and Cifelli, 2000). Such a relationship poses a substantial biogeographic problem, however, because SANUs are unknown outside South America in the Paleogene (during most of which South America was isolated) and perissodactyls are not known from South America until late in the Cenozoic. Even if the closest living relatives of SANUs are perissodactyls, it is possible that other archaic ungulates for which we do not have molecular data are even closer to perissodactyls than are SANUs.

CONCLUSIONS

Finding *Cambaytherium* in the lower Eocene of India, dating from near or before the collision with Asia, was unexpected

and sheds new light on the origin of the mammalian order Perissodactyla. Although *Cambaytherium* was initially interpreted as a bunodont perissodactyl, now that most of its anatomy is known it proves to be far more interesting. The anatomy of *Cambaytherium* is a mosaic of derived features that typify perissodactyls, superimposed on plesiomorphic traits characteristic of archaic ungulates such as phenacodontids. This description applies to the dentition and nearly every postcranial skeletal element. Indeed, many elements exhibit an amalgam of phenacodontid-like and perissodactyl features or have features that are more or less intermediate in morphology between those of phenacodontids or other condylarths and basal perissodactyls. Taken together, these features reflect a subcursorial animal whose modifications for running are more derived than those of phenacodontids but less specialized than those of early perissodactyls. Overall, the perissodactyl imprint on the anatomy is stronger (e.g., fused mandibular symphysis, twinned metaconids on lower molars, m3 with extended third lobe, alternating tarsus with astragalus with concave navicular facet and narrow cuboid facet) and at first glance might appear to place *Cambaytherium* as a primitive, bunodont perissodactyl. But in other ways the skeleton differs from those of all known perissodactyls in retaining plesiomorphic traits: more robust limb elements and more generalized proportions, a long humeral deltopectoral crest, a distal humeral articulation lacking the lateral articular shelf, short antebrachium, probably pentadactyl manus and pes, short and robust metapodials, and relatively short and wide tarsus with a wide astragalar trochlea and retained astragalar foramen. Bunodonty is probably plesiomorphic as well. Whereas some of these features might be interpreted as secondary generalizations, most of them would have required highly unlikely reversals from even the most plesiomorphic state in basal Perissodactyla; therefore, they attest to the primitive state of *Cambaytherium*. Large upper molar conules and a tendency toward accessory cuspules, especially on third molars, could be autapomorphic traits. This combination indicates that *Cambaytherium* is more closely related to perissodactyls than to other major clades, but that it remains just outside that clade. The dental and gnathic evidence also demonstrates a sister-group relationship between cambaytheriids and anthracobunids, thus supporting the clade Anthracobunia. We recognize this plesiomorphic clade as sister to conventional crown group Perissodactyla and unite the two in a new superordinal clade Perissodactylamorpha.

Three species of *Cambaytherium* have been found in the Cambay Shale Formation. They differ significantly in size: small (*C. gracilis*), medium-sized (*C. thewissi*), and large (*C. marinus*). Most specimens are referable to *C. thewissi*. The sample of *C. thewissi* exhibits considerable variation in size and dental morphology, sometimes even on opposite sides of the same individual; however, the very restricted temporal and spatial distribution of most of the sample supports assignment of these specimens to a single species, *C. thewissi*. Several lines of evidence point to the possibility of sexual dimorphism in *Cambaytherium*, although it remains inconclusive.

As the most primitive perissodactylamorphs, cambaytheres offer insight on the morphology of the perissodactyl ancestor. In particular, they suggest that the common ancestor of perissodactyls and anthracobunians had bunodont cheek teeth, rather than lophodont molars as has been hypothesized in recent years (Hooker, 1989; Ting, 1993). In addition, *Cambaytherium* suggests that the hind limb may have modified toward cursoriality prior to the forelimb and that the astragalus, in particular, achieved its diagnostic saddle-shaped navicular facet prior to other tarsal specializations. The perissodactylamorph ancestor was also apparently pentadactyl, and its first metatarsal had already rotated posteriorly to articulate with Mt III, as in extant *Tapirus*.

The presence of such a primitive form as *Cambaytherium* in the lower Eocene of India requires reconsideration of the place of

origin and initial radiation of Perissodactyla. It suggests that the stem perissodactyl was not a lophodont form from central Asia but more likely was a bunodont taxon that inhabited southern or southwestern Asia. Such a form might have reached India, giving rise to *Cambaytherium* and to earliest perissodactyls, which then dispersed to the Laurasian landmass near the start of the PETM or just before. Dispersal to Europe might have occurred to the west via the Oman/Kohistan/Ladakh arc (or similar land bridges), or to southwestern Asia via island arcs or sweepstakes routes across the narrowing Neotethys. Basal perissodactyls in southwest Asia would have been positioned to disperse to Europe across the Turgai Straits during low sea level stand around the PETM, as hypothesized by Hooker (2015).

The occurrence of *Cambaytherium* on India at a time (~54.5 Ma) near or perhaps prior to its collision with Asia indicates that India and nearby parts of southwest Asia played a significant role in the origin and/or early diversification of perissodactyls. This supports, in part, Krause and Maas's (1990) hypothesis that Perissodactyla might have originated on the Indian Plate during its northward drift. It now seems highly improbable, however, that perissodactyl ancestral stock reached India before it separated from Madagascar in the Late Cretaceous. In view of its probable derivation from Laurasian condylarths, it is much more likely that *Cambaytherium* or its ancestor reached India during the Paleocene or earliest Eocene, but whether it came from Africa, Arabia, or southern or southwest Asia, and by what route, remains uncertain. The direction of dispersal, and the number of dispersal events involving perissodactyla-morphs, is also unknown. What *is* known is that once Perissodactyla diverged, dispersal across Laurasia was abrupt and rapid at the onset of the PETM, taking place in a matter of thousands to a few tens of thousands of years at most (e.g., Smith et al., 2006). This situation has complicated efforts to pinpoint the geographic center of origin of Perissodactyla.

Any of the scenarios just mentioned would require that close relatives of cambaytheres also occurred in the source area (probably south or southwestern Asia), but as yet no such fossils are known from those areas. If paleogeographic models suggesting that central India was near or south of the equator at the time of *Cambaytherium* (e.g., Clementz et al., 2011) are accurate, then it seems increasingly likely that cambaythere forebears reached India from Afro-Arabia or southwest Asia during brief episodes of land contact during the Paleocene. Moreover, the restriction of Anthracobunia to the Indian subcontinent also implies that *Cambaytherium* or its ancestor evolved on India or was present in adjacent areas and that Perissodactyla also evolved in this region.

ORCID

Kenneth D. Rose ⓘ http://orcid.org/0000-0003-0326-9171
Luke T. Holbrook ⓘ http://orcid.org/0000-0001-5179-3053
Kishor Kumar ⓘ http://orcid.org/0000-0003-0875-9735
Rajendra S. Rana ⓘ http://orcid.org/0000-0002-2366-1181
Rachel H. Dunn ⓘ http://orcid.org/0000-0002-1647-2796
Katrina E. Jones ⓘ http://orcid.org/0000-0003-1088-0497
Thierry Smith ⓘ http://orcid.org/0000-0002-1795-2564

LITERATURE CITED

Adatte, K. H., H. Khozyem, J. E. Spangenberg, B. Samant, and G. Keller. 2014. Response of terrestrial environment to the Paleocene-Eocene Thermal Maximum (PETM), new insights from India and NE Spain. Rendiconti Online della Società Geologica Italiana 31:5–6.

Ali, J. R., and J. C. Aitchison. 2008. Gondwana to Asia: plate tectonics, paleogeography, and the biological connectivity of the Indian subcontinent from the Middle Jurassic through the latest Eocene (165–35 Ma). Earth-Science Reviews 88:145–166.

Alimohammadian, H., A. Sahni, R. Patnaik, R. S. Rana, and H. Singh. 2005. First record of an exceptionally diverse and well preserved amber-embedded biota from Lower Eocene (~52 Ma) lignites, Vastan, Gujarat. Current Science 89:1328–1330.

Argot, C. 2012. Postcranial analysis of a carnivoran-like archaic ungulate: the case of *Arctocyon primaevus* (Arctocyonidae, Mammalia) from the Late Paleocene of France. Journal of Mammalian Evolution 20:83–114.

Asher, R. J., M. J. Novacek, and J. H. Geisler. 2003. Relationships of endemic African mammals and their fossil relatives based on morphological and molecular evidence. Journal of Mammalian Evolution 10:131–194.

Bai, B., Y.-Q. Wang, and J. Meng. 2010. New craniodental materials of *Litolophus gobiensis* (Perissodactyla, "Eomoropidae") from Inner Mongolia, China and phylogenetic analysis of Eocene chalicotheres. American Museum Novitates 3688:1–27.

Bai, B., Y.-Q. Wang, and J. Meng. 2018. The divergence and dispersal of early perissodactyls as evidenced by early Eocene equids from Asia. Communications Biology 115:1–10.

Bai, B., J. Meng, Y.-Q. Wang, H.-B. Wang, and L. Holbrook. 2017. Osteology of the middle Eocene ceratomorph *Hyrachyus modestus* (Mammalia, Perissodactyla). Bulletin of the American Museum of Natural History 413:1–68.

Bajpai, S., and J. J. Head. 2007. An early Eocene palaeopheid snake from Vastan lignite mine, Gujarat, India. Gondwana Geological Magazine 22(2):85–90.

Bajpai, S., and V. V. Kapur. 2004. Oldest known gobiids from Vastan Lignite Mine (early Eocene), District Surat, Gujarat. Current Science 87:433–435.

Bajpai, S., and V. V. Kapur. 2008. Earliest Cenozoic frogs from the Indian subcontinent: implications for out-of-India hypothesis. Journal of the Palaeontological Society of India 53:65–71.

Bajpai, S., V. V. Kapur, and J. G. M. Thewissen. 2009. Creodont and condylarth from the Cambay Shale (early Eocene, ~55–54 ma), Vastan Lignite Mine, Gujarat, western India. Journal of the Palaeontological Society of India 54:103–109.

Bajpai, S., D. P. Das, V. V. Kapur, B. N. Tiwari, and S. S. Srivastava. 2007. Early Eocene rodents (Mammalia) from Vastan Lignite Mine, Gujarat, western India. Gondwana Geological Magazine 22(2):91–95.

Bajpai, S., V. V. Kapur, J. G. M. Thewissen, D. P. Das, and B. N. Tiwari. 2006. New Early Eocene cambaythere (Perissodactyla, Mammalia) from the Vastan Lignite Mine (Gujarat, India) and an evaluation of cambaythere relationships. Journal of the Palaeontological Society of India 51:101–110.

Bajpai, S., V. V. Kapur, J. G. M. Thewissen, B. N. Tiwari, and D. P. Das. 2005a. First fossil marsupials from India: early Eocene *Indodelphis* n. gen. and *Jaegeria* n. gen. from Vastan Lignite Mine, District Surat, Gujarat. Journal of the Palaeontological Society of India 50:147–151.

Bajpai, S., V. V. Kapur, D. P. Das, B. N. Tiwari, N. Saravanan, and R. Sharma. 2005b. Early Eocene land mammals from Vastan Lignite Mine, District Surat (Gujarat), western India. Journal of the Palaeontological Society of India 50:101–113.

Bajpai, S., R. F. Kay, B. A. Williams, D. P. Das, V. V. Kapur, and B. N. Tiwari. 2008. The oldest Asian record of Anthropoidea. Proceedings of the National Academy of Sciences of the United States of America 105:11093–11098.

Bajpai, S., V. V. Kapur, J. G. M. Thewissen, D. P. Das, B. N. Tiwari, R. Sharma, and N. Saravanan. 2005c. Early Eocene primates from Vastan Lignite Mine, Gujarat, western India. Journal of the Palaeontological Society of India 50:43–54.

Beard, K. C. 1993. Phylogenetic systematics of the Primatomorpha, with special reference to Dermoptera; pp. 129–150 in F. S. Szalay, M. J. Novacek, and M. C. McKenna (eds.), Mammal Phylogeny—Placentals. Springer, New York.

Beard, K. C. 1998. East of Eden: Asia as an important center of taxonomic origination in mammalian evolution; pp. 5–39 in K. C. Beard and M. R. Dawson (eds.), Dawn of the Age of Mammals in Asia. Bulletin of Carnegie Museum of Natural History 34. Pittsburgh, Pennsylvania.

Bemis, K. E., J. C. Tyler, W. E. Bemis, K. Kumar, R. S. Rana, and T. Smith. 2017. A gymnodont fish jaw with remarkable molariform teeth from the early Eocene of Gujarat, India (Teleostei, Tetraodontiformes). Journal of Vertebrate Paleontology 37:e1369422.

Bertram, J. E. A., and A. Gutmann. 2009. Motions of the running horse and cheetah revisited: fundamental mechanics of the transverse and rotary gallop. Journal of the Royal Society Interface 6:549–559.

Biswas, S. K. 1987. Regional tectonic framework, structure and evolution of the western marginal basins of India. Tectonophysics 135:307–327.

Boszczyk, B. M., A. A. Boszczyk, and R. Putz. 2001. Comparative and functional anatomy of the mammalian lumbar spine. Anatomical Record 264:157–168.

Bowen, G. J., W. C. Clyde, P. L. Koch, S. Ting, J. Alroy, T. Tsubamoto, Y.-Q. Wang, and Y. Wang. 2002. Mammalian dispersal at the Paleocene/Eocene boundary. Science 295:2062–2065.

Bronnert, C., E. Gheerbrant, M. Godinot, and G. Métais. 2018. A primitive perissodactyl (Mammalia) from the early Eocene of Le Quesnoy (MP7, France). Historical Biology 30:237–250.

Buckley, M. 2015. Ancient collagen reveals evolutionary history of the endemic South American 'ungulates.' Proceedings of the Royal Society B: Biological Sciences 282:20142671.

Butler, P. M. 1956. The skull of *Ictops* and a classification of the Insectivora. Proceedings of the Zoological Society of London 126:453–481.

Campbell, B. 1936. The comparative myology of the forelimb of the hippopotamus, pig and tapir. American Journal of Anatomy 59:201–247.

Chandra, P. K., and L. R. Chowdhary. 1969. Stratigraphy of the Cambay Basin. Bulletin Oil and National Gas Commission (ONGC), Dehradun, India 6:37–50.

Chatterjee, S., A. Goswami, and C. R. Scotese. 2013. The longest voyage: tectonic, magmatic, and paleoclimatic evolution of the Indian plate during its northward flight from Gondwana to Asia. Gondwana Research 23:238–267.

Chatterjee, S., C. R. Scotese, and S. Bajpai. 2017. Indian plate and its epic voyage from Gondwana to Asia: its tectonic, paleoclimatic and paleobiogeographic evolution. Geological Society of America 529:1–147.

Clementz, M., S. Bajpai, V. Ravikant, J. G. M. Thewissen, N. Saravanan, I. B. Singh, and V. Prasad. 2011. Early Eocene warming events and the timing of terrestrial faunal exchange between India and Asia. Geology 39:15–18.

Colbert, M. 2005. The facial skeleton of the early Oligocene *Colodon* (Perissodactyla, Tapiroidea). Palaeontologia Electronica 8(1):12A. Available at https://palaeo-electronica.org/2005_1/colbert12/issue1_05.htm

Coombs, W. P., Jr., and M. C. Coombs. 1979. *Pilgrimella*, a primitive Asiatic perissodactyl. Zoological Journal of the Linnean Society 65:185–192.

Cooper, L. N., E. R. Seiffert, M. Clementz, S. I. Madar, S. Bajpai, S. T. Hussain, and J. G. M. Thewissen. 2014. Anthracobunids from the middle Eocene of India and Pakistan are stem perissodactyls. PLoS ONE 9:e109232.

Cope, E. D. 1884. The Vertebrata of the Tertiary formations of the West. Report of the U.S. Geological Survey of the Territories, Volume 3:1–1009.

Copley, A., J.-P. Avouae, and J.-Y. Royer. 2010. India-Asia collision and the Cenozoic slow down of the Indian plate: implications for the forces driving plate motions. Journal of Geophysical Research 115: B0310. doi: 10.1029/2009JB006634.

Court, N. 1992. The skull of *Arsinoitherium* (Mammalia, Embrithopoda) and the higher order interrelationships of ungulates. Palaeovertebrata 22:1–43.

Damuth, J. 1990. Problems in estimating body masses of archaic ungulates using dental measurements; pp. 229–253 in J. Damuth and B. J. MacFadden (eds.), Body Size in Mammalian Paleobiology: Estimation and Biological Implications. Cambridge University Press, Cambridge, U.K.

Dashzeveg, D., and J. J. Hooker. 1997. New ceratomorph perissodactyls (Mammalia) from the Middle and Late Eocene of Mongolia: their implications for phylogeny and dating. Zoological Journal of the Linnaean Society 120:105–138.

Davis, D. D. 1964. The giant panda. A morphological study of evolutionary mechanisms. Fieldiana Zoology Memoirs 3:1–339.

Dean, C. M. 1987. Growth layers and incremental markings in hard tissues; a review of the literature and some preliminary observations about enamel structure in *Paranthropus boisei*. Journal of Human Evolution 16:157–172.

Dehm, R., and T. Oettingen-Spielberg. 1958. Paläontologische und geologische Untersuchungen in Tertiär von Pakistan. 2. Die mitteleocänen Säugetiere von Ganda Kas bei Basal in Nordwest-Pakistan. Abhandlungen Bayerischen. Akademie der Wissenschaften, Mathematisch-Naturwissenschaftliche Klasse 91:1–54.

Ding, L., M. Qasim, I. A. K. Jadoon, M. A. Khan, Q. Xu, F. Cai, H. Wang, U. Baral, and Y. Yue. 2016. The India-Asia collision in north Pakistan: insight from the U–Pb detrital zircon provenance of Cenozoic foreland basin. Earth and Planetary Science Letters 455:49–61.

Dirks, W., R. L. Anemone, P. A. Holroyd, D. J. Reid, and P. Walton. 2009. Phylogeny, life history and the timing of molar crown formation in two archaic ungulates, *Meniscotherium* and *Phenacodus* (Mammalia, 'Condylarthra'); pp. 3–8 in T. Koppe, G. Meyer, and K. W. Alt (eds.), Comparative Dental Morphology. Karger, Basel, Switzerland.

Domning, D. P., C. E. Ray, and M. C. McKenna. 1986. Two new Oligocene desmostylians and a discussion of tethytherian systematics. Smithsonian Contributions to Paleobiology 59:1–56.

Ducrocq, S., A. N. Soe, B. Bo, M. Benammi, Y. Chaimanee, T. Tun, T. Thein, and J.-J. Jaeger. 2000. First record of an Anthracobunidae (Mammalia, ?Tethytheria) from the Eocene of the Pondaung Formation, Myanmar. Comptes Rendus de l'Académie des Sciences, Paris, Sciences de la Terre et des Planètes 330:725–730.

Dunn, R. H., K. D. Rose, R. S. Rana, K. Kumar, A. Sahni, and T. Smith. 2016. New euprimate postcrania from the early Eocene of Gujarat, India, and the strepsirrhine-haplorhine divergence. Journal of Human Evolution 99:25–51.

Dutta, S., S. M. Tripathi, M. Mallick, R. P. Matthews, P. F. Greenwood, M. R. Rao, and R. E. Summons. 2011. Eocene out-of-India dispersal of Asian dipterocarps. Review of Palaeobotany and Palynology 166:63–68.

Eriksson, T. 2001. AutoDecay ver. 5.0 (program distributed by the author). Bergius Foundation, Royal Swedish Academy of Sciences, Stockholm, Sweden.

Evans, H. E., and G. C. Christensen. 1979. Miller's Anatomy of the Dog, second edition. W. B. Saunders, Philadelphia, Pennsylvania, 1181 pp.

Fischer, M. S. 1986. Die Stellung der Schliefer (Hyracoidea) im phylogenetischen System der Eutheria. Zugleich ein Beitrag zur Anpassungsgeschichte der Procaviidae. Courier Forschungsinstitut Senckenberg 84:1–132.

Fischer, M. S. 1989. Hyracoids, the sister-group of perissodactyls; pp. 37–56 in D. R. Prothero and R. M. Schoch (eds.), The Evolution of Perissodactyls. Oxford University Press, New York.

Fischer, M. S., and P. Tassy. 1993. The interrelation between Proboscidea, Sirenia, Hyracoidea, and Mesaxonia: the morphological evidence; pp. 217–234 in F. S. Szalay, M. J. Novacek, and M. C. McKenna (eds.), Mammal Phylogeny: Placentals. Springer, New York.

Fisher, R. E., K. M. Scott, and V. L. Naples. 2007. Forelimb myology of the pygmy hippopotamus (*Choeropsis liberiensis*). The Anatomical Record 290:673–693.

Fisher, R. E., B. Adrian, M. Barton, J. Holmgren, and S. Y. Tang. 2009. The phylogeny of the red panda (*Ailurus fulgens*): evidence from the forelimb. Journal of Anatomy 215:611–635.

Folie, A., R. S. Rana, K. D. Rose, A. Sahni, K. Kumar, L. Singh, and T. Smith. 2013. Early Eocene frogs from Vastan Lignite Mine, Gujarat, India. Acta Palaeontologica Polonica 58:511–524.

Franzen, J. L. 1989. Origin and systematic position of the Palaeotheriidae; pp. 102–108 in D. R. Prothero and R. M. Schoch (eds.), The Evolution of Perissodactyls. Oxford University Press, New York.

Franzen, J. L. 2007. Eozäne Equoidea (Mammalia, Perissodactyla) aus der Grube Messel bei Darmstadt (Deutschland). Funde der Jahre 1969–2000. Schweizerische Paläontologische Abhandlungen 127:1–245.

Franzen, J. L., and J. Habersetzer. 2017. Complete skeleton of *Eurohippus messelensis* (Mammalia, Perissodactyla, Equoidea) from the early middle Eocene of Grube Messel (Germany). Palaeobiodiversity and Palaeoenvironments 97:807–832.

Frischauf, C., R. Gockert, N. Kavcik-Graumann, and G. Rabeder. 2016. "Kiskevély Knives" indicate the menu of Alpine cave bears: comparative studies on wedge shaped defects of canines and incisors. International Cave Bear Symposium Proceedings 2016:14–17.

Froehlich, D. J. 1999. Phylogenetic systematics of basal perissodactyls. Journal of Vertebrate Paleontology 19:140–159.

Froehlich, D. J. 2002. Quo vadis eohippus? The systematics and taxonomy of the early Eocene equids (Perissodactyla). Zoological Journal of the Linnean Society 134:141–256.

Garg, R., K. Ateequzzaman, V. Prasad, S. K. M. Tripathi, I. B. Singh, A. K. Jauhri, and S. Bajpai. 2008. Age-diagnostic dinoflagellate cysts from lignite-bearing sediments of the Vastan lignite mine, Surat District, Gujarat, western India. Journal of the Palaeontological Society of India 53:99–105.

Gazin, C. L. 1953. The Tillodontia: an early Tertiary order of mammals. Smithsonian Miscellaneous Collections 121(10):1–110.

Gazin, C. L. 1965. A study of the early Tertiary condylarthran mammal *Meniscotherium*. Smithsonian Miscellaneous Collections 149(2):1–98.

Getty, R. 1975. Sisson and Grossman's The Anatomy of the Domestic Animals. W. B. Saunders, Philadelphia, Pennsylvania, 2,130 pp.

Gheerbrant, E. 2009. Paleocene emergence of elephant relatives and the rapid radiation of African ungulates. Proceedings of the National Academy of Sciences of the United States of America 106:10717–10721.

Gheerbrant, E., B. Bouya, and M. Amaghzaz. 2012. Dental and cranial anatomy of *Eritherium azzouzorum* from the Paleocene of Morocco, earliest known proboscidean mammal. Palaeontographica, Abteilung A: Paläozoologie–Stratigraphie 297:151–183.

Gheerbrant, E., D. P. Domning, and P. Tassy. 2005b. Paenungulata (Sirenia, Proboscidea, Hyracoidea, and relatives); pp. 84–105 in K. D. Rose and J. D. Archibald (eds.), The Rise of Placental Mammals: Origins and Relationships of the Major Extant Clades. Johns Hopkins University Press, Baltimore, Maryland.

Gheerbrant, E., A. Filippo, and A. Schmitt. 2016. Convergence of afrotherian and laurasiatherian ungulate-like mammals: first morphological evidence from the Paleocene of Morocco. PLoS ONE 11:e0157556.

Gheerbrant E., J. Sudre, and H. Cappetta. 1996. A Palaeocene proboscidean from Morocco. Nature 383:68–71.

Gheerbrant, E., J. Sudre, P. Tassy, M. Amaghzaz, B. Bouya, and M. Iarochène. 2005a. Nouvelles données sur *Phosphatherium escuilliei* (Mammalia, Proboscidea) de l'Éocène inférieur du Maroc, apports à la phylogénie des Proboscidea et des ongulés lophodontes. Geodiversitas 27:239–333.

Gingerich, P. D. 1974. Size variability of the teeth in living mammals and the diagnosis of closely related sympatric fossil species. Journal of Paleontology 48:895–903.

Gingerich, P. D. 1976. Cranial anatomy and evolution of early Tertiary Plesiadapidae (Mammalia, Primates). University of Michigan Papers on Paleontology 15:1–141.

Gingerich, P. D. 1977. A small collection of fossil vertebrates from the middle Eocene Kuldana and Kohat formations of Punjab (Pakistan). Contributions from the Museum of Paleontology, The University of Michigan 24:190–203.

Gingerich, P. D. 1986. Early Eocene *Cantius torresi*—oldest primate of modern aspect from North America. Nature 320:319–321.

Gingerich, P. D. 1989. New earliest Wasatchian mammalian fauna from the Eocene of northwestern Wyoming: composition and diversity in a rarely sampled high-floodplain assemblage. University of Michigan Papers on Paleontology 28:1–97.

Gingerich, P. D. 1991. Systematics and evolution of early Eocene Perissodactyla (Mammalia) in the Clarks Fork Basin, Wyoming. Contributions from the Museum of Paleontology, The University of Michigan 28:181–213.

Gingerich, P. D. 2006. Environment and evolution through the Paleocene-Eocene thermal maximum. Trends in Ecology and Evolution 21:246–253.

Gingerich, P. D. 2010. Mammalian faunal succession through the Paleocene-Eocene Thermal Maximum (PETM) in western North America. Vertebrata PalAsiatica 48:308–327.

Gingerich, P. D., S. G. Abbas, and M. Arif. 1997. Early Eocene *Quettacyon parachai* (Condylarthra) from the Ghazij Formation of Baluchistan (Pakistan): oldest Cenozoic land mammal from South Asia. Journal of Vertebrate Paleontology 17:629–637.

Gingerich, P. D., D. E. Russell, and N. A. Wells. 1990. Astragalus of *Anthracobune* (Mammalia, Proboscidea) from the early–middle Eocene of Kashmir. Contributions from the Museum of Paleontology, The University of Michigan 28:71–77.

Gingerich, P. D., M. Arif, I. H. Khan, and S. G. Abbas. 1998. First early Eocene land mammals from the upper Ghazij Formation of the Sor Range, Baluchistan; pp. 1–17 in M. I. Ghaznavi, S. M. Raza, and M. T. Hasan (eds.), Siwaliks of South Asia. Proceedings of the Third GEOSAS Workshop held at Islamabad, Pakistan, March 1997. Geological Survey of Pakistan, Islamabad, Pakistan.

Gingerich, P. D., M. Arif, I. H. Khan, W. C. Clyde, and J. I. Bloch. 1999. *Machocyon abbasi*, a new early Eocene quettacyonid (Mammalia, Condylarthra). Contributions from the Museum of Paleontology, The University of Michigan 30:233–250.

Gingerich, P. D., M. Arif, I. H. Khan, M. Ul-Haq, J. I. Bloch, W. C. Clyde, and G. F. Gunnell. 2001. Gandhera Quarry, a unique mammalian faunal assemblage from the early Eocene of Baluchistan (Pakistan); pp. 251–262 in G. F. Gunnell (ed.), Eocene Biodiversity: Unusual Occurrences and Rarely Sampled Habitats. Kluwer Academic/Plenum Publishers, New York.

Ginsburg, L., K. H. Durrani, A. M. Kassi, and J.-L. Welcomme. 1999. Discovery of a new Anthracobunidae (Tethytheria, Mammalia) from the lower Eocene lignite of the Kach-Harnai area in Baluchistan (Pakistan). Comptes Rendus de l'Académie des Sciences. Série 2, Sciences de la Terre et Planètes 328:209–213.

Goloboff, P., J. S. Farris, and K. Nixon. 2008. TNT: a free program for phylogenetic analysis. Cladistics 24:774–786.

Granger, W. 1908. American Eocene horses. Bulletin of the American Museum of Natural History 24:221–264.

Halpert, A. P., F. A. Jenkins Jr., and H. Franks. 1987. Structure and scaling of the lumbar vertebrae in African bovids (Mammalia, Artiodactyla). Journal of Zoology 211:239–258.

Hermanson, J. W., and B. J. MacFadden. 1992. Evolutionary and functional morphology of the shoulder region and stay-apparatus in fossil and extant horses (Equidae). Journal of Vertebrate Paleontology 12:377–386.

Hildebrand, M. 1959. Motions of the running cheetah and horse. Journal of Mammalogy 40:481–495.

Holbrook, L. T. 1999. The phylogeny and classification of tapiromorph perissodactyls (Mammalia). Cladistics 15:331–350.

Holbrook, L. T. 2001. Comparative osteology of early Tertiary tapiromorphs (Mammalia, Perissodactyla). Zoological Journal of the Linnean Society 132:1–54.

Holbrook, L. T. 2009. Osteology of *Lophiodon* Cuvier, 1822 (Mammalia, Perissodactyla) and its phylogenetic implications. Journal of Vertebrate Paleontology 29:212–230.

Holbrook, L. T. 2014. On the skull of *Radinskya* (Mammalia) and its phylogenetic position. Journal of Vertebrate Paleontology 34:1203–1215.

Holbrook, L. T. 2015. The identity and homology of the postprotocrista and its role in molarization of upper premolars of Perissodactyla (Mammalia). Journal of Mammalian Evolution 22:259–269.

Holbrook, L. T., and J. B. LaPergola. 2011. A new genus of perissodactyl (Mammalia) from the Bridgerian of Wyoming, with comments on basal perissodactyl phylogeny. Journal of Vertebrate Paleontology 31:895–901.

Holland, W. J., and O. A. Peterson. 1914. The osteology of the Chalicotheroidea, with special reference to a mounted skeleton of *Moropus elatus* Marsh, now installed in the Carnegie Museum. Memoirs of the Carnegie Museum 3:189–406.

Hooker, J. J. 1984. A primitive ceratomorph (Perissodactyla, Mammalia) from the early Tertiary of Europe. Zoological Journal of the Linnean Society 82:229–244.

Hooker, J. J. 1989. Character polarities in early perissodactyls and their significance for *Hyracotherium* and infraordinal relationships; pp. 79–101 in D. R. Prothero and R. M. Schoch (eds.), The Evolution of Perissodactyls. Oxford University Press, New York.

Hooker, J. J. 1994. The beginning of the equoid radiation. Zoological Journal of the Linnean Society 112:29–63.

Hooker, J. J. 1996. Mammalian biostratigraphy across the Paleocene-Eocene boundary in the Paris, London and Belgian basins; pp. 205–218 in R. W. O'B. Knox, R. M. Corfield, and R. E. Dunay (eds.), Correlation of the Early Paleogene in Northwest Europe. Geological Society Special Publication 101. The Geological Society, London.

Hooker, J. J. 2005. Perissodactyla; pp. 199–214 in K. D. Rose and J. D. Archibald (eds.), The Rise of Placental Mammals: Origins and Relationships of the Major Extant Clades. Johns Hopkins University Press, Baltimore, Maryland.

Hooker, J. J. 2010. The Mammal Fauna of the Early Eocene Blackheath Formation of Abbey Wood, London. Monograph of the Palaeontographical Society, London, 162 pp. + 4 pls.

Hooker, J. J. 2015. A two-phase mammalian dispersal event across the Paleocene-Eocene transition. Newsletters on Stratigraphy 48:201–220.

Hooker, J. J., and M. E. Collinson. 2012. Mammalian faunal turnover across the Paleocene-Eocene boundary in NW Europe: the roles of displacement, community evolution and environment. Austrian Journal of Earth Sciences 105:17–28.

Hooker, J. J., and D. Dashzeveg. 2003. Evidence for direct mammalian faunal interchange between Europe and Asia near the Paleocene-Eocene boundary; pp. 479–500 in S. L. Wing, P. D. Gingerich, B. Schmitz, and E. Thomas (eds.), Causes and Consequences of Globally Warm Climates in the Early Paleogene. Geological Society of America Special Paper 369. Boulder, Colorado.

Hooker, J. J., and D. Dashzeveg. 2004. The origin of chalicotheres (Perissodactyla, Mammalia). Palaeontology 47:1363–1386.

Howell, A. B. 1944. Speed in Animals. University of Chicago Press, Chicago, Illinois, 270 pp.

Hu, X., E. Garzanti, T. Moore, and I. Raffi. 2015. Direct stratigraphic dating of India-Asia collision onset at the Selandian (middle Paleocene, 59 ± 1 Ma). Geology 43:859–862.

Hu, X., E. Garzanti, J. Wang, W. Huang, W. An, and A. Webb. 2016. The timing of India-Asia collision onset—facts, theories, controversies. Earth-Science Reviews 160:264–299.

Hussain, S. T. 1975. Evolutionary and functional anatomy of the pelvic limb in fossil and recent Equidae (Perissodactyla, Mammalia). Anatomia, Histologia, Embryologia 4:179–222.

Iakovleva, A. I., H. Brinkhuis, and C. Cavagnetto. 2001. Late Palaeocene–early Eocene dinoflagellate cysts from the Turgay Strait, Kazakhstan; correlations across ancient seaways. Palaeogeography, Palaeoclimatology, Palaeoecology 172:243–268.

IBM Corp. 2017. IBM SPSS Statistics for Windows, version 25.0. IBM Corp., Armonk, New York.

International Commission on Zoological Nomenclature. 2012. International Code of Zoological Nomenclature, fourth edition. Available at www.iczn.org/the-code/the-international-code-of-zoological-nomenclature/the-code-online. Accessed August 15, 2018.

International Committee on Veterinary Gross Anatomical Nomenclature. 2012. Nomina Anatomica Veterinaria, fifth edition, revised. Editorial Committee of ICVGAN, Hannover, Germany.

Jenkins, F. A., Jr., and S. M. Camazine. 1977. Hip structure and locomotion in ambulatory and cursorial carnivores. Journal of Zoology, London 181:351–370.

Jones, K. E. 2015a. Evolutionary allometry of lumbar shape in Felidae and Bovidae. Biological Journal of the Linnean Society London 116:721–740.

Jones, K. E. 2015b. Preliminary data on the effect of osseous anatomy on ex vivo joint mobility in the equine thoracolumbar region. Equine Veterinary Journal 48:502–508.

Jones, K. E. 2016. New insights on equid locomotor evolution from the lumbar region of fossil horses. Proceedings of the Royal Society B: Biological Sciences 283:20152947.

Jones, K. E., and L. T. Holbrook. 2016. The evolution of lateral accessory articulations in the lumbar region of perissodactyls. Journal of Vertebrate Paleontology. doi: 10.1080/02724634.2016.1224892.

Kapur, V. V., and S. Bajpai. 2015. Oldest south Asian tapiromorph (Perissodactyla, Mammalia) from the Cambay Shale Formation, western India, with comments on its phylogenetic position and biogeographic implications. The Paleobotanist 64:95–103.

Kapur, V. V., D. P. Das, S. Bajpai, and G. V. R. Prasad. 2017a. First mammal of Gondwanan lineage in the early Eocene of India. Comptes Rendus Palevol 16:721–737.

Kapur, V. V., D. P. Das, S. Bajpai, and G. V. R. Prasad. 2017b. Corrigendum to "First Mammal of Gondwanan lineage in the early Eocene of India" [C. R. Palevol, Kapur et al. 16 (2017)]. Comptes Rendus Palevol 16:820.

Kitts, D. B. 1956. American *Hyracotherium* (Perissodactyla, Equidae). Bulletin of the American Museum of Natural History 110:1–60.

Kneepkens, A. F. L. M., D. M. Badoux, and A. A. MacDonald. 1989. Descriptive and comparative myology of the forelimb of the Babirusa (*Babyrousa babyrussa* L., 1758). Anatomia, Histologia, Embryologia 18:349–365.

Koenigswald, W. von. 1997. Brief survey of the enamel diversity at the schmelzmuster level in Cenozoic placental mammals; pp. 137–161 in W. von Koenigswald and P. Sander (eds.), Tooth Enamel Microstructure. Balkema, Rotterdam, The Netherlands.

Koenigswald, W. von, and K. D. Rose. 2005. The enamel microstructure of the early Eocene pantodont *Coryphodon* and the nature of the zigzag-enamel. Journal of Mammalian Evolution 12:419–432.

Koenigswald, W. von, L. T. Holbrook, and K. D. Rose. 2011. Diversity and evolution of Hunter-Schreger band configuration in tooth enamel of perissodactyl mammals. Acta Palaeontologica Polonica 56:11–32.

Koenigswald, W. von, K. D. Rose, L. T. Holbrook, K. Kumar, R. S. Rana, and T. Smith. 2018. Mastication and enamel structure in *Cambaytherium*, a perissodactyl-like ungulate from the early Eocene of India. Palaeontologische Zeitschrift 92:671–680.

Kondrashov, P., and S. G. Lucas. 2012. Nearly complete skeleton of *Tetraclaenodon* (Mammalia, Phenacodontidae) from the early Paleocene of New Mexico: morpho-functional analysis. Journal of Paleontology 86:25–43.

Koob, T. J., and J. H. Long. 2000. The vertebrate body axis: evolution and mechanical function. American Zoologist 40:1–18.

Krause, D. W., and M. C. Maas. 1990. The biogeographic origins of late Paleocene–early Eocene mammalian immigrants to the Western Interior of North America; pp. 71–105 in T. M. Bown and K. D. Rose (eds.), Dawn of the Age of Mammals in the Northern Part of the Rocky Mountain Interior, North America. Geological Society of America Special Paper 243. Boulder, Colorado.

Kumar, K. 1991. *Anthracobune aijiensis* nov. sp. (Mammalia: Proboscidea) from the Subathu Formation, Eocene from NW Himalaya, India. Geobios 24:221–239.

Kumar, K., H. Singh, and R. S. Rana. 2011. Ichnospecies *Teredolites longissimus* and teredinid body fossils from the Early Eocene of India—taphonomic and palaeoenvironmental implications. Ichnos 18:57–71.

Kumar, K., K. D. Rose, R. S. Rana, L. Singh, T. Smith, and A. Sahni. 2010. Early Eocene artiodactyls (Mammalia) from western India. Journal of Vertebrate Paleontology 30:1245–1274.

Ladevèze, S., P. Missiaen, and T. Smith. 2010. First skull of *Orthaspidotherium edwardsi* (Mammalia, Condylarthra) from the late Paleocene of Berru (France) and phylogenetic affinities of the enigmatic European family Pleuraspidotheriidae. Journal of Vertebrate Paleontology 30:1559–1578.

Luckett, W. P. 1993. An ontogenetic assessment of dental homologies in therian mammals; pp. 182–204 in F. S. Szalay, M. J. Novacek, and M. C. McKenna (eds.), Mammal Phylogeny: Mesozoic Differentiation, Multituberculates, Monotremes, Early Therians, and Marsupials. Springer, New York.

Macdonald, A. A., and A. F. L. M. Kneepkens. 1995. Descriptive and comparative myology of the hindlimb of the babirusa (*Babyrousa babyrussa* L. 1758). Anatomia, Histologia, Embryologia 24:197–207.

MacFadden, B. J. 1976. Cladistic analysis of primitive equids, with notes on other perissodactyls. Systematic Zoology 25:1–14.

MacPhee, R. D. E. 1994. Morphology, adaptations, and relationships of *Plesiorycteropus*, and a diagnosis of a new order of eutherian mammals. Bulletin of the American Museum of Natural History 220:1–214.

Mallick, M., S. Dutta, P. F. Greenwood, and N. Bertram. 2009. Pyrolytic and spectroscopic studies of Eocene resin from Vastan Lignite Mine, Cambay Basin, western India. Journal Geological Society of India 74:16–22.

Mao, F.-Y., Y.-Q. Wang, Q. Li, and X. Jin. 2016. New records of archaic ungulates from the Lower Eocene of Sanshui Basin, Guangdong, China. Historical Biology 28:787–802.

Marsh, O. C. 1884. Dinocerata. A Monograph of an Extinct Order of Gigantic Mammals. Monographs of the United States Geological Survey 10, Washington, D.C., 237 pp.

Matthew, W. D. 1915. A revision of the Lower Eocene Wasatch and Wind River faunas. Part I: Order Ferae (Carnivora). Suborder Creodonta. Bulletin of the American Museum of Natural History 34:1–103.

Matthew, W. D. 1917. Absence of the pollex in Perissodactyla. Bulletin of the American Museum of Natural History 37:573–577.

Matthew, W. D. 1937. Paleocene faunas of the San Juan Basin, New Mexico. Transactions of the American Philosophical Society (new series) 30:1–510.

Mayr, G., R. S. Rana, A. Sahni, and T. Smith. 2007. Oldest fossil avian remains from the Indian subcontinental plate. Current Science 92:1266–1269.

Mayr, G., R. S. Rana, K. D. Rose, A. Sahni, K. Kumar, and T. Smith. 2013. New specimens of the early Eocene bird *Vastanavis* and the inter-relationships of stem group Psittaciformes. Paleontological Journal 47:1308–1314.

Mayr, G., R. S. Rana, K. D. Rose, A. Sahni, K. Kumar, L. Singh, and T. Smith. 2010. *Quercypsitta*-like birds from the early Eocene of India (Aves, ?Psittaciformes). Journal of Vertebrate Paleontology 30:467–478.

McCann, T. 2010. Chenier plain sedimentation in the Palaeogene of western India. Zeitschrift der Deutschen Gesellschaft fur Geowissenschaften 161:335–351.

McKenna, M. C. 1975. Fossil mammals and early Eocene North Atlantic land continuity. Annals of the Missouri Botanical Garden 62:335–353.

McKenna, M. C., and S. K. Bell. 1997. Classification of Mammals above the Species Level. Columbia University Press, New York, 631 pp.

McKenna, M. C., M. Chow, S. Ting, and Z.-X. Luo. 1989. *Radinskya yupingae*, a perissodactyl-like mammal from the late Paleocene of China; pp. 24–36 in D. R. Prothero and R. M. Schoch (eds.), The Evolution of Perissodactyls. Oxford University Press, New York.

Mead, J. G., and R. E. Fordyce. 2009. The therian skull: a lexicon with emphasis on the odontocetes. Smithsonian Contributions to Zoology 627:1–249.

Meng, J., C. Wang, and X. Zhao. 2012. India-Asia collision was at 24° N and 50 Ma: palaeomagnetic proof from southernmost Asia. Scientific Reports 2:925.

Meng, J., R. Zhai, and A. Wyss. 1998. The late Paleocene Bayan Ulan fauna of Inner Mongolia, China; pp. 148–185 in K. C. Beard and M. R. Dawson (eds.), Dawn of the Age of Mammals in Asia. Bulletin of Carnegie Museum of Natural History 34. Pittsburgh, Pennsylvania.

Meredith, R. W., J. Janecka, J. Gatesy, O. A. Ryder, C. A. Fisher, E. C. Teeling, A. Goodbla, E. Eizirik, T. L. L. Simão, T. Stadler, D. L. Rabosky, R. L. Honeycutt, J. J. Flynn, C. M. Ingram, C. Steiner, T. L. Williams, T. J. Robinson, A. Burk-Herrick, M. Westerman, N.

A. Ayoub, M. S. Springer, and W. J. Murphy. 2011. Impacts of the Cretaceous terrestrial revolution and KPg extinction on mammal diversification. Science 334:521–524.

Missiaen, P., and P. D. Gingerich. 2012. New early Eocene tapiromorph perissodactyls from the Ghazij Formation of Pakistan, with implications for mammalian biochronology in Asia. Acta Palaeontologica Polonica 57:21–34.

Missiaen, P., and P. D. Gingerich. 2014. New basal Perissodactyla (Mammalia) from the Lower Eocene Ghazij Formation of Pakistan. Contributions from the Museum of Paleontology, The University of Michigan 32:139–160.

Missiaen, P., G. F. Gunnell, and P. D. Gingerich. 2011a. New Brontotheriidae (Mammalia, Perissodactyla) from the early and middle Eocene of Pakistan, with implications for mammalian paleo-biogeography. Journal of Paleontology 85:665–677.

Missiaen, P., F. Quesnel, C. Dupuis, J.-Y. Storme, and T. Smith. 2013. The earliest Eocene mammal fauna of the Erquelinnes Sand Member near the French-Belgian border. Geologica Belgica 16:262–273.

Missiaen, P., K. D. Rose, R. S. Rana, K. Kumar, and T. Smith. 2011b. Revision of *Indobune* and *Cambaytherium* from the early Eocene of Vastan (India), and their affinities with anthracobunid and perissodactyl mammals. Journal of Vertebrate Paleontology 31 (Program and Abstracts):159.

Mohan, M. 1995. Cambay basin—a promise of oil and gas potential. Journal of the Palaeontological Society of India 40:41–47.

Mones, A. 1989. Nomen dubium versus nomen vanum. Journal of Vertebrate Paleontology 9:232–234.

Muizon, C. de, and R. L. Cifelli. 2000. The "condylarths" (archaic Ungulata, Mammalia) from the early Paleocene of Tiupampa (Bolivia): implications on the origin of South American ungulates. Geodiversitas 22:47–150.

Muller, J. 1935. The orbitotemporal region of the skull of the Mammalia. Archives Néerlandaises de Zoologie 1:118–259.

Murie, J. 1872. On the Malayan tapir, *Rhinochoerus sumatranus* (Gray). Journal of Anatomy and Physiology 6:131–169.

Murphy, W. J., E. Eizirik, W. E. Johnson, Y. P. Zhang, O. A. Ryder, and S. J. O'Brien. 2001. Molecular phylogenetics and the origins of placental mammals. Nature 409:614–618.

Nagori, M. L., S. C. Khosla, and S. R. Jakhar. 2013. Middle Eocene Ostracoda from the Tadkeshwar Lignite Mine, Cambay Basin, Gujarat. Journal of the Geological Society of India 81:514–520.

Nolf, D., R. S. Rana, and H. Singh. 2006. Fish otoliths from the Ypresian (early Eocene) of Vastan, Gujarat, India. Bulletin de l'Institut Royal des Sciences Naturelles de Belgique, Sciences de la Terre, Belgium 76:105–118.

Novacek, M. J. 1986. The skull of leptictid insectivorans and the higher-level classification of eutherian mammals. Bulletin of the American Museum of Natural History 183:1–112.

Novacek, M. J., and A. R. Wyss. 1986. Higher-level relationships of the Recent eutherian orders: morphological evidence. Cladistics 2:257–287.

O'Leary, M. A., and K. D. Rose. 1995. Postcranial skeleton of the early Eocene mesonychid *Pachyaena* (Mammalia: Mesonychia). Journal of Vertebrate Paleontology 15:401–430.

O'Leary, M. A., J. I. Bloch, J. J. Flynn, T. J. Gaudin, A. Giallombardo, N. P. Giannini, S. L. Goldberg, B. P. Kraatz, Z.-X. Luo, J. Meng, X. Ni, M. J. Novacek, F. A. Perini, Z. S. Randall, G. W. Rougier, E. J. Sargis, M. T. Silcox, N. B. Simmons, M. Spaulding, P. M. Velazco, J. R. Wible, and A. L. Cirranello. 2013. The placental mammal ancestor and the post-K-Pg radiation of placentals. Science 339:662–667.

Osborn, H. F. 1898. Remounted skeleton of *Phenacodus primaevus*. Comparison with Euprotogonia. Bulletin of the American Museum of Natural History 10:159–164.

Otts, C. 1991. Postural and locomotor capabilities in the phenacodontid condylarths (Mammalia). Ph.D. dissertation, University of Arizona, Tucson, Arizona, 566 pp.

Owen, R. 1848. Description of teeth and portions of jaws of two extinct Anthracotherioid quadrupeds (*Hyopotamus vectianus* and *Hyop. bovinus*) discovered by the Marchioness of Hastings in the Eocene deposits on the NW coast of the Isle of Wight: with an attempt to develope Cuvier's idea of the Classification of Pachyderms by the number of their toes. Quarterly Journal of the Geological Society of London 4:103–141.

Pandey, J., N. P. Singh, B. R. Krishna, D. D. Sharma, A. K. Parakh, and S. S. Nath. 1993. Lithostratigraphy of Cambay Basin. Document III,

Keshav Dev Malviya Institute of Petroleum Exploration Publication, Oil and Natural Gas Commission, Dehradun 1:1–166.

Paul, S., J. Sharma, B. D. Singh, P. K. Saraswati, and S. Dutta. 2015. Early Eocene equatorial vegetation and depositional environment: biomarker and palynological evidences from a lignite-bearing sequence of Cambay Basin, western India. International Journal of Coal Geology 149:77–92.

Pilgrim, G. E. 1940. Middle Eocene mammals from northwest Pakistan. Proceedings of the Zoological Society of London, Series B 110:127–152.

Prasad, G. V. R., and S. Bajpai. 2008. Agamid lizards from the early Eocene of western India: oldest Cenozoic lizards from South Asia. Palaeontologia Electronica 11.1.4A.

Prasad, V., A. Farooqui, S. K. M. Tripathi, and B. Thakur. 2009. Evidence of Late Palaeocene-Early Eocene equatorial rain forest refugia in southern Western Ghats, India. Journal of Biosciences 34:777–797.

Prasad, V., I. B. Singh, S. Bajpai, R. Garg, B. Thakur, A. Singh, N. Saravanan, and V. V. Kapur. 2013. Palynofacies and sedimentology-based high-resolution sequence stratigraphy of the lignite-bearing muddy coastal deposits (early Eocene) in the Vastan Lignite Mine, Gulf of Cambay, India. Facies 59:737–761.

Prothero, D. R., E. M. Manning, and M. Fischer. 1988. The phylogeny of the ungulates; pp. 201–234 in M. J. Benton (ed.), The Phylogeny and Classification of the Tetrapods. 2: Mammals. Clarendon Press, Oxford, U.K.

Punekar, J., and P. K. Saraswati. 2010. Age of the Vastan lignite in context of some oldest Cenozoic fossil mammals from India. Journal of the Geological Society of India 76:63–68.

Radinsky, L. B. 1963a. Origin and early evolution of North American Tapiroidea. Bulletin Yale Peabody Museum 17:1–106.

Radinsky, L. B. 1963b. The perissodactyl hallux. American Museum Novitates 2145:1–8.

Radinsky, L. B. 1965a. Evolution of the tapiroid skeleton from *Heptodon* to *Tapirus*. Bulletin of the Museum of Comparative Zoology 134:69–106.

Radinsky, L. B. 1965b. Early Tertiary Tapiroidea of Asia. Bulletin of the American Museum of Natural History 129:181–264.

Radinsky, L. B. 1966. The adaptive radiation of the phenacodontid condylarths and the origin of the Perissodactyla. Evolution 20:408–417.

Radinsky, L. B. 1969. The early evolution of the Perissodactyla. Evolution 23:308–328.

Rage, J.-C., A. Folie, R. S. Rana, H. Singh, K. D. Rose, and T. Smith. 2008. A diverse snake fauna from the early Eocene of Vastan Lignite Mine, Gujarat, India. Acta Palaeontologica Polonica 53:391–403.

Rana, R. S., K. Kumar, and H. Singh. 2004. Vertebrate fauna from the subsurface Cambay Shale (Lower Eocene), Vastan Lignite Mine, Gujarat, India. Current Science 87:1726–1733.

Rana, R. S., M. Augé, A. Folie, K. D. Rose, K. Kumar, L. Singh, A. Sahni, and T. Smith. 2013. High diversity of acrodontan lizards in the Early Eocene Vastan Lignite Mine of India. Geologica Belgica 16:290–301.

Rana, R. S., K. Kumar, G. Escarguel, A. Sahni, K. D. Rose, T. Smith, H. Singh, and L. Singh. 2008. An ailuravine rodent from the lower Eocene Cambay Formation at Vastan, western India, and its palaeobiogeographic implications. Acta Palaeontologica Polonica 53:1–14.

Rana, R. S., K. Kumar, S. P. Zack, F. Solé, K. D. Rose, P. Missiaen, L. Singh, A. Sahni, and T. Smith. 2015. Craniodental and postcranial morphology of *Indohyaenodon raoi* from the early Eocene of India, and its implications for ecology, phylogeny, and biogeography of hyaenodontid mammals. Journal of Vertebrate Paleontology. doi: 10.1080/02724634.2015.965308.

Rangarajan, S. 2008. A case for revisiting the evolutionary history of pericratonic Cambay basin, India; pp. 123–129 in Seventh International Conference and Exposition on Petroleum Geophysics, Hyderabad, 2008. Society of Petroleum Geologists of India.

Rao, K. L. N. 1969. Lithostratigraphy of the Paleogene succession of Southern Cambay Basin. Bulletin Oil and National Gas Commission (ONGC), Dehradun, India 6:24–37.

Rao, M. R., A. Sahni, R. S. Rana, and P. Verma. 2013. Palynostratigraphy and depositional environment of Vastan Lignite Mine (Early Eocene), Gujarat, western India. Journal Earth System Science 122:289–307.

Rasmussen, D. T., M. Gagnon, and E. L. Simons. 1990. Taxeopody in the carpus and tarsus of Oligocene Pliohyracidae (Mammalia: Hyracoidea) and the phyletic position of hyraxes. Proceedings of the National Academy of Sciences of the United States of America 87:4688–4691.

Ray, C. E., D. P. Domning, and M. C. McKenna. 1994. A new specimen of *Behemotops proteus* (Order Desmostylia) from the marine Oligocene of Washington. Proceedings of the San Diego Museum of Natural History 29:205–222.

Richards, M. W., and A. G. Watson. 1991. Development and variation of the lateral vertebral foramen of the atlas in dogs. Anatomia, Histologia, Embryologia 20:363–368.

Rose, K. D. 1981. The Clarkforkian Land-Mammal Age and mammalian faunal composition across the Paleocene-Eocene boundary. University of Michigan Papers on Paleontology 26:1–197.

Rose, K. D. 1990. Postcranial skeletal remains and adaptations in early Eocene mammals from the Willwood Formation, Bighorn Basin, Wyoming; pp. 107–133 in T. M. Bown and K. D. Rose (eds.), Dawn of the Age of Mammals in the Northern Part of the Rocky Mountain Interior. Geological Society of America Special Paper 243. Boulder, Colorado.

Rose, K. D. 1996. Skeleton of early Eocene *Homogalax* and the origin of Perissodactyla. Palaeovertebrata 25:243–260.

Rose, K. D., R. H. Dunn, and L. Grande. 2014a. A new pantolestid skeleton from the early Eocene Fossil Butte Member, Green River Formation (Wyoming), and skeletal ontogeny in Pantolestidae (Mammalia, Pantolesta). Journal of Vertebrate Paleontology 34:932–940.

Rose, K. D., L. T. Holbrook, and W. P. Luckett. 2018a. Deciduous premolars of Eocene Equidae and their phylogenetic significance. Historical Biology 30:89–118.

Rose, K. D., R. S. Rana, A. Sahni, and T. Smith. 2007. A new adapoid primate from the early Eocene of India. Contributions from the Museum of Paleontology, The University of Michigan 31:379–385.

Rose, K. D., K. Kumar, R. S. Rana, A. Sahni, and T. Smith. 2013. New hypsodont tillodont (Mammalia: Tillodontia) from the early Eocene of India. Journal of Paleontology 87:842–853.

Rose, K. D., A. E. Chew, R. H. Dunn, M. J. Kraus, H. C. Fricke, and S. P. Zack. 2012. Earliest Eocene mammalian fauna from the Paleocene-Eocene Thermal Maximum at Sand Creek Divide, southern Bighorn Basin, Wyoming. University of Michigan Papers on Paleontology 36:1–122.

Rose, K. D., R. S. Rana, A. Sahni, K. Kumar, L. Singh, and T. Smith. 2009a. First tillodont from India: additional evidence for an early Eocene faunal connection between Europe and India? Acta Palaeontologica Polonica 54:351–355.

Rose, K. D., V. B. DeLeon, P. Missiaen, R. S. Rana, A. Sahni, L. Singh, and T. Smith. 2008. Early Eocene lagomorph (Mammalia) from western India and the early diversification of Lagomorpha. Proceedings of the Royal Society London B: Biological Sciences 275:1203–1208.

Rose, K. D., R. H. Dunn, K. Kumar, J. M. G. Perry, K. A. Prufrock, R. S. Rana, and T. Smith. 2018b. New fossils from Tadkeshwar Mine (Gujarat, India) increase primate diversity from the early Eocene Cambay Shale. Journal of Human Evolution 122:93–107.

Rose, K. D., R. S. Rana, A. Sahni, K. Kumar, P. Missiaen, L. Singh, and T. Smith. 2009b. Early Eocene primates from Gujarat, India. Journal of Human Evolution 56:366–404.

Rose, K. D., T. Smith, R. S. Rana, A. Sahni, H. Singh, P. Missiaen, and A. Folie. 2006. Early Eocene (Ypresian) continental vertebrate assemblage from India, with description of a new anthracobunid (Mammalia, Tethytheria). Journal of Vertebrate Paleontology 26:219–225.

Rose, K. D., L. T. Holbrook, R. S. Rana, K. Kumar, K. E. Jones, H. E. Ahrens, P. Missiaen, A. Sahni, and T. Smith. 2014b. Early Eocene fossils suggest that the mammalian order Perissodactyla originated in India. Nature Communications 5:5570.

Russell, D. E. 1964. Les mammifères Paléocènes d'Europe. Mémoires du Muséum National d'Histoire Naturelle Série C, Sciences de la Terre, tome XIII:1–324.

Rust, J., H. Singh, R. S. Rana, T. McCann, L. Singh, K. Anderson, N. Sarkar, P. C. Nascimbene, F. Stebner, J. C. Thomas, M. S. Kraemer, C. J. Williams, M. S. Engel, A. Sahni, and D. Grimaldi. 2010. Biogeographic and evolutionary implications of a diverse paleobiota in amber from the early Eocene of India. Proceedings of the National Academy of Sciences of the United States of America 107:18360–18365.

Sahni, A., and S. K. Khare. 1973. Additional Eocene mammals from the Subathu Formation of Jammu and Kashmir. Journal of the Palaeontological Society of India 17:31–49.

Sahni, A., and K. Kumar. 1980. Lower Eocene Sirenia, *Ishatherium subathuensis*, gen. et. sp. nov. from the type area, Subathu Formation, Subathu, Simla Himalayas, H.P. Journal of the Palaeontological Society of India 23–24:132–135.

Sahni, A., P. K. Saraswati, R. S. Rana, K. Kumar, H. Singh, H. Alimohammadian, N. Sahni, K. D. Rose, L. Singh, and T. Smith. 2006. Temporal constraints and depositional palaeoenvironments of the Vastan lignite sequence, Gujarat: analogy for the Cambay Shale hydrocarbon source rock. Indian Journal of Petroleum Geology 15:1–20.

Samanta, A., A. Sarkar, M. K. Bera, J. Rai, and S. S. Rathore. 2013. Late Paleocene-early Eocene carbon isotope stratigraphy from a near-terrestrial tropical section and antiquity of Indian mammals. Journal of Earth System Science 122:163–171.

Scotese, C. R. 2006. Paleomap project. Available at www.scotese.com. Accessed November 15, 2018.

Scott, K. M. 1983. Prediction of body weight of fossil Artiodactyla. Zoological Journal of the Linnean Society 77:199–215.

Scott, K. M. 1990. Postcranial dimensions of ungulates as predictors of body mass; pp. 301–336 in J. Damuth and B. J. MacFadden (eds.), Body Size in Mammalian Paleobiology: Estimation and Biological Implications. Cambridge University Press, Cambridge, U.K.

Scott, W. B. 1888. On some new and little known creodonts. Journal of the Academy of Natural Sciences of Philadelphia 9:155–185.

Seiffert, E. R. 2007. A new estimate of afrotherian phylogeny based on simultaneous analysis of genomic, morphological, and fossil evidence. BMC Evolutionary Biology 7:224.

Serra-Kiel, J., L. Hottinger, E. Caus, K. Drobne, C. Ferrandez, A. K. Jauhri, G. Less, R. Pavlovec, J. Pignatti, J. M. Samsó, H. Schaub, E. Sirel, A. Strougo, Y. Tambareau, J. Tosquella, and E. Y. Zakrevskaya. 1998. Larger foraminiferal biostratigraphy of the Tethyan Paleocene and Eocene. Bulletin de la Société Géologique de France 169:281–299.

Shelley, S. L., T. E. Williamson, and S. L. Brusatte. 2018. The osteology of *Periptychus carinidens*: a robust, ungulate-like placental mammal (Mammalia: Periptychidae) from the Paleocene of North America. PLoS ONE 13:e0200132.

Silva, M., and J. A. Downing. 1995. CRC Handbook of Mammalian Body Masses. CRC Press, Boca Raton, Florida, 359 pp.

Simpson, G. G. 1940. Mammals and land bridges. Journal of the Washington Academy of Sciences 30:137–163.

Simpson, G. G. 1945. The principles of classification and a classification of mammals. Bulletin of the American Museum of Natural History 85:1–350.

Simpson, G. G. 1947. Holarctic mammalian faunas and continental relationships during the Cenozoic. Bulletin of the Geological Society of America 58:613–688.

Simpson, G. G., A. Roe, and R. C. Lewontin. 1960. Quantitative Zoology. Harcourt, Brace and Company, New York, 440 pp.

Singh, H., M. Prasad, K. Kumar, and S. K. Singh. 2011. Paleobotanical remains from the Paleocene–Lower Eocene Vagadkhol Formation, western India and their climatic and phytogeographic implications. Palaeoworld 20:332–356.

Singh, H., M. Prasad, K. Kumar, and S. K. Singh. 2015. Early Eocene macroflora and associated palynofossils from the Cambay Shale Formation, Western India: phytogeographic and palaeoclimatic implications. Palaeoworld 24:293–323.

Singh, H., B. Samant, T. Adatte, and H. Khozyem. 2014. Diverse palynoflora from amber and associated sediments of Tarkeshwar lignite mine, Surat district, Gujarat, India. Current Science 106:930–932.

Singh, H., M. Prasad, K. Kumar, R. S. Rana, and S. K. Singh. 2010. Fossil fruits from Early Eocene Vastan Lignite, Gujarat, India: taphonomic and phytogeographic implications. Current Science 98:1625–1632.

Slijper, E. J. 1946. Comparative biologic-anatomical investigations on the vertebral column and spinal musculature of mammals. Verhandelingen der Koninklijke Nederlandse Akademie van Wetenschappen, Afdeeling Natuurkunde, Tweede Reeks 42:1–128.

Sloan, R. E. 1969. Cretaceous and Paleocene terrestrial communities of western North America. Proceedings of the North American Paleontological Convention E:427–453.

Smith, T., K. D. Rose, and P. D. Gingerich. 2006. Rapid Asia-Europe-North America geographic dispersal of earliest Eocene primate *Teilhardina* during the Paleocene-Eocene Thermal Maximum. Proceedings of the National Academy of Sciences of the United States of America 103:11223–11227.

Smith, T., J. Habersetzer, N. B. Simmons, and G. F. Gunnell. 2012. Systematics and paleobiogeography of early bats; pp. 23–66 in G. F. Gunnell and N. B. Simmons (eds.), Evolutionary History of Bats: Fossils, Molecules and Morphology. Cambridge University Press, Cambridge, U.K.

Smith, T., R. S. Rana, P. Missiaen, K. D. Rose, A. Sahni, H. Singh, and L. Singh. 2007. High bat (Chiroptera) diversity in the Early Eocene of India. Naturwissenschaften 94:1003–1009.

Smith, T., F. Solé, P. Missiaen, R. S. Rana, K. Kumar, A. Sahni, and K. D. Rose. 2015. First early Eocene tapiroid from India and its implication for the paleobiogeographic origin of perissodactyls. Palaeovertebrata 39(2):e5.

Smith, T., K. Kumar, R. S. Rana, A. Folie, F. Solé, C. Noiret, T. Steeman, A. Sahni, and K. D. Rose. 2016. New early Eocene vertebrate assemblage from western India reveals a mixed fauna of European and Gondwanan affinities. Geoscience Frontiers 7:969–1001.

Solé, F., E. De Bast, H. Legendre, R. S. Rana, K. Kumar, K. D. Rose, and T. Smith. In press. New specimens of *Frugivastodon* (Mammalia: Apatotheria) from the early Eocene of India confirm its apatemyid status and elucidate dispersal of Apatemyidae; in G. V. R. Prasad and R. Patnaik (eds.), Biological Consequences of Plate Tectonics: New Perspectives on Post-Gondwanaland Break-up–A Tribute to Ashok Sahni, in Vertebrate Paleobiology and Paleoanthropology series. Springer.

Solounias, N., M. Danowitz, E. Stachtiaris, A. Khurana. M. Araim, M. Sayegh, and J. Natale. 2018. The evolution and anatomy of the horse manus with an emphasis on digit reduction. Royal Society Open Science 5:e171782.

Sondaar, P. Y. 1968. The osteology of the manus of fossil and recent Equidae with special reference to phylogeny and function. Verhandelingen der Koninklijke Nederlandse Akademie van Wetenschappen, Afdeeling Natuurkunde, Eerste Reeks 25:1–76.

Sperber, G. H. 2017. Dental wear: attrition, erosion, and abrasion—a palaeo-odontological approach. Dentistry Journal 5(2):e19.

Stefen, C. 1997. Differentiations in Hunter-Schreger bands of carnivores; pp. 123–136 in W. von Koenigswald and P. M. Sander (eds.), Tooth Enamel Microstructure. A. A. Balkema, Rotterdam, The Netherlands.

Sudhakar, R., and D. N. Basu. 1973. A reappraisal of the Paleogene stratigraphy of southern Cambay Basin. Bulletin of the Oil and Natural Gas Commission 10:55–76.

Swofford, D. L. 2003. PAUP*: Phylogenetic Analysis Using Parsimony (*and Other Methods), version 4.0b10a. Sinauer Associates, Sunderland, Massachusetts.

Szalay, F. S. 1969. Mixodectidae, Microsyopidae, and the insectivore-primate transition. Bulletin of the American Museum of Natural History 140:193–330.

Tassy, P. 1981. Le crâne de *Moeritherium* (Proboscidea, Mammalia) de l'Eocène de Dor el Talha (Libye) et le problème de la classification phylogénétique du genre dans les Tethytheria McKenna, 1975. Bulletin du Muséum National d'Histoire Naturelle, Paris 4:87–147.

Tassy, P., and J. Shoshani. 1988. The Tethytheria: elephants and their relatives; pp. 283–315 in M. J. Benton (ed.), The Phylogeny and Classification of the Tetrapods, Volume 2. Clarendon Press, Oxford, U.K.

Thewissen, J. G. M. 1990. Evolution of Paleocene and Eocene Phenacodontidae (Mammalia, Condylarthra). University of Michigan Papers on Paleontology 29:1–107.

Thewissen, J. G. M., and D. P. Domning. 1992. The role of phenacodontids in the origin of the modern orders of ungulate mammals. Journal of Vertebrate Paleontology 12:494–504.

Ting, S.-Y. 1993. A preliminary report on an early Eocene mammalian fauna from Hengdong, Hunan Province, China. Kaupia 3:201–207.

Tong, Y.-S., J.-W. Wang, and J. Meng. 2004. *Olbitherium millenariusum*, a new perissodactyl-like archaic ungulate (Mammalia) from the early Eocene Wutu Formation, Shandong. Vertebrata PalAsiatica 42:27–38.

Tsubamoto, T., S. T. Tun, N. Egi, M. Takai, N. Shigehara, A. N. Soe, A. K. Aung, and T. Thein. 2003. Reevaluation of some ungulate mammals from the Eocene Pondaung Formation, Myanmar. Paleontological Research 7:219–243.

Ungar, P. S. 2010. Mammalian Teeth: Origin, Evolution, and Diversity. The Johns Hopkins University Press, Baltimore, Maryland, 304 pp.

Van Valen, L. 1966. Deltatheridia, a new order of mammals. Bulletin of the American Museum of Natural History 132:1–126.

Welker, F., M. Collins, J. Thomas, M. Wadsley, S. Brace, E. Cappellini, S. Turvey, M. Reguero, J. Gelfo, A. Kramarz, J. Burger, J. Thomas-Oates, D. Ashford, P. Ashton, K. Rowsell, D. Porter, B. Kessler, R.

Fischer, C. Baessmann, S. Kaspar, J. Olsen, P. Kiley, J. Elliott, C. Kelstrup, V. Mullin, M. Hofreiter, E. Willerslev, J.-J. Hublin, L. Orlando, I. Barnes, and R. MacPhee. 2015. Ancient proteins resolve the evolutionary history of Darwin's South American ungulates. Nature 522:81–84.

Wells, N. A., and P. D. Gingerich. 1983. Review of Eocene Anthracobunidae (Mammalia, Proboscidea) with a new genus and species, *Jozaria palustris*, from the Kuldana Formation of Kohat (Pakistan). Contributions from the Museum of Paleontology, The University of Michigan 26:117–139.

West, R. M. 1971. Deciduous dentition of the early Tertiary Phenacodontidae (Condylarthra, Mammalia). American Museum Novitates 2461:1–37.

West, R. M. 1980. Middle Eocene large mammal assemblage with Tethyan affinities, Ganda Kas region, Pakistan. Journal of Paleontology 54:508–533.

West, R. M. 1983. South Asian Middle Eocene moeritheres (Mammalia: Tethytheria). Annals of Carnegie Museum 52:359–373.

Westbury, M., S. Baleka, A. Barlow, S. Hartmann, J. Paijmans, A. Kramarz, A. Forasiepi, M. Bond, J. Gelfo, M. Reguero, P. López-Mendoza, M. Taglioretti, F. Scaglia, A. Rinderknecht, W. Jones, F. Mena, G. Billet, C. de Muizon, J. Aguilar, R. MacPhee, and M. Hofreiter. 2015. A mitogenomic timetree for Darwin's enigmatic South American mammal *Macrauchenia patachonica*. Nature Communications 8:15951.

Wible, J. R. 1987. The eutherian stapedial artery: character analysis and implications for superordinal relationships. Zoological Journal of the Linnean Society 91:107–135.

Wible, J. R., G. W. Rougier, M. J. Novacek, and R. J. Asher. 2009. The eutherian mammal *Maelestes gobiensis* from the Late Cretaceous of Mongolia and the phylogeny of Cretaceous Eutheria. Bulletin of the American Museum of Natural History 327:1–123.

Williams, P. L. (ed.). 1995. Gray's Anatomy, thirty-eighth edition. Churchill Livingstone, Edinburgh, U.K., 2092 pp.

Williamson, T. E., and S. G. Lucas. 1992. *Meniscotherium* (Mammalia, "Condylarthra") from the Paleocene-Eocene of western North America. Bulletin of the New Mexico Museum of Natural History and Science 1:1–75.

Wood, A. R., R. M. Bebej, C. L. Manz, D. L. Begun, and P. D. Gingerich. 2011. Postcranial functional morphology of *Hyracotherium* (Equidae, Perissodactyla) and locomotion in the earliest horses. Journal of Mammalian Evolution 18:1–32.

Wortman, J. L. 1894. Osteology of *Patriofelis*, a middle Eocene creodont. Bulletin of the American Museum of Natural History 6:129–165.

Wortman, J. L. 1896. Species of *Hyracotherium* and allied perissodactyls from the Wasatch and Wind River beds of North America. Bulletin of the American Museum of Natural History 8:81–111.

Wyss, A. R., and J. J. Flynn. 1993. A phylogenetic analysis and definition of the Carnivora; pp. 32–52 in F. S. Szalay, M. J. Novacek, and M. C. McKenna (eds.), Mammal Phylogeny: Placentals. Springer, New York.

Wyss, A., and J. Meng. 1996. Application of phylogenetic taxonomy to poorly resolved crown clades: a stem-modified node-based definition of Rodentia. Systematic Biology 45:559–568.

Youlatos, D. 2003. Osteological correlates of tail prehensility in carnivorans. Journal of Zoology, London 259:423–430.

Zack, S. P., K. D. Rose, L. T. Holbrook, K. Kumar, R. S. Rana, and T. Smith. 2019. An enigmatic new ungulate-like mammal from the early Eocene of India. Papers in Palaeontology. doi: 10.1002/spp2.1288.

Zhang, Y.-P. 1978. Two new genera of condylarthran phenacolophids from the Paleocene of Nanxiong Basin, Guangdong. Vertebrata PalAsiatica 16:267–274.

Zhou, X., W. J. Sanders, and P. D. Gingerich. 1992. Functional and behavioral implications of vertebral structure in *Pachyaena ossifraga* (Mammalia, Mesonychia). Contributions from the Museum of Paleontology, The University of Michigan 28:289–319.

Zhu, D. C., Q. Wang, Z. D. Zhao, S. L. Chung, P. A. Cawood, Y. Niu, S. A. Liu, F. Y. Wu, and X. X. Mo. 2015. Magmatic record of India-Asia collision. Scientific Reports 5:14289.

APPENDIX 1. DOI links to illustrated specimens (micro-CT scans) hosted on Morphosource (www.morphosource.org/) as Project ID P750. **Abbreviations**: **L**, left; **Mc**, metacarpal; **Mt**, metatarsal; **R**, right.

Taxon	Specimen	Element	Figure	Zipped .tiff stack	Surface mesh
Cambaytherium gracilis	GU 9017	L Mt III	76K–P	doi:10.17602/M2/M78979	doi:10.17602/M2/M78980
	GU 9019	R Dentary with m2-3 and associated m1	21	Dentary doi:10.17602/M2/M155089 m1 doi:10.17602/M2/M155202	Dentary doi:10.17602/M2/M158523 m1 doi:10.17602/M2/M158522
	GU 9206	R Proximal ulna	55F	doi:10.17602/M2/M79153	doi:10.17602/M2/M79154
	WIF/A 4208	R Ulna	55E	doi:10.17602/M2/M79155	doi:10.17602/M2/M79156
	WIF/A 4212	R Dentary with m3	33D–F	doi:10.17602/M2/M78983	doi:10.17602/M2/M78984
	WIF/A 4235	Rp4	33A–C	doi:10.17602/M2/M79003	doi:10.17602/M2/M79004
	WIF/A 4239	RP4	33G–I	doi:10.17602/M2/M79005	doi:10.17602/M2/M79006
	WIF/A 4244	L Radius	55G	doi:10.17602/M2/M79017	doi:10.17602/M2/M79018
	WIF/A 4256	L Mc III	59F–J	doi:10.17602/M2/M84624	doi:10.17602/M2/M84355
	WIF/A 4263	L Astragalus	72Q–U	doi:10.17602/M2/M78777	doi:10.17602/M2/M78765
Cambaytherium marinus	GU 841	L Mt II	78	doi:10.17602/M2/M78967	doi:10.17602/M2/M78968
	GU 8052	L Distal tibia	71F–J	doi:10.17602/M2/M79125	doi:10.17602/M2/M79126
Cambaytherium thewissi	GU 10	Canine	25E–I	doi:10.17602/M2/M84600	doi:10.17602/M2/M83825
	GU 224	Canine	25O–S	doi:10.17602/M2/M78857	doi:10.17602/M2/M78858
	GU 274	R Radius	55B	doi:10.17602/M2/M79011	doi:10.17602/M2/M79012
	GU 275	R Mt IV	77A–F	doi:10.17602/M2/M79182	doi:10.17602/M2/M79183
	GU 280	Proximal phalanx	62A–C	doi:10.17602/M2/M80132	doi:10.17602/M2/M80133
	GU 292	R Mc II	58A–F	doi:10.17602/M2/M79191	doi:10.17602/M2/M79192
	GU 294	R Lunar	56J–N	doi:10.17602/M2/M79199	doi:10.17602/M2/M79200
	GU 295	R Lunar	56E–I	doi:10.17602/M2/M79205	doi:10.17602/M2/M79206
	GU 296	R Cuneiform	57A–D	doi:10.17602/M2/M79207	doi:10.17602/M2/M79208
	GU 297	R Navicular	75A–D	doi:10.17602/M2/M80134	doi:10.17602/M2/M80135
	GU 300	R Distal fibula	70D–G	doi:10.17602/M2/M79209	doi:10.17602/M2/M79210
	GU 333	L Pisiform	57E–H	doi:10.17602/M2/M79211	doi:10.17602/M2/M79212
	GU 402	Skull	15A–E	doi:10.17602/M2/M83533	doi:10.17602/M2/M83529
	GU 403	Mandible	15F, 17	doi:10.17602/M2/M78959	doi:10.17602/M2/M78960
	GU 403-1	Incisor	24J–M	doi:10.17602/M2/M84602	doi:10.17602/M2/M84603
	GU 403-2	Incisor	24N–R	doi:10.17602/M2/M84604	doi:10.17602/M2/M84605
	GU 404	LdP1	36D–F	doi:10.17602/M2/M78944	doi:10.17602/M2/M78945
	GU 404	LP2	36A–C	doi:10.17602/M2/M78947	doi:10.17602/M2/M78948
	GU 404	LP3–M3	36A–C	doi:10.17602/M2/M78949	doi:10.17602/M2/M78950
	GU 404	RP2	36A–C	doi:10.17602/M2/M78951	doi:10.17602/M2/M78953
	GU 404	RP3-M3	36A–C	doi:10.17602/M2/M78952	doi:10.17602/M2/M78956
	GU 407	Canine	25J–N	doi:10.17602/M2/M78859	doi:10.17602/M2/M78860
	GU 409	Ldp1	27I–K	doi:10.17602/M2/M84606	doi:10.17602/M2/M84339
	GU 626-1	Incisor	24A–D	doi:10.17602/M2/M84607	doi:10.17602/M2/M84357
	GU 626-2	Incisor	24E–I	doi:10.17602/M2/M84608	doi:10.17602/M2/M84358
	GU 730	Cranium	16	doi:10.17602/M2/M83513	doi:10.17602/M2/M83512
	GU 735	L Mt III	76E–J	doi:10.17602/M2/M79213	doi:10.17602/M2/M79214
	GU 739	L Distal tibia	71A–E	doi:10.17602/M2/M79123	doi:10.17602/M2/M79124
	GU 768	L Cuboid	75E–I	doi:10.17602/M2/M79411	doi:10.17602/M2/M79412
	GU 770	L Astragalus	72A–E, K; 73C, D	doi:10.17602/M2/M78760	doi:10.17602/M2/M78761
	GU 772	L Distal calcaneus	74E–I	doi:10.17602/M2/M79413	doi:10.17602/M2/M79414
	GU 773	Atlas	44A–F	doi:10.17602/M2/M78769	doi:10.17602/M2/M78770
	GU 774	Axis	45	doi:10.17602/M2/M78773	doi:10.17602/M2/M78774
	GU 775	C5	47A–F	doi:10.17602/M2/M83658	doi:10.17602/M2/M83648
	GU 776	R Canine	26A–E	doi:10.17602/M2/M78898	doi:10.17602/M2/M78900
	GU 776	L Canine	26F–J	doi:10.17602/M2/M78897	doi:10.17602/M2/M78899
	GU 780	R Astragalus	72F–J, L	doi:10.17602/M2/M78762	doi:10.17602/M2/M78763
	GU 782	Atlas	44G–K	doi:10.17602/M2/M78771	doi:10.17602/M2/M78772
	GU 783	C7/T1	47G–L	doi:10.17602/M2/M78775	doi:10.17602/M2/M78776
	GU 786	Lumbar vertebra	49F–J	doi:10.17602/M2/M79427	doi:10.17602/M2/M79428
	GU 787	Lumbar vertebra	49A–E	doi:10.17602/M2/M79425	doi:10.17602/M2/M79426
	GU 788	Thoracic vertebra	48	doi:10.17602/M2/M79021	doi:10.17602/M2/M79022
	GU 792	Canine	25A–D	doi:10.17602/M2/M84619	doi:10.17602/M2/M83830
	GU 809	R Proximal humeral epiphysis	54A–D	doi:10.17602/M2/M78937	doi:10.17602/M2/M78938
	GU 821	R Proximal Mt III	76A–D	doi:10.17602/M2/M79429	doi:10.17602/M2/M79430
	GU 822	L Mc IV	60	doi:10.17602/M2/M79431	doi:10.17602/M2/M79432
	GU 824	Caudal vertebra	51	doi:10.17602/M2/M78915	doi:10.17602/M2/M78917
	GU 825a	Caudal vertebra	52G–L	doi:10.17602/M2/M84626	doi:10.17602/M2/M84627
	GU 825b	Caudal vertebra	52M–R	doi:10.17602/M2/M84628	doi:10.17602/M2/M84629
	GU 828	Proximal phalanx	62H–K	doi:10.17602/M2/M79433	doi:10.17602/M2/M79434
	GU 829	Proximal phalanx	62L–P	doi:10.17602/M2/M79435	doi:10.17602/M2/M79436
	GU 831	R Mt IV	77G–L	doi:10.17602/M2/M79437	doi:10.17602/M2/M79438
	GU 833	Canine	25T–X	doi:10.17602/M2/M78886	doi:10.17602/M2/M78887
	GU 834	R Distal humerus	54E–I	doi:10.17602/M2/M78957	doi:10.17602/M2/M78958
	GU 835	R Scaphoid	56A–D	doi:10.17602/M2/M79439	doi:10.17602/M2/M79440

(*Continued*)

Continued.

Taxon	Specimen	Element	Figure	Zipped .tiff stack	Surface mesh
	GU 842	L Proximal radius	55C	doi:10.17602/M2/M79013	doi:10.17602/M2/M79014
	GU 844	Intermediate phalanx	63F–J	doi:10.17602/M2/M79441	doi:10.17602/M2/M79442
	GU 845	Intermediate phalanx	63K–O	doi:10.17602/M2/M79443	doi:10.17602/M2/M79444
	GU 847	R Mc V	61A–F	doi:10.17602/M2/M78971	doi:10.17602/M2/M78972
	GU 1217	R Mc III	59A–E	doi:10.17602/M2/M80061	doi:10.17602/M2/M80062
	GU 1676	Incisor	23A–E	doi:10.17602/M2/M84601	doi:10.17602/M2/M84336
	GU 1701	Dentary	18	doi:10.17602/M2/M83547	doi:10.17602/M2/M83540
	GU 1704	R Mc V	61G–L	doi:10.17602/M2/M78975	doi:10.17602/M2/M78976
	GU 7003	Axis	46	doi:10.17602/M2/M83647	Centrum: doi:10.17602/M2/M83646 Spinous process: doi:10.17602/M2/M83645
	GU 7004	Mandible with Rp2-m3, Lp2-m2, symphysis	9	Rp2-m3 doi:10.17602/M2/M154753 Lp3-m2 doi:10.17602/M2/M154600 Symphysis with Lp2 doi:10.17602/M2/M154918	Rp2-m3 doi:10.17602/M2/M158524 Lp3-m2 doi:10.17602/M2/M158475 Symphysis with Lp2 doi:10.17602/M2/M158525
	GU 7005	R Proximal ulna	55A–D	doi:10.17602/M2/M79143	doi:10.17602/M2/M79151
	GU 7007	L Mc II	58G–L	doi:10.17602/M2/M78977	doi:10.17602/M2/M78978
	GU 7008	Proximal phalanx	62D–G	doi:10.17602/M2/M80063	doi:10.17602/M2/M80064
	GU 7009	Intermediate phalanx	63A–E	doi:10.17602/M2/M80065	doi:10.17602/M2/M80066
	GU 7015	Rdp1	27E–H	doi:10.17602/M2/M84620	doi:10.17602/M2/M84621
	GU 7019	R Distal radius	55D	doi:10.17602/M2/M79015	doi:10.17602/M2/M79016
	GU 7021	Terminal phalanx	64A, B	doi:10.17602/M2/M80067	doi:10.17602/M2/M80068
	GU 7023	RdP3-4	37	doi:10.17602/M2/M78995	doi:10.17602/M2/M78996
	GU 8017	Caudal vertebra	52A–F	doi:10.17602/M2/M84622	doi:10.17602/M2/M83822
	GU 8018	L Patella	70A–C	doi:10.17602/M2/M80069	doi:10.17602/M2/M80070
	GU 8020	LdP1	27A–D	doi:10.17602/M2/M78999	doi:10.17602/M2/M79000
	GU 8023	Incisor	23J–N	doi:10.17602/M2/M84614	doi:10.17602/M2/M84615
	GU 8026	Incisor	23T–X	doi:10.17602/M2/M84616	doi:10.17602/M2/M84617
	GU 8029	Intermediate phalanx	63P–T	doi:10.17602/M2/M80136	doi:10.17602/M2/M80137
	GU 8030	Incisor	23Y–BB	doi:10.17602/M2/M84611	doi:10.17602/M2/M84612
	GU 8033	Incisor	23F–I	doi:10.17602/M2/M84609	doi:10.17602/M2/M84353
	GU 8034	Incisor	23O–S	doi:10.17602/M2/M84613	doi:10.17602/M2/M84348
	GU 9002	Symphysis	10	doi:10.17602/M2/M158471	doi:10.17602/M2/M158472
	GU 9006	Lp4	31A–C	doi:10.17602/M2/M78997	doi:10.17602/M2/M78998
	WIF/A 1190	L Calcaneus	73I, J 74A–D	doi:10.17602/M2/M80071	doi:10.17602/M2/M80072
	WIF/A 1192	L Magnum	57I–M	doi:10.17602/M2/M80073	doi:10.17602/M2/M80074
	WIF/A 4216	L Astragalus	72M–P	doi:10.17602/M2/M83521	doi:10.17602/M2/M83514
	WIF/A 4219	RM3	39E	doi:10.17602/M2/M78987	doi:10.17602/M2/M78988
	WIF/A 4220	RM3	39D–F	doi:10.17602/M2/M78990	doi:10.17602/M2/M78991
	WIF/A 4221	RM3	39A–C	doi:10.17602/M2/M78992	doi:10.17602/M2/M78993
	WIF/A 4255	Lp4	31D–F	doi:10.17602/M2/M79007	doi:10.17602/M2/M79008
	WIF/A 4264	Lp4	31G–I	doi:10.17602/M2/M79009	doi:10.17602/M2/M79010

APPENDIX 2. Description of characters and states used in parsimony analyses, with additional discussion of selected characters.

Each character used in the parsimony analyses for this study is described, including various states and their scores. Citations indicate sources with similar (not necessarily identical) characters, with the number of the appropriate character from a given study given after the colon. Note that in most cases the character used here is a modified version of a character from a given source, and in some cases a character from another source is cited that only partly corresponds to the character in question for this study. In other cases, a single character in this study might relate to multiple characters in another source.

The matrix for this study is an expanded version of the one used by Rose et al. (2014b). Whereas the matrix of Rose et al. (2014b) focused on perissodactyls and included only a few representative afrotheres, that of Cooper et al. (2014), who also addressed anthracobunid and cambaythere relationships, had essentially the converse focus. The matrix of Cooper et al. (2014) was modified from Barrow et al. (2010), which was based on Seiffert (2007). Thus, the Cooper et al. (2014) matrix focused on afrotheres and included only a few perissodactyls. For this study, we expanded the representation of afrotheres, as well as including additional laurasiatheres and representatives of Euarchontoglires, in order to more fully test the position of cambaytheres. We also expanded the number of characters, including a large number drawn from Seiffert (2007), primarily to address afrothere relationships.

(1) Posterior nasal: narrow, not contacting lacrimal (0); broad transverse suture with frontal (1). (Holbrook, 1999:C2, 2001:C2, 2009:1; Froehlich, 2002:4; Seiffert, 2007:321, 322; Kondrashov and Lucas, 2012:77; Rose et al., 2014b:1)

In eutherians, the most widespread condition involves narrow nasals that generally don't contact the lacrimals but do intrude between the frontal bones. This condition typically means that the maxilla and frontal contact each other on the rostrum, separating the lacrimal and nasal; Seiffert (2007:321) essentially scored nasal-lacrimal contact as an expression of maxilla-frontal contact.

Nasolacrimal contact is found in most perissodactyls, as well as a number of other mammals, including many

marsupials. However, the nature of this contact is qualitatively different in perissodactyls and derives from the distinctive shape of their nasal bones. In many marsupials, such as *Didelphis*, the two nasal bones form a diamond shape and the lateral corners of the diamond extend to contact the lacrimal. The posterior end of the nasals intrudes between the frontal bones. In perissodactyls, the nasals are posteriorly broad and have a nearly transverse suture with the frontal bones, such that the nasals are more or less triangular in shape, both individually and as a pair. The posterolateral corners of this triangle often make contact with the lacrimal bones. Although the contact is absent in some taxa, such as *Tapirus*, the general shape of the nasals is conserved.

(2) Length of postorbital portion of skull: shorter than preorbital portion (0); about equal to preorbital portion (1); longer than preorbital portion (2). (Froehlich, 2002:14; Rose et al., 2014b:2)

     The relative lengths of the preorbital and postorbital regions of the skull vary considerably among mammals, although the most common condition among the taxa examined here is the two regions being roughly equal in length. Froehlich (1999, 2002) included this character to distinguish brontotheriids, which generally have a relatively short preorbital region, from other perissodactyls.

(3) Position of orbits: over molars (0); over premolars or more anterior (1). (Fischer and Tassy, 1993:56; Seiffert, 2007:318; Kondrashov and Lucas, 2012:86; Rose et al., 2014b:3)

     The position of the orbits has been used as a possible synapomorphy of tethytheres, where the orbits are placed more anteriorly compared with many other mammals (e.g., Fischer and Tassy, 1993).

(4) Premaxilla ascending process: contacts nasals (0); ascending process present, no nasal contact (1). (Novacek, 1986:4; Novacek and Wyss, 1986:68; Court, 1992:2; Holbrook, 1999:C4, 2001:C4, 2009:2; Colbert, 2005:60; Rose et al., 2014b:4)

     In many mammals, the premaxilla alone forms the posterior or lateral border of the narial opening and contacts the nasal dorsally. In some taxa, the premaxilla does not contact the nasal, and as a consequence the maxilla forms part of the narial border. There are (at least) two different conditions where this is observed. In some instances, the ascending process of the premaxilla is still quite prominent but no longer contacts the nasal due to some change in the nature of the narial opening, such as the opening becoming deeply retracted, as in *Tapirus*. In this case, the premaxilla is still prominent and often is more robust in order to house the incisor arcade without the additional structural support of the surrounding bones. In the second condition, the ascending process is greatly reduced, and this largely accounts for its lack of contact with the nasal. This is typical of rhinocerotids, in which the premaxilla in general is much reduced.

(5) Orientation of caudal border of premaxilla: vertical (0); dorsocaudally oblique resulting in tapering of dorsocaudal portion (1). (Seiffert, 2007:315)

(6) Caudal extent of premaxilla: short, not approaching frontal (0); extends caudally to approach or contact frontal (1). (Seiffert, 2007:320)

     In some mammals, such as proboscideans, sirenians, and rodents, the ascending ramus is so robust and posteriorly extensive that it approaches or even contacts the frontal.

(7) Incisive foramen: paired (0); single median (1). (Court, 1992:3; Thewissen and Domning, 1992:18; Holbrook, 1999:C5, 2001:C5, 2009:3; Colbert, 2005:70; Seiffert, 2007:298; Rose et al., 2014b:5)

     The incisive foramen houses the incisive duct and is a paired bilateral structure, such that mammals typically possess two foramina. The left and right incisive foramina can fuse into a single, large median opening, as in *Tapirus*.

(8) Rostral opening of infraorbital foramen: over or rostral to P2 (0); over P3 (1); over P4 (2); over M1 (3); over M2 or M3 (4). (Holbrook, 1999:C7, 2001:C7; Colbert, 2005:67; Seiffert, 2007:311; Ladevèze et al., 2010:23; Kondrashov and Lucas, 2012:76)

     The typical position of the infraorbital foramen in mammals is over the upper premolars; in perissodactyls, it is usually found over P3.

(9) Tuber maxillae: weak or absent in adult (0); prominent in adult (1). (Fischer and Tassy, 1993:67; Froehlich, 2002:9; Rose et al., 2014b:6)

     In a number of groups, including perissodactyls, the portion of the maxilla that accommodates the posterior molars forms a tuberosity that extends into the orbit, forming its anteroventral floor.

(10) Orbital portion of maxilla: separated from frontal (0); contacting frontal (1). (Thewissen and Domning, 1992:16; Froehlich, 2002:6; Ladevèze et al., 2010:20; Kondrashov and Lucas, 2012:73; Rose et al., 2014b:7)

     The orbital portion of the maxilla is often separated from the frontal by the palatine and lacrimal, which contact each other. This condition is considered to be ancestral for mammals (Butler, 1956; Novacek and Wyss, 1986; Thewissen and Domning, 1992). In some mammals, including some perissodactyls, the maxilla has expanded between the palatine and the lacrimal to contact the frontal.

(11) Sphenopalatine foramen position: middle of orbit (0); near maxillary foramen (1). (Holbrook, 2009:4; Rose et al., 2014b:8)

     In many mammals, including many perissodactyls, the sphenopalatine foramen is positioned in the middle of the orbit. In some taxa, such as *Equus*, the sphenopalatine foramen is positioned much more anteriorly and lies near to the maxillary foramen.

(12) Common recess for sphenopalatine foramen and dorsal palatine foramen: present (0); absent (1). (Novacek, 1986:20; Thewissen and Domning, 1992:19; Seiffert, 2007:302)

     In a number of mammals, including *Phenacodus*, these two foramina share a common depression in the palatine. In other mammals, such as perissodactyls, these two foramina are separate and not found in a common depression, a condition that Novacek (1986) considered to be derived. Thewissen and Domning (1992) considered the polarity of this feature to be ambiguous.

(13) Contribution of ascending lamina of palatine in orbit: forms significant part of medial orbital wall (0): very small or absent from medial orbital wall (1). (Novacek, 1986:21; Seiffert, 2007:32; Rose et al., 2014b:97)

     In most mammals, including perissodactyls, the palatine is a distinct component of the orbital mosaic, contacting the frontal and either the maxilla or the lacrimal. In some mammals, such as proboscideans, the palatine is essentially absent from the orbit and has no contact with either the frontal or the lacrimal.

(14) Contact of palatine and frontal in orbit: absent (0); present (1). (Seiffert, 2007:326)

(15) Palatal vacuities: present (0); absent (1). (Seiffert, 2007:328; Rose et al., 2014b:10)

Palatal vacuities (or palatal fenestrae) are found in many marsupials but are uncommon in eutherians. Macroscelideans are one of the exceptions.

(16) Postpalatine torus: present (0); absent or weak (1). (Seiffert, 2007:304)

(17) Position of caudal border of palatines: rostral to or at mesial edge of M3 (0); at or just caudal to distal edge of M3 (1); well caudal of M3 (2). (Seiffert, 2007:305)

(18) Facial exposure of lacrimal: large or moderate, not contacting nasal (0); large or moderate, contacting nasal (1); small, not contacting nasal (2); absent (3). (Novacek, 1986:22; Court, 1992:8, 9; Holbrook, 1999:C3, 2001:C3, 2009:5; Froehlich, 2002:4; Rose et al., 2014b:11)

In most perissodactyls, the lacrimal has a significant facial process. In many mammals, including some perissodactyls, the lacrimal has very little exposure on the rostrum; instead, it is confined to the anterior rim of the orbit. In those perissodactyls that have a reduced lacrimal exposure, nasolacrimal contact is generally lost.

(19) Lacrimal foramen: absent (0); present, opening on facial portion of lacrimal (1); present, opening on orbital rim (2); present, opening within orbit (3). (Seiffert, 2007:306)

(20) Lacrimal tubercle: absent or indistinct (0); distinctly present (1). (Novacek, 1986:24; Thewissen and Domning, 1992:15; Froehlich, 2002:5; Seiffert, 2007:307; Ladevèze et al., 2010:21; Kondrashov and Lucas, 2012:74)

The lacrimals of some mammals, including perissodactyls, possess a small but distinct tubercle.

(21) Supraorbital process: absent, region over orbit does not project laterally from sagittal plane (0); present, short (1); present, long and extending ventrally (2). (Ladevèze et al., 2010:19; Kondrashov and Lucas, 2012:72; Rose et al., 2014b:12)

(22) Supraorbital foramen or notch: present (0); absent (1). (Holbrook, 1999:C9, 2001:C9, 2009:6; Rose et al., 2014b:13)

The supraorbital process of mammals sometimes possesses a notch or foramen that transmits the supraorbital neurovascular bundle. The conditions of either a notch or a foramen are related ontogenetically; a notch forms in the anterior edge of the supraorbital process then deepens and eventually closes anteriorly later in life. This can be observed in an ontogenetic series of skulls of *Equus*.

(23) Sinus canal and cranio-orbital foramen: canal and foramen absent (0); canal present, foramen opens cranial or lateral to sphenorbital fissure (1); canal present, foramen confluent with ethmoid foramen (2); canal present, foramen confluent with sphenorbital fissure (3). (Froehlich, 2002:3; Seiffert, 2007:331)

(24) Crista orbitotemporalis: absent (0); short, not extending rostrally beyond orbital foramina (1); long, extending rostrally into cranial part of orbit (2). (Seiffert, 2007:333)

(25) Optic foramen: anteriorly placed (0); posteriorly placed (1). (Hooker, 1989:2, 1994:33; Froehlich, 2002:7; Hooker and Dashzeveg, 2003:33, 2004:33; Holbrook, 2009:7; Rose et al., 2014b:14)

MacFadden (1976) was the first to use the posterior placement of the optic foramen as a synapomorphy for equids, at that time including *Hyracotherium*. In this condition, the optic foramen lies very close to the posteroventral group of orbital foramina: the anterior lacerate foramen (or sphenorbital fissure), the foramen rotundum, and the anterior opening of the alisphenoid canal. In most perissodactyls, and in many other mammals, the optic foramen is positioned more anteriorly, so that a distinct gap is present between it and the posteroventral foramina. The orbit is not well preserved in many fossils, and even with little distortion it can be difficult to interpret this character.

(26) Suboptic foramen: absent (0); present (1). (Seiffert, 2007:334)

(27) Ethmoid foramen: absent (0); present, rostral to sphenorbital fissure (1); within sphenorbital fissure (2); dorsal to optic foramen (3). (Thewissen and Domning, 1992:20; Seiffert, 2007:340)

Presence of this foramen is considered to be ancestral for mammals.

(28) Sphenorbital fissure: separate from foramen rotundum (0); confluent with foramen rotundum (1). (Novacek, 1986:33; Court, 1992:1; Thewissen and Domning, 1992:249; Froehlich, 2002:10; Seiffert, 2007:329; Ladevèze et al., 2010:15; Kondrashov and Lucas, 2012:84; Rose et al., 2014b:15)

In perissodactyls, these two foramina are separate and, along with the anterior opening of the alisphenoid canal, form the posteroventral group of orbital foramina. The confluence of these two foramina is considered to be the ancestral condition for placental mammals (Muller, 1935; Novacek, 1986; Thewissen and Domning, 1992).

(29) Contact of frontal and alisphenoid in orbit: absent (0); short (1); long (2). (Seiffert, 2007:335)

(30) Alisphenoid canal (posterior opening): present (0); absent (1). (Novacek, 1986:34; Court, 1992:20; Thewissen and Domning, 1992:25; Seiffert, 2007:336; Ladevèze et al., 2010:13; Kondrashov and Lucas, 2012:80; Rose et al., 2014b:16)

The presence of an alisphenoid canal is considered to be ancestral for placental mammals (Novacek, 1986; Thewissen and Domning, 1992), including perissodactyls. In extant macroscelideans, the canal is very short, and in *Rhynchocyon* it is variable, being separated from the foramen ovale by only a thin sliver of bone when present.

(31) Posterior opening of alisphenoid canal: separate from foramen ovale (0); in common depression with foramen ovale (1). (Ladevèze et al., 2010:14; Rose et al., 2014b:17)

(32) Foramen ovale: separate (0); confluent with middle lacerate foramen (1). (Hooker, 1989:1; Froehlich, 2002:12; Colbert, 2005:82; Holbrook, 2009:8; Rose et al., 2014b:18)

In perissodactyls, the alisphenoid forms the anterior border of the middle lacerate foramen, which lies anterior to the petrosal. In most perissodactyls, and in many mammals, the foramen ovale lies anterior to the middle lacerate foramen, completely enclosed in the alisphenoid bone. In a number of perissodactyls, these two foramina have become confluent. In some cases, a thin spine of bone projecting posteriorly demarcates the boundary between the two foramina, whereas in other cases there is essentially no obvious osteological indication that this opening represents two foramina. For the purposes of this study, these two conditions where the foramina are confluent are treated as a single state. MacFadden (1976) considered this feature to be a synapomorphy of equids (in which he included palaeotheriids).

(33) Foramen ovale position: anterior to glenoid fossa (0); medial to glenoid fossa (1). (Seiffert, 2007:337; Ladevèze et al., 2010:12; Rose et al., 2014b:19)

(34) Alisphenoid contribution to bulla: absent (0); present (1). (Seiffert, 2007:363)

(35) Tympanic process of basisphenoid: absent or weak (0); large (1). (Seiffert, 2007:353)

(36) Orbital portion of parietal: contacting alisphenoid (0); not contacting alisphenoid (1). (Court, 1992:14; Rose et al., 2014b:20)

In some perissodactyls, the parietal extends into the orbit and contacts the alisphenoid bone. In others, the frontal and squamosal contact each other in the posterior part of the orbit, precluding contact between the parietal and the alisphenoid.

(37) Zygomatic arch: complete (0); incomplete (1). (Seiffert, 2007:343)

(38) Anterior extent of jugal and zygomatic portion of maxilla: jugal extends anteriorly, forms anteroventral border of orbit (0); zygomatic portion of maxilla large, jugal more posterior and does not contribute to anteroventral border of orbit (1). (Court, 1992:11; Fischer and Tassy, 1993:32; Seiffert, 2007:313; Rose et al., 2014b:21)

In perissodactyls, the rostral portion of the jugal is robust and contacts the lacrimal bone, contributing to the anterior rim of the orbit. In some mammals, the rostral portion of the jugal is reduced and does not extend to the lacrimal.

(39) Posterior extent of jugal: strong, contributes to anterior portion of glenoid fossa (0); strong, extends to posterior border of glenoid fossa without contributing to articular surface (1); weak, splint-like, extends to anterior edge of glenoid fossa (2). (Novacek and Wyss, 1986:61; Court, 1992:12; Fischer and Tassy, 1993:34; Froehlich, 2002:11; Seiffert, 2007:348; Rose et al., 2014b:22)

In marsupials, some eutherians, and various early mammals, the articular surface of the mandibular fossa extends onto the jugal. In many eutherians, the mandibular fossa is restricted to the squamosal.

(40) Zygomatic process of squamosal: narrow (0); laterally expanded (1). (Novacek and Wyss, 1986:67; Court, 1992:10; Fischer and Tassy, 1993:58; Seiffert, 2007:345; Rose et al., 2014b:23)

Tassy (1981) and Novacek and Wyss (1986) described this condition as a derived feature of tethytheres. In other mammals, the squamosal portion of the zygomatic arch is less robust and more ventrally positioned.

(41) Preglenoid process: absent (0); present (1). (Holbrook, 2009:9; Ladevèze et al., 2010:18; Kondrashov and Lucas, 2012:78; Rose et al., 2014b:24)

In most perissodactyls, the anterior border of the mandibular fossa is relatively flat. In some taxa, notably palaeotheriids, the anterior edge is expanded ventrally into a mediolaterally elongated tuberosity, termed here the preglenoid process.

(42) Postglenoid process: absent or indistinct (0); small bump (1); dorsoventrall tall (2); recurved (3). (Seiffert, 2007:351)

(43) Postglenoid process orientation: facing anteriorly (0); facing anterolaterally (1). (Holbrook, 1999:C11, 2001:C11, 2009:10; Colbert, 2005:86; Rose et al., 2014b:25)

Most perissodactyls have a postglenoid process that is generally blunt or peg-like and faces roughly anteriorly. Some perissodactyls, such as ceratomorphs, have a postglenoid process that faces more medially.

(44) Postglenoid foramen: present (0); absent (1). (Court, 1992:21; Holbrook, 1999:C10, 2001:C10, 2009:11; Colbert, 2005:81; Seiffert, 2007:352; Kondrashov and Lucas, 2012:82; Rose et al., 2014b:26)

The postglenoid foramen is found in a wide variety of mammals, including many fossil perissodactyls, although it is absent in living forms. Prothero et al. (1988) considered loss or reduction of the postglenoid foramen to be a synapomorphy of a clade including cetaceans, tethytheres, hyracoids, perissodactyls, and a number of fossil taxa.

(45) Posttympanic process: about the same size as postglenoid process (0); shortened relative to postglenoid process (1). (Holbrook, 1999:C13, 2001:C13, 2009:12; Rose et al., 2014b:27)

The posttympanic process forms the posterior border of the external auditory meatus, and it is about the same length dorsoventrally as the postglenoid process in most perissodactyls. In some taxa, notably chalicotheres, the posttympanic process is shorter and does not extend as far ventrally as the postglenoid process. This may be related to the development of a prominent auditory bulla in these taxa.

(46) Exposure of mastoid: broad, posterior (0); narrow, lateral (1); absent (amastoidy) (2). (Novacek, 1986:60; Novacek and Wyss, 1986:60; Court, 1992:36; Thewissen and Domning, 1992:32; Froehlich, 2002:13; Seiffert, 2007:370; Holbrook, 2009:13; Ladevèze et al., 2010:7; Rose et al., 2014b:28)

The mastoid portion of the periotic typically is exposed on the posterior aspect of the skull in mammals. In perissodactyls, the only exposure of the mastoid on the surface of the skull is a narrow triangular portion on the lateral aspect of the braincase, between the squamosal and the exoccipital bones. In some other taxa, no mastoid exposure is visible on the skull surface, a condition termed amastoidy. Amastoidy is characteristic of tethytheres and hyracoids and has been used as evidence of a close relationship between these taxa, but the condition also occurs in a number of other mammals groups.

(47) Mastoid foramen: present, between mastoid and occipital-supraoccipital (0); absent (1). (Seiffert, 2007:369; Ladevèze et al., 2010:16; Kondrashov and Lucas, 2012:81; Rose et al., 2014b:29)

(48) Posttemporal (or percranial) canal: present at petrosal-squamosal suture, canal continues within suture (0); absent (1). (Ladevèze et al., 2010:17; Rose et al., 2014b:30)

Wible (1987) and MacPhee (1994) discussed the comparative anatomy of the percranial canal, which houses the great diploetic artery. MacPhee (1994) demonstrated the distinction between the percranial canal and the mastoid foramen, with which it is often confused.

(49) Tympanic roof: present, formed by squamosal, alisphenoid, or both (0); absent (piriform fenestra) (1). (Seiffert, 2007:357)

(50) Epitympanic sinus: absent (0); present (1). (Seiffert, 2007:358)

(51) Petrosal surface: smooth (0); ridged with a distinct rostral tympanic process (1). (Ladevèze et al., 2010:1)

(52) Subarcuate fossa: deep (0); shallow (1); absent (2). (Seiffert, 2007:365)

(53) Perilymphatic foramen: absent, divided into fenestra cochleae and aqueductus cochleae (0); present, undivided (1). (Seiffert, 2007:359)

(54) Aqueductus cochleae: dorsal (0); ventral, slit-like (1); ventral, not slit-like (2); absent (3). (Ladevèze et al., 2010:2)

(55) Tegmen tympani: uninflated, forms thin lamina lateral to facial nerve canal (0); inflated, forms barrel-shaped ossification lateral to facial nerve canal (1). (Ladevèze et al., 2010:3)

(56) Fossa for tensor tympani: shallow, anteroposteriorly elongate (0); circular pit, no groove (1). (Ladevèze et al., 2010:4)

(57) Sulcus for internal carotid artery: transpromontorial, forms anteroposterior groove on promontorium (0); absent (1). (Ladevèze et al., 2010:5; Kondrashov and Lucas, 2012:79; Rose et al., 2014b:31)

(58) Sulcus for proximal stapedial artery: present, forms groove that branches from transpromontorial sulcus anteromedial to fenestrae vestibuli and cochleae (0); absent (1). (Ladevèze et al., 2010:6; Rose et al., 2014b:32)

(59) Arterial canals on petrosal: absent (0); present, enclose internal carotid artery on promontorium or distal to stapes (1). (Seiffert, 2007:368)

(60) Rostral tympanic process of petrosal: tall, contributes to entrance of internal carotid artery, articulates with basisphenoid, or both (0); absent (1). (Seiffert, 2007:367)

(61) Caudal tympanic process of petrosal: absent, small, or only shields fenestra cochleae ventrally (0); large, shields fenestra cochleae, contributes to bulla, or both (1). (Seiffert, 2007:366)

(62) Tympanic process or medial section of caudal tympanic process of petrosal: absent (0); present but short (1); present and long, posteriorly developed, contacting or almost reaching tympanohyal and forming enclosure for facial nerve (2). (Ladevèze et al., 2010:8)

(63) Tympanic aperture of hiatus Fallopii: absent (0); present (1). (Ladevèze et al., 2010:9; Rose et al., 2014b:33)

(64) Lateral section of caudal tympanic process of petrosal: tiny or absent (0); well developed and separates stylomastoid foramen into two passages, one for facial nerve, one for auricular branch of vagus (1). (Ladevèze et al., 2010:10)

(65) Foramen for ramus superior of stapedial artery: present, through petrosal or petrosal squamosal suture on dorsolateral edge of epitympanic recess (0); present and anterolateral, through basioccipital (1); absent (2). (Ladevèze et al., 2010:11; Rose et al., 2014b:34)

(66) Ectotympanic: not attached (0); attached (1); attached and forms bulla (2). (Holbrook, 2009:14; Rose et al., 2014b:35)

The ectotympanic takes a number of forms among mammals, from a small, horseshoe-shaped bone loosely attached to the skull to a large hollow globe forming some or all of the auditory bulla and fused to the skull. In fossils, the ectotympanic is rarely preserved unless it forms a firmly attached bulla, although its presence may be inferred by facets on the petrosal or other parts of the ear region. Loosely attached ectotympanics vary among extant mammals, but in fossils (and sometimes even in extant mammals), when the ectotympanic is simply not preserved, it is often impossible to infer more than that it was present and not firmly attached. Thus, the states used here have been simplified to accommodate the uncertainty in fossils.

(67) Entotympanic: absent (0); small (1); large with significant contribution to bulla (2). (Seiffert, 2007:364)

(68) Bones enclosing foramen magnum: supraoccipital and exoccipitals (0); only exoccipitals (1). (Seiffert, 2007:372)

(69) Hypoglossal foramen: present (0); absent (1). (Court, 1992:38; Fischer and Tassy, 1993:35; Seiffert, 2007:334; Rose et al., 2014b:36)

Court (1992) interpreted the absence of a hypoglossal foramen as a synapomorphy of proboscideans and embrithopods.

(70) Height of mandibular condyle: below level of dentition (0); even with superior aspect of dentition (1); substantially superior to dentition (2). (Seiffert, 2007:286; Ladevèze et al., 2010:22; Kondrashov and Lucas, 2012:75; Rose et al., 2014b:37)

(71) Coronoid canal of dentary: absent (0); present (1). (Seiffert, 2007:280; Kondrashov and Lucas, 2012:83; Rose et al., 2014b:38)

(72) Lateral coronoid crest: weak or absent (0); well developed (1).

In some mammals, a crest is present on the lateral side of the horizontal ramus of the dentary that is continuous with the anterior edge of the coronoid process of the dentary. This crest defines the anterior edge of the masseteric fossa. In some mammals, such as some condylarths, the crest is especially prominent and projects laterally.

(73) Ventral border of mandibular angle: not expanded, inflected medially (0); not expanded, not inflected (1); expanded posteroventrally (2). (Seiffert, 2007:272)

(74) Number of thoracic vertebrae: 13 or fewer (0); 15 (1); 16 (2); 17 (3); 18 or more (4). (Fischer and Tassy, 1993:74; Seiffert, 2007:182; Rose et al., 2014b:39)

(75) Number of lumbar vertebrae: 3 (0); 4 (1); 5 (2); 6 (3); 7 (4); 8+ (5). (Thewissen and Domning, 1992:37; Froehlich, 2002:109; Seiffert, 2007:184)

(76) Orientation of lumbar spines: cranial (0); dorsal (1); caudal (2). (Seiffert, 2007:185)

(77) Number of sacral vertebrae: three or fewer (0); four (1); five (2); six (3). (Thewissen and Domning, 1992:38; Froehlich, 2002:110; Seiffert, 2007:188; Rose et al., 2014b:40)

(78) Number of vertebrae in sacroiliac joint: 1 (0); 2 (1); 3 (2); 4 (3). (Seiffert, 2007:189)

(79) Fusion of spines on caudal-most two sacral vertebrae: absent (0); present (1). (Seiffert, 2007:190)

(80) Clavicle: present (0); absent (1). (Seiffert, 2007:173)

(81) Acromion process of scapula: present (0); absent (1). (Holbrook, 1999:P1, 2001:P1, 2009:15; Seiffert, 2007:178)

(82) Shape of scapular glenoid fossa: flat (0); ventrally expanded (1); hook-like (2). (Seiffert, 2007:175; Rose et al., 2014b:41)

(83) Coracoid process of scapula: absent or not elongate (0); long and medially inflected (1). (Seiffert, 2007:176)

(84) Metacromion process of scapula: present (0); absent (1). (Seiffert, 2007:177)

(85) Relative size of supraspinous and infraspinous fossae of scapula: supraspinous larger than infraspinous (0); both fossae about equal (1); infraspinous larger than supraspinous (2). (Seiffert, 2007:179)

(86) Shape of cranial margin of scapula: arched, convex (0); flat (1). (Seiffert, 2007:180)

(87) Proximal projection of greater tuberosity of humerus: distal to humeral head (0); at about the level of the humeral head (1); proximal to humeral head (2). (Seiffert, 2007:191)

(88) Bicipital groove of humerus: simple (0); with distinct 'facet' (1). (Holbrook, 2009:16; Rose et al., 2014b:42)

In some palaeotheriids, the bicipital groove of the proximal humerus has a distinct smooth area resembling an articular facet.

(89) Ridge from deltopectoral crest extending onto distal anterior shaft of humerus: present (0); absent (1). (Rose et al., 2014b:43)

(90) Supinator crest of humerus: well developed and prominent (0); present but restricted to distal third of shaft (1); weak or absent (2). (Kondrashov and Lucas, 2012:45; Rose et al., 2014b:44)

(91) Lateral articular shelf (capitular tail) of humerus: absent or indistinct (0); present, tapered distally (1); present, extended distally (2). (Holbrook, 2009:17; Rose et al., 2014b:45)

(92) Placement of lateral articular shelf of humerus: at distal edge of capitulum (0); more proximal (1). (Seiffert, 2007:195)

(93) Proximolateral part of lateral articular shelf of humerus: flat or convex (0); concave and elaborated (1). (Rose et al., 2014b:46)

(94) Entepicondylar foramen: present (0); absent (1). (Holbrook, 1999:P3, 2001:P3, 2009:18; Froehlich, 2002:113; Seiffert, 2007:196; Ladevèze et al., 2010:44; Rose et al., 2014b:47)

(95) Position of entepicondylar foramen relative to trochlea: confluent with medial edge of trochlea (0); separate from medial edge of trochlea (1). (Seiffert, 2007:197)

(96) Medial epicondyle of humerus: very prominent, expands medially (0); prominent but not expanded (1); weak or absent (2). (Seiffert, 2007:193; Kondrashov and Lucas, 2012:44; Rose et al., 2014b:48)

(97) Supratrochlear foramen of humerus: absent (0); present (1). (Froehlich, 2002:112; Seiffert, 2007:203; Kondrashov and Lucas, 2012:43; Rose et al., 2014b:49)

(98) Capitulum of humerus: round (0); gently keeled (1); distinctly, sharply keeled (2). (Holbrook, 1999:P4, 2001:P4; Rose et al., 2014b:50)

(99) Proximal radius: with single fossa for humeral capitulum and trochlea (0); with separate fossae for capitulum and trochlea (1). (Ladevèze et al., 2010:45; Rose et al., 2014b:51)

(100) Proportions of head of radius: low width to depth ratio (0); high width to depth ratio (1). (Rose et al., 2014b:52)

(101) Lateral process of proximal radius: absent or weak (0); present (1). (Holbrook, 1999:P5, 2001:P5; Rose et al., 2014b:53)

(102) Articular surface of lateral process of proximal radius: shallowly concave (0); shallowly convex (1). (Rose et al., 2014b:54)

(103) Extent of proximal ulnar facet on posterior aspect of proximal radius: restricted to lateral half of face (0); extending medially as narrow strip across width of head (1). (Rose et al., 2014b:55)

(104) Shape of lateral process of proximal radius: not beveled (0); beveled to accommodate capitular tail (lateral articular shelf) (1). (Rose et al., 2014b:56)

(105) Styloid process of distal radius: distinct and projecting distally (0); weak or absent (1). (Rose et al., 2014b:57)

(106) Facets on distal radius: single concave fossa (0); split into separate scaphoid and lunar fossae (1). (Ladevèze et al., 2010:46; Rose et al., 2014b:58)

(107) Articular surface of distal radius: restricted to distal face (0); convex extension onto distopalmar surface (1). (Rose et al., 2014b:59)

(108) Orientation of olecranon process of ulna: proximal (0); posterior (1); medial (2). (Seiffert, 2007:205)

(109) Fusion of radius and ulna: absent (0); present (1). (Seiffert, 2007:207)

(110) Articulation between ulna and lunar: absent (0); present (1). (Seiffert, 2007:211)

(111) Contact between lunar and unciform: present (0); absent (1). (Fischer and Tassy, 1993:24; Froehlich, 2002:114; Seiffert, 2007:218; Rose et al., 2014b:60)

(112) Contact between lunar and trapezoid: absent (0); present (1). (Fischer and Tassy, 1993:25; Froehlich, 2002:114; Rose et al., 2014b:61)

(113) Centrale: present as separate ossification (0); absent or fused to scaphoid (1). (Seiffert, 2007:212; Ladevèze et al., 2010:47; Rose et al., 2014b:62)

(114) Trapezium: present (0); absent (1). (Seiffert, 2007:221)

(115) Contact between cuneiform and fifth metacarpal: absent (0); present (1). (Seiffert, 2007:216)

(116) Contact between unciform and third metacarpal: present (0); absent (1). (Seiffert, 2007:217)

(117) First metacarpal: present (0); absent (1). (Seiffert, 2007:224; Rose et al., 2014b:63)

The ancestral condition for mammals is five digits on the manus, with proximal, middle, and terminal phalanges on digits II to IV and proximal and terminal phalanges on the pollex (digit I). Digit reduction has occurred multiple times in mammalian evolution, and can include shortening of the digit without loss of elements, loss of distal elements, reduction of the size and functionality of the metacarpal, and finally loss of the entire metacarpal. Digit reduction typically involves initial reduction of the toes farthest from the midline of the manus and further reduction proceeding with digits closer to the midline. Thus, digit I is often the earliest digit to exhibit reduction in a lineage.

The disposition of digit I is known with certainty in taxa for which the skeleton in general is well known, particularly extant taxa. In some extinct taxa, the presence or absence of at least the first metacarpal can be inferred based on the presence or absence of facets on bones that articulate with it, namely, the trapezium and the medial side of the proximal second metacarpal. Such a facet exists on Mc II of *Cambaytherium thewissi*, and for that reason it is scored here as retaining the first metacarpal (state 0). No perissodactyl exhibits such a facet.

(118) Fifth manual digit: present with phalanges (0); present without phalanges (1); absent (2). (Holbrook, 2009:19; Rose et al., 2014b:64)

As with manual digit I, the ancestral condition for mammals is a functional digit V, with proximal, middle, and terminal phalanges. Like digit I, digit V often is one of the earliest manual digits to exhibit reduction in a digit-reducing lineage. In perissodactyls, digit V is present with phalanges ancestrally, although it is generally smaller than digits II to IV. Reduction and functional loss of this digit has occurred multiple times in perissodactyl history (Holbrook, 2001). Even when the digit itself is not preserved, the presence of Mc V can often be inferred from the proximal Mc IV, which will bear facets and a concavity on its lateral side to accommodate Mc V. Mc IV of *Cambaytherium thewissi* exhibits this evidence for Mc V. Although there is no direct evidence of phalanges, we have scored *Cambaytherium thewissi* as (0) for the purposes of this analysis.

(119) Anterior iliac crest: round (0); slightly concave or straight (1); deeply concave (2). (Holbrook, 1999:P7, 2001:P7; Froehlich, 2002:111; Rose et al., 2014b:65)

(120) Anterior inferior iliac spine: absent (0); present (1). (Seiffert, 2007:227)

(121) Ileopectineal tubercle: absent (0); present (1). (Seiffert, 2007:228)

(122) Epipubic bones: present (0); absent (1). (Seiffert, 2007:225)

(123) Fovea capitis of femur: centrally located (0); marginal (1). (Froehlich, 2002:117; Seiffert, 2007:237; Holbrook, 2009:20; Kondrashov and Lucas, 2012:53; Rose et al., 2014b:66)

(124) Femoral neck: absent (0); present (1). (Seiffert, 2007:240)

(125) Height of greater trochanter of femur: lower than head (0); about even with head (1); higher than head (2). (Froehlich, 2002:116; Seiffert, 2007:236; Holbrook, 2009:21; Ladevèze et al., 2010:48; Kondrashov and Lucas, 2012:50; Rose et al., 2014b:67)

(126) Orientation of lesser trochanter of femur: medially (0); posteromedially (1). (Kondrashov and Lucas, 2012:51; Rose et al., 2014b:68)

(127) Size of third trochanter of femur: small (0); large (1); absent (2). (Kondrashov and Lucas, 2012:52; Rose et al., 2014b:69)

(128) Supracondylar fossa of femur: absent (0); present (1). (Holbrook, 1999:P10, 2001:P10, 2009:22; Rose et al., 2014b:70)

(129) Trochlear ridges of distal femur: subequal (0); medial expanded with tuberosity (1). (Holbrook, 1999:P9, 2001:P9, 2009:23; Rose et al., 2014b:71)

(130) Ossified patella: absent (0); present (1). (Rose et al., 2014b:72)

(131) Medial malleolus of tibia: forms well-developed medial wall (0); prominent anteriorly, reduced and beveled posteriorly (1). (Rose et al., 2014b:73)

(132) Posterior process and median ridge of distal articulation of tibia: absent (0); present (1). (Rose et al., 2014b:74)

(133) 'Beaked' distal tibia articulation: absent (0); present (1). (Seiffert, 2007:248)

(134) Proximal fusion between tibia and fibula: absent (0); present (1). (Seiffert, 2007:246)

(135) Distal fusion between tibia and fibula: absent (0); present (1). (Seiffert, 2007:247; Kondrashov and Lucas, 2012:54)

(136) Astragalar canal: present (0); absent (1). (Fischer and Tassy, 1993:27; Hooker, 1994:35; Froehlich, 2002:123; Hooker and Dashzeveg, 2003:35, 2004:35; Ladevèze et al., 2010:49; Kondrashov and Lucas, 2012:62; Rose et al., 2014b:75)

(137) Orientation of trochlear ridges of astragalus: not oblique (essentially vertical) (0); oblique (1). (Rose et al., 2014b:76)

(138) Depth of trochlear groove of astragalus: nearly flat to concave (0); shallow groove, less than 25% of trochlea width (1); deep groove, more 25% of trochlear width (2). (Ladevèze et al., 2010:50; Kondrashov and Lucas, 2012:60; Rose et al., 2014b:77)

(139) Distal extent of medial trochlear ridge of astragalus: separate from distal edge of astragalus (0); reaching distal edge of astragalus (1). (Froehlich, 2002:120; Rose et al., 2014b:78)

(140) Height of lateral ridge of astragalus: at same level as medial trochlear ridge (0); extending proximal to medial trochlear ridge (1). (Seiffert, 2007:252)

(141) Articulation between lateral trochlear ridge of astragalus and distal fibula: poorly developed (0); sharply defined and interlocking (1). (Seiffert, 2007:253)

(142) Cotylar fossa of astragalus: absent (0); present (1). (Seiffert, 2007:259; Ladevèze et al., 2010:54; Kondrashov and Lucas, 2012:63; Rose et al., 2014b:79)

(143) Lateral process of astragalus: small (0); large and shelf-like (1). (Kondrashov and Lucas, 2012:56; Rose et al., 2014b:80)

(144) Tuberculum mediale of astragalus: absent (0); present (1). (Fischer and Tassy, 1993:28; Seiffert, 2007:260; Rose et al., 2014b:81)

(145) Squatting facet on dorsal side of astragalar neck: absent (0); present (1). (Ladevèze et al., 2010:53; Rose et al., 2014b:82)

(146) Shape and position of sustentacular facet of astragalus: oval and medial (0); angular and wide (1). (Ladevèze et al., 2010:51)

(147) Sustentacular facet of astragalus: separate from distal calcaneal and ectal facets (0); confluent with distal calcaneal facet (1); 'J'-shaped (2); confluent with ectal facet (3). (Holbrook, 1999:P13, 2001:P13, 2009:24; Colbert, 2005:88; Rose et al., 2014b:83)

(148) Posterior tubercle of medial trochlear facet of astragalus: small (0); protruding (1); extending proximomedially (2). (Rose et al., 2014b:84)

(149) Proximal calcaneal facet of astragalus: without distoectal lappet (0); with distoectal lappet (1). (Rose et al., 2014b:85)
     In some perissodactyls, there is a distal extension of the proximal calcaneal facet from the ectal part of its distal edge.

(150) Navicular facet of astragalus: spherical or convex (0); saddle-shaped (1); trochleated (2). (Hooker, 1994:34; Holbrook, 1999:P15, 2001:P14, 2009:25; Froehlich, 2002:118; Hooker and Dashzeveg, 2003:34, 2004:34; Seiffert, 2007:262; Ladevèze et al., 2010:52; Rose et al., 2014b:86)

(151) Contact between astragalus and cuboid: absent or negligible (0); present and well developed (1). (Froehlich, 2002:122; Seiffert, 2007:251; Kondrashov and Lucas, 2012:55)

(152) Lateral groove on calcaneus: present, broad (0); absent or indistinct (1). (Rose et al., 2014b:87)

(153) Plantar tubercle of calcaneus: absent or weak (0); prominent (1). (Seiffert, 2007:268)

(154) Articulation of calcaneus and distal fibula: present (0); absent (1). (Seiffert, 2007:269)

(155) Orientation of astragalar facet of calcaneus in lateral view: sloping proximally, with no angle formed within facet (0); sloping slightly proximally, facet has a rounded angle within it (1); perpendicular to long axis, facet forms sharp angle (2). (Rose et al., 2014b:88)

(156) Orientation of astragalar facet of calcaneus in anterior view: oriented at angle to long axis (0); oriented perpendicular to long axis (1); elongated along long axis (2). (Rose et al., 2014b:89)

(157) Shape of facet of sustentaculum of calcaneus: round or oval (0); narrow, straight on lateral edge (1). (Rose et al., 2014b:90)

(158) Orientation of distal edge of calcaneus between sustentaculum and cuboid facet: makes wide angle with long axis (0); makes acute angle with long axis (1); expanded into distal shelf that forms right angle (2). (Rose et al., 2014b:91)

(159) Shape of cuboid facet of calcaneus: not crescent-shaped (0); crescent-shaped (1). (Rose et al., 2014b:92)

(160) Peroneal tuberosity of calcaneus: large (0); present, moderate, projecting distally (1); small, indistinct, or absent (2). (Seiffert, 2007:265; Ladevèze et al., 2010:55; Kondrashov and Lucas, 2012:70; Rose et al., 2014b:93)

(161) Anterior contact between navicular and calcaneus: absent (0); present (1). (Rose et al., 2014b:94; Seiffert, 2007:267)

(162) Plantar process of navicular: present and prominent (0); weak or absent (1). (Seiffert, 2007:264; Rose et al., 2014b:95)

(163) Navicular and proximal ectocuneiform facets of cuboid: not confluent (0); confluent with distinct ridge (1). (Rose et al., 2014b:96)

(164) Entocuneiform: medially placed (0); posteriorly placed (1); absent (2). (Holbrook, 2009:26; Rose et al., 2014b:97)

(165) Entocuneiform and mesocuneiform: separate (0); fused (1). (Rose et al., 2014b:98)

(166) Mesocuneiform and navicular facets of entocuneiform: along anterior margin (0); mesocuneiform facet posterolateral to navicular facet (1). (Rose et al., 2014b:99)

(167) Cuboid: not contacting Mt III (0); contacts Mt III (1). (Froehlich, 2002:124; Holbrook, 2009:27; Rose et al., 2014b:100)

(168) First metatarsal: present with phalanges (0); present without phalanges, medially positioned (1); small and lacking phalanges, articulating with posterior Mt III (2); absent (3). (Holbrook, 1999:P16, 2001:P15; Dashzeveg and Hooker, 1997:3; Froehlich, 2002:125; Colbert, 2005:84; Seiffert, 2007:270; Ladevèze et al., 2010:57; Kondrashov and Lucas, 2012:71; Rose et al., 2014b:101)

     As with the manus, the ancestral condition for mammals is five digits on the pes, each with proximal and terminal phalanges, as well as middle phalanges on digits II to V. Digit reduction has occurred multiple times in mammalian evolution and typically follows the pattern described for the manus, where reduction begins with the toes farthest from the midline and proceeds inward.

     In contrast to the tetradactyl manus, which is ancestral for perissodactyls, a functionally tridactyl pes is ancestral for the order and found in essentially all perissodactyls except later horses. Although digits II to IV constitute the part of the pes

that contacts the substrate in locomotion, many perissodactyls do retain a vestige of the first metatarsal. Radinsky (1963b) demonstrated that a vestigial first metatarsal is present in living tapirs and in many fossil taxa and that this is the ancestral condition for the order.

In some groups, such as later rhinocerotids, the Mt I vestige may fuse to the entocuneiform, and in others, such as later horses, it might be lost entirely. Because the entocuneiform is rotated posteriorly, Mt I, when present, comes to lie adjacent to the posterior process extending from the proximal Mt III, bracing the tarsus posteriorly and providing an origin, at least in extant *Tapirus*, for the contrahentes muscles (Radinsky, 1963b). The contact between Mt I and Mt III is such that the posterior process of the proximal Mt III bears a facet for Mt I when the latter is present in this posterior position. Thus, the presence of Mt I can often be inferred based on the presence of the facet on Mt III. Such a facet is present on Mt III of *Cambaytherium thewissi*; therefore, we have scored this taxon as (2).

(169) Fifth metatarsal: present with phalanges (0); present without phalanges (1); absent (2). (Dashzeveg and Hooker, 1997:3; Holbrook, 1999:P16, 2001:P15; Froehlich, 2002:125; Colbert, 2005:84; Seiffert, 2007:271; Ladevèze et al., 2010:58; Kondrashov and Lucas, 2012:71; Rose et al., 2014b:102)

As with digit I, presence of pedal digit V with three phalanges is ancestral for mammals, and, because it and digit I are the farthest from the midline of the foot, it frequently exhibits reduction in those lineages where digit reduction is a trend. Even if digit V is not preserved in a fossil, a facet on the lateral aspect of the proximal Mt IV might indicate its presence.

Virtually no perissodactyl displays any evidence of Mt V, with two exceptions. Franzen (2007) reported a vestigial Mt V in the articulated pes of *Eurohippus messelensis* (here combined with *Propalaeotherium*) from Grube Messel. Wood et al. (2011) reported a similar structure in the articulated pes of *Arenahippus grangeri*. In both cases, the putative Mt V is a small, irregularly shaped knob of bone situated on the plantar aspect of the pes. Interestingly, neither study reported the presence of a vestigial Mt I—although Wood et al. indicated a possible Mt I facet on the entocuneiform—and it is possible that the bone identified as Mt V is actually Mt I, perhaps slightly displaced. The exact relationship of the alleged Mt V to other metatarsals, especially to Mt III, is not clear from the figures, and in both specimens there are difficulties in interpreting the pes: the *Eurohippus* specimen, like other Messel specimens, is articulated and embedded in resin in a way that limits what is visible, whereas the *Arenahippus* pes appears to be in a concretion and only visualized through computed tomography. It is notable that Franzen (2007) did not report the presence of Mt V in *Propalaeotherium*, which is known from equally well-preserved material as *Eurohippus*. Given the uncertainty regarding these elements, in this study Mt V of *Arenahippus* is scored as unknown ('?') and that of *Propalaeotherium* as absent (2).

The proximal Mt IV of *Cambaytherium thewissi* bears a narrow facet on its lateral aspect that we interpret as a facet for Mt V. Given the small size of the facet, we interpret Mt V as not well developed, and we therefore provisionally score it as present without phalanges (1).

(170) Distal phalanges: laterally compressed, as claws (0); dorsoventrally compressed, as hooves (1). (Kondrashov and Lucas, 2012:49; Rose et al., 2014b:103)

(171) Canine size: large (0); small (1); absent (2). (Hooker, 1989:10; Colbert, 2005:2; Seiffert, 2007:14, 16, 97, 98; Kondrashov and Lucas, 2012:23; Rose et al., 2014b:104)

Upper and lower canines are present in a number of early perissodactyls, as well as in many of the outgroups, and are presumably ancestral.

(172) Postcanine diastema: short (0); long (1); absent (2). (Hooker, 1989:15, 1994:32; Holbrook, 1999:D4, 2009:28; Froehlich, 2002:17; Hooker and Dashzeveg, 2003:32; Ladevèze et al., 2010:24, 34; Rose et al., 2014b:105)

Perissodactyls, like many mammals, typically have a gap between the canine and the anterior-most premolar. In the earliest perissodactyls, the gap is relatively short, but many later perissodactyls have a long postcanine diastema, more than twice the length of the anterior-most premolar. This lengthening may occur through changes in facial proportions, loss of anterior premolars, or both. In some taxa, there is no gap between the canine and the anterior-most premolar.

(173) Cusp relief of cheek teeth: sharp, generally conical (0); tall, bunodont cusps with little or no loph development (1); low, bunodont to bunolophodont (2); well-developed lophodonty with high lophs (3). (Kondrashov and Lucas, 2012:11; Rose et al., 2014b:106)

(174) Cheek tooth enamel surface: smooth (0); rugose (1). (Seiffert, 2007:85; Rose et al., 2014b:107)

(175) Fifth premolar: present (0); absent (1). (Seiffert, 2007:48, 101; Rose et al., 2014b:108)

The ancestral dental formula for eutherians is now reconstructed as including five premolars in the upper and lower jaws, based on a number of discoveries of Cretaceous eutherians (Wible et al., 2009). Given that four or fewer upper and lower premolars characterizes almost all extant and Cenozoic mammals, there is some question of what premolar position was lost initially. For the purposes of this study, we only scored the presence or absence of a fifth premolar without specifying which position is lost.

(176) First upper incisor: present (0); absent (1). (Seiffert, 2007:87)

(177) First or central upper incisor size: larger than second upper incisor (0); about equal to second upper incisor (1); smaller than second upper incisor (2). (Seiffert, 2007:88; Kondrashov and Lucas, 2012:85)

(178) Second upper incisor: present (0); absent (1). (Seiffert, 2007:90)

(179) Third upper incisor: present (0); absent (1). (Seiffert, 2007:92)

(180) Fourth upper incisor: present (0); absent (1). (Seiffert, 2007:94)

(181) Fifth upper incisor: present (0); absent (1). (Seiffert, 2007:95)

The ancestral number of upper incisors for therians is five, as seen in polyprotodont marsupials and some Cretaceous eutherians. Like many other living eutherians orders, perissodactyls have three or fewer upper incisors. (Holbrook, 1999:D1)

(182) Diastema between last upper incisor and upper canine: absent or short (0); longer than length of canine (1); longer than twice length of canine (2). (Seiffert, 2007:96)

(183) Number of roots of upper canine: 1 (0); 2 (1); 3 (2). (Seiffert, 2007:97)

(184) Metacone on upper canine: absent (0); present (1). (Seiffert, 2007:99)

(185) First upper premolar: present with diastema (0); present without diastema (1); absent (2). (Hooker, 1989:11; Holbrook, 1999:D5, 2009:29; Froehlich, 2002:18, 20; Hooker and Dashzeveg, 2004:20, 52; Seiffert, 2007:102; Ladevèze et al., 2010:25; Rose et al., 2014b:109)

In the taxa considered here, either the first upper premolar is positioned with short diastemata anterior and posterior to it or, as in the perissodactyls *Isectolophus* and *Heptodon*, there is no gap between P1 and P2. Some taxa lack a tooth at this position. Note that, in most mammals, the identity of the tooth at this position, when present, is usually a retained deciduous first upper premolar. Replacement of dP1 by a permanent P1 occurs in some taxa, including some perissodactyls, but replacement does not appear to occur in any Eocene perissodactyl lineages (Rose et al., 2018a). Given the difficulties in establishing the exact identity of the tooth retained at the first upper premolar locus in fossil taxa, for the purposes of this character for this study, no distinction is made between dP1 and P1.

(186) First upper premolar protocone: absent (0); small (1); large (2). (Seiffert, 2007:104)

(187) First upper premolar metacone: absent (0); small (1); large (2). (Seiffert, 2007:105)

(188) First upper premolar hypocone: absent (0); present (1). (Dashzeveg and Hooker, 1997:17; Colbert, 2005:28; Seiffert, 2007:106)

(189) P2: present (0); absent (1). (Seiffert, 2007:108)

(190) Diastema posterior to P2: absent (0); long (greater than P3 length) (1); short (less than or equal to P3 length) (2). (Rose et al., 2014b:110)

(191) P2 protocone: absent (0); small (1); large (2). (Seiffert, 2007:110)

(192) P2 metacone: absent (0); present, small, close to paracone (1); present, about as large as and separate from paracone (2). (Seiffert, 2007:111; Holbrook, 2009:30; Rose et al., 2014b:111)

(193) P2 metacone position: close to paracone (0); distant from paracone (1). (Froehlich, 2002:22; Seiffert, 2007:111; Rose et al., 2014b:112)

(194) P2 hypocone: absent (0); smaller than protocone (1); as large or larger than protocone (2). (Froehlich, 2002:21; Seiffert, 2007:112; Holbrook, 2009:31; Rose et al., 2014b:113)

As is the case with other premolars, when P2 is molarized, it possesses two lingual cusps, serially homologous with the protocone and hypocone of the upper molars. The historical homology of these cusps is less clear, particularly in perissodactyls, and Froehlich (1999, 2002), Holbrook (2009), and Rose et al. (2014b) avoided the issue of historical homology of these cusps by simply identifying the number of lingual cusps present. Seiffert (2007) specified the presence or absence of the hypocone (as well as its size), because in his taxonomic set it is generally clearer that the last lingual cusp to form is the distal one, i.e., the hypocone. We adopt Seiffert's description of this character here, with the caveat that it is possible that neither of the lingual cusps of the molarized P2 of some perissodactyls is historically homologous with the P2 hypocone of other taxa.

(195) P2 mesostyle: absent (0); present (1). (Seiffert, 2007:114)

(196) P3 size: smaller or nearly equal to P4 (0); larger than P4 (1). (Rose et al., 2014b:114)

(197) P3 parastyle: protruding, P3 mesial edge concave (0); not protruding, P3 mesial edge convex (1). (Rose et al., 2014b:115)

(198) P3 paraconule: absent or indistinct (0); present (1); present and lingually positioned (2). (Hooker, 1989:17, 1994:30; Froehlich, 2002:23, 25; Hooker and Dashzeveg, 2003:30, 2004:30; Seiffert, 2007:118; Holbrook, 2009:32; Rose et al., 2014b:116)

Granger (1908) argued that molarization of P3 in early equids involves enlargement and lingual displacement of the paraconule, which comes to assume a position that is serially homologous with the protocone of the upper molars. The cusp that is historically homologous with the protocone in the unmolarized P3 of early Eocene equids is distally positioned and thus is serially homologous with the upper molar hypocone. This pattern of cusp development and homology in P3 is distinct from what is observed in P4, where the last cusp to develop is the distal lingual cusp, or hypocone. In equids with fully molarized premolars, such as *Mesohippus*, P3 resembles the upper molars to the degree that it possesses a serial homolog of the upper molar paraconule, which in Granger's interpretation would be a neomorph. For the purposes of this study, *Mesohippus* is scored based on Granger's argument, with the caveat that this introduces an assumption regarding homologies that presumes that *Mesohippus* follows the equid pattern.

(199) P3 preparaconule crista: in line with connection to protocone (0); angled more buccally than connection to protocone (1). (Rose et al., 2014b:117)

(200) P3 metacone: absent (0); present, much smaller than paracone (1); present, comparable in size to paracone (2). (Hooker, 1989:30, 1994:29; Froehlich, 2002:29; Hooker and Dashzeveg, 2003:29, 2004:29; Seiffert, 2007:116; Kondrashov and Lucas, 2012:2; Rose et al., 2014b:118)

(201) P3 metaconule: absent or indistinct (0); present, small relative to paraconule (1); present, similar in size to paraconule (2). (Hooker, 1989:22; Froehlich, 2002:30; Seiffert, 2007:119; Rose et al., 2014b:119)

(202) P3 metaloph: absent, metaconule separate from ectoloph and protocone (0); metaconule connected to protocone but not to ectoloph (1); metaconule connects to ectoloph but not to protocone (2); metaloph complete but weak (3); metaloph complete and prominent (4). (Rose et al., 2014b:120)

(203) P3 protocone: absent (0); present (1). (Seiffert, 2007:115; Rose et al., 2014b:121)

(204) P3 endoprotocrista: absent (0); present, distal ridge (1); present, forming hypocone (2). (Hooker, 1989:19; Froehlich, 2002:27; Hooker and Dashzeveg, 2004:50; Rose et al., 2014b:122)

Holbrook (2015) established that the crest sometimes identified as the postprotocrista in perissodactyl premolars is actually a different crest, which he termed the endoprotocrista. Whereas the postprotocrista typically connects the protocone and the metaconule, the endoprotocrista extends distally and well lingual of the metaconule, instead often giving rise at its distal end to the hypocone. Thus, the endoprotocrista contributes to one of the modes of premolar molarization observed in perissodactyls.

(205) P3 hypocone: absent (0); small (1); large (2). (Seiffert, 2007:117)

(206) P3 mesostyle: absent (0); present (1). (Seiffert, 2007:121)

(207) P3 stylocone: absent (0); present (1). (Seiffert, 2007:123)

(208) P4 protocone: absent or indistinct (0); present, close to paracone in size (1). (Seiffert, 2007:128; Kondrashov and Lucas, 2012:3; Rose et al., 2014b:123)

(209) P4 paraconule: large and distinct (0); small (1); indistinct (2). (Hooker, 1989:24; Froehlich, 2002:31; Seiffert, 2007:132; Holbrook, 2009:33; Kondrashov and Lucas, 2012:7; Rose et al., 2014b:124)

(210) P4 preparaconule crista orientation: toward parastyle (0); toward paracone (1). (Rose et al., 2014b:125)

(211) P4 metacone: present, distinctly smaller than paracone (0); present, about equal in size to paracone (1); absent (2). (Seiffert, 2007:129; Ladevèze et al., 2010:27; Rose et al., 2014b:126)

(212) P4 metaconule: present, similar in size to paraconule (0); present, significantly smaller than paraconule (1); absent or indistinct (2). (Hooker, 1989:27; Froehlich, 2002:33; Hooker and Dashzeveg, 2004:47; Seiffert, 2007:133; Holbrook, 2009:34; Rose et al., 2014b:127)

(213) P4 metaconule position: distal to line connecting protocone and metacone (0); on line connecting protocone and metacone (1); mesial to line connecting protocone and metacone (2). (Hooker and Dashzeveg, 2004:49; Rose et al., 2014b:128)

(214) P4 endoprotocrista: absent (0); present as ridge joined to protocone (1); present, forming hypocone (2). (Hooker, 1989:25; Froehlich, 2002:35; Hooker and Dashzeveg, 2004:46; Rose et al., 2014b:129).
See comment under character 204.

(215) P4 metaloph: absent, no connections between protocone (or hypocone), metaconule, and ectoloph (0); metaconule connects to ectoloph, but not protocone or hypocone (1); metaconule connects to protocone or hypocone, but not ectoloph (2); metaloph complete but low or weak (3); metaloph complete and high (4). (Hooker and Dashzeveg, 2004:48; Rose et al., 2014b:130)

(216) P4 hypocone: absent (0); present, weak or poorly separated from protocone (1); present, strong and separate from protocone (2). (Seiffert, 2007:130; Rose et al., 2014b:131)

(217) P4 mesostyle: absent (0); small (1); large (2). (Seiffert, 2007:136)

(218) P4 ectostyle: absent (0); present (1). (Seiffert, 2007:134)

(219) P4 stylocone: absent (0); present (1). (Seiffert, 2007:137)

(220) P3 and P4 metacone position: distal to paracone (0); distolingual to paracone (1). (Hooker, 1989:28; Froehlich, 2002:37; Rose et al., 2014b:132)

(221) P3–4 cross-lophs: not 'U'-shaped (0); 'U'-shaped (1). (Hooker, 1989:21; Holbrook, 1999:D7, 2009:35; Rose et al., 2014b:133)
Radinsky (1965b) noted that the cross-lophs of the upper premolars of lophialetids formed a 'U'-shaped structure. In other early perissodactyls that are more lophodont, like most ceratomorphs, these lophs form a 'V'.

(222) M1 size: smaller or nearly equal to M2 (0); larger than M2 (1). (Fischer and Tassy, 1993:9; Seiffert, 2007:168; Rose et al., 2014b:134)

(223) M1 ectocingulum: absent (0); present but broken at paracone (1); present and continuous (2). (Hooker, 1994:20; Froehlich, 2002:43; Seiffert, 2007:150; Rose et al., 2014b:135)

(224) M2 ectocingulum: absent (0); present but broken on paracone (1); present and continuous (2). (Hooker, 1994:20; Froehlich, 2002:43; Seiffert, 2007:150; Rose et al., 2014b:136)

(225) Upper molar centrocrista: poorly developed (0); present, buccally flexed (1); present, not flexed (2). (Hooker, 1989:32, 1994:10; Froehlich, 2002:48, 52; Hooker and Dashzeveg, 2003:10, 2004:10; Seiffert, 2007:153; Holbrook, 2009:36; Rose et al., 2014b:137)

(226) Upper molar mesostyle: absent (0); weak, cingular (1); strong (2). (Hooker, 1989:33, 62, 1994:11; Froehlich, 2002:46; Hooker and Dashzeveg, 2003:11, 2004:11; Seiffert, 2007:157; Holbrook, 2009:37; Rose et al., 2014b:138)

(227) Upper molar paracone: not flattened (0); flattened buccally (1); pinched (2). (Hooker, 1989:54; Froehlich, 2002:47; Holbrook, 2009:38; Rose et al., 2014b:139)

(228) Lingual crest on upper molar paracone: absent (0); present (1). (Rose et al., 2014b:140)
In some perissodactyls, the lingual aspect of the upper molar paracone forms a short crest running lingually. This crest is distal to and separate from the protoloph.

(229) Upper molar metacone: not flattened (0); flattened buccally (1); part of convex ectoloph (2). (Hooker, 1989:35, 55; Dashzeveg and Hooker, 1997:4; Froehlich, 2002:50; Hooker and Dashzeveg, 2004:45; Colbert, 2005:8, 9, 10; Holbrook, 2009:39; Rose et al., 2014b:141)

(230) Upper molar metacone: tilting vertical, in line with paracone (0); metacone lingually tilted (1). (Hooker, 1989:55; Dashzeveg and Hooker, 1997:5; Froehlich, 2002:48; Hooker and Dashzeveg, 2004:44; Rose et al., 2014b:142)

(231) M1–2 postmetacrista: weak or absent (0); present and in line with paracone and metacone (1); present and buccally deflected (2). (Hooker, 1989:49, 61, 1994:23; Dashzeveg and Hooker, 1997:13, 15; Froehlich, 2002:60, 62; Hooker and Dashzeveg, 2003:23, 2004:23; Colbert, 2005:25, 27; Seiffert, 2007:167; Rose et al., 2014b:144)

(232) M3 postmetacrista: weak or absent (0); present and in line with paracone and metacone (1); present and buccally deflected (2).

(233) Upper molar protocone and hypocone shape: vertical (0); mesially recurved (1). (Hooker, 1989:66; Froehlich, 2002:51; Rose et al., 2014b:145)

(234) Upper molar paraconules: large and distinct (0); small or indistinct (1); merged into protoloph (2). (Hooker, 1989:36; Holbrook, 1999:D9, 2009:40; Froehlich, 2002:41, 42; Seiffert, 2007:159; Rose et al., 2014b:146)

(235) Upper molar paraconule position: midway between paracone and protocone (0); closer to protocone (1); closer to paracone (2). (Hooker, 1989:38; Rose et al., 2014b:147)

(236) M1–2 postparaconule crista: absent (0); present (1). (Seiffert, 2007:160)

(237) Upper molar metaconules: present (0); very small (1); absent (2). (Hooker, 1989:51, 53, 1994:9; Holbrook, 1999:D10, 2009:41; Froehlich, 2002:49; Hooker and Dashzeveg, 2003:9, 2004:9; Seiffert, 2007:161; Rose et al., 2014b:148)

(238) Upper molar metaconules or corresponding part of metalophs: on line between metacone and hypocone (0); mesial to line connecting metacone and hypocone (1). (Hooker, 1989:63, 1994:7; Hooker and Dashzeveg, 2003:7, 2004:7; Ladevèze et al., 2010:31; Rose et al., 2014b:149)

(239) Upper molar parastyles: small (0); large, teardrop-shaped (1); form crest with paracone (2); absent or no more than expansion of cingulum, much lower than paracone (3). (Hooker, 1994:24; Dashzeveg and Hooker, 1997:7; Holbrook, 1999:D8, 2009:42; Froehlich, 2002:38; Hooker and Dashzeveg, 2003:24, 2004:24; Seiffert, 2007:160; Rose et al., 2014b:150)

(240) Main mass of upper molar parastyle: in line with paracone and metacone (0); buccal to line connecting paracone and metacone (1). (Froehlich, 2002:40; Holbrook, 2009:43; Rose et al., 2014b:151)

(241) Upper molar parastyles: not recurved (0); distally recurved (1). (Hooker and Dashzeveg, 2004:42; Holbrook, 2009:44; Rose et al., 2014b:152)

(242) M2 stylocone: absent (0); present (1). (Seiffert, 2007:149)

(243) M3 parastyle: similar to that of M1–2 (0); projecting buccally (1). (Hooker, 1989:65; Hooker and Dashzeveg, 2004:43; Holbrook, 2009:45; Rose et al., 2014b:153)

(244) M1–2 paracone and metacone sizes: paracone distinctly larger than metacone (0); paracone and metacone about same size (1). (Ladevèze et al., 2010:28; Rose et al., 2014b:154)

(245) Upper molar preparaconule crista: toward parastyle (0); toward paracone, does not join (1); joined with paracone (2). (Hooker, 1994:2; Froehlich, 2002:55; Hooker and Dashzeveg, 2003:2, 2004:2; Holbrook, 2009:46; Rose et al., 2014b:155)

(246) Upper molar ectoloph-metaloph junction: anterior to metacone, separate (0); anterior to metacone, premetaconule crista bends back to join (1); joins at metacone (2). (Hooker, 1989:47, 1994:8; Dashzeveg and Hooker, 1997:9; Holbrook, 1999:D15, 2009:47; Froehlich, 2002:59; Colbert, 2005:18, 19, 20; Rose et al., 2014b:156)

(247) M1–2 postprotocrista: absent (0); weak (1); strong (2). (Seiffert, 2007:145)

(248) M1–2 hypocone: absent (0); present (1). (Hooker, 1989:52; Hooker and Dashzeveg, 2003:22, 2004:22; Seiffert, 2007:156; Ladevèze et al., 2010:32; Rose et al., 2014b:157)

(249) M2 posthypocrista: absent or indistinct (0); distinct, short, and mesiobuccally directed (1); distinct, long, and mesially directed (2); distinct, long, mesiobuccally directed, forming basin distal to metaloph (3). (Dashzeveg and Hooker, 1997:10; Rose et al., 2014b:158)

(250) M2 lingual cingulum: absent (0); present only as ridge spanning central valley (1); present, except at hypocone (2); present across entire lingual face (3). (Dashzeveg and Hooker, 1997:11; Colbert, 2005:22, 23; Ladevèze et al., 2010:30; Rose et al., 2014b:159)

(251) Buccal crest or cusp of upper molar hypocone: absent (0); present (1). (Rose et al., 2014b:160)
   In cambaytheres, the upper molar hypocones typically have either a crest that extends buccally or a cusp positioned buccal to the hypocone, giving it a 'doubled' appearance. The buccal cusp is distinct from and distal to the metaconule. Likewise, the buccal crest is distinct from the metaloph (or where the metaloph would be based on the metaconule position) and is not angled mesiobuccally as the metaloph typically is. The buccal crest is considered here to be formed by the merging of the buccal cusp; thus, we score the cusp and crest as representing the same basic morphology.

(252) M3 presence: present (0); absent (1). (Seiffert, 2007:169)

(253) Upper M3 size: distinctly smaller than M2 (0); about same size as M2 (1); distinctly larger than M2 (2). (Hooker, 1994:25; Froehlich, 2002:67; Hooker and Dashzeveg, 2003:25, 2004:25; Seiffert, 2007:169; Ladevèze et al., 2010:33; Kondrashov and Lucas, 2012:9; Rose et al., 2014b:161)

(254) M3 metacone: similar to that of M2 (0); lingually shifted (1); lingually shifted to nearly touching hypocone (2). (Froehlich, 2002:61; Holbrook, 2009:48; Rose et al., 2014b:162)

(255) M3 hypocone: absent (0); present, but distinctly smaller than M3 protocone (1); present, similar in size to M3 protocone (2). (Hooker, 1989:52; Hooker and Dashzeveg, 2003:22, 2004:22; Rose et al., 2014b:163)

(256) M3 hypocone position: at about same level as protocone (0); buccally shifted relative to protocone (1); lingually shifted relative to protocone (2). (Rose et al., 2014b:164)

(257) M3 hypostyle: absent (0); small or narrow cingulum (1); large shelf or cusp (2); posthypocrista continuous with postmetacrista, enclosing basin (3). (Rose et al., 2014b:165)

(258) M1–2: square or longer than broad (0); broader than long (1). (Hooker, 1994:21; Froehlich, 2002:64; Hooker and Dashzeveg, 2003:21, 2004:21; Holbrook, 2009:49; Rose et al., 2014b:166)

(259) First lower incisor: present (0); absent (1). (Seiffert, 2007:2)

(260) Second lower incisor: not tusk-like (0); enlarged, procumbent, and tusk-like (1); absent (2). (Seiffert, 2007:5; Rose et al., 2014b:167)

(261) Third lower incisor: present (0); absent (1). (Seiffert, 2007:9)

(262) Distal cusp on i3: absent (0); present (1); multicuspate (2). (Hooker, 1989:8; Colbert, 2005:4; Seiffert, 2007:10; Holbrook, 2009:50; Rose et al., 2014b:168)
   In most perissodactyls, i3 is a simple tooth with essentially a single cusp. In some taxa, such as *Lophialetes*, the distal portion of the tooth forms a small cusp, giving the impression of a thumb on a mitten (Radinsky, 1965b). Hooker (1989) considered the presence of this cusp to be ancestral for perissodactyls, but the polarity of this feature is ambiguous at best. Froehlich (1999, 2002) mistakenly described and scored this character for the upper third incisor.

(263) Fourth lower incisor: present (0); absent (1). (Seiffert, 2007:12)
   The ancestral number of upper incisors for therians is four, as seen in polyprotodont marsupials and some Cretaceous eutherians. Like many other living eutherian orders, perissodactyls have three or fewer lower incisors.

(264) Diastema between last lower incisor and lower canine: absent (0); shorter than length of canine (1); longer than but less than twice the length of lower canine (2); at least twice the length of lower canine (3). (Seiffert, 2007:13)

(265) Diastema between lower canine and adjacent premolar: absent (0); at least half as long but no longer than length of lower canine (1); longer than length of lower canine (2). (Seiffert, 2007:17)

(266) First lower premolar: present with short diastema (0); present with no diastema (1); absent (2). (Holbrook, 1999:D6, 2009:51; Froehlich, 2002:18; Hooker and Dashzeveg, 2004:32, 53; Colbert, 2005:49; Seiffert, 2007:18; Ladevèze et al., 2010:35; Rose et al., 2014b:169)
   As is the case for the first upper premolar, in the taxa considered here, the first lower premolar, when present, either is positioned with short diastemata anterior and posterior to it or, as in the perissodactyls *Isectolophus* and *Heptodon*, abuts the second lower premolar. Some taxa lack a tooth at this position. Note that, in most mammals, the identity of the tooth at this position, when present, is usually a retained deciduous first lower premolar. Replacement of dp1 by a permanent p1 occurs in some taxa, including some perissodactyls, but replacement does not appear to occur in any Eocene perissodactyl lineages (Rose et al., 2018a). Given that establishing the exact identity of the tooth retained at the first lower premolar locus is not always possible in fossil taxa, for the purposes of this character for this study no distinction is made between dp1 and p1.

(267) First lower premolar paraconid: absent or indistinct (0); present and distinct (1). (Seiffert, 2007:20)

(268) First lower premolar metaconid: absent or indistinct (0); present and distinct (1). (Seiffert, 2007:21)

(269) First lower premolar entoconid: absent (0); present (1). (Seiffert, 2007:22)

(270) p2: present (0); absent (1). (Seiffert, 2007:23)

(271) Post-p2 diastema: absent (0); short (less than or equal to p3) (1); long (greater than p3) (2). (Hooker and Dashzeveg, 2004:54; Rose et al., 2014b:170)

(272) p2 paraconid: absent (0); large and distinct without paralophid (1); present with paralophid (2); paralophid forming loop enclosing mesial basin (3). (Seiffert, 2007:25; Rose et al., 2014b:171)

(273) p2 metaconid: absent (0); very small swelling on protoconid slope (1); distinct, small, and distolingual to protoconid (2); large and lingual to protoconid (3). (Seiffert, 2007:26; Rose et al., 2014b:172)

(274) p2 talonid: shelf or ridge with no distinct cusps (0); small, medially placed hypoconid present (1); large, medially placed hypoconid with well-developed metalophid (2); large, buccally placed hypoconid with well-developed metalophid, entoconid absent (3); large, buccally placed hypoconid with well-developed metalophid, entoconid present (4). (Seiffert, 2007:27, 28; Rose et al., 2014b:173)

(275) p3 paraconid: absent or indistinct (0); present but small (1); present, large and distinct (2); part of well-developed paralophid (3). (Dashzeveg and Hooker, 1997:23; Hooker and Dashzeveg, 2003:31, 2004:31; Colbert, 2005:50; Seiffert, 2007:29)

(276) p3 metaconid: absent (0); present, close to protoconid (1); present, closer to margin of tooth than to protoconid (2). (Dashzeveg and Hooker, 1997:22; Froehlich, 2002:69, 70; Colbert, 2005:51; Seiffert, 2007:30; Holbrook, 2009:52; Ladevèze et al., 2010:36; Rose et al., 2014b:174)

(277) p3 metaconid size: less than half the height of protoconid (including absent) (0); more than half the height of protoconid but still distinctly smaller (1); about equal in size to protoconid (2). (Rose et al., 2014b:175)

(278) p3 hypoconid: small (0); large (1); absent (2). (Froehlich, 2002:72; Seiffert, 2007:31; Rose et al., 2014b:176)

(279) p3 entoconid: absent (0); present, distinctly smaller than hypoconid (1); present, comparable in size to hypoconid (2). (Fischer and Tassy, 1993:13; Seiffert, 2007:32; Rose et al., 2014b:177)

(280) p3 paraconid or paralophid: paraconid not distinct, paralophid no more than short, mesial preprotocristid (0); paraconid distinct cusp, with or without paracristid (1); paralophid well developed without distinct paraconid, defines valley between paralophid and metaconid/protoconid (2). (Seiffert, 2007:29; Rose et al., 2014b:178)

(281) p4 paraconid and paralophid: absent (0); distinct cusp, with or without paracristid (1); paralophid well developed without paraconid, mesially or mesiolingually directed (2); paralophid well developed without paraconid, extends lingually close to mesial wall (3). (Seiffert, 2007:35; Rose et al., 2014b:179)

(282) p4 width: distinctly narrower than m1 (0); as wide or almost as wide as m1 (1); wider than m1 (2). (Kondrashov and Lucas, 2012:28; Rose et al., 2014b:180)

(283) p4 metaconid: absent (0); present, much smaller than protoconid (1); present, about same size as protoconid (2); present, taller than protoconid (3). (Seiffert, 2007:36; Ladevèze et al., 2010:37; Kondrashov and Lucas, 2012:26; Rose et al., 2014b:181)

(284) p4 metaconid position: transverse (i.e., directly lingual) relative to protoconid (0); distal to protoconid (1).

(285) p4 hypoconid: absent or indistinct (0); present but less than half the height of protoconid (1); present and greater than half the height of protoconid (2). (Seiffert, 2007:40)

(286) p4 hypoconid position: lingually placed (0); centrally placed (1); buccally placed (2). (Seiffert, 2007:43)

(287) p4 entoconid: absent or weak (0); present and distinct (1). (Froehlich, 2002:75; Seiffert, 2007:39; Holbrook, 2009:53; Rose et al., 2014b:182)

(288) Ratio of p4 length to m1 length: greater than 1 (0); at least 0.8 but less than 1 (1); less than 0.8 (2). (Seiffert, 2007:49; Froehlich, 2002:78)

(289) m1 and m2 occlusal area: m1 area greater than m2 area (0); m1 and m2 about equal in area (1); m1 area less than m2 area (2). (Seiffert, 2007:51)

(290) Lower m3 size: larger than m2 in area (0); about equal in size to m2 (1); smaller than m2 in area (2); m3 absent (3). (Seiffert, 2007:81; Ladevèze et al., 2010:39)

(291) m1 paraconid or paralophid: distinct, separate paraconid cusp (0); distinct paraconid at lingual end of paralophid appressed to protolophid (1); paralophid extending lingually without distinct paraconid, separate from metaconid (2); paralophid extending lingually and connected to mesial crest from metaconid (3); paralophid extending mesiolingually with valley between it and protolophid (4); short lingually extending paralophid and buccally extending crest from metaconid meeting at mid-protolophid (5); paraconid and paralophid absent or indistinct (6). (Froehlich, 2002:86; Seiffert, 2007:57, 58; Ladevèze et al., 2010:38; Rose et al., 2014b:183)

(292) m3 protolophid shape: straight (0); buccal portion angled more distolingually than lingual portion (1); lingual portion angled more distolingually than rest (2). (Rose et al., 2014b:184)

(293) Lower molar protolophid notch: deeply notched nearly to base of cusps (0); shallowly notched to flat (1). (Hooker, 1994:5; Froehlich, 2002:89; Hooker and Dashzeveg, 2003:5, 2004:5; Seiffert, 2007:74; Holbrook, 2009:55; Ladevèze et al., 2010:41; Rose et al., 2014b:185)

(294) Lower molar twinned metaconids: absent (0); present (1). (Hooker, 1989:37, 1994:3, 4; Holbrook, 1999:D13, 2009:54; Froehlich, 2002:83, 84; Hooker and Dashzeveg, 2003:3, 2004:3; Rose et al., 2014b:186)

     Hooker (1994) made a distinction between metastylids and twinned metaconids on lower cheek teeth of perissodactyls and supported this by noting the presence of both cusps in certain perissodactyl taxa.

(295) Lower molar protolophid connection to metaconid: protolophid connects to mesial metaconid or between mesial and distal metaconids (0); protolophid connects exclusively to distal metaconid (1). (Rose et al., 2014b:187)

     This character applies only to taxa that exhibit twinned metaconids.

(296) Lower molar metaconid buttress: absent (0); lingual (1); buccal (2). (Hooker and Dashzeveg, 2003:13, 2004:13; Seiffert, 2007:54; Rose et al., 2014b:188)

     Hooker and Dashzeveg (2003, 2004) used the term 'metaconid buttress' for a crest extending from the metaconid either distally or labiodistally. Seiffert (2007) described variation in lower molar postmetacristids that, at least in part, matches the morphology described by Hooker and Dashzeveg (2003, 2004).

(297) Mesial crest of lower molar metaconid: present (0); absent (1). (Hooker and Dashzeveg, 2004:41; Seiffert, 2007:78; Rose et al., 2014b:189)

(298) Height of lower molar metaconids: lower than protoconids (0); about equal to height of protoconids (1); higher than protoconids (2). (Seiffert, 2007:59)

(299) Lower molar metastylids: strong (0); weak (1); absent (2). (Hooker, 1994:6; Froehlich, 2002:85; Hooker and Dashzeveg, 2003:6, 2004:6; Seiffert, 2007:54; Rose et al., 2014b:190)

Hooker (1994) distinguished between metastylids and twinned metaconids, arguing that both were present in some perisso-dactyl taxa. Seiffert (2007) included the development of metastylids as part of his character states for lower molar metacristids.

(300) Lower molar cristid obliqua: oblique, contacts middle of protolophid (0); oblique, contacts lingual cusps (1); longitudinal (2); absent (3). (Hooker, 1994:14; Holbrook, 1999:D12, 2009:56; Froehlich, 2002:80; Hooker and Dashzeveg, 2003:14, 2004:14; Seiffert, 2007:72; Rose et al., 2014b:191)

(301) m2 cristid obliqua shape: straight (0); bowed buccally (1); bowed buccally forming continuous arc with hypolophid (2); bowed lingually (3). (Hooker and Dashzeveg, 2003:4, 2004:4; Rose et al., 2014b:192)

(302) m3 cristid obliqua shape: straight (0); bowed buccally (1); forming continuous arc with hypolophid (2); bowed lingually (3). (Hooker and Dashzeveg, 2003:4, 2004:4; Rose et al., 2014b:193)

(303) Height of cristid obliqua within valley between trigonid and talonid: cristid obliqua very low or interrupted, valley wide and deep (0); valley filled or reduced by cristid obliqua or encroaching bases of cusps (1). (Seiffert, 2007:71; Rose et al., 2014b:194)

(304) Lower molar talonid height: much lower than trigonid (0); about same height as trigonid (1). (Seiffert, 2007:55; Kondrashov and Lucas, 2012:29; Rose et al., 2014b:195)

(305) Lower molar talonid length: talonid absent (0); shorter than trigonid (1); longer than trigonid (2). (Seiffert, 2007:63)

(306) Lower molar hypoconids: present (0); absent (1). (Seiffert, 2007:62)

(307) Lower molar entoconids: present (0); absent (1). (Seiffert, 2007:60)

(308) m3 hypolophid: incomplete (0); complete, lingual and buccal cristids about equal (1); complete, buccal cristid longer than lingual (2). (Hooker, 1994:28; Froehlich, 2002:91; Hooker and Dashzeveg, 2003:28, 37, 2004:28, 37; Holbrook, 2009:58; Rose et al., 2014b:196)

(309) m3 hypolophid shape: straight (0); buccal portion angled more distolingually than lingual portion (1); slightly concave distally (2); lingual portion angled more distobuccally than buccal portion (3). (Rose et al., 2014b:197)

(310) Lower molar posthypocristid: present (0); absent (1). (Dashzeveg and Hooker, 1997:26; Froehlich, 2002:96, 97; Colbert, 2005:41; Rose et al., 2014b:198)

(311) Lower molar postentocristid: absent (0); present (1). (Hooker, 1989:44; Froehlich, 2002:96, 97; Rose et al., 2014b:199)

(312) m1 postentoconulid: absent (0); present as separate cusp (1); present and connected by crest to hypoconulid (2).

(313) m3 postentoconulid: absent (0); present, small (1); present, large (2); medial extension of lophoid loop (3). (Fischer and Tassy, 1993:3; Rose et al., 2014b:200)

Some taxa exhibit a cusp lingual to the hypoconulid. This is particularly evident on m3 in anthracobunids, cambaytheres, early proboscideans, and desmostylians, but it is sometimes present on m1 (see character 312). This cusp has been referred to by a number of terms, including as a 'twinned heel' (West, 1980), 'doubled' or 'twinned' hypoconulid (Wells and Gingerich, 1983), 'entoconid II' (Domning et al., 1986), or 'postentoconulid' (Shoshani, 1988; Fischer and Tassy, 1993; Gheerbrant et al., 2005b). For the purposes of character descriptions, we use the term 'postentoconulid' to refer to a cusp lingual to the hypoconulid.

The size of this cusp can approach that of the hypoconulid in some cases, giving the impression of a 'twinned' hypoconulid, and this condition has been used in the past as evidence of a close relationship between anthracobunids and proboscideans (West, 1980) or between anthracobunids and tethytheres (Wells and Gingerich, 1983; Fischer and Tassy, 1993). This is the condition scored here as '2.' A smaller but still distinct version of this cusp is observed in some early perissodactyls, particularly more buno-dont forms, and this condition is scored as '1.' Furthermore, more lophodont early perissodactyl taxa typically lack a distinct cusp in this position but instead have a lophoid hypoconulid that forms a tight 'U' shape, with a shorter lingual arm in the same position as the distinct postentoconulid in other taxa. We treat this loph as an expression of the postentoconulid and score it as '3' for those taxa that possess it.

(314) m1 and m2 hypoconulids: large (0); small (1); absent or cingular (2); form enlarged cingular shelf (3). (Froehlich, 2002:98; Seiffert, 2007:61; Ladevèze et al., 2010:40; Rose et al., 2014b:201)

(315) m1 and m2 hypoconulid position: buccal (0); medial (1); lingual (2). (Froehlich, 2002:99; Rose et al., 2014b:202)

(316) m2 hypoconulid: separate from hypolophid (0); closely appressed to hypolophid (1). (Froehlich, 2002:95; Rose et al., 2014b:203)

(317) m3 hypoconulid: present, large (0); small (1); absent or reduced to cingulum (2). (Hooker, 1989:59, 60; Dashzeveg and Hooker, 1997:16; Holbrook, 1999:D14, 2009:59; Froehlich, 2002:100, 101, 102; Colbert, 2005:40; Seiffert, 2007:80; Ladevèze et al., 2010:43; Rose et al., 2014b:204)

(318) m3 hypoconulid position: completely distal to hypoconid and entoconid (0); between hypoconid and entoconid, forming part of hypolophid where present (1). (Rose et al., 2014b:205)

(319) m3 hypoconulid connection: separate (0); joining mid-hypolophid (1); joins postcristid from hypoconid (2); joins postcristid from entoconid (3). (Holbrook, 2009:60; Rose et al., 2014b:206)

(320) Lower molar entoconulid: distinct (0); indistinct or absent (1). (Hooker, 1994:16; Hooker and Dashzeveg, 2003:16, 2004:16; Rose et al., 2014b:207)

The entoconulid is a cusp just mesial to the entoconid, usually forming as a swelling of the precristid of the entoconid.

(321) Enamel prism decussation: horizontal (0); vertical (1); radial enamel without Hunter-Schreger bands (2). (Rose et al., 2014b:208)

Koenigswald et al. (2011) discussed the variation in enamel microstructure observed in perissodactyls, with an emphasis on prism decussation and the orientations of Hunter-Schreger bands (HSB) that result from differences in decussation. Although there is considerable variation in enamel microstructure across Mammalia (e.g., Koenigswald, 1997), non-perissodactyls often lack HSB and possess non-decussating radial enamel.

Vertical decussation of enamel prisms is an unusual feature that is often evident as tiny but macroscopic ridges on the occlusal surface of the enamel. Among perissodactyls, vertical decussation is present in rhinocerotoids. In some rhinocerotoid taxa, both vertical and horizontal decussation is present in different layers of the enamel, a condition that Koenigswald et al. (2011) termed 'compound.' Compound enamel is present in *Hyrachyus* and the early rhinocerotid *Uintaceras*, and it is also present in depere-etellids. For this study, we score a taxon exhibiting any vertical decussation, including the compound condition, as having state 1.

APPENDIX 3. Measurements (in mm) of upper teeth of *Cambaytherium*. Group designations are for MANOVA comparing different samples: A, *C. thewissi* from Vastan Mine; B, *C. thewissi* from Mangrol; C, *C. thewissi* from Tadkeshwar; D, *C. gracilis* from Tadkeshwar. **Abbreviations**: **ant**, anterior; **bucc**, buccal; **L**, length; **ling**, lingual; **Lt**, left; **max**, maximum; **post**, posterior; **R**, right; **W**, width. *Estimate from broken edges; excluded from statistics.

Specimen no.	Group	P1L	P1W	P2L	P2W	P3L	P3W	P4L	P4W	M1Lbucc	M1Want	M1Wpost
GU 5	A							9.85	12.3	10.95	12.15	11.5
GU 12	A											
GU 18	A									10.6	11.5	10.8
GU 202	A									10.25	10.9	10.6
GU 204	A							10.3	12.35			
GU 402 Lt	A	8.65	5.1									
GU 402 R	A	8.3	5.1	11.95	8.2	11.15	11.85	9.65	11.8	11.05	11.4	11
GU 404 Lt	A	9.45	6.15	13.3	8.5	11.7	12.25	10.4	12.75	12.05	13.3	12.45
GU 404 R	A			13.35	8.55	11.8	12	10.1	12.6	11.8	13	12.6
GU 412	A							10.9	12.65			
GU 413	A									11.35	12.25	11.85
GU 415	A							9.35	12.15			
GU 417	A											
GU 418*	A											
GU 424	A									12.2	13.55	13.1
GU 425	A											
GU 426	A					10.55	11.55					
GU 430	A							9.25	13.1			
GU 661	A					10.95	12.2	9.85	12.8			
GU 662	A							8.9	11.2			
GU 663	A							9.7	11.9			
GU 665	A											
GU 730 Lt	A									11.25	12	11
GU 730 R	A									11.05	11.35	
GU 731	A									11.65	12.8	12.05
GU 732	A							9.8	11.75			
GU 784	A									11.9	13.4	12.8
GU 785	A											
GU 1221	A											
GU 1222	A									10.9	12.1	11.9
GU 1223	A									11.3	12.2	11.6
GU 1516	A											
GU 1615	A									11.6	12.5	12.9
GU 1616	A											
GU 1672	A											
GU 1683	A			11.35	9.7							
GU 1702a Lt	A			13.3	8.6							
GU 1702a R	A							11.2	14.4			
GU 1702b Lt	A											
GU 1702c Lt	A											
GU 1702d R	A					12.85	12.5	10.65	12.85			
GU 1708	A							9.25	12.05			
GU 1727	A			12.6*	9.6	11.15	12.95	10.6	13.75			
GU 1728 Lt	A											
GU 1728 R	A											
GU 8003	A									11.25	12.65	12.25
GU 8012	A											
GU 8015	A	8.65	6									
GU 8019	A			11.75	8.9							
GU 8020	A	9.8	5.7									
GU 8039	A											
WIF/A 1193	A											
WIF/A 1194	A											
WIF/A 1195	A											
WIF/A 1196	A											
WIF/A 1197	A											
WIF/A 1199	A											
GU 7002	B					11.2	11.95					
GU 7011	B											
GU 7012	B											
GU 7013	B							14.2	15.65			
GU 7022	B							10.4	13.5	11.25	12.4	11.5
GU 7023	B											
GU 9202	C							10.4	11.9	11		
WIF/A 4217	C							10.2	12.65	10.85	13.4	12.8
WIF/A 4219	C											
WIF/A 4220	C											
WIF/A 4221	C											
GU 9007	D					7.95	8.2					
GU 9008	D											
WIF/A 4213	D	5.4	3.0	7.1	5.4	7.6	8.3					

Continued.

Specimen no.	Group	P1L	P1W	P2L	P2W	P3L	P3W	P4L	P4W	M1Lbucc	M1Want	M1Wpost
WIF/A 4214	D							7.65	9.75			
WIF/A 4215	D			7.35	5.7							
WIF/A 4238	D											
WIF/A 4239	D							8.2	9.7			
WIF/A 4240	D							8.1	9.9			
WIF/A 4241	D											
WIF/A 4242	D											
WIF/A 4243	D											
WIF/A 4265	D			7.1	5.55	8.15	9	7.6	9.6	8.4	10	9.55

Specimen no.	Group	M2L	M2Want	M2Wpost	M3Lbucc	M3Lling	M3Wmax	dP3L	dP3W
GU 5	A							9.1	8
GU 12	A	12.4	14.65	14.2					
GU 18	A								
GU 202	A								
GU 204	A								
GU 402 Lt	A								
GU 402 R	A	12.35	14.35	13.55					
GU 404 Lt	A	12.95	14.65	13.65	10.55	11.1	14.2		
GU 404 R	A	13.1	14.9	14.2	10.85	11.75	14.1		
GU 412	A								
GU 413	A								
GU 415	A								
GU 417	A	12.5	14.05	12.7					
GU 418*	A				9.4	10.5	11.8		
GU 424	A								
GU 425	A				9.75	11.25	12.9		
GU 426	A								
GU 430	A								
GU 661	A								
GU 662	A								
GU 663	A								
GU 665	A	11.6	14.15	13.4					
GU 730 Lt	A							10	8.45
GU 730 R	A								
GU 731	A								
GU 732	A								
GU 784	A								
GU 785	A				12.3	14.3	14.6		
GU 1221	A				10.8	11.9	14.25		
GU 1222	A								
GU 1223	A								
GU 1516	A				10.5	12.7	15.3		
GU 1615	A								
GU 1616	A	12.8	13.9	13.7					
GU 1672	A				10.3	13.35	13.95		
GU 1683	A								
GU 1702a Lt	A	12.3	14.3	14.6	12	13.85	14.2		
GU 1702a R	A				11.05	13.75	14.3		
GU 1702b Lt	A	14.1	15.9	14.85	10.9	12.65	14		
GU 1702c Lt	A				11.45	13.9	14.3		
GU 1702d R	A				12	13.25	14.4		
GU 1708	A								
GU 1727	A	12.55	15.1	13.7	11.35	12.75	14.25		
GU 1728 Lt	A	12.7	15.2	14	11.6	12.7	14.1		
GU 1728 R	A	12.9	15.25	13.9	11.1	12.75	14.1		
GU 8003	A								
GU 8012	A				12.3	13.5	14.9		
GU 8015	A								
GU 8019	A								
GU 8020	A								
GU 8039	A							9.6	7.9
WIF/A 1193	A	14.3	17	15.4					
WIF/A 1194	A				11.15	13	14.45		
WIF/A 1195	A	12.9	15.25	14.25					
WIF/A 1196	A	14	17.3						
WIF/A 1197	A	13.1	14.85	13.9					
WIF/A 1199	A							9.8	8.25
GU 7002	B	12.3	14.25	13.45					
GU 7011	B				11.1	12.8	14.55		
GU 7012	B				11.15	12.3	14.2		
GU 7013	B								
GU 7022	B								

138 Rose et al.—*Cambaytherium* from the lower Eocene of India

Continued.

Specimen no.	Group	M2L	M2Want	M2Wpost	M3Lbucc	M3Lling	M3Wmax	dP3L	dP3W
GU 7023	B							9.45	8.1
GU 9202	C	12.25	14.55	13.6	11.55	13.95	14.4		
WIF/A 4217	C	11.6	15.3	14.1					
WIF/A 4219	C				12.5	14.7	14.15		
WIF/A 4220	C				12	14.7	15.3		
WIF/A 4221	C				12.7	14.25	14.3		
GU 9007	D								
GU 9008	D				8.45	9.55	10.4		
WIF/A 4213	D								
WIF/A 4214	D	9.45	11.8	10.75	8.1	9.05	10.8		
WIF/A 4215	D								
WIF/A 4238	D								
WIF/A 4239	D								
WIF/A 4240	D								
WIF/A 4241	D	8.55	10.2	9.6					
WIF/A 4242	D				8.7	10	10.5		
WIF/A 4243	D				8	9.6	11.2		
WIF/A 4265	D	9.25	11.2	10.3	8.85	9.55	11		

Specimen no.	Group	dP4L	dP4Want	dP4Wpost	P3L/W	P4L/W
GU 5	A	8.85	9.5	8.75		0.8
GU 12	A					
GU 18	A					
GU 202	A					
GU 204	A					0.83
GU 402 Lt	A					
GU 402 R	A				0.94	0.82
GU 404 Lt	A				0.96	0.82
GU 404 R	A				0.98	0.8
GU 412	A					0.86
GU 413	A					
GU 415	A					0.77
GU 417	A					
GU 418*	A					
GU 424	A					
GU 425	A					
GU 426	A				0.91	
GU 430	A					0.71
GU 661	A				0.9	0.77
GU 662	A					0.79
GU 663	A					0.82
GU 665	A					
GU 730 Lt	A	9.8	9.6	9.1		
GU 730 R	A	10	10.05	9.3		
GU 731	A					
GU 732	A					0.83
GU 784	A					
GU 785	A					
GU 1221	A					
GU 1222	A					
GU 1223	A					
GU 1516	A					
GU 1615	A					
GU 1616	A					
GU 1672	A					
GU 1683	A					
GU 1702a Lt	A					
GU 1702a R	A					0.78
GU 1702b Lt	A					
GU 1702c Lt	A					
GU 1702d R	A				1.03	0.83
GU 1708	A					0.77
GU 1727	A				0.86	0.77
GU 1728 Lt	A					
GU 1728 R	A					
GU 8003	A					
GU 8012	A					
GU 8015	A					
GU 8019	A					
GU 8020	A					
GU 8039	A					
WIF/A 1193	A					
WIF/A 1194	A					

(*Continued*)

Continued.

Specimen no.	Group	dP4L	dP4Want	dP4Wpost	P3L/W	P4L/W
WIF/A 1195	A					
WIF/A 1196	A					
WIF/A 1197	A					
WIF/A 1199	A					
GU 7002	B				0.94	
GU 7011	B					
GU 7012	B					
GU 7013	B					0.91
GU 7022	B					0.77
GU 7023	B	9.65	9.4	9.05		
GU 9202	C					
WIF/A 4217	C					
WIF/A 4219	C					
WIF/A 4220	C					
WIF/A 4221	C					
GU 9007	D					
GU 9008	D					
WIF/A 4213	D					
WIF/A 4214	D					
WIF/A 4215	D					
WIF/A 4238	D	8.3				
WIF/A 4239	D					
WIF/A 4240	D					
WIF/A 4241	D					
WIF/A 4242	D					
WIF/A 4243	D					
WIF/A 4265	D					

APPENDIX 4. Measurements (in mm) of lower teeth of *Cambaytherium*. Group designations are for MANOVA comparing different samples: A, *C. thewissi* from Vastan Mine; B, *C. thewissi* from Mangrol; C, *C. thewissi* from Tadkeshwar; D, *C. gracilis* from Tadkeshwar. **Abbreviations**: **dent ML**, dentary thickness below m1; **est**, estimated; **L**, length; **Lt**, left; **MD**, mandibular depth measured buccally at point indicated; **R**, right; **tal**, talonid; **tri**, trigonid; **W**, width. *From Vastan Mine, just below Lignite 1, probably TAD-2 equivalent; analyzed in group C.

Specimen no.	Group	p1L	p1W	p2L	p2W	p3L	p3W	p4L	p4W	m1L	m1Wtri	m1Wtal
GU 2	A											
GU 3	A											
GU 203	A									11.5	8	7
GU 221	A			13.75	7.75							
GU 222	A	8.2	4.9									
GU 401	A											
GU 403 Lt	A	7.2	4.25							11.2	7.85	7.95
GU 403 R	A	7.15	4.5					10.2	8.4	11.1	7.8	7.7
GU 414	A							10.55	7.5			
GU 427	A			13.1	6.95							
GU 659	A											
GU 660	A			13.55	8							
GU 664	A											
GU 674	A											
GU 733	A											
GU 734	A											
GU 736	A											
GU 776	A					12.8	8.6	10.55	7.95	11.6	8.3	7.75
GU 823	A											
GU 1515	A											
GU 1593	A											
GU 1594	A	7.9	4.5									
GU 1595	A											
GU 1596	A											
GU 1597	A											
GU 1598	A											
GU 1671	A							11.5	8.15/8.75			
GU 1679	A							11.5	8.8/9.3			
GU 1682	A											
GU 1700	A											
GU 1701	A											
GU 1709	A			12.4	7.3							
GU 1710	A			13.75	8.3	13.1		11	8.4	11.6	8.35	8.5
GU 1711	A									12.2	8.5	8.3
GU 7015	A	8.8	5.15									
GU 8004	A											

(*Continued*)

Continued.

Specimen no.	Group	p1L	p1W	p2L	p2W	p3L	p3W	p4L	p4W	m1L	m1Wtri	m1Wtal
GU 8005	A											
GU 8007	A											
GU 8008	A			14.65	8.8							
GU 8009	A							10.25	7.0/7.50			
GU 8010	A											
GU 8011	A											
GU 8014 Lt	A											
GU 8014 R	A											
GU 8031	A	6.8	4.4									
GU 8032	A											
GU 8041	A			14.9	8.4							
WIF/A 1198	A									11.65	8.6	8.45
WIF/A 4255	A							10.6	8.15/8.3			
WIF/A 4264	A							10.4	7.55/8.15			
GU 7001	B					12	7.6	10.4	7.2	11.8	7.9	7.6
GU 7004 Lt	B			13.9	8.7	13.3	9	10.85	8.6	12.9	8.6	8.25
GU 7004 R	B			13.9	8.95	13.1	9	10.75	8.7	12.35	8.75	8.3
GU 7017	B					13	8.4					
GU 7018	B							11.8	8.65			
GU 9006	C							11.6	8.2			
WIF/A 1200	C						8.55	11.2	8.4			
WIF/A 4222	C											
WIF/A 4223	C											
WIF/A 4224	C											
WIF/A 4232	C			12.4	8.35							
WIF/A 4233	C									12.5	10.05	9.6
WIF/A 4234	C											
GU 9001 TYPE	D					8.25	5.7	8.25	6.5	9.5	6.2	6.2
GU 9009	D									9.5	6.25	6.05
GU 9010	D							8.6	6.05			
GU 9019	D									9.5	6	5.9
WIF/A 4210	D			7.35	4.15	8.9	5.4	8.6	6.15	9.5	6.35	6.2
WIF/A 4211	D							8.5	6.45	9.4	6.2	6.3
WIF/A 4212	D											
WIF/A 4235	D							8.05	5.9			
WIF/A 4236	D							8.9	6.65			
WIF/A 4237	D											
GU 7016								12.7	9.8			
GU 8013*												

Specimen no.	Group	m2L	m2Wtri	m2Wtal	m3L	m3Wtri	m3Wtal	dp2L	dp2W	dp3L	dp3W
GU 2	A							9.75	4.4		
GU 3	A							10.45	5.4		
GU 203	A										
GU 221	A										
GU 222	A										
GU 401	A	13	9.1	8.9	14.7	8.5	7.4				
GU 403 Lt	A	12.9	9.35	8.8							
GU 403 R	A	12.65	9.3	8.75							
GU 414	A										
GU 427	A										
GU 659	A							9.7	4.85		
GU 660	A										
GU 664	A									11.45	5.55
GU 658	A				18.5	10.35	8.6				
GU 733	A									10.45	4.55
GU 734	A										
GU 736	A									11.45	5.65
GU 776	A	12.7	9.1	8.6							
GU 823	A				15.8	9.2	8.3				
GU 1515	A				19	9.9	9.6				
GU 1593	A							10	5		
GU 1594	A										
GU 1595	A	13.8	10	9.8	16.8	10.4	8.9				
GU 1596	A	13.2	9.3	8.6	16.6	9.25	8.3				
GU 1597	A				18.05	9.2	8.8				
GU 1598	A	14	8.8								
GU 1671	A										
GU 1679	A										
GU 1682	A									11.6	5.15
GU 1700	A	13.4	9.75	9.35	16.05	10.3	8.95				
GU 1701	A							10.2	4.65	11.5	5
GU 1709	A										

(*Continued*)

Continued.

Specimen no.	Group	m2L	m2Wtri	m2Wtal	m3L	m3Wtri	m3Wtal	dp2L	dp2W	dp3L	dp3W
GU 1710	A	13.6	9	9.15							
GU 1711	A	12.4	9.3	9.4	16.1	9.8	8.9				
GU 7015	A										
GU 8004	A	13.5	9.15	8.65							
GU 8005	A									10.25	4.35
GU 8007	A									11.5	5.15
GU 8008	A										
GU 8009	A										
GU 8010	A				15.8	9.3	8.5				
GU 8011	A				16.2	9.1	7.85				
GU 8014 Lt	A	14	9	8.4							
GU 8014 R	A	13.4	9.4	8.4							
GU 8031	A										
GU 8032	A							9.3	4.75		
GU 8041	A										
WIF/A 1198	A										
WIF/A 4255	A										
WIF/A 4264	A										
GU 7001	B	12.1	8.65	8.1	16.05	8.9	8.25				
GU 7004 Lt	B	13.6	9.6	9.65							
GU 7004 R	B	13.35	9.8	9.7	17.25	10	8.85				
GU 7017	B										
GU 7018	B										
GU 9006	C										
WIF/A 1200	C	14.95	10.05	10.4							
WIF/A 4222	C				15.4	10.1	9.15				
WIF/A 4223	C				17.75	10.9	10.6				
WIF/A 4224	C	13.5	9.95	9.7							
WIF/A 4232	C										
WIF/A 4233	C										
WIF/A 4234	C									11.35	6.1
GU 9001 TYPE	D	10.25	7.3	6.9	12.9	7.75	7.2				
GU 9009	D										
GU 9010	D										
GU 9019	D	10.2	7.25	7.35	12.1	7.4	7.2				
WIF/A 4210	D	10.9	7.5	7.25	12.35	7.45	6.75				
WIF/A 4211	D				13.3	8.2	7.2				
WIF/A 4212	D				12.85	7.35	6.65				
WIF/A 4235	D										
WIF/A 4236	D										
WIF/A 4237	D	10.75	7.35	6.95							
GU 7016											
GU 8013*		14.9	10.5	9.6							

Specimen no.	Group	dp4L	dp4Wtri	dp4Wtal	MD p3tal	MD m2tri	dent ML m1
GU 2	A						
GU 3	A						
GU 203	A						
GU 221	A						
GU 222	A						
GU 401	A						
GU 403 Lt	A						
GU 403 R	A					27.7	12.6
GU 414	A						
GU 427	A						
GU 659	A						
GU 660	A						
GU 664	A						
GU 658	A						
GU 733	A						
GU 734	A	10.7	6.25	6.15			
GU 736	A	11.05	7.15	7	20.7		
GU 776	A				30.85	35.2	14.8
GU 823	A						
GU 1515	A						
GU 1593	A						
GU 1594	A						
GU 1595	A					40 est	
GU 1596	A					31.8	
GU 1597	A						
GU 1598	A						
GU 1671	A						
GU 1679	A						

(*Continued*)

Continued.

Specimen no.	Group	dp4L	dp4Wtri	dp4Wtal	MD p3tal	MD m2tri	dent ML m1
GU 1682	A						
GU 1700	A					32.1	17.5
GU 1701	A				18.8		
GU 1709	A						
GU 1710	A						
GU 1711	A					34.3	15.05
GU 7015	A						
GU 8004	A						
GU 8005	A						
GU 8007	A						
GU 8008	A						
GU 8009	A						
GU 8010	A						
GU 8011	A						
GU 8014 Lt	A						
GU 8014 R	A						
GU 8031	A						
GU 8032	A						
GU 8041	A						
WIF/A 1198	A						
WIF/A 4255	A						
WIF/A 4264	A						
GU 7001	B				23.75		10.4
GU 7004 Lt	B						
GU 7004 R	B						12.25
GU 7017	B						
GU 7018	B						
GU 9006	C						
WIF/A 1200	C				26.2	30.3	16
WIF/A 4222	C						
WIF/A 4223	C						
WIF/A 4224	C						
WIF/A 4232	C						
WIF/A 4233	C						
WIF/A 4234	C						
GU 9001 TYPE	D				18.5	19.7	9.05
GU 9009	D						
GU 9010	D						
GU 9019	D						
WIF/A 4210	D					22	10.5
WIF/A 4211	D						11.2
WIF/A 4212	D						
WIF/A 4235	D						
WIF/A 4236	D						
WIF/A 4237	D						
GU 7016							
GU 8013*							

FIGURE A1. Size distribution of p3 in *Cambaytherium*. **Abbreviations**: **L**, length; **W**, width.

FIGURE A2. Size distribution of m3 in *Cambaytherium*. **Abbreviations**: **L**, length; **Wtri**, trigonid width; **Wtal**, talonid width.
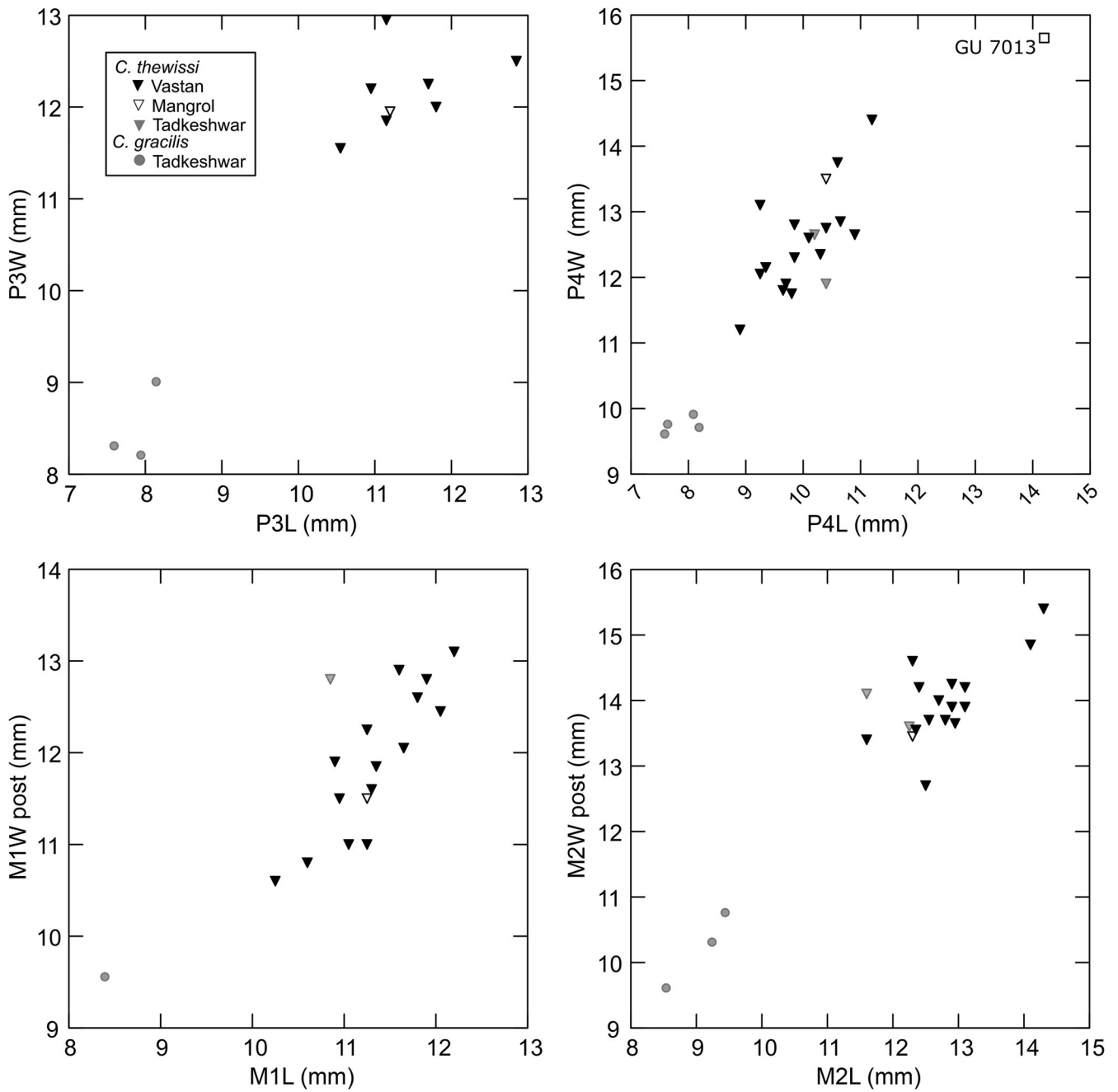
FIGURE A3. Upper teeth size distributions in *Cambaytherium*. **Abbreviations**: **L**, length; **W**, width; **Wpost**, posterior width of M2.

APPENDIX 5. Summary measurements (in mm) and statistics for upper and lower teeth of *Cambaytherium thewissi* (Vastan and Mangrol mines). **Abbreviations**: **ant**, anterior; **bucc**, buccal; **Dent ML**, mediolateral thickness of dentary; **L**, length; **ling**, lingual; **max**, maximum; **MD**, mandibular depth; **post**, posterior; **tal**, talonid; **tri**, trigonid; **W**, width.

Statistic	P1L	P1W	P2L	P2W	P3L	P3W	P4L	P4W
N of cases	2	2	6	6	8	8	17	17
Minimum	8.65	5.70	11.35	8.20	10.55	11.55	8.90	11.20
Maximum	9.80	6.00	13.35	9.70	12.85	12.95	11.20	14.40
Arithmetic mean	9.23	5.85	12.50	8.74	11.42	12.16	10.01	12.58
Standard deviation	0.813	0.212	0.915	0.520	0.701	0.429	0.638	0.799
Coefficient of variation	8.8	3.6	7.3	5.9	6.1	3.5	6.4	6.4
Shapiro-Wilk statistic	—	—	0.808	0.865	0.900	0.968	0.979	0.973
Shapiro-Wilk P-value	—	—	0.070	0.205	0.290	0.886	0.947	0.861

Statistic	M1L	M1Want	M1Wpost	M2L	M2Want	M2Wpost	M3Lbucc	M3Lling	M3Wmax
N of Cases	17	17	16	17	17	16	20	20	20
Minimum	10.25	10.90	10.60	11.60	13.90	12.70	9.40	10.50	11.80
Maximum	12.20	13.55	13.10	14.30	17.30	15.40	12.30	14.30	15.30
Arithmetic mean	11.32	12.32	11.87	12.87	15.00	13.97	11.08	12.70	14.12
Standard deviation	0.512	0.756	0.779	0.706	0.964	0.635	0.766	1.003	0.765
Coefficient of variation	4.5	6.1	6.6	5.5	6.4	4.5	6.9	7.9	5.4
Shapiro-Wilk statistic	0.979	0.972	0.962	0.914	0.862	0.965	0.964	0.958	0.742
Shapiro-Wilk P-value	0.948	0.854	0.698	0.118	0.016	0.760	0.622	0.502	0.000

Statistic	DP3L	DP3W	DP4L	DP4Want	DP4Wpost
N of cases	5	5	4	4	4
Minimum	9.10	7.90	8.85	9.40	8.75
Maximum	10.00	8.45	10.00	10.05	9.30
Arithmetic mean	9.59	8.14	9.58	9.64	9.05
Standard deviation	0.344	0.216	0.504	0.287	0.227
Coefficient of variation	3.6	2.7	5.3	3.0	2.5
Shapiro-Wilk statistic	0.987	0.970	0.872	0.870	0.963
Shapiro-Wilk P-value	0.969	0.875	0.305	0.296	0.797

Statistic	p1L	p1W	p2L	p2W	p3L	p3W	p4L	p4W	m1L	m1Wtri	m1Wtal
N of cases	6	6	9	9	6	5	13	13	10	10	10
Minimum	6.8	4.25	12.4	6.95	12	7.6	10.2	7	11.1	7.8	7
Maximum	8.8	5.15	14.9	8.95	13.3	9	11.8	8.8	12.9	8.75	8.5
Arithmetic mean	7.642	4.6	13.767	8.128	12.883	8.52	10.796	8.081	11.79	8.265	7.98
Standard deviation	0.732	0.324	0.747	0.688	0.462	0.576	0.514	0.598	0.549	0.352	0.472
Coefficient of variation	9.6	.7	5.4	8.5	3.6	6.8	4.8	7.4	4.7	4.3	5.9
Shapiro-Wilk statistic	0.938	0.909	0.95	0.942	0.808	0.871	0.894	0.917	0.929	0.906	0.906
Shapiro-Wilk P-value	0.645	0.432	0.685	0.608	0.069	0.269	0.112	0.229	0.435	0.255	0.257

Statistic	m2L	m2Wtri	m2Wtal	m3L	m3Wtri	m3Wtal	dp2L	dp2W	dp3L	dp3W
N of Cases	16	16	15	13	13	13	6	6	7	7
Minimum	12.1	8.65	8.1	14.7	8.5	7.4	9.3	4.4	10.25	4.35
Maximum	14	10	9.8	19	10.4	9.6	10.45	5.4	11.6	5.65
Arithmetic mean	13.225	9.288	8.95	16.685	9.554	8.554	9.9	4.842	11.171	5.057
Standard deviation	0.558	0.365	0.528	1.216	0.608	0.555	0.406	0.34	0.566	0.478
Coefficient of variation	4.2	3.9	5.9	7.3	6.4	6.5	4.1	.7	5.1	9.5
Shapiro-Wilk statistic	0.958	0.973	0.943	0.928	0.931	0.958	0.986	0.975	0.707	0.938
Shapiro-Wilk P-value	0.621	0.891	0.427	0.323	0.355	0.719	0.977	0.923	0.004	0.617

Statistic	dp4L	dp4Wtri	dp4Wtal	MD at p3tal	MD at m2tri	Dent ML at m1
N of cases	2	2	2	4	6	6
Minimum	10.7	6.25	6.15	18.8	27.7	10.4
Maximum	11.05	7.15	7	30.85	40	17.5
Arithmetic mean	10.875	6.7	6.575	23.525	33.517	13.767
Standard deviation	0.247	0.636	0.601	5.292	4.105	2.516
Coefficient of variation	2.3	9.5	9.1	22.5	12.2	18.3
Shapiro-Wilk statistic	—	—	—	0.919	0.973	0.972
Shapiro-Wilk P-value	—	—	—	0.534	0.915	0.903

APPENDIX 6. Summary measurements (in mm) and statistics for upper and lower teeth of *Cambaytherium thewissi* (Tadkeshwar Mine). **Abbreviations**: **ant**, anterior; **bucc**, buccal; **Dent ML**, mediolateral thickness of dentary; **L**, length; **ling**, lingual; **max**, maximum; **MD**, mandibular depth; **post**, posterior; **tal**, talonid; **tri**, trigonid; **W**, width.

Statistic	P4L	P4W	M1L	M1Want	M1Wpost	M2L	M2Want	M2Wpost	M3Lbucc	M3Lling	M3Wmax
N of cases	2	2	2	1	1	2	2	2	4	4	4
Minimum	10.20	11.90	10.85	13.40	12.80	11.60	14.55	13.60	11.55	13.95	14.15
Maximum	10.40	12.65	11.00	13.40	12.80	12.25	15.30	14.10	12.70	14.70	15.30
Arithmetic mean	10.30	12.28	10.93	13.40	12.80	11.93	14.93	13.85	12.19	14.40	14.54
Standard deviation	0.141	0.530	0.106	—	—	0.460	0.530	0.354	0.517	0.367	0.519
Coefficient of variation	1.4	4.3	1.0	—	—	3.9	3.6	2.6	4.2	2.6	3.6
Shapiro-Wilk statistic	—	—	—	—	—	—	—	—	0.952	0.860	0.807
Shapiro-Wilk P-value	—	—	—	—	—	—	—	—	0.726	0.262	0.116

Statistic	p2L	p2W	p3W	p4L	p4W	m1L	m1Wtri	m1Wtal	m2L	m2Wtri	m2Wtal
N of cases	1	1	1	2	2	1	1	1	3	3	3
Minimum	12.40	8.35	8.55	11.20	8.20	12.50	10.05	9.60	13.50	9.95	9.60
Maximum	12.40	8.35	8.55	11.60	8.40	12.50	10.05	9.60	14.95	10.50	10.40
Arithmetic mean	12.40	8.35	8.55	11.40	8.30	12.50	10.05	9.60	14.45	10.17	9.90
Standard deviation	—	—	—	0.283	0.141	—	—	—	0.823	0.293	0.436
Coefficient of variation	—	—	—	2.5	1.7	—	—	—	5.7	2.9	4.4
Shapiro-Wilk statistic	—	—	—	—	—	—	—	—	0.776	0.881	0.842
Shapiro-Wilk P-value	—	—	—	—	—	—	—	—	0.058	0.328	0.220

Statistic	m3L	m3Wtri	m3Wtal	dp3L	dp3W	MD at p3tal	MD at m2tri	Dent ML at m1
N of cases	2	2	2	1	1	1	1	1
Minimum	15.40	10.10	9.15	11.35	6.10	26.20	30.30	16.00
Maximum	17.75	10.90	10.60	11.35	6.10	26.20	30.30	16.00
Arithmetic mean	16.58	10.50	9.88	11.35	6.10	26.20	30.30	16.00
Standard deviation	1.662	0.566	1.025	—	—	—	—	—
Coefficient of variation	10.0	5.4	10.4	—	—	—	—	—
Shapiro-Wilk statistic	—	—	—	—	—	—	—	—
Shapiro-Wilk P-value	—	—	—	—	—	—	—	—

APPENDIX 7. Summary of body mass (BM) estimates (kg) for *Cambaytherium* by element and species, based on Scott's (1990) suoid and all-ungulate regressions. *Measurements taken (see Table 3).

| Element	Specimen number	Locality	Measure*	BM (Suoid-only)	BM (All-ungulate)
C. thewissi					
Humerus	GU 270	Vastan	H5	35.21	36.21
Humerus	GU 737	Vastan	H3, H5	30.96	27.05
Humerus	GU 778	Vastan	H3	22.28	16.03
Humerus	GU 809	Vastan	H3	22.91	16.42
Humerus	GU 834	Vastan	H5, H7, H8	21.01	21.95
Humerus	GU 7006	Vastan	H4, H5	25.86	23.40
Humerus	WIF/A 4262	TAD-2	H7, H8	14.43	15.02
Radius	GU 274	Vastan	R2, R3, R6	16.62	11.06
Radius	GU 771	Vastan	R2, R3	17.57	13.20
Radius	GU 842	Vastan	R2, R3	22.54	16.26
Radius	GU 7019	Mangrol	R6	24.52	8.54
Radius	GU 8051	Vastan	R6	15.95	5.91
Femur	GU 198	Vastan	F5	22.60	19.29
Femur	WIF/A 2262	TAD-1	F6, F7	15.02	12.65
Femur	WIF/A 4207	TAD-1	F2, F3, F5, F6, F7	19.15	15.15
Femur	WIF/A 4258	TAD-2	F6, F7	17.56	14.82
Femur	WIF/A 4259	TAD-2	F6, F7	22.96	19.03
Tibia	GU 278	Vastan	T4, T5	33.99	22.40
Tibia	GU 739	Vastan	T4, T5, T6, T7	13.31	10.50
Tibia	GU 779	Vastan	T6, T7	16.31	12.24
Tibia	GU 9207	TAD-2	T4, T5, T6, T7	23.17	16.97
Tibia	GU 9211	TAD-2	T6, T7	21.49	15.80
C. gracilis					
Humerus	GU 9018	TAD-2	H7, H8	7.10	7.67
Radius	WIF/A 4244	TAD-2	R2, R3, R6	7.87	5.34
Femur	GU 9208	TAD-2	F3, F5, F6, F7	12.23	10.77
Femur	GU 9210	TAD-2	F3, F5, F6, F7	10.21	9.09
Femur	WIF/A 4257	TAD-2	F6, F7	12.04	9.70
C. marinus					
Femur	GU 7026	Mangrol	F2, F3	157.99	115.31
Tibia	GU 8052	Vastan	T4, T5	90.75	57.64
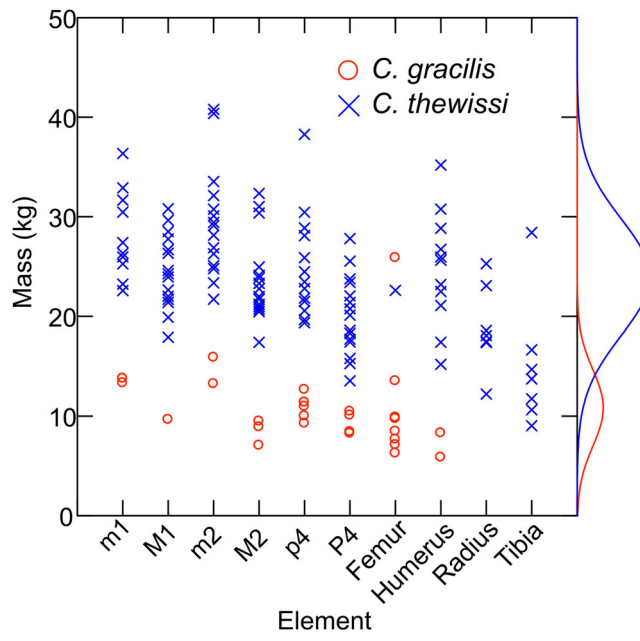
FIGURE A4. Predicted body mass of *Cambaytherium* based on each specimen of each element used for body mass estimation. Curves at right show distribution of mass estimates across elements for each species (*C. thewissi* above, *C. gracilis* below).